

British Columbia Geological Survey
Ministry of Energy and Mines
www.em.gov.bc.ca/geology

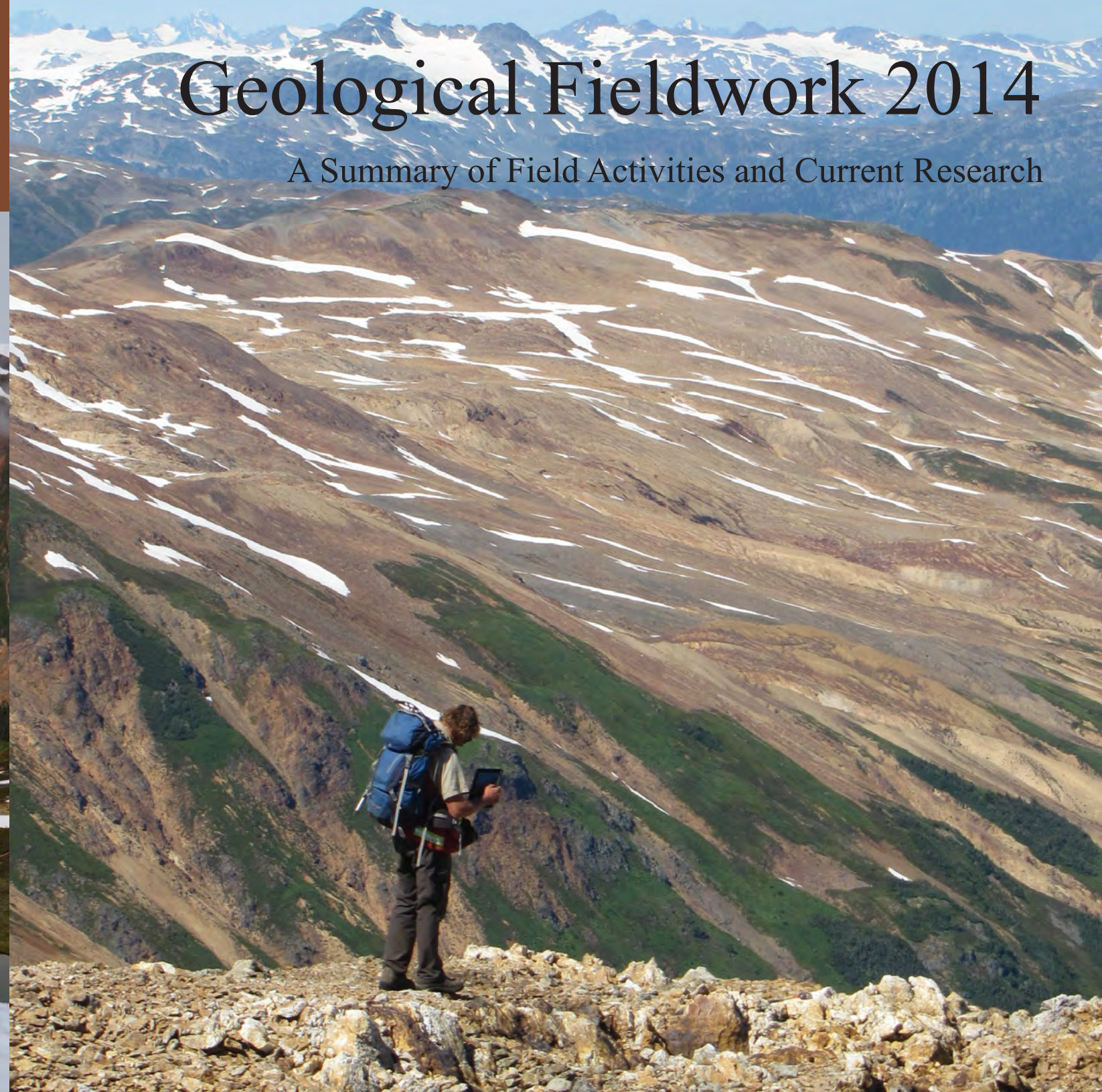


Ministry of
Energy and Mines



Geological Fieldwork 2014

A Summary of Field Activities and Current Research





Ministry of
Energy and Mines



Geological Fieldwork 2014

A Summary of Field Activities and Current Research

Ministry of Energy and Mines
British Columbia Geological Survey

Paper 2015-1

Ministry of Energy and Mines Mines and Mineral Resources Division British Columbia Geological Survey

Recommended citation format for individual papers:

Rukhlov, A.S., Han, T., Nelson, J., Hickin, A., and Ferri, F., 2015. Carlin-type geochemical signal in lake and stream sediments from the Kechika trough, north-central British Columbia. In: Geological Fieldwork 2014, British Columbia Ministry of Energy and Mines, British Columbia Geological Survey Paper 2015-1, pp. 165-188.

Front Cover: Upper 'Lake' ridge in the Snippaker Creek area. In the foreground, Early Jurassic plagioclase-phyric diorite dikes of the Lehto suite intrude Stuhini volcanoclastic rocks. Immediately beyond, Sericite Ridge hosts a broad zone of quartz-sericite-pyrite alteration. See Kyba, J. and Nelson, J.L., 2015. Stratigraphic and tectonic framework of the Khyber-Sericite-Pins mineralized trend, lower Iskut River, northwest British Columbia, this volume. **Photo by JoAnne Nelson.**

Back Cover: Snippaker Creek area, looking west from 'Lake' ridge and the Lehto pluton at the Sky fault system, which juxtaposes strongly quartz-sericite-pyrite-chlorite replaced rocks on Sericite Ridge (foreground) with highly strained, less altered sedimentary rocks (background) along a northwest-southeast trend near the toe of an unnamed glacier. See Kyba, J. and Nelson, J.L., 2015. Stratigraphic and tectonic framework of the Khyber-Sericite-Pins mineralized trend, lower Iskut River, northwest British Columbia, this volume. **Photo by Adrian Hickin.**

This publication is available, free of charge, from the British Columbia Geological Survey website:
<http://www.em.gov.bc.ca/Mining/Geoscience/PublicationsCatalogue/Fieldwork>

British Columbia Cataloguing in Publication Data

Main entry under title:

Geological Fieldwork: - 1974 -

Annual.

Issuing body varies

Vols. for 1978-1996 issued in series: Paper / British Columbia. Ministry of Energy, Mines and Petroleum Resources; vols. for 1997 - 1998, Paper / British Columbia. Ministry of Employment and Investment; vols. for 1999-2004, Paper / British Columbia. Ministry of Energy and Mines; vols. for 2005-2009, Paper / British Columbia. Ministry of Energy, Mines and Petroleum Resources; vols. for 2010, Paper / British Columbia. Ministry of Forests, Mines and Lands; vols. for 2011, Paper / British Columbia. Ministry of Energy and Mines; vols. for 2012- , Paper / British Columbia. Ministry of Energy, Mines and Natural Gas; vols. for 2014- , Paper / British Columbia. Ministry of Energy and Mines.

Includes Bibliographical references.

ISSN 0381-243X=Geological Fieldwork

1. Geology - British Columbia - Periodicals. 2. Mines and mineral resources - British Columbia - Periodicals. 3. Geology - Fieldwork - Periodicals. 4. Geology, Economic - British Columbia - Periodicals. 5. British Columbia. Geological Survey Branch - Periodicals. I. British Columbia. Geological Division. II. British Columbia. Geological Survey Branch. III. British Columbia. Geological Survey Branch. IV. British Columbia. Dept. of Mines and Petroleum Resources. V. British Columbia. Ministry of Energy, Mines and Petroleum Resources. VI. British Columbia. Ministry of Employment and Investment. VII. British Columbia Ministry of Energy and Mines. VIII. Series: Paper (British Columbia. Ministry of Energy, Mines and Petroleum Resources). IX. Series: Paper (British Columbia. Ministry of Employment and Investment). X. Series: Paper (British Columbia Ministry of Energy and Mines). XI. Series: Paper (British Columbia Ministry of Energy, Mines and Petroleum Resources). XII. Series: Paper (British Columbia Ministry of Forests, Mines and Lands). XIII. Series: Paper (British Columbia Ministry of Energy and Mines). XIV. Series: Paper (British Columbia Ministry of Energy, Mines and Natural Gas). XV. Series: Paper (British Columbia Ministry of Energy and Mines).

QE187.46 622.1'09711 C76-083084-3 (Rev.)

Victoria
British Columbia
Canada

January 2015

Foreword

Geological Fieldwork 2014

This is the 40th edition of Geological Fieldwork, a volume of peer-reviewed papers that present the results of geological research conducted by the British Columbia Geological Survey (BCGS) and its partners in 2014. The papers address various aspects of British Columbia's geology, with many highlighting the mineral wealth of the Province. The annual Geological Fieldwork publication is one way that the BCGS helps to unlock this mineral wealth by providing comprehensive, objective, and up-to-date geoscience information, advice, and knowledge to the minerals industry.

The BCGS underwent considerable renewal this year with the addition of 7 new permanent staff to fill both new positions and several longstanding vacancies.

British Columbia Geological Survey activity highlights

Research

- Fieldwork and in-house laboratory studies continued on three projects that are part of the Geological Survey of Canada's (GSC) Targeted Geoscience Initiative program (TGI-4).
- Initiatives on the metallogeny of porphyry deposits in British Columbia continued with industry colleagues and the GSC as part of a renewed Geo-mapping for Energy and Minerals program (GEM-2).
- A new geochemical initiative on indicator minerals began with a joint team of five researchers from the School of Earth and Ocean Sciences (University of Victoria) and the BCGS.
- BCGS geologists published three Geoscience Maps, fifteen Open Files, eleven Geofiles, nine Information Circulars, thirteen external papers, and seven interagency publications.

Outreach at conferences and workshops

- Survey geologists presented at conferences and workshops including Roundup, PDAC, GSA, KEG, GACMAC, Minerals South, Minerals North, FOSS4G, Cordilleran Tectonics Workshop, and the Smither's Rock Talk.
- BCGS staff chaired two technical sessions and presented numerous talks and posters at the Geological Society of America (GSA) 2014 Annual Meeting in Vancouver. This was the first time in 16 years that the GSA held its annual meeting outside of the United States and over 7,000 delegates were in attendance.
- The newest generation of MapPlace, the Survey's web service, was tested by clients at a workshop held at the Minerals South Conference in Nelson.

Data archiving and access

- Clients can now access over 34,000 company mineral assessment reports using the online ARIS database.
- The Property File database now features more than 54,000 documents online.
- MINFILE continues to expand with 14,000 occurrences recorded. In the past two and half years, updates to 5,900 occurrences included 1,700 new entries.
- The Regional Geochemical Survey (RGS) database was re-compiled from the original published sources into a MS Access database to remove inconsistencies. The new database now contains 64,828 samples covering 80% of the province.
- The Provincial litho-geochemical database, last released in 2005, underwent retrofitting and updating to improve data quality.

Renewal

- The BCGS's Mineral Development Office in Vancouver underwent a complete renovation in 2014, just in time for the arrival of its new Director, Gordon Clarke.

Awards

- The 2013-2014 Fraser Institute's global ranking of geological databases ranked MapPlace third again in 2014. Since 2005, MapPlace has consistently been ranked in the top ten, including two first place placements.

Stephen M. Rowins
Chief Geologist & Executive Director
British Columbia Geological Survey



Table of Contents

Hickin, Adrian S., Jones, Larry D., Rowins, Stephen M., and Clarke, Gordon: British Columbia Geological Survey annual program review 2014-2015.....	1
Schiarizza, Paul: Geological setting of the Granite Mountain batholith, south-central British Columbia	19
Kyba, Jeff and Nelson, JoAnne: Stratigraphic and tectonic framework of the Khyber-Sericite-Pins mineralized trend, lower Iskut River, northwest British Columbia.....	41
Febbo, Gayle E., Kennedy, Lori A., Savell, Michael, Creaser, Robert A., and Friedman, Richard M.: Geology of the Mitchell Au-Cu-Ag-Mo porphyry deposit, northwestern British Columbia, Canada	59
Cutts, J.A., McNicoll, V.J., Zagorevski, A., Anderson, R.G., and Martin, K.: U-Pb geochronology of the Hazelton Group in the McTagg anticlinorium, Iskut River area, northwestern British Columbia	87
Han, Tian and Nelson, JoAnne: Mapping hydrothermally altered rocks with Landsat 8 imagery: A case study in the KSM and Snowfield zones, northwestern British Columbia.....	103
Ryan, James J., Nelson, JoAnne, and van Staal, Cees: Fieldwork in the Sylvester allochthon, Cassiar Mountains, British Columbia: Investigations of the Rapid River tectonite and the Slide Mountain terrane	113
Mihalynuk, Mitchell G., Diakow, Larry J., Logan, James M., and Friedman, Richard M.: Preliminary geology of the Shrimpton Creek area (NTS 092H/15E, 16W) Southern Nicola Arc Project.....	129
Rukhlov, Alexei S., Han, Tian, Nelson, JoAnne, Hickin, Adrian, and Ferri, Filippo: Carlin-type geochemical signal in lake and stream sediments from the Kechika trough, north-central British Columbia.....	165
Mackay, D.A.R., Simandl, G.J., Luck, P., Grcic, B., Li, C., Redfearn, M., and Gravel, J.: Concentration of carbonatite indicator minerals using a Wilfley gravity shaking table: A case history from the Aley carbonatite, British Columbia, Canada.....	189
Appendix: British Columbia Geological Survey publications, 2014.....	197

British Columbia Geological Survey annual program review 2014-2015

Adrian S. Hickin^{1, a}, Larry D. Jones¹, Stephen M. Rowins¹, and Gordon Clarke²

¹ British Columbia Geological Survey, Ministry of Energy and Mines, Victoria, BC, V8W 9N3

² British Columbia Geological Survey, Ministry of Energy and Mines, Vancouver, BC, V6Z 2G3

^a corresponding author: Adrian.Hickin@gov.bc.ca

Recommended citation: Hickin, A.S., Jones, L.D., Rowins, S.M., and Clarke, G., 2015. British Columbia Geological Survey annual program review. In: Geological Fieldwork 2014, British Columbia Ministry of Energy and Mines, British Columbia Geological Survey Paper 2015-1, pp. 1-17.

1. Introduction

This annual review highlights the activities of the British Columbia Geological Survey (BCGS) in 2014, providing a summary of projects, events, and accomplishments. In 2015, the BCGS will celebrate 120 years of service to British Columbia and the mineral exploration industry. Throughout this long history, the core role of the Survey has been to link government, the minerals industry, and British Columbians to the Province's geology and mineral resources (see The British Columbia Geological Survey, IC2014-7¹). In support of this core role, the Survey is committed to:

- creating, maintaining, and delivering geoscience knowledge to lead informed decision making
- attracting companies and individuals to explore British Columbia for new mineral and coal resources
- acting as the public steward of mineral and coal resources for current and future generations
- guiding public policy by providing assessments on the nature and economic health of mineral exploration and mining activities

The BCGS is responsible for documenting, assessing and archiving the geology and related mineral and coal resources of the Province. The Survey strives to be a leader in public government geoscience, providing data and knowledge to all stakeholders through traditional reports, maps, databases, and resident expertise, but also through innovative web-based delivery. The BCGS is a branch in the Mines and Mineral Resources Division of the Ministry of Energy and Mines. It is headquartered in Victoria, on south Vancouver Island. The Survey is led by Stephen Rowins, the Chief Geologist and Executive Director, and consists of three sections: 1) Cordilleran Geoscience; 2) Resource Information; and 3) the Mineral Development Office (MDO).

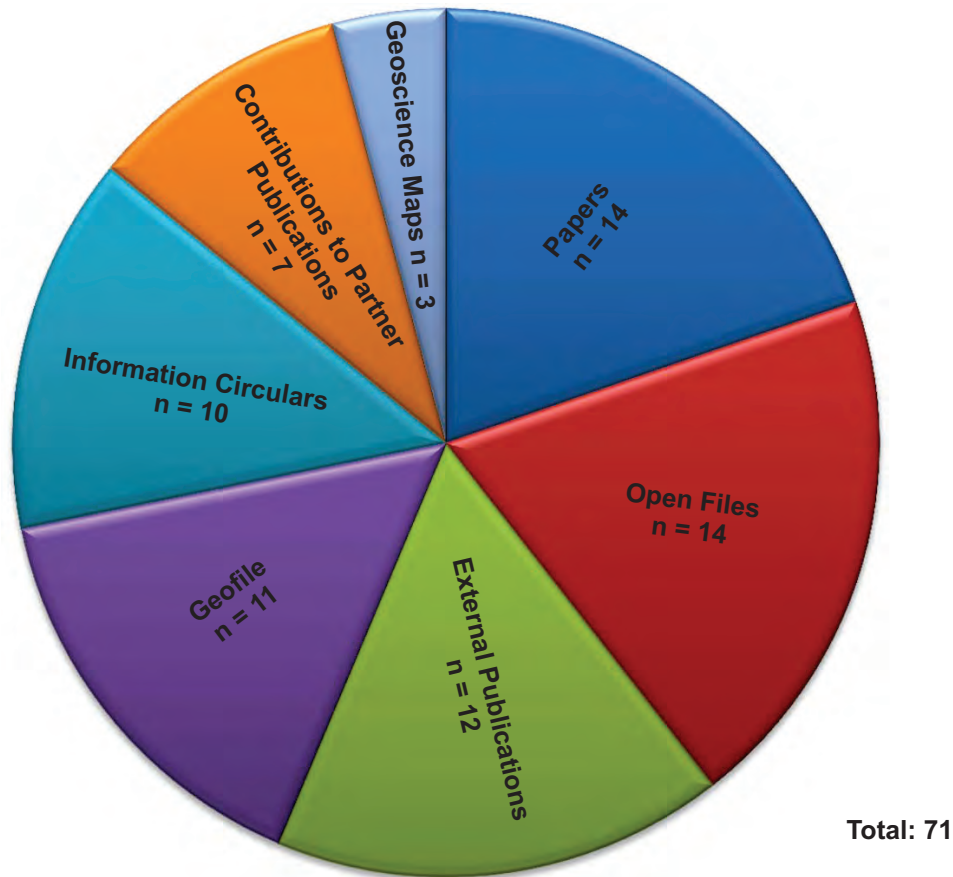
The Cordilleran Geoscience Section, led by Adrian Hickin, is responsible for generating new geoscience knowledge largely

through field-based surveys and targeted mineral deposit studies. Larry Jones directs the Resource Information Section, which is responsible for maintaining and developing the provincial geoscience databases and disseminating geoscience data online. Since 1947, the Resource Information Section has been responsible for evaluating and archiving assessment reports filed by the exploration and mining industry. These reports provide information on geological, geophysical, and geochemical activities related to mineral exploration in BC. Most reports are available online from the ARIS (Assessment Report Indexing System) website. The Mineral Development Office (MDO) is the Survey's Vancouver office and is led by Gordon Clarke. Vancouver is a centre of excellence for global mineral exploration and is the headquarters for more than 800 exploration and mining companies. As the technical marketing arm of the Survey, the MDO is well positioned to connect the exploration community with mineral and coal opportunities, geoscience products of the BCGS, and outputs of the Regional Geologist Program.

The British Columbia Geological Survey provides free web-based access to all of its geoscience outputs. In 2014, the Survey produced 71 new publications (Fig. 1; see Appendix, this volume) the results of which were presented at regional, national, and international scientific meetings and conferences. All publications, data releases, conference presentations, websites, and databases on MapPlace (MINFILE, ARIS, COALFILE, Property File) are profiled annually at the Association for Mineral Exploration in BC (AMEBC) Mineral Exploration Roundup in Vancouver and the Prospectors and Developers Association of Canada (PDAC) meeting in Toronto. Survey products are also distributed at regional geoscience meetings across the province throughout the year.

In January 2015, the Ministry of Energy and Mines and the British Columbia Geological Survey will inaugurate the 'BC Pavilion' at the Vancouver Convention Centre, the new venue for the Mineral Exploration Roundup. Designed as a one-stop venue for Roundup delegates to discuss the business of mineral exploration with government personnel, the Pavilion will be staffed by representatives from the BCGS, Mineral Titles

¹ British Columbia Geological Survey. Information Circular 2014-7, www.empr.gov.bc.ca/Mining/Geoscience/PublicationsCatalogue/InformationCirculars/Pages/IC2014-7.aspx



Types of Publications by the British Columbia Geological Survey

Papers: This series is reserved for reviews and final thematic or regional works. *Geological Fieldwork, our annual review of field activities and current research, is released as the first Paper of each year.

Geoscience Maps: This series is the BCGS vehicle for publishing final maps.

Open Files: These maps and reports present the interim results of ongoing research, particularly mapping projects.

GeoFiles: These publications enable rapid release of extensive data tables from ongoing geochemical, geochronologic, and geophysical work. As such, they serve the same function as data repositories provided by many journals, providing immediate access to raw data from specific projects.

Information Circulars: These publications provide accessible geoscience information to a broad audience in government, industry, and the general public. Included in the Information Circular series are the annual Provincial Overview of Mining and Exploration, **Exploration and Mining in British Columbia, and the Coal Industry Overview.

Contributions to partner publications: This category included reports, maps, and other products published by another agency such as the Geological Survey of Canada or Geoscience BC, but have received contributions from British Columbia Geological Survey staff.

External publications: These are contributions to the peer reviewed literature and published in a recognized national or international scientific journal.

*The count refers to the total number of article included in Geological Fieldwork.

**Although five articles are included in Exploration and Mining in British Columbia, the volume is counted as a single Information Circular.

Fig. 1. British Columbia Geological Survey publications in 2014.

Branch, Health, Safety and Permitting Branch, FrontCounter BC, and DataBC. The new space will afford the Survey and sister government organizations with the opportunity to present program highlights, geoscience information, and new exploration opportunities, and assist delegates with permitting and tenuring issues.

2. Partnerships

Limited government resources combined with a challenging global investment climate mean that collaborative geoscience partnerships are necessary to maximize the effectiveness of BCGS projects. In 2014, the BCGS collaborated with the Geological Survey of Canada, universities, Geoscience BC, and industry to deliver diverse geoscience projects, some of which are described below. Please contact Adrian Hickin (Director, Cordilleran Geoscience; Adrian.Hickin@gov.bc.ca) for details about partnering with the Survey.

2.1. Geological Survey of Canada

The BCGS and the Geological Survey of Canada (GSC) continue to collaborate closely on both large and small geoscience projects. In 2014, the Province engaged in two main collaborations: the fourth iteration of the Targeted Geoscience Initiative (TGI4) program; and the second iteration of the Geo-mapping for Energy and Minerals (GEM 2) program.

2.1.1. Targeted Geoscience Initiative 4

The TGI4 program provides geoscience knowledge to effectively target buried mineral deposits. The past 30 years have seen a marked decline in proven and probable mineral reserves in Canada (Duke, 2010). As surface discoveries decline, exploration efforts are directed at targets under deep cover. The aims of the program are to: 1) develop robust means of determining if a geological system may contain deeply buried ore (system fertility) and providing a direction to that ore (exploration vectors), thereby reducing investment risk and cost; and 2) develop new and improved geoscience knowledge and techniques to better understand, model, and detect mineral systems. The BCGS has partnered with the GSC on three TGI4 projects: 1) Specialty metals; 2) Orogenic Ni-Cu-PGE; and 3) Porphyry indicator minerals (PIMs) in till. These projects are described in following sections.

2.1.2. Geo-mapping for Energy and Minerals 2

The GSC launched the first phase of a five-year Geo-mapping for Energy and Minerals (GEM) program in 2008. During this phase, the BCGS participated in several initiatives as part of the “EDGES” project (Fig. 2). The goal of EDGES was to outline resource-rich environments in the exotic terranes that accreted to the western flank ancestral North America. BCGS contributions included mapping projects on BC’s north coast, Kutcho region, central BC (QUEST compilation) and northwest BC (Sutlahine). The second phase of GEM, a seven-year program (2013-2020), was announced in August 2013. The BCGS is participating in the Cordilleran Regional project (Fig. 2), which

involves the geological surveys of Yukon, Alaska, BC and the Canadian Government. Multidisciplinary field-based studies in poorly understood areas will focus on bedrock geology, crustal architecture, Cordilleran tectonics, and metallogeny to help drive the discovery of new mineral deposits and increase known resources. In addition, surficial geology and glacial history studies will provide vital knowledge for mineral exploration in covered regions. Initial work will be directed at western and southern Yukon and northernmost British Columbia through three themes, or “activities” including: 1) Crustal Blocks, 2) Porphyry Transition, and 3) Cache Creek (Fig. 2). Each activity will begin with a short field reconnaissance to identify priority areas and develop more substantive studies. Surficial geology activities will be integrated with bedrock mapping, facilitating mineral exploration in glaciated and unglaciated drift-covered areas of the Yukon.

2.2. Ministry of Energy and Mines-University of Victoria Partnership (MEM-UVic Partnership)

The goal of this partnership is to support research projects and student training that will benefit UVic, MEM and the energy and mining sectors in BC. Since 2003, the partnership has funded 37 research projects, 25 student projects, and 45 student Co-op positions. Additional funding to the partnership in 2012 supported six new four-month Co-op term positions with the BCGS, three joint research projects, and a project aimed at engaging youth through minerals and mining education.

2.3. Geoscience BC-Targeting Resources for Exploration and Knowledge (TREK)

The Targeting Resources for Exploration and Knowledge (TREK) Project, initiated in 2013, focuses on the northern Interior Plateau. This is an underexplored region with complex and thick sediment and volcanic cover. The first phase of the TREK geochemistry component was a collaboration between the BCGS and Geoscience BC. In 2013 the BCGS completed its contribution to the project through the development, supervision, and production of basal till potential maps. The till potential maps highlight where basal till is most likely to occur, and were used to plan and implement the TREK project till geochemical sampling program. In 2014, ten basal till potential maps of the TREK project area were co-published with Geoscience BC (see Appendix, this volume). In addition, Travis Ferbey, a senior Quaternary geologist with the BCGS, assisted in training Geoscience BC till sampling field crews to use these maps and recognize basal till, which is the ideal media for drift prospecting.

3. Cordilleran Geoscience Section

The Cordilleran Section is responsible for generating new geoscience knowledge through field-based studies, regional mapping, and targeted geoscience projects. The portfolio of projects is developed to balance both short- and long-term needs of the exploration community, thereby stimulating and maintaining a prosperous mineral exploration and investment

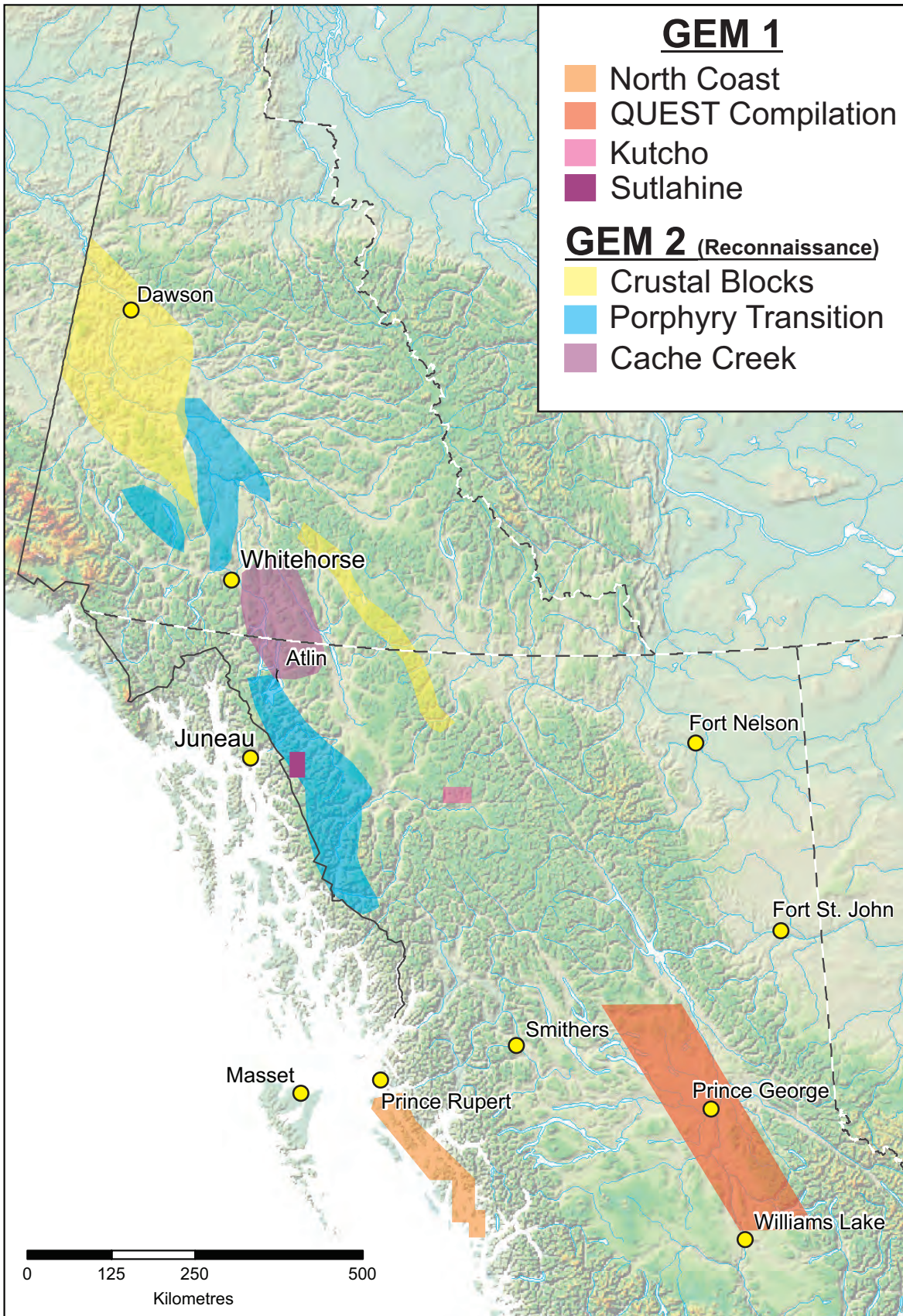


Fig. 2. Location of collaborative projects between the Geological Survey of Canada and the British Columbia Geological Survey through the Geo-mapping for Energy and Minerals (GEM) 1 and 2.

industry in British Columbia. The BCGS continues to have an important role in spurring activity as the exploration industry continues to face financial challenges. BCGS projects yield new geoscience maps, geological models, and exploration targets, thus contributing toward making BC a preferred destination for new investment in minerals and coal resources.

3.1. 2013-2014 Projects

The Cordilleran Section projects cover four general themes: 1) BC Porphyry Initiatives; 2) Exploration Methods; 3) Mineral Deposit Studies; and 4) Regional Synthesis and Map Compilations. Many of these projects are advanced multi-year investigations. The following section highlights 2014 activities (Fig. 3).

3.1.1. BC Porphyry Deposits Initiative

Much of British Columbia's metal endowment occurs in Cu-Mo-Au calc-alkaline and alkalic porphyry deposits genetically related to Late-Triassic to Early Jurassic island arc magmatism (Logan and Mihalynuk, 2014). The BC Porphyry Deposits Initiative, which began in 2012, is directed at: 1) determining the ages and structural controls on arc magmatism and porphyry pluton emplacement; 2) establishing the geological framework of major porphyry trends; and 3) developing new exploration techniques to aid in the discovery of buried or blind deposits. The main project areas (Fig. 4) are in the Intermontane arc complex, focusing on the Nicola Arc in the Quesnel terrane (BC interior plateau) and in Stikine terrane (northwest BC).

3.1.1.1. Nicola Arc

The Nicola Arc consists of three temporally distinct, north-trending plutonic belts that may represent the eastward migration of the Mesozoic arc magmatism (Fig. 5; Logan and Mihalynuk, 2014). This belt of rocks is particularly important to British Columbia's mineral wealth, hosting active mines such as Copper Mountain, Highland Valley, New Afton, and Gibraltar.

3.1.1.1.1. Southern Nicola Arc Project (2013-2015)

Lead by Mitch Mihalynuk and supported by Larry Diakow, the Southern Nicola Arc Project (SNAP) is remapping the geology between Princeton and Merritt (Fig. 6) to refine the stratigraphic, structural, and mineral deposit evolution of the Quesnel terrane. Results of this two-year project are reported by Mihalynuk et al. (2014) and in this volume. New mapping, geochronology, and geochemistry have added detail to the geology between the Allison Lake pluton and the Osprey Lake batholith and identified a number of new mineral occurrences (Fig. 7).

3.1.1.1.2. Gibraltar Mine and the Granite Mountain Batholith (2013-2015)

Gibraltar Mine began production in 1972 targeting Cu-Mo mineralization hosted in the Granite Mountain batholith (Late Triassic). Despite a long production history, the origin of the

deposit has been contentious (Ash and Riveros, 2001), and it has remained unclear if it formed in the Cache Creek terrane or the Quesnel terrane. New mapping, stratigraphic, geochronologic, and paleontologic studies by Paul Schiarizza were directed at resolving the question. Work in 2013 (Schiarizza, 2014) and in 2014 (see Schiarizza, this volume) demonstrates that the Granite Mountain batholith cuts rocks characteristic of Quesnel terrane and is part of a Late Triassic magmatic belt that includes the Guichon Creek batholith, which hosts the Highland Valley Cu deposit.

3.1.1.1.3. Porphyry indicator minerals in till, central British Columbia (TG14; 2010-2015)

Alain Plouffe (GSC) and Travis Ferbey (BCGS) are developing surficial geochemical and mineralogical methods for detecting buried porphyry-style mineralization in drift-covered areas. This project aims to define the key components of till that are enriched with porphyry indicator minerals and retain a porphyry trace element chemistry following a history of erosion from a mineralized outcrop, subglacial transport, and near-surface oxidation. Glacial dispersal of heavy minerals and till matrix are being studied at the Highland Valley, Gibraltar, and Mount Polley mines, and the advanced-stage Woodjam project. A critical part of the study is applying surficial geological mapping and observations of ice-flow indicators to reconstruct the glacial and ice-flow histories at each site. These ice-flow histories will be applied to the interpretation of geochemical and mineralogical dispersal patterns in till.

3.1.1.2. Porphyry Transitions (GEM 2; 2013-2018)

Paired belts of calc-alkaline and alkalic porphyry deposits that are genetically linked to early Mesozoic arc magmatism are documented in the southern Quesnel terrane and, potentially, parts of the more northerly Stikine terrane (Logan and Mihalynuk, 2014). The temporal and geochemical characteristics of the belts are reasonably well constrained in southern Quesnel terrane (Mihalynuk et al. this volume; Schiarizza, this volume), but they remain ambiguous in Stikine terrane (Zagorevski, et al., 2014). The transition from calc-alkaline to alkaline magmatism (e.g., Logan and Mihalynuk 2014) reflects changes in subduction geometry and/or melting regime of lithosphere below the arc. Mitch Mihalynuk (BCGS) and Alex Zagorevski (GSC) are co-leading a project that aims to develop and update the regional geologic framework for magmatism in the Stikine and Yukon-Tanana terrane by characterizing volcanic and intrusive rocks across the BC-Yukon border (Fig. 8). Activities in 2014 were directed at reconnaissance-level work that sets the stage for the larger study and focuses on constraining the age and petrology of Late Triassic to Early Jurassic plutons (Zagorevski, et al., 2014).

3.1.1.3. Structural and stratigraphic control of porphyry mineralization in the Snip-Bronson area (2014)

This project is a continuation of work begun in 2013 in the KSM-Brucejack area near the McTagg anticlinorium

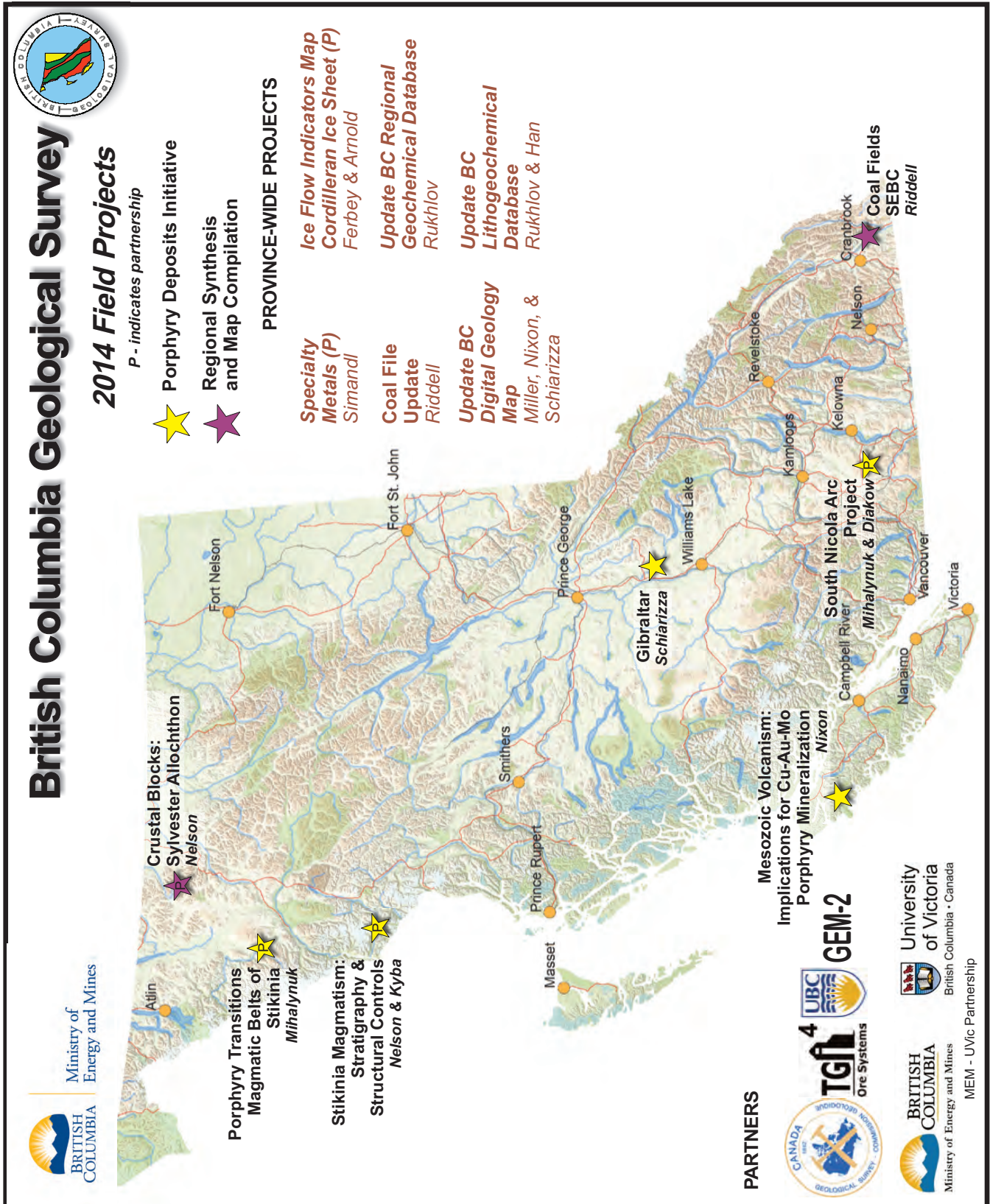


Fig. 3. British Columbia Geological Survey field projects in 2014.

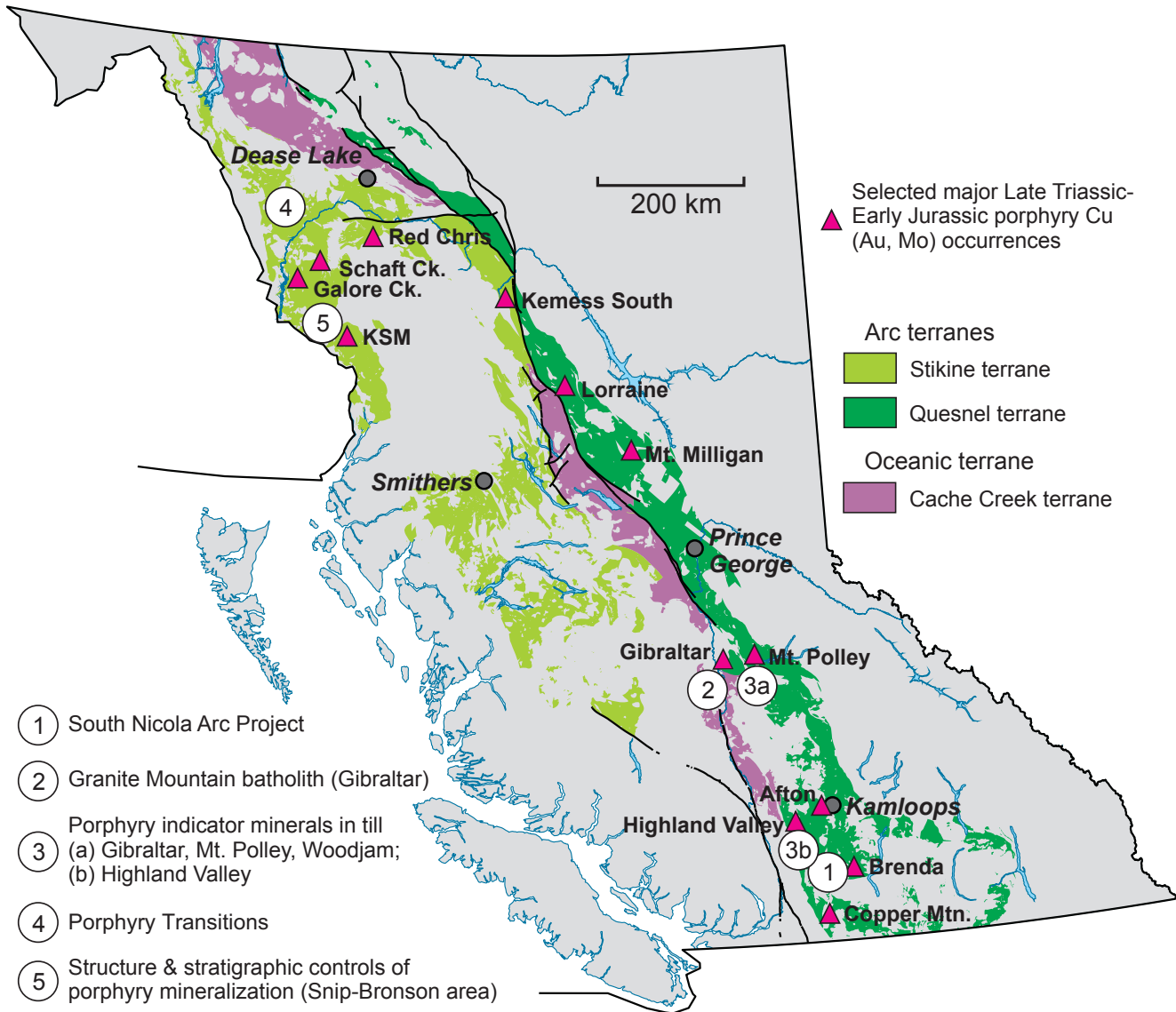


Fig. 4. Location of BC Porphyry Initiative project areas and the main porphyry terranes in British Columbia (i.e. Quesnel and Stikine terranes).

(Nelson and Kyba, 2014). The work is directed at establishing stratigraphic and structural controls on latest Triassic to Early Jurassic porphyry and related mineralisation. A key stratigraphic element, the unconformity between the Stuhini Group (Upper Triassic) and the Hazelton Group (Upper Triassic to Lower Jurassic), represents tectonic interruption and modification of arc magmatism in Stikinia. Also important to orebody location and form are long-lived, multiply-reactivated faults, such as the north-striking Sulphurets fault, which defines the eastern boundary of the McTagg anticlinorium. To the west, south of the lower Iskut River, a set of prominent alteration zones, Early Jurassic intrusions, and porphyry-related epigenetic vein occurrences (the ‘Bronson corridor’) are associated with the sub-Hazelton Group unconformity. Structural trends here are at a high angle to the generally north-trending grain in the KSM-

Brucejack area. They control the west-northwest-trending mineralized belt, and are thus of pre-mineral origin. JoAnne Nelson and Jeff Kyba aim to extend the understanding of the interaction of synmagmatic structures and Hazelton basins and volcanic centres into the western Iskut River area (Fig. 9; see Kyba and Nelson, this volume).

3.1.2. Exploration Methods

3.1.2.1. Carlin-type Gold in BC (2013)

Led by Alexei Rukhlov, this project uses regional stream-sediment geochemistry to detect Carlin-type gold deposits in northern British Columbia. Statistically robust treatment of multi-element geochemical data successfully demonstrates $Au \pm As \pm Hg \pm Tl \pm Sb$ enrichment in stream and lake sediments from the Kechika trough, a long-lived (Neoproterozoic to

Nicola Arc Project

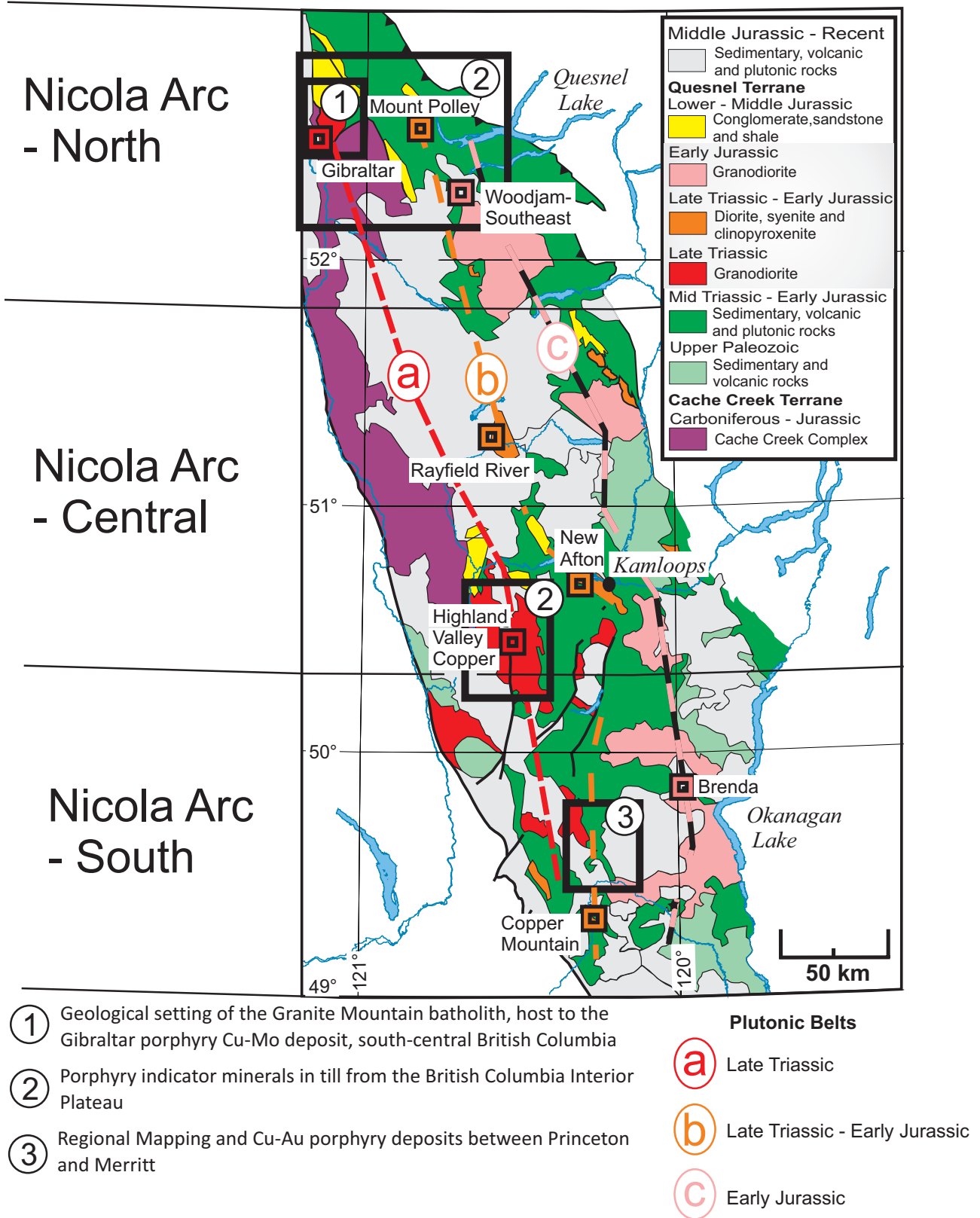


Fig. 5. Location of the Nicola Arc project areas. Generalized geology of southern Quesnellia modified from Logan and Mihalynuk (2013).

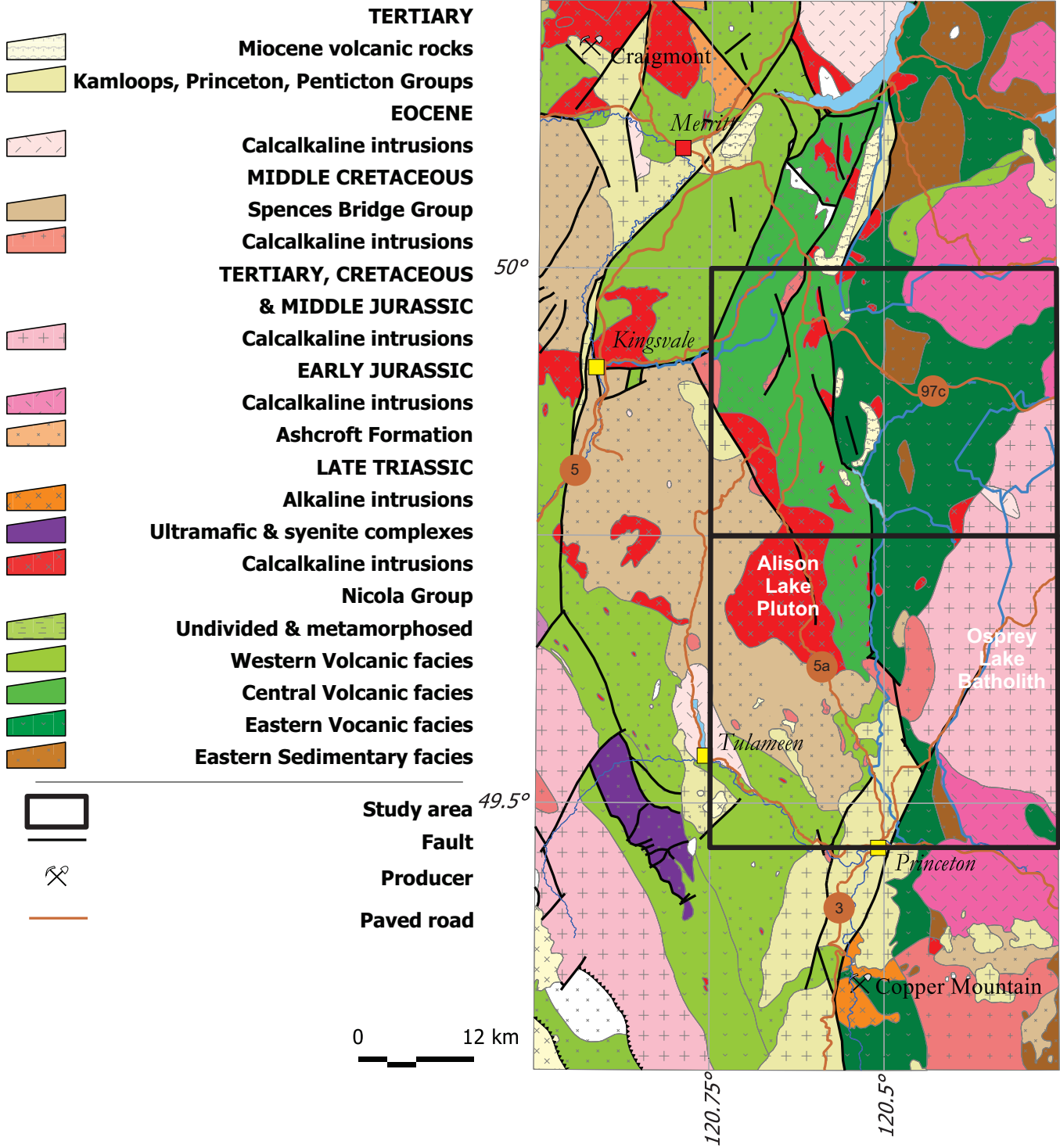


Fig. 6. Generalized geology of the Southern Nicola Arc Project (SNAP) area (from Mihalynuk et al. this volume).



Fig. 7. Geological mapping in the Southern Nicola Arc study area.



Fig. 8. Reconnaissance mapping and geochronological sampling in the northern British Columbia, part of the Porphyry Transitions project under the collaborative GSC-BCGS GEM 2 Cordilleran Regional program.

Paleozoic) deep-water basin in north-central British Columbia. A similar enrichment is found in stream sediments sourced from recently discovered Carlin-type gold and realgar occurrences in Rackla belt in the Selwyn basin of east-central Yukon. The Kechika trough may hold potential for Carlin-type deposits (Rukhlov et al., this volume).

3.1.2.2. Trace Element Systematics of Hydrothermal Apatite in Major Mineral Deposits (MEM-UVic Partnership; 2013-2014)

This project is developing a new exploration tool for concealed deposits using the abundances of trace elements in hydrothermal apatite associated with all the major mineral deposit types. This is a joint research project between the University of Victoria and the BCGS. The project draws on the expertise of Dr. Mao Mao (MEM-UVic Research Scientist),



Fig. 9. Geological mapping and stratigraphic studies on Snippaker Ridge above the Bronson Airstrip, Iskut River area, northern British Columbia.

Dr. Alexei Rukhlov (BCGS), Dr. Stephen Rowins (BCGS), Dr. Laurence Coogan (UVic), and Dr. Jody Spence (UVic) and is funded through the MEM-UVic Partnership. The development of analytical protocols for the measurement of trace element abundances in hydrothermal and magmatic apatites using laser ablation inductively-coupled plasma mass spectrometry (LA-ICPMS) has allowed for the discrimination of hydrothermal apatites from different mineral deposits and different host-rocks. This study will provide a powerful exploration technique in till-covered terrains. Apatite was chosen for this study because it is a common accessory mineral in igneous, metamorphic and sedimentary rocks, and most types of mineral deposits.

3.1.2.3. Lead Isotopes (2013-2014)

Alexei Rukhlov, with support from Travis Ferbey, is testing the application of lead isotopes in till silt and clay fractions to explore for massive sulphide deposits in glaciated terrains where conventional geochemical techniques are inconclusive. Lead isotopic ratios provide a unique way to fingerprint distinct bedrock sources (e.g., mineralization vs background) even in cases where elemental abundances in tills derived from these sources show little contrast. Due to a large difference in Pb isotopic ratios between anomalous and background samples (several %), this technique may not require expensive state-of-the-art precision to highlight a volcanogenic-massive-sulphide (VMS) signal in basal till. Basal till and rock samples, including

the VMS ores from the Seneca deposit (Chehalis River valley; hosted in Middle Jurassic Harrison Lake Formation), were analysed for conventional geochemical and isotopic analyses at three different laboratories to test different extraction and analytical techniques. The project confirmed the method for mineral exploration in northern Cordillera, where most VMS deposits are as young as Mesozoic, and that results from commercial ICP-MS are consistent with those derived from more sophisticated, and expensive, techniques.

3.1.3. Mineral Deposits

3.1.3.1. Specialty Metals (TGI4; 2010-2015)

The BCGS and the GSC continued to collaborate on this five-year Province and nation-wide study of specialty metals and rare earth elements. Specialty metals are uncommon, nonferrous metals used in small quantities (typically < 150,000 tonnes/year or derived from geographically restricted areas). The Specialty Metals Program is led by BCGS Geologist George Simandl and is an important contribution to Natural Resources Canada's TGI4 program. It has two major components: 1) reviewing ore deposits and their mineral economics in Canada; and 2) developing techniques to guide exploration toward ore-grade zones in host deposits. Fieldwork for this project was completed in 2013. In 2014 most efforts were directed at processing stream-sediment samples and developing cost effective, efficient and rapid specialty metal specific (Nb, Ta, and REE) indicator mineral-based vectoring method that involves Quantitative Evaluation of Minerals by SCANNing electron microscopy (QEMSCAN). This technique could be used by industry to follow-up on anomalies detected by regional geochemical surveys. To be effective, new specialty metal specific discrimination diagrams have been developed. Recent work focused on carbon, oxygen, and sulfur stable isotope studies of carbonatite-related mineralization and future work will involve the characterization of carbonatite mineralizing systems. The results of the Specialty Metals project will aid exploration and development of these strategic metal resources.

3.1.3.2. Orogenic Ni-Cu-PGE (TGI4; 2010-2015)

The Ni-Cu-PGE-Cr Ore Systems project is part of the GSC's Intrusion Related Ore Systems Targeted Geoscience Initiative (TGI4) and is in its concluding year. The British Columbia component is a collaborative effort between the BCGS, GSC, and the University of British Columbia. The project is examining the potential for orthomagmatic Ni-Cu-PGE sulphide deposits hosted by mafic-ultramafic intrusions at convergent margins. The aim is to establish mineral deposit models and exploration criteria for poorly understood magmatic sulphide environments in Cordilleran-style orogenic settings: 1) orthopyroxene-rich ultramafic intrusions like Giant Mascot, BC's only past-producing nickel mine (1958-74); and 2) Alaskan-type intrusions such as Turnagain, which has a world-class resource of low-grade nickel. The project is supporting the thesis work of two MSc students at the University of British Columbia.

3.1.4. Regional Synthesis

3.1.4.1. Ice-flow map of Cordilleran Ice Sheet (GEM 2; 2013-2018)

Large areas of northern British Columbia, southern Yukon, and southeast Alaska lack detailed surficial geology maps. Hence glacial transport histories are poorly understood in these areas, hindering effective mineral exploration. Preliminary surficial geoscience studies, including Province-scale compilations of ice-flow features (Ferbey et al., 2013) have revealed glacial-flow history complexities that need to be resolved for drift prospecting programs to be successful. As part of the GEM 2 program, a revised Quaternary ice-flow compilation for the entire Cordilleran Ice Sheet, including Yukon and Alaska, is underway. Once completed, Travis Ferbey and Holly Arnold will fill gaps in current mapping using the BCGS' recently acquired Summit Evolution photogrammetric 3D workstations (Fig. 10), the Provinces inventory of digital stereo models, and newly acquired digital satellite and high-level airphoto stereo models.

3.1.4.2. Coal Field Compilation Maps (2012-2015)

Despite declining coal prices and a reduction in the number of operating coal mines in BC (which dropped from nine to six in 2014), production remained steady, dipped only slightly from 31 million tonnes (in 2013) to a forecasted production of about 29 million tonnes in 2014. Coal remains an important mined commodity in British Columbia and at 46%, coal is the single largest contributor to the total mine production value in British Columbia (IC2015-3²). As a result, demand for information about BC coalfields and the value of the coal industry continues. To address this, BCGS coal geologist



Fig. 10. BCGS geomorphologist mapping surficial geology on the recently acquired Summit Evolution photogrammetric 3D workstations.

² British Columbia coal industry overview 2014, Information Circular 2015-3, www.empr.gov.bc.ca/Mining/Geoscience/PublicationsCatalogue/InformationCirculars/Pages/IC2015-3.aspx

Janet Riddell has generated coalfield compilation maps that will provide comprehensive information about the geology, production history, and major projects in BC coal-producing regions. The first compilation is for coalfields in the southeast part of the Province. To make the information accessible to a wide range of interested parties, the maps are designed for both technical and lay-person use.

4. Resource Information Section

The BCGS is the custodian of Province-wide geological data, including bedrock geology, surficial geology, mineral occurrences, and multi-element geochemistry from rock, till, stream sediment, and water samples. This information resides in free web-based databases that are integrated with MapPlace, the BCGS online service that allows clients to browse, visualize, and analyze multidisciplinary geoscience data and create custom maps (Table 1). The data and derived products provide baseline geological information for mineral exploration, environmental assessment, and land use planning (see Information Circular IC2014-9³). In particular, they increase exploration effectiveness by enabling users to efficiently gather regional information useful for property-scale evaluation, and help explorers advance projects without duplicating previous work.

4.1. MapPlace and database activities

Since 1995, MapPlace has provided open geoscience data and custom map-making tools to aid in the discovery of deposits and the assessment of mineral potential in British Columbia. MapPlace's unique, interactive applications and tools assist in investment decision making. MapPlace continues to provide clients with efficiencies in research time, data costs, and

analysis. Data themes and applications available on MapPlace include mineral potential, bedrock and surficial geology, publications, mineral and coal tenure, MINFILE, assessment reports, geochemistry, and geophysical surveys. Steven Zhao, Yao Cui, and Pat Desjardins continue to develop the next generation of MapPlace with testing of the new version of MapGuide Open Source. 'MapPlace 20/20' has demonstrated impressive performance, displaying province-wide bedrock geology, geochemistry data and mineral titles within seconds.

MapPlace, database applications, and recent technological advances were presented at several meetings including: Mineral Exploration Roundup in Vancouver, Prospector and Developers Association of Canada (PDAC) in Toronto, Society of Economic Geologists (SEG) in Whistler, Kamloops Exploration Group (KEG) in Kamloops, Free and Open Source Software for Geospatial (FOSS4G) in Portland, Oregon, Geological Society of America (GSA) in Vancouver, and a well-received workshop on the new MapPlace convened by Pat Desjardins, Sarah Meredith-Jones, and Deanna Miller at Minerals South in Nelson.

ARIS is the searchable database of over 34,000 assessment reports submitted to the Ministry of Energy and Mines, in compliance with the Mineral Tenure Act (MTA) Regulations (Fig. 11a). These reports summarized results from exploration programs on mineral claims. After a one-year confidentiality period, the reports become an open resource for planning mineral exploration, investment, research, land use, and resource management. Between 1967 and 2013, about \$2.6 billion of reported work has been captured in ARIS. The Ministry maintains a library of 916 Coal Assessment Reports submitted by exploration companies and dating from 1900 (Fig. 11b). COALFILE contains details of coal exploration reports including data from 11,595 boreholes, 500 bulk samples, 957 maps, 3415 trenches. A search engine leads clients to a summary page for each coal assessment report and links to the complete report. The data are spatially referenced on MapPlace and are available for download as an MS Access database. Ted

³ Online databases at the British Columbia Geological Survey, Information Circular 2014-9, www.empr.gov.bc.ca/Mining/Geoscience/PublicationsCatalogue/InformationCirculars/Pages/IC2014-9.aspx

Table 1. British Columbia Geological Survey databases.

MapPlace	www.mapplace.ca
ARIS	www.empr.gov.bc.ca/Mining/Geoscience/ARIS
MINFILE	www.empr.gov.bc.ca/MINING/GEOSCIENCE/MINFILE
COALFILE	www.empr.gov.bc.ca/Mining/Geoscience/Coal/CoalBC/Pages/CoalDataReports.aspx
Mineral Titles Online (MTO)	www.empr.gov.bc.ca/TITLES/MINERALTITLES
Publication Catalogue	www.empr.gov.bc.ca/MINING/GEOSCIENCE/PUBLICATIONSCATALOGUE
Regional Stream Sediment Geochemistry ¹	www.empr.gov.bc.ca/Mining/Geoscience/Geochemistry/RegionalGeochemistry
Lithochemical Database ²	www.empr.gov.bc.ca/Mining/Geoscience/PublicationsCatalogue/GeoFiles/Pages/2005-14.aspx

^{1,2} Currently being updated

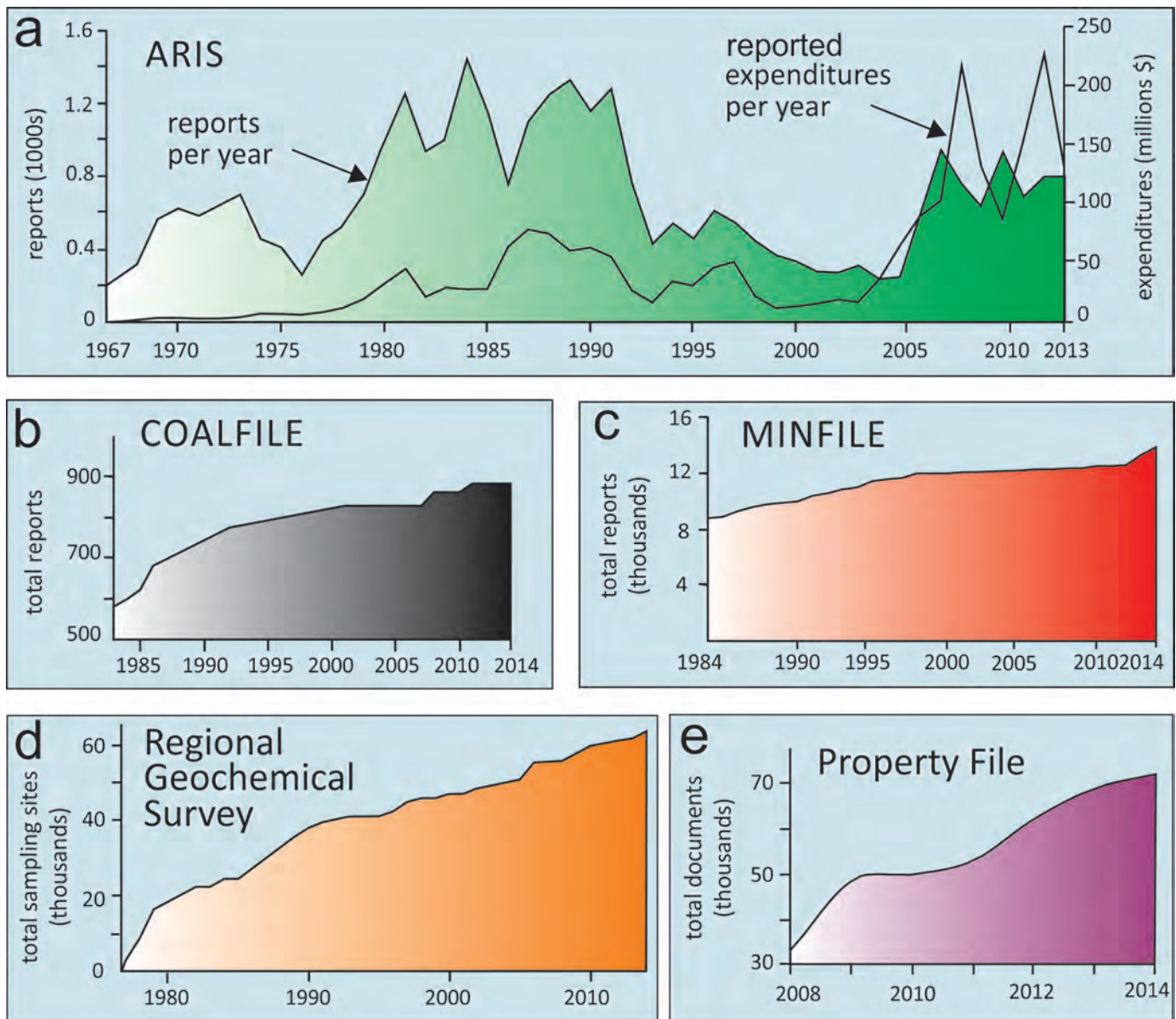


Fig. 11. Growth of some British Columbia Geological Survey databases.

Fuller and Jessica Norris review and manage the ARIS and COALFILE reports and databases.

MINFILE contains geological, location, and economic information on almost 14,000 occurrences and is updated continuously. In the last two and half years, updates to 5900 occurrences included 1700 new entries (Fig. 11c). Using the web-enabled MINFILE search application, users can query by location, identification number, mineralogy, commodity, host rock, deposit type, geological setting age, production, and references. MINFILE links with MapPlace, ARIS and Property File. Sarah Meredith-Jones is the primary contact for MINFILE: Sara.Meredithjones@gov.bc.ca.

The provincial geochemical databases hold field and geochemical data from multi-media surveys conducted by the Geological Survey of Canada (GSC), the British Columbia

Geological Survey, Geoscience BC (GBC), and contractors. The databases are updated regularly and contain results from: 1) the Regional Geochemical Survey program (RGS) including analyses from stream-sediment, lake-sediment, moss, and water samples (Fig. 11d); 2) till surveys; and 3) rock samples collected during the course of mapping projects. The RGS database provides representative geochemical data for catchment basins upstream of sample sites. Samples of fine-grained sediment are typically collected from lakes and streams at an average density of 1 site per 10-13 km². Data catalogued include determinations for up to 63 analytes, field observations, and sample locations. In 2014, Alexei Rukhlov (Provincial Geochemist) and Mustafa Naziri updated and overhauled the RGS database. Currently, the RGS database contains results from 64,828 samples covering over 80 percent of the

province. Previous RGS database versions had inconsistent and conflicting rules for reporting missing values (nulls) and values below the minimum detection limit. These issues severely downgraded the original data quality in the database with potential for misleading interpretations. To address these problems the RGS data were re-compiled from the original published sources using a new standardized data file structure, and are now available for download in a MS Access database.

The provincial litho-geochemical database, last released in 2005, is being retrofitted to improve data quality, enhance data access and retrieval, and update with new data. Tian Han (BCGS Digital Information Scientist) has developed a new simplified data model. Holly Arnold, Mustafa Naziri, and Alexei Rukhlov are updating the database with new analysis produced since 2005 and reviewing archive data to ensure that it has been captured. The team has improved QA/QC, and included links from the data to sources in the BCGS publication catalogue.

Property File is a collection of over 54,000 government, university, personal, and industry documents donated to the British Columbia Geological Survey over the last 150 years (Fig. 11e). Previously available only in hard copy, these documents can now be searched for and downloaded from the Property File database. Property File contains: unpublished reports; theses; field notes; company prospectuses; correspondence; hand-drawn maps; claim maps; mine plans; photographs; and geological, geochemical, geophysical, and drill data. A new Property File layer was posted MapPlace, linking to over 80,000 documents in 7221 sites. The BC Geological Survey accepts donations to Property File and interested parties should contact Kirk Hancock (kirk.hancock@gov.bc.ca).

The BCGS continues to process and integrate geological maps into the province-wide digital geology database, using a 'geologic framework data' (GFD) model (Cui, 2014). In 2014, the GFD model was enhanced and database applications were developed to further automate map integration. Deanna Miller (under the direction of Yao Cui) worked to integrate four maps compiled by Graham Nixon for northern Vancouver Island.

5. Mineral Development Office

The BC Mineral Development Office (MDO) in Vancouver is the technical marketing arm of the British Columbia Geological Survey and the Ministry of Energy and Mines. Its location in downtown Vancouver provides the domestic and international minerals industry with a point of contact for Survey activities, access to government geoscience products, and advice on mineral and coal opportunities in the Province. MDO staff geologists deliver technical presentations at major geoscience meetings, mining conferences, and investment missions. These formal activities are regularly accompanied by informal meetings with individuals and companies that require expert opinion on BC geology, its operating mines, and up-to-date information on the status of exploration projects in the Province.

Primary outputs of the MDO are publications aimed at audiences ranging from large foreign investors through to

independent domestic entrepreneurs. These publications are distributed widely at conferences, business meetings, over the counter, and online. In 2014, an updated version of the 'Opportunities to Explore' document was released in both English and Mandarin. This non-technical publication is designed for new investors who want to learn more about existing and potential exploration and mining opportunities in the Province. Opportunities to Explore is an example of a sector-specific document produced by the MDO that is used by other government agencies (i.e., Ministry of International Trade) to promote trade and investment in BC's mining sector.

The MDO oversees and coordinates the creation of exploration and mining summary documents from the Regional Geologist program, maintaining a legacy that dates back to 1874 with the Annual Reports of the Minister of Mines. The third annual version of the 'Coal Industry Overview' (IC2014- 5⁴) was released in early 2014; publication of this volume will continue on an annual basis (see IC2015-3⁵ for the 2014 review).

After a decade long hiatus, the inventory of gold in the province was updated and released in early 2014 (IC2014- 4⁶) as 'Gold Resources and Production in British Columbia (1890-2013)'. The circular includes a 2,000,000-scale map and spreadsheet. The map shows gold occurrences by deposit type and grade category. The project highlighted a significant increase in gold inventories in the Province over the ten-year period since the last inventory.

6. Regional Geologists Program

The Regional Geologists (formerly District Geologists) program was created in the early 1970s to facilitate economic development in the mineral exploration and mining sector. The British Columbia Regional Geologists represent the provincial government on geological matters at a regional level and capture information on industry activity in their jurisdictions. Within their communities, they provide advice and information on exploration trends, possible investment opportunities, land use processes, First Nation capacity building, public outreach and other key deliverables of government.

7. Staffing announcements

The survey welcomed back Melanie Mitchell, our Branch Coordinator, whose post was ably filled by Janet Hughes, now

⁴ British Columbia coal industry overview 2013, Information Circular 2014-5, www.empr.gov.bc.ca/Mining/Geoscience/PublicationsCatalogue/InformationCirculars/Pages/IC2014-5.aspx

⁵ British Columbia coal industry overview 2014, Information Circular 2015-3, www.empr.gov.bc.ca/Mining/Geoscience/PublicationsCatalogue/InformationCirculars/Pages/IC2015-3.aspx

⁶ Northcote, B., Madu, B., Schroeter, T., and Li, G., 2014. Gold production and resources in British Columbia, 1890-2013. resources and production in British Columbia (1890-2013), Information Circular 2014-4, www.empr.gov.bc.ca/Mining/Geoscience/PublicationsCatalogue/InformationCirculars/Pages/IC2014-4.aspx

at the Ministry of Environment. GIS Geoscientist Deanna Miller replaced Fiona Katay who left the BCGS to assume the role of Regional Geologist in Cranbrook. Jessica Norris joined the Resource Information Section as the new coal and mineral assessment geoscientist. The Survey welcomed a new Director to the Mineral Development Office in Vancouver. Gordon Clark replaced outgoing Director Bruce Madu who left the public service to join Geoscience BC, a non-governmental organization that provides grants and contracts to consultants to undertake geoscience projects of direct interest to the minerals industry. Two long-time members of the BCGS team recently retired. Jim Logan, who started with the BCGS in 1989, retired in early 2014 (Fig. 12). Pat Desjardins who joined the Survey in 1986, leaves in early 2015 (Fig. 13).

The Survey is saddened by the passing of Allan Wilcox and alumnus Ward Kilby. Allan joined the Survey in 1981 and was well known throughout the BC exploration industry for his role as compliance officer for mineral assessment reporting. Allan passed away in May. Ward Kilby retired from the Survey in 2000, but remained a very active alumnus and continued to

collaborate with the Resource Information Section on many database projects. Ward passed away in June.

Acknowledgment

We thank George Owsiacski of Total Earth Science Services for desktop publishing of this volume.

References

- Ash, C.H. and Riveros, C.P., 2001. Geology of the Gibraltar copper–molybdenite deposit, east-central British Columbia (93B/9). In: Geological Fieldwork 2000, British Columbia Ministry of Energy and Mines, British Columbia Geological Survey Paper 2001-1, pp. 119-133.
- Cui, Y., 2014. Integration and delivery of British Columbia digital geology. British Columbia Ministry of Energy and Mines, British Columbia Geological Survey GeoFile 2014-9 (poster).
- Duke, J.M., 2010. Government geoscience to support mineral exploration: public policy rationale and impact. Prospectors and Developers Association of Canada, Toronto, Ontario, 64 pages.
- Ferbey, T., Arnold, H. and Hickin, A.S., 2013. Ice-flow indicator compilation, British Columbia. British Columbia Ministry of Energy and Mines, British Columbia Geological Survey, Open File



Fig. 12. Jim Logan at his desk at the BCGS in the late 1980s (top) and in the field in 2012 (bottom).



Fig. 13. Pat Desjardins at Cordilleran Roundup in the late 1980s (top) and at the BCGS open in 2013 (bottom).

- 2013-06, scale 1: 650 000.
- Logan, J.M. and Mihalynuk, M.G., 2013. Bonaparte gold: another 195 Ma porphyry Au-Cu deposit in southern British Columbia? In: Geological Fieldwork 2012, British Columbia Ministry of Energy, Mines, and Natural Gas, British Columbia Geological Survey Paper 20013-1, pp. 71-80.
- Logan, J.M., and Mihalynuk, M.G., 2014. Tectonic controls on Early Mesozoic paired alkaline porphyry deposit belts (Cu-Au ± Ag-Pt-Pd-Mo) within the Canadian Cordillera. *Economic Geology*, 109, 827-858.
- Mihalynuk, M.G., Logan, J.M., Diakow, L.J., Friedman, R.M., and Gabites, J., 2014. Southern Nicola Arc Project (SNAP): Preliminary results. In: Geological Fieldwork 2013, British Columbia Ministry of Energy and Mines, British Columbia Geological Survey Paper 2014-1, pp. 29-57.
- Nelson, J. and Kyba, J., 2014. Structural and stratigraphic control of porphyry and related mineralization in the Treaty Glacier – KSM – Brucejack – Stewart trend of western Stikinia. In: Geological Fieldwork 2013, British Columbia Ministry of Energy and Mines, British Columbia Geological Survey Paper 2014-1, pp. 111-140.
- Schiarizza, P., 2014. Geological setting of the Granite Mountain batholith, host to the Gibraltar porphyry Cu-Mo deposit, south-central British Columbia. In: Geological Fieldwork 2013, British Columbia Ministry of Energy and Mines, British Columbia Geological Survey Paper 2014-1, pp. 95-110.
- Zagorevski, A, Mihalynuk, M.G., Joyce, N., and Martin, K., 2014. Characterization of volcanic and intrusive rocks across the British Columbia – Yukon border Gem 2 Cordillera. Geological Survey of Canada, Open File 7697, 10 pages.

In Memoriam

Allan Frederick Wilcox (1947-2014)

Allan graduated from Carleton University in 1971 and worked for Noranda, Manitoba Department of Mines, the Geological Survey of Canada, and Indian and Northern Affairs Canada. He joined the British Columbia Geological Survey in 1981. Allan was instrumental in developing and implementing the first MINFILE, an electronic database of mineral occurrences, and the Assessment Report Indexing System (ARIS). He expertly guided the compliance of mineral assessment reporting by the exploration community. Over the past thirty years, Allan built strong working relationships with clients and was highly respected in the industry. Allan's valuable contribution to Survey geoscience culminated in being part of the MapPlace team that was a 2012 finalist in the Premier Award category for Innovation (MapPlace-World Leader in Geospatial Technology Innovation, Attracting Global Mineral Industry Investment). For many years, Allan volunteered and sat on the board of directors for community theatres and cultural societies and could commonly be seen at a local arena, assisting disabled attendees. Allan passed away peacefully in May 2014.



In Memoriam

Ward E. Kilby (1954-2014)

Ward graduated from the University of Alberta with a M.Sc. in 1978 and worked for several resource companies before joining the BCGS in 1982. Ward held positions of Senior Coal Geologist and Manager of Mineral Potential and GIS until 2000. While at the Survey, Ward began developing MapPlace and brought many of the geoscience databases to the exploration community through visualization and query tools. In large part owing to Ward's efforts, the Province has consistently been ranked in the top ten of the Fraser Institute's Global Ranking of Geological Databases. After leaving the Survey in 2000, Ward consulted with Cal Data Ltd, making great advancements in remote sensing, data management and analysis, web-mapping development, and resource assessments. Ward served on technical advisory committees for Geoscience BC and the BCGS. In 2008, he received the Meritorious Achievement Award from APEGBC and was part of the BCGS team that was a 2012 finalist in the Premier Award category for Innovation (MapPlace-World Leader in Geospatial Technology Innovation, Attracting Global Mineral Industry Investment). Ward passed away on June 30, 2014.



Geological setting of the Granite Mountain batholith, south-central British Columbia

Paul Schiarizza^{1, a}

¹ British Columbia Geological Survey, Ministry of Energy and Mines, 300-865 Hornby Street, Vancouver, BC, V6Z 2G3

^a corresponding author: Paul.Schiarizza@gov.bc.ca

Recommended citation: Schiarizza, P., 2015. Geological setting of the Granite Mountain batholith, south-central British Columbia. In: Geological Fieldwork 2014, British Columbia Ministry of Energy and Mines, British Columbia Geological Survey Paper 2015-1, pp. 19-39.

Abstract

The Granite Mountain mapping project, initiated in 2013 and continued in 2014, was implemented to clarify the contact relationships and terrane affinity of the Granite Mountain batholith (Late Triassic), host to the Gibraltar porphyry Cu-Mo deposit. The batholith is included in Quesnel terrane because, on its northeast margin, it intrudes the slightly older Burgess Creek stock, which itself intrudes an assemblage of Upper Triassic sedimentary and volcanic rocks correlated with the Nicola Group, the defining stratigraphic unit of Quesnel terrane. These Nicola rocks have yielded Late Triassic conodonts from one locality, and consist mainly of volcanogenic sandstone (locally gritty to pebbly), intercalated with conglomerate, mafic and felsic volcanic breccia, siltstone, limestone and basalt. The Nicola rocks, and possibly the northern part of the Granite Mountain batholith, are overlain by a younger assemblage that includes slate, siltstone, sandstone and conglomerate, and is correlated with the Dragon Mountain succession (Lower to Middle Jurassic), another characteristic element of Quesnel terrane. A narrow belt of rocks along the southwest margin of the Granite Mountain batholith is assigned to the Cuisson Lake unit. It consists mainly of chlorite schist, foliated limestone and skarn, and was derived from a succession of feldspathic volcanoclastic ±volcanic rocks intercalated with limestone. These rocks were previously included in the Cache Creek Complex, but herein are correlated with the Nicola Group. The Granite Mountain batholith, and rocks of the Nicola Group, Cuisson Lake unit, Burgess Creek stock, and Dragon Mountain succession, form a panel of Quesnel rocks that is bounded to the east and south by rocks of Cache Creek terrane. The eastern boundary is an unexposed north-northwest striking fault that may record more than 20 km of sinistral strike slip. The southern boundary of the Quesnel panel is an east-trending fault that juxtaposes the Cuisson Lake unit against Early Cretaceous tonalite of the Sheridan Creek stock, which apparently intrudes Cache Creek rocks farther south. This structure is inferred to be a south-dipping thrust or reverse fault that formed in conjunction with greenschist facies metamorphism and the development of south-dipping foliations in the Sheridan Creek stock, the Cuisson Lake unit, and the southern part of the Granite Mountain batholith.

Keywords: Granite Mountain batholith, Burgess Creek stock, Late Triassic, tonalite, diorite, Nicola Group, Cache Creek Complex, Dragon Mountain succession, Sheridan Creek stock, Gibraltar porphyry Cu-Mo deposit, Quesnel terrane, Cache Creek terrane

1. Introduction

In 2013, the British Columbia Geological Survey initiated a two-year bedrock-mapping project to clarify the geological setting, terrane affinity, and structural history of the Granite Mountain batholith (Late Triassic), which hosts the Gibraltar porphyry Cu-Mo deposit (Fig. 1). This project builds on the work of Ash et al. (1999a, b), who challenged the long-held view (Drummond et al., 1976; Bysouth et al., 1995) that the Granite Mountain batholith was part of Cache Creek terrane. Instead, Ash et al. (1999a, b) proposed that the batholith is part of Quesnel terrane, and that it was juxtaposed against Cache Creek rocks along post-Triassic faults. Furthermore, Ash et al. (1999a, b) argued that ductile shear zones in the Gibraltar deposit formed during this post-Triassic deformation, suggesting that Gibraltar might not be a porphyry deposit, or at least that mineralization had been significantly remobilized.

Mapping in 2013 covered a small area on the northeast margin of the Granite Mountain batholith, where volcanoclastic rocks that Tipper (1978) assigned to a Jurassic siliciclastic assemblage were re-interpreted by Ash et al. (1999a, b) as Nicola Group (Late Triassic) of Quesnel terrane. The main

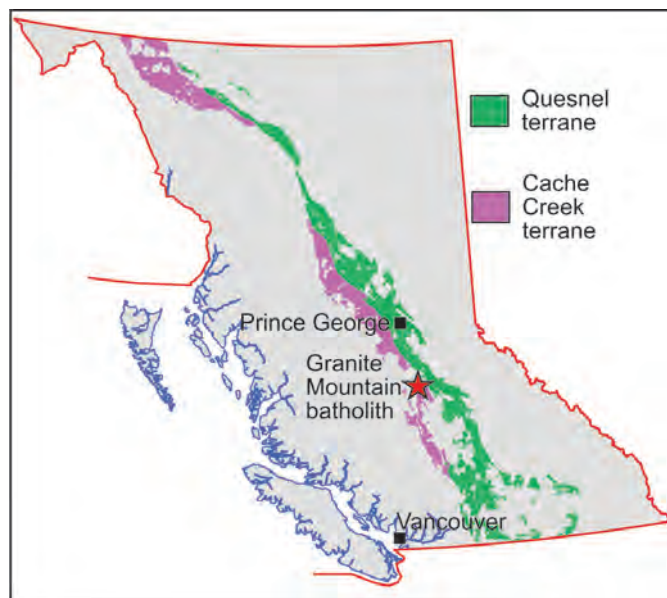


Fig. 1. Location of the Granite Mountain batholith and distribution of Quesnel and Cache Creek terranes in British Columbia.

conclusion was that these rocks are part of the Nicola Group (Schiarizza, 2014). Mapping in 2014 encompassed the entire Granite Mountain batholith, including rocks that are in contact with it to the north, east and south (Fig. 2), and confirmed that the Granite Mountain batholith is in a panel of Quesnel terrane.

2. Regional setting

The Granite Mountain batholith outcrops on the Fraser Plateau, seven to eighteen kilometres east of the Fraser River, within the traditional territories of the Northern Secwepemc to Qelmučw and Tsilhqot' in First Nations (Fig. 2). The community of McLeese Lake, on Highway 97, is 10 km south-southwest of the Gibraltar ore deposits, and is linked to the mine site by paved road. Networks of logging and Forest Service roads occur throughout the region and provide good access to most parts of the Granite Mountain map area.

Previous studies that have contributed to the geologic interpretation of the Granite Mountain area include: regional mapping of the Quesnel River (93B) map area by Tipper (1959, 1978); geological mapping of the Granite Mountain batholith by Panteleyev (1978) and Ash et al. (1999a, b); and detailed studies of geology and mineralization within and near the Gibraltar deposits by Sutherland Brown (1958, 1967, 1974), Eastwood (1970), Simpson (1970), Drummond et al. (1973, 1976), Bysouth et al. (1995), Raffle (1999), Ash and Riveros (2001), Oliver et al. (2009), Harding (2012), van Straaten et al. (2013), and Mostaghimi et al. (2014).

Quesnel terrane is an important metallogenic province that occurs along most of the length of the Canadian Cordillera (Fig. 1; Nelson et al., 2013). It is characterized by a Late Triassic to Early Jurassic magmatic arc complex that formed along or near the continental margin of western North America. Quesnel terrane is flanked to the east by Proterozoic and Paleozoic siliciclastic, carbonate, and volcanic rocks of pericratonic affinity and locally, an intervening marginal basin assemblage comprising mid to Late Paleozoic oceanic basalt and chert of Slide Mountain terrane. Late Paleozoic through mid-Mesozoic oceanic rocks of Cache Creek terrane are west of Quesnel terrane, and are interpreted as part of the accretion-subduction complex that was responsible for generating the Quesnel magmatic arc.

At the latitude of McLeese Lake, rocks of Quesnel terrane crop out mainly in a northwest-trending, 30 km-wide belt, 20 km east of the Granite Mountain batholith (Fig. 2). The terrane is represented mainly by Middle to Upper Triassic volcanic and sedimentary rocks of the Nicola Group, together with abundant Late Triassic to Early Jurassic calcalkaline and alkaline intrusions (Logan et al., 2010). Lower to Middle Jurassic siliciclastic sedimentary rocks along the western margin of the terrane, assigned to the Dragon Mountain succession (Logan and Moynihan, 2009), were derived from, and deposited on, Quesnel terrane (Petersen et al., 2004; Logan and Moynihan, 2009).

The Cache Creek Complex includes exposures of chert, argillite, basalt, limestone, sandstone, gabbro, and serpentinite

west of the main Quesnel belt (Logan et al., 2010). The complex is not well dated in the McLeese Lake area, although one limestone exposure, 10 km east of the southern part of the Granite Mountain batholith, yielded Permian fossils (Tipper, 1978). Contiguous, but better-studied parts of the Cache Creek Complex to the south and north, include rocks ranging from Carboniferous to Early Jurassic (Cordey and Read, 1992; Read, 1993; Struik et al., 2001).

The Granite Mountain batholith is exposed north of McLeese Lake. It occurs west of the main Quesnel terrane belt, but is inferred to comprise the south end of a separate, north-trending panel of Quesnel rocks that is faulted against Cache Creek terrane to the east and south (Fig. 2). This panel also includes Late Triassic volcanoclastic and volcanic rocks correlated with the Nicola Group, exposed on the northeast margin of the Granite Mountain batholith, and conglomerates and finer-grained rocks correlated with the Lower to Middle Jurassic Dragon Mountain succession.

Granitic rocks that postdate the Late Triassic-Early Jurassic intrusions of Quesnel terrane include Middle Jurassic plutons within Quesnel and Cache Creek terranes north and northeast of the Granite Mountain batholith, and Early Cretaceous stocks in Cache Creek terrane south of the batholith (Fig. 2). The youngest rocks in the region include Eocene volcanic and local sedimentary rocks, Oligocene-Pliocene siliciclastic sequences along parts of the Fraser River, and widespread Miocene-Pleistocene basalt of the Chilcotin Group (Fig. 2).

3. Geologic units of the Granite Mountain area

The Granite Mountain area (Fig. 3) is underlain mainly by a north-trending belt of rocks assigned to Quesnel terrane, including the Nicola Group (Middle and Upper Triassic), the Burgess Creek stock (Late Triassic), the Granite Mountain batholith (Late Triassic), and the Dragon Mountain succession (Lower to Middle Jurassic). Rocks included in the Cache Creek Complex (Cache Creek terrane) form a poorly exposed belt east of the Quesnel rocks. A narrow belt of rocks, mainly chlorite schist, limestone, and skarn, along the south and southwest margin of the Granite Mountain batholith is referred to as the Cuisson Lake unit, and is tentatively correlated with the Nicola Group. Early Cretaceous tonalite of the Sheridan Creek stock is the southernmost unit in the map area, and is in fault contact with the Cuisson Lake unit and the Granite Mountain batholith.

3.1. Nicola Group

Rocks reassigned to Nicola Group on lithostratigraphic grounds (Ash et al., 1999a; Schiarizza, 2014) are exposed in the northern part of the map area, where they are cut by the Burgess Creek stock and are overlain, structurally and/or stratigraphically, by the Dragon Mountain succession (Fig. 3). Originally, the Nicola rocks were included in the upper (Lower to Middle Jurassic) part of the Quesnel River Group by Tipper (1978), and were assigned to an unnamed unit of suspected Early Jurassic age by Panteleyev (1978).

In the map area, the Nicola Group consists of sandstone

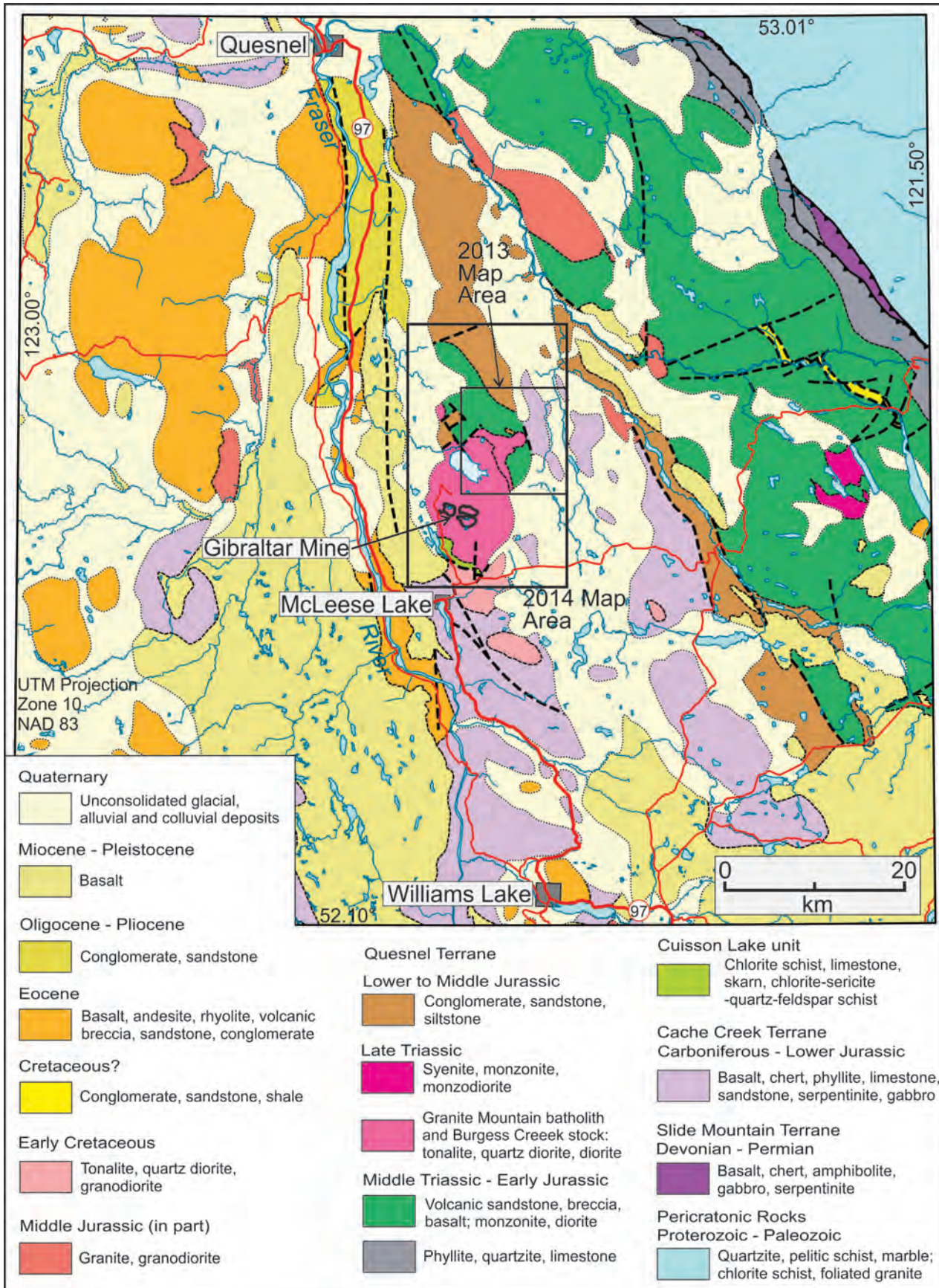


Fig. 2. Geological map of the area between Williams Lake and Quesnel, showing the location and setting of the Granite Mountain batholith.

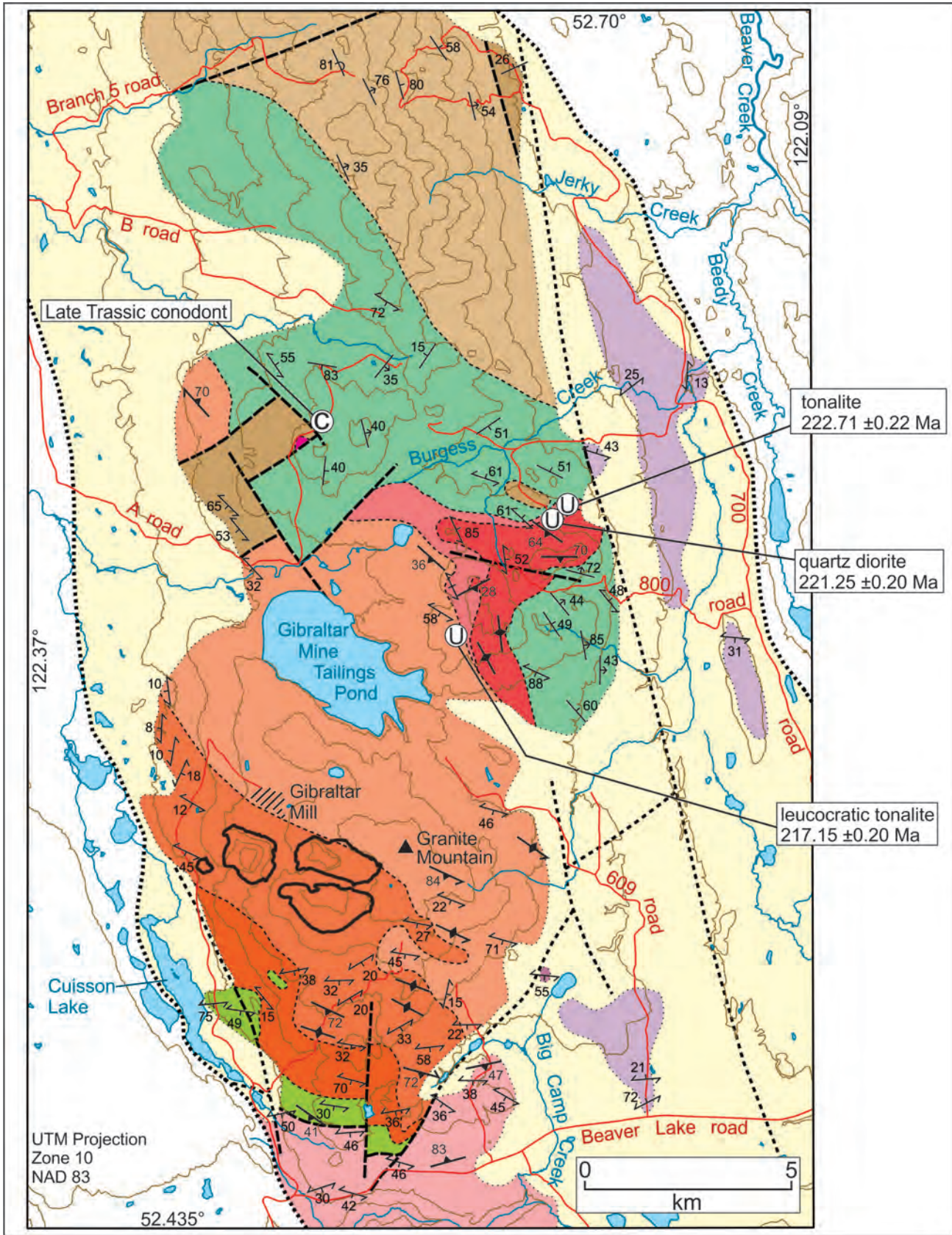


Fig. 3a. Geology of the Granite Mountain map area, based on 2013 and 2014 fieldwork. U-Pb zircon ages from Richard Friedman, University of British Columbia, written communication March 2014; conodont identification by M.J. Orchard, Geological Survey of Canada, written communication April 2014. Heavy black lines delineate Gibraltar mine pit areas.



Fig. 3b. Legend for Fig. 3a.

and gritty to pebbly sandstone, with local intercalations of conglomerate, mafic and felsic volcanic breccia, siltstone, limestone, and basalt (Schiarizza, 2014). Most of the group was mapped in 2013; the 2014 program expanded the known Nicola Group distribution a few km northward (Fig. 3) where small scattered outcrops of green feldspathic sandstone, gritty to pebbly sandstone, and conglomerate are typical of the predominant rock types in better exposed sections to the south (see Schiarizza, 2014 for detailed descriptions).

Paleontologic and geochronologic data corroborate assigning these rocks to the Nicola Group. Five limestone samples collected during the 2013 field season were processed for conodonts at the Geological Survey of Canada's microfossil laboratory in Vancouver. One of these samples, collected 4 km north of the Gibraltar tailings pond (Fig. 3), from a unit comprising narrow limestone lenses interleaved with green volcanic sandstone (Fig. 4), yielded a single conodont fragment, identified as *Norigondolella* cf. *navicula*, of probable Lower Norian age (M.J. Orchard, Geological Survey of Canada, written communication, April 2014). Furthermore, a sample collected by Jim Logan (British Columbia Geological Survey) from this same locality in 2005 yielded a conodont fragment of Middle or Late Triassic age (Orchard, 2006; GSC Loc. No. C-307484). Moreover, samples from the Burgess Creek stock, which clearly intrudes the sedimentary succession (Schiarizza, 2014), have yielded Late Triassic U-Pb zircon ages (Fig. 3; see below), demonstrating that the rocks reassigned to the Nicola Group are pre-Jurassic.

3.2. Burgess Creek stock

The Burgess Creek stock comprises a heterogeneous assemblage of tonalites, quartz diorites, and diorites that intrude the Nicola Group on the northeast margin of the Granite Mountain batholith (Fig. 3). The stock was first mapped and named by Panteleyev (1978) who considered it to be younger than the Granite Mountain batholith. Bysouth et al. (1995) also



Fig. 4. Nicola Group limestone interbedded with green volcanic sandstone, 4 km north of the Gibraltar tailings pond.

mapped it as a younger unit, but Ash et al. (1999a, b) concluded that these rocks were part of the batholith, and referred to them as border phase quartz diorite (unit EJGb). Schiarizza (2014) mapped the Burgess Creek stock and Granite Mountain batholith as separate entities, but did not establish which was older. U-Pb zircon geochronology on samples collected during the 2013 field season show that rocks from the Burgess Creek stock are 4-5 Ma older than the adjacent Granite Mountain phase of the batholith (see below). The term Burgess Creek stock continues to be used herein, although it could be considered a relatively old border phase of the batholith, as suggested by Ash et al. (1999a, b).

The Burgess Creek stock was shown as a single unit by Schiarizza (2014), but here is subdivided into two units: a mixed unit that includes tonalite, quartz diorite and diorite phases; and a tonalite unit consisting almost entirely of leucocratic tonalite (Fig. 3). The mixed unit includes most rocks assigned to the Burgess Creek stock by Schiarizza (2014). The tonalite unit partially envelops the mixed unit to the west, northwest and north, and includes some rocks previously assigned to the stock, and some, in the northwest, that were previously included in the Granite Mountain batholith (Schiarizza, 2014).

The tonalite unit consists of light grey, light grey-weathered, medium- to coarse-grained, equigranular hornblende-biotite tonalite. It is typically leucocratic, with 7-10% mafic minerals (hornblende > biotite), 30-40% quartz, and 50-60% plagioclase, although varieties with up to 15% mafic minerals are not uncommon. Leucotonalite, with only a few per cent chloritized mafic grains, forms local narrow dikes or poorly-defined patches with indistinct contacts with the enclosing tonalite.

The mixed unit of the Burgess Creek stock includes tonalite, quartz diorite, diorite and leucotonalite. Tonalite is predominant, and includes leucocratic varieties, very similar to those of the tonalite unit, as well as darker varieties that contain up to 30% mafic minerals (Fig. 5). A less abundant, but equally widespread, phase comprises greenish-grey,



Fig. 5. Mafic tonalite, mixed unit, northwestern part of the Burgess Creek stock.

light brownish-grey-weathered, medium- to coarse-grained hornblende-biotite quartz diorite. It typically contains 20-30% mafic minerals, 5-10% quartz, and 60-70% plagioclase, but quartz content is highly variable, such that some rocks are diorites and others are mafic tonalites. Locally, this phase contains irregular mafic patches several centimetres to tens of centimetres in size, consisting mainly of hornblende and magnetite, intergrown with minor amounts of quartz and plagioclase. A third component of the mixed unit comprises fine-grained diorite, consisting of hornblende (30-40%) and plagioclase. It is most common as screens and xenoliths within tonalite, but is the main rock type in some exposures along the southeast margin of the stock. It is typically equigranular, but locally displays a porphyritic texture, with phenocrysts of hornblende and/or plagioclase scattered through a fine-grained dioritic groundmass. The youngest component of the mixed unit is leucotonalite, which occurs as dikes, commonly 1-30 cm thick but locally much thicker, that cut all other rock types. The dikes consist of quartz and plagioclase with only a few per cent chloritized mafic minerals. They display a variety of textures, including fine-grained aplitic, coarse-grained with pegmatitic patches, and porphyritic, comprising phenocrysts of quartz \pm plagioclase \pm hornblende in a fine-grained leucotonalite groundmass.

A sample of leucocratic tonalite, collected from the tonalite unit along the northeast margin of the Burgess Creek stock yielded a U-Pb zircon age of 222.71 ± 0.22 Ma, and a sample of quartz diorite, collected from the mixed unit 350 m to the southwest, yielded a U-Pb zircon age of 221.25 ± 0.20 Ma (Richard Friedman, University of British Columbia, written communication March 2014). These determinations establish a Late Triassic age for the Burgess Creek stock. The fact that the tonalite yielded an older age than the quartz diorite was unexpected, as tonalites within the mixed unit, which are similar in appearance to the dated tonalite of the tonalite unit, commonly display crosscutting relationships indicating they are younger than the quartz diorite phase. The radiometric ages suggest there are tonalites of multiple ages within the stock.

The Burgess Creek stock is in contact with the Nicola Group to the north and southeast, and with the Granite Mountain phase of the Granite Mountain batholith to the west. The stock cuts across Nicola Group stratigraphy, and an intrusive contact is exposed in an outcrop along its southern margin near the east end of the stock. This intrusive relationship is corroborated by observations elsewhere, including dikes of tonalite and quartz diorite cutting the Nicola Group near the contact, xenoliths of Nicola rock in the stock near the contact, and a zone of skarn-altered rocks in the Nicola Group along the southeastern margin of the stock (Schiarizza, 2014). The contact between the Burgess Creek stock and the Granite Mountain batholith is well constrained east of the Gibraltar tailings pond. Although the contact is covered, indications of faulting are lacking, and the Granite Mountain phase is inferred to cut the Burgess Creek stock on geochronologic grounds (Fig. 3; see below).

3.3. Granite Mountain batholith

The Granite Mountain batholith is mainly exposed in a northwest elongate, 15 x 10 km, elliptical area (Fig. 3). As recognized by previous workers (Panteleyev, 1978; Ash et al., 1999a, b; Bysouth et al., 1995), the batholith is subdivided into three northwest-trending map units that become progressively more felsic from southwest to northeast. The units, following the terminology of Bysouth et al. (1995) are: Border phase (quartz diorite); Mine phase (tonalite); and Granite Mountain phase (leucocratic tonalite). A fourth phase, also recognized by previous workers, comprises leucotonalite, which occurs as dikes that intrude all three map units.

A large part of the batholith, including the Gibraltar open pits, the tailings pond, and all the area in between, was not examined in this study because of industrial activity related to the Gibraltar Mine. The contact between the Mine phase and the Granite Mountain phase in this area is based on the map of Ash et al. (1999b).

3.3.1. Border phase

The Border phase consists mainly of light to medium greenish-grey, brownish-grey-weathered, medium- to coarse-grained quartz diorite, locally grading to diorite or tonalite. It consists of saussuritic plagioclase accompanied by 25-40% chloritized hornblende, and 2-15% quartz. Textures are equigranular, typically weakly to strongly foliated, and rarely isotropic (Fig. 6). In two isolated exposures, several km apart, the unit comprises complex mixtures of fine, medium and coarse-grained hornblende diorite to quartz diorite, cut by veins and dikes of leucocratic quartz diorite. Elsewhere, the quartz diorite typically displays a uniform composition at the scale of an individual outcrop, although it is commonly cut by dikes of the leucotonalite phase.

3.3.2. Mine phase

The Mine phase occurs northeast of the Border phase, and hosts the orebodies at the Gibraltar Mine. It comprises medium- to coarse-grained, equigranular, isotropic to well-foliated tonalite, commonly with 15-25% chloritized mafic grains (mainly or entirely hornblende) and 25-30% quartz, together with saussuritic plagioclase, sericite and epidote (Fig. 7). More mafic varieties, with 25-35% chloritized mafic minerals and 15-25% quartz are common in the southeastern part of the unit, and leucocratic rocks, with 15% mafic grains and subequal proportions of quartz and plagioclase occur locally near the contact with the Granite Mountain phase. Compositions are typically uniform in any given area, but a few outcrops in the southeastern part of the unit contain complex mixtures of different tonalite phases, defined by variations in grain size and modal abundance of quartz and mafic minerals. Contacts with the border phase are not well exposed, but Mine phase tonalites near the contact are generally mafic-rich and quartz-poor, suggesting it is gradational.

Oliver et al. (2009) reported that a sample of Mine phase tonalite yielded a U-Pb zircon laser ablation age of 211.9



Fig. 6. Quartz diorite, Border phase of the Granite Mountain batholith, 3.8 km east-southeast of the south end of Cuisson Lake.



Fig. 7. Tonalite, Mine phase of the Granite Mountain batholith, 3 km southeast of the Granite Lake pit.

± 4.3 Ma. To establish more precise crystallization ages, samples collected in 2014 have been submitted for U-Pb zircon geochronology using the CA-TIMS method (Chemical Abrasion-Thermal Ionization Mass Spectroscopy).

3.3.3. Granite Mountain phase

The Granite Mountain phase is the predominant component of the Granite Mountain batholith, forming more than half its areal extent. It comprises light grey, light grey to white-weathered, isotropic to well-foliated, coarse-grained leucocratic tonalite. A typical rock in the southern part of the unit contains approximately equal proportions of quartz and plagioclase, and 10-12% chloritized mafic minerals (Fig. 8). To the north, quartz is slightly more abundant than plagioclase, and commonly forms very coarse (8-12 mm) aggregates. These quartz-rich tonalites commonly have 5-10% mafic minerals, with more biotite than hornblende.



Fig. 8. Leucocratic tonalite, Granite Mountain phase of the Granite Mountain batholith, 450 m southeast of Granite Mountain.

The contact between the Granite Mountain and Mine phases appears to be gradational where it is fairly well constrained southeast of the Gibraltar mine. A traverse from the Granite Mountain phase (10% mafics, equal proportions of plagioclase and quartz) into the Mine phase shows, first, a slight increase in mafic content (15% mafics, equal proportions of plagioclase and quartz), and then a further increase in mafic content coupled with a decrease in quartz (20% mafics, 35% quartz, 45% plagioclase). The Granite Mountain phase is differentiated from the tonalite unit of the Burgess Creek stock (equally leucocratic), because the latter unit has less quartz and is finer grained.

Exposures of leucocratic tonalite 5 km north-northwest of the Gibraltar tailings pond are tentatively assigned to the Granite Mountain phase, but are separated from the main part of the Granite Mountain batholith by a fault-bounded block containing exposures of the slate-sandstone unit of the Dragon Mountain succession. This outlier may be connected to the main part of the batholith at depth, because a vertical diamond drill hole collared in Dragon Mountain rocks in the west-central part of the fault block extended through the sedimentary succession to end in tonalite that was correlated with the Granite Mountain phase (Barker and Grubisa, 1994, Hole 94-3).

A sample of coarse-grained, quartz-rich leucocratic tonalite, collected from the Granite Mountain phase west of the Burgess Creek stock in 2013, yielded a U-Pb zircon CA-TIMS age of 217.15 ± 0.20 Ma (Fig. 3; Richard Friedman, University of British Columbia, written communication March 2014). Ash and Riveros (2001) reported that the Granite Mountain batholith has a magmatic age of 215 ± 0.8 Ma, apparently from a U-Pb zircon determination on a sample collected from the Granite Mountain phase 1.5 km north-northeast of the Gibraltar mill site (Ash et al., 1999a). Oliver et al. (2009) reported that a sample from the Granite Mountain phase yielded a U-Pb zircon laser ablation age of 209.6 ± 6.3 Ma.

3.3.4. Leucotonalite dikes

Leucotonalite dikes with a variety of textures, but characterised by low (0-5%) mafic content, are a ubiquitous but volumetrically minor component of the Granite Mountain batholith, and are found in all three map units. They are commonly equigranular, fine (aplitic) to coarse-grained, variably oriented, and a few centimetres to tens of centimetres thick (Fig. 9). Porphyritic varieties contain quartz \pm plagioclase phenocrysts, several mm in size, in a groundmass of mainly finer quartz and plagioclase. Thick quartz-plagioclase porphyry units, several tens of metres wide, occur locally in the Border phase and Mine phase.

Ash and Riveros (2001) reported that leucotonalite dikes in the Pollyanna pit of the Gibraltar Mine yielded a U-Pb age of 212 ± 0.4 Ma, without providing details. A sample collected in 2014, from a thick quartz-plagioclase porphyry dike that cuts Mine Phase tonalite 4 km southeast of the Gibraltar Mine, was submitted for U-Pb zircon geochronology using CA-TIMS.

3.4. Dragon Mountain succession

Lower to Middle Jurassic sedimentary rocks in the region that were included in the upper part of the Quesnel River Group by Tipper (1978), were referred to as the Dragon Mountain succession by Logan and Moynihan (2009). The succession is well represented by a belt of exposures that extends from near Quesnel southward to the northern part of the Granite Mountain map area (Fig. 2). Logan and Moynihan (2009) showed that, near Quesnel, these rocks rest stratigraphically above the Nicola Group. They subdivided the Dragon Mountain succession into two units: a lower unit of mainly phyllite and siltstone; and an upper unit of predominantly conglomerate. These same two units are recognized in the Granite Mountain map area.

3.4.1. Slate-sandstone unit

The slate-sandstone unit is juxtaposed against the Nicola Group and the Granite Mountain batholith in a fault-bounded



Fig. 9. Leucotonalite dikes cutting Mine phase tonalite, Granite Mountain batholith, 2.5 km southeast of the Granite Lake pit.

block north-northwest of the Gibraltar tailings pond; forms a small outlier north of the Burgess Creek stock; and is exposed in a narrow fault-bounded sliver against the conglomerate unit at the north end of the 700 road (Fig. 3). The unit consists mainly of dark grey slate with laminae and thin interbeds of lighter grey siltstone and, less commonly beds of fine- to medium-grained yellowish-brown-weathered quartz-rich sandstone (Fig. 10). Locally, in the fault block northwest of the Gibraltar tailings pond, the unit also includes poorly defined beds of pebble conglomerate. The conglomerate contains subrounded to subangular clasts of intermediate to mafic volcanic rock, quartz-phyric rhyolite, and uncommon fine- to medium-grained tonalite. The clasts are supported by a mixed matrix that includes foliated sericite and chlorite, and sand-sized quartz, feldspar and rock fragments.

The basal contact of the slate-sandstone unit is not exposed in the Granite Mountain map area, but the small outlier north of the Burgess Creek stock is inferred to rest unconformably above the Nicola Group, and the rocks north-northwest of the Gibraltar tailings pond are, at least in part, above the Granite Mountain batholith. The latter interpretation is based on a diamond drill hole in the west-central part of the fault block, which was collared in Dragon Mountain rocks but extended through the sedimentary succession to end in tonalite correlated with the Granite Mountain phase (Barker and Grubisa, 1994, Hole 94-3). The slate-sandstone unit is undated in the Granite Mountain map area, but 13 km to the north, along the French Creek road, it contains Early Jurassic (Late Pliensbachian) fossils (Petersen et al., 2004; Logan and Moynihan, 2009).

3.4.2. Conglomerate unit

The conglomerate unit of the Dragon Mountain succession forms a single northwest trending belt in the northern part of the map area. Rocks in the belt dip and young to the east. They occur above the Nicola Group, exposed to the southwest, and are apparently truncated to the east by an unexposed north-northwest trending fault that separates them from the Cache Creek Complex. In contrast to the Nicola Group the unit consists of coarse conglomerate over stratigraphic intervals of many hundreds of metres and contains a highly diverse clast suite, including coarse-grained tonalite. Green feldspathic sandstone, which forms 10-15% of the unit, is not readily distinguished from sandstones in the underlying Nicola Group.

The conglomerates generally weather to a light brown or brownish-green, but locally are light purplish-grey. They contain angular to subrounded pebbles and cobbles in a sandy matrix that includes feldspar, quartz and lithic grains (Fig. 11). The clasts consist mainly of light grey to green volcanic rocks with various combinations of plagioclase, hornblende and pyroxene phenocrysts, but fine-grained, equigranular, diorite, quartz diorite and tonalite, dark green mafic volcanic rocks and quartz-phyric rhyolite are also represented. Less common clasts include limestone, chert, and coarse-grained equigranular tonalite. The conglomerate forms massive intervals, many tens of metres thick, with little or no apparent stratification. Local



Fig. 10. Decimetre- to mm-scale sandstone-siltstone-mudstone fining-upward sequences with abundant soft-sediment deformation structures; slate-sandstone unit of the Dragon Mountain succession, 550 m north of the Burgess Creek stock.



Fig. 11. Conglomerate, Dragon Mountain succession, conglomerate unit, north end of the 700 road.

well-stratified intervals include thick to very thick beds of moderately sorted pebble-cobble conglomerate, intercalated with thin to medium beds of sandstone, pebbly sandstone and siltstone. These stratified intervals commonly contain graded beds and cut-and-fill features that show tops-to-the-east.

The conglomerate unit dips and youngs to the east-northeast, away from the underlying Nicola Group. The base of the unit is not exposed, and is not well constrained. Of note, however, is the apparent absence of the slate-sandstone unit, which typically forms the base of the Dragon Mountain succession (Logan and Moynihan, 2009). This suggests that the western boundary of the conglomerate unit might be a fault which has cut out the basal part of the succession.

3.5. Early Jurassic? gabbro

Dark green, coarse-grained gabbro forms an isolated exposure

a short distance southeast of the A road, about 3.6 km north of the Gibraltar tailings pond (Fig. 3). The gabbro displays an isotropic texture and consists of clinopyroxene (70%, 3-6 mm), fewer and smaller plagioclase grains, and 1-2% biotite flakes. Locally it is cut by narrow veins of fine-grained leucocratic diorite. Contacts are not exposed, but the gabbro is apparently in a fault block underlain mainly by the slate-sandstone unit of the Dragon Mountain succession. It is suspected to have intruded these Lower Jurassic rocks, based on correlation with an ultramafic-mafic intrusive unit that intrudes the slate-sandstone unit where it was intersected in exploration diamond drill holes cored 3.5 km to the southwest (Barker and Grubisa, 1994). Similar gabbro is a component of Early Jurassic Alaskan-type ultramafic-mafic intrusive complexes that are scattered throughout Quesnel terrane in central and southern British Columbia (Logan et al., 2010; Schiarizza et al., 2013).

3.6. Cache Creek Complex

The Cache Creek Complex underlies the eastern part of the map area, but is not well exposed. Good exposures occur along parts of Burgess Creek, but outcrops elsewhere are small and widely scattered. The exposures consist mainly of chert, limestone and basalt. Chert is most common, is grey to greenish-grey, and occurs as lenses and layers, $\leq 1-6$ cm thick, separated by partings and thin interbeds of grey phyllite or slate (Fig. 12). Limestone is finely crystalline, medium to dark grey, and weathers light or medium grey. Along Burgess Creek it forms centimetre- to metre-scale lenses and layers interleaved with chert, but exposures southeast of the lake at the head of Big Camp Creek may represent a limestone unit many tens of metres thick. Small exposures of medium to dark green, rusty-brown-weathered basalt occur along the 609 road, along Burgess Creek, and in cutblocks south of the Burgess Creek logging road. The latter exposures are heavily altered with carbonate, and locally contain fragments and lenses of grey limestone.

An isolated set of exposures northwest of the small lake



Fig. 12. Chert and phyllite, Cache Creek Complex, Burgess Creek.

at the head of Big Camp Creek (Fig. 3) includes grey chert with a sugary recrystallized texture, and rusty hornfels consisting mainly of actinolite, epidote, biotite and quartz, with disseminated pyrrhotite and pyrite. These rocks are cut by a unit of greenish-grey hornblende-plagioclase porphyry.

3.7. Cuisson Lake unit

The Cuisson Lake unit, consisting mainly of chlorite schist, limestone and skarn, forms a narrow belt in the southwestern part of the map area, between the Granite Mountain batholith and the Sheridan Creek stock. These rocks were considered part of the Cache Creek Complex by Drummond et al. (1976), Panteleyev (1978) and Bysouth et al. (1995). Ash et al. (1999a) interpreted the unit as an intensely deformed and recrystallized mafic phase of the Granite Mountain batholith, but Ash and Riveros (2001) revised this interpretation to suggest that it might include both melanocratic phases of the Granite Mountain batholith and basaltic volcanic rocks of the Cache Creek Complex. Most rocks in the unit are well foliated and recrystallized, such that protolith mineralogy and texture are not preserved. Current mapping suggests that the unit is derived mainly from a succession of feldspathic volcanoclastic±volcanic rocks intercalated with limestone that is locally altered to skarn. The unit also includes sericite-chlorite-quartz-plagioclase schists that may have been derived from quartz dioritic intrusive rocks.

The most common component of the Cuisson Lake unit is green, well-foliated schist consisting mainly of fine-grained chlorite, epidote, actinolite, plagioclase, calcite and quartz (Fig. 13). Narrow lenses of epidote-calcite are commonly oriented parallel to the schistosity, and dark green 1-3 mm clots of porphyroblastic actinolite occur locally. Relict grains of plagioclase (< 2 mm) are variably altered with sericite, epidote and calcite and, although common, may only be obvious in thin section. At one locality in the central part of the belt, relict grains of plagioclase (accompanied by rare quartz) display variations in abundance and size that define a vague stratification,



Fig. 13. Chlorite schist, Cuisson Lake unit, 1.8 km east-southeast of the south end of Cuisson Lake.

suggesting derivation from a feldspar-rich siliciclastic rock. A bedded protolith is also suggested at a nearby outcrop, 400 m to the southeast, where the schist locally displays what appear to be primary 1-2 mm laminae.

Light-grey finely crystalline limestone is common in the central and eastern parts of the Cuisson Lake belt, where it forms a series of lenses or layers intercalated with chlorite schist (Fig. 14). Platy foliation within the limestone, concordant to schistosity in adjacent chlorite schists, is defined by narrow partings of chlorite±sericite. Narrow lenses of magnetite and/or specularite skarn, variably mineralized with chalcopyrite, are associated with the limestone in the central part of the belt, forming the Iron Mountain mineral occurrence. Skarn is more extensive in the northwestern part of the belt, east of central Cuisson Lake, where it forms the predominant rock type across the entire width of the unit. The skarn here is massive, contains epidote, actinolite, garnet, chlorite, calcite and quartz (Fig. 15), and is commonly cut by veins containing quartz, chlorite, calcite and epidote.

Light grey to greenish-grey sericite-chlorite-quartz plagioclase schists are a relatively minor component of the Cuisson Lake unit, but occur locally along the entire length of

the belt. These schists consist mainly of well-foliated sericite, chlorite and fine-grained recrystallized quartz, but also include single and multiple grains (<2 mm) of relict plagioclase, variably altered with calcite, epidote and sericite. They commonly occur near the contact with the Granite Mountain batholith, and may have been derived from quartz dioritic intrusive rocks.

The contact between the Cuisson Lake unit and the Granite Mountain batholith is not exposed, and is closely constrained in only two places, near the northwest and east ends of the belt. It is suspected to be an intrusive contact because: 1) evidence of faulting where it is closely constrained is lacking; 2) sericite-chlorite-quartz plagioclase schists in the unit may represent quartz dioritic dikes related to the Granite Mountain batholith; and 3) a small exposure of skarn enveloped by quartz diorite, east of the north end of the unit (Fig. 3), may be an enclave of the Cuisson Lake unit within the batholith. The southern contact of the Cuisson Lake unit, with the Sheridan Creek stock, is likewise not exposed, but is inferred to be a south-dipping fault. This interpretation is based mainly on a marked increase in foliation intensity, and local development of mylonitic fabrics, in both units as the contact is approached.

Most previous interpretations correlate the Cuisson Lake unit with the Cache Creek Complex. Observations presented here suggest that it was derived mainly from feldspathic volcanoclastic±volcanic rocks intercalated with limestone. Hence a more likely correlation is with the Nicola Group of Quesnel terrane.

3.8. Sheridan Creek stock

Light grey, isotropic to well foliated tonalite in the southern part of the map area is part of the Sheridan Creek stock (Early Cretaceous). Most of the tonalite has a fairly uniform composition, comprising 20% hornblende, 25-35% quartz and 45-55% plagioclase (Fig. 16). It is typically medium grained (2-3 mm grain size), but oversized prismatic hornblende crystals, up to 8 mm long, are characteristic. Fine-grained leucocratic tonalite to quartz diorite locally forms narrow dikes or irregular patches in the predominant tonalite phase, and a relatively melanocratic (25% hornblende) fine- to medium-grained quartz diorite is the main phase at one isolated exposure in the northwestern part of the stock.

The north side of the Sheridan Creek stock is juxtaposed against the Cuisson Lake unit. The contact is not exposed, but is inferred to be a south-dipping fault because south-dipping foliation in both units intensifies, with local development of mylonitic fabrics, as the contact is approached. The stock is apparently hosted by the Cache Creek Complex, which crops out to the east and south (Fig. 2; Ash et al. 1999b), but contacts are not exposed. Ash and Riveros (2001) reported that the stock yielded a U-Pb zircon age of 108.1 ±0.6 Ma.

4. Structural geology of the Granite Mountain area

Mesoscopic structural features and contact relationships within the Granite Mountain map area will be discussed in terms of three domains: a northern domain, which includes



Fig. 14. Limestone, Cuisson Lake unit, 2.2 km east-southeast of the south end of Cuisson Lake.

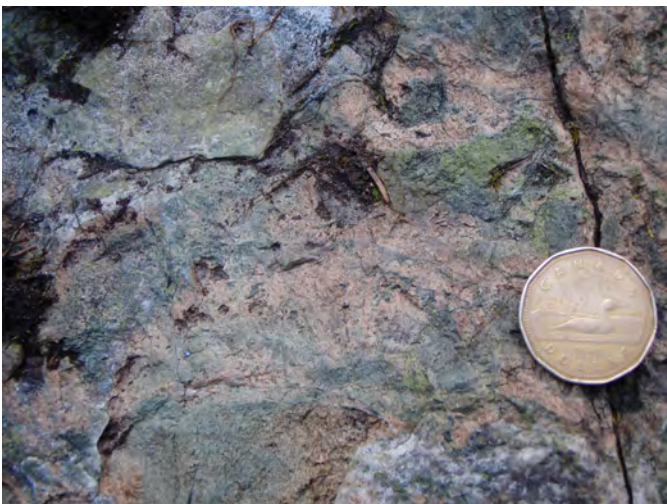


Fig. 15. Skarn, Cuisson Lake unit, 300 m east of central Cuisson Lake.



Fig. 16. Hornblende tonalite, Sheridan Creek stock, 4 km southeast of the lake at the head of Big Camp Creek.

the Nicola Group, Burgess Creek stock and Dragon Mountain succession; a southern domain, which includes the Granite Mountain batholith, the Cuisson Lake unit, and the Sheridan Creek stock; and an eastern domain which comprises the Cache Creek Complex. Subsequent sections will discuss the map-scale faults within the area, and a final section presents a brief structural synopsis which places the structures in a regional context.

The structural geology of the Gibraltar mine, which was not examined during the present study, is not discussed. A detailed structural analysis of the Gibraltar deposit is ongoing (Mostaghimi et al., 2014).

4.1. Northern domain

The southern part of the Nicola Group comprises a fairly uniform, right-way-up homoclinal panel that dips at moderate angles to the east-northeast (Fig. 3). This panel is crosscut at a high angle by the eastern part of the Burgess Creek stock. Bedding orientations are more variable in the poorly-exposed central and northern parts of the Nicola belt, indicating structural complications that are not understood. The Nicola Group is overlain to the northeast, structurally or stratigraphically, by the conglomerate unit of the Dragon Mountain succession which, like Nicola rocks to the south, forms a homoclinal panel that dips and youngs to the east-northeast. Bedding in the small outlier of the Dragon Mountain slate-sandstone unit south of Burgess Creek is folded, but dips are gentle and mainly southwest to northwest, in contrast to nearby Nicola exposures, which dip at moderate angles to the northeast. The slate-sandstone unit also dips gently within the fault block to the west, although bedding observations are rare.

The characteristic well-developed slaty cleavage of the Dragon Mountain slate-sandstone unit dips steeply, mainly to the northeast but locally to the southwest, and is axial planar to mesoscopic folds of bedding which, together with bedding-cleavage intersection lineations, plunge gently to the

northwest. In one exposure northwest of the Gibraltar tailings pond, the southwest-dipping slaty cleavage is deformed by south to southeast-plunging mesoscopic folds and crenulations, and an associated east-dipping crenulation cleavage. A weak to moderately developed cleavage, also with steep dips to the northeast or southwest, cuts siltstone, limestone, and some breccia units of the Nicola Group, but is not developed in most units of the group, nor in the Dragon Mountain conglomerate unit. The cleavage, typically defined by oriented chlorite and/or sericite, is accentuated by variably flattened lithic fragments in breccia units. Mesoscopic folds were observed at only one locality in the Nicola Group, south of the Burgess Creek stock. Here, folds developed in uncleaved, thin- to medium-bedded volcanic sandstone plunge at moderate angles to the north and verge to the west (north-striking, steeply-dipping short limbs enclosed by moderately east-northeast-dipping long limbs).

The Burgess Creek stock locally displays a weak, northeast to southwest-dipping foliation, parallel to, and presumably the same age as, cleavage within the Nicola Group and Dragon Mountain slate-sandstone unit. The stock also contains local narrow, steeply dipping, high-strain zones, defined by well foliated, locally mylonitic rock, ranging from 40 cm to 30 m wide. These zones occur in the mixed unit, are typically near and parallel to its margins, and are crosscut by younger tonalite and leucotonalite phases of the stock. They are inferred to have formed during emplacement and construction of the stock. A well-foliated zone that dips gently to the southeast in the west-central part of the stock is probably younger (Fig. 3). It is localized within a quartz porphyry unit, and locally displays C-S fabrics indicating northwest-directed thrust movement.

4.2. Southern domain

The southern domain comprises the Granite Mountain batholith, the Cuisson Lake unit and the Sheridan Creek stock. These rocks are characterized by a foliation that dips at moderate to gentle angles to the south. This foliation (S1) is strong throughout the Cuisson Lake unit, but is of variable intensity in plutonic rocks of the Granite Mountain batholith and Sheridan Creek stock, and is typically weak to absent in the northern part of the Granite Mountain phase. Weakly foliated plutonic rocks display an isotropic igneous texture overprinted by discontinuous sericite foliae, and may show a slight flattening of chloritized mafic clots. Strongly foliated rocks (Fig. 17) comprise anastomosing networks of sericite-rich and chlorite-rich foliae that enclose lenses of flattened quartz and saussuritic (but internally unstrained) plagioclase. These foliations accommodated mainly flattening strain, but in two locations in the Granite Mountain phase, southeast of Granite Mountain, local zones of well-foliated rock display C-S fabrics showing top-to-the-north shear. Outcrops of both the Cuisson Lake unit and Sheridan Creek stock, near their mutual contact, display similar extremely strong foliations, but unequivocal kinematic indicators were not observed.

The S1 foliation in the Granite Mountain batholith is locally cut by a crenulation cleavage that strikes east-southeast



Fig. 17. Mine phase tonalite with well-developed, gently dipping S1 foliation, Gibraltar Mine road.

and dips steeply, mainly to the south-southwest. Associated crenulation lineations, and rare mesoscopic folds of S1, plunge gently to the southeast. In one Mine phase exposure, 1.9 km south-southeast of Granite Mountain, there are two crenulation cleavages at a low angle to one another; one strikes 098° and dips steeply south, and the other, younger cleavage strikes 118° and is vertical. Schists within the Cuisson Lake unit locally display a southeast-plunging crenulation lineation that may be equivalent to those seen in the Granite Mountain batholith. South-plunging kink folds and crenulations, with north-striking, steeply-dipping axial surfaces, appear to be younger structures, and were observed to deform schists of the Cuisson Lake unit and a south-dipping high-strain zone in the Sheridan Creek stock.

Narrow, steeply dipping high-strain zones with east-southeast trends are a striking but relatively uncommon feature in Granite Mountain and Mine phase rocks east, south and southwest of Granite Mountain (Fig. 3). They range from 10 cm to 10 m wide, clearly crosscut the S1 foliation, and have an orientation that is similar to the local crenulation cleavage in these rocks. The zones are up to 10 m wide in the Granite Mountain phase, where they typically display features (C-S fabrics and shear bands) indicating sinistral shear (Fig. 18). High-strain zones in the Mine phase (Fig. 19) are typically less than 1 m wide; most do not display clear indications of non-coaxial strain, although one narrow zone that cuts a quartz-feldspar porphyry dike in the Mine phase, 5.1 km south of Granite Mountain, accommodated dextral shear.

4.3. Eastern domain

The eastern domain, comprising the Cache Creek Complex, includes well-foliated chert-phyllite units, as well as limestone and basalt, which show little or no foliation. The fabric of the chert units is composite, and is defined by platy layers and lenses of chert and a well-developed phyllitic cleavage, in the thin phyllite interbeds, which is typically parallel to the chert layers.



Fig. 18. Southeast striking, steeply dipping sinistral shear zone in leucocratic tonalite of the Granite Mountain phase, 1 km southeast of Granite Mountain. Note shear bands extending diagonally from top right to middle left. Looking down on flat outcrop surface with top of photo facing southwest.



Fig. 19. High-strain zone, dipping steeply to the south-southwest, cutting weakly foliated Mine phase tonalite, 4.2 km southwest of Granite Mountain. View is to the east.

In addition, chert-phyllite units commonly display narrow slip surfaces at a low angle to this foliation, which define local truncations and discontinuities of the chert layering (Fig. 12). Narrow limestone lenses in predominantly chert intervals along Burgess Creek are parallel to the foliation and, where contacts are observed, appear to be bounded by narrow shear zones.

Foliation in the eastern domain most commonly dips at low to moderate angles to the north. It is deformed by north to northwest-plunging mesoscopic folds along the southern part of the 609 road, and by east-southeast-plunging folds on the low ridge south of the 800 road, where the foliation dips mainly to the south. Gently dipping foliation along Burgess Creek is locally cut by two weak crenulation cleavages, one dipping steeply south and the other dipping steeply to the east-southeast.

4.4. East-trending faults

An east trending fault is inferred to mark the contact between the Cuisson Lake unit and the Sheridan Creek stock in the southwestern part of the map area (Fig. 3) because a south-dipping foliation in both units becomes progressively stronger (locally mylonitic), as the contact is approached. It may be a north-directed thrust fault, because similar south-dipping foliation in the Granite Mountain phase to the north locally grades into a C-S mylonite that shows top-to-the-north sense of shear.

An east-southeast trending fault is inferred from an apparent 300 m sinistral offset of the southern contact of the Burgess Creek stock (Fig. 3). Farther west, within the stock, this fault offsets the contact between the mixed unit and the tonalite unit. The orientation of this structure is similar to the sinistral high-strain zones mapped in the Granite Mountain phase to the south, but it is unknown if they are the same age.

4.5. Northeast-trending faults

A prominent northeast-trending fault in the southern part of the map area truncates the Cuisson Lake unit, an east-trending fault that bounds the Cuisson Lake unit to the south, and the Border and Mine phases of the Granite Mountain batholith (Fig. 3). The fault juxtaposes these units against the Sheridan Creek stock to the southeast. The northeast extension of this fault apparently separates the Granite Mountain phase of the batholith from the Cache Creek Complex. Sinistral movement along this fault is inferred from the distribution of Sheridan Creek tonalite, and because several outcrop-scale sinistral faults with similar strikes, and steep to moderate southeast dips, are in the Sheridan Creek stock near the inferred fault trace.

Northeast-trending faults in the area north of the Gibraltar tailings pond are inferred from truncations of map units and topographic lineaments, but were not directly observed. Predominantly normal-sense movement is inferred on the faults that bound the slate-sandstone unit of the Dragon Mountain succession. Near the north boundary of the map area, an east-northeast trending fault with sinistral and/or north-side-down movement is inferred from the truncation of the contact between the Nicola Group and Dragon Mountain conglomerate unit.

4.6. North and north-northwest trending faults

A north-trending fault in the southern part of the map area marks a 750 m offset of the Cuisson Lake unit and adjacent map units. The fault is not exposed, but the apparent offset of the south-dipping map units suggests dextral and/or west-side-down displacement. The Cuisson Lake unit is also offset by a north-northwest trending fault 2300 m farther west, which was defined, in part, by diamond drilling of the Sawmill mineral deposit. This structure dips at moderate angles to the west, and is thought to have more than 300 m of west-side-down displacement (Bysouth et al., 1995). Northwest-trending faults inferred north of the Gibraltar tailings pond show offsets and juxtapositions of map units that suggest some combination of

dextral and/or west-side-down vertical displacements. North to north-northwest striking outcrop-scale faults in this area, and in the Granite Mountain batholith to the south, commonly show a dextral component.

A major north-northwest trending fault that may not be related to those described previously is inferred to separate rocks of Quesnel terrane, including the Dragon Mountain succession, the Nicola Group, and Burgess Creek stock, from the Cache Creek Complex to the east. This fault is notable because it reverses the regional arrangement of these terranes, in which Cache Creek rocks are typically west of Quesnel terrane. One possible explanation is that this structure marks a Middle Jurassic or younger sinistral offset of the previously established terrane boundary. Weak support for this interpretation comes from near the west end of the Cache Creek exposures along Burgess Creek, where a prominent vertical fault that strikes 160, parallel to the trace of the major fault inferred to the west, has well-developed calcite slickenfibres that indicate sinistral slip (Fig. 20).

4.7. Regional significance of structures

The major structural features of the northern domain (steeply dipping, northwest striking foliation and associated folds) are parallel to the structural grain of the Cordillera, and probably formed during Cordilleran-wide contractional deformation that began in the early Middle Jurassic. These structures postdate local syn-plutonic high-strain zones in the Burgess Creek stock, which likely formed during Late Triassic construction of the Quesnel arc. The major structural feature of the southern domain (south-dipping foliation in the Sheridan Creek stock, the Cuisson Lake unit, and the southern part of the Granite Mountain batholith) likely formed during structural juxtaposition of the Sheridan Creek stock with rocks of Quesnel terrane during Cretaceous or younger structural reworking of the Quesnel-Cache Creek boundary. This juxtaposition may have formed in concert with sinistral displacement along the



Fig. 20. South-southeast striking vertical fault with calcite slickenfibres showing sinistral sense of shear; Cache Creek Complex, Burgess Creek. View is to the west.

north-northwest trending fault at the Quesnel-Cache Creek boundary in the eastern part of the map area. Structures in the Cache Creek Complex (eastern domain) bear no obvious relationship to those within the north and south domains. They may include structures that initially formed during accumulation as a subduction-related accretionary complex in the Triassic and Early Jurassic, variably overprinted during younger tectonic events. The youngest structures in the map area (north to northwest trending faults with mainly dextral and/or west-side-down displacement, and northeast trending faults with sinistral and/or vertical displacement) are probably related to Cretaceous to Eocene Cordilleran-wide strike-slip tectonics (Struik, 1993).

5. Mineral occurrences

Mineralization at the Gibraltar Mine is hosted in Mine phase tonalite of the Granite Mountain batholith, but porphyry-style mineral occurrences are also known in the Border phase and the Granite Mountain phase. Copper mineralization also occurs within the Cuisson Lake unit adjacent to the batholith, and at several locations within the Nicola Group near the Burgess Creek stock (Fig. 21).

5.1. Gibraltar Mine

The Gibraltar Cu-Mo deposit includes four open pits, Granite Lake (MINFILE 093B 013), Pollyanna (MINFILE

093B 006), Gibraltar East (MINFILE 093B 012) and Gibraltar West (MINFILE 093B 007), and adjacent mineralized zones, including Gibraltar North (MINFILE 093B 011), which have yet to be exploited (Fig. 21). The mine operated from 1972 to 1998, was shut down from 1999 to 2003, has been in production since it was reopened by Taseko Mines Ltd. in 2004, and has a projected mine life extending to 2037 (van Straaten et al., 2013). Production from 1972 to 1998 was 322 million short tons grading 0.367% Cu, and from 2004 to the first quarter of 2011 was 77 million short tons grading 0.324% Cu and 0.010% Mo (van Straaten et al., 2013).

The Gibraltar deposits are described by Sutherland Brown (1974), Simpson (1970), Drummond et al. (1973, 1976), Bysouth et al. (1995), Ash and Riveros (2001), Oliver et al. (2009), Harding (2012), van Straaten et al. (2013), and Mostaghimi et al. (2014). Mineralization consists mainly of disseminated and vein-hosted chalcopyrite, but also includes molybdenite, mainly in quartz veins, minor amounts of bornite in the east, and substantial amounts of sphalerite in the northwest. Re-Os radiometric ages on molybdenite, reported by Harding (2012), are Late Triassic and range from 210.1 ± 0.9 Ma to 215.0 ± 1.0 Ma. These determinations, similar to the age of the host batholith, together with the styles of vein and disseminated mineralization, are consistent with an origin as a calcalkaline porphyry deposit (Oliver et al., 2009; van Straaten et al., 2013). A unique feature of the Gibraltar deposits however, is a strong association of ore with high-strain zones, including south-dipping foliations and south-dipping top-to-the-north shear zones. These structures are considered by many to be the same age as the mineralization (Drummond et al., 1976; Bysouth et al., 1995; Oliver et al., 2009), but Ash et al. (1999a, b) suggested that the deformation is younger. The relationship between mineralization and deformation is currently under investigation (Mostaghimi et al., 2014).

5.2. Rick (MINFILE 093B 062)

The Rick occurrence is in Mine Phase tonalite 1-2 km north of the Gibraltar North zone (Fig. 21). Copper and zinc mineralization was discovered in 1998 during an exploration program covering the southern part of the Copper Ace property for United Gunn Resources Ltd. (Payne, 1999b; Ash et al., 1999a). Diamond drill programs carried out by Copper Ridge Explorations Inc. in 2006 (3 holes) and 2007 (13 holes) were focused on coincident soil and geophysical anomalies in an area measuring about 1200 m east-west by 800 m north-south, which includes the mineralized outcrops (Dawson, 2007; Hodge and Dawson, 2008). Thirteen of fourteen holes drilled in this area intersected copper mineralization, but some contained only minor disseminations, and in others mineralized intersections were narrow. Mineralization comprises chalcopyrite \pm molybdenite, as disseminations and in quartz veins, and locally includes bornite or sphalerite. Significant gold values were returned from some narrow intervals, including 0.425 g/t Au and 3.43% Cu over 1.6 m in hole CA-06-02 (Dawson, 2007), and 6.3 g/t Au and 684 ppm Cu over 0.5 m in hole

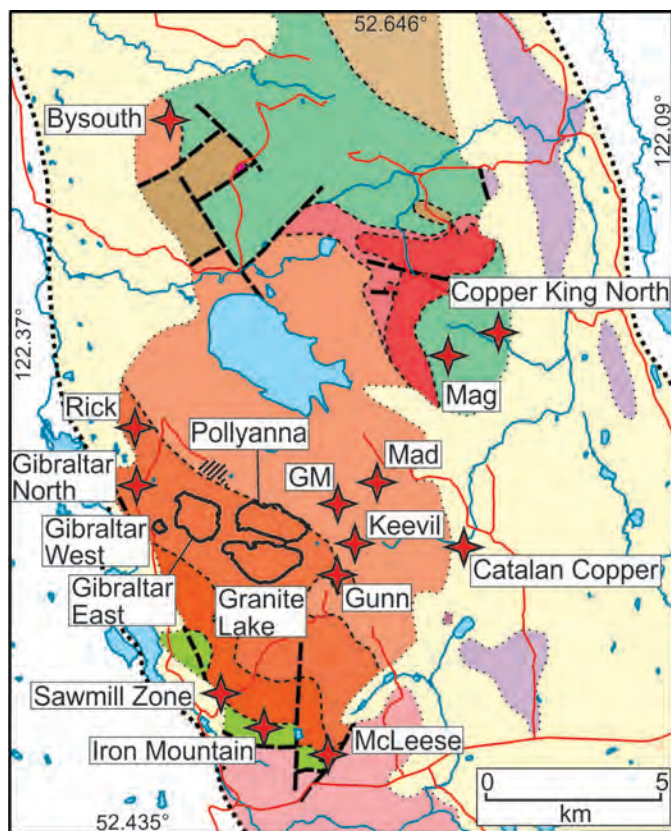


Fig. 21. Main mineral occurrences in the Granite Mountain map area. Base map is derived from Fig. 3.

CA07-09 (Hodge and Dawson, 2008).

5.3. Gunn (MINFILE 093B 003)

The Gunn prospect comprises porphyry-style copper-molybdenum mineralization in Mine phase tonalite about 1 km east of the Granite Lake pit. This area was explored by Gunn Mines Ltd. in the late 1960s, and the geology and mineralization is briefly described by Cannon (1968) and Eastwood (1970). Mineralization encountered during current mapping comprises sheeted veinlets, 1-2 mm wide and spaced 2-6 cm apart, consisting mainly of pyrite, chalcopyrite, chlorite and sericite. The sheeted veinlets dip steeply south, and are in Mine phase tonalite, which displays a weak foliation dipping gently south. The same outcrop includes a south-dipping quartz vein, 5-16 cm wide that contains patches of heavily-disseminated molybdenite, and local blebs of chalcopyrite along its margins.

5.4. Sawmill zone (MINFILE 093B 051)

The Sawmill zone is along the south margin of the Granite Mountain batholith, about 1 km east of the south end of Cuisson Lake. Mineralization was first intersected in diamond drill holes cored in 1979, which targeted a large I.P. anomaly. Subsequent drill programs by Gibraltar Mines Ltd. have outlined a resource (non-NI-43-101 compliant) reported as 75.5 million short tons grading 0.244% copper (Bysouth et al., 1995). Mineralization is in Border phase quartz diorite, along its contact with the Cuisson Lake unit, but is also hosted in local units of tonalite, similar to Mine phase tonalite, and quartz porphyry (Bysouth, 1990). It consists mainly of pyrite, chalcopyrite and molybdenite in veins and shears accompanied by quartz, chlorite, carbonate, sericite and epidote. Gypsum veins, containing chalcopyrite and minor bornite, also occur (Bysouth, 1990). The mineralized zone is truncated to the west by a west-dipping fault, referred to as the Sawmill fault, suspected to have more than 300 m of west-side-down displacement (Bysouth et al., 1995).

5.5. McLeese (MINFILE 093B 050)

The McLeese occurrence comprises copper mineralization hosted mainly in Border phase quartz diorite near the southeastern tip of the Granite Mountain batholith. Mineralization was discovered and explored with trenches and short diamond drill holes during exploration carried out by Sheridan Copper Mines Ltd. and Granite Mountain Mines Ltd. in 1970 and 1971 (Meyer, 1971a, b). It comprises chalcopyrite, pyrite, malachite and azurite that occur in east-striking vertical fracture zones, as disseminations along foliation planes and, locally, in quartz veins adjacent to gently dipping shears (Meyer, 1971a, b). Border phase quartz diorite is the main host, but the adjacent Cuisson Lake unit hosts rare mineralized quartz veins (Meyer, 1971a). Traverses through this area in 2014 encountered minor amounts of chalcopyrite and malachite disseminated in quartz diorite.

5.6. Keevil (MINFILE 093B 002) and GM

The Keevil and GM occurrences comprise substantial zones of

porphyry-style Cu-Mo mineralization in the Granite Mountain phase, east and northeast of the Gibraltar Mine. The Keevil occurrence was explored by Keevil Mining Group Ltd. in the 1960s. Mineralization is mainly in an northeast-trending zone, about 650 m long by 120 m wide, and includes chalcopyrite and malachite disseminated in foliated and sheared tonalite, malachite as coatings on joint surfaces, and molybdenite, locally with chalcopyrite and malachite, in quartz veins that are up to 1 m thick (Armstrong, 1968; Eastwood, 1970).

The GM occurrence is 1-1.5 km north-northwest of the Keevil zone. This mineralization was intersected in diamond drill holes cored by Boliden Westmin Ltd. (owner, at that time, of the Gibraltar Mine) in 1998. This drill program was designed to test a large chargeability anomaly that had been outlined by an I.P. geophysical survey conducted in 1997 (Rydman, 1998). Four of five vertical holes intersected significant mineralization, consisting mainly of chalcopyrite, pyrite and molybdenite in quartz veins. An oxide zone, with significant amounts of malachite, azurite, cuprite, tenorite and limonite, was encountered in two of the holes, and three holes intersected chalcocite in a near-surface supergene enrichment zone (Rydman, 1998). An array of recent drill pads attests to subsequent exploration of this occurrence, but results have not been made public.

5.7. Mad (MINFILE 093B 052)

The Mad showing is in the Granite Mountain phase about 1.3 km east-northeast of the GM occurrence. It comprises a few occurrences of copper sulphides, presumably chalcopyrite, that were located during a soil geochemical survey conducted over the Mad claim group by Exeter Mines Ltd. in 1973 (Mark, 1973).

5.8. Bysouth (MINFILE 093B 061)

The Bysouth occurrence is 5.3 km north of the Gibraltar tailings pond, in tonalite that is mapped as an outlier of the Granite Mountain phase. It comprises two separate mineralized zones, one with molybdenite and the other with chalcopyrite. The molybdenum mineralization was encountered in a diamond drill hole cored by Gibraltar Mines Ltd. in 1986 on their Ze claim group. Drill hole 86-65 intersected silicified tonalite which enclosed a 30 m zone of leucotonalite cut by molybdenite-bearing quartz veins (Bysouth, 1987). Copper mineralization consists of pyrite, chalcopyrite, malachite and azurite in a silicified breccia zone that cuts tonalite about 100 m south of drill hole 86-65 (Ash et al., 1999a; Reid, 2005). This area was explored with a diamond drill program conducted by Bell Resources Corporation in 2004, who had optioned the Copper Ace North claims from Copper Ridge Explorations Inc. These drill holes intersected variably altered intrusive units, locally with anomalous concentrations of Mo and Cu, but did not encounter the high-grade breccia zone exposed at surface (Reid, 2005).

5.9. Iron Mountain (MINFILE 093B 004)

The Iron Mountain occurrence comprises a series of iron oxide-rich skarn lenses in the Cuisson Lake unit, 1-2.5 km east-southeast of the south end of Cuisson Lake. They were staked as the Iron Mountain group in 1952, and have seen intermittent exploration by a number of operators, mainly in the 1950s and 1960s (Sutherland Brown, 1958; Philp, 1968). The skarn lenses consist of specular hematite or magnetite, with lesser amounts of epidote, garnet, clinopyroxene, chalcocopyrite and malachite (Sutherland Brown, 1958). Individual lenses range from a few cm to 2 m wide, and occur over a strike length of about 1500 m along the north side of the Cuisson Lake unit (Sutherland Brown, 1958).

5.10. Catalan Copper (MINFILE 093B 068)

The Catalan Copper occurrence, 2 km north of the lake at the head of Big Camp Creek, comprises copper and molybdenum mineralization that was intersected in a diamond drill hole cored by Stikine Gold Corporation in 2007. The hole (CC-07-04) was drilled to test a linear magnetic anomaly on the AP claim group. It intersected foliated andesitic volcanic rocks cut by an intrusive suite that includes feldspar porphyry, diorite and quartz diorite. The mineralization comprises pyrite, chalcocopyrite and minor molybdenite that form disseminations, veinlets and stockworks in the volcanic rocks (Mirko et al., 2007).

The Catalan Copper occurrence is in a covered area east of the Granite Mountain batholith. Rocks intersected in diamond drill hole CC-07-04 are likely Nicola Group cut by an intrusive suite related to the Burgess Creek stock. Diamond drill hole CC-07-01, cored 300 m to the east, intersected rocks that are probably part of the Cache Creek Complex, described by Mirko et al. (2007) as *mélange*, comprising incoherent graphitic argillite with blocks of limestone. These two drill holes are inferred to constrain the location of a north-trending fault contact between Quesnel and Cache Creek terranes.

5.11. Mag and Copper King North

The Mag and Copper King North are minor occurrences of chalcocopyrite in the Nicola Group southeast of the Burgess Creek stock. The Mag occurrence includes mineralization encountered in two diamond drill holes cored by Gibraltar Mines Ltd. in 1985, to test an I.P. anomaly that was spatially associated with exposures of magnetite-epidote-garnet skarn on the Mag claim group (Bysouth, 1985). These holes encountered minor amounts of chalcocopyrite in quartz-carbonate veins and quartz-epidote-chlorite-carbonate-cemented breccia (Bysouth, 1985). This area was explored as part of the Copper King property for United Gunn Resources Ltd. in the late 1990s. Payne (1999a) reports that minor amounts of disseminated pyrite and chalcocopyrite occur in a package of silicified limestones and volcaniclastic rocks, which is apparently a southward extension of the skarn zone.

The Copper King North occurrence, 1.5 km northeast of the Mag occurrence, was identified during exploration of

the Copper King property for United Gunn Resources Ltd. in 1998. The mineralization is described as disseminations and stringers of chalcocopyrite in intensely silicified lapilli tuff (Payne, 1999a). Grab samples contain up to 13967 ppm Cu, but the mineralization was described as spotty, lacking lateral continuity (Payne, 1999a).

6. Discussion

6.1. Terrane affinity of the Granite Mountain batholith

The Granite Mountain batholith is interpreted to be part of Quesnel terrane. This interpretation is based mainly on its association with rocks that are correlated with the Nicola Group (Upper Triassic) the main stratigraphic unit of Quesnel terrane. The Nicola correlation is mainly lithologic (Schiarizza 2014), but is corroborated by Late Triassic conodonts extracted from the succession at one locality and geochronologic data from bounding plutons. The Nicola rocks are intruded by the Burgess Creek stock (Late Triassic), which is in turn intruded by the Granite Mountain phase of the Granite Mountain batholith. The basal unit of the Dragon Mountain succession overlies the Nicola Group north of the Burgess Creek stock, and in the fault block northwest of the Gibraltar tailings pond it apparently overlies the Granite Mountain batholith (Barker and Grubisa, 1994). This relationship provides an additional link between the Granite Mountain batholith and Quesnel terrane, as regional studies suggest that the Dragon Mountain succession represents an intra-Quesnel basin that was derived from, and deposited on, older units of Quesnel terrane (Petersen et al., 2004; Logan and Moynihan, 2009).

Rocks along the southwest margin of the Granite Mountain batholith have commonly been interpreted as Cache Creek rocks altered during batholith emplacement. These rocks are assigned to the Cuisson Lake unit and are suspected, but not proven, to have been intruded by the Border phase of the Granite Mountain batholith. They were derived from a succession of feldspathic volcaniclastic=volcanic rocks intercalated with limestone, and it is suggested herein that they are more readily correlated with the Nicola Group than the Cache Creek Complex. This correlation corroborates assignment of the Granite Mountain batholith to Quesnel terrane.

Hornfelsed Cache Creek rocks form an isolated set of exposures northwest of the lake at the head of Big Camp Creek. These rocks are a little more than 1 km from exposures of the Granite Mountain batholith, and this spatial relationship might be considered evidence for an intrusive relationship. This interpretation is rejected because strong evidence elsewhere shows that the batholith intruded Nicola rocks. The hornfelsed Cache Creek rocks are inferred to be separated from the Granite Mountain batholith by an extension of the northeast-striking fault mapped to the southwest (Fig. 3). The metamorphic overprint may have been caused by hornblende-plagioclase porphyry intrusions identified in the same set of exposures, or the Sheridan Creek stock. It is suspected that these rocks are part of a structural-metamorphic domain, recognized by Ash et al. (1999a, b), that is spatially associated with the Sheridan

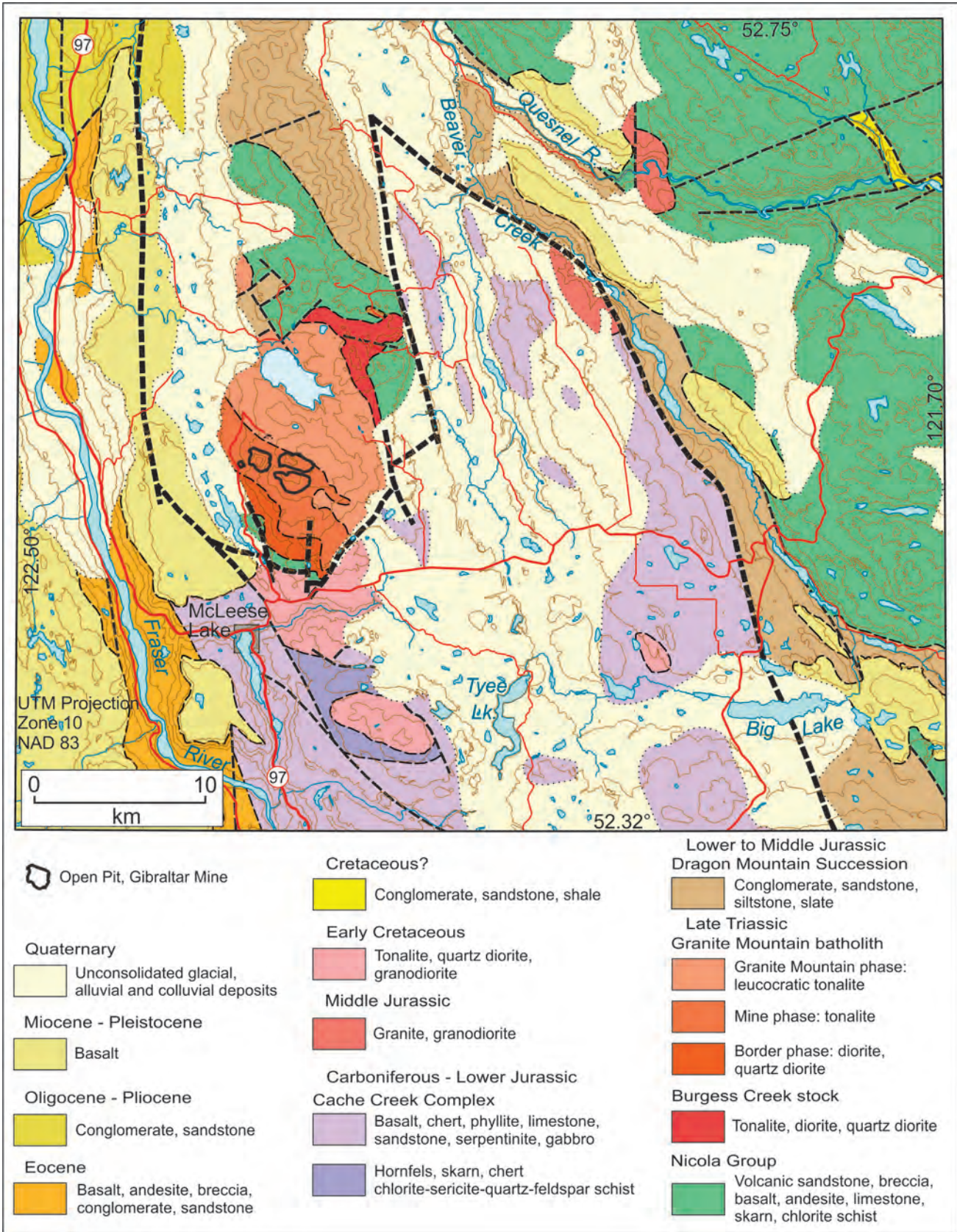


Fig. 22. Geologic map of the Granite Mountain batholith and surrounding area. Based on Tipper (1959, 1978), Ash et al. (1999b), Logan et al. (2010), and this study. Bold dashed line denotes fault segments, projected above Neogene and Quaternary cover, that form the boundary between Quesnel and Cache Creek terranes.

Creek stock and a correlative stock to the south (Fig. 22).

The Granite Mountain batholith is a Late Triassic arc pluton (Oliver et al., 2009). Quesnel is an arc terrane characterized by Upper Triassic arc-derived volcanic and sedimentary rocks, and Late Triassic to Early Jurassic calc-alkalic and alkalic arc plutons. Assigning the Granite Mountain batholith to the Quesnel arc places it in a more appropriate setting than an accretionary complex (Cache Creek). Furthermore, as part of the Quesnel arc system, the Granite Mountain batholith conforms and contributes to a pattern defined by parallel belts of calc-alkalic or alkalic plutons that become progressively younger from west to east (Fig. 21 of Schiarizza, 2014). The Granite Mountain batholith is part of a western belt of Late Triassic calc-alkalic plutons that also includes the Guichon Creek batholith, 250 km to the south-southeast, host to the Highland Valley Cu-Mo porphyry deposits.

6.2. Structural relationship to Cache Creek terrane

The Nicola Group (including the Cuisson Lake unit), Burgess Creek stock, Granite Mountain batholith, and Dragon Mountain succession form a coherent panel of rocks that is part of Quesnel terrane. This panel is bounded to the east by a north-tapering wedge of Cache Creek rocks. This relationship indicates significant local shuffling of the terrane boundary because, regionally, Cache Creek terrane occurs to the west of Quesnel terrane (Fig. 22). Accordingly, the contact between the Quesnel panel and the Cache Creek wedge is inferred to be a significant north-northwest trending fault that records more than 20 km of sinistral strike-slip displacement, as required to restore the southern end of the Quesnel block to the northern termination of the Cache Creek wedge (Fig. 22). This fault is not exposed, and no obvious strike extensions are apparent in adjacent map areas, although Logan (2008) documented local northwest-trending sinistral fault zones in Quesnel terrane along the Cottonwood River, 50 km north-northwest of the Granite Mountain map area.

The southern boundary of the Quesnel panel is, in part, defined by the east-trending fault that marks the contact between the Cuisson Lake unit and the Sheridan Creek stock in the southwestern part of the map area. The Cuisson Lake unit is correlated with the Nicola Group, and the Sheridan Creek stock apparently intrudes the Cache Creek Complex, so this fault forms the boundary between Quesnel and Cache Creek terranes. This fault is truncated by a northeast-trending sinistral fault to the east, and is locally offset by northerly trending faults with dextral and/or west-side-down displacements. The east-west contact is inferred to be a fault because the south-dipping foliation in both units becomes progressively stronger, and is locally mylonitic, as the contact is approached. It is suspected to be a south-dipping thrust or reverse fault because the south-dipping foliation tracks northward into the Granite Mountain batholith, where it locally grades into a C-S mylonite that shows top-to-the-north sense of shear. The fault is mid-Cretaceous or younger because it cuts the Early Cretaceous Sheridan Creek stock. Temperatures were sufficiently high to

generate greenschist facies mineral assemblages in the foliated rocks affected by the deformation.

7. Conclusions

The Late Triassic Granite Mountain batholith, host to the Gibraltar porphyry Cu-Mo deposit, is part of Quesnel terrane. It, and associated rocks of the Nicola Group, Nicola-correlative Cuisson Lake unit, Burgess Creek stock and Dragon Mountain succession, form a panel of Quesnel rocks, 15 km wide, that is partially enveloped by exposures of Cache Creek terrane. The southern boundary of this panel is an inferred east-striking fault that juxtaposes the Cuisson Lake unit against Early Cretaceous tonalite of the Sheridan Creek stock. South-dipping foliations in the Sheridan Creek stock, the Cuisson Lake unit, and the southern part of the Granite Mountain batholith formed at the same time as this fault. The eastern boundary of the Quesnel panel is an unexposed north-northwest striking fault that juxtaposes it against the Cache Creek Complex. This fault cuts rocks as young as the Lower to Middle Jurassic Dragon Mountain succession, but its age, dip and movement history are not well constrained. Map-scale relationships suggest that it is a sinistral fault with at least 20 km of displacement.

Acknowledgments

I thank Mark Ralph and Lori Kennedy for their cheerful assistance during fieldwork; and Mark and Vicki for providing accommodation on McLeese Lake. I also thank Richard Friedman for providing radiometric dates, and Mike Orchard for extracting and identifying conodonts. Chris Ash made important observations in the late 1990s that set the table for this study. Lawrence Aspler provided a thorough review that improved the paper.

References cited

- Armstrong, C.M., 1968. Geological survey of a portion of the GM mineral claim group, Cariboo Mining Division, Granite Mountain area, McLeese Lake, B.C. British Columbia Ministry of Energy and Mines, British Columbia Geological Survey Assessment Report 1596, 32 p.
- Ash, C.H., Rydman, M.O., Payne, C.W., and Panteleyev, A., 1999a. Geological setting of the Gibraltar mine, south-central British Columbia (93B/8, 9). In: Exploration and Mining in British Columbia 1998, British Columbia Ministry of Energy and Mines, pp. A1-A15.
- Ash, C.H., Panteleyev, A., MacLennan, K.L., Payne, C.W., and Rydman, M.O., 1999b. Geology of the Gibraltar mine area, NTS 93B/8, 9. British Columbia Ministry of Energy and Mines, British Columbia Geological Survey Open File 1999-7; scale 1:50 000.
- Ash, C.H., and Riveros, C.P., 2001. Geology of the Gibraltar copper-molybdenite deposit, east-central British Columbia (93B/9). In: Geological Fieldwork 2000, British Columbia Ministry of Energy and Mines, British Columbia Geological Survey Paper 2001-1, pp. 119-133.
- Barker, G.E., and Grubisa, G.G., 1994. Diamond drill report on the Ze claim group, Cariboo Mining Division, 93B/9W. British Columbia Ministry of Energy and Mines, British Columbia Geological Survey Assessment Report 23496, 69 p.
- Bysouth, G.D., 1985. Diamond drill report on the Mag Group, Cariboo Mining Division, 93B/8. British Columbia Ministry of Energy and Mines, British Columbia Geological Survey

- Assessment Report 13784, 24 p.
- Bysouth, G.D., 1987. Diamond drill report on the Ze Group, Cariboo Mining Division, 93B/9. British Columbia Ministry of Energy and Mines, British Columbia Geological Survey Assessment Report 15764, 28 p.
- Bysouth, G.D., 1990. Diamond drill report on the Sawmill zone, Cariboo Mining Division, 93B/8. British Columbia Ministry of Energy and Mines, British Columbia Geological Survey Assessment Report 20514, 55 p.
- Bysouth, G.D., Campbell, K.V., Barker, G.E., and Gagnier, G.K., 1995. Tonalite-trondhjemite fractionation of peraluminous magma and the formation of syntectonic porphyry copper mineralization, Gibraltar mine, central British Columbia. In: Schroeter, T.G. (Ed.), *Porphyry deposits of the northwestern cordillera of North America*, Canadian Institute of Mining, Metallurgy and Petroleum, Special Volume 46, pp. 201-213.
- Cannon, R.W., 1968. Geological report, percussion drilling, Granite Mountain; McLeese Lake. British Columbia Ministry of Energy and Mines, British Columbia Geological Survey Assessment Report 1641, 30 p.
- Cordey, F., and Read, P.B., 1992. Permian and Triassic radiolarian ages from the Cache Creek Complex, Dog Creek and Alkali Lake areas, southwestern British Columbia. In: *Current Research, Part E*, Geological Survey of Canada Paper 92-1E, pp. 41-51.
- Dawson, J.G., 2007. Diamond drilling report on the Copper Ace property, NTS 93B/9, Cariboo Mining Division, British Columbia. British Columbia Ministry of Energy and Mines, British Columbia Geological Survey Assessment Report 29283, 72 p.
- Drummond, A.D., Tennant, S.J., and Young, R.J., 1973. The interrelationship of regional metamorphism, hydrothermal alteration and mineralization at the Gibraltar Mines copper deposit in B.C. *Canadian Institute of Mining and Metallurgy Bulletin*, 66, 48-55.
- Drummond, A.D., Sutherland Brown, A., Young, R.J., and Tennant, S.J., 1976. Gibraltar – regional metamorphism, mineralization, hydrothermal alteration and structural development. In: Sutherland Brown, A. (Ed.), *Porphyry deposits of the Canadian Cordillera*, Canadian Institute of Mining and Metallurgy, Special Volume 15, pp. 195-205.
- Eastwood, G.E.P., 1970. McLeese Lake: Geology of the Granite Mountain stock. In: *Geology, Exploration and Mining in British Columbia 1969*, British Columbia Department of Mines and Petroleum Resources, pp. 162-172.
- Harding, B., 2012. The characterization of molybdenum mineralization at the Gibraltar mines Cu-Mo porphyry, central British Columbia. B.Sc. thesis, Queen's University, 52 p.
- Hodge, J.L., and Dawson, J.G., 2008. 2007 diamond drilling and geophysical report, Copper Ace Cu-Au-Mo property, Cariboo Mining Division, NTS 93B/9, British Columbia. British Columbia Ministry of Energy and Mines, British Columbia Geological Survey Assessment Report 29862, 223 p.
- Logan, J.M., 2008. Geology and mineral occurrences of the Quesnel terrane, Cottonwood map sheet, central British Columbia (NTS 093G/01). In: *Geological Fieldwork 2007*, British Columbia Ministry of Energy, Mines and Petroleum Resources, British Columbia Geological Survey Paper 2008-1, pp. 69-86.
- Logan, J.M., and Moynihan, D.P., 2009. Geology and mineral occurrences of the Quesnel River map area, central British Columbia (NTS 093B/16). In: *Geological Fieldwork 2008*, British Columbia Ministry of Energy, Mines and Petroleum Resources, British Columbia Geological Survey Paper 2009-1, pp. 127-152.
- Logan, J.M., Schiarizza, P., Struik, L.C., Barnett, C., Nelson, J.L., Kowalczyk, P., Ferri, F., Mihalynuk, M.G., Thomas, M.D., Gammon, P., Lett, R., Jackaman, W., and Ferbey, T., 2010. Bedrock geology of the QUEST map area, central British Columbia. British Columbia Ministry of Energy, Mines and Petroleum Resources, British Columbia Geological Survey Geoscience Map 2010-1; scale 1:500 000 (also Geoscience BC, Report 2010-5; Geological Survey of Canada, Open File 6476).
- Mark, D.G., 1973. Geochemical report on a soil sample survey, Mad claim group, McLeese Lake area, Cariboo Mining Division, B.C. British Columbia Ministry of Energy and Mines, British Columbia Geological Survey Assessment Report 4506, 27 p.
- Meyer, W., 1971a. Report on McLeese, Tor and Bob claims – McLeese Lake area, B.C., Cariboo Mining Division. British Columbia Ministry of Energy and Mines, British Columbia Geological Survey Property File Document 014233, 19 p.
- Meyer, W., 1971b. Progress report on McLeese Lake property. British Columbia Ministry of Energy and Mines, British Columbia Geological Survey Property File Document 014234, 12 p.
- Mirko, J.M., Bowen, B., and Middleton, M., 2007. Diamond drilling assessment report on the Catalan Copper property, McLeese Lake area, BC. British Columbia Ministry of Energy and Mines, British Columbia Geological Survey Assessment Report 29294, 31 p.
- Mostaghimi, N., Kennedy, L.A., and Gabites, J., 2014. Geological setting, structural geology and timing of deformation at the Gibraltar Cu-Mo porphyry deposit, Cariboo region, British Columbia. *Geological Society of America, Abstracts with Programs*, 46, 6, 588.
- Nelson, J., Colpron, M., and Israel, S., 2013. The Cordillera of British Columbia, Yukon and Alaska: tectonics and metallogeny. In: Colpron, M., Bissig, T., Rusk, B., and Thompson, J.F.H., (Eds.), *Tectonics, Metallogeny, and Discovery - the North American Cordillera and similar accretionary settings*. Society of Economic Geologists, Special Publication 17, pp. 53-109.
- Oliver, J., Crozier, J., Kamionko, M., and Fleming, J., 2009. The Gibraltar Mine, British Columbia. A billion tonne deep copper-molybdenum porphyry system: structural style, patterns of mineralization and rock alteration. In: *Association for Mineral Exploration British Columbia, 2009 Mineral Exploration Roundup, Program with Abstracts*, pp. 35-36.
- Orchard, M.J., 2006. Report on conodonts and other microfossils, Quesnel Lake (93A); Report No. MJO-2006-1, Geological Survey of Canada, Paleontological report on samples collected by J. Logan, British Columbia Geological Survey.
- Payne, C.W., 1999a. Geophysical and soil geochemical report on the Copper King property, CK2, CK3, CK4, CK8 and CK9 claims, NTS 93B/8, 9, Cariboo Mining Division, British Columbia. British Columbia Ministry of Energy and Mines, British Columbia Geological Survey Assessment Report 25793, 65 p.
- Payne, C.W., 1999b. Geophysical and soil geochemical report on the Copper Ace property, CA1, CA2, CA3, CA4, CA5 and CA6 claims, NTS 93B/9, Cariboo Mining Division, British Columbia. British Columbia Ministry of Energy and Mines, British Columbia Geological Survey Assessment Report 25794, 67 p.
- Petersen, N.T., Smith, P.L., Mortensen, J.K., Creaser, R.A., and Tipper, H.W., 2004. Provenance of Jurassic sedimentary rocks of south-central Quesnellia, British Columbia: implications for paleogeography. *Canadian Journal of Earth Sciences*, 41, 103-125.
- Panteleyev, A., 1978. Granite Mountain project (93B/8). In: *Geological Fieldwork 1977*, British Columbia Ministry of Energy, Mines and Petroleum Resources, British Columbia Geological Survey Paper 1978-1, pp. 39-42.
- Philp, R.H.D., 1968. Geochemical survey report on the Brenda, Mayday, Maybe, Ted and Tell claims of Ensbrook Mines Ltd. (NPL). British Columbia Ministry of Energy and Mines, British Columbia Geological Survey Assessment Report 1873, 11 p.
- Raffle, K.J., 1999. Structure, deformation and element mobility of the Gibraltar Cu-Mo Mine, south-central British Columbia. B.Sc. thesis, The University of British Columbia, 58 p.
- Read, P.B., 1993. Geology of northeast Taseko Lakes map area, southwestern British Columbia. In: *Current Research, Part A*, Geological Survey of Canada Paper 93-1A, pp. 159-166.
- Reid, R.E., 2005. Copper Ace North project, Cariboo Mining

- Division, British Columbia, NTS 093B/9W: 2004 diamond drill program. British Columbia Ministry of Energy and Mines, British Columbia Geological Survey Assessment Report 27759, 123 p.
- Rydman, M., 1998. Diamond drill report on the GM mineral claim group, Cariboo Mining Division, 93B/9E, 9W. British Columbia Ministry of Energy and Mines, British Columbia Geological Survey Assessment Report 25542, 104 p.
- Schiarizza, P., 2014. Geological setting of the Granite Mountain batholith, host to the Gibraltar Cu-Mo porphyry deposit, south-central British Columbia. In: Geological Fieldwork 2013, British Columbia Ministry of Energy and Mines, British Columbia Geological Survey Paper 2014-1, pp. 95-110.
- Schiarizza, P., Israel, S., Heffernan, S., Boulton, A., Bligh, J., Bell, K., Bayliss, S., Macauley, J., Bluemel, B., Zuber, J., Friedman, R.M., Orchard, M.J., and Poulton, T.P., 2013. Bedrock geology between Thuya and Woodjam creeks, south-central British Columbia, NTS 92P/7, 8, 9, 10, 14, 15, 16; 93A/2, 3, 6. British Columbia Ministry of Energy, Mines and Natural Gas, British Columbia Geological Survey Open File 2013-05; 4 sheets, scale 1:100 000.
- Simpson, R.Y., 1970. Geology of the Gibraltar – Pollyanna copper deposit. B.Sc. thesis, The University of British Columbia, 43 p.
- Struik, L.C., 1993. Intersecting intracontinental Tertiary transform fault systems in the North American Cordillera. *Canadian Journal of Earth Sciences*, 30, 1262-1274.
- Struik, L.C., Schiarizza, P., Orchard, M.J., Cordey, F., Sano, H., MacIntyre, D.G., Lapierre, H., and Tardy, M., 2001. Imbricate architecture of the upper Paleozoic to Jurassic oceanic Cache Creek Terrane, central British Columbia. *Canadian Journal of Earth Sciences*, 38, 495-514.
- Sutherland Brown, A., 1958. Williams Lake: McLeese - Cuisson lakes area. In: Annual Report of the Minister of Mines for 1957, British Columbia Department of Mines, pp. 14-18.
- Sutherland Brown, A., 1967. Geology of the Granite Mountain – Cuisson Lake area. In: Annual Report of the Minister of Mines and Petroleum Resources for 1966, British Columbia Ministry of Mines and Petroleum Resources, pp. 121-124.
- Sutherland Brown, A., 1974. Gibraltar Mine (93B-12, 13). In: Geology, Exploration and Mining in British Columbia 1973, British Columbia Ministry of Energy, Mines and Petroleum Resources, pp. 299-318.
- Tipper, H.W., 1959. Quesnel, British Columbia. Geological Survey of Canada, Map 12-1959; scale 1:253 440.
- Tipper, H.W., 1978. Northeastern part of Quesnel (93B) map-area, British Columbia. In: Current Research, Part A, Geological Survey of Canada, Paper 78-1A, pp. 67-68.
- van Straaten, B.I., Oliver, J., Crozier, J., and Goodhue, L., 2013. A summary of the Gibraltar porphyry copper-molybdenum deposit, south-central British Columbia, Canada. In: Logan, J. and Schroeter, T. G. (Eds.), Porphyry systems of central and southern BC: Prince George to Princeton, Society of Economic Geologists Field Trip Guidebook 43, pp. 55-66.

Stratigraphic and tectonic framework of the Khyber-Sericite-Pins mineralized trend, lower Iskut River, northwest British Columbia

Jeff Kyba^{1, a} and JoAnne Nelson²

¹ Ministry of Energy and Mines, Smithers, BC, V0J 2N0

² British Columbia Geological Survey, Ministry of Energy and Mines, Victoria, BC, V8W 9N3

^a corresponding author: Jeff.Kyba@gov.bc.ca

Recommended citation: Kyba, J. and Nelson, J.L., 2015. Stratigraphic and tectonic framework of the Khyber-Sericite-Pins mineralized trend, lower Iskut River, northwest British Columbia. In: Geological Fieldwork 2014, British Columbia Ministry of Energy and Mines, British Columbia Geological Survey Paper 2015-1, pp. 41-58.

Abstract

The Khyber-Sericite-Pins trend is part of the ‘Bronson corridor’, a belt of mineralization in northwest Stikinia that extends southeast from the past-producing Snip and Johnny Mountain gold mines. Within the mineralized belt, a series of Early Jurassic (195-190 Ma) plutons, stocks and dikes of the Lehto plutonic suite cut stratified Stuhini Group and Hazelton Group rocks. Large quartz-sericite-pyrite (QSP) alteration zones and precious-metal veins and stockworks are spatially associated with the intrusive suite. The corridor is bounded to the southwest by the Sky fault system, a 20 kilometre-long set of normal faults and reactivated post-mineral reverse faults. Notable among the latter is the Khyber reverse fault, which forms the immediate hanging wall to intense QSP alteration and mineralization at the Khyber-Inel prospects. Previous workers distinguished between the Stuhini and Hazelton groups on chronostratigraphic grounds, placing the contact at the Triassic-Jurassic boundary (201 Ma). In contrast, we use lithostratigraphic criteria, and place the base of the Hazelton Group at an angular unconformity cut into Stuhini Group volcanoclastic rocks that is overlain by a distinctive Upper Norian conglomerate-bearing siliciclastic unit, herein referred to as the Snippaker unit. The Snippaker unit consists of polymictic conglomerate, arkose, and siltstone. It is compositionally mature relative to Stuhini Group strata beneath the unconformity. Coeval with Late Triassic porphyry deposits of Stikinia such as Red Chris, the unit records the termination of Stuhini arc volcanoclastic sedimentation and erosional unroofing of the Stuhini Group. Very coarse, immature lower Hazelton Group conglomerates near the Sky fault zone south of Mt. Johnny indicate steep local slopes and clast contributions from a variety of nearby sources. Previously brecciated hypabyssal intrusive clasts in one of the deposits suggest deposition proximal to a pencontemporaneous fault. The structural and stratigraphic setting of the Khyber-Sericite -Pins trend closely resembles that of the Kerr-Sulphurets-Mitchell-Brucejack porphyry-epithermal camp. The Sky fault system appears to have played a similar role to that of the Sulphurets thrust and its precursor basin-bounding faults, in localizing Early Jurassic intrusion and mineralization. The Khyber reverse fault, with its highly QSP-altered footwall, is a close analogue to the Sulphurets thrust fault. In both cases, Cretaceous thrust reactivation was facilitated by mechanically weak, highly altered, clay-sericite-rich rocks.

Keywords: Bronson corridor, KSP trend, Iskut River area, Stikinia, Cu-Au porphyries, Snippaker unit, Hazelton Group, Early Jurassic

1. Introduction

The Khyber-Sericite-Pins mineralized trend of northwest Stikinia is on the south side of the Iskut River, southeast of the past-producing Snip and Johnny Mountain gold mines (Figs. 1, 2). It is part of the northwest-trending ‘Bronson corridor’ (Metcalf and Moors, 1992), in which an unusual concentration of intrusion-related mineral occurrences and broad alteration zones are spatially associated with a belt of plutons, stocks, and dikes of the Lehto suite (Fig. 3; Early Jurassic, ca 195-190 Ma, U-Pb zircon, Lewis et al., 2001). Investigations by Nelson and Kyba (2014) in the KSM-Brucejack camp, about 40 km to the east (Fig. 2), documented details of the Hazelton Group and allied intrusive host rocks. We focused on basal units in the Hazelton Group and the sub-Hazelton unconformity, and recognized reactivated basin structures, particularly the Sulphurets fault. Herein we continue our analysis of the lower Hazelton Group and structural controls on mineralization, emphasizing the unconformity between the Stuhini Group (Upper Triassic) and the Hazelton Group (Upper Triassic to Lower Jurassic) and a system of faults on the southwest flank

of the Bronson corridor.

2. Mineralization in the Bronson corridor

Of the 58 known MINFILE occurrences in the Bronson corridor, most are precious metal-rich polymetallic and intrusion-related veins and skarns. Combined past gold production from Snip and Johnny Mountain totalled over one million (1,106,163) ounces from 712,990 tonnes between 1989 and 1999. The best-known porphyry prospect in the area is the Red Bluff stock, which has been genetically linked to the Snip vein (Fig. 3; Rhys, 1995). The concentration of intrusion-related mineralization linked to Early Jurassic plutons, which are coeval with, and texturally and compositionally similar to, intrusions at the Stewart camp (Mitchell porphyry suite at Kerr-Sulphurets-Mitchell or KSM, and ‘Premier Porphyry’), suggests that undiscovered porphyry deposits may exist in the Bronson corridor. Other indications include broad, intense quartz-sericite-pyrite alteration zones (Alldrick et al., 1990; Fig. 3) and regionally elevated gold and copper values in stream sediments (British Columbia Geological Survey Regional

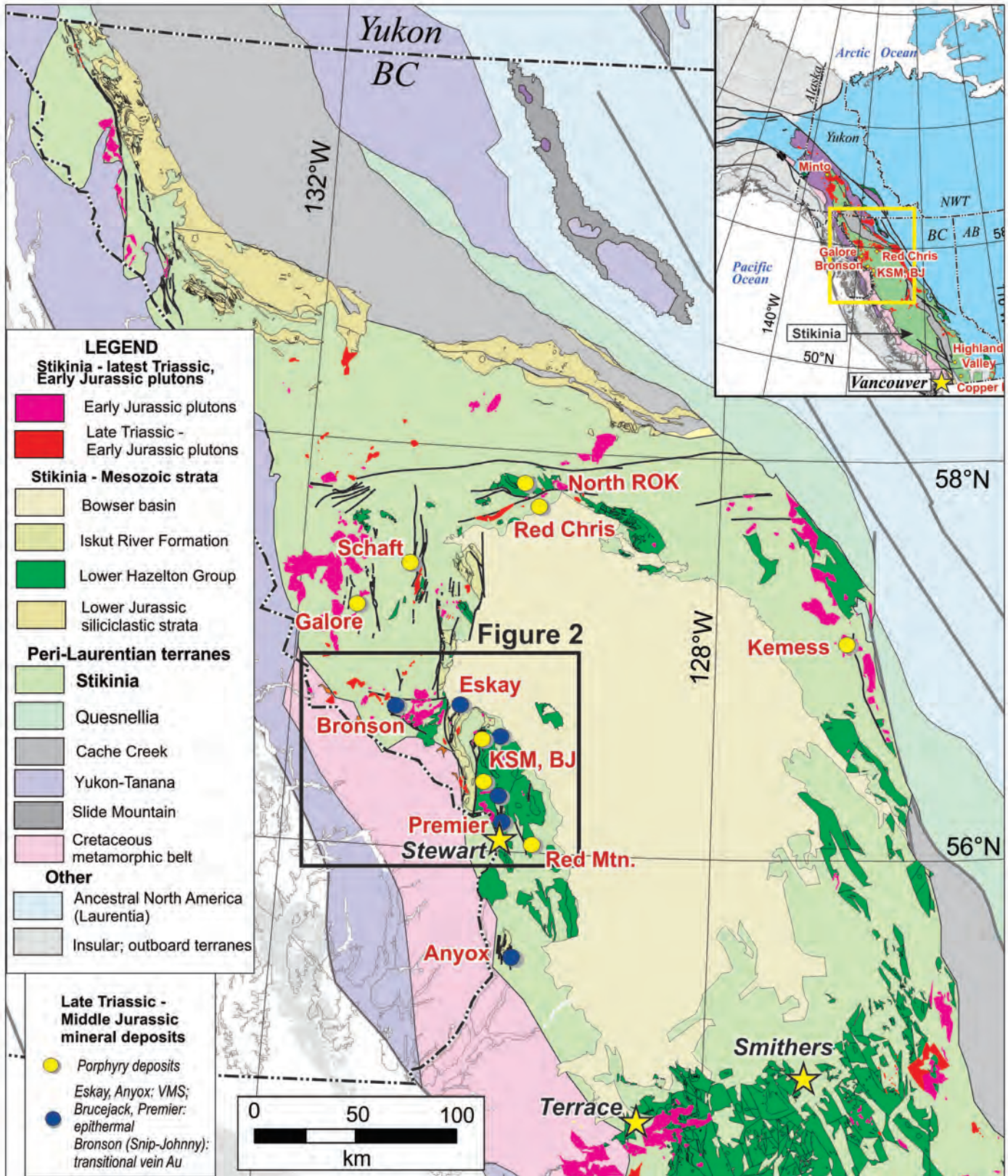


Fig. 1. Triassic and Jurassic geology and major mineral occurrences of northern Stikinia.

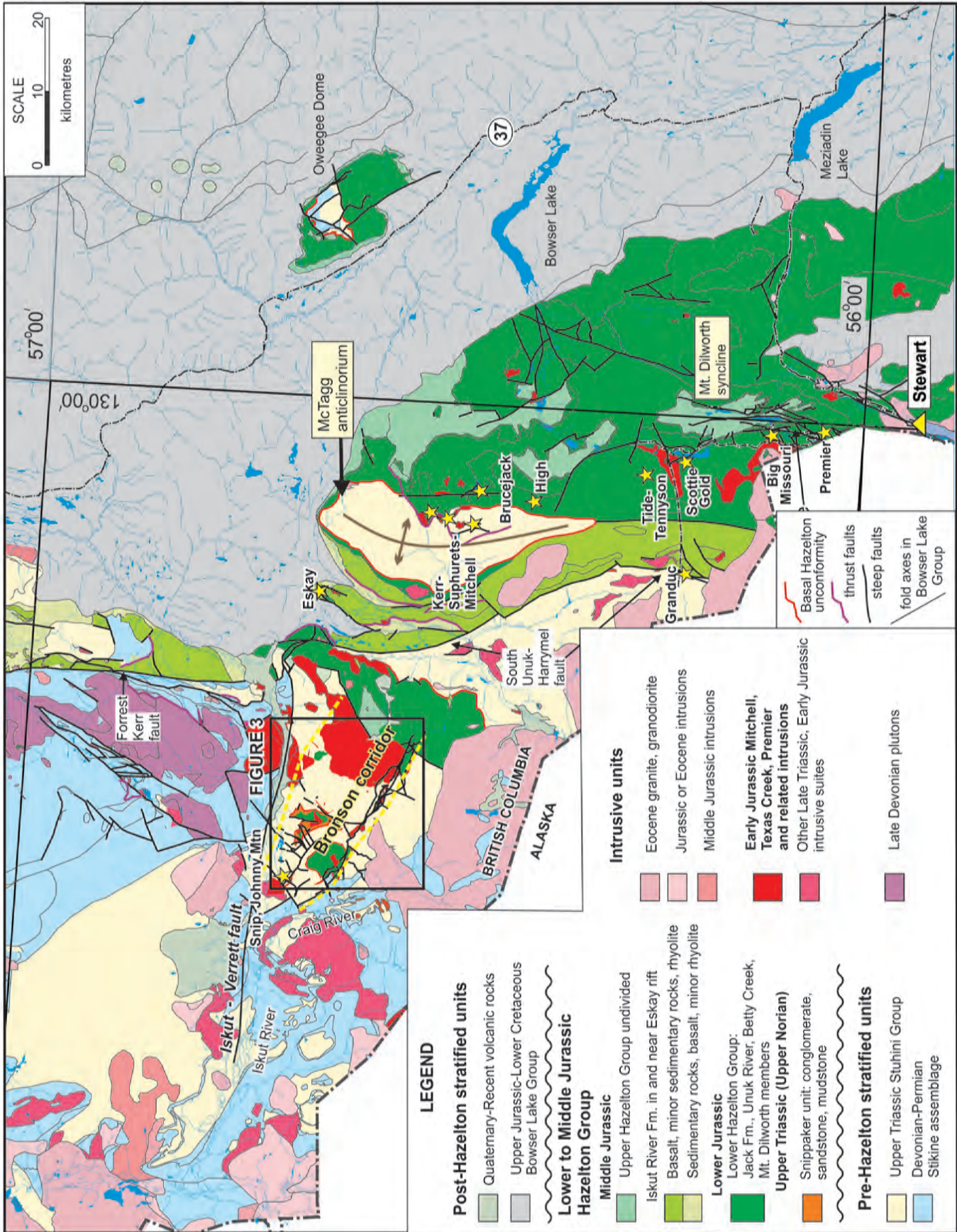


Fig. 2. Geology of lower Iskut River area and Bronson corridor, western Stikinia.

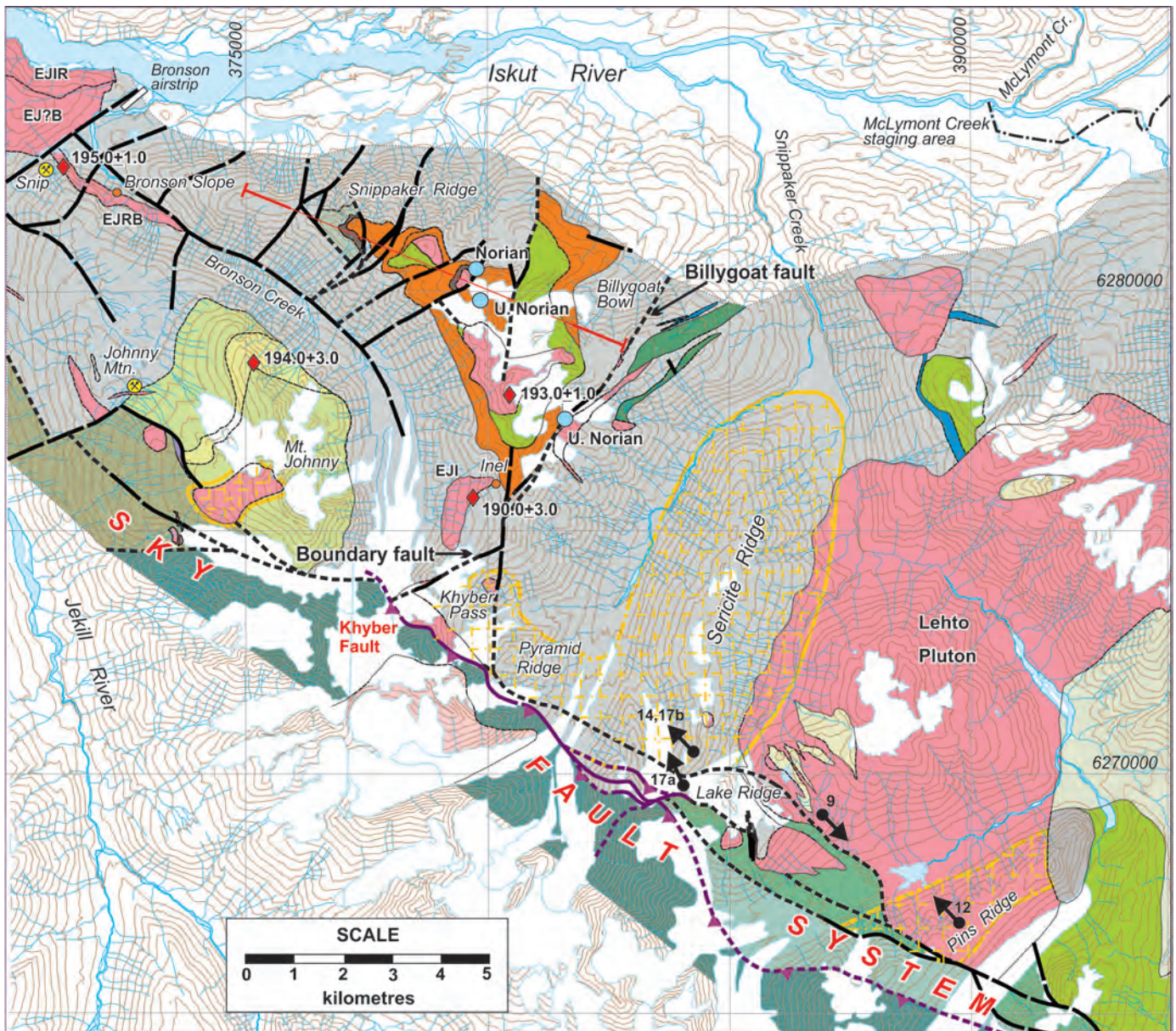


Fig. 3. Geology of the Bronson corridor and Khyber-Sericite Ridge-Pins trend. Mapping by J. Kyba and J.L. Nelson, 2014; other contacts compiled from Lewis (2013), with some subdivisions of Stuhini Group omitted for clarity. UTM Zone 9N, NAD 83.

Geochemical Survey). In 2014, Colorado Resources conducted district-scale exploration including geologic, geochemical, and geophysical surveys followed by drilling that tested for porphyry copper-gold and related precious metal prospects. Convenient helicopter access to the area is now possible from a staging area at the newly commissioned Alta Gas McLymont power project, 17 km east of the Bronson airstrip (Fig. 3).

3. Stratigraphy of the Stuhini and Hazelton groups; Lehto plutonic suite

The study area is underlain mainly by stratified rocks of the Stuhini Group (Upper Triassic) and Hazelton Group (Upper Triassic to Lower Jurassic) and by Early Jurassic plutons and smaller bodies that are considered comagmatic with

Hazelton Group volcanic units. Epiclastic and volcanoclastic rocks of the Stuhini Group are unconformably overlain by siliciclastic, volcanic, and volcanoclastic rocks of the Hazelton Group (Fig. 4). In contrast to previous studies (Alldrick et al., 1990; Metcalfe and Moors, 1993; Lewis 2013), we assign a siliciclastic unit immediately above the unconformity, which contains Norian and Upper Norian fossils (Nadaraju and Smith 1992; Nadaraju and Lewis, 2001), to the Hazelton Group, introducing the informal name ‘Snippaker unit’. The Snippaker unit is overlain by the ‘volcanoclastic unit’, which locally cuts through the Snippaker section to lie directly on Stuhini Group rocks. Lewis et al. (2001) reported a U-Pb zircon age of ca. 193 Ma for this volcanoclastic unit.

Stuhini and Hazelton strata along the Bronson corridor are

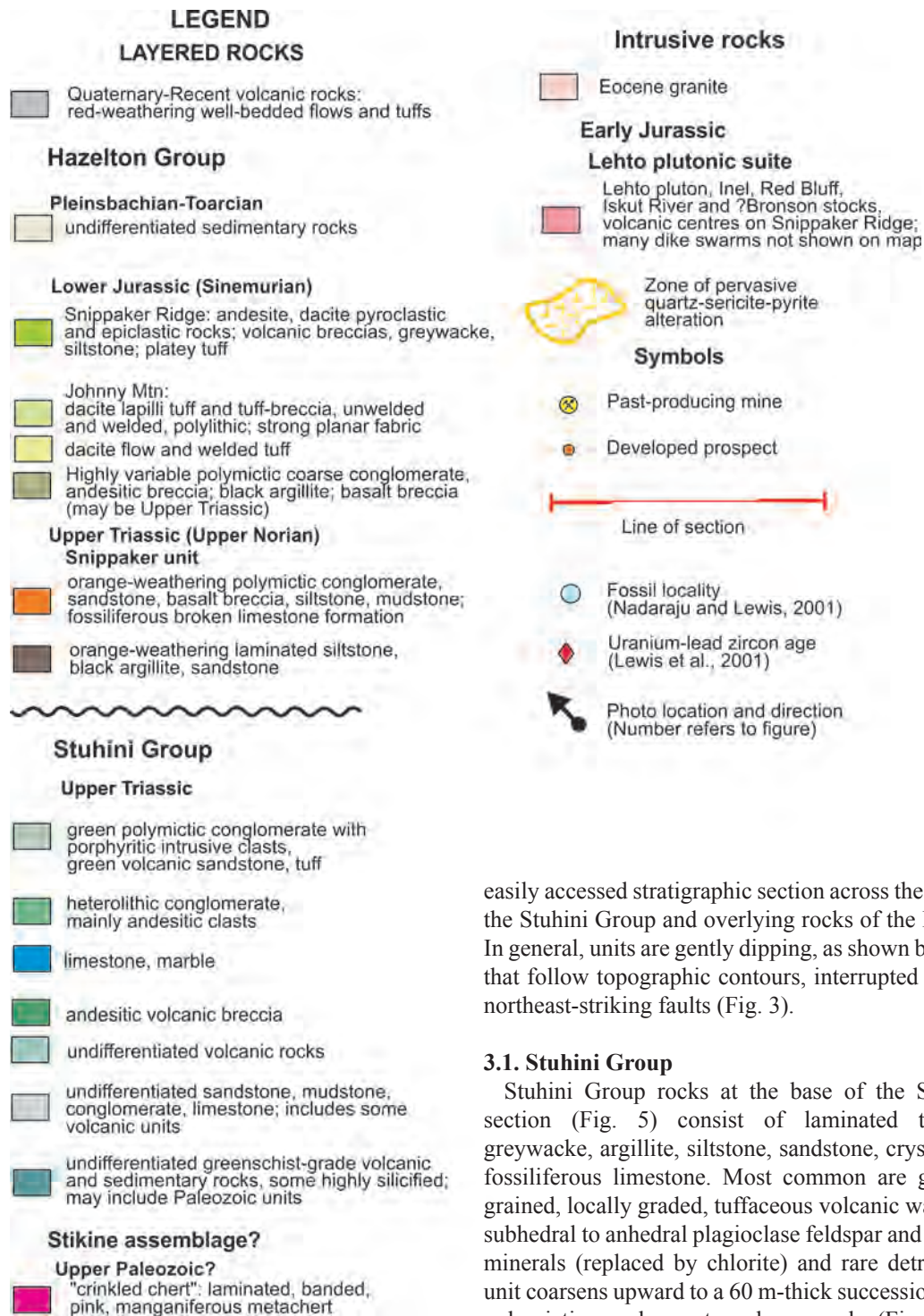


Fig. 3. Continued.

cut by diorite, quartz diorite, and monzodiorite plutons, plugs and dikes of the Lehto suite (Fig. 3; Early Jurassic, ca 190-195 Ma, U-Pb zircon, Lewis et al., 2001). It includes the main Lehto pluton, a northeast-trending body 5 kilometres wide and 10 kilometres long, and the Inel, Red Bluff, and Iskut River stocks.

Snippaker Ridge (Fig. 4a) provides the best exposed and most

easily accessed stratigraphic section across the contact between the Stuhini Group and overlying rocks of the Hazelton Group. In general, units are gently dipping, as shown by major contacts that follow topographic contours, interrupted by minor, steep, northeast-striking faults (Fig. 3).

3.1. Stuhini Group

Stuhini Group rocks at the base of the Snippaker Ridge section (Fig. 5) consist of laminated to thick-bedded greywacke, argillite, siltstone, sandstone, crystal tuff, and rare fossiliferous limestone. Most common are grey-green, fine-grained, locally graded, tuffaceous volcanic wackes containing subhedral to anhedral plagioclase feldspar and up to 10% mafic minerals (replaced by chlorite) and rare detrital quartz. This unit coarsens upward to a 60 m-thick succession of interbedded polymictic conglomerate and greywacke (Fig. 5a). Rounded to subangular clasts, up to several decimetres in long dimension and supported by a siltstone-sandstone matrix, include microdiorite, plagioclase-phyric felsic intrusive rocks, fine-grained mafic volcanic rocks, carbonate rocks, quartz-sericite-pyrite (QSP) altered fragments, vein quartz, and minor chert. Conglomerate beds are locally graded and up to 5 meters thick.

At the Khyber Pass prospect (Fig. 3), coarse-grained rocks in the upper part of the Stuhini Group include a 125-150 m thick unit of framework-intact monomictic conglomerate, which

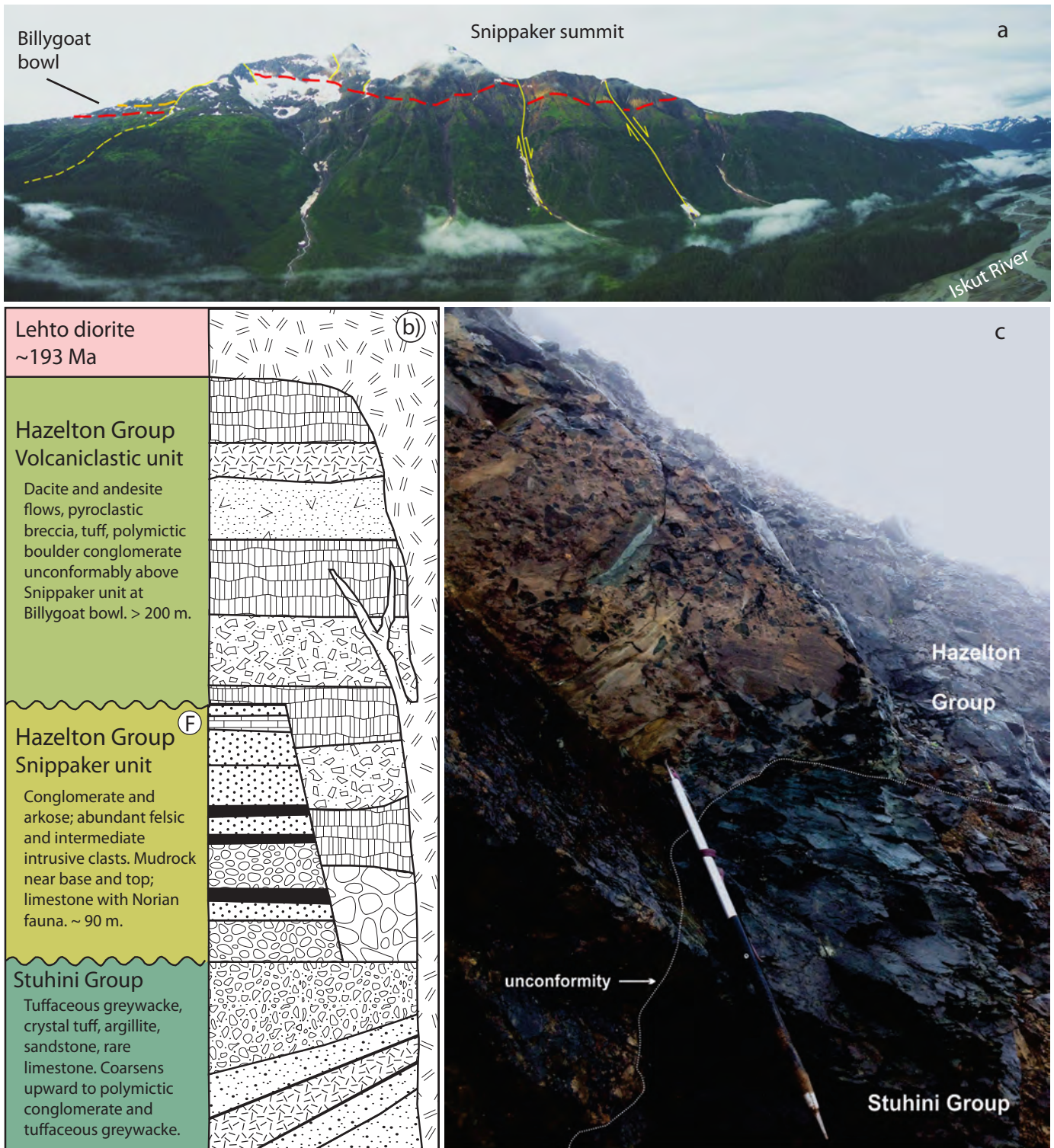


Fig. 4. Snippaker Ridge stratigraphy. **a)** Snippaker Ridge looking toward southwest. Elevation difference from valley floor to summit is ca. 2000 m. Dashed red line marks unconformity between Stuhini Group and overlying Hazelton Group. **b)** Schematic section. **c)** Angular unconformity between Stuhini Group mafic tuff and overlying matrix-supported conglomerate of the Hazelton Group, Billygoat bowl. Angular fragments of the immediately subjacent, weakly foliated, dark green Stuhini mafic tuff are incorporated in the conglomerate together with greywacke and laminated volcanic mudstone clasts from elsewhere in the Stuhini Group. 381979 E, 6278421 N.



Fig. 5. Stuhini Group. **a)** Uppermost Stuhini polymictic pebbly granulestone, western Snippaker Ridge. Most pale-coloured clasts are of high-level intrusive origin. Dark clasts are basalt. 376110 E, 6281460 N. **b)** Tuffaceous greywacke. Scale in cm.

contains well-rounded pyroxene-bearing clasts, that transitions to a unit of conglomerate in which diverse clast types float in a volcanic wacke matrix. The base of this epiclastic succession is an important local exploration guide, because gold-silver and zinc mineralization tends to focus along it (Jim Oliver personal communication, 2014).

3.2. Hazelton Group

3.2.1. Snippaker unit (new informal name)

In previous studies, siliciclastic rocks of Upper Norian age at high elevations on Snippaker Ridge were assigned to the Stuhini Group, based on the concept that the Stuhini-Hazelton contact should be placed at the Triassic-Jurassic (ca. 201 Ma; International Commission on Stratigraphy, 2014) boundary (Tipper and Richards, 1976). A revision is suggested here, because these strata lie unconformably above the Stuhini Group

and display a different sedimentary style. We consider them to be the lowest unit of the Hazelton Group, and introduce the name ‘Snippaker unit’ to differentiate them from volcaniclastic rocks higher in the Hazelton section. The base of the Snippaker unit is a mildly angular unconformable surface that forms a slight bench in the cliffs on the north side of the ridge and corresponds to a distinct colour change, from dull-toned Stuhini Group rocks to bright orange rocks of the Snippaker unit (Fig. 4a). Bedding in the underlying Stuhini Group is truncated along the unconformity,

The Snippaker unit is a siliclastic succession, approximately 90 m thick, that includes conglomerate, arkose, siltstone, laminated argillite and locally, limestone with Upper Norian fauna (Fig. 4b). Iron carbonate cement weathers orange, in strong contrast to the grey-green of the underlying volcanosedimentary Stuhini Group. The thickest and most distinctive beds of the unit are polymictic conglomerates containing decimetre- to metre-scale arkosic sandstone lenses and beds. (Fig. 6). The conglomerates contain well-rounded clasts (30-80%) in an arkosic matrix. Clast types include felsic and intermediate plagioclase-phyric intrusive rocks, aphanitic quartz, grey and dark grey chert, weak to moderate QSP-replaced tonalite, argillite, fossiliferous limestone, and rare woody debris. A fossiliferous limestone olistolith containing Upper Norian corals, brachiopods, gastropods, sponges, and ammonites occurs within the conglomerate. Mudstone-siltstone intervals with minor interbedded iron carbonate-cemented sandstone and conglomerate occur near the base and top of the Snippaker unit. Minor crystal ash tuff and at least one basalt breccia also occur within this unit; they share the typical orange-weathering iron carbonate cement.

3.2.2. Lower Jurassic volcaniclastic unit

The sub-volcaniclastic unit (ca. 193 Ma, Lewis et al., 2001) unconformity bevels into the Snippaker unit (Fig. 3), although locally the contact is paraconformable. At Billygoat bowl six kilometers southeast of Snippaker Ridge (Fig. 3), the basal conglomerate of the volcaniclastic unit lies in direct contact with Stuhini group rocks, above an angular unconformity (Fig. 4c). At the Inel prospect (Fig. 3), mafic crystal tuffs and fragmental rocks overlie Stuhini Group rocks along an unconformity that is locally marked by a zone of ankerite-rich alteration (Jim Oliver, personal communication, 2014).

At Snippaker Peak, the volcaniclastic unit consists of dacite and andesite flows and related pyroclastic breccias. Two kilometers east of Snippaker Peak, it comprises polymictic boulder, cobble and pebble conglomerate, interbedded polyolithic tuff breccias, and greywacke. Conglomerate units contain 70% rounded to angular clasts including fine-grained mafic and intermediate volcanic rocks and intermediate to felsic crowded plagioclase-phyric intrusive rocks in a litharenite matrix (Figs. 7, 8). Above the basal conglomerate at Billygoat bowl, the sequence consists mainly of pale maroon ash-lapilli tuffs with sparse clasts of intermediate intrusive rocks, aphanitic quartz, and fine-grained mafic volcanic rocks.



Fig. 6. Hazelton Group, Snippaker unit. **a)** Polymictic framework-intact conglomerate. Light clasts are felsic to intermediate high-level intrusive and silicified rocks; dark clasts are chert. Weathered-out clasts are limestone. 377358 E, 6281369 N. **b)** Polymictic pebbly conglomerate layer, with local ankeritic cement, cut into underlying sandstones.

3.2.3. Lehto plutonic suite on Snippaker Ridge

Most of the peaks on Snippaker Ridge are underlain by small elliptical hypabyssal intrusive bodies, with long axes less than 0.5 km, of coherent diorite, quartz diorite and monzodiorite (Fig. 3). The bodies are generally porphyritic, and contain plagioclase, hornblende and lesser potassium feldspar phenocrysts. Intrusive phases intermingle with surrounding volcaniclastic units: contacts are locally defined by transition zones in which coherent, crowded plagioclase-phyric intrusions pass into mixed zones where they are cut by, and grade into, intrusive breccias, and then into polymictic, crudely bedded breccias that appear to be volcaniclastic. Dikes up to 3 m wide intrude the surrounding Hazelton volcanic units. Due to their shapes and contact relationships, the elliptical bodies are interpreted to be the remains of volcanic pipes that fed the volcaniclastic unit on Snippaker Ridge. They are part of the Lehto suite, and represent the highest subvolcanic level of intrusion.



Fig. 7. Hazelton Group volcaniclastic unit polymictic pebble-cobble conglomerate, Billygoat bowl. The pinkish felsic intrusive clasts are texturally similar to the small plugs on top of Snippaker Ridge, which are interpreted as feeders to the volcaniclastic sequence. 381430 E, 6280469 N.



Fig. 8. Hazelton Group volcaniclastic unit at Billygoat bowl. Interbedded polymictic conglomerate and pebbly sandstone with local carbonate cement.

3.2.4. Hazelton Group stratigraphy and synvolcanic intrusion on Mt. Johnny

3.2.4.1. Basal conglomerate south of Mt. Johnny

A remarkable section of coarse conglomeratic rocks is exposed in extensive, recently deglaciated outcrops in the valley below the south side of Mt. Johnny (Fig. 3). The unit has an observed thickness of over 200 m near the toe of the glacier, and probably extends many hundreds of metres on Mt. Johnny above and below treeline to the west. It consists mainly of sharp-based boulder-cobble conglomerate and breccia in beds 5-25 m thick. Sorting is poor, and angular to subangular clasts float in a matrix of sand, mud and locally, minor carbonate. Some beds show crude grading. The unit also includes rare thin lenses of framework-intact pebble-cobble conglomerates containing rounded clasts (Fig. 9a), and sandstones with local



Fig. 9. Hazelton conglomeratic unit south of Mt. Johnny. **a)** Polymictic conglomerate containing andesite, hypabyssal intrusive, chert and minor limestone clasts. **b)** Coral-head clast in monomictic breccia of fossiliferous limestone. 373839 E, 6275103 N.

cross stratification.

Nested coarse conglomeratic lenses contain markedly different clast populations. Clast types include felsic to intermediate hypabyssal intrusive rocks, andesite, basalt, limestone, coral, vein quartz, chert, intraformational sandstone and siltstone, QSP-altered rocks, and brecciated intrusive rock. Most beds contain a diverse clast suite, but some consist mostly of one clast type. A striking example is a conglomerate containing wispy-shaped coral fragments that are supported in a micritic matrix (Fig. 9b); clast shapes imply fragmentation before complete induration. This bed lies between layers of polymictic, matrix-supported boulder conglomerate containing andesite and hypabyssal intrusive clasts and a single green (Paleozoic?) chert block three metres across.

Thirty metres downsection from the coral clast-bearing conglomerate is a nearly monomictic, matrix-supported boulder conglomerate that contains clasts up to 3 m in diameter that were derived from a brecciated plagioclase-phyric diorite. Internal breccia textures vary from clasts with a jig-saw-fit, to clasts that

are slightly rotated, to clasts that are isolated; hairline fractures and breccia fragments are cemented by grey cryptocrystalline silica with clay and silt impurities (Fig. 10). White quartz veins cut across the both fragments and cement in one breccia clast (Fig. 10b) indicating that the breccia from which the clast was derived was indurated sufficiently to maintain fractures. However, some clasts display jagged reentrants (Fig. 10a), and some of the larger clasts are surrounded by swarms of small fragments in zones that transition from intact breccia to a clast-dense periphery to trains of centimeter-scale angular fragments, suggesting that induration was inadequate in some of the source breccia to prevent clasts from dismembering during transport. We interpret that the clasts were derived from variably cemented fault breccias that originated due to movement along a shallow-level brittle fault. Angular, metre-scale, matrix-supported clasts consisting almost entirely of probable fault breccia imply that the unit records near-source mass flow sedimentation, likely from collapse of a syndepositional fault scarp.

A bifurcating polymictic clastic dike, 10 cm to >1 m wide, with subrounded clasts floating in a mudstone matrix, cuts sharply through a ca.15 m thick layer of clast-poor, matrix-supported andesite block breccia (Fig. 11). Its clast population differs from the surrounding unit in that it contains both volcanic and laminated sandstone-siltstone intraclasts. The excess pore pressures that lead to fluidization of unconsolidated sediment and injection of conglomeratic dikes are most commonly generated by seismic events (e.g., Jolly and Lonergan, 2002) consistent with the idea of syndepositional faulting.

In summary, the Mount Johnny conglomerates record repeated mass flows that were derived from diverse sources, including high-level intrusive bodies, carbonate bodies, chert, volcanic rocks and, significantly, fault breccia. The thickness of the conglomeratic section (200 m minimum), the thickness of individual depositional units (5-25 m), and extremely large (up to 3 m) angular clasts point to near-source sedimentation and significant relief. This relief was likely generated and maintained by syndepositional faulting, such as is evident in the beds containing clasts of fault-brecciated diorite. It remains unclear if the Mount Johnny conglomerates are equivalent to the Snippaker unit or to the basal conglomerates at the Billygoat bowl section. We collected samples for detrital zircon geochronology to determine the maximum age of deposition.

3.2.4.2. Lower Jurassic Hazelton volcanic sequence and pluton, upper Mt. Johnny

The upper slopes of Mt. Johnny are underlain by a felsic volcanoclastic sequence of lapilli tuffs and tuff breccias, with one thick bed of coherent rhyolite or dacite that has yielded a ca. 194 Ma U-Pb zircon age (Fig. 3; Lewis et al., 2001). The tuffs contain a range of felsic clast types, including angular white coherent dacite and green lithic fragments, flattened lapilli, and crowded feldspar-phyric hypabyssal intrusive and propylitically altered rocks, in a fine crystal-ash matrix. On the upper southern slope of Mt. Johnny the felsic volcanoclastic section is cut by a strongly altered microtonalite body 1 by 2 kilometres across

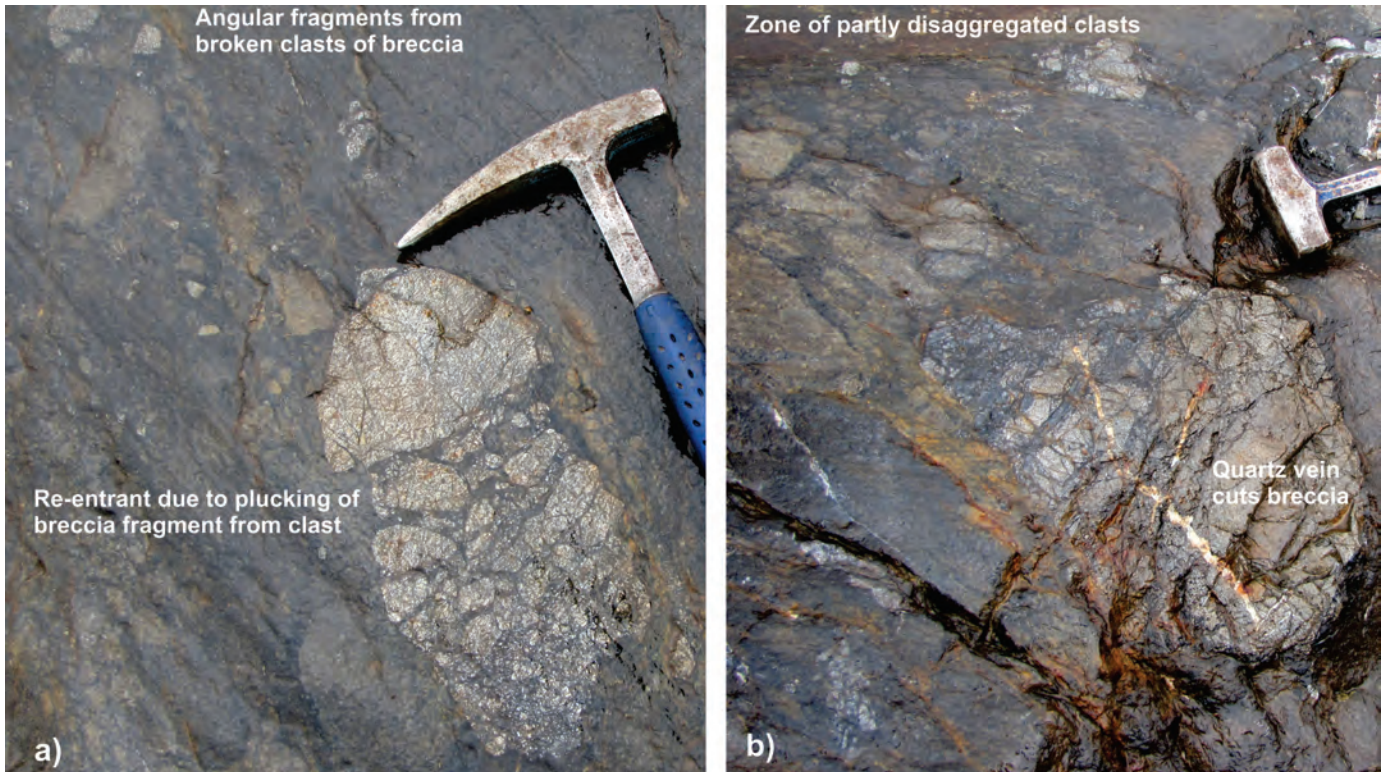


Fig. 10. a) Clast of cataclastically brecciated porphyritic diorite, healed with dark silica. **b)** Clast of brecciated porphyritic diorite, with post-brecciation but pre-sedimentation quartz veins. Note irregular shape of clast; stronger unbrecciated diorite resists mechanical breakage. Top centre shows incipient breakage of breccia clasts. 373844 E, 6275046 N.



Fig. 11. Margin of polymictic pebble dike in foreground cutting brown-weathering conglomerate. Note sandstone-siltstone intraclast. 373801 E, 6275016 N.

that has not been recognized in previous mapping (Fig. 3). Moderate to strong QSP alteration is pervasive. Hydrothermal and intrusive breccias in and around the body host broad areas of silicification and quartz stockwork veins that contain rare fine-grained visible gold and a show weak, patchy malachite stains on fractures. This body may have been an intrusive feeder to the surrounding felsic volcanoclastic edifice, given

the presence of hypabyssal and altered clasts in some of the units. It may be coeval with a ca. 192 Ma plagioclase-phyric dike near the Johnny Mtn. mine portal, which is interpreted as a subvolcanic equivalent to the volcanoclastics and flows (Lewis et al., 2001).

South of Mt. Johnny, the volcanoclastic sequence is underlain by coarse conglomerates. Although contact relationships are obscured by deformation and thick vegetation cover, interlayering of rocks with diagnostic volcanoclastic textures and conglomerates indicate a transitional, albeit faulted, boundary. North and west of the Johnny Mtn. mine, the conglomeratic unit is missing and the felsic volcanoclastic unit directly overlies thinly-bedded mudstone and greywacke of the Stuhini Group.

4. The Sky fault system

Our structural study focused on the southwestern margin of intense quartz-sericite-pyrite alteration, intrusion, and mineralization along the Bronson corridor (Fig. 2, Alldrick et al., 1990). We refer to this margin as the Sky fault system, following informal usage for strands near Mt. Johnny (Fig. 3; Rhys, 1995). The system includes significant normal and reverse structures. Near its southeastern extent, on Pins Ridge (Fig. 3), most strands show normal-sense motion except for one short reverse section (Fig. 12). To the northwest, between Sericite Ridge and Khyber Pass, reverse strands become more important.



Fig. 12. View of the Sky fault system cutting Stuhini Group rocks on Pins Ridge, looking southeast from Lake Ridge (see Fig. 3 for location). Steeply northeast-dipping normal-sense shear zones (yellow) on higher part of the ridge separate panels with low-angle normal shear zones. A single thrust fault (red) forms the hanging wall of strong quartz-sericite-pyrite alteration in ‘Pins bowl’.

4.1. Pins Ridge

The Pins Ridge segment of the Sky fault system is over 1 km wide (Figs. 3, 12). On its southwest margin, a normal fault cuts upper greenschist facies-grade Stuhini Group volcanic breccias in which pyroxenes are replaced by coarse crystalline actinolite. To the northeast, within the fault zone, consistent C-S kinematic indicators on chlorite shears document normal-sense, northeast-side-down displacement. The absence of actinolite neoblasts may indicate that the shearing occurred during retrograde, lower-temperature metamorphism. A plagioclase-phyrlic dike crosscuts the shear fabric along an argillite-basalt breccia contact, but is locally sheared along its margins, indicating that it was emplaced late in the shearing event (Figs. 13a, b). It has been sampled for uranium-lead zircon geochronology. The concentration of Lehto suite intrusive rocks increases toward the northeast, with accompanying hornfelsing of Stuhini volcanoclastic rocks. Locally, epidote fills veins and replaces phenocrysts in Lehto suite rocks, including hornblende diorite dikes with epidote-replaced megacrysts of euhedral plagioclase up to 4 cm long and 2 cm wide (Fig. 14). This ‘pistachio diorite’ also occurs farther west as part of the main Lehto pluton on the Lake Ridge and as dikes on Sericite Ridge. Both quartz-sericite-pyrite alteration zones and normal faults are cut by a late reverse fault of small interpreted displacement that forms the hanging wall of alteration in ‘Pins bowl’ (Fig. 12).

4.2. Lake Ridge

Northwest of Pins Ridge, reverse faults begin to become more prominent. At Lake Ridge, the Sky fault system narrows to about 700 m (Figs. 3, 15). A reverse fault bounds the southwestern

flank of this segment, but the northeast fault block displays C-S fabrics indicating normal movement. Strain is distributed; gently dipping zones of intense fabrics are separated by 100 metre-scale panels of less deformed rock. The zones of strong flattening focus pyrite-epidote and lesser quartz-sericite-pyrite alteration and dike emplacement. This demonstrates that the normal-sense distributed shear system was in existence prior to, and at least in part controlled, intrusion of the Lehto suite and accompanying mineralization.

4.3. Sericite Ridge

At Sericite Ridge, the Sky fault system narrows to less than 400 m (Fig. 3). Reverse faults overprint earlier normal structures and fabrics. This is the most southeasterly occurrence of a north-vergent reverse fault in the immediate hanging wall of strong quartz-sericite-pyrite alteration. The hanging wall of the gently southwest-dipping ($123/20^\circ$) reverse fault is marked by strong chlorite-silica-pyrite-replaced volcanoclastic rock (Fig. 16). Approximately 100 m into the footwall, hornblende diorite, plagioclase porphyry diorite and aplite dikes are cut by curvilinear brittle shears of widely varying orientations with slickenfibres and zones of cataclasis. These features mark a distributed brittle fault zone that post-dates intrusion and alteration. Farther to the northeast, normal-sense fabrics are preserved locally in QSP-chlorite-replaced Stuhini volcanoclastic rocks. A swarm of intersecting west-northwesterly dikes of Lehto suite ‘pistachio diorite’ and other plagioclase-phyrlic phases cuts QSP- and propylitically altered rock. North of the Sky fault system, the remainder of the northeast-trending Sericite Ridge shows strong pervasive QSP

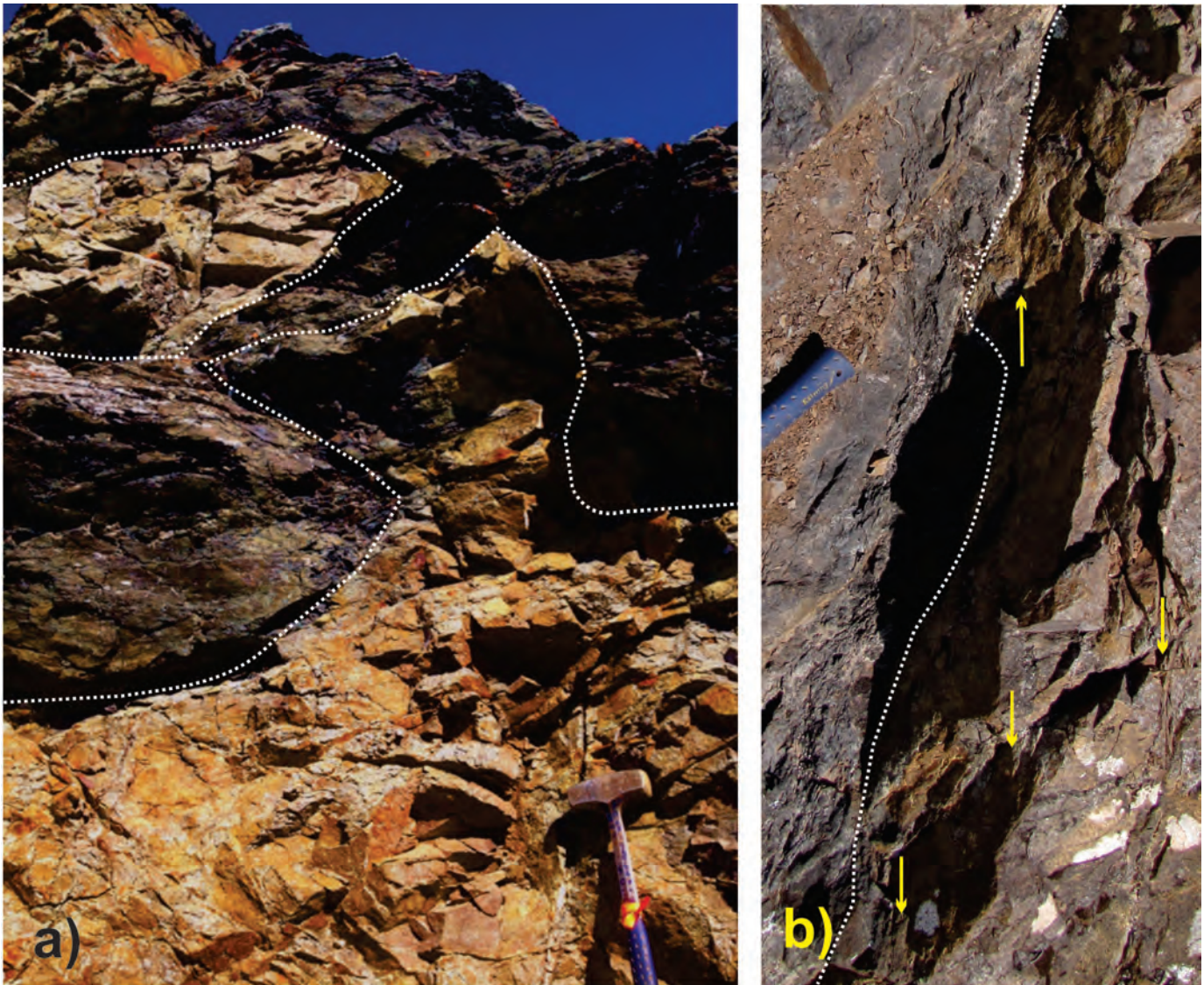


Fig. 13. a) Plagioclase-phyric dike intruding normal-sense shear zone that separates argillite from volcanoclastic protolith, Stuhini Group, upper Pins Ridge. Dike apophyses cut across hanging wall and foot wall. b) Close-up of dike margin to show internal weak, sporadic shear fabric (arrows). 388175 E, 6265759 N.

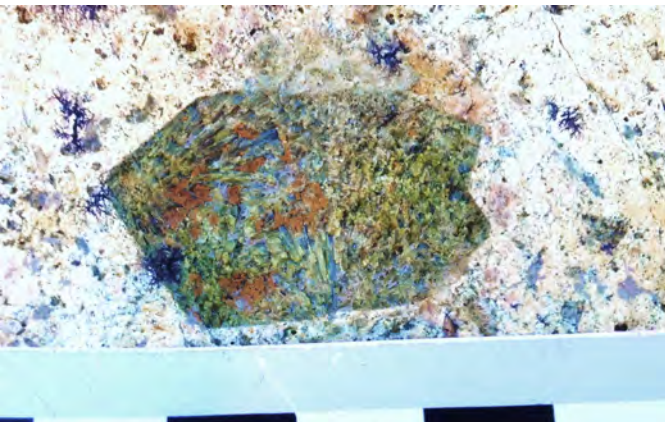


Fig. 14. Plagioclase megacryst replaced by radiating crystalline epidote, the 'pistachio diorite' phase of the Lehto pluton, Pins Ridge. Identical textures also occur in the main body of the pluton on Lake Ridge, and on Sericite Ridge and Pyramid. Scale in cm. 389715 E, 6266563 N.

alteration (Fig. 3). This zone parallels the northwestern contact of the main Lehto pluton.

4.4. Pyramid Ridge

At Pyramid Ridge, northwest of Sericite Ridge, the Sky fault system further narrows to about 200 m. The Khyber reverse fault ($143/70^\circ$) outcrops as a planar surface separating strongly QSP-replaced rock in the footwall from hornfelsed, siliceous volcanic rocks and meta-chert in the hanging wall (Fig. 17). The hanging wall rocks are unlike any others observed in the area. They display strong pervasive silica replacement and patchy red-brown biotite hornfels, and likely represent volcanoclastic protoliths overprinted by regional and contact metamorphism. Unlike other zones of hornfelsed volcanic rocks, primary features beyond centimeter-scale layering are lacking. The most distinctive textural variant is a matrix-supported breccia with angular clasts of aphanitic quartz (Fig. 18). These hanging

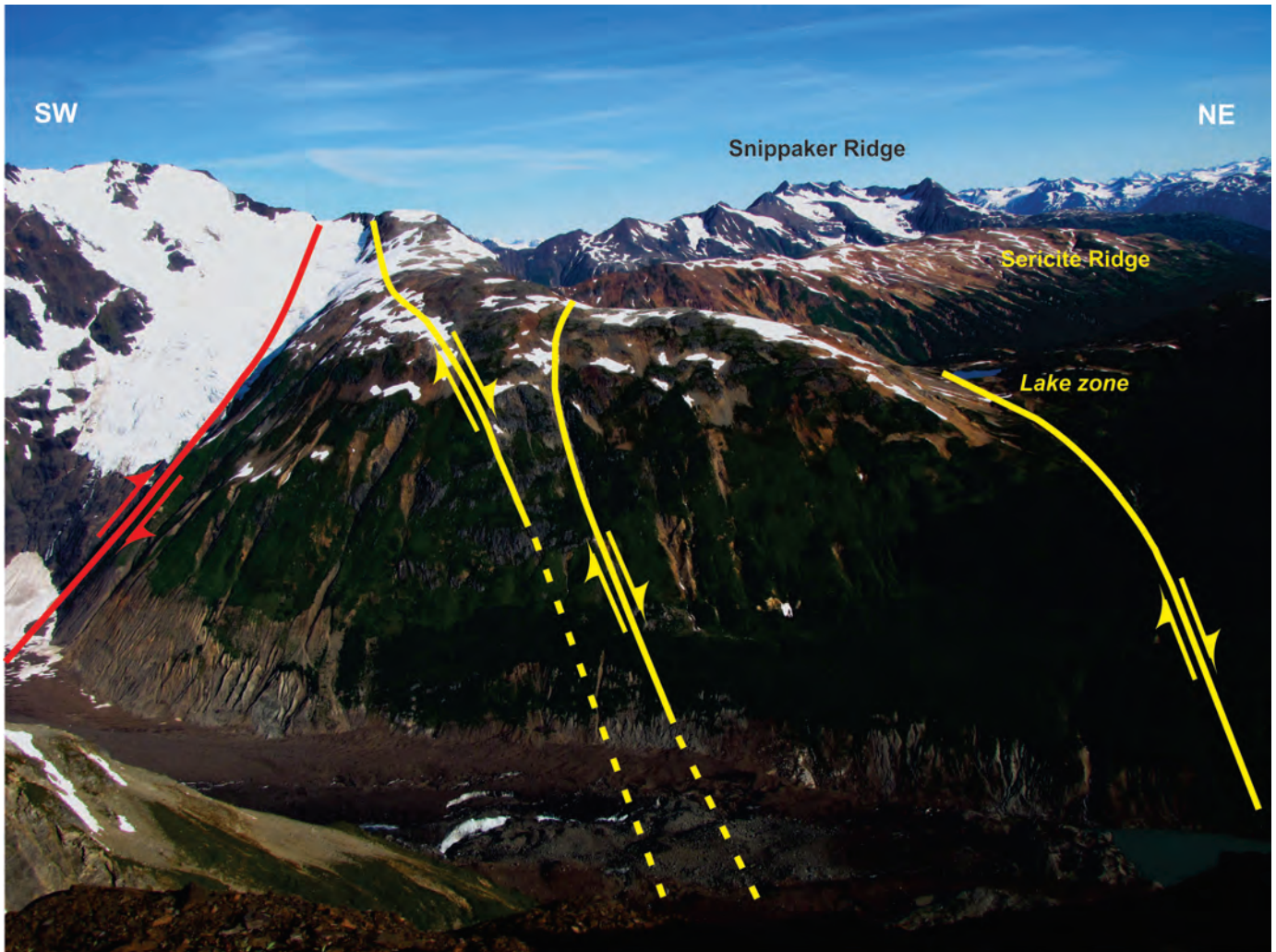


Fig. 15. Lake Ridge area, looking northwest from Pins Ridge (see Fig. 3 for location). Inferred thrust fault through glacier joins Khyber fault to west. Sericite Ridge in background.



Fig. 16. Sheared, chlorite-sericite-quartz-pyrite-altered rock in Khyber fault zone, Sericite Ridge. Scale in cm. 384023 E, 6269865 N.

wall rocks may have been derived from the Stuhini Group or the Stikine assemblage (Paleozoic).

4.5. Khyber Pass, Inel and the Boundary-Billygoat fault system

At Khyber Pass, about 1.5 km to the northwest, the Khyber fault ($140/40^\circ$) truncates the northeast-trending ($045-060^\circ$), southeast-dipping ($75-85^\circ$) Boundary-Billygoat fault (Fig. 3; Jim Oliver personal communication, 2014). This fault divides the Khyber from the Inel prospects and appears to have exerted control on intrusion and mineralization. The Boundary fault zone hosts a concentration of fine-grained mafic sills and dikes, and dense quartz-chlorite-sulphide stockworks and sheeted veins with gold-silver-zinc mineralization. The number and volume of intrusive bodies and the intensity of alteration and mineralization increase toward the Sky fault system and Khyber reverse fault (Jim Oliver personal communication, 2014). Dikes in the immediate footwall of the Sky fault system are sub-parallel to it. Many intrusive rocks are strongly altered and occur with strong copper and gold mineralized zones. Gold is commonly identified along the margins of orthoclase-phyric dikes and in sheeted quartz veins in larger dioritic intrusions.

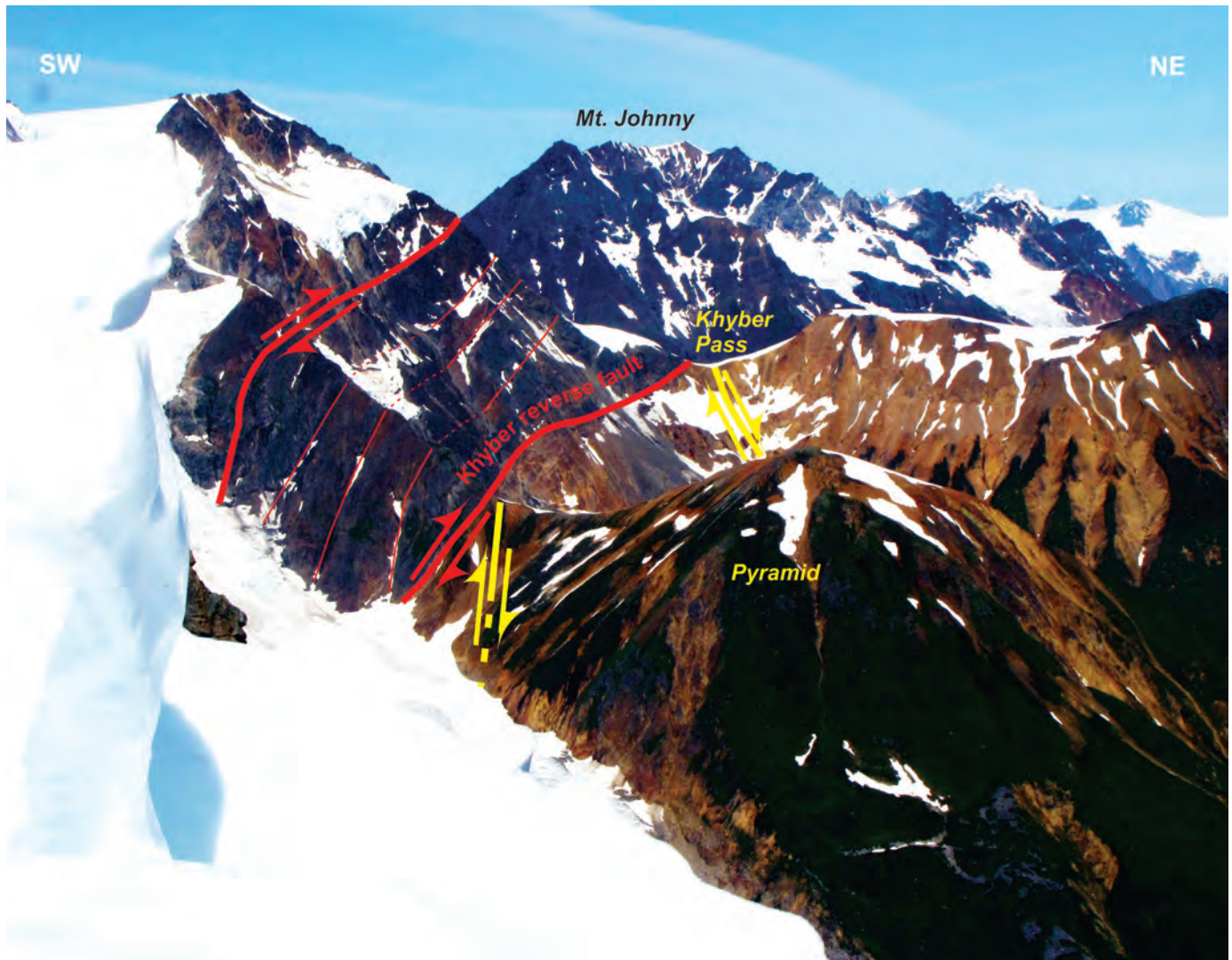


Fig. 17. The Sky fault system in the Pyramid-Khyber Pass area from the southeast (see Fig. 3 for location). The Khyber reverse fault marks the hanging wall of strong quartz-sericite-pyrite alteration. Structural form lines are shown in the hanging wall. Normal-sense faults in the footwall are truncated by the Khyber fault.



Fig. 18. Breccia with aphanitic quartz clasts in the hanging wall of the Khyber fault at Pyramid Ridge. Scale in cm. 379818 E, 6272105 N.

The Boundary fault is offset by the Inel fault, and continues as a well-defined structure, the Billygoat fault, at least 8 kilometres to the northeast. On the ridge south of Billygoat bowl, the fault zone is occupied by a swarm of Lehto dikes, gabbros, monzonites, ‘pistachio diorites’ and aplites. Stuhini Group wall rocks are propylitically altered with patchy epidote and pyrite. The structural block immediately southeast of the fault has been tilted to a steep, northeasterly orientation parallel to the fault trace, as shown by the distribution of Stuhini layered units (Fig. 3 and Lewis, 2013). Presence of Lehto-suite dikes indicates that the Boundary-Billygoat faults, like the Sky fault, were active in Early Jurassic time.

4.6. South of Mt. Johnny

The Sky fault system is well exposed at recently deglaciated outcrops on the south side of Mt. Johnny (Fig. 3), where it is expressed as a 400 m wide zone of penetrative foliation and

anastomosing mylonites developed in coarse conglomerates of the lower Hazelton Group. In one instance, a dextral sense of shear on a foliation of $315/64^\circ$ is shown in deformed conglomerate (Fig. 19a). The conglomerates also display down-dip stretching lineations but lack macroscopic kinematic indicators. Nearby, a set of sigmoidal quartz veins indicates dextral displacement toward 280° . Alteration intensity is greatest in the most strained rocks. Most pervasive replacements include well-foliated red-brown, fine-grained biotite and green chlorite, and clots of pyrite. Alteration styles include matrix replacement, clast replacement, vein selvages, and fracture fills. Quartz \pm carbonate \pm pyrite veins up to 5 cm wide are common throughout; they have been affected by both ductile and brittle deformation.

Several plagioclase-phyric dikes up to 3 m wide crosscut and also intrude along the shear-related fabrics. Dike margins are typically irregular on centimeter as well as metre scales (Fig. 19b). One dike displays a weak subsolidus fabric defined by foliated chlorite, suggesting late synkinematic emplacement. We collected a geochronological sample of this dike to establish the time of faulting.

The felsic volcanic units on upper Johnny Mountain contain a gently dipping penetrative flattening fabric that parallels compositional layering and the basal contact of the sequence. Lineations plunge gently to the WNW; they are parallel to the axes of upright folds mapped in the underlying Stuhini Group (Lewis, 2013). The origin of the layer-parallel fabric is unclear, given that faults and fabrics elsewhere tend to be steep. Kinematic indicators were not recognized.

5. Discussion

5.1. Hazelton Group stratigraphy and Hazelton-Stuhini relationships

The sedimentary succession at Snippaker Ridge records the termination of volcanoclastic sedimentation related to the Stuhini arc, erosional unroofing of Stuhini Group rocks, and subsequent Hazelton arc volcanism. We place the sub-Hazelton Group unconformity beneath the Snippaker unit, which includes Upper Norian fauna, in contrast to Tipper and Richards (1976) who separated the Stuhini and Hazelton groups chronostratigraphically, at the ca. 201 Ma Jurassic-Triassic boundary. This revision is consistent with examples of Late Triassic lower Hazelton rocks elsewhere in Stikinia. The oldest Hazelton unit in the Spatzizi area is the ca. 206 Ma Griffith Creek volcanics, which overlie a conglomerate containing Triassic and Permian limestone clasts (Thorkelson et al., 1995). Upper Norian fossil fauna were reported from above the basal Hazelton unconformity at Kinskuch Lake near Kitsault (Cordey et al., 1992), and near Terrace, the base of the Telkwa Formation is ca. 205 Ma old (Barresi et al., in press). The onset of deposition of basal Hazelton rocks above the unconformity seems to have varied not only across western Stikinia, but also on a more local scale. On the flanks of the McTagg anticlinorium about 40 km east of the Bronson area (Fig. 2), Lower Jurassic (201-191 Ma; Hettangian-Sinemurian)



Fig. 19. a) Mylonitic zone in conglomerate, sigma porphyroclasts show dextral sense of shear; one possible delta clast indicated. 373851 E / 6275019 N; **b)** Quartz-feldspar porphyry dike (bottom) cutting well-foliated conglomerate. Note irregular, non-planar margin indicated by white arrow. 373530 E, 6274904 N.

conglomeratic rocks of the Jack Formation unconformably overlie the Stuhini Group (Nelson and Kyba, 2014). Cessation of Stuhini volcanism was followed by the creation of a landscape of highlands and basins. Onset of Hazelton deposition and volcanism varied throughout the terrane, in response to local topography and magma sources.

The second unconformity observed at Billygoat bowl and elsewhere on Snippaker Ridge indicates the onset of Early Jurassic volcanism. This episode is likely co-magmatic with the ca. 193 Ma Lehto plutonic suite and coeval with the nearby copper-gold porphyry intrusions at Kerr-Sulphurets-Mitchell-Iron Cap (Fig. 2). The Lehto plutonic suite appears to have been the thermal driver for mineralization observed in the Bronson corridor, as indicated by the close spatial association of intrusions, alteration zones and mineralization; the occurrence of intrusive-hosted veins at Inel; the Red Bluff porphyry occurrence; and an Early Jurassic lead isotopic model age

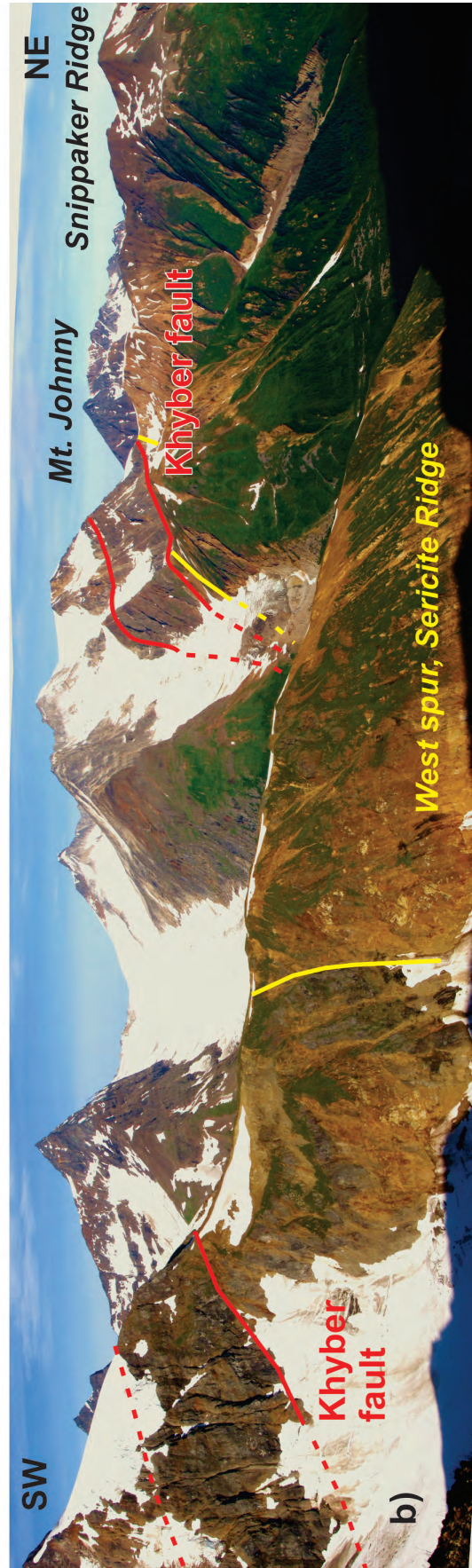


Fig. 20. a) View of Sky fault and Snippaker Ridge from Sericite Ridge (See Fig. 3 for location); b) Looking northwest from top of Sericite Ridge along Sky fault toward Pyramid and Khyber Pass. Shows continuity of Khyber fault from Khyber Pass to Sericite Ridge.

from the Snip mine (Rhys, 1995). The configuration of nested unconformities and related intrusive systems is analogous to that observed at the porphyry-hosting Tampakan stratavolcanic complex in the Philippines (Rohrlach, 2002).

5.2. The Sky fault system: influence on Early Jurassic intrusion, alteration and mineralization

Our analysis of the Sky fault system suggests that the Bronson corridor of alteration and mineralization (Metcalf and Moors, 1992) was controlled by regional structures. Normal faulting, emplacement of Lehto intrusive rocks, and alteration appear to be genetically related, as indicated by synkinematic dikes (Fig. 13) and the increased intensity of QSP alteration, polymetallic mineralization, and dike density at the Inel and Khyber prospects toward the Sky fault system. South of Mt. Johnny, the coarse mass-flow conglomerate section of the basal Hazelton Group coincides with the Sky fault trace. It reflects local steep topography; the presence of healed fault-breccia fragments as predominant clasts in one of the deposits suggests relief along penecontemporaneous fault scarps.

In this study, we have observed many instances of normal-sense motion on strands of the Sky fault system. However, the stress regime during the Early Jurassic may not have been purely extensional. There is limited evidence of dextral-sense motion on the Sky fault south of Mt. Johnny. Detailed underground structural study of the Snip vein showed that it formed during normal-oblique (dextral) motion on the minor west-northwesterly, southeast-dipping fault zone that hosts it (Rhys, 1995). Northeasterly faults and trends of intrusions and alteration zones are an important feature of the Bronson corridor. These include the Boundary-Billygoat fault, the Lehto pluton, and the 4 kilometre-wide zone of QSP alteration on Sericite Ridge that parallels the western margin of the pluton for 10 kilometres. All are truncated against the Sky fault system. The exploitation of northeasterly structures by intrusions is consistent with Early Jurassic northwest-southeast extension along the axis of the Bronson trend coeval with faulting along its southern margin. Thus, there may have been a transcurrent component in the fault regime.

Part of the Sky fault system was reactivated as a set of reverse faults after emplacement of the Lehto plutonic suite and associated alteration. Reverse fault movement increases in importance along strike from southeast to northwest. At Pins and Lake ridges, reverse faulting is limited, but northwest of Sericite Ridge, displacement on the Khyber reverse strand increases. At Pyramid and Khyber Pass the Khyber fault is a single southwesterly, steeply-dipping surface that separates strongly QSP altered rocks in the footwall from greenschist grade rocks in the hanging wall (Figs. 20a, b). The southeastern tip-line of the Khyber reverse fault is close to Sericite Ridge and the southeastern limit of broad-scale QSP alteration that extends from Sericite Ridge through Pyramid and Khyber Pass (Fig. 3). We consider that the mechanically weakened, clay-sericite-rich altered rocks provided convenient glide surfaces for thrust reactivation during regional shortening. The only

limit we have on the timing of thrust reactivation is that it was post-Early Jurassic. Nonetheless, the style of deformation corresponds closely to the Skeena fold and thrust belt in the KSM-Brucejack area. In particular, the Khyber reverse fault closely resembles the Sulphurets thrust fault, with strongly QSP-altered Early Jurassic and older rocks in its footwall and weakly altered Triassic and older strata in its hanging wall (Nelson and Kyba, 2014).

6. Conclusions

The Bronson corridor is prospective for porphyry and related precious metal mineralization as indicated by past production and recent (2014) discoveries. Late Triassic siliciclastic rocks of the Snippaker unit record uplift and erosional unroofing of the Stuhini arc before the main episode of Hazelton Group volcanism. The Lehto pluton, as shown in the Lewis (2013) compilation, is a large, northeast-trending, uniform intrusive body. More detailed observations show a wider diversity of phases, and distribution of Lehto plutonic rocks throughout the belt in small, high-level intrusive centers (e.g., Snippaker Ridge and Mt. Johnny) and as dikes near the Sky fault system. Analysis of the Sky fault system indicates that early normal faults, likely genetically related to alteration, mineralization, and Lehto plutonism, reactivated in a thrust sense during post-Early Jurassic regional shortening. The Sky fault system likely formed close to the boundary of a rift-type basin and enhanced circulation of hydrothermal fluids generated during Lehto suite plutonism to form the deposits of the Bronson corridor. The coeval Early Jurassic Mitchell intrusions, responsible for the KSM deposits, occupy a similar structural position in a basin now in the immediate footwall of the Sulphurets Fault (Nelson and Kyba, 2014).

Acknowledgments

Our understanding of the Khyber-Sericite Ridge-Pins Ridge area benefitted greatly from field interaction with the Colorado Resources exploration team, particularly Jim Oliver, who contributed descriptions of the Khyber Pass-Inel area to this paper. Colorado Resources and Seabridge Resources aided in field logistics. Wes Luck of Fireweed Helicopters provided superb piloting in difficult conditions. We are grateful for Pete Kossey's hospitality at his camp on Bronson strip.

References

- Alldrick, D.J., Britton, J.M., MacLean, M.E., Hancock, K.D., Fletcher, B.A., and Hiebert, S.N. 1990. Geology and mineral deposits of the Snippaker area, NTS 104B/6E, 104B/7W, 104B/10W, 104B/11E. British Columbia Ministry of Energy, Mines and Petroleum Resources, Open File 1990-16, scale: 1:50,000.
- Barresi, T., Nelson, J.L., Dostal, J. and Friedman, R. in press. Evolution of the Hazelton arc, British Columbia: Stratigraphic, geochronological and geochemical constraints on a Late Triassic-Early Jurassic arc and Cu-Au porphyry belt. *Canadian Journal of Earth Science*.
- British Columbia Geological Survey Regional Geochemical Survey. <http://www.empr.gov.bc.ca/Mining/Geoscience/Geochemistry/RegionalGeochemistry/Pages/default.aspx> (Accessed November,

- 2014).
- Cordey, F., Greig, C.J. and Orchard, M.J., 1992. Permian, Triassic and Middle Jurassic microfaunal associations, Stikine terrane, Oweegee and Kinskuch areas, northwestern British Columbia. In: Current Research, Part E, Geological Survey of Canada, Paper 92-1E, 107-116.
- International Commission on Stratigraphy, 2014. International stratigraphic chart, v2014/2. <http://www.stratigraphy.org/index.php/ics-chart-timescale> (accessed November, 2014).
- Jolly, R.J.H., and Lonergan, L., 2002. Mechanisms and controls on the formation of sand intrusions. *Journal of the Geological Society of London*, 159, 605-617.
- Lewis, P.D., Mortensen, J.K., Childe, F., Friedman, R., Gabites, J., Ghosh, D. and Bevier, M.L. 2001. Geochronology Data Set. In: Lewis, P.D., Toma, A., Tosdal, R.M., eds., *Metallogenesis of the Iskut River area, northwestern British Columbia*. Mineral Deposit Research Unit, University of British Columbia, Special Publication Number 1, Chapter 9, 89-96.
- Lewis, P.D. 2013. Iskut River Area Geology, Northwest British Columbia (104B/08, 09, 10 & part of 104B/01, 07, 11). Geoscience British Columbia Report 2013-05; 3 1:50,000-scale maps.
- Metcalfé, P. and Moors, J.G. 1993. Refinement and local correlation of the upper Snippaker Ridge section, Iskut River area, B.C. (104B/10W and 11E). In: *Geological Fieldwork 1992*, British Columbia Ministry of Energy, Mines and Petroleum Resources, Paper 1993-1, 335-340.
- Nadaraju, G.T. and Lewis, P.D. 2001. Biogeochronological data set. In: Lewis, P.D., Toma, A., Tosdal, R.M., eds., *Metallogenesis of the Iskut River area, northwestern British Columbia*; Mineral Deposit Research Unit, University of British Columbia, Special Publication Number 1, Chapter 8, 85-88.
- Nadaraju, G.T. and Smith, P.I. 1992. Jurassic biochronology in the Iskut River map area, British Columbia: A progress report. In: *Current Research Part A*, Geological Survey of Canada, Paper 1992-1A, 333-335.
- Nelson, J.L. and Kyba, 2014. Structural and stratigraphic control if porphyry and related mineralization in the Treaty Glacier – KSM – Brucejack – Stewart trend of northwestern Stikinia. In: *Geological Fieldwork 2013*, British Columbia Ministry of Energy and Mines, BC Geological Survey Paper 2014-1, 111-140.
- Rhys, D.A. 1995. The Red Bluff gold-copper porphyry and associated precious and base metal veins, northwestern British Columbia. In: *Porphyry Deposits of the Northwestern Cordillera of North America*, T.G. Schroeter, ed., Canadian Institute of Mining and Metallurgy Special Volume 46, 838-850.
- Rohrlach, B.D. 2002. Tectonic evolution, petrochemistry, geochronology and palaeohydrology of the Tampakan porphyry and high-sulphidation epithermal Cu-Au deposit, Mindanao, Philippines. Unpublished PhD Thesis, Australian National University, Canberra, Australia.
- Thorkelson, D.J., Mortensen, J.K., Marsden, H. and Taylor, R.P. 1995. Age and tectonic setting of Early Jurassic episodic volcanism along the northeastern margin of the Hazelton trough, northern British Columbia. In: Miller, D.M. and Busby, C., *Jurassic Magmatism and Tectonics of the North American Cordillera*, Geological Society of America Special Paper 299, p. 83-94.
- Tipper, H.W. and Richards, T.A. 1976. Jurassic stratigraphy and history of north-central British Columbia. *Geological Survey of Canada, Bulletin 270*, 73 p.

Geology of the Mitchell Au-Cu-Ag-Mo porphyry deposit, northwestern British Columbia, Canada

Gayle E. Febbo^{1, a}, Lori A. Kennedy², Michael Savell³, Robert A. Creaser⁴, and Richard M. Friedman⁵

¹ Mineral Deposit Research Unit, University of British Columbia, Vancouver, BC, V6T 1Z4

² Department of Earth, Ocean and Atmospheric Science, 2020-2207 Main Mall, University of British Columbia, Vancouver, BC, V6T 1Z4

³ Seabridge Gold Inc., 106 Front Street East, Suite 400, Toronto, ON, M5A 1E1

⁴ The 1-26 Earth Sciences Building, University of Alberta, Edmonton, AB, T6G 2R3

⁵ Pacific Centre for Isotopic and Geochemical Research, University of British Columbia, Vancouver, BC, V6T 1Z4

^a corresponding author: Gayle.Febbo@gmail.com

Recommended citation: Febbo, G.E., Kennedy, L.A., Savell, M., Creaser, R.A., and Friedman, R.M., 2015. Geology of the Mitchell Au-Cu-Ag-Mo porphyry deposit, northwestern British Columbia, Canada. In: Geological Fieldwork 2014, British Columbia Ministry of Energy and Mines, British Columbia Geological Survey Paper 2015-1, pp. 59-86.

Abstract

The Mitchell Au-Cu-Ag-Mo porphyry deposit, hosted by Early Jurassic volcanosedimentary and intrusive rocks in the Stikine terrane of northwestern British Columbia, is considered the largest undeveloped gold resource in Canada. It contains 1740 Mt of measured and indicated resource grading 0.61 g/t Au, 0.17% Cu, 3.1 g/t Ag, and 58 ppm Mo based on a 0.5 gold-equivalent gram per tonne cut-off. The deposit is genetically related to multiple diorite intrusions (Sulphurets suite) that cut sedimentary and volcanic rocks of the Stuhini Group (Upper Triassic) and sandstones, conglomerates, and andesitic rocks of the Jack Formation (basal Hazelton Group; Lower Jurassic). Mineralization and accompanying alteration and stockwork proceeded in four stages. Hosted by Phase 1 plutons (196.0 ± 2.9 Ma and 189 ± 2.8 Ma), Stage 1 sheeted veins and stockwork contain most of the copper-gold mineralization and potassic and propylitic alteration. A Stage 2 disseminated and stockwork-hosted molybdenum halo (190.3 ± 0.8 Ma; Re-Os) is peripheral and contiguous with the core copper-gold system. It is associated with phyllic alteration and is temporally related to a Phase 2 pluton (192.2 ± 2.8 Ma) that outcrops central to the halo. Stage 3 consists of poorly mineralized massive pyrite veins associated with advanced argillic alteration and is related to Phase 3 diorite, diatreme breccia emplacement and intrusion breccia dikes. Stage 4 consists of high-level, gold-rich veins that are lateral to, and overprint, the main deposit. The geochemistry of the Sulphurets intrusions, nature and extent of alteration assemblages, high silica content of the ore zone and Mo mineralization, indicate that the Mitchell porphyry is calc-alkalic rather than alkalic. The subalkaline Sulphurets suite is here interpreted as the progenitor to the Mitchell deposit, rather than the alkaline Premier suite. The Premier and Sulphurets suites accompanied siliciclastic sedimentation and andesitic volcanism recorded by the Jack Formation. The deposit was deformed during development of the Skeena fold and thrust belt (mid-Cretaceous) and is now exposed in an erosional window beneath the Mitchell thrust fault, which separates it from its interpreted offset (Snowfield deposit) in the hanging wall to the southeast.

Keywords: Mitchell, Snowfield, Cu-Au porphyry, Kerr-Sulphurets-Mitchell, KSM, Sulphurets district, Iskut, Triassic-Jurassic porphyry, Jack Formation

1. Introduction

The Mitchell Cu-Au-Ag-Mo porphyry deposit is in the Stikine terrane of northwestern British Columbia (Fig. 1). Together, the Kerr-Sulphurets-Mitchell porphyry deposits (KSM), the Brucejack high-grade gold deposit, and the Snowfield porphyry deposit are hosted in volcanosedimentary rocks of the Stuhini Group (Triassic) and unconformably overlying volcanosedimentary strata and allied plutonic rocks of the Hazelton Group (Lower Jurassic; Fig. 2). Part of the Sulphurets district, these deposits lie at the northern end of a 60 km long north-northwest trending Cu-Au porphyry and related mineralization trend that extends south to the town Stewart (Fig. 2). The origin of the trend has been ascribed to Jurassic faults that controlled sedimentation of the Jack

Formation (basal Hazelton Group; Henderson et al., 1992; Lewis, 2001; Nelson and Kyba, 2014), which partly hosts mineralization at KSM, Snowfield and Brucejack.

The Mitchell deposit, delineated by extensive drilling that began in 2006, is considered the largest undeveloped gold resource in Canada (Visual Capitalist, 2013). Although porphyry-related mineralization in the Mitchell zone has been studied for over 50 years (e.g., Kirkham, 1963; Margolis, 1993; Aldrick and Britton, 1991; Lewis, 1992), detailed deposit-scale documentation has hitherto been lacking. Herein we present new field, petrographic, geochemical, and geochronologic data to document relationships between sedimentation, plutonism, alteration, vein paragenesis, mineralization, and deformation.

2. Geologic setting

The Quesnel and Stikine arc terranes are part of the Intermontane Belt of the Canadian Cordillera, geographically

Errata to the printed version of this paper were corrected January, 2019.

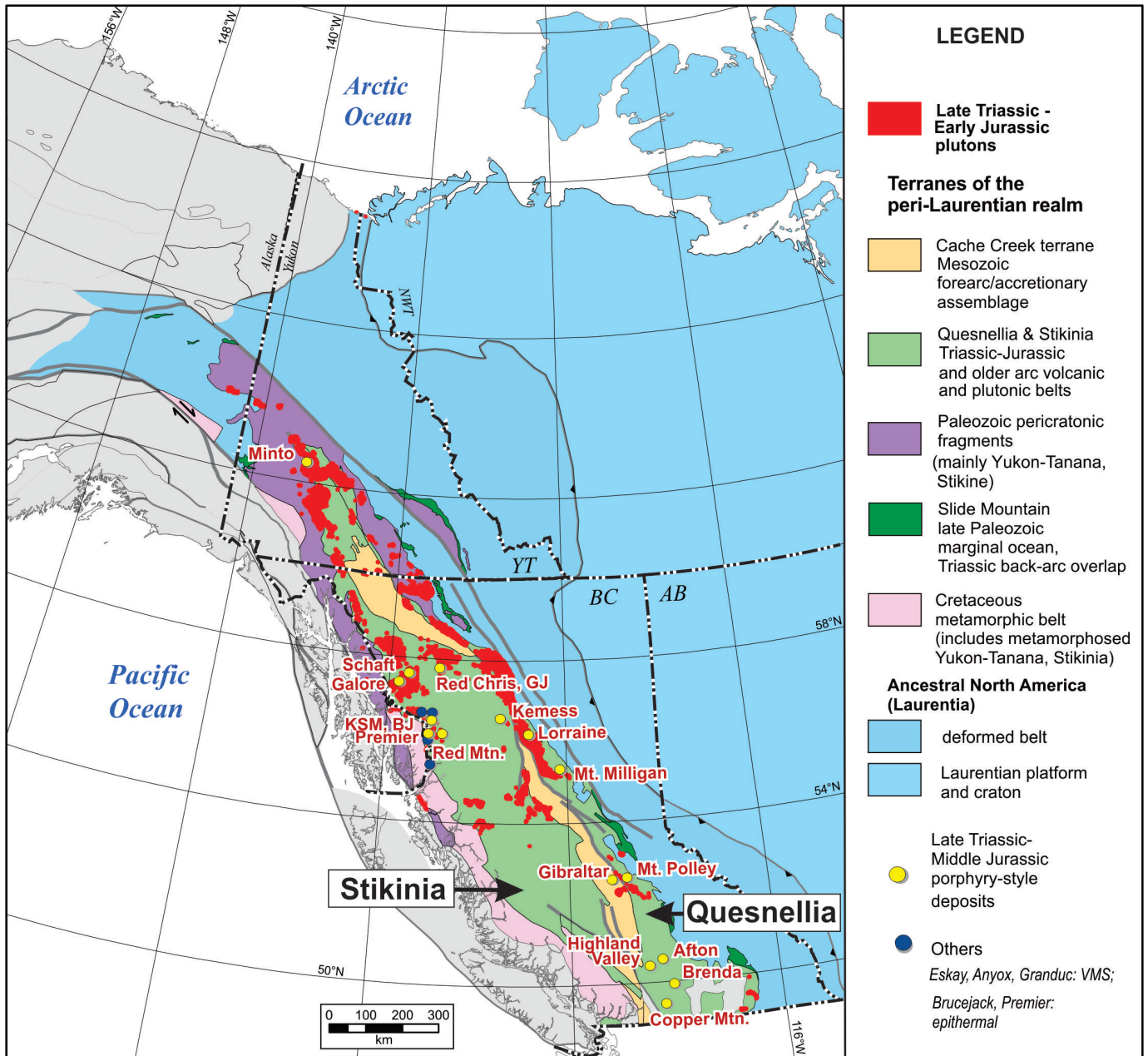


Fig. 1. Tectonic setting of Kerr-Sulphurets-Mitchell (KSM) deposits and other Triassic-Jurassic porphyry and related deposits in Quesnellia and Stikinia (from Nelson and Kyba, 2014).

inboard of the Cost Plutonic Complex and separated from each other by primitive arc and oceanic rocks of the Cache Creek terrane (Fig. 1). Long-lived arc magmatism across Stikinia and Quesnellia during the Late Triassic to Early Jurassic generated paired belts of alkalic and calc-alkalic porphyry deposits that extend for 2,000 km along the axis of the Canadian Cordillera (Logan and Mihalynuk, 2014). These deposits are both alkalic (e.g., Afton-Ajax, Copper Mountain, Mount Polly and Galore Creek) and calc-alkalic (e.g., Gibraltar, Schaft Creek and Kemess). Porphyry deposits of the Sulphurets district are along the western margin of the Stikine terrane (Fig. 1) with mineralization ages between 197 and 190 Ma (Bridge,

1993; Margolis, 1993; this study). Gold mineralization in the Sulphurets district spans ~12 Ma as indicated by high-grade gold-silver at Brucejack (ca. 185 Ma) superimposed onto older porphyry mineralization (192-190 Ma; Pretium Resources, 2013).

The Stikine terrane comprises three unconformity-bounded island arc volcanosedimentary successions that span 200 Ma. These include the Stikine assemblage (Devonian to Mississippian; Anderson, 1989; Greig, 1992; Logan et al., 2000), the Stuhini and Takla groups (Middle to Late Triassic), and the Hazelton Group (Late Triassic to Middle Jurassic). Mesozoic plutonic suites (Figs. 1, 2) include Stikine and

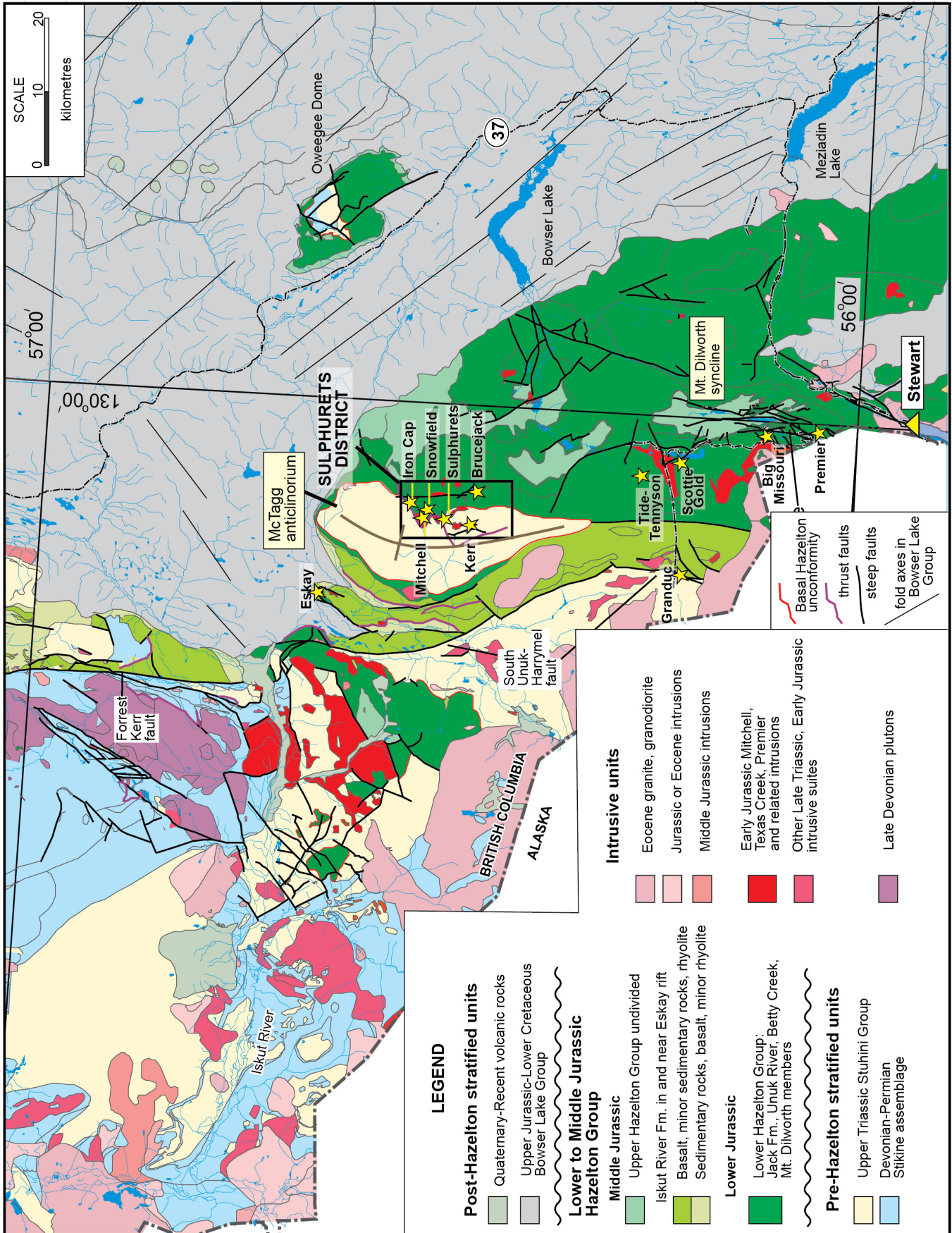


Fig. 2. Western Iskut region geology. The Stewart-Sulphurets district trend extends from the Premier deposit ~ 60 km north to the Sulphurets district (from Nelson and Kyba, 2014).

Copper Mountain (Late Triassic, coeval and comagmatic with the Stuhni Group), Texas Creek (coeval and comagmatic with the Hazelton Group; Early Jurassic), Three Sisters (Middle Jurassic). Gold-rich deposits are associated with both the Late Triassic and Early Jurassic intrusive suites in northwestern Stikinia. Between Stewart and the Sulphurets district (Fig. 2) these deposits coincide with a belt of 195-187 Ma Texas Creek plutons (Alldrick, 1993; Logan and Mihalynuk, 2014). The Premier intrusions are an important subset of the Texas Creek plutons named for the synmineral dike occurrences in the Premier mine area near Stewart (Alldrick, 1993). Premier suite rocks are defined in the Stewart area by the presence of potassium feldspar megacrysts and plagioclase phenocrysts ('two-feldspar porphyry') in a fine-grained groundmass (Alldrick, 1993). East of the Sulphurets district, the Bowser Lake Group is a molassoid sedimentary succession containing debris derived from the collision of the Intermontane terranes and the edge of ancestral North America (Evenchick et al., 2007). The area was deformed by mid-Cretaceous sinistral transpression that gave rise to the Skeena fold and thrust belt, an extensive NE-verging zone of shortening that extends across most of the northern Intermontane Belt (Evenchick, 2001). The Sulphurets district is on the eastern limb of the McTagg anticlinorium, a north-trending mid-Cretaceous structural culmination (Fig. 2). The anticlinorium is bounded in part by outward-vergent thrust faults, including the east-vergent Sulphurets fault, structurally above the Mitchell deposit (Figs. 2, 3).

3. Sulphurets district geology

3.1. Stratigraphy

The Sulphurets district is underlain predominantly by Stuhini Group bedded sedimentary rocks and Hazelton Group siliciclastic rocks that interfinger with massive and fragmental andesites, and related Mitchell plutons (Lewis, 2013; Figs. 3-5). Drill holes in the western Sulphurets district intersected maroon radiolarian chert from surface to depths of 200 m that are interpreted to be Stikine assemblage (Nelson, pers. comm., 2014). The chert is located in the bottom of the valley in the hinge area of the McTagg anticlinorium and represents the lowest stratigraphic level identified in the McTagg.

Stuhini Group rocks comprise thinly bedded mudstone, graphitic mudstone, and lesser calcareous mudstone, and felsic tuff. The uppermost Stuhini Group unit immediately beneath the sub-Hazelton Group unconformity consist of felsic volcanic stratified tuffs, fragmental and coherent rocks (Fig. 5).

The base of the Hazelton Group is an angular unconformity that cuts into previously folded Stuhini Group rocks, marking a significant regional hiatus in volcanism and an episode of uplift and erosion (e.g., Nelson and Kyba, 2014). The unconformity is overlain by polymictic conglomerates with felsic intrusive and extrusive clasts and quartz-rich arkoses of the Jack Formation, a unique basal Hazelton unit that is restricted to the periphery of the McTagg anticlinorium (Nelson and Kyba, 2014). In the KSM area, the conglomerate commonly contains black mudstone intraclasts, clasts of black chert, felsic

and intermediate volcanic rock, crowded feldspar porphyry intrusive rock and bedded mudstone. In the Sulphurets district, Jack Formation strata interfinger with, and pass gradationally to, andesitic breccias, flows, and tuffs (Nelson and Kyba, 2014).

Subaerial andesite and dacite volcanic and volcanoclastic strata overlie the Jack Formation in the Brucejack area. They were included in the Betty Creek Formation by Lewis (2013). A thin unit of Middle Jurassic fossiliferous mudstone, also assigned to the Betty Creek Formation, outcrops east of the Iron Cap deposit.

3.2. Plutonism

Small Early Jurassic porphyritic diorite to syenite bodies referred to as the Mitchell intrusions cut the Stuhini and Hazelton groups in the Sulphurets district, and are considered part of the Texas Creek plutonic suite (Kirkham, 1963; Alldrick and Britton, 1988, 1991). We recognize two suites modified from Alldrick and Britton's (1991) 'one-feldspar' Sulphurets Glacier porphyry and 'two-feldspar' Premier porphyry identified in the Sulphurets district (see also Alldrick, 1993). Crowded, coarse-grained Premier intrusions are cut by uncrowded, relatively fine-grained Sulphurets intrusions. The Premier suite, consisting of diorite, monzonite, granite, syenite and quartz syenite, are crowded porphyry intrusions that are commonly medium to coarse grained and contain minor porphyry mineralization. West of the Sulphurets zone and above the Sulphurets thrust, diorite margins to monzonite plugs are interpreted to indicate that the diorite is the oldest phase of the Premier suite (Fig. 3). In the northern Mitchell valley, Premier suite syenite cuts monzonite and monzonite cuts diorite in drill core. Monzonite and syenite intrusions are cut in drill core by the Sulphurets suite diorite and related stockwork and alteration in the Iron Cap area. The Sulphurets suite, consisting of diorite to monzonite porphyry, are fine to medium grained. The Sulphurets suite is a partial host to all porphyry deposits in the district and were emplaced before, during, and after mineralization. Current geochronological data (Table 1) and cross cutting relationships suggest that the Premier suite magmatism preceded, and possibly overlapped with, the Sulphurets suite.

3.3. Structure

The Kerr, Sulphurets, Snowfield, and Iron Cap porphyry deposits are in the footwall of the Sulphurets fault (Fig. 3.), an east-vergent thrust that marks the eastern margin of the McTagg anticlinorium (Fig. 2). Both of these regional structures are interpreted to be kinematically linked to the Skeena fold and thrust belt (Kirkham and Margolis, 1995). The Mitchell thrust fault is a prominent splay of the Sulphurets thrust that separates the Snowfield and Iron Cap zones in its hanging wall from the Mitchell zone in its footwall (e.g., Savell and Threlkeld, 2013; Nelson and Kyba, 2014). Rocks in the Sulphurets area have been affected by folding, faulting, penetrative cleavage formation, and low-grade regional metamorphism (Kirkham, 1963; Henderson et al., 1992; Margolis, 1993). Beds in the

Table 1. Radiometric ages for Mitchell intrusions and related molybdenite mineralization in the Sulphurets district (¹laser ablation, ²TIMS).

Sub-district	Location	Stage	Suite	Unit	Sample	Method	Age	+	-	Reference
Brucejack	Bridge zone	-	-	hornblende porphyritic diorite	93-PL-185	U-Pb zircon ²	182.1	4.8	14.2	Lewis et al., 2001
Brucejack	Bridge zone	-	-	post-mineral mafic dike	-	U-Pb zircon ¹	182.7	1	1	Pretium Resources, 2013
Brucejack	south of Hanging Glacier	-	-	k-feldspar megacrystic dike	KQ-90-152	U-Pb zircon ²	188	0.5	0.5	McNicoll and Kirkham, in Kirkham and Margolis, 1995
Snowfield	east of Snowfield	post-3	-	k-feldspar megacrystic plagioclase-hornblende porphyry	S238	U-Pb zircon ²	189.6	2.2	2.2	Margolis, 1993
Mitchell	423312E 6265278N	1	Sulphurets	hornblende-plagioclase diorite porphyry	GF-13-02	U-Pb zircon ¹	189.9	2.8	2.8	this study
Brucejack	Bridge zone	-	n/a	molybdenite in vein	-	Re-Os	190.2	0.8	0.8	Pretium Resources, 2013
Mitchell	DDH M-10-116, 214.6 m	2	n/a	molybdenite in vein	M-10-116	Re-Os	190.3	0.8	0.8	this study
Brucejack	west of Hanging Glacier	-	Sulphurets	albite-hornblende porphyry	KQ-90-154C	Pb-Pb	191.4	5.3	5.3	Mortensen and Kirkham, in Kirkham and Margolis, 1995
Brucejack	Bridge zone (DDH SU-151)	-	n/a	molybdenite in vein	-	Re-Os	191.5	0.8	0.8	Pretium website, 2013
Sulphurets	Montgomery (Main Copper)	-	Premier	feldspar porphyry, monzonite to syenite	-	U-Pb zircon ²	191.8	6.5	1	Macdonald, in Kirkham and Margolis, 1995
Mitchell	DDH M-07-49, 320 m	2	Sulphurets	hornblende-plagioclase diorite porphyry	M-07-49	U-Pb zircon ¹	192.2	2.8	2.8	this study
Mitchell	southwest of Mitchell Glacier	pre-1	Premier	quartz syenite	S462	U-Pb zircon ²	192.7	5.4	3.6	Margolis, 1993
Mitchell	North of Mitchell glacier	pre-1	Premier	trachytoid syenite to aplitic granite porphyry	KQ-89-890/90A	U-Pb zircon ²	193.9	0.5	0.5	Mortensen and Kirkham, in Kirkham and Margolis, 1995
Brucejack	south of Hanging Glacier	-	Sulphurets	altered plagioclase-hornblende porphyry	KQ-90-151A	U-Pb zircon ²	194	1	1	McNicoll and Kirkham, in Kirkham and Margolis, 1995
Brucejack	west of West zone	-	-	k-feldspar megacrystic porphyry	93-PL-187	U-Pb zircon ²	194	3.7	0.6	Lewis et al., 2001
Kerr	Kerr deposit	-	-	k-feldspar megacrystic, plagioclase-hornblende porphyry	00-lskut	U-Pb zircon ²	195	1.5	1.5	Bridge, 1993
Mitchell	DDH M-11-123, 621 m	1	Sulphurets	diorite porphyry	M-11-123	U-Pb zircon ¹	196	2.9	2.9	this study
Sulphurets	Raewyn zone	-	Premier	altered quartz monzonite	-	U-Pb zircon ²	196	17	32	Macdonald, in Kirkham and Margolis, 1995
Kerr	western Kerr deposit	-	-	syenodiorite, symmetrical	Iskut-lapp	U-Pb zircon ²	197	3	3	Bridge, 1993

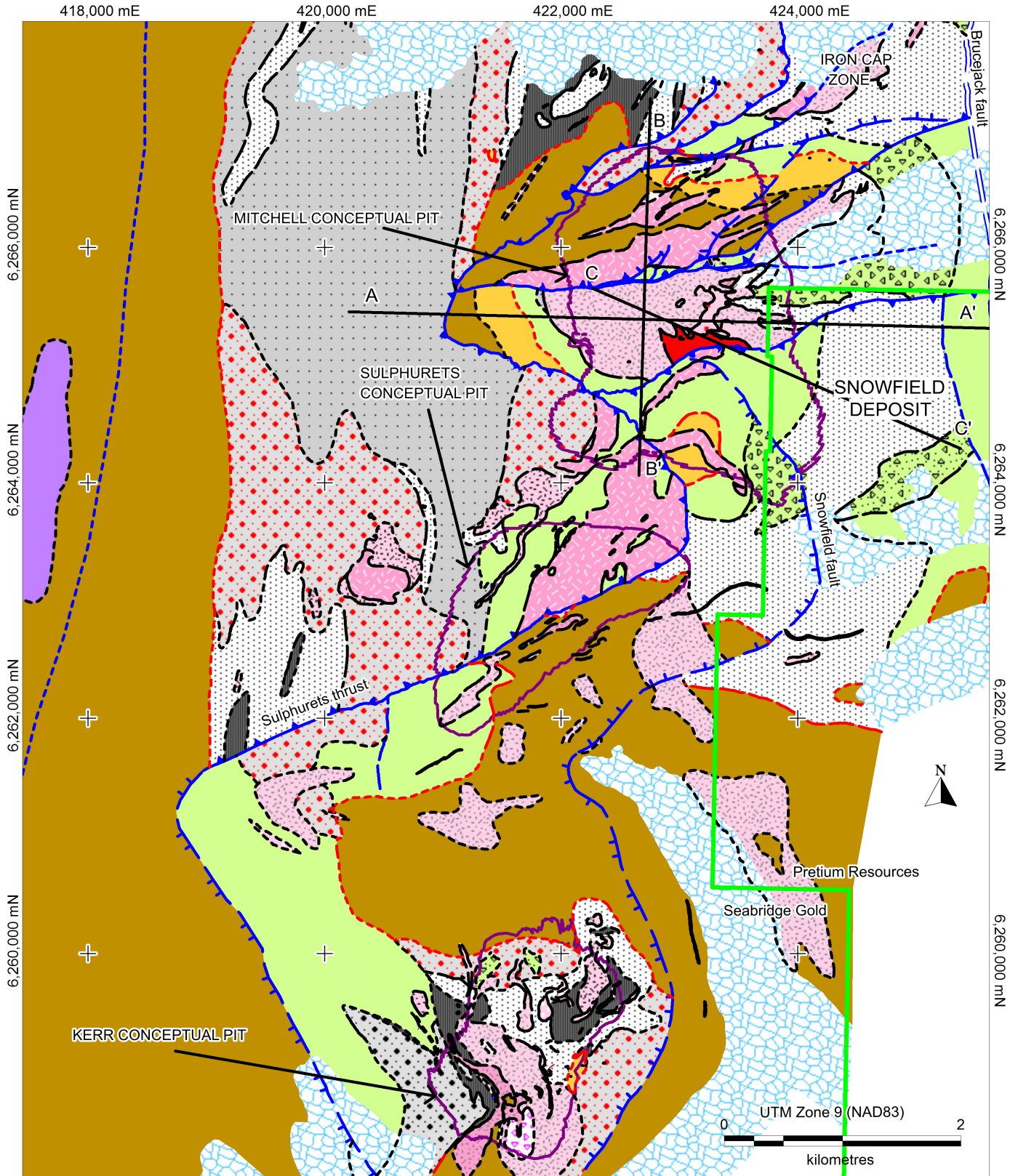


Fig. 3. Geology of the KSM property, showing the conceptual pit boundaries for Mitchell, Sulphurets and Kerr and the Snowfield and Iron Cap zones. For section A-A' refer to Figure 7a, for section B-B' refer to Figure 7b and for section C-C' refer to Figure 23. For lithology legend refer to Figure 4.

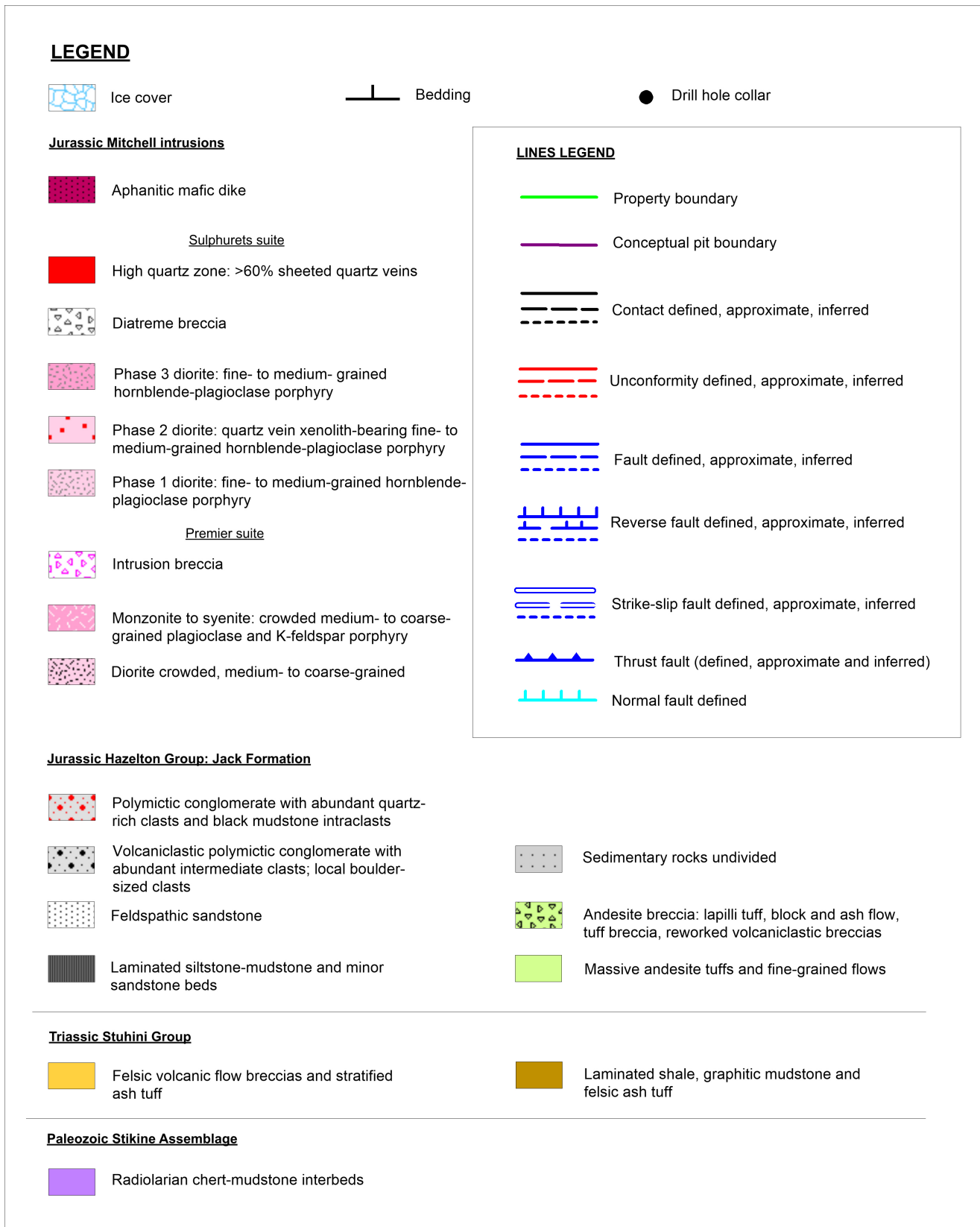


Fig. 4. Legend for Figures 3, 5, 7a, 7b, 8 and 21.

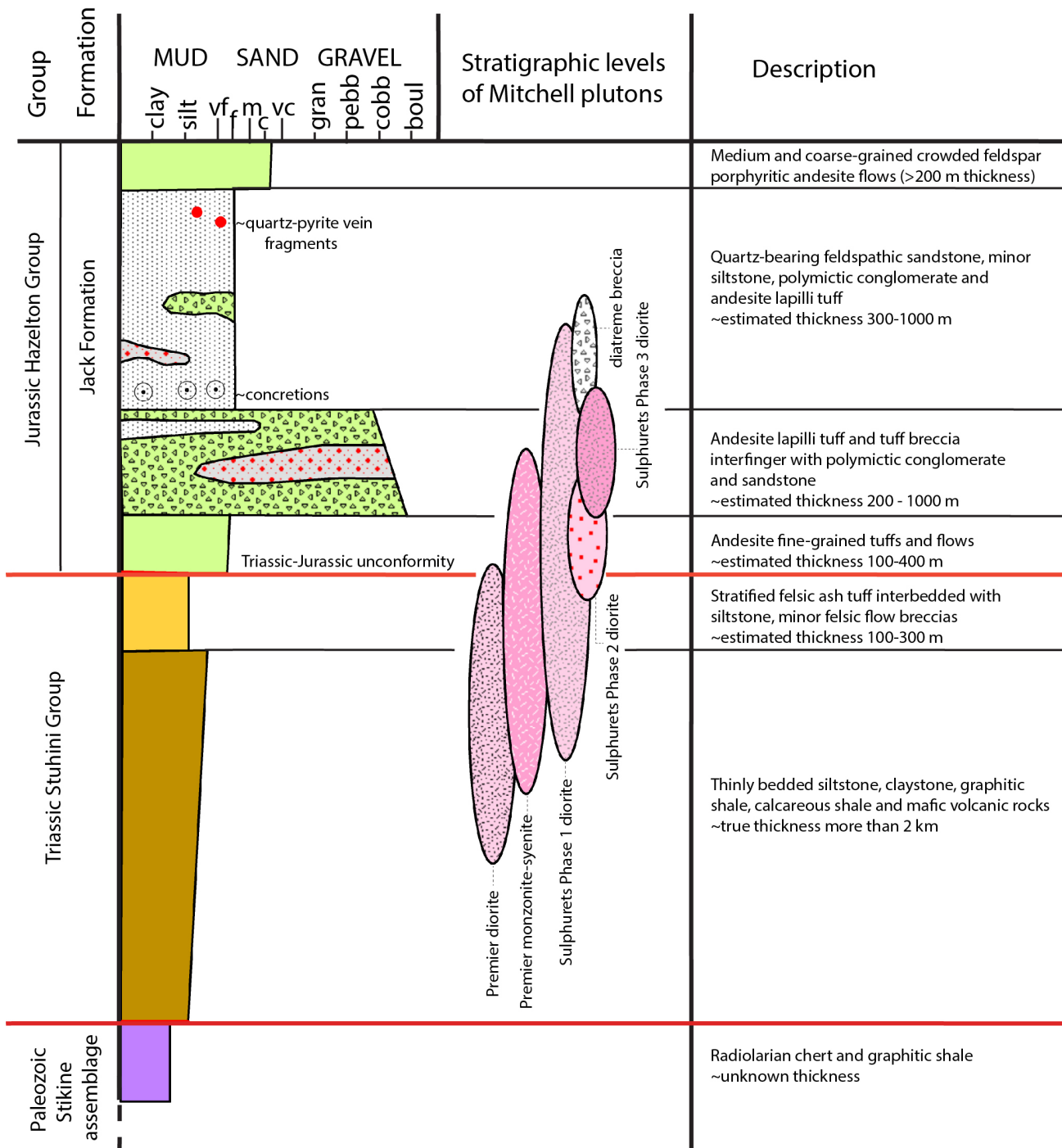


Fig. 5. Stratigraphy of the Mitchell-Snowfield area. For lithology refer to Figure 4.

district are generally north striking with moderate to steep dips and have been deformed into upright buckle folds, also related to Skeena fold and thrust belt deformation (Kirkham and Margolis, 1995). Two fold geometries are documented in the district: 1) north-northwest-plunging buckle folds with a related axial planar cleavage (Bridge, 1993; Kramer, 2014); and 2) west-plunging buckle folds, with a variably developed steep, north-dipping pressure solution cleavage (Kirkham,

1963; Margolis, 1993; this study). Although Margolis (1993) suggested that east-west striking cleavage in the Mitchell-Snowfield area may have developed as a post-emplacment fabric in the Jurassic, orthogonal fold trends in the Brucejack area may record progressive mid-Cretaceous deformation (C. Greig, pers. comm., 2014). Altered rocks at Kerr, Mitchell, Snowfield and Brucejack in particular are characterized by a strong pervasive pressure solution cleavage, folded veins, and

5-70% flattening compared to Sulphurets and Iron Cap, which have poorly developed deformation fabrics. Kirkham (1963) directly correlated cleavage development, degree of alteration, and abundance of micaceous minerals.

3.4. Mineralization

The Sulphurets district contains five undeveloped porphyry deposits (Kerr, Sulphurets, Snowfield, Mitchell and Iron Cap) and the high-grade epithermal Brucejack deposit (Fig. 2) with compliant estimates of mineral reserves and resources. Seabridge Gold Inc. claims cover the KSM property (Kerr, Sulphurets, Mitchell, and Iron Cap); Pretium Resources Inc. claims cover the Snowfield and Brucejack deposits. At surface, the Kerr deposit is hosted by Stuhini Group volcanosedimentary rocks, Jack Formation sandstone, and Sulphurets plutons; at depths of 0.5-1 km, it is intrusion hosted. The Sulphurets deposit is a tabular-shaped, northwest dipping ore body hosted in Jack Formation sandstone, andesite volcanic rocks, and subordinate Sulphurets suite monzodiorite to diorite dikes and sills. The Iron Cap and Snowfield deposits are hosted by Jack Formation sandstone, interfingering andesite volcanoclastic rocks, and Sulphurets suite intrusions.

The Mitchell deposit is largely hosted in Sulphurets suite diorite stocks. It lies in the footwall of the Mitchell thrust, and is considered equivalent to the Snowfield deposit which, in the hanging wall of the Mitchell thrust, is offset ca. 1.6 km to the southeast (Savell and Threlkeld, 2013). The KSM deposits have a measured and indicated resource of 2.78 billion tonnes at 0.55 g/t Au, 0.21% Cu, 2.9 g/t Ag and 55 ppm Mo (0.5 g/t gold equivalent cut off; Seabridge Gold, 2014). The Snowfield deposit hosts an additional measured and indicated resource of 1.37 billion tonnes at 0.59 g/t Au, 1.72 g/t Ag, 0.10% Cu and 85.5 ppm Mo (0.3 g/t gold equivalent cut off; Pretium Resources, 2011). The high-grade Valley of the Kings deposit (Brucejack project) contains a measured and indicated resource of 15.3 million tonnes at 17.6 g/t gold and 14.3 g/t Ag (5 g/t gold equivalent cut off; Pretium Resources, 2014).

The Snowfield deposit is underlain by andesite flow breccias and interbedded volcanoclastic arenite (Margolis, 1993) that host most of the mineralization. These rocks are intruded by pre-mineralization Sulphurets suite diorite and Premier suite quartz-syenite (192.7 ± 5.4 - 3.5 Ma; U-Pb, zircon; Margolis, 1993). Mineralization at Snowfield is divided into four stages (Margolis, 1993): Stage-1) deep, chalcopyrite-bearing potassic alteration flanked by propylitic alteration and Cu-Au enriched quartz-stockwork; Stage-2) high-level quartz-sericite-pyrite-chlorite-molybdenite-tourmaline; Stage-3) high-level advanced argillic alteration and deeper massive pyrite veins containing Bi-Te-Sn; and Stage-4) predominantly high-level, gold-rich vein and disseminated mineralization enriched in Ag-Pb-Zn-Ba-Sb-Hg-Cd-Te. Herein we adopt the Margolis (1993) scheme for the Mitchell deposit. Nelson and Kyba (2014) assigned quartz-rich arenites in the Snowfield area to the Jack Formation. Polymictic Jack Formation conglomerate outcrops west of the

Snowfield alteration zone (Nelson and Kyba, 2014). Argillic-altered sandstones in the upper part of the Jack Formation in the Snowfield area contain pebbles of banded quartz-pyrite vein fragments (Fig. 6a), indicating predepositional mineralization. Sulphurets suite porphyry plugs (Nelson and Kyba, 2014) contain Jack Formation sandstone xenoliths indicating that intrusion followed sedimentation. However, the Sulphurets suite porphyry is overprinted by alteration and mineralization (Margolis, 1993) and also contains clasts of chalcopyrite-bearing quartz veins (Margolis, 1993). In short, the mineralizing system appears to have been active before, during, and after deposition of the Jack Formation.

4. The Mitchell deposit

The Mitchell deposit is centred around a dense cluster of Mitchell porphyry diorites that cut the Stuhini Group and basal Hazelton Group (Jack Formation, Figs. 5, 8). Three pulses of Sulphurets suite diorite form a crudely elliptical 2 x 1 km outcrop with sills and dikes extending to the east. Multiple stocks of uniform medium-grained hornblende-plagioclase porphyritic diorite grade into coarse-grained porphyritic K-feldspar-hornblende-plagioclase diorite at depth (Figs. 7a, b). The deposit is characterized by episodic intrusion, stockwork and cannibalization of previously emplaced diorite and stockwork into later-stage intrusion breccias and diatremes. Deeper-level potassic and transitional potassic alteration in the western part of the map area grade into higher-level intermediate argillic and chloritic alteration in the central part which, in turn, grades to phyllic and clay alteration farther east. This alteration pattern is flanked by propylitic and albitic alteration that together with core alteration assemblages define a >4 km diameter alteration halo that is truncated by the Sulphurets thrust to the west and by the Brucejack fault to the east.

4.1. Lithologic units

4.1.1. Stuhini Group (Triassic)

The Stuhini Group is the oldest unit exposed in the Mitchell area (Fig. 8). The most abundant lithologies are cm-scale bedded siltstone, graphitic shales and less common calcareous mudstones intersected in drill core. Lesser amounts of dolostone and limestone are identified in drill core in the Mitchell mineralized zone (Hansley, 2008) and are of unknown thickness and extent. A unit of rhythmically bedded felsic tuff and siltstone assigned to Stuhini Group was intersected in drill core (Fig. 6b) in the western part of the map area, beneath the Mitchell thrust. Similar rocks outcrop north and south of the Mitchell zone above the Mitchell thrust fault (Fig. 8), and the unit appears to be >200 m thick. In the northwestern Mitchell valley, Jack Formation conglomerates contain clasts of a quartz-feldspar porphyritic flow breccia that were likely derived from an identical breccia body immediately beneath the unconformity (Fig. 6c). Ubiquitous felsic clasts in the Jack Formation were likely derived from similar rocks (J. Nelson, pers. comm., 2014).

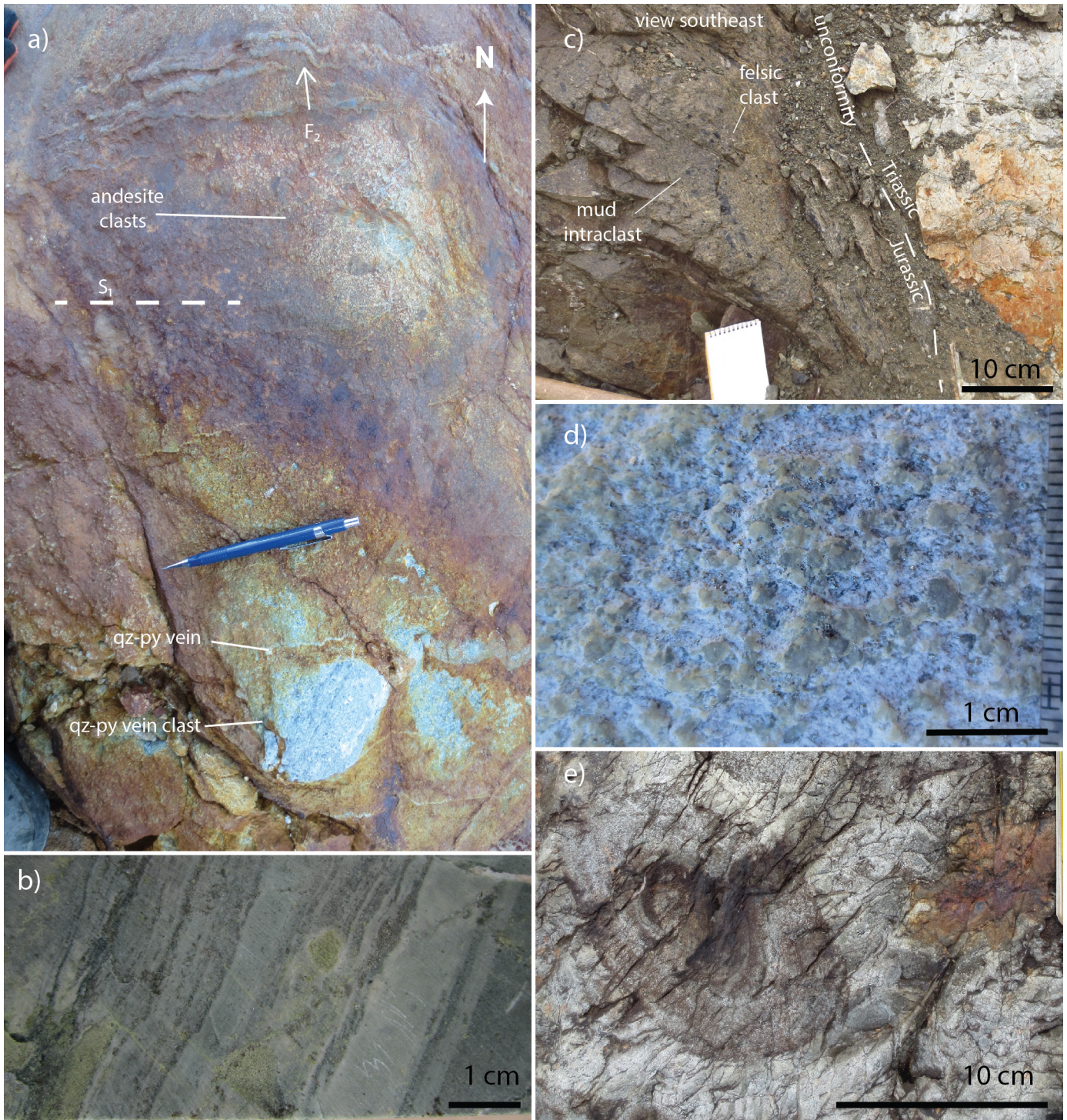


Fig. 6. Mitchell zone and surrounding area rocks. **a)** Jack Formation conglomeratic sandstone in the Snowfield zone with andesite and quartz-pyrite vein clasts. S_1 and veins folded by F_2 , 424583 E, 6264244 N. **b)** Pale Stuhini Group felsic ash tuff interbedded with siltstone (drill core, M-07-42, 348.7 m). **c)** Jack Formation conglomerate contains felsic flow breccia clasts derived from subjacent Stuhini Group, 421431 E, 6266817 N. **d)** Phyllic- and clay-altered Jack Formation feldspathic sandstone of the Mitchell zone, 424861 E 6265572 N. **e)** Elliptical concretionary structure in Jack Formation sandstone with concentric banding defined by albite-chlorite-chalcopyrite-pyrite, 424475 E 6266436 N.

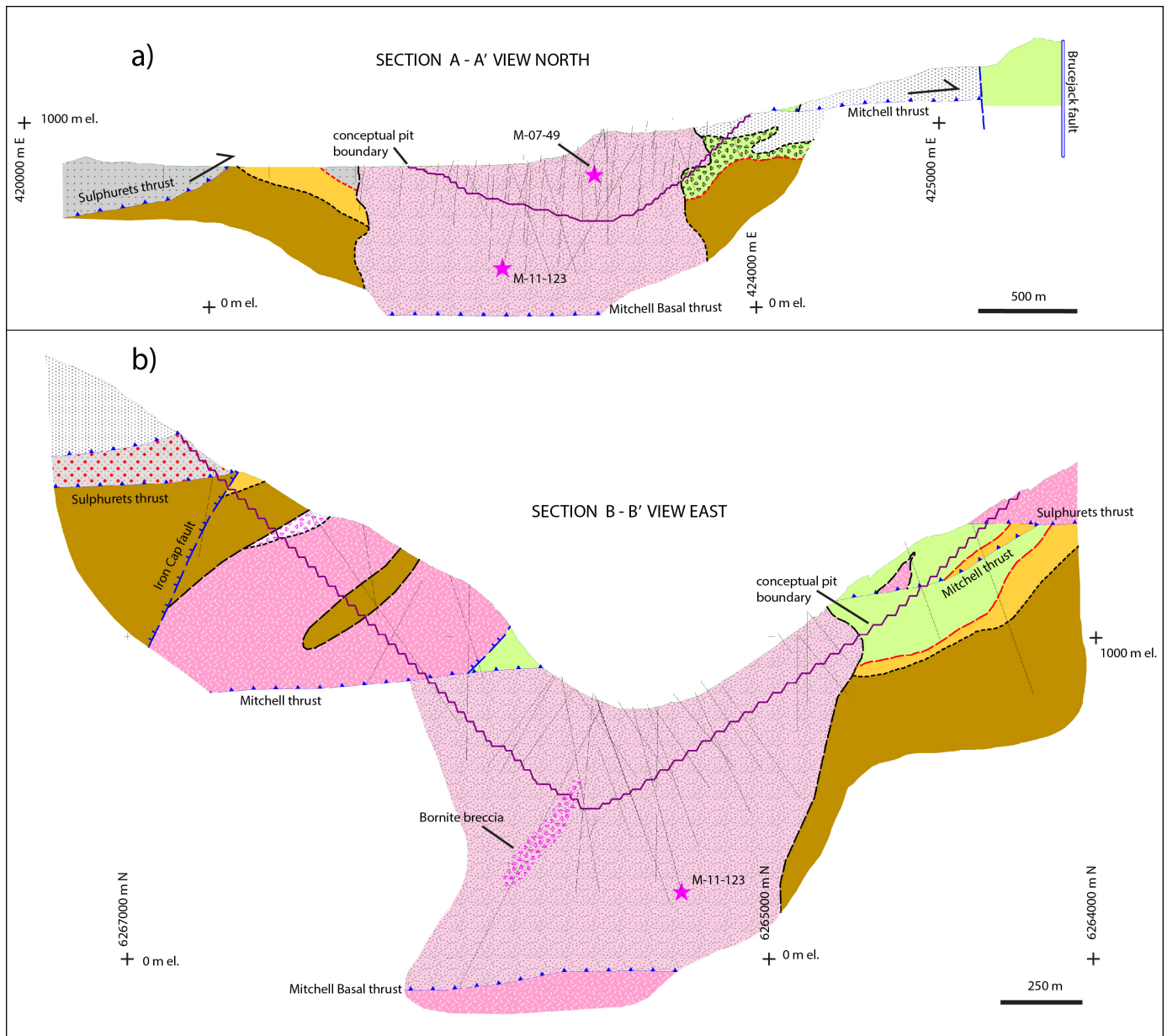


Fig. 7. Cross sections across KSM property (see Fig. 3 for locations): **a)** A-A' east-west, **b)** B-B' north-south. For lithology legend, refer to Figure 4.

4.1.2. Hazelton Group (Late Triassic to Middle Jurassic)

Beneath the Mitchell thrust fault east of the Mitchell deposit (Fig. 8), the Jack Formation is represented by a unit of massive feldspathic sandstone (Fig. 6d). The sandstone contains 10-45% quartz and 50-70% feldspar and is typically very fine grained to fine grained, but with rare granule fragments. The unit is 300 m to 1 km thick and has gradational contacts with conglomerate and andesite lapilli tuff. Rarely, the sandstones contain lenses of conglomerate up to 10 m thick with felsic volcanic, black chert and intermediate volcanic clasts in a sandstone matrix. In the northeastern Mitchell zone, bedding in the lower part of the sandstone unit is locally defined by high concentrations of concretionary structures with concentric

bands of chalcopyrite-pyrite-chlorite-albite (Fig. 6e). Some concretions contain small amounts of carbonate. The intensity of hydrothermal minerals in concretionary structures relates to intensity of pervasive and mottled chalcopyrite-pyrite-chlorite-albite in sandstone and to the proximity to Sulphurets dikes. If the concretionary structures are a product of diagenesis that contained carbonate cement, then mineralization post-dates both sandstone deposition and diagenesis.

Jack Formation sandstone is intruded by pre- to post-mineral Sulphurets diorite and is intensely altered to albite, quartz-sericite-pyrite and muscovite-illite in all outcrops beneath the Mitchell thrust fault. Alteration is characterized by partial to complete replacement of feldspar and interstitial carbonate by

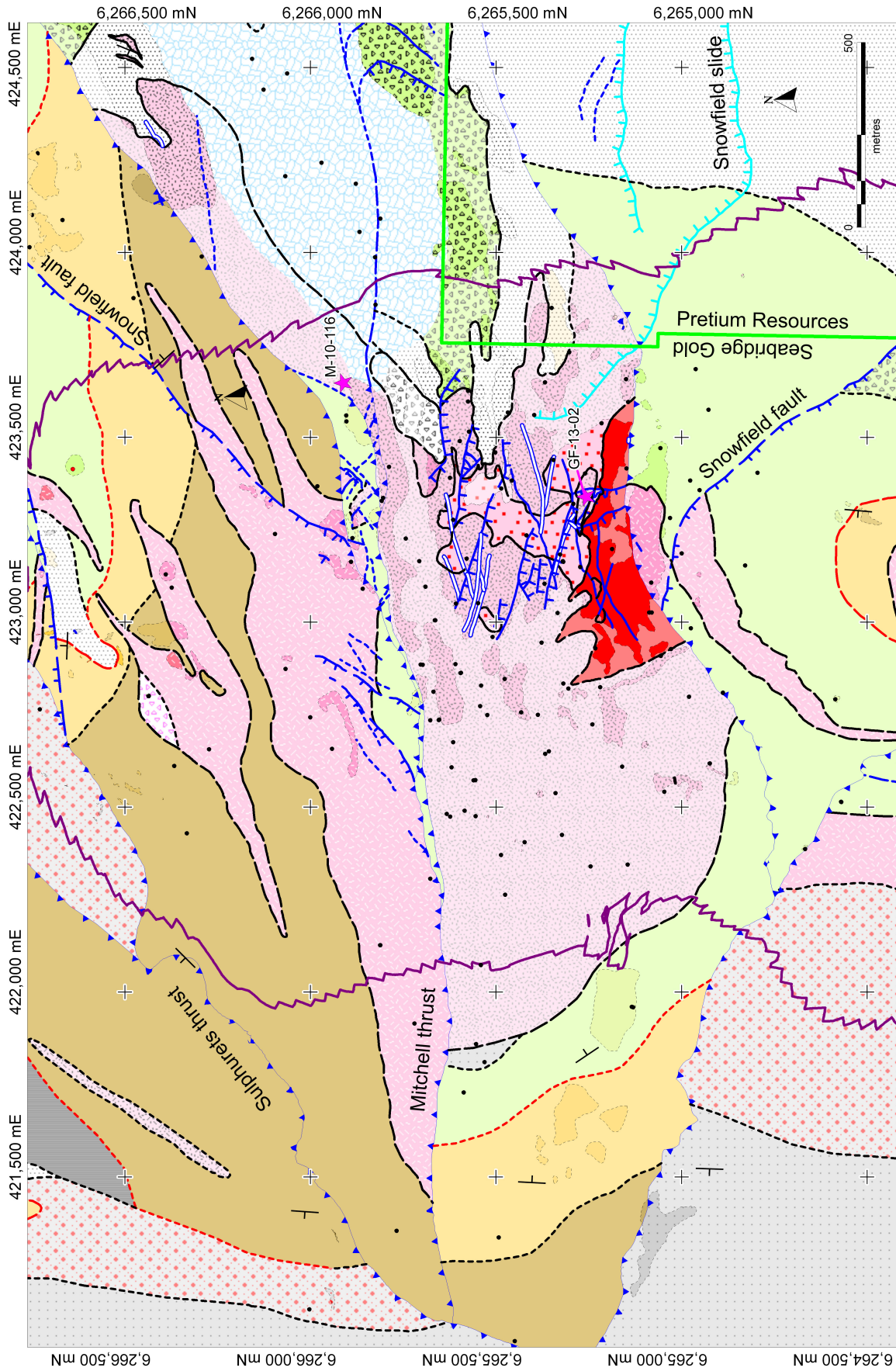


Fig. 8. Geology of the Mitchell zone and surrounding area. Geochronologic sample GF-13-02 from outcrop, M-10-116 from drill core. For legend, refer to Figure 4.

hydrothermal minerals. Quartz grains in altered sandstone are subrounded to angular and fractures in grains are commonly filled with pyrite and chalcopyrite.

Andesite volcanic rocks in the Mitchell zone outcrop beneath the Mitchell thrust fault east of the Mitchell intrusions (Fig. 8). They comprise three general types that are broadly laterally equivalent: 1) lapilli-sized breccia; 2) tuff-breccia; and 3) feldspar-phyric flows. The breccias are well sorted, massive, and contain abundant (60-85%) 1-2 cm porphyritic juvenile clasts with aspect ratios that range from 1:1 to 2:1 (Fig. 9a). Clast sizes tend to be uniform within individual layers, and many of the clasts have concavo-convex shapes and margins with flame-like projections. The breccias interfinger with sandstone layers and locally contain a sandstone matrix. The deposits are interpreted to record subaqueous phreatomagmatic volcanic eruptions, as indicated by the porphyritic textures and irregular clast boundaries, coeval with sandstone sedimentation. Andesite tuff breccia deposits contain poorly sorted, 50-80%, angular, porphyritic clasts that range from ~1 cm to more than 1 m in a massive tuffaceous matrix (Fig. 9b). They display local stratification and rare sigmoidal shaped fiamme fragments. Fragments typically have aspect ratios of 1:1 to 5:1. Sections with >1 m clast sizes are interpreted to be near-vent deposits. The deposits are interpreted to be block and ash flows due to their poor sorting, tuffaceous matrix and the angular, large monolithic andesite clasts.

Andesite flows and flow breccias outcrop in the most easterly Mitchell zone beneath the Mitchell thrust and west of the Brucejack fault (Fig. 8), where they probably represent the highest parts of the section. Fine-grained plagioclase-hornblende-phyric flows near the sandstone contact grade into overlying crowded, coarse-grained (up to 1 cm), feldspar-phyric flows. A lava tube, ca. 2 m in diameter, outcrops in the transition between fine- and coarse-grained intermediate flow sequences. The tube is defined by concentric flow banding that is truncated by a subhorizontal erosional surface and overlain locally by a coherent andesite flow and flow breccia (Fig. 9c).

The andesites host stockwork and disseminated mineralization and are cut by Sulphurets suite diorite intrusions. The andesites are interpreted to be coeval with the Premier suite intrusions because: 1) of their stratigraphic position within the basal Hazelton Group; 2) of their spatial association with Premier intrusions; and 3) at Snowfield they contain hypabyssal syenite clasts with a pink K-feldspar matrix (J. Nelson, pers. comm., 2013). Above the Mitchell thrust, offset equivalents of the andesite strata of the Mitchell zone are locally cut by Premier suite syenite and monzonite in drill core and Sulphurets suite diorite in outcrop (Fig. 8).

4.1.3. Premier intrusive suite

Premier suite intrusions outcrop in the immediate hanging wall of the Mitchell thrust fault (Figs. 8, 7b). Premier suite plutons are characteristically phaneritic with crowded oscillatory zoned plagioclase and common pink or maroon K-feldspar phenocrysts (Figs. 10a, b). Dioritic varieties are

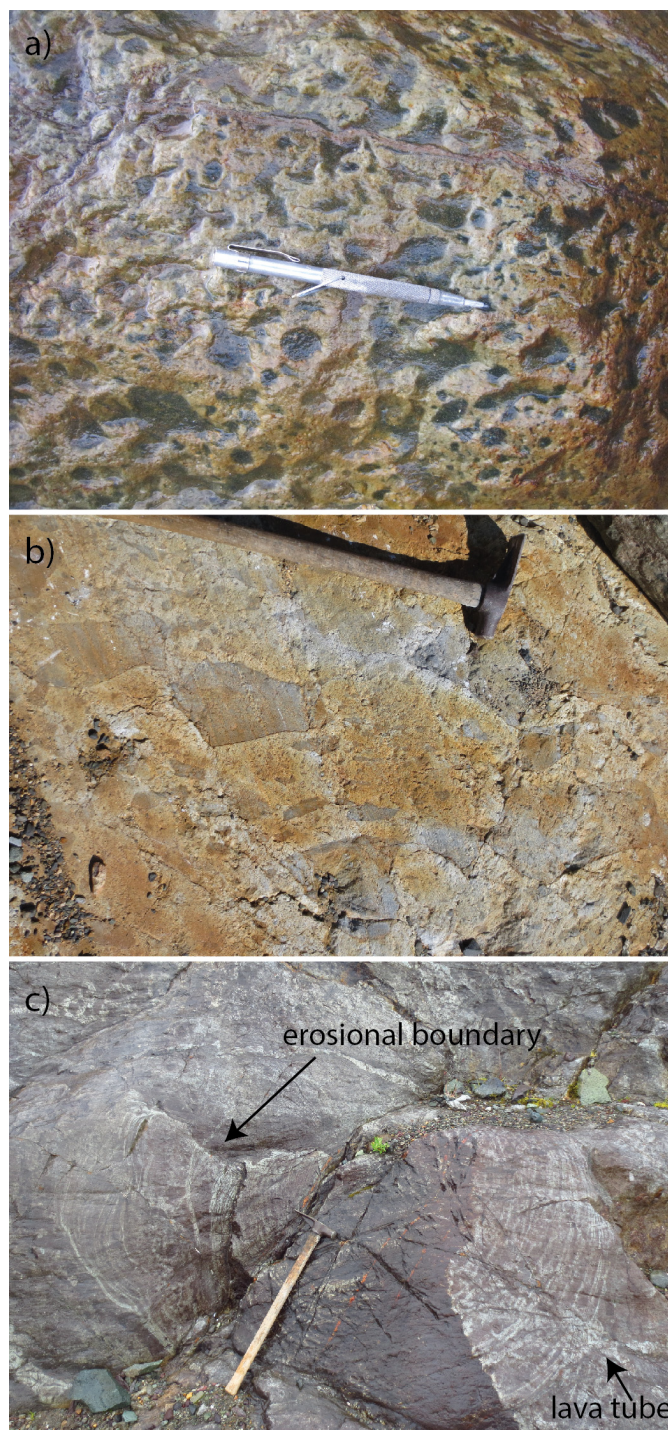


Fig. 9. Mitchell zone Jack Formation andesite. **a)** Chlorite and quartz altered phreatomagmatic andesite lapilli tuff, 424000 E, 6265584 N. **b)** Andesite block breccia, 424950 E, 6265755 N. **c)** Lava tube with concentric bands cut by overlying andesite flow breccia, 424874 E, 6266646 N.

crowded biotite-pyroxene-hornblende-plagioclase phyric, medium- to coarse-grained porphyries that outcrop in the southwestern Mitchell valley above the Sulphurets thrust fault (Fig. 3). Monzonite varieties are commonly coarse grained, crowded with oscillatory zoned plagioclase, pink K-feldspar

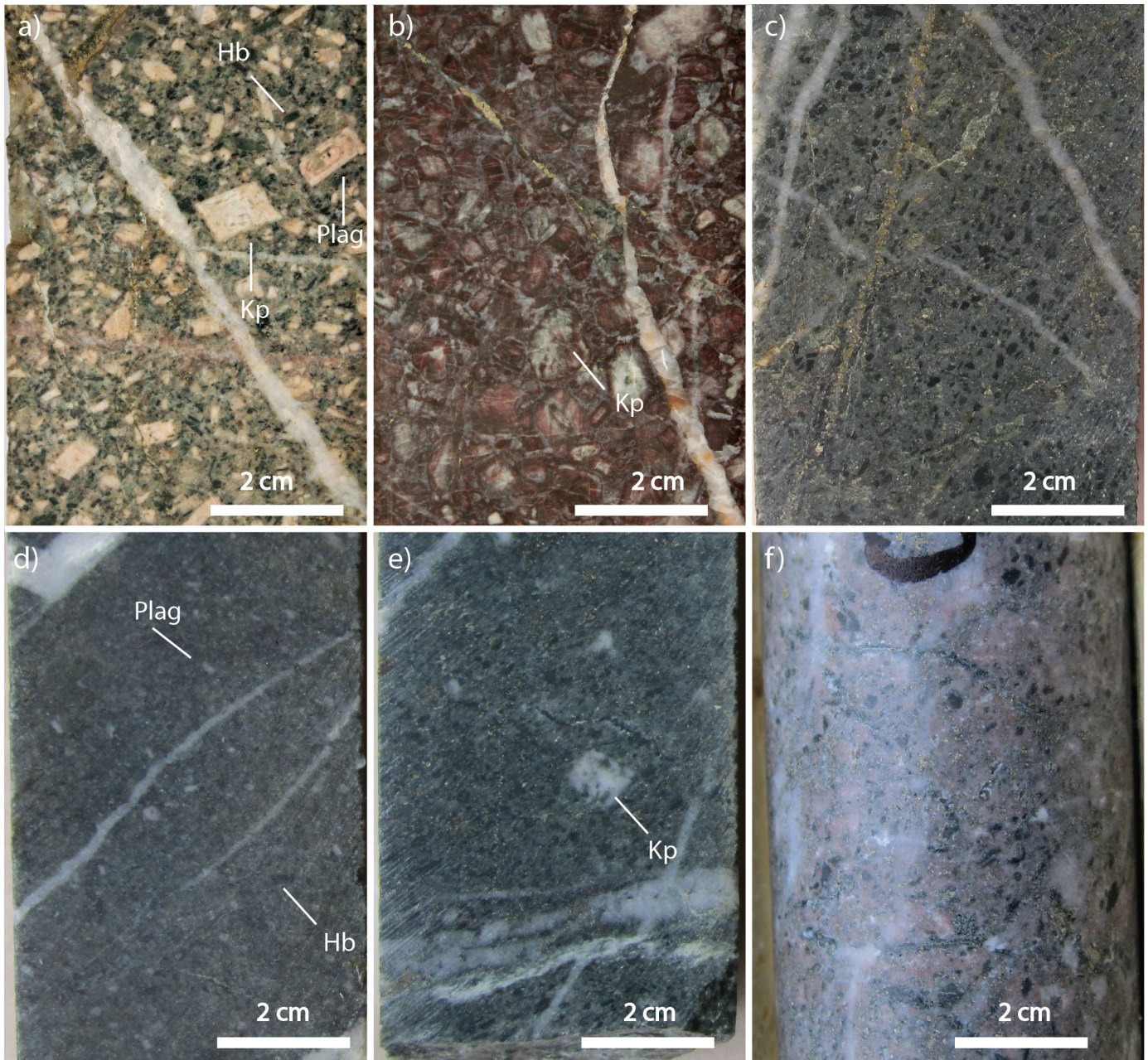


Fig. 10. Mitchell intrusions; Premier and Sulphurets suites (Jurassic). **a)** Premier suite; coarse-grained, crowded monzonite porphyry. Hb- hornblende; Plag- plagioclase; Kp- K-feldspar. Drill core M-06-23, 54 m. **b)** Premier suite; red hematite dusted coarse-grained, syenite. Plag- plagioclase; Kp- K-feldspar. Drill core M-12-129, 895 m. **c)** Sulphurets suite; Phase 1 diorite with chloritized hornblende and plagioclase phenocrysts. Drill core M-07-58, 690.5m. **d)** Sulphurets suite; Phase 1 medium-grained diorite; Hb- hornblende; Plag- plagioclase. Drill core M-07-42, 50 m. **e)** Sulphurets suite; Phase 1 bimodal porphyry diorite contains 1% coarse-grained K-feldspar (Kp) phenocrysts in a hornblende-plagioclase, medium-grained diorite porphyry. Drill core M-07-25, 456.6m. **f)** Phase 1 diorite with k-feldspar-altered groundmass and chlorite-altered mafic phenocrysts. Drill core M-11-126, 336.5 m.

phenocrysts up to 2 cm, hornblende up to 1 cm, biotite and trace quartz phenocrysts (Fig. 10a). Syenitic varieties (Fig. 10b) are commonly maroon to red, contain from 40-65% perthitic K-feldspar phenocrysts, oscillatory zoned plagioclase phenocrysts, local quartz phenocrysts, and lack mafic primary minerals (Kirkham, 1963; Simpson, 1983).

4.1.4. Sulphurets intrusive suite and related breccia bodies

Sulphurets suite plutons in the Mitchell deposit are diorite in composition. Compared to the Premier suite diorite, they are more uniform in texture and composition, and are notably finer grained and less crowded (Figs. 10c-d). Based on field observations, we distinguish three phases of diorite. Phase 1 includes diorite in contact with country rock and Phase 2 is a

plug that crosscuts Phase 1 rocks and contains quartz-pyrite-chalcopyrite veins as xenoliths. A breccia body and small breccia dikes cut Phase 2 rocks but are cut by a small Phase 3 plug.

4.1.4.1. Phase 1 diorite

Phase 1 diorite is the most voluminous of the three Sulphurets intrusions. It cuts bedded sedimentary rocks of the Stuhini Group and both cuts and interfingers with Jack Formation sandstone and andesite breccia (Fig. 8). The margins of the diorite contain xenoliths of sedimentary rocks. The country rock adjacent to the intrusions has albite alteration and local skarn alteration mineralogy (see below). Phase 1 diorite is a partial host to the high quartz zone (Fig. 8) near the southern contact area and is interpreted to have been emplaced prior to or possibly synchronous with the high quartz zone that is cut by Phase 2 diorite. (Fig. 8). Phase 1 diorite is remarkably homogeneous in composition and texture and is characterized by partial to complete hydrothermal replacement of plagioclase and replacement of hornblende phenocrysts (Figs. 10c, e, f). A narrow diorite sill intersected in drill core along the western margin of the Mitchell zone is relatively unaltered and provides primary texture information (Fig. 10d). This sill contains 20-30% plagioclase (An_{10} - An_{20}) phenocrysts (up to 3 mm) 1-10% K-feldspar (up to 1 mm), 5% hornblende phenocrysts (up to 3 mm), trace biotite (ca. 1 mm) and trace apatite. At depth, diorite contains up to 1% K-feldspar oikocrysts 1-1.5 cm in diameter in local coarser intervals (Fig. 10e). Inclusions in the K-feldspar oikocryst include 20% anorthite, 5% hornblende, 1% clinopyroxene and trace garnet. Where Phase 1 diorite is cut by veins with relatively sharp boundaries, we infer emplacement before mineralization. Where mineralized veins in the diorite are disarticulated, fluidal shaped, and irregular, which suggests incomplete diorite crystallization, we infer synmineralization emplacement.

4.1.4.2. Phase 2 diorite

The Phase 2 intramineral diorite plug contains quartz vein xenoliths, cuts Phase 1 diorite and the high quartz zone (Fig. 11a) and occupies the core of the deposit (Fig. 8). It is distinguished on surface by a contact breccia, sparser (10-20%) quartz veins than Phase 1, and uniformly high concentrations of quartz vein xenoliths (Fig. 11b). Contacts between Phase 1 and Phase 2 are most clearly identified where Phase 2 rocks cut the high quartz zone, with quartz zone xenoliths in the contact breccia (Fig. 11a) and by internally stockworked Phase 1 diorite xenoliths (Fig. 11c). Elsewhere, contacts are inferred by transitions from higher to lower quartz stockwork coupled with an increase in quartz vein xenoliths.

4.1.4.3. Diatreme breccia

A ca. 100 x 300 m, northeast-trending complex breccia body interpreted to be the root zone of a diatreme breccia, outcrops in the northeastern Mitchell zone (Fig. 8). It cuts Phase 2 diorite on its southern margin, and cuts sandstone and andesite on its

southeastern margin, but is cut by Phase 3 diorite at its western margin where indistinct boundaries to xenoliths of the diatreme within Phase 3 diorite are interpreted to indicate an unlifted breccia at the time of Phase 3 magmatism (Fig. 11d). On the west, clast sizes are up to 20 cm in diameter, on the east clasts are generally <2 cm across. Clasts include: 1) andesite volcanic fragments that are 1-2 cm in diameter, fine-grained, porphyritic, and angular (Figs. 12a, b); 2) quartz-rich sandstones that are subrounded and <3 mm in diameter; 3) porphyritic diorite(?), that display amoeboid shapes and 2-6 cm in diameter; 4) quartz-pyrite±chalcopyrite veins, 0.5-3 cm in diameter (Fig. 12b); and 5) mineralized quartz stockworked diorite (Fig. 12a) that are subrounded and 2-20 cm in diameter. Concentrations of quartz stockworked diorite clasts can make up 80% of the rock in the western 'bone breccia' outcrop (Fig. 12a; see also Fig. 20 in Kyba and Nelson, 2014) but decrease eastward. Clasts of andesite or diorite are flattened to form local banding that is at an angle to the overprinting pervasive foliation (Fig. 12b). The breccia is overprinted by 1-5% quartz-chalcopyrite-molybdenite stockwork. Late quartz-pyrite stringers with tourmaline alteration halos are common, and tourmaline is locally in the groundmass. The groundmass displays weak chlorite and sericitic alteration, but subtle porphyritic textures in thin section suggest a magmatic origin.

We interpret that the breccia formed as a subvertical diatreme pipe that now plunges steeply to the west, and that the eastward decrease in clast sizes reflects increasing distance from source rocks. Cross-cutting relationships suggest that the pipe was emplaced during the waning stages of Phase 2 plutonism, and/or the early stages of Phase 3 plutonism. Emplacement of the diatreme pipe coincided with the waning of latest molybdenite-rich, porphyry-type mineralization and cessation of stockwork veining. The quartz stockwork dense 'bone breccia' outcrop is interpreted to be an intact root zone to the diatreme breccia that is penetrated by intrusion breccia dikes (see also Nelson and Kyba, 2014).

4.1.4.4. Intrusion breccia dikes

Small (20-50 cm wide; 2-20 m long) intrusion breccia dikes cut sandstone, Phase 1 and 2 diorite, and the diatreme breccia and they are cut by Phase 3 diorite. The dikes are distributed about the margins of and emanate from, Phase 3 diorite. Boundaries are commonly sharp and irregular, and dike traces anastomose. Where dikes cut sandstone, clasts of chert, rounded siliceous pebbles and angular mineralized quartz veins are in a tourmalinized porphyritic groundmass (Fig. 13c). Where dikes cut the diorite, clasts are predominantly quartz vein fragments and quartz stockworked diorite fragments. Where dikes cut the diatreme breccia, they contain clasts of quartz stockworked diorite, angular diorite(?) porphyry, and quartz veins in a tourmalinized groundmass. The clast compositions in these three examples appear to directly reflect cannibalization of the host lithologies. Breccia dikes are cut by pyrite-quartz veins with tourmaline halos and tourmaline is commonly observed in the groundmass of the dikes (Fig. 13c). A particularly notable

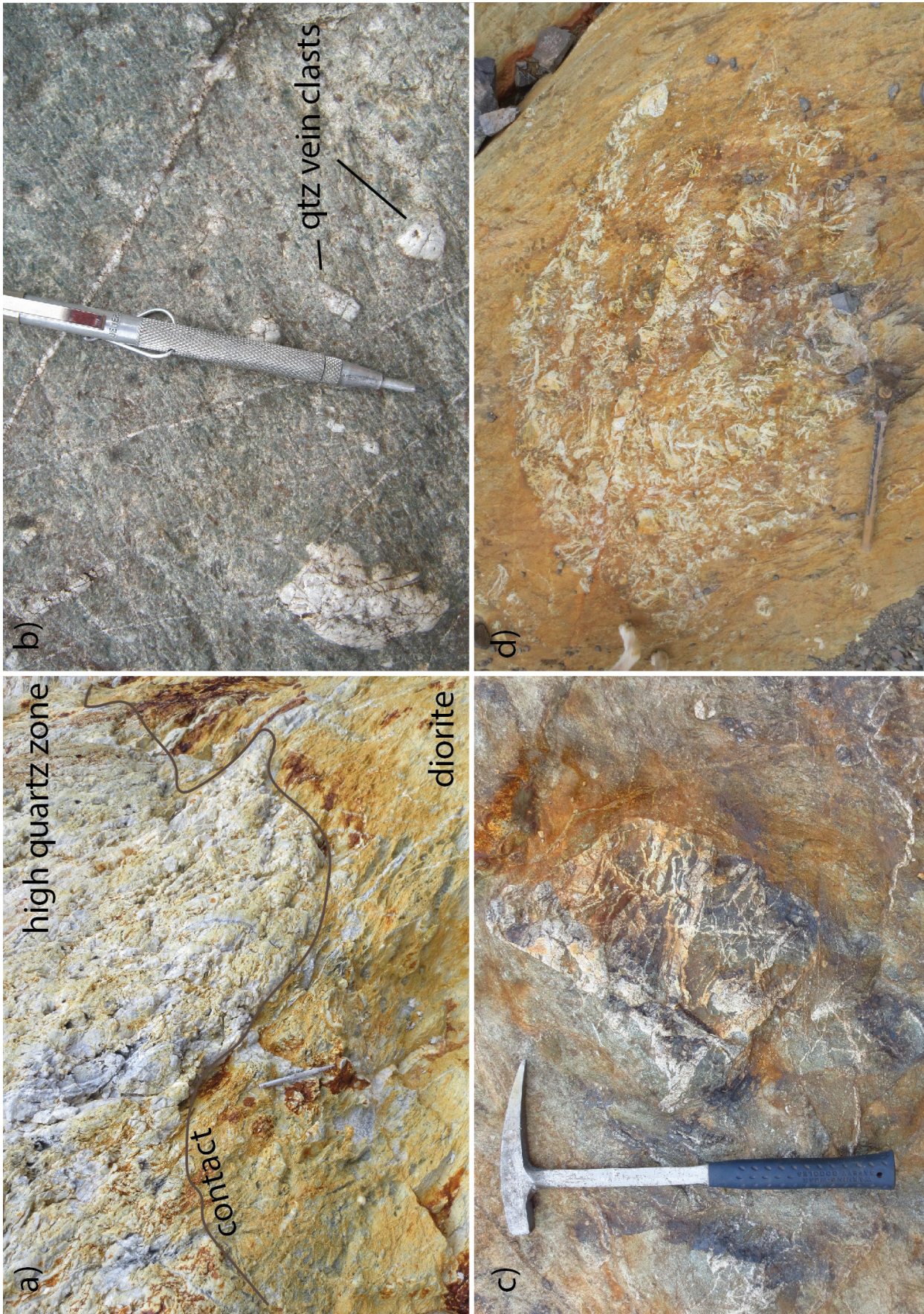


Fig. 11. Sulphurets suite diorite breccia. **a)** Contact between Phase 2 phyllic altered diorite and high quartz zone, 423353 E, 6265193 N. **b)** Angular quartz vein xenoliths in Phase 2 diorite, 422958 E, 6265505 N. **c)** Xenolith of Phase 1 diorite (with internal quartz stockwork veins abruptly truncated at clast boundary) in Phase 2 diorite, 423300 E, 6265575 N. **d)** Clast of diatreme breccia in Phase 3 diorite, 423391 E, 6265661 N.

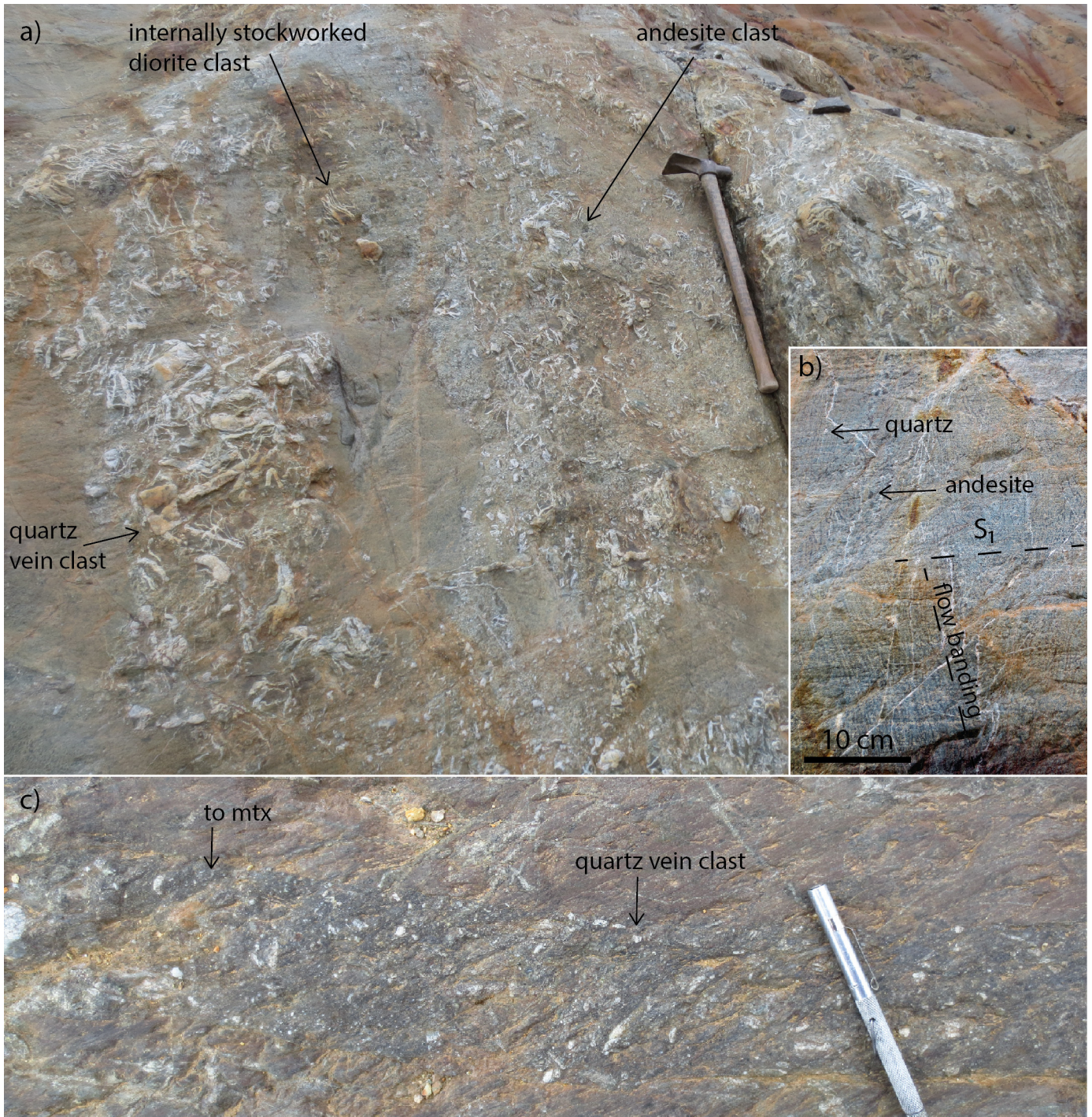


Fig. 12. Diatreme breccia and intrusion breccia dike in outcrop. **a)** Dense internally stockworked diorite clasts, quartz vein and andesite fragments 423469 E, 6265628 N. **b)** Irregular flow banding in the diatreme breccia is locally at a high angle to steeply dipping main cleavage (S_1), 423511 E, 6265640 N. **c)** Intrusion breccia dike with tourmalinized groundmass, containing quartz-chalcopryrite-pyrite vein clasts, 423575 E, 6265533 N.

3 m thick breccia dike that intrudes the diatreme breccia is cut by Phase 3 diorite. The breccia dikes are interpreted to have been emplaced during the early stages of Phase 3 diorite intrusion as they emanate from the Phase 3 plug and are locally cut by it.

4.1.4.5. Phase 3 diorite

A small (50 x 125 m) plug of Phase 3 diorite cuts the western end of the diatreme breccia (Fig. 8) and intrusion breccia dikes, and is overprinted only by minor quartz-pyrite-tourmaline stringers. The plug is most easily distinguished by a near lack (<1%) of quartz veins, and by abundant clasts of quartz

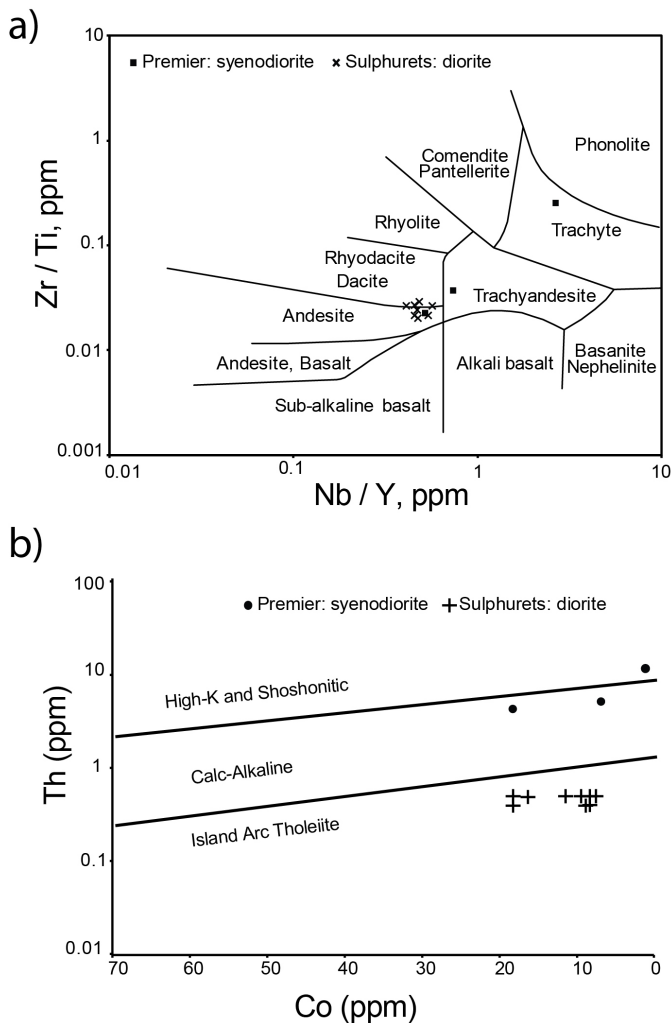


Fig. 13. Geochemistry of the Mitchell intrusions (Premier and Sulphurets suites). **a)** Zr/Ti vs Nb/Y diagram (Winchester and Floyd, 1977) and **b)** Th vs Co diagram (Hastie et al., 2007).

stockworked diorite (up to 20 cm), clasts of diatreme breccia (>1 m, Fig. 11c) and clasts of breccia dikes. The plug is assigned intermineral status because it post-dates Stage 2 stockwork and pre-dates Stage 3 pyrite stringers described below.

4.2. Geochemistry of the Premier and Sulphurets intrusions

On plots of immobile elements (Fig. 13a), most intrusions of the Mitchell deposit plot in the andesite (diorite) field, although some plugs border the dacite (monzonite) field. Compositions of the Premier and Sulphurets suites are comparable, although the younger phases of Premier magmatism trend toward the trachyte (syenite) fields. Kirkham (1963) attributed this compositional differentiation to fractional crystallization, with composite intrusions resulting from progressive crystallization from diorite to monzonite to syenite over time. The Premier and Sulphurets suites display separate trend lines on a Co versus Th plot (Fig. 13b), which shows the Premier to be more alkaline. Overlapping crystallization ages of the Premier and Sulphurets suites (Table 1) suggest that they may have been emplaced in separate but kindred crustal chambers.

4.3. Alteration

Adopting the alteration scheme developed for the Snowfield deposit by Margolis (1993), we recognize three stages of alteration in the Mitchell deposit (Table 2).

4.3.1. Stage 1

Stage 1 potassic alteration is characterized by equigranular textures and a simpler, less dense quartz vein stockwork in the western Mitchell zone (Fig. 14) and in the central, deeper regions of the drilled extents of the Mitchell intrusion. Secondary biotite, K-feldspar (Fig. 10f), magnetite, albite, anhydrite, chlorite, phengite are commonly preserved. The potassic assemblage transitions laterally and upwards (into stratified wall rocks) to transitional potassic, a calcite-epidote-chlorite distal propylitic (Fig. 6b) and hornfels alteration that contains epidote, albite, cordierite and carbonates, and quartz veins diminish in volume. The transitional potassic alteration (Fig. 14), characterized by quartz, chlorite, anhydrite, magnetite, biotite and several episodes of quartz stockwork veins, is outboard of the core potassic alteration zone and inboard of the propylitic zone. Here, fine, shreddy textures and rutile inclusions commonly observed in chlorite suggest that chlorite replaces some of the secondary biotite. Local zones of skarn mineral assemblages, including magnetite, diopside, zoisite, garnet and epidote occur, farther outboard in the hornfelsed host rocks.

Table 2. Summary of mineralization, alteration, vein and plutonic stages and phases.

Stage	Plutonism	Alteration	Mineralization	Veins	Age
1	Phase 1	potassic, transitional potassic, propylitic, albitic	Cu-Au core zone	5-95% by volume quartz-pyrite-chalcopyrite veining, sheeted high quartz zone	196.0 ± 2.9 Ma - 190.3 ± 0.8 Ma
2	Phase 2	phyllic	Mo envelope, additional Cu-Au	<10% by volume quartz-pyrite-chalcopyrite-molybdenite veining	190.3 ± 0.8 Ma
3	Phase 3	advanced argillic	n/a	massive pyrite veins	<190.3 ± 0.8 Ma
4	n/a	n/a	high grade Au-Ag-Cu-Pb-Zn	epithermal	185(?) Ma

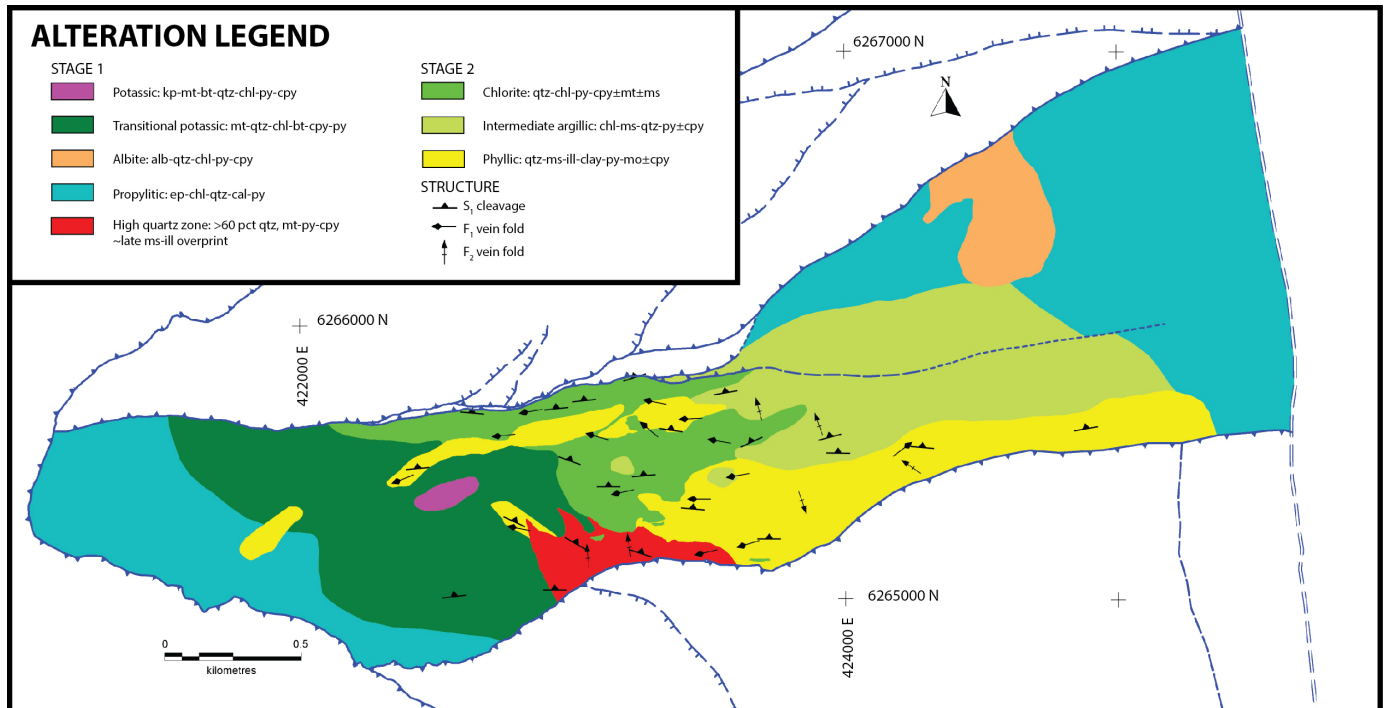


Fig. 14. Alteration map for the Mitchell zone. Alteration above the Mitchell thrust fault is not plotted.

4.3.2. Stage 2

Secondary phyllic alteration overprints the primary alteration (Fig. 14) and consists of quartz, sericite, illite, and chlorite accompanied by quartz stockwork veins (Figs. 9b, 11a). The degree of overprint ranges from spaced, metre scale, fracture-controlled replacement in deeper regions of the porphyry (observed in drill core), to pervasive overprint in the eastern and upper levels of the deposit. Intense phyllic alteration in the eastern Mitchell zone is defined by bleached to pale grey or yellow rocks entirely lacking in mafic minerals and magnetite (Fig. 6d).

4.3.3. Stage 3

Stage 3 advanced argillic alteration includes kaolinite, pyrophyllite and rutile in southeastern Mitchell zone. High pyrite concentrations are spatially associated with this alteration type, but lack significant gold and copper mineralization.

4.4. Vein paragenesis

Adopting the vein paragenesis scheme developed for the Snowfield deposit by Margolis (1993), Stage 1 veins comprise mm- to cm-scale stockwork to sheeted veins (Figs. 15a-c) that make up 5-95% of the host rock and are composed of chalcopyrite-pyrite-quartz±magnetite±K-feldspar±chlorite. The high quartz zone, formed during Stage 1, is characterized by 1-2 cm thick, sheeted quartz veins that strike east-northeast and dip steeply to the north (Fig. 15b). The high quartz zone is tabular in shape and grades into lower quartz vein abundance stockwork to the west. To the north, the high quartz zone is cut by Phase 2 diorite. In general, Stage 1 veins have uniform

mineralogy, lack alteration halos (Fig. 15c) and are part of a protracted stockwork event that overlapped with emplacement of Phase 1 diorite. At deeper levels Stage 1 stockwork displays diffuse boundaries and contain more magnetite and K-feldspar but are interpreted to be part of the same progressive stockwork event that is responsible for the vast majority of veins in the deposit. Stage 1 veins are temporally associated with early potassic and propylitic alterations (Margolis, 1993).

Stage 2 molybdenite-rich vein and stockwork bodies are distributed in a halo about the core copper-gold mineralized zone and are composed of quartz-pyrite-molybdenite±chalcopyrite±chlorite±sericite±fluorite±anhydrite. The veins are more typically stockwork-style and are not sheeted in the Mitchell zone. Molybdenite-bearing veins (Fig. 15d) are generally associated with smaller volumes of quartz veins compared to Stage 1 veins. Stage 2 veins are spatially distributed with phyllic alteration assemblages (Fig. 14). A bornite-bearing hydrothermal stockwork and breccia body intersected in drill core (Fig. 7b) is interpreted as Stage 2. The breccia body overprints Stage 1 stockwork and is cut by Stage 3 pyrite veins and a late, narrow diorite sill interpreted as Phase 3. The bornite breccia is interpreted to be up to ca. 100 m thick tabular to pipe-like body that plunges steeply to the north. Contact margins of the breccia contain clasts of Phase 1 quartz stockwork and diorite, and the core areas contain banded, stockwork and breccia textures with clasts and matrix composed of hydrothermal gangue and sulphide minerals. Clasts in the breccia are commonly lenticular and irregular and are interpreted to have been coeval with the matrix because the mineralogy of both is comparable. X-ray diffraction determinations of gangue and

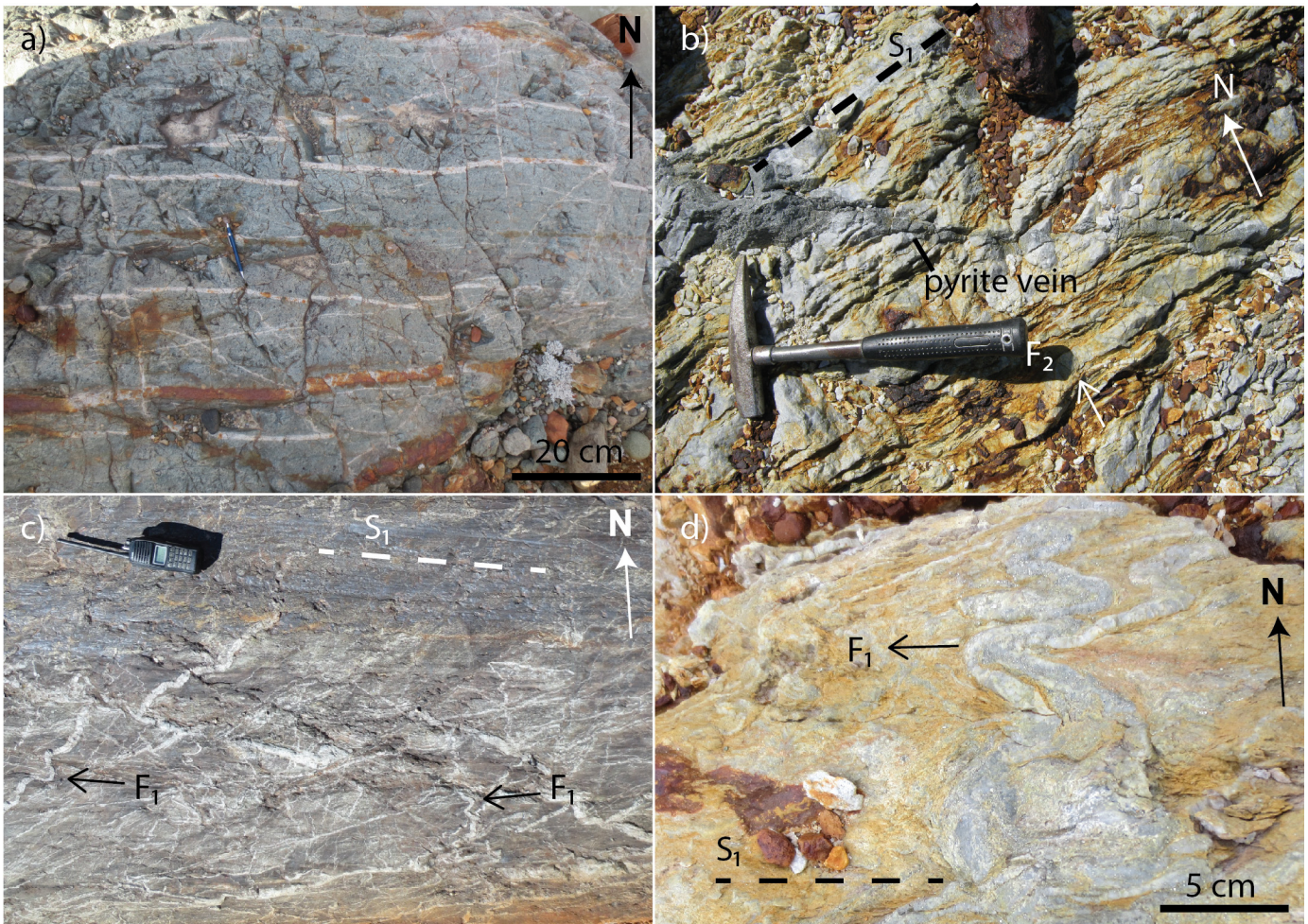


Fig. 15. Quartz stockwork and vein fold geometry in the Mitchell zone. **a)** Planar Stage 1 quartz-K-feldspar-magnetite-chalcopyrite veins in potassic altered diorite, 422532 E, 6265370 N. **b)** Sheeted Stage 1 veins of the high quartz zone parallel main cleavage (S_1) with cross cutting Stage 3 related pyrite vein, 423150 E, 6265155 N. **c)** Open F_1 folded quartz veins in chlorite-quartz altered sandstone formed during the first phase of deformation, 423493 E, 6265539 N. **d)** Tight to isoclinal folded molybdenite-quartz veins and related pervasive cleavage formed in intense phyllic altered rocks during the first phase of deformation (F_1, S_1), 423832 E, 6265290 N.

sulphide mineralogy in the breccia indicates: quartz, anhydrite, fluorite, calcite, gypsum, muscovite, illite, apatite, anatase, albite and chlorite together with pyrite, chalcopyrite, bornite, molybdenite, tennantite, enargite, sphalerite and traces of magnetite. The bornite breccia body preserves all four stages of mineralization with Stage 1 stockwork preceding breccia emplacement, and Stage 3 and Stage 4 veins and breccias cutting the body. Bornite and molybdenite disseminations in the same veins suggest that the bornite breccia is temporally associated with Stage 2 molybdenite mineralization. Anhydrite-fluorite-bornite-chalcopyrite assemblages in the bornite body also resemble the Stage 2 molybdenite veins peripheral to the core zone, which contain anhydrite and fluorite.

Stage 3 massive pyrite veins cut all phases of diorite, Stage 2 molybdenite veins, the high quartz zone (Fig. 15b) and the bornite breccia. Massive pyrite veins in the Mitchell zone are 1 mm to 3 cm wide and contain 60-95% medium- to coarse-pyrite grains. Gangue minerals are commonly quartz and muscovite that, together with disseminated pyrite, extend into

the country rock as a halo to the vein. Pyrite contains small inclusions of sphalerite, galena, chalcopyrite and tennantite. Margolis (1993) interpreted massive pyrite veins to be related to acid-sulphate style advanced-argillic alteration in the eastern Mitchell zone and the Snowfield gold zone. The late timing of our Stage 3 veins is consistent with this interpretation.

Stage 4 high-grade gold veins contain quartz, barite, calcite, and manganian calcite gangue minerals, with banded sulphides that include galena, sphalerite, tetrahedrite, electrum and tennantite. Stage 4 veins cut sandstone in the eastern part of the deposit, the bornite breccia and Stage 3 massive pyrite veins. Veins display sharp margins and euhedral to banded textures consistent with an epithermal origin. Minor bornite mineralization in Stage 4 veins that cut the bornite body is interpreted to have been remobilized during veining.

4.5. Mineralization

Most of the disseminated and vein-controlled copper and gold mineralization is related to Stage 1 alteration and Phase 1

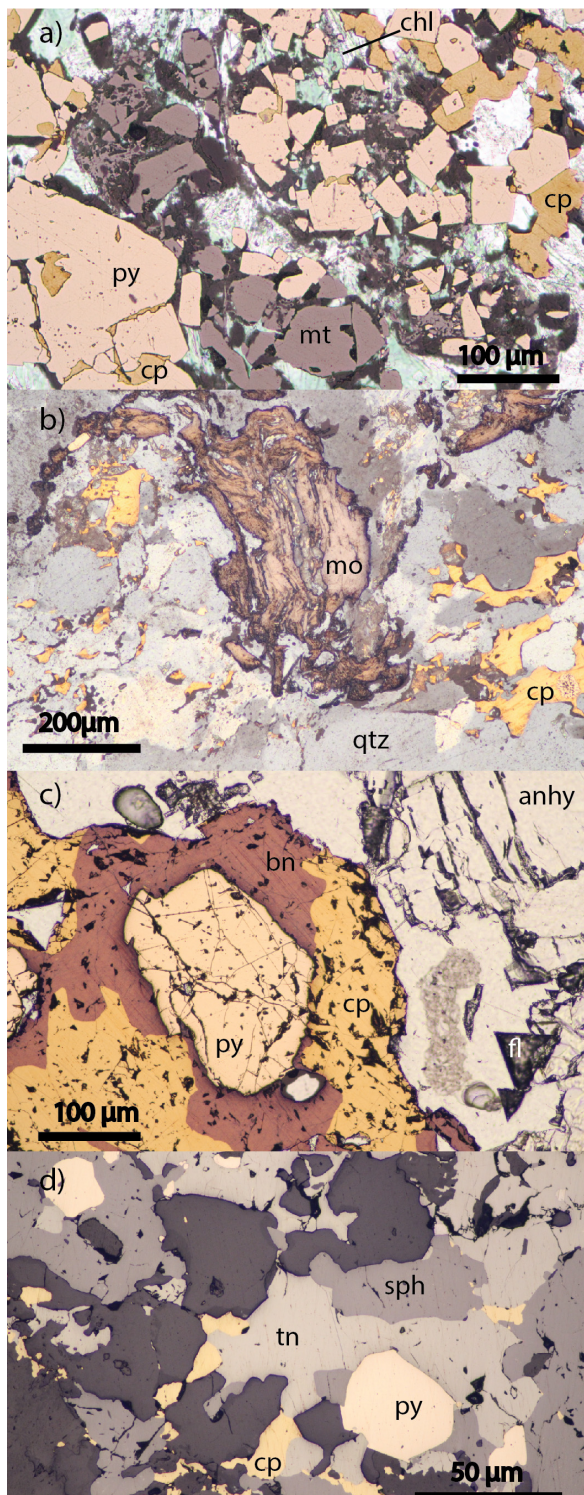


Fig. 16. Microtextures of chalcopyrite mineralization. **a)** Stage 1 cp: chalcopyrite with mt: magnetite and chl: chlorite replaces pyrite, reflected and plane polarized light, M-07-55, 255 m. **b)** Stage 2 mo: molybdenite and cp: chalcopyrite in quartz vein, reflected and cross polarized light M-08-70, 329 m. **c)** bn: bornite and cp: chalcopyrite replace py: pyrite and are spatially associated with anhy: anhydrite and fl: fluorite, reflected and plane polarized light, M-08-67, 251.3 m. **d)** Early py: pyrite is partially replaced by cp: chalcopyrite-sph: sphalerite-tn: tennantite in Stage 4 barite-quartz vein, reflected light, M-07-26, 212.6 m.

diorite plutonism. Chalcopyrite rims and replaces pyrite, occurs as inclusions in pyrite and as inclusions in and replacements of magnetite (Fig. 16a). Chalcopyrite and pyrite are inversely related; chalcopyrite to pyrite ratios generally decrease from the core outwards. Gold is microscopic and typically occurs as inclusions in sulphides or at sulphide grain boundaries. Copper and gold values are positively correlated and are notably homogeneous in their relative grade. Gold grades in general are proportional to the volume percent of quartz veins.

A molybdenum-rich shell envelopes the copper-gold core and is interpreted to have formed with Stage 2 phyllic alteration assemblages (Margolis, 1993) and Phase 2 diorite. The molybdenite to copper ratio increases from the core of the deposit outward. In the eastern, shallow levels of the system, molybdenite veins lack chalcopyrite. Although Stage 2 stockwork and mineralization are devoid of chalcopyrite at Snowfield (Margolis, 1993), we observed chalcopyrite and molybdenite-bearing veins in the transition zone between the core copper-gold and the molybdenite-rich shell at Mitchell (Fig. 16b).

Higher than average grades of copper and gold are intersected in the bornite breccia body and are interpreted to be the result of progressive upgrading during Stages 1 through 4 hydrothermal activity. Elevated copper grades correspond to high bornite to chalcopyrite ratios and are interpreted to have been introduced with anhydrite-fluorite-quartz (Fig. 16c).

High-grade Au-Ag-Pb-Zn-Cu mineralization associated with Stage 4 low sulphidation-type veins are superposed onto earlier (Stage 1-3) porphyry system stockwork and breccia bodies. Unlike porphyry-related mineralization, veins related to Stage 4 tend to have much higher tennantite to chalcopyrite ratios (Fig. 16d), higher gold and silver values, and visible sphalerite, galena and electrum grains. We consider that the veins are genetically related to porphyry emplacement and that their timing may correlate with porphyry-related epithermal mineralization at Brucejack (ca. 185 Ma; Pretium Resources, 2013). Epithermal veins cutting earlier stockwork zones suggest that uplift occurred between Stages 3 and 4. The Stage 4 veins lack significant mineralization in the drilled resource area but offer potential in the eastern Mitchell area.

4.6. Structure the Mitchell deposit

Three phases of progressive deformation related to mid-Cretaceous transpression and the formation of the Skeena fold and thrust belt, structurally modify the Mitchell deposit. The first phase is defined by a pervasive east-trending, near-vertical S_1 foliation, manifested by aligned chlorite and muscovite. Below the Mitchell thrust, the S_1 foliation (Fig. 17a) is subparallel to the sheeted Stage 1 quartz veins. Quartz veins are commonly folded into F_1 folds (Fig. 17b) that plunge steeply to the west, similar to the overall plunge of the orebody. West-northwest to west-southwest striking, steeply dipping predominantly sinistral strike slip faults (Fig. 8) are interpreted to have formed before and, possibly during the development of S_1 fabrics. S_1 foliation, in particular the limbs of F_1 folds, are

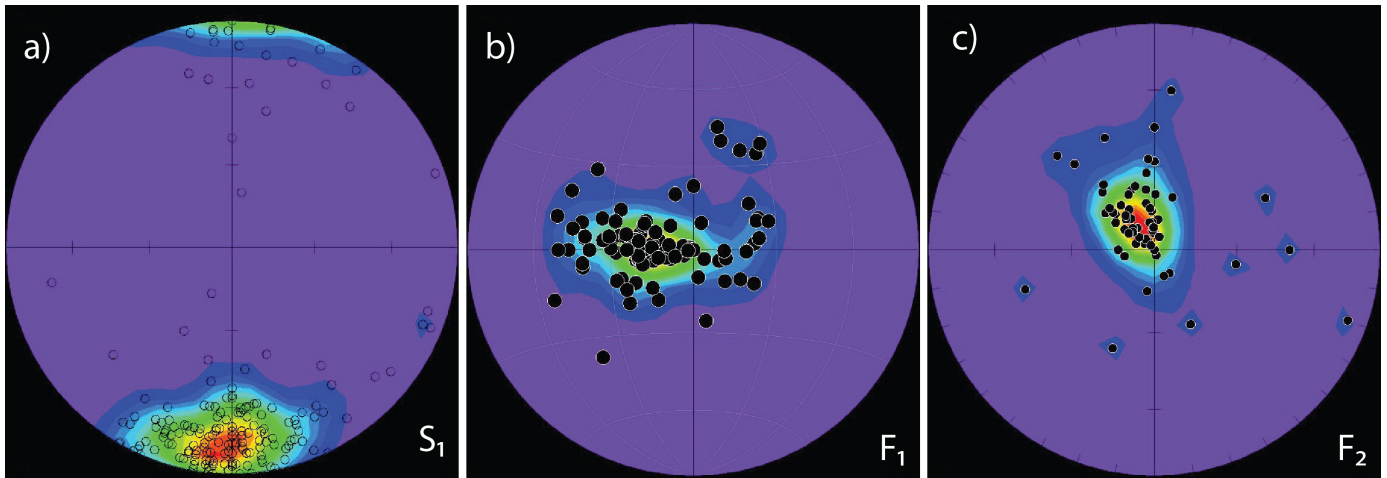


Fig. 17. a) Poles to S_1 cleavage. b) F_1 fold axes. c) F_2 fold axes.

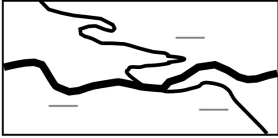
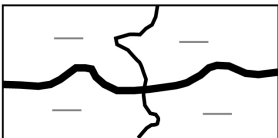
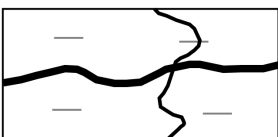
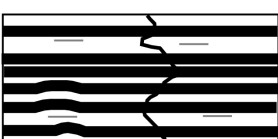
Alteration	Estimated flattening	Example	Folds
phyllitic	50-70%		F_1 tight to isoclinal, F_2 gentle-open
intermediate argillic	20-50%		F_1 open-isoclinal, F_2 gentle-open
chlorite	20-40%		F_1 open, F_2 gentle
high quartz zone	10-30%		rare F_1 due to E-W vein geometry, gentle F_2
transitional potassic	5-10%		F_1 folds in thin veins
potassic and propylitic	0%		none

Fig. 18. Qualitative estimate of strain for altered rocks of the Mitchell zone as indicated by F_1 and F_2 fold morphology.

locally overprinted by steep north-northwest plunging, gentle-open F_2 folds (deformation phase 2; Fig. 17c).

Fold geometry is a function of alteration type (Fig. 18). Isoclinal F_1 folds in quartz veins are in intensely phyllic altered rocks; close folds are in, chlorite and intermediate argillic altered rocks, and folds are lacking in potassic altered rocks. Veins of the high quartz zone are sheeted and preferentially develop F_2 folds due to their east-west striking trends. Foliation is very well developed in the predominantly phyllic altered southeastern parts of the Mitchell zone and is poorly developed to non-existent in the western, potassic and transitional potassic areas (Fig. 14).

The Mitchell thrust fault (deformation phase 3; 110.2 ± 2.3 Ma; Ar-Ar illite; Margolis, 1993) is curvilinear, dips shallowly to the northwest and offsets the steeply plunging deposit ca. 1600 m to the southeast. The Mitchell thrust is in the footwall of the Sulphurets thrust and is interpreted as a younger, in-sequence foreland-propagating fault. The Mitchell thrust clearly truncates the east-west striking sheeted quartz veins and the subparallel east-west striking S_1 cleavage. The ore deposit is further imbricated by smaller thrust and reverse faults (Fig. 8) that are likely kinematically linked with the Mitchell thrust. Mineralization in the Mitchell deposit is offset at ca. 900 m depth by a 20 m thick deformation zone named here as the Mitchell Basal thrust observed in holes M-08-62 and M-08-67 (Figs. 7a, b).

5. Geochronology of the Mitchell deposit

Two Phase 1 and one Phase 2 medium-grained dioritic samples from the Sulphurets suite were collected for U-Pb zircon geochronology. One vein sample of molybdenite from the Mitchell deposit was collected from drill core for Re-Os geochronology.

5.1. Analytical methods: U-Pb zircon

Zircon analysis was by laser ablation-inductively coupled plasma-mass spectrometry (LA-ICP-MS) at the University of British Columbia's Pacific Centre for Isotopic and Geochemical Research; detailed methods are described by Tafti et al. (2009).

5.2. Analytical methods: Re-Os (molybdenite)

A molybdenite mineral separate was produced by metal-free crushing followed by gravity and magnetic concentration methods. Methods used for molybdenite analysis are described in detail by Selby & Creaser (2004) and Markey et al. (2007). The ^{187}Re and ^{187}Os concentrations in molybdenite were determined by isotope dilution mass spectrometry using Carius-tube, solvent extraction, anion chromatography and negative thermal ionization mass spectrometry techniques. A mixed double spike containing known amounts of isotopically enriched ^{185}Re , ^{190}Os , and ^{188}Os analysis is used. Isotopic analysis is made using a ThermoScientific Triton mass spectrometer by Faraday collector. Total procedural blanks for Re and Os are less than <3 picograms and 2 picograms, respectively, which are insignificant for the Re and Os concentrations in molybdenite.

The Chinese molybdenite powder HLP-5 (Markey et al., 1998), is analyzed as a standard. For this control sample over a period of two years, an average Re-Os date of 221.56 ± 0.40 Ma (1SD uncertainty, $n=10$) is obtained. This Re-Os age date is identical to that reported by Markey et al. (1998) of 221.0 ± 1.0 Ma. The age uncertainty is quoted at 2σ level, and includes all known analytical uncertainty, including uncertainty in the decay constant of ^{187}Re .

5.3. Results

5.3.1. Sample M-11-123; Phase 1 diorite

A medium-grained, potassic altered, Phase 1 diorite (sample M-11-123; Fig. 19a) sampled from a depth of 621 m yielded an age 196.0 ± 2.9 Ma (Fig. 19a). The intrusion is interpreted to be intramineral as it is host to Stage 1 related veins that are irregularly shaped, have diffuse boundaries, and are disarticulated. The sampled intrusion is diorite in composition from whole rock geochemistry (Fig. 13a). The porphyry contains 35% sericitized anorthitic plagioclase (0.5-2 mm in diameter), 7% K-feldspar (1-5 mm in diameter) with inclusions of hornblende in an altered, fine-grained groundmass (Fig. 20a). The sampled area is overprinted by pervasive and vein-controlled secondary K-feldspar, quartz, biotite, chlorite, magnetite, pyrite and chalcopyrite.

5.3.2. Sample GF-13-02; Phase 1 diorite

A medium-grained, chlorite and phyllic altered, Phase 1 diorite that outcrops adjacent to the high quartz zone (sample GF-13-02; 423312E, 6265278N; Fig. 8) yielded an age of 189 ± 2.8 Ma (Fig. 19b). The diorite is interpreted as a host rock to the high quartz zone in this location because there are no clasts of sheeted quartz veins in the intrusion and it appears to grade into the high quartz zone. The sampled intrusion is diorite in composition from whole rock geochemistry (Fig. 13a). The porphyry contains 35% sericitized laths interpreted to be replaced plagioclase (1-2 mm in diameter), 8% chlorite rhombohedral aggregates interpreted to be replaced hornblende (0.5-1 mm in diameter) and 5% equant anhedral K-feldspar partially replaced to sericite (2-3 mm diameter) in an altered, fine-grained groundmass (Fig. 20b). The intrusion is overprinted by Stage 2 sericite-chlorite-pyrite alteration with disseminations of secondary magnetite, trace chalcopyrite, 2% pyrite and ~10% quartz-chalcopyrite-pyrite veins by volume.

5.3.3. Sample M-07-49; Phase 2 diorite

A sample (M-07-49, 320 m; Fig. 7a) of fine-grained, Phase 2 diorite plug that cuts the high quartz zone and is overprinted by Stage 2 phyllic alteration yields an age of 192.2 ± 2.8 Ma (Fig. 19c). The high quartz zone that is cut by the plug contains 60-90% quartz-pyrite-chalcopyrite veins in the contact area. The sampled intrusion is diorite in composition from whole rock geochemistry (Fig. 13a) and contains 1-10% quartz vein xenoliths that are most abundant in the contact areas. The porphyry contains 30% sericitized laths (ca. 1 mm long) interpreted to be replaced plagioclase, 5% chlorite aggregates

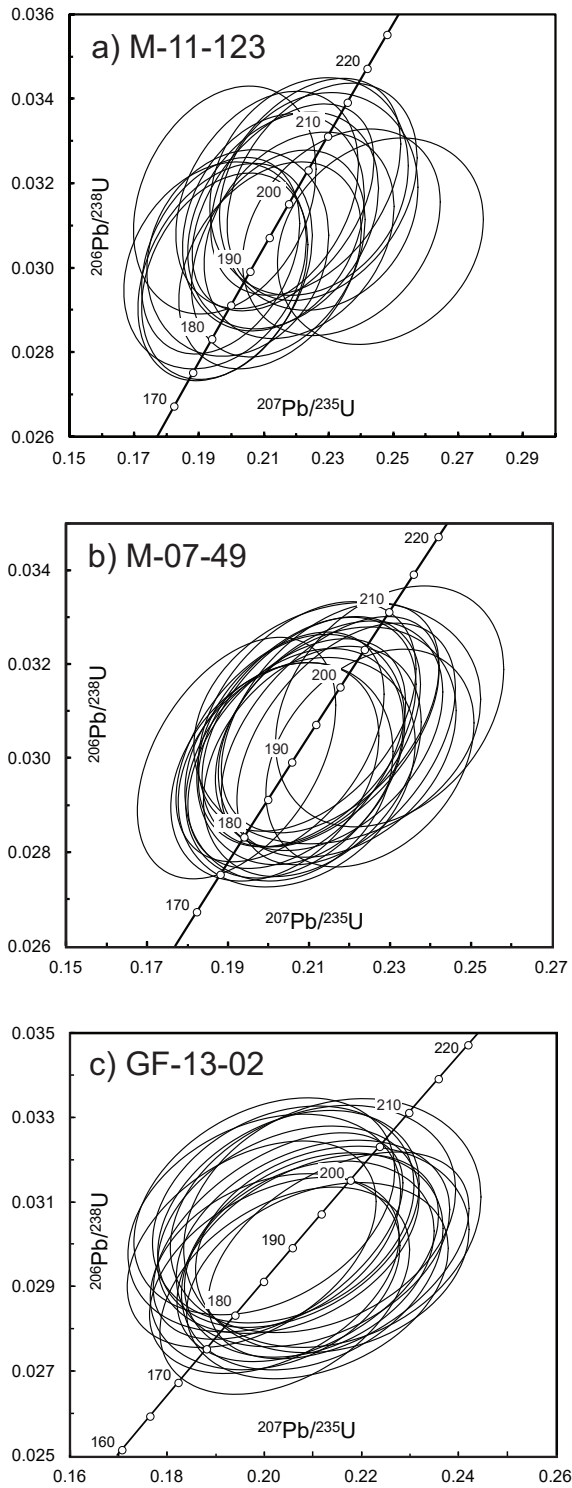


Fig. 19. U-Pb concordia diagrams for Sulphurets suite diorite in the Mitchell deposit. **a)** Sample M-11-123, **b)** sample M-07-49 and **c)** sample GF-13-02. See Figs. 7a, b, 8 for sample locations.

interpreted to be replaced hornblende, and 5% anhedral inclusion-rich K-feldspar in a fine-grained groundmass (Fig. 20c). The intrusion is overprinted by Stage 2 sericite-chlorite-pyrite alteration with 1% secondary magnetite, trace chalcopyrite and stringers of anhydrite and calcite.

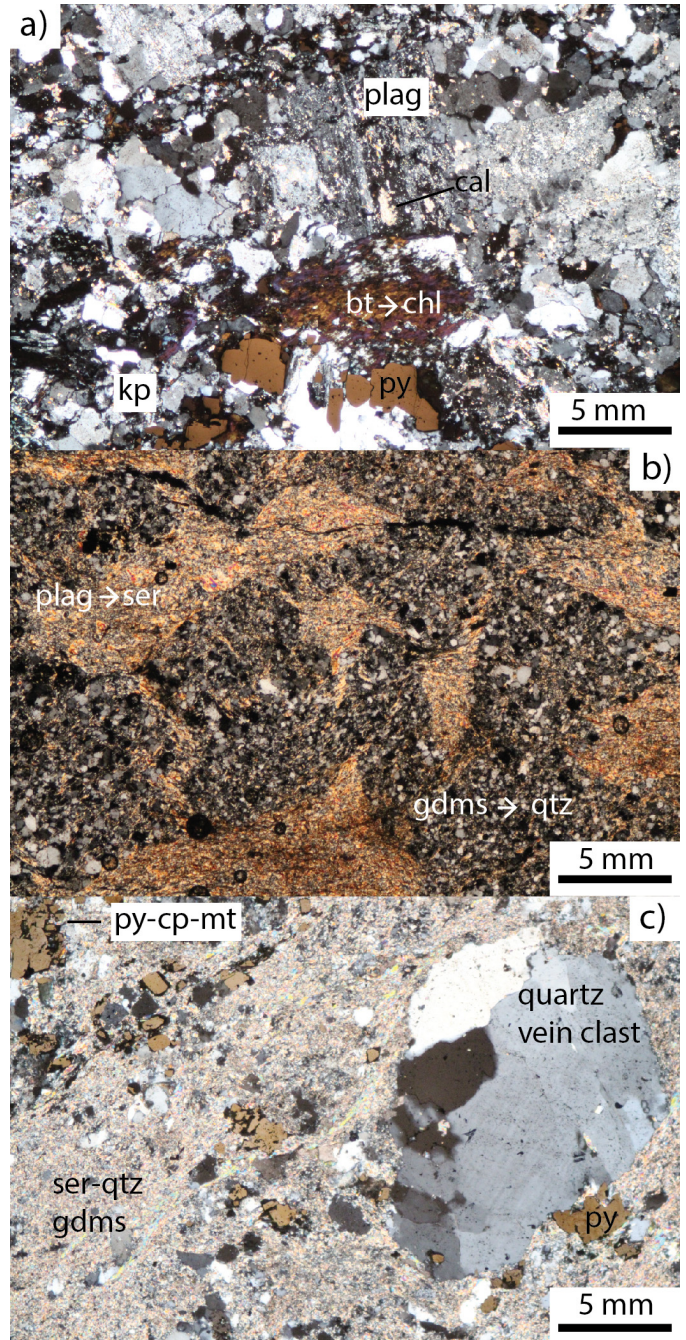


Fig. 20. Photomicrographs of the three dated Mitchell intrusions. **a)** Primary plag: plagioclase altered to cal: calcite, kp: K-feldspar replacement of groundmass and plagioclase, secondary bt: biotite replaced to chl: chlorite, sample M-11-123. **b)** Plagioclase ghosts are defined by sericite domains (plag->ser) and groundmass consists of quartz altered domains (gdms->qtz), sample GF-13-02. **c)** Phenocrysts and groundmass completely replaced by sericite-quartz (ser-qtz gdms), quartz vein clast (high quartz zone) and pyrite-chalcopyrite-magnetite (py-cp-mt) accompanies alteration, sample M-07-49.

5.3.4. Sample M-10-116, Stage 2 molybdenite vein (Re-Os)

Molybdenite in a sample (M-10-116, 214.6 m; Fig. 8) from a Stage 2 quartz-pyrite vein with yellow sericite alteration haloes in intensely sericite-pyrite-chlorite altered andesite breccia

yielded an Re-Os age of 190.3 ± 0.8 Ma. The vein host rock contains juvenile porphyritic angular andesite fragments ca. 60% clasts ca. 1 cm in diameter with <1% subrounded granule-sized felsic clasts. The host rock is intensely altered to sericite-pyrite-chlorite and is well foliated. The molybdenite-bearing vein is 3-4 mm wide with wavy margins, is parallel to foliation and contains a thin (1 mm) selvage of white and yellow sericite alteration. The vein contains 75% grey-white microcrystalline quartz, 15% blue-grey elongate molybdenite disseminations, 8% brass-yellow anhedral to subhedral pyrite disseminations (<0.2 mm) and 2% sericite.

5.3.5. Geochronologic summary

Phase 1 plutonism and Stage 1 alteration and copper-gold mineralization are bracketed between 196.0 ± 2.9 Ma and 189.9 ± 2.8 Ma. The crystallization age of Phase 2 rocks is 192.2 ± 2.8 Ma, close to the age of molybdenite mineralization (190.3 ± 0.8 Ma), which we consider records Stage 2 alteration and mineralization. Advanced argillic, Stage 3 and Phase 3 plutonism are interpreted to be younger than 190.3 ± 0.8 Ma.

6. Discussion

6.1. Evolution of the Mitchell deposit

The most significant mineralization and alteration event (Stage 1) was coeval with Phase 1 Sulphurets diorite intrusion, potassic and propylitic alteration, and the formation of a copper-gold core zone (Fig. 21a; Table 2). An east-striking, steeply dipping sheeted high quartz zone (>60% volume of quartz) is developed in the contact area between Phase 1 diorite and Stuhini Group rocks or overlying Jack Formation (Fig. 21a). A Stage 2 molybdenite shell envelopes a Phase 2 Sulphurets diorite plug in the core region of the deposit related to overprinting phyllic and intermediate argillic alteration. The alteration developed laterally in Jack Formation sandstone and penetrated along fractured stockwork zones at deeper levels (Fig. 21b; Table 2). The molybdenite shell is contiguous with the core zone copper-gold stockwork emplaced during Stage 1 and Stage 2 events. Poorly mineralized massive Stage 3 pyrite veins are temporally related to a small Phase 3 Sulphurets diorite plug advanced argillic alteration in the southeastern Mitchell zone, and widespread advanced argillic alteration in the Snowfield zone (Fig. 21c; Table 2). Stage 3 alteration lacks

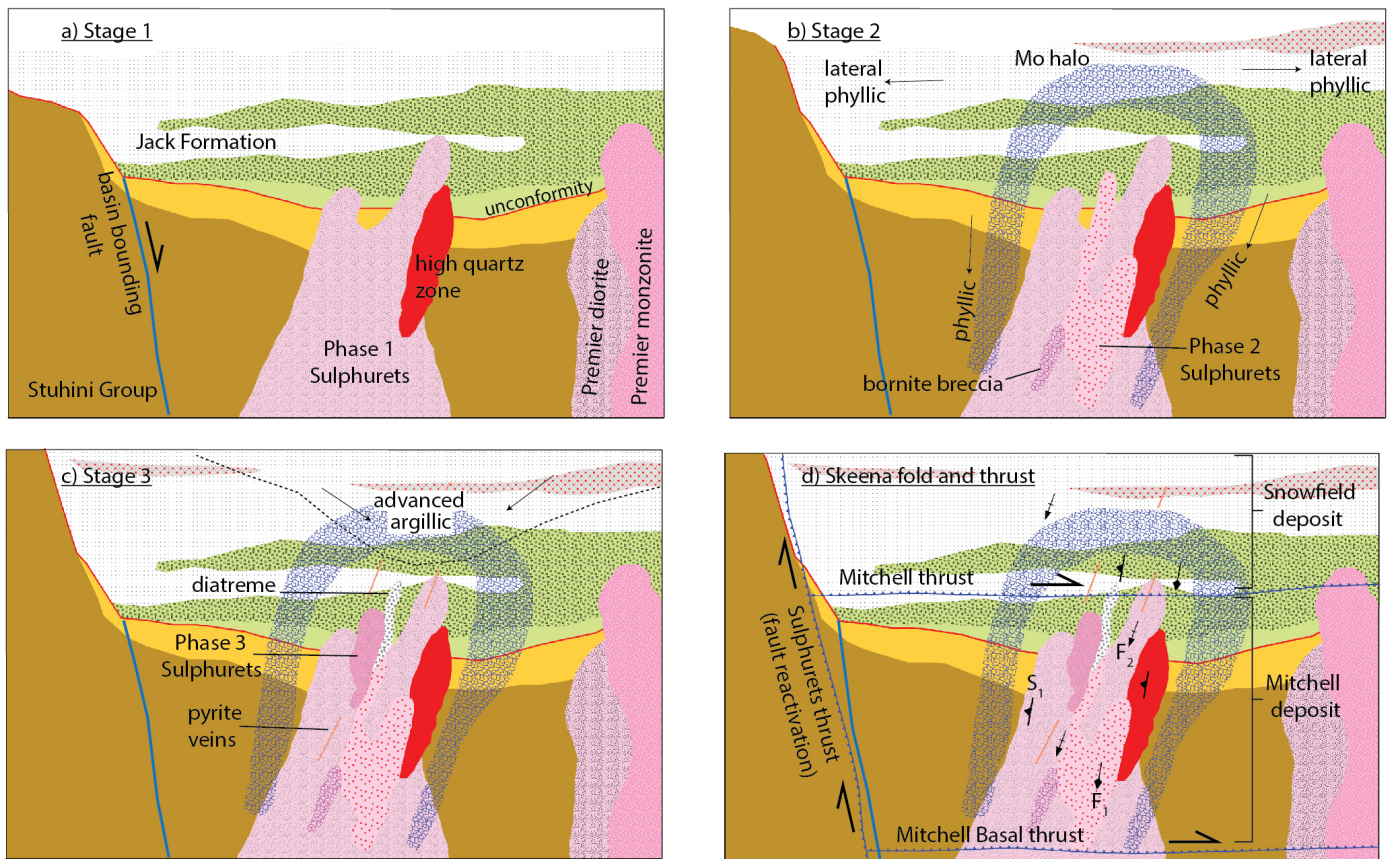


Fig. 21. Model for the evolution of the Mitchell deposit. **a)** Stage 1 alteration and mineralization is related to emplacement of Phase 1 diorite and the high quartz zone after Premier diorite and monzonite intrusion; **b)** Stage 2 phyllic alteration is related to a molybdenite-rich envelope, Phase 2 diorite and the bornite breccia; **c)** Stage 3 advanced argillic alteration at shallow levels is related to massive pyrite veins, Phase 3 diorite and the diatreme breccia; **d)** Mid-Cretaceous deformation related to Skeena fold and thrust belt; S_1 pervasive cleavage F_1 , F_2 folds and D_3 Mitchell thrust, Mitchell Basal thrust and the Sulphurets thrust.

significant mineralization. Epithermal textures in Stage 4 veins suggest uplift during a hiatus of hydrothermal activity between Stages 3 and 4.

In the mid-Cretaceous, three phases of progressive deformation modified the deposit. Pervasive east-west striking S_1 cleavage and associated steeply west-plunging F_1 folds are overprinted by steeply north-plunging F_2 fold trends similar to the McTagg Anticlinorium, and the Mitchell thrust fault separated the Snowfield and Mitchell zones (Fig. 21d).

6.2. The Mitchell deposit: a calc-alkalic porphyry

The shallower porphyry deposits of the Sulphurets district have been variously classified as alkalic and calc-alkalic. For example, Logan and Mihalynuk (2014) referred to the Kerr deposit as calc-alkalic Bissig and Cooke (2014) designated the KSM deposits as a whole as silica-saturated alkalic. At Sulphurets, quartz veins and molybdenum content are considered characteristic of calc-alkaline magmatism whereas the composition of the intrusions and alteration types are more typical of alkalic systems (Fowler and Wells, 1995). Ditson et al. (1995) suggested the core chlorite with phyllic alteration halo at Kerr is atypical of British Columbia porphyry deposits and does not fit either alkalic or calc-alkalic models. Margolis (1993) interpreted early Cu-Au mineralization at Snowfield as a result of alkaline magmatism and related molybdenum and sericitic alteration (uncommon to alkaline systems) to a younger overprint. Pretium Resources (2013) considers epithermal high grade gold veins at Brucejack to be genetically related to alkaline Cu-Au porphyry mineralization at KSM.

Although the Mitchell deposit shares characteristics with alkalic porphyry systems, such as relatively high gold grades and magnetite in alteration assemblages (Bissig and Cooke,

2014), we consider the Mitchell a calc-alkalic porphyry deposit because: 1) the Sulphurets suite is subalkaline; 2) phyllic and clay alteration assemblages are abundant, 3) alteration assemblages contain high pyrite concentrations throughout; 4) alteration is extensive (>4 km wide; Fig. 14); 5) silica contents in the ore zone are high (5-95% volume quartz veins); 6) it contains economically significant molybdenum mineralization; and 7) of the scale of the deposit (>4.5 billion tonnes of inferred resources combining the Mitchell and Snowfield; Pretium Resources, 2011; Seabridge Gold, 2014).

6.3. The relationship between the Snowfield and Mitchell deposits

The Snowfield deposit occupies the hanging wall of the Mitchell thrust fault ca. 1.6 km east-southeast of the Mitchell deposit and is interpreted to be the shallower continuation of the Mitchell deposit (Fig. 21). We base this interpretation on the following: 1) metal zonation patterns indicate a core zone of elevated copper and gold with a shell of molybdenum-rich ore common to both deposits separated by the Mitchell thrust (Fig. 22; Savell and Threlkeld, 2013); 2) the Snowfield mineralization is hosted in Mitchell intrusions and Jack Formation quartz-bearing sandstone and conglomerate in the highest stratigraphic levels of the Mitchell zone; 3) the Snowfield deposit is composed predominantly of phyllic and argillic alteration assemblages whereas in the Mitchell deposit phyllic alteration is limited to shallow and easterly regions and penetrations at depth suggesting continuity of alteration assemblages between the two deposits. Margolis (1993) considered the advanced argillic alteration intensity in the Snowfield stockwork as evidence that it is a shallower system than the Mitchell stockwork. The Mitchell-Snowfield system

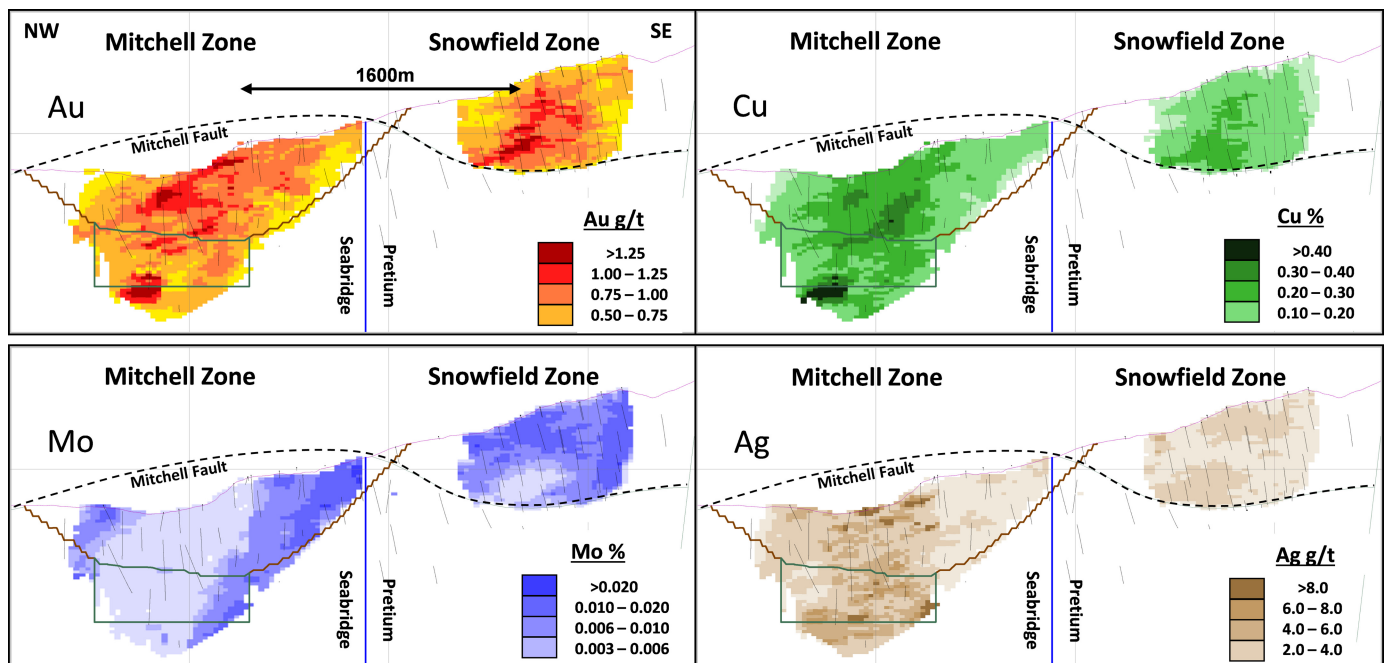


Fig. 22. Au, Cu, Ag and Mo metal grades of the Mitchell and Snowfield deposit, after Savell and Threlkeld (2013).

is interpreted as a north-plunging, fault-dissected ore body that grades from Jack Formation sandstone hosted stockwork on surface in the Snowfield deposit to intrusion-hosted stockwork at depth in the Mitchell deposit.

7. Conclusion

The calc-alkalic Mitchell deposit formed during emplacement of Sulphurets suite dioritic magmatism and is interpreted to be the deeper levels of a once contiguous, gigantic porphyry deposit that included the structurally offset Snowfield deposit. The Mitchell-Snowfield mineral system was likely active for at least 2 million years. Mineralization is related to Sulphurets suite plagioclase-hornblende intrusions that cut and overprint earlier Premier suite monzonite and syenite intrusions. Three new U-Pb zircon ages for the Sulphurets suite diorite and a Re-Os molybdenite age indicate that magmatic-hydrothermal mineralizing processes started after 196.0 ± 2.9 Ma and ended before 189.9 ± 2.8 Ma.

Acknowledgments

This research was made possible by a generous financial contribution from Seabridge Gold Inc to LAK in addition to in-kind support throughout the project. We are grateful to the Seabridge Gold management team especially: Rudi Fronk, Bill Threlkeld, Tim Dodd, Peter Erwich, James Freeman and Tom Kraft for the tremendous support and involvement in the research project. GEF is grateful to Pretium Resources Inc, namely Ken McNaughton, Charlie Grieg and Warwick Board, for permission to map parts of the Mitchell and Snowfield deposits and for valuable input throughout the project. Many thanks to Paul Wojdak and JoAnne Nelson for discussions about the Mitchell zone, which have contributed much to our understanding of the deposit. This manuscript was greatly improved by detailed and thoughtful reviews by Lawrence Aspler, JoAnne Nelson, and Jim Logan.

References cited

- Alldrick, D.J., 1993. Geology and metallogeny of the Stewart mining camp, northwestern British Columbia, British Columbia Ministry of Energy, Mines and Petroleum Resources, British Columbia Geological Survey Bulletin 85, 105 p.
- Alldrick, D.J., and Britton, J.M., 1988. Geology and mineral deposits of the Sulphurets area. British Columbia Ministry of Energy, Mines and Petroleum Resources, British Columbia Geological Survey Bulletin 85, 105 p.
- Alldrick, D.J., and Britton, J.M., 1991. Sulphurets area geology. British Columbia Ministry of Energy, Mines and Petroleum Resources, British Columbia Geological Survey Open File 1991-21, 1:20,000 scale.
- Anderson, R.G., 1989. A stratigraphic, plutonic, and structural framework for the Iskut River map area, northwestern British Columbia; in Current Research, Part E, Geological Survey of Canada, Paper 89-1E, pp. 145-154.
- Bissig, T., and Cooke, D.R., 2014. Introduction to the Special Issue devoted to alkalic porphyry Cu-Au and epithermal Au deposits: Economic Geology, Special Issue on Alkalic Porphyry Deposits, 109, pp. 819-825.
- Bridge, D.J., 1993. The deformed Early Jurassic Kerr copper-gold porphyry deposit, Sulphurets gold camp, northwestern British Columbia, unpublished M.Sc. thesis, University of British Columbia.
- Disson, G.M., Wells, R.C., and Bridge, D.J., 1995. Kerr: The geology and evolution of a deformed porphyry copper-gold deposit, northwestern British Columbia. In: Porphyry Deposits of the Northwestern Cordillera of North America, T.G. Schroeter, (Ed.), Canadian Institute of Mining, Metallurgy and Petroleum, Special Volume 46, pp. 509-523.
- Evenchick, C.A., 2001. Northeast-trending folds in the western Skeena Fold Belt, northern Canadian Cordillera: a record of Early Cretaceous sinistral plate convergence: Journal of Structural Geology, 23, 1123-1140.
- Evenchick, C.A., McMechan, M.E., McNicoll, V.J., and Carr, S.D., 2007. A synthesis of the Jurassic-Cretaceous tectonic evolution of the central and southeastern Canadian Cordillera: exploring the links across the orogeny. In: Sears, J.W., Harms, T.A., and Evenchick, C.A., (Eds.), Whence the mountains? Inquiries into the evolution of orogenic systems. A volume in honour of Raymond A. Price. Geological Society of America, Special Paper 433, pp. 117-145.
- Fowler, B.P., and Wells, R.C., 1995. The Sulphurets Gold zone, northwestern British Columbia, Porphyry Deposits of the Northwestern Cordillera of North America, Schroeter, T.G., (Ed.), Canadian Institute of Mining, Metallurgy and Petroleum, Special Volume 46, pp. 484-498.
- Greig, C.J., 1992. Fieldwork in the Oweegee and Snowslide ranges and Kinskuch Lake area, Northwestern BC. In: Current Research, Part A. Geological Survey Paper 92-1A, pp. 145-155.
- Hansley, P., 2008. Petrography of samples from the Kerr-Sulphurets-Mitchell property, Petrographic Consultants International Inc., unpublished report prepared for Seabridge Gold Inc.
- Hastie, A.R., Kerr, A.C., Pearce, J.A., and Mitchell, S.F., 2007. Classification of altered volcanic island arc rocks using immobile trace elements: development of the Th-Co discrimination diagram. Journal of Petrology, 48, 2341-2357.
- Henderson, J.R., Kirkham, R.V., Henderson, M.N., Payne, J.G., Wright, T.O., and Wright, R.L., 1992. Stratigraphy and structure of the Kerr-Sulphurets area, British Columbia, Current Research, Part A, Geological Survey of Canada, Paper 92-1A, pp. 323-335.
- Kirkham, R.V., 1963. The geology and mineral deposits in the vicinity of the Mitchell and Sulphurets glaciers, Northwest British Columbia, unpublished M.Sc.thesis, University of British Columbia, 142 p.
- Kirkham, R.V., and Margolis, J., 1995. Overview of the Sulphurets area, northwestern British Columbia, Porphyry Deposits of the Northwestern Cordillera of North America, Schroeter, T.G., (Ed.), Canadian Institute of Mining, Metallurgy and Petroleum, Special Volume 46, pp. 473-483.
- Kramer, R., 2014. Structural geology of the Kerr Deposit Iskut-Stikine region, British Columbia, unpublished B.Sc. thesis, University of British Columbia.
- Lewis, P.D., 1992. Structural Evolution of the Iskut River Area: Preliminary results. Mineral Deposit Research Unit, The University of British Columbia Annual Technical Report-Year 2, pp. 2.1-2.21.
- Lewis, P.D., 2001. Geological maps of the Iskut River area. In: Lewis, P.D., Toma, A., and Tosdal, R.M., (Eds.), Metallogenesis of the Iskut River area, northwestern British Columbia. Mineral Deposit Research Unit, Special Publication Number 1, 77-83.
- Lewis, P.D., Mortensen, J.K., Childe, F., Friedman, R., Gabites, J., Ghosh, D., and Bevier, M.L., 2001. Geochronology data set in the Iskut River area-progress and problems: metallogenesis of the Iskut River area, northwestern British Columbia, Mineral Deposit Research Unit, Special Publication Number 1, pp. 89-96.
- Lewis, P.D., 2013. Iskut River area geology, northwest British Columbia. Geoscience British Columbia Report 2013 -05, 3

- 1:50,000 scale maps, legend and notes.
- Logan, J.M., Drobe, J.R., and McClelland, W.C., 2000. Geology of the Forrest Kerr-Mess Creek area, northwest British Columbia (NTS 104B/10, 15 & 104/G2 & 7W). British Columbia Ministry of Energy, Mines and Petroleum Resources, British Columbia Geological Survey Bulletin 104, 163 p.
- Logan, J.M., and Mihalynuk, M.G., 2014. Tectonic controls on early Mesozoic paired alkaline porphyry deposit belts (Cu-Au+Ag-Pt-Pd-Mo) within the Canadian Cordillera: Economic Geology, Special Issue on Alkalic Porphyry Deposits, 109, 827-858.
- Markey, R., Stein, H.J., Hannah, J.L., Zimmerman, A., Selby, D., and Creaser, R.A., 2007. Standardizing Re-Os geochronology: a new molybdenite reference material (Henderson, USA) and stoichiometry of Os salts. *Chemical Geology*, 244, 74-87.
- Markey, R., Stein, H., and Morgan, J., 1998. Highly precise Re-Os dating for molybdenite using fusion and NTIMS. *Talanta*, 45, 935-946.
- Margolis, J., 1993. Geology and intrusion-related copper-gold mineralization, Sulphurets, British Columbia, unpublished Ph.D. thesis, University of Oregon, 289 p.
- Nelson, J., and Kyba, J., 2014. Structural and stratigraphic control of porphyry and related mineralization in the Treaty Glacier-KSM-Brucejack-Stewart trend of western Stikinia. In: *Geological Fieldwork 2013*, British Columbia Ministry of Energy and Mines, British Columbia Geological Survey Paper 2014-1, pp. 111-140.
- Pretium Resources, 2011. Snowfield project website: <http://www.pretium.com>. Snowfield mineral resource summary, February, 2011.
- Pretium Resources, 2013. Brucejack project website: <http://www.pretium.com>. Report on Brucejack property geology, April, 2013.
- Pretium Resources, 2014. Brucejack project website: <http://www.pretium.com>. Brucejack project reserves and resources summary, June, 2014.
- Savell, M., and Threlkeld, B., 2013. The KSM project-a cluster of porphyry related, deformed and dismembered Au-Cu-Mo deposits displaying a transition from deep porphyry to shallow vein environments, Seabridge Gold Inc. website: http://seabridgegold.net/pdf/geology/KSM_Geology_update_Sep_2013.pdf.
- Seabridge Gold, 2014. Reserves and resources website: <http://seabridgegold.net>. Mineral reserves and resources, March 11, 2014.
- Selby, D., and Creaser, R.A., 2004. Macroscale NTIMS and microscale LA-MC-ICP-MS Re-Os isotopic analysis of molybdenite: testing spatial restrictions for reliable Re-Os age determinations, and implications for the decoupling of Re and Os within molybdenite. *Geochimica et Cosmochimica Acta*, 68, 3897-3908.
- Simpson, T.M., 1983. The geology and hydrothermal alteration of the Sulphurets deposits, Northwest British Columbia, unpublished M.Sc. thesis, University of British Columbia, 99 p.
- Tafti, R., and Mortensen, J.K., 2009. Jurassic U-Pb and Re-Os ages for the newly discovered Xietongmen Cu-Au porphyry district, Tibet, PRC: implications for metallogenic epochs in the southern gangdese belt. *Economic Geology*, 104, 127-136.
- Visual Capitalist, 2013. Global gold mine and deposit rankings 2013 website: <http://www.visualcapitalist.com/wp-content/uploads/2013/11/global-gold-mine-and-deposit-rankings-2013.pdf>.
- Winchester, J.A., and Floyd, P.A., 1977. Geochemical discrimination of different magma series and their differentiation products using immobile elements. *Chemical Geology*, 20, 325-343.

U-Pb geochronology of the Hazelton Group in the McTagg anticlinorium, Iskut River area, northwestern British Columbia

J.A. Cutts¹, V.J. McNicoll^{1,a}, A. Zagorevski^{1,a}, R.G. Anderson², and K. Martin³

¹ Geological Survey of Canada, 601 Booth St., Ottawa, ON, K1A 0E8

² Geological Survey of Canada, 1500 - 605 Robson St., Vancouver, BC, V6B 5J3

³ Department of Earth Sciences, University of Ottawa, 120 University Private, Ottawa, ON K1N 6N5

^a corresponding authors: vmnicol@nrcan.gc.ca and azagorev@nrcan.gc.ca

Recommended citation: Cutts, J.A., McNicoll, V.J., Zagorevski, A., Anderson, R.G., and Martin, K., 2015. U-Pb geochronology of the Hazelton Group in the McTagg anticlinorium, Iskut River area, northwestern British Columbia. In: Geological Fieldwork 2014, British Columbia Geological Survey Paper 2015-1, pp. 87-101.

Abstract

Early to Middle Jurassic rocks of the Hazelton Group are extensively mineralized, including the precious metal-rich Eskay Creek deposit that is hosted by bimodal volcanic successions in the Eskay rift. In this study, we present U-Pb zircon ages of seven Hazelton Group volcanic, epiclastic and hypabyssal rocks to establish the absolute ages of Hazelton Group units in the McTagg anticlinorium, east of the Eskay Creek deposit. A felsic volcanoclastic sample from the Brucejack Lake member (Betty Creek Formation) yielded a 187.1±1.9 Ma U-Pb crystallization age that is consistent with previous fossil and U-Pb age determinations. Six samples from the Bruce Glacier member (Iskut River/Salmon River Formation) yielded U-Pb crystallization ages of 178.5±1.8, 174.6±1.8, 174.4±1.7, 174.7±1.8, 173.6±1.7, and 173.3±1.8 Ma. These ages indicate that volcanic rocks coeval with the Eskay member occur in the McTagg anticlinorium, as far south as Mt. Dilworth.

Keywords: Hazelton Group, Eskay Rift, Betty Creek Formation, Iskut River Formation, Salmon River Formation, Bruce Glacier, Treaty Ridge, geochronology

1. Introduction

The Canadian Cordillera is endowed with abundant and diverse mineral deposits. Mineralization includes Cu±Au±Mo porphyry, volcanogenic massive sulphide, gold stockwork, shear-hosted vein, hydrothermal breccia, and replacement deposits that range in age from Devonian-Mississippian to Eocene (Nelson and Colpron, 2007; Nelson et al., 2013). Most prospects and deposits in northwestern British Columbia are hosted by Triassic to Middle Jurassic volcano-sedimentary and plutonic rocks of the Stikine terrane (Fig. 1). The nature of Triassic to Middle Jurassic magmatism in the northern Stikine terrane changed over time, resulting in episodic emplacement of calc-alkaline, alkaline, and tholeiitic magmas (e.g., Souther, 1972; Anderson, 1993; Logan et al., 2000). The late Early Jurassic transition from calc-alkaline to tholeiitic magmatism in the Hazelton Group (Lower to Middle Jurassic) is perhaps one of the most profound changes in magmatic character (Alldrick et al., 2005 and references therein). This change was caused by rifting of the Hazelton arc complex, which led to development of the Eskay rift (Fig. 2; Anderson and Thorkelson, 1990). It also represents a change to predominantly submarine volcanism and sedimentation and a change from porphyry and epithermal to volcanogenic massive sulphide mineralization. Constraining the age and tectonic significance of this change is critical for understanding the tectonics of the northwestern Cordillera and the distribution of Mesozoic mineral deposits.

The Hazelton Group (Tipper and Richards, 1976) hosts epithermal deposits in Lower Jurassic units and volcanogenic massive sulphides in Middle Jurassic units, including the

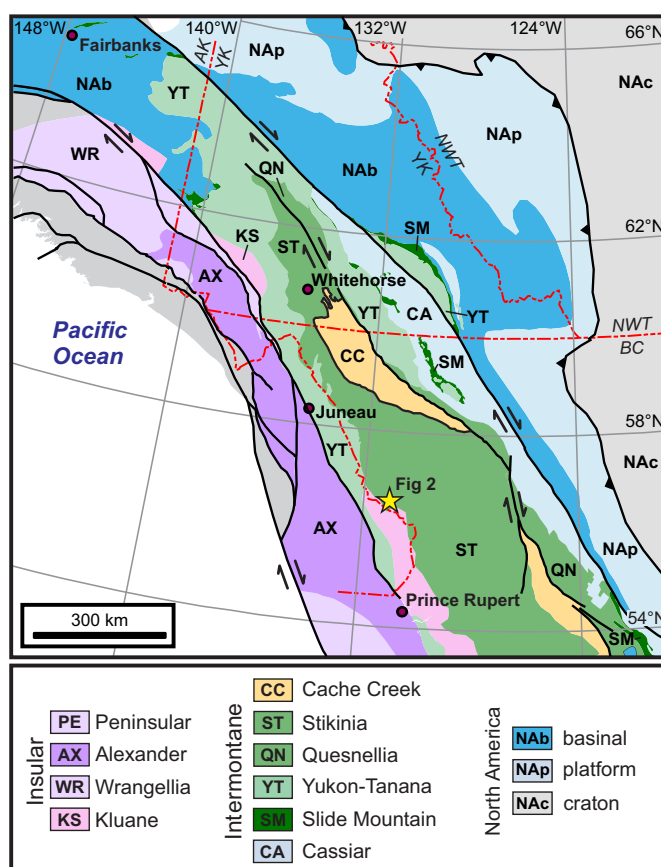


Fig. 1. Terranes of the northern Cordillera (after Colpron and Nelson, 2011). Iskut River area (star) is in the Stikine terrane (Paleozoic to Mesozoic).

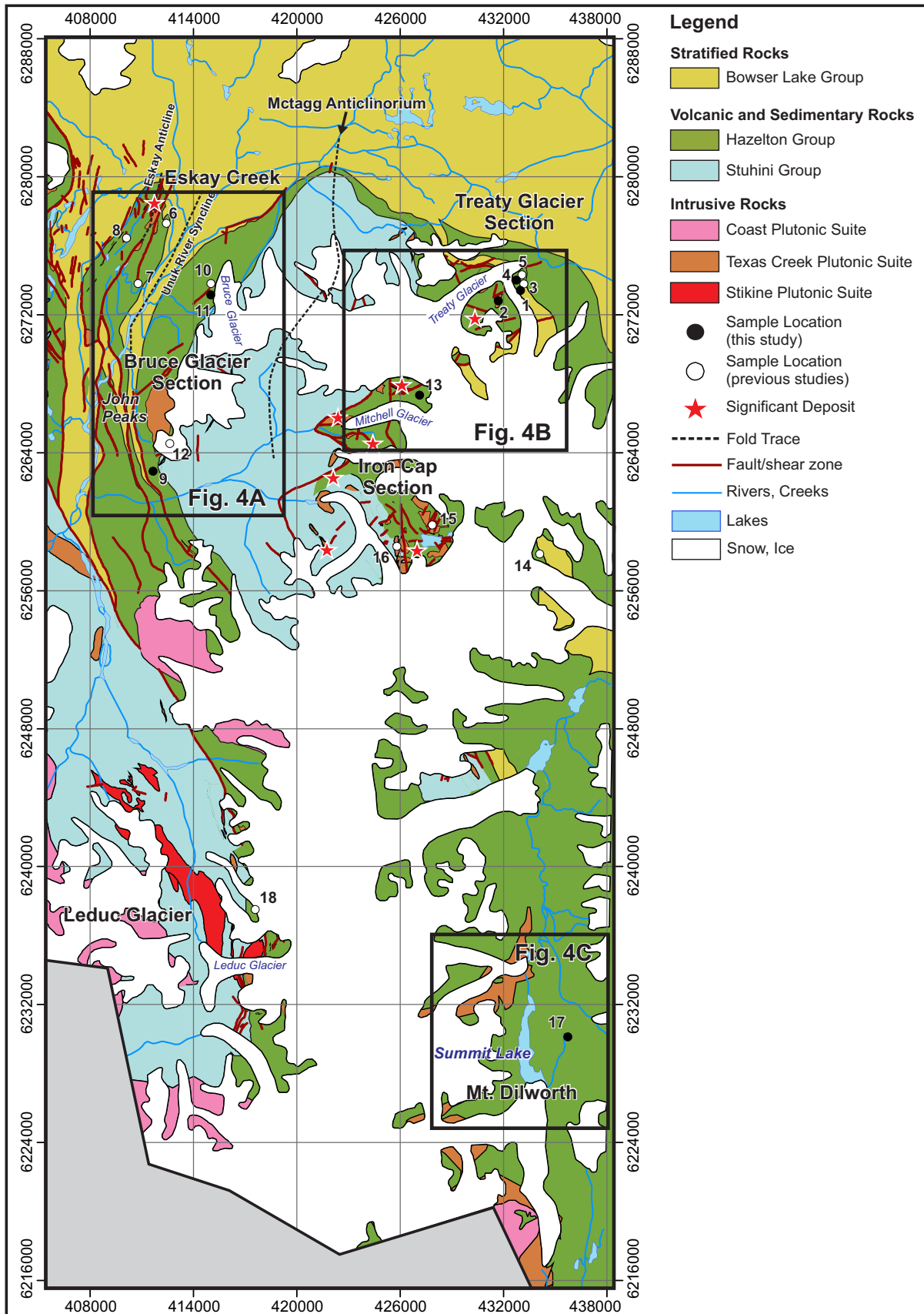


Fig. 2. Simplified geological map of the Iskut River area (modified from Lewis 2013). Numbers refer to ages of volcanic and hypabyssal rocks summarized in Table 1. UTM zone 9, NAD 83.

Au-rich Eskay Creek volcanogenic massive sulphide deposit (Roth et al., 1999 and references therein) and the Iron Cap, Mitchell, Sulphurets, Kerr, Snowfields, and Valley of Kings Cu-Au porphyry deposits (Nelson and Kyba, 2014). The rift stratigraphy of the Hazelton Group forms a northerly trend (Anderson and Thorkelson, 1990). Understanding the regional distribution of this stratigraphy and the underlying regional-scale controls on mineralization has been hampered by a lack of geochronological data from outside of known deposit areas. Herein, we present Sensitive High Resolution Ion Microprobe II (SHRIMP II) data on volcanic, epiclastic, and hypabyssal samples from the Hazelton Group on the limbs of the McTagg anticlinorium, east of the Eskay Creek deposit (Fig. 2; Roth et al., 1999; Nelson and Kyba, 2014, and references therein). Our main goal is to better understand the stratigraphy and timing of the key volcano-sedimentary Hazelton Group units with potential to host economic deposits. We integrate these data into the compilation map of Lewis (2013) and extend definitive occurrences of rocks around the McTagg anticlinorium that are coeval with the Eskay member.

2. Regional geology

The study area is in the Stikine terrane (Paleozoic to Mesozoic) of northwestern British Columbia (Figs. 1, 2). The oldest rocks in the Stikine terrane are included in the Stikine assemblage (Devonian to Permian, Monger, 1977). The Stikine assemblage comprises predominantly Mississippian arc and backarc volcanic, epiclastic, and plutonic rocks that are overlain by Pennsylvanian to Permian limestone and chert (e.g., Brown et al., 1991; Logan et al., 2000; Mihalynuk et al., 2012). The Stikine assemblage is unconformably overlain by Triassic rocks of the Stuhini Group and intruded by the Stikine and Copper Mountain plutonic suites (e.g., Brown et al., 1991; Logan et al., 2000; Mihalynuk et al., 2012). The Stuhini Group comprises characteristic augite-phyric volcanic and volcanoclastic rocks, sedimentary rocks, and minor felsic volcanic rocks. Stuhini Group volcanic rocks and related intrusions have yielded ca. 223 to 213 Ma crystallization ages (U-Pb zircon; Lewis et al., 2001; Logan et al., 2000) and Carnian-Norian fossil collections (Logan et al., 2000). Overall, the Stuhini Group and related plutonic suites have been interpreted to have formed in an intra-oceanic arc setting; however, Upper Triassic alkalic magmatism with Precambrian inheritance (Bevier and Anderson, 1991) suggests a more complex tectonic setting. Stuhini Group magmatism ended in the Late Triassic and was followed by erosion, exhumation of plutonic complexes, development of a regional angular unconformity (Brown et al., 1996; Logan et al., 2000; Lewis, 2013; Kyba and Nelson, 2015), initiation of Labarge Group deposition to the north (Gabrielse, 1998), and initiation of Hazelton Group deposition and consanguineous plutonism in northwestern British Columbia (Anderson, 1993; Thorkelson et al., 1995; Brown et al., 1996; Logan et al., 2000; Mihalynuk et al., 2012; Nelson and Kyba, 2014).

2.1. Hazelton Group

The Hazelton Group is aerially extensive in the Stikine terrane of northwestern British Columbia, from the Smithers-Hazelton area in the south, through the Iskut region of central-northern Stikinia and extending north into southern Yukon (e.g. Tipper and Richards, 1976; Thorkelson et al. 1995, Hart, 1997; Lowey, 2004). Regionally, it consists of a lower and upper part. The lower Hazelton Group is arc-related, whereas the upper Hazelton Group records arc demise, regional subsidence, and local development of the Eskay rift (Gagnon et al., 2012).

The following summary of the Iskut area is from Lewis (2013) and Nelson and Kyba (2014). The Hazelton Group is exposed in a series of north-northeast trending anticlines and synclines (Fig. 2). The lower Hazelton Group is divided into the Jack and Betty Creek formations (Lewis 2013), although the divisions are not universally agreed upon (Fig. 3; see Table 1 in Nelson and Kyba, 2014). Unconformably overlying Stuhini Group rocks, the Jack Formation consists of conglomerate, sandstone, and siltstone with limey interbeds. Fossil collections from the Jack Formation yielded ammonites that are diagnostic of Upper Hettangian to Lower Sinemurian age (Lewis, 2013). The overlying Betty Creek Formation includes predominantly volcanic and volcanoclastic strata of the Unuk River member (andesitic), the Brucejack Lake member (dacitic to rhyolitic), and predominantly siliciclastic and carbonate rocks of the Treaty Ridge member (Lewis, 2013). The Unuk River and Brucejack Lake members may be, in part, laterally equivalent and have yielded ca. 194-185 Ma U-Pb ages (Table 1, Fig. 3; Lewis, 2013). The overlying Treaty Ridge member yielded Upper Pliensbachian to Upper Aalenian fossil collections, suggesting a significant gap in magmatism prior to onset of upper Hazelton Group magmatism (Lewis, 2013). Nelson and Kyba (2014) include the Treaty Ridge member in the upper Hazelton Group.

The upper Hazelton Group comprises bimodal volcanic rocks that overlie the Treaty Ridge member (Fig. 3). These rocks were assigned to the Salmon River Formation by Lewis (2013) and Iskut River Formation by Gagnon et al. (2012) and Nelson and Kyba (2014). Gagnon et al. (2012) proposed that the term 'Salmon River Formation' be formally abandoned because it was inaccurately defined in its type area and confused with the Bowser Lake Group. For clarity however, we retain the term here so that our samples can be readily cross referenced with units on the Lewis (2013) compilation. The Salmon River Formation (Figs. 4, 5) is divided into the Bruce Glacier member (predominantly felsic volcanic rocks), the Troy Ridge member (predominantly tuffs and other sedimentary rocks), the John Peak member (predominantly mafic volcanic rocks) and the Eskay member (predominantly felsic volcanic rocks). The Bruce Glacier member is distinguished geochemically from the Eskay member on the basis of Al-Ti-Zr ratios (Childe, 1996; Roth et al., 1999; Lewis, 2013). Nelson and Kyba (2014) retained these members, but followed Gagnon et al. (2012) and included the Bruce Glacier, John Peaks, and Eskay members in the Iskut River Formation of the upper Hazelton Group.

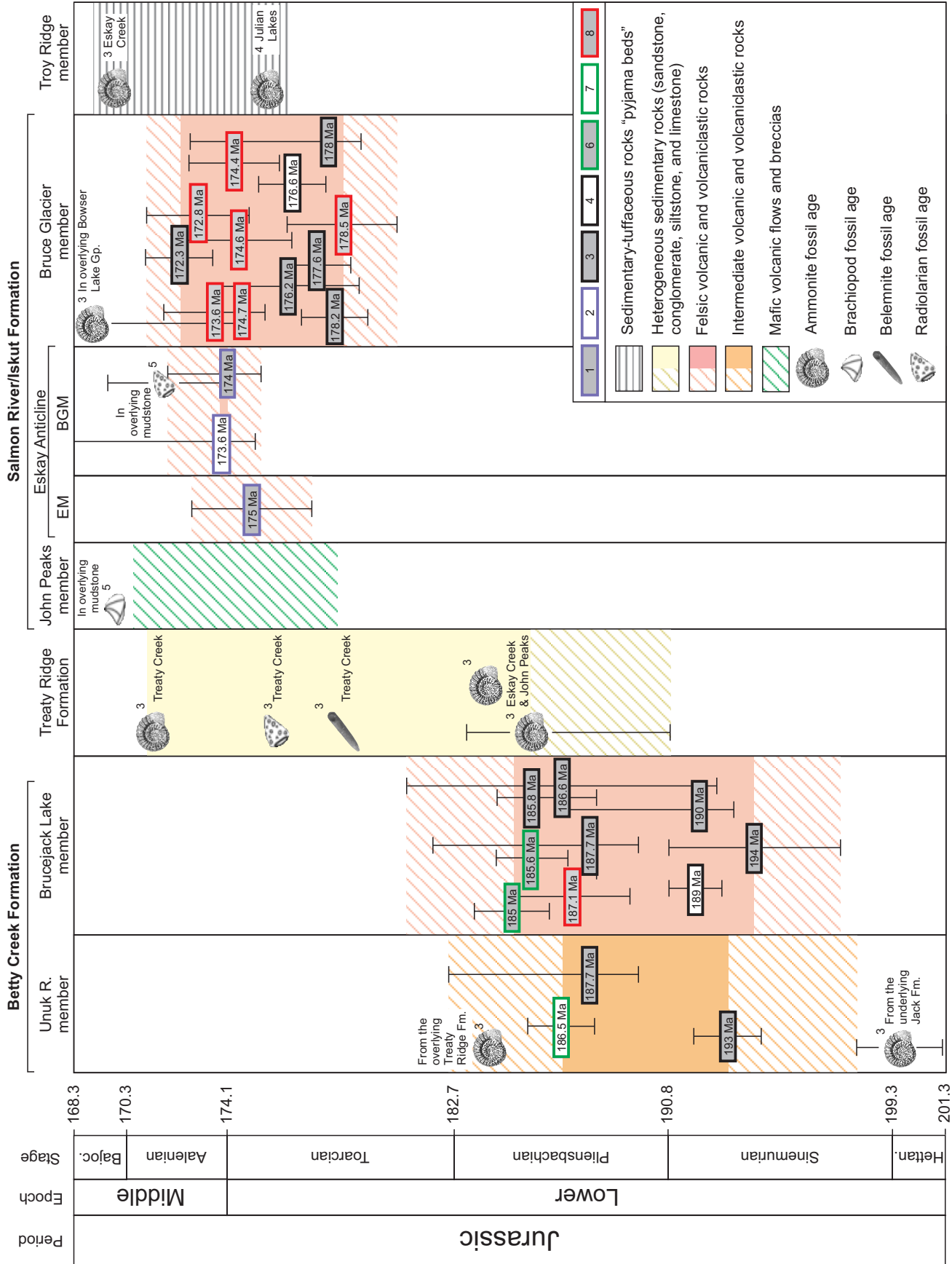


Fig. 3. U-Pb and fossil ages from the Hazelton Group in the Iskut River area summarized from 1 – Childe, 1994; 2 – Lewis et al., 2001; 3 – Lewis et al., 2001; 4 – Evenchick et al., 2001; 5 – Gagnon et al., 2012; 6 – Macdonald, 1993; 7 – Macdonald et al., 1996; 8 – This study. EM = Eskey member, BGM = Bruce Glacier member. Stage boundaries are from Cohen et al. (2013).

Table 1. Geochronology data for volcanic and hypabyssal rocks in the Iskut River area.

#	Unit	Rock Type	Age (Ma)	Reference
Bruce Glacier Section				
9	Bruce Glacier member	Felsic volcanoclastic	174.6 ± 1.8	This Study
10	Bruce Glacier member	Dacite flow	176.2 ± 2.2	Lewis et al. 2001
11	Bruce Glacier member	Spherulitic rhyolite	178.5 ± 1.8	This Study
12	Brucejack Lake member	Felsic crystal tuff	190 +5/-1	Lewis et al. 2001
Iron Cap Section				
13	Bruce Glacier member	Felsic volcanoclastic	173.3 ± 1.8	This Study
14	Bruce Glacier member	Dacite to rhyolite flow	178 +5/-1	Lewis et al. 2001
15	Brucejack Lake member	Kspar megacrystic flow	187.7 +5.8/-1.5	Lewis et al. 2001
16	Brucejack Lake member	Rhyolite flow	194 ± 3	Lewis et al. 2001
Treaty Glacier Section				
1	Bruce Glacier member	Feldspar-phyric rhyolite	173.3 ± 1.8	This Study
2	Bruce Glacier member	Hypabyssal flowbanded rhyolite	174.4 ± 1.7	This Study
3	Bruce Glacier member	Dacite-rhyolite pyroclastic flow	177.6 ± 1.0	Lewis et al. 2001
4	Brucejack Lake member	Alkali-feldspar porphyritic volcanoclastic	187.1 ± 1.9	This Study
5	Unuk member	Andesite-dacite pyroclastic flow	187.7 +5.3/-1.5	Lewis et al. 2001
Mt. Dilworth				
17	Bruce Glacier member	Felsic volcanoclastic	173.6 ± 1.7	This Study
Eskay Creek				
6	Bruce Glacier member	Dacite flow	173.6 +5.6/-0.5	Childe 1994
7	Eskay Rhyolite member	Rhyolite breccia and tuffs	174 +2/-1	Childe 1996
8	Bruce Glacier member	Flow-banded rhyolite	175 ± 2	Childe 1996
Leduc Glacier				
17	Brucejack Lake member	Dacite breccia	186.6 ± 5.6	Lewis et al. 2001

These upper Hazelton units have yielded 178-172 Ma U-Pb ages and Upper Toarcian to Bajocian fossils (Table 1, Fig. 3; Lewis, 2013). The Hazelton Group is conformably overlain by siliciclastic cover rocks of the Bowser Lake Group (Evenchick et al., 2010; Gagnon et al., 2012).

3. U-Pb Geochronology

Seven samples were collected and analyzed from the Bruce Glacier, Iron Cap, Treaty Ridge, and Mt. Dilworth areas of the McTagg anticlinorium (Fig. 2), including at or near the type sections of Hazelton Group members (see Lewis 2013 and Nelson and Kyba 2014). The upper Hazelton Group samples analyzed herein display low Al/Ti ratios (Anderson, unpublished data) indicating affinity with the Bruce Glacier member rather than the Eskay member (e.g., Childe, 1996; Roth et al., 1999). U-Pb SHRIMP data are presented in Table 2 and Figure 6.

3.1. Analytical procedures

SHRIMP II (Sensitive High Resolution Ion MicroProbe) analyses were conducted at the Geological Survey of Canada using analytical procedures described by Stern (1997), with standards and U-Pb calibration methods following Stern and

Amelin (2003). Heavy mineral concentrates were prepared from the samples using standard mineral separation techniques, including: crushing, grinding, hydrogravimetric Wilfley™ table, and heavy liquid separation. This was followed by final separation of the zircon grains by magnetic susceptibility using a Frantz™ isodynamic separator and hand-picking. Zircons from the samples and fragments of the GSC laboratory zircon standard (z6266 zircon, with $^{206}\text{Pb}/^{238}\text{U}$ age = 559 Ma) and a secondary zircon standard (Temora 2) were cast in an epoxy grain mount (see Table 2 for GSC mount number), polished with diamond compound to reveal the grain centers, and photographed in transmitted light. Internal features of the zircons (such as zoning, structures, and alteration) were characterized in back-scattered electron (BSE) and cathodoluminescence (CL) modes using a Zeiss Evo 50 scanning electron microscope (SEM). Mount surfaces were evaporatively coated with 10 nm of high purity Au. Analyses were conducted using an O⁻ primary beam, projected onto the zircons with an elliptical 17 μm x 23 μm spot (K120). The count rates of ten masses including background were sequentially measured over 6 scans with a single electron multiplier and a pulse counting system with deadtime of 23 ns. Off-line data processing used customized in-house software. The SHRIMP analytical data are presented in Table 2, where

Table 2. U/Pb SHRIMP Analytical Data.

Spot name	U (ppm)	Th (ppm)	Th/U	Pb (ppm)	²⁰⁶ Pb/ ²⁰⁶ Pb	f206	²⁰⁶ Pb/ ²⁰⁶ Pb ± 2σ	²⁰⁶ Pb/ ²⁰⁶ Pb ± 2σ	²⁰⁷ Pb/ ²³⁵ U ± 2σ	²⁰⁶ Pb/ ²³⁸ U	²⁰⁶ Pb/ ²³⁸ U ± 2σ	Corr Coeff	²⁰⁷ Pb/ ²⁰⁶ Pb	²⁰⁷ Pb/ ²⁰⁶ Pb ± 2σ	Ages (Ma) ± 1σ		
															²⁰⁶ Pb/ ²³⁸ U	²⁰⁶ Pb/ ²³⁸ U	
04-ATSK-106-L01 (z8335): spherulitic rhyolite, Bruce Glacier member (GSC grain mount IP345³)																	
8335-5.1	418	156	0.39	12	1	0.0001129	0.00196	0.130	0.006	0.2014	0.0100	0.0283	0.0004	0.366	0.0516	180	2
8335-11.1	1230	325	0.27	34	0	0.0000100	0.00017	0.091	0.003	0.1950	0.0046	0.0279	0.0004	0.506	0.0009	178	2
8335-31.1	1816	608	0.35	50	0	0.0000100	0.00017	0.108	0.002	0.1929	0.0028	0.0279	0.0003	0.502	0.0005	177	2
8335-32.1	1454	440	0.31	41	2	0.0000495	0.00086	0.096	0.002	0.1918	0.0051	0.0283	0.0003	0.492	0.0011	180	2
8335-33.1	1273	432	0.35	37	3	0.0001010	0.00175	0.099	0.002	0.1939	0.0047	0.0292	0.0004	0.482	0.0008	185	3
8335-34.1	1186	400	0.35	33	0	0.0000100	0.00017	0.107	0.003	0.1958	0.0034	0.0283	0.0003	0.502	0.0006	180	2
8335-36.1	1112	333	0.31	31	0	0.0000100	0.00017	0.099	0.002	0.1975	0.0035	0.0281	0.0004	0.509	0.0006	179	2
8335-37.1	1059	292	0.28	29	5	0.0002031	0.00352	0.101	0.004	0.1992	0.0072	0.0276	0.0004	0.523	0.0017	176	2
8335-40.1	678	188	0.29	18	3	0.0002017	0.00350	0.087	0.004	0.1845	0.0074	0.0275	0.0003	0.487	0.0018	175	2
8335-41.1	960	367	0.39	26	1	0.0000406	0.00070	0.069	0.001	0.1901	0.0110	0.0281	0.0003	0.491	0.0027	179	2
8335-42.1	1064	332	0.32	29	4	0.0001617	0.00280	0.097	0.004	0.1891	0.0070	0.0281	0.0003	0.489	0.0016	179	2
8335-44.1	1137	354	0.32	32	3	0.0001189	0.00206	0.097	0.003	0.1895	0.0058	0.0283	0.0003	0.475	0.0013	180	2
8335-46.1	790	244	0.32	21	4	0.0001949	0.00338	0.101	0.003	0.1858	0.0051	0.0274	0.0003	0.511	0.0012	174	2
8335-47.1	1313	421	0.33	37	2	0.0000623	0.00108	0.107	0.002	0.1955	0.0051	0.0283	0.0004	0.586	0.0011	180	2
8335-51.1	1327	367	0.29	37	1	0.0000457	0.00079	0.091	0.004	0.1916	0.0067	0.0283	0.0006	0.651	0.0013	180	3
8335-55.1	1203	315	0.27	33	1	0.0000245	0.00042	0.083	0.004	0.2001	0.0042	0.0285	0.0003	0.636	0.0008	181	2
8335-56.1	1311	325	0.26	36	6	0.0001957	0.00339	0.084	0.004	0.1837	0.0050	0.0285	0.0003	0.506	0.0011	181	2
04-ATSL-042-L01 (z8337): felsic volcanoclastic rock, Bruce Glacier member (GSC grain mount IP345³)																	
8337-1.1	196	74	0.39	6	1	0.0002095	0.00363	0.138	0.015	0.2025	0.0247	0.0286	0.0005	0.263	0.0514	182	3
8337-4.1	1499	443	0.31	42	3	0.0000698	0.00121	0.097	0.002	0.1931	0.0048	0.0281	0.0003	0.555	0.0011	179	2
8337-5.1	294	87	0.31	8	2	0.0002825	0.00490	0.096	0.014	0.1896	0.0209	0.0274	0.0004	0.502	0.0054	174	2
8337-13.1	155	35	0.23	4	1	0.00001456	0.00252	0.098	0.019	0.2107	0.0316	0.0274	0.0004	0.259	0.0558	174	3
8337-18.1	255	59	0.24	7	1	0.0001264	0.00219	0.089	0.009	0.2095	0.0159	0.0271	0.0003	0.286	0.0562	172	2
8337-21.1	96	36	0.39	3	2	0.0008253	0.01430	0.154	0.026	0.2735	0.0504	0.0337	0.0006	0.217	0.0589	0.0107	213
8337-40.1	207	62	0.31	6	2	0.0004803	0.00832	0.109	0.011	0.1916	0.0173	0.0272	0.0004	0.277	0.0511	173	2
8337-41.1	346	116	0.35	10	0	0.0000415	0.00072	0.117	0.013	0.2178	0.0199	0.0276	0.0004	0.284	0.0574	173	2
8337-42.1	208	52	0.26	6	2	0.0003621	0.00628	0.092	0.015	0.2027	0.0235	0.0276	0.0004	0.236	0.0532	176	2
8337-43.1	171	35	0.21	4	4	0.0008921	0.01546	0.064	0.011	0.1845	0.0179	0.0271	0.0004	0.264	0.0494	172	2
8337-44.1	706	224	0.33	19	4	0.0002201	0.00381	0.106	0.004	0.1852	0.0070	0.0274	0.0003	0.403	0.0490	174	2
8337-46.1	665	236	0.37	18	6	0.0003551	0.00615	0.110	0.008	0.1908	0.0103	0.0279	0.0003	0.319	0.0496	177	2
8337-62.1	297	102	0.35	8	5	0.0007427	0.01287	0.114	0.011	0.1874	0.0143	0.0274	0.0004	0.294	0.0496	174	2
8337-63.1	174	41	0.24	5	3	0.0007368	0.01277	0.083	0.012	0.2004	0.0201	0.0278	0.0004	0.258	0.0523	177	2
8337-64.1	921	238	0.27	25	7	0.0003068	0.00532	0.085	0.004	0.1861	0.0069	0.0280	0.0004	0.476	0.0482	178	2
8337-65.1	339	93	0.28	9	1	0.0001183	0.00205	0.111	0.010	0.2257	0.0162	0.0274	0.0003	0.294	0.0597	175	2
04-AT0-1001-L01 (z8567): lapilli tuff, Bruce Glacier member (GSC grain mount IP357³)																	
8567-3.1	308	138	0.46	9	3	0.0004428	0.00767	0.157	0.012	0.1973	0.0195	0.0273	0.0004	0.251	0.0524	174	2
8567-5.1	180	82	0.47	5	6	0.0013849	0.02400	0.135	0.020	0.1688	0.0276	0.0270	0.0004	0.221	0.0453	172	3
8567-7.1	122	32	0.28	3	0	0.0000100	0.00017	0.141	0.014	0.2528	0.0091	0.0275	0.0004	0.512	0.0668	175	3
8567-8.1	179	52	0.30	5	0	0.0000100	0.00017	0.117	0.008	0.2138	0.0074	0.0269	0.0005	0.622	0.0577	171	3
8567-10.1	458	158	0.36	13	2	0.0001864	0.00323	0.119	0.007	0.2069	0.0109	0.0282	0.0004	0.351	0.0532	179	2
8567-14.1	187	56	0.31	5	5	0.0011380	0.01972	0.067	0.021	0.1559	0.0306	0.0271	0.0004	0.206	0.0418	172	3
8567-15.1	459	147	0.33	12	3	0.0003248	0.00563	0.102	0.009	0.1783	0.0121	0.0273	0.0004	0.308	0.0475	173	2
8567-17.1	144	48	0.34	4	3	0.0009831	0.01704	0.110	0.024	0.1815	0.0327	0.0270	0.0006	0.236	0.0487	172	3
8567-21.1	245	123	0.52	7	5	0.0003296	0.00571	0.113	0.012	0.1972	0.0169	0.0272	0.0004	0.304	0.0526	173	3
8567-22.1	176	54	0.32	5	4	0.0008801	0.01525	0.156	0.016	0.1676	0.0178	0.0270	0.0004	0.256	0.0450	172	2
8567-70.1	192	112	0.60	5	0	0.0008616	0.01493	0.099	0.014	0.1819	0.0208	0.0271	0.0004	0.264	0.0488	172	3
8567-71.1	257	106	0.42	7	6	0.0000980	0.00014	0.223	0.016	0.2251	0.0243	0.0270	0.0004	0.262	0.0604	172	3
8567-70.1	192	112	0.60	5	0	0.0009742	0.01688	0.138	0.012	0.1767	0.0206	0.0271	0.0004	0.242	0.0474	172	2
8567-82.1	238	91	0.40	7	2	0.0004197	0.00727	0.137	0.019	0.2110	0.0275	0.0286	0.0005	0.243	0.0535	182	3

Table 2. Continued.

Spot name	U (ppm)	Th (ppm)	Th/U	Pb (ppm)	²⁰⁴ Pb	²⁰⁶ Pb/ ²⁰⁶ Pb	²⁰⁶ Pb/ ²⁰⁶ Pb	²⁰⁶ Pb/ ²⁰⁶ Pb	²⁰⁷ Pb/ ²³⁵ U	²⁰⁶ Pb/ ²³⁸ U	Corr Coeff	²⁰⁷ Pb/ ²⁰⁶ Pb	²⁰⁷ Pb/ ²⁰⁶ Pb	Ages (Ma) ± 1σ ¹ ²⁰⁶ Pb/ ²³⁸ U	Ages (Ma) ± 1σ ² ²¹⁰ Pb/ ²³⁸ U				
04-ATSK-008-L01 (z8330): spherulitic rhyolite, Bruce Glacier member (GSC grain mount IP345³)																			
8336-2.1	132	54	0.42	4	1	0.003259	0.00565	0.146	0.015	0.2225	0.0282	0.0317	0.0006	0.0509	0.0063	201	3	201	3
8336-3.1	401	89	0.23	10	4	0.0004007	0.00694	0.065	0.006	0.1697	0.0097	0.0271	0.0003	0.0454	0.0025	173	2	173	2
8336-4.1	293	56	0.20	7	42	0.0056797	0.09844	-0.022	0.032	0.0783	0.0558	0.0265	0.0005	0.0215	0.0152	168	3	173	3
8336-5.1	309	61	0.20	8	2	0.003403	0.00590	0.064	0.010	0.1819	0.0157	0.0274	0.0004	0.0481	0.0040	174	2	175	2
8336-6.1	335	68	0.21	9	2	0.002844	0.00493	0.065	0.007	0.1840	0.0120	0.0274	0.0004	0.0486	0.0030	175	2	175	2
8336-7.1	458	113	0.26	12	2	0.002156	0.00374	0.081	0.005	0.1930	0.0091	0.0280	0.0004	0.0323	0.0022	178	2	178	2
8336-8.1	662	274	0.43	21	0	0.0000100	0.00017	0.150	0.003	0.2208	0.0052	0.0306	0.0004	0.0523	0.0009	194	3	194	3
8336-9.1	270	52	0.20	7	0	0.0000100	0.00017	0.074	0.003	0.2072	0.0070	0.0273	0.0004	0.0551	0.0015	173	3	172	3
8336-12.1	723	193	0.28	20	2	0.0001336	0.00232	0.094	0.006	0.1942	0.0171	0.0281	0.0016	0.0500	0.0030	179	10	179	10
8336-13.1	277	57	0.21	7	1	0.0001702	0.00295	0.073	0.012	0.1867	0.0201	0.0276	0.0004	0.0490	0.0051	176	3	176	3
8336-17.1	310	58	0.19	8	3	0.003484	0.00604	0.059	0.008	0.1877	0.0117	0.0278	0.0004	0.0489	0.0029	177	3	177	3
8336-18.1	221	41	0.19	6	2	0.0003788	0.00657	0.062	0.013	0.1989	0.0223	0.0280	0.0005	0.0515	0.0056	178	3	178	3
8336-21.1	275	54	0.20	7	1	0.0001585	0.00275	0.068	0.008	0.1867	0.0115	0.0271	0.0003	0.0500	0.0029	172	2	172	2
8336-23.1	165	99	0.62	6	2	0.0003107	0.00538	0.203	0.016	0.2564	0.0299	0.0344	0.0006	0.0541	0.0061	218	4	217	4
8336-26.1	320	66	0.21	8	2	0.0002649	0.00459	0.070	0.012	0.1897	0.0180	0.0274	0.0004	0.0257	0.0047	174	2	174	2
8336-33.1	305	62	0.21	8	0	0.0000548	0.00095	0.073	0.008	0.1943	0.0135	0.0273	0.0003	0.0516	0.0035	174	2	173	2
8336-35.1	268	51	0.20	7	3	0.0005335	0.00925	0.050	0.011	0.1784	0.0162	0.0278	0.0004	0.0465	0.0041	177	2	178	2
8336-36.1	430	117	0.28	12	0	0.0000100	0.00017	0.097	0.005	0.2024	0.0125	0.0284	0.0010	0.0517	0.0024	181	6	180	6
04-ATSK-004-L01 (z8392): felsic volcanoclastic rock, Bruce Glacier member (GSC grain mount IP345³)																			
8392-5.1	309	131	0.44	9	3	0.0004185	0.00725	0.149	0.010	0.2109	0.0163	0.0289	0.0004	0.0529	0.0039	184	3	183	3
8392-12.1	854	352	0.43	24	6	0.0002789	0.00483	0.135	0.005	0.1872	0.0078	0.0279	0.0003	0.0486	0.0019	178	2	178	2
8392-15.1	337	119	0.36	9	3	0.0003418	0.00592	0.129	0.009	0.2057	0.0120	0.0277	0.0004	0.0539	0.0030	176	2	175	2
8392-16.1	236	70	0.31	6	5	0.0009088	0.01575	0.107	0.015	0.2003	0.0234	0.0270	0.0004	0.0539	0.0061	172	3	171	2
8392-21.1	394	124	0.33	11	4	0.0004587	0.00795	0.106	0.007	0.1895	0.0113	0.0273	0.0004	0.0504	0.0029	173	2	173	2
8392-22.1	539	168	0.32	14	4	0.0003206	0.00556	0.107	0.007	0.1831	0.0102	0.0266	0.0003	0.0499	0.0027	169	2	169	2
8392-23.1	385	115	0.31	10	4	0.0004966	0.00861	0.094	0.009	0.1862	0.0124	0.0271	0.0003	0.0499	0.0032	172	2	172	2
8392-24.1	782	265	0.35	21	6	0.0003409	0.00591	0.111	0.005	0.1845	0.0076	0.0274	0.0003	0.0489	0.0019	174	2	174	2
8392-26.1	173	50	0.30	4	5	0.0013426	0.02327	0.080	0.017	0.1814	0.0259	0.0268	0.0004	0.0491	0.0069	171	3	170	2
8392-27.1	327	108	0.34	9	3	0.0003550	0.00615	0.117	0.007	0.2008	0.0117	0.0272	0.0004	0.0536	0.0030	173	2	172	2
8392-28.1	483	138	0.30	13	4	0.0003766	0.00653	0.101	0.006	0.1919	0.0093	0.0273	0.0003	0.0510	0.0023	174	2	173	2
8392-29.1	255	70	0.28	7	7	0.0011725	0.02032	0.086	0.011	0.1694	0.0177	0.0270	0.0004	0.0455	0.0046	172	2	172	2
8392-30.1	222	53	0.25	6	5	0.0009356	0.01621	0.070	0.020	0.1941	0.0322	0.0282	0.0004	0.0499	0.0082	179	3	179	2
8392-31.1	1009	127	0.13	28	6	0.0002423	0.00420	0.040	0.005	0.2015	0.0087	0.0297	0.0003	0.0492	0.0020	189	2	189	2
8392-43.1	635	212	0.34	18	2	0.0001266	0.00219	0.112	0.007	0.2044	0.0113	0.0277	0.0003	0.0536	0.0028	176	2	175	2
8392-47.1	606	202	0.35	17	6	0.0004075	0.00706	0.108	0.006	0.1914	0.0111	0.0279	0.0003	0.0498	0.0028	177	2	177	2

Notes:

Spot name follows the convention x-y-z; where x = lab number, y = grain number, z = spot number
 Uncertainties reported at one sigma and are calculated by numerical propagation of all known sources of error (Stern, 1997).
¹ 206-corrected ages; ² 207-corrected ages (Stern 1997)
³ GSC grain mounts IP345, IP350, and IP357: spot size - 17µm x 23µm (K120); calibration error = 1.0%

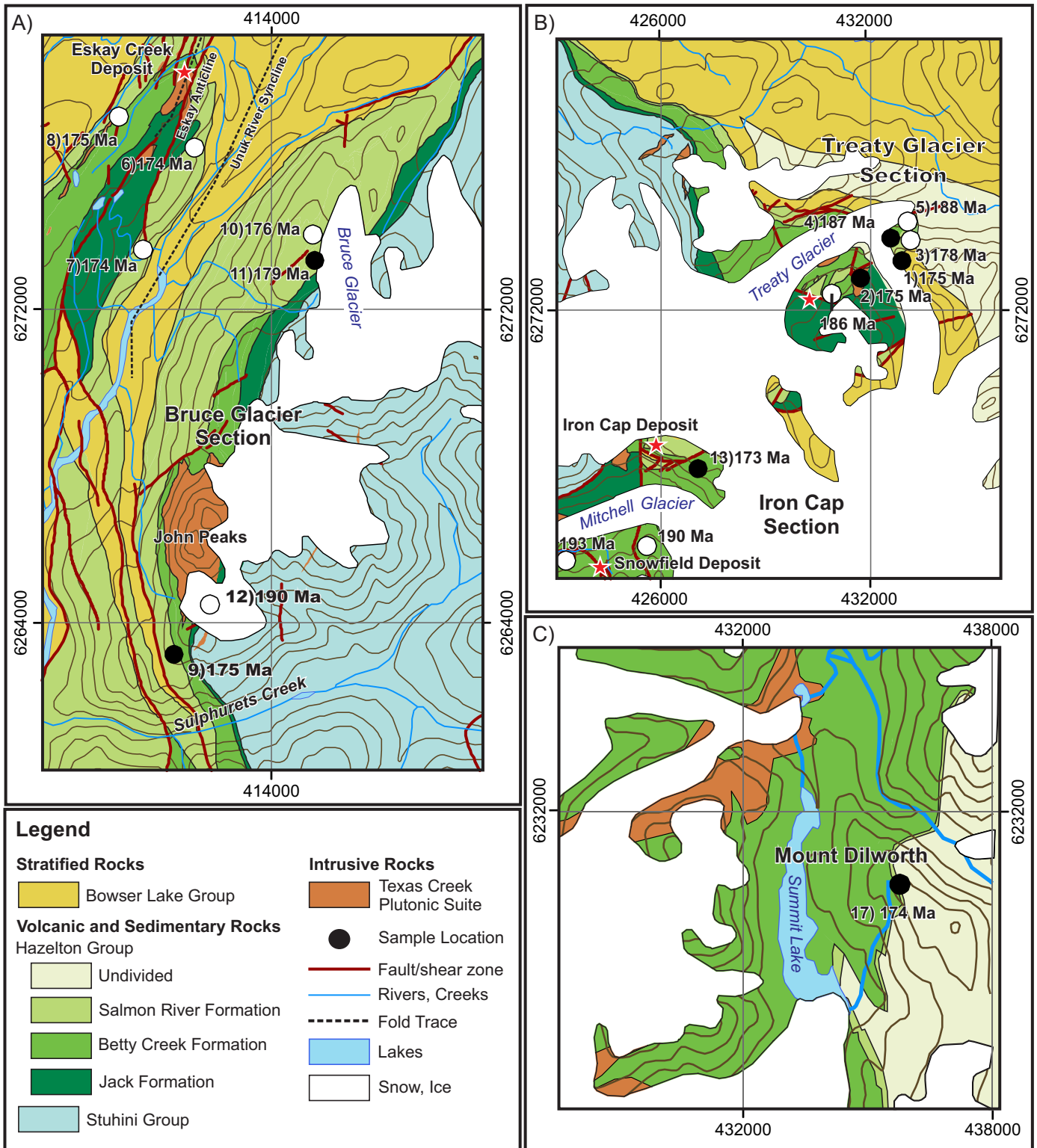


Fig. 4. Simplified geological maps (modified from Lewis, 2013). **a)** Bruce Glacier area. **b)** Iron Cap-Treaty Glacier area. **c)** Mt. Dilworth area. Numbers refer to ages of volcanic and hypabyssal rocks in the Iskut River area (Table 1). UTM zone 9, NAD 83.

the 1σ external errors of $^{206}\text{Pb}/^{238}\text{U}$ ratios incorporate a 1.0% error in calibrating the standard zircon (Stern and Amelin, 2003). A fractionation correction was not applied to the Pb-isotope data; common Pb correction used the Pb composition

of the surface blank (Stern, 1997). The 207-corrected $^{206}\text{Pb}/^{238}\text{U}$ ages of analyses overlapping concordia were used to calculate weighted means and construct cumulative probability plots (Fig. 6). Weighted means were calculated using Isoplot v.

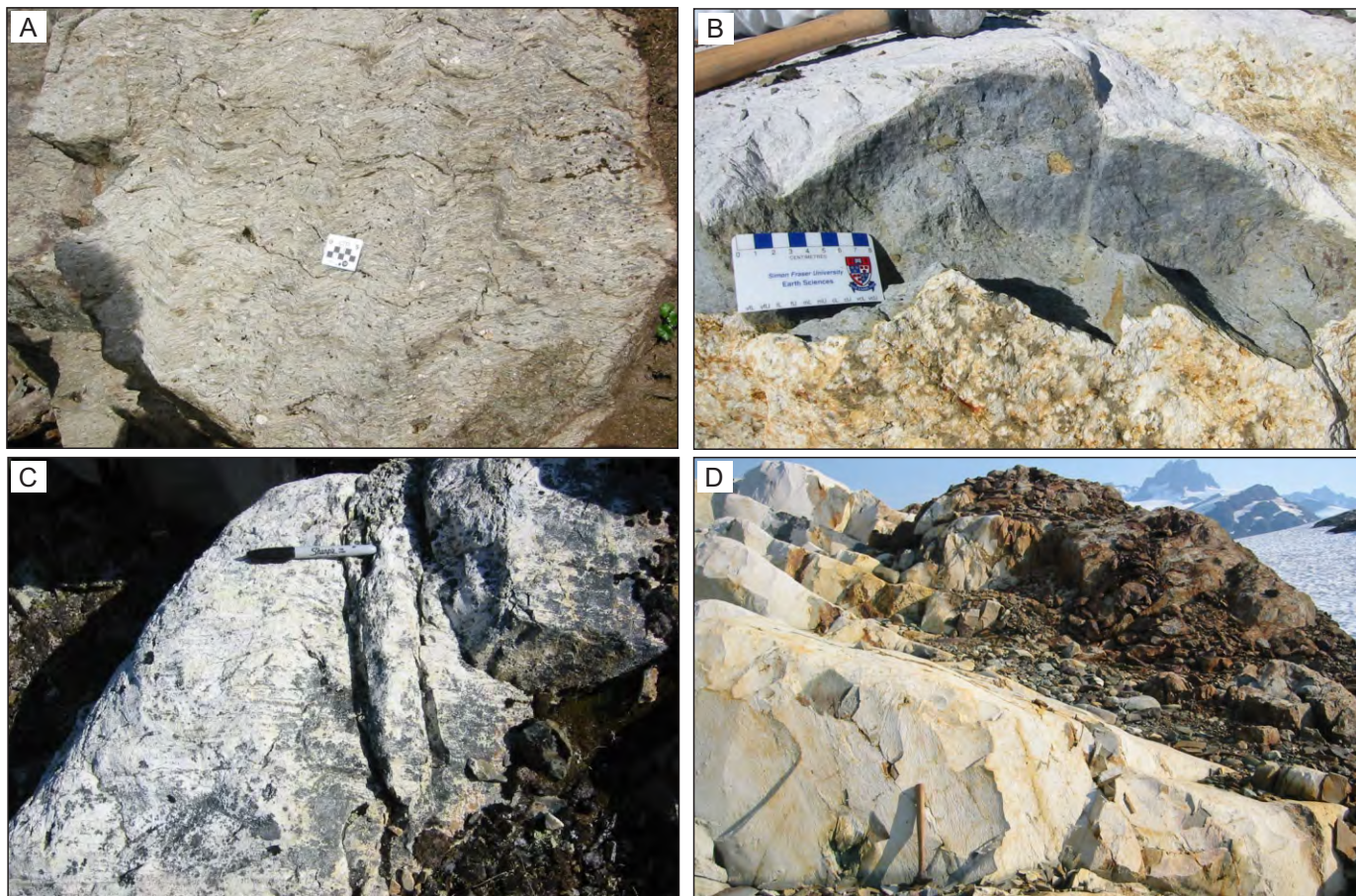


Fig. 5. Representative photographs of analyzed samples. **a)** Thick unit of foliated and crenulated, monolithic, felsic lapilli tuff of the Bruce Glacier member (Sample 04-ATSL-042-L01; z8337). **b)** Felsic lapilli tuff in the Iron Cap area (Sample 04-AT-1001-L01; z8567). **c)** Spherulitic, flow-banded rhyolite from Treaty Ridge (Sample 04-ATSK-008-L01; z8336). **d)** Felsic tuff in the Mt. Dilworth area (Sample 04-ATSK-004-L01; z8392).

3.0 (Ludwig, 2003) with errors on the ages quoted at the 2σ level and cumulative probability plots were constructed using AGEDISPLAY (Sircombe, 2004).

3.2. Bruce Glacier area

3.2.1. 04-ATSK-106-L01 (z8335): Spherulitic rhyolite, Bruce Glacier member

In the Bruce Glacier section (Fig. 4a), the Stuhini Group is unconformably overlain by the Jack Formation, which is in turn unconformably overlain by the Bruce Glacier member (Lewis 2013; see also Fig. 3 in Nelson and Kyba 2014). West of the McTagg anticlinorium, the base of the Bruce Glacier member is an angular unconformity that cuts through the Treaty Ridge and Unuk River members (Lewis 2013). We collected a sample of spherulitic rhyolite considered to be typical of the Bruce Glacier member along Bruce Glacier, northeast of John Peaks and east of Unuk River (Fig. 4a). The sample yielded two size populations of zircon. One consists of clear, colourless, euhedral prism tips $\sim 150 \mu\text{m}$ long, with abundant fractures, rare inclusions, and faint to strong oscillatory growth zoning typical of magmatic zircons. The second consists of clear, colourless, euhedral prismatic crystals, prism tips and tabular grains

$\sim 100 \mu\text{m}$ long, lacking visible fractures or inclusions. These grains display faint oscillatory growth and sector zoning, both typical of magmatic zircons (Fig. 6a). Excluding one analysis interpreted to be inherited (analysis 8335-33.1, Table 2), sixteen analyses from both populations yielded a mean $^{206}\text{Pb}/^{238}\text{U}$ age of 178.5 ± 1.2 (MSWD = 1.2). Taking into account the error associated with the zircon standards, the crystallization age of the rhyolite is interpreted as 178.5 ± 1.8 Ma (Fig. 6a).

3.2.2. 04-ATSL-042-L01 (z8337): Felsic volcanoclastic rock, Bruce Glacier member

South of John Peaks, the Stuhini Group is overlain by the Jack Formation at a well-exposed, sharp, angular unconformity (Fig. 4a; Lewis 2013). The Jack Formation is in turn overlain by the Brucejack, Unuk River and Treaty Ridge members of the Betty Creek Formation. Bruce Glacier member felsic volcanic rocks overlie the Betty Creek Formation above an angular unconformity (Fig. 4a; Lewis 2013). We collected a sample of monolithic, felsic lapilli tuff from the Bruce Glacier member (Fig. 5a). The sample yielded two size populations of zircon. The first population comprises $50\text{--}100 \mu\text{m}$, clear, colourless, subhedral prismatic grains and prism fragments with rounded

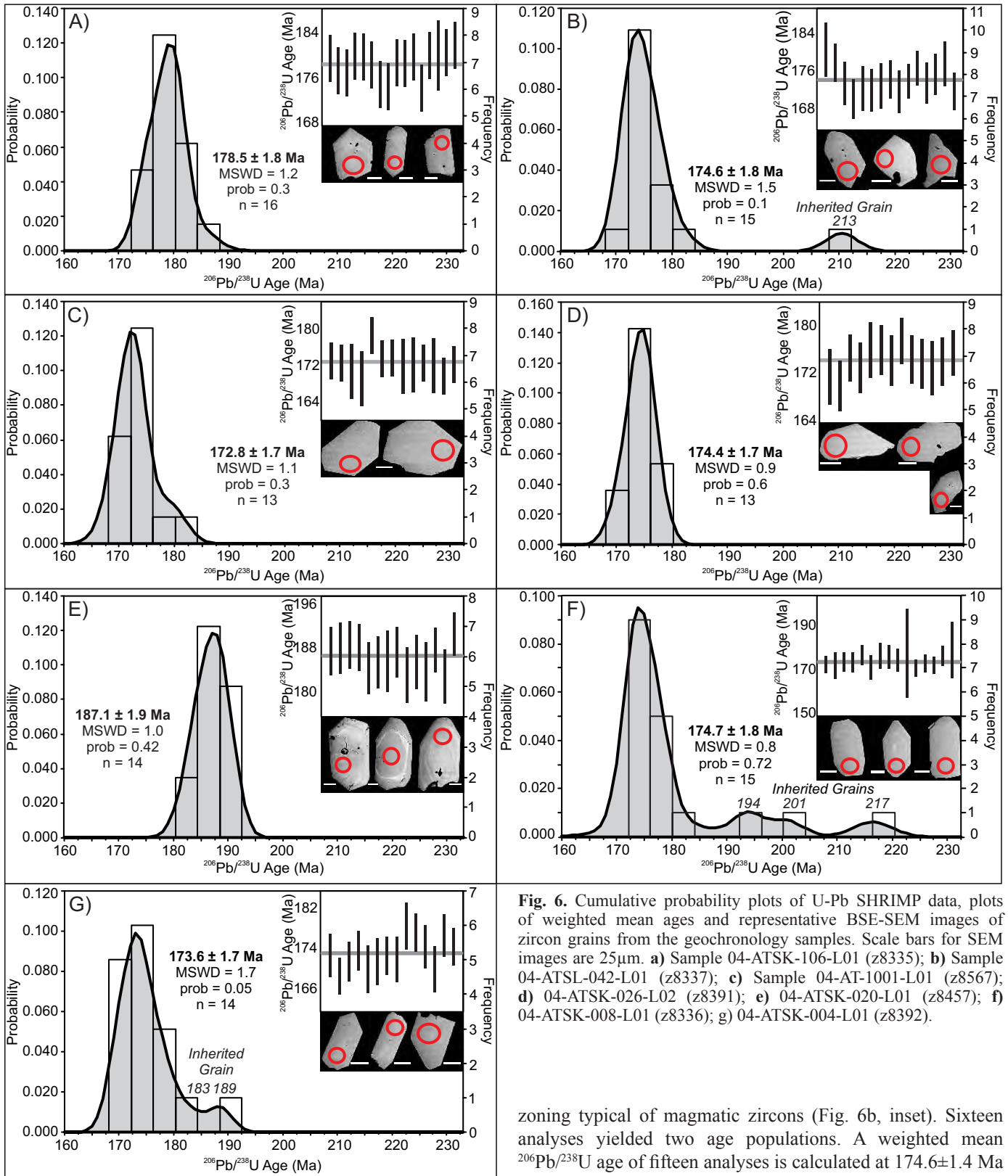


Fig. 6. Cumulative probability plots of U-Pb SHRIMP data, plots of weighted mean ages and representative BSE-SEM images of zircon grains from the geochronology samples. Scale bars for SEM images are 25µm. **a)** Sample 04-ATSK-106-L01 (z8335); **b)** Sample 04-ATSL-042-L01 (z8337); **c)** Sample 04-AT-1001-L01 (z8567); **d)** 04-ATSK-026-L02 (z8391); **e)** 04-ATSK-020-L01 (z8457); **f)** 04-ATSK-008-L01 (z8336); **g)** 04-ATSK-004-L01 (z8392).

tips, and rare to abundant fractures. The second comprises 150–200 µm, clear, colourless, euhedral to subhedral prismatic grains with rare fractures and inclusions. Both populations lack

zoning typical of magmatic zircons (Fig. 6b, inset). Sixteen analyses yielded two age populations. A weighted mean $^{206}\text{Pb}/^{238}\text{U}$ age of fifteen analyses is calculated at 174.6 ± 1.4 Ma (MSWD=1.5). Taking into consideration the error associated with the zircon standards, the crystallization age of the felsic tuff is interpreted as 174.6 ± 1.8 Ma (Fig. 6b). A single unzoned prism fragment (analysis 8337-21.0, Table 2) yielded ca. 213 Ma age and is interpreted to be inherited (Fig. 6b).

3.3. Iron Cap area

3.3.1. 04-AT-1001-L01 (z8567): Lapilli tuff, Bruce Glacier member

The ca. 195 Ma Iron Cap intrusion and related volcanoclastic rocks that host the Iron Cap porphyry Cu-Au deposit (Kirkham and Margolis, 1995) are unconformably overlain by the Treaty Ridge member (Middle Jurassic; Lewis et al., 2001) west of the Brucejack fault (Fig. 4b; see Fig. 5 in Nelson and Kyba, 2014). East of the Brucejack fault, the Treaty Ridge member is absent and Unuk River member andesitic rocks are unconformably overlain by the Bruce Glacier member (Fig. 4b). A sample from a unit of flow-banded felsic lapilli tuff was collected to test its correlation with the Bruce Glacier member (Fig. 5b). The sample yielded abundant zircon grains ranging in size from 50-100 μm with variable morphologies, including euhedral to subhedral prismatic grains and prism fragments and sparse euhedral to subhedral, tabular grains. Some grains display oscillatory growth zoning typical of magmatic zircons (Fig. 6c). Excluding one analysis interpreted to be xenocrystic (analysis 8567-82.1, Table 2), thirteen analyses yielded a weighted mean $^{206}\text{Pb}/^{238}\text{U}$ age of 172.8 ± 1.2 Ma (MSWD = 1.1). Taking into account the error associated with the zircon standards, the crystallization age of the lapilli tuff is interpreted as 172.8 ± 1.7 Ma (Fig. 6c).

3.4. Treaty Glacier area

3.4.1. 04-ATSK-026-L02 (z8391): Flow-banded rhyolite, feeder to Bruce Glacier member?

Southeast of the Treaty Glacier, on the Treaty Nunatak, hypabyssal felsic dykes and stocks, assigned by Lewis (2013) to the Texas Creek plutonic suite, intrude a southeast-younging succession of sedimentary rocks and pillow basalts interpreted as the Treaty Ridge and John Peaks members (Fig. 4b; Lewis, 2013). A sample of hypabyssal flow-banded rhyolite was collected to establish the age of these intrusive rocks and to provide a minimum age for the volcano-sedimentary rocks that are assigned to the Treaty Ridge member. The sample yielded abundant zircon grains that are clear, colourless, stubby, prismatic crystals 75-100 μm long, with rare fractures and inclusions. Some grains display oscillatory growth zoning typical of magmatic zircons (Fig. 6d), and some have possible inherited cores that were not analyzed. Thirteen analyses yielded a weighted mean $^{206}\text{Pb}/^{238}\text{U}$ age of 174.4 ± 1.1 Ma (MSWD = 0.9). Taking into consideration the error associated with the zircon standards, the crystallization age of the rhyolite and related felsic stocks is interpreted as 174.4 ± 1.7 Ma (Fig. 6d). It is significantly younger than the Texas Creek suite, and corresponds to ages of nearby felsic rocks of the Bruce Glacier member.

3.4.2. 04-ATSK-020-L01 (z8457): Felsic volcanoclastic rock, Brucejack Lake member

The base of Treaty Ridge, south of Treaty Creek, exposes volcanic rocks of the lower Hazelton Group that were included in the Unuk River member by Lewis (2013). These rocks are

overlain by the Treaty Ridge, John Peaks, and Bruce Glacier members (Fig. 4b). A sample of alkali feldspar-phyric felsic volcanoclastic rock was collected from near the base of exposed section. The sample yielded abundant zircon grains including clear, colourless subhedral to euhedral, tabular prismatic crystals and prism fragments, 50-100 μm long, that contain many fractures and inclusions. These grains are either unzoned or display oscillatory growth zoning typical of magmatic zircons (Fig. 6e). A weighted mean of the $^{206}\text{Pb}/^{238}\text{U}$ ages of fourteen analyses is calculated at 187.1 ± 1.2 Ma (MSWD=1.0). Taking into account the error associated with the zircon standards, the crystallization age of the felsic volcanic is interpreted as 187.1 ± 1.9 Ma (Fig. 6e).

3.4.3. 04-ATSK-008-L01 (z8336): Spherulitic rhyolite, Bruce Glacier member

We collected a sample of fine-grained, feldspar-phyric, spherulitic rhyolite from the Bruce Glacier member upsection from sample 04-ATSK-020-L01 (see above, Fig. 5c). The sample yielded abundant zircon grains that are 50-100 μm long and include clear, colourless, euhedral to subhedral tabular prisms, with rare fractures and local inclusions. Some grains display strong oscillatory growth zoning typical of magmatic zircons (Fig. 6f). Fifteen analyses yielded a weighted mean $^{206}\text{Pb}/^{238}\text{U}$ age of 174.7 ± 1.2 Ma (MSWD=0.8). Taking into account the error associated with the zircon standards, the crystallization age of the rhyolite is taken to be 174.7 ± 1.8 Ma (Fig. 6f). Three zircon grains yielded significantly older ages, which are interpreted to be inherited. Inherited analyses of ca. 194 and 200 Ma ages (analyses 8336-8.1 and 8336-23.1) were from euhedral to subhedral prismatic grains lacking evidence of inherited cores. A rounded grain with a possible older core yielded an age of ca. 218 Ma (analysis 8336-2.1; Fig. 6f).

3.5. Mt. Dilworth area

3.5.1. 04-ATSK-004-L01 (z8392): Felsic volcanoclastic rock, Bruce Glacier Member

North of Mt. Dilworth and east of Summit Lake, the Betty Creek Formation is overlain by a continuous unit of dacitic volcanoclastic rocks that extends over 20 kilometres along strike (Fig. 4c). This unit was assigned to the Mt. Dilworth Formation by Alldrick (1991, 1993). Its age was poorly constrained by a single Toarcian macrofossil collection from an overlying limestone unit (Alldrick, 1993), and a ca. 178 Ma U-Pb age with complicated systematics (ATP-Troy Ridge, in Lewis et al., 2001). As evidence began to emerge of the Middle Jurassic (ca. 174-176 Ma) age of the Eskay and Bruce Glacier members, Lewis (2001) considered that the Mt. Dilworth Formation was significantly older than originally defined and discontinued use of the term in the Iskut area. A sample of a volcanoclastic rock (Fig. 5d) was collected to determine the age of magmatism in the Mt. Dilworth area and to test its correlation with other felsic units of the Hazelton Group (i.e. Brucejack and Bruce Glacier members). The sample yielded abundant zircon grains that are 50-100 μm long and include clear, colourless, euhedral

prismatic crystals and prism fragments with rounded tips, no fractures and few inclusions, and elongate prisms up to 150 μm long. Some grains display oscillatory growth zoning typical of magmatic zircons (Fig. 6g). Fourteen analyses yielded a weighted mean $^{206}\text{Pb}/^{238}\text{U}$ age of 173.6 ± 1.7 Ma (MSWD=1.7), which is interpreted as the crystallization age of the felsic volcanic rock (Fig. 6g). Two inherited zircon analyses include a core of a subhedral rounded grain (analysis 8392-5.1: Table 2) with an age of ca. 183 Ma and an oscillatory growth zoned euhedral prism (analysis 8392-31.1: Table 2) with an age of ca. 189 Ma.

4. Discussion

In this study, we present U-Pb zircon data from seven Hazelton Group samples to establish the absolute ages of volcano-sedimentary units in the McTagg anticlinorium, east of the Eskay Creek deposit (Tables 1, 3). One sample of felsic volcanoclastic rock documents the age of the Brucejack Lake member of the Betty Creek Formation at Treaty Ridge. Six samples limit the spatial and temporal extent of the Bruce Glacier member of the Iskut River Formation.

4.1. Brucejack Lake Member

The Treaty Ridge section exposes a continuous stratigraphic sequence from the Unuk River member to the Treaty Ridge, John Peaks and Bruce Glacier members (Fig. 3b). Alkali feldspar porphyritic felsic volcanoclastic rock from near the base of the exposed section yielded a 187.1 ± 1.9 Ma crystallization age (Table 2) confirming Brucejack Lake member epiclastic units, which may interfinger with andesites of the Unuk River member. This age closely agrees with the ca. 188 Ma age from this section reported by Lewis et al. (2001). Elsewhere, the Brucejack Lake and Unuk River members and their hypabyssal equivalents yielded ca. 194 to 185 Ma

U-Pb zircon crystallization ages (Macdonald, 1993; Lewis et al. 2001), indicating that magmatism spanned ca. 5 to 10 m.y. (Fig. 3).

The underlying Jack Formation yielded Hettangian ammonites (Lewis et al. 2001) consistent with ca. 194 to 185 Ma U-Pb ages from the overlying Betty Creek Formation. However, there appears to be a several m.y. hiatus prior to onset of Unuk and Brucejack Lake member volcanism (Fig. 3). Pliensbachian ammonites in the overlying Treaty Ridge Member (Fig. 3) suggest either that Treaty Ridge sedimentation immediately followed cessation of Sinemurian to Pliensbachian Betty Creek Formation magmatism or that Treaty Ridge deposition occurred in an area that was isolated from the products of Betty Creek Formation volcanism.

4.2. Bruce Glacier Member

Bruce Glacier member felsic volcanic and epiclastic rocks are exposed along the east limb of the Eskay anticline and on both limbs of the McTagg anticlinorium (Fig. 2). Samples from the type locality at Bruce Glacier yielded 178.5 ± 1.8 Ma and 174.6 ± 1.8 Ma ages (Table 2, Fig. 3a) indicating that magmatism spanned ca. 1 to 7 m.y. Bruce Glacier member volcanic and hypabyssal rocks in the Iron Cap, Treaty Glacier, and Mt. Dilworth areas yielded ca. 175 to 173 Ma ages (Table 2; Figures 3b,c). Older Bruce Glacier member felsic rocks appear to be more commonly dacitic whereas younger rocks tend to be rhyolitic. Previous samples of the Bruce Glacier member volcanic and hypabyssal rocks equivalents have yielded ca. 178 to 173 Ma U-Pb zircon crystallization ages (Fig. 3; Macdonald, 1993; Lewis et al., 2001). Both our results and previous ages indicate magmatism either spanned ca. 5 to 9 m.y. or occurred in several discrete pulses.

Based on zircon inheritance and Sm-Nd isotopic data, Childe (1996) suggested that underlying Mesozoic and Paleozoic arcs

Table 3. Sample summary.

Sample Number	Lab Number	UTM		Unit Name	Rock Description	Interpreted Age	Inherited Ages
		E	N				
Bruce Glacier area							
04-ATSK-106-L01	8335	415112	6273249	Bruce Glacier member	Spherulitic rhyolite	178.5 ± 1.8 Ma	ca. 186 Ma
04-ATSL-042-L01	8337	411626	6263187	Bruce Glacier member	Felsic volcanoclastic rock	174.6 ± 1.8 Ma	ca. 213 Ma
Iron Cap area							
04-AT-1001-L01	8567	427059	6267454	Bruce Glacier member	Felsic volcanoclastic rock	173.3 ± 1.8 Ma	ca. 181 Ma
Treaty Glacier area							
04-ATSK-026-L02	8391	431695	6272917	Bruce Glacier member	Hypabyssal flowbanded rhyolite	174.4 ± 1.7 Ma	
04-ATSK-020-L01	8457	432437	6274000	Brucejack Lake member	Alkali feldspar porphyritic volcanoclastic rock	187.1 ± 1.9 Ma	
04-ATSK-008-L01	8336	432873	6273418	Bruce Glacier member	Feldspar-phyric rhyolite	174.7 ± 1.8 Ma	ca. 194 Ma, ca. 200 Ma, ca. 217 Ma
Mt. Dilworth area							
04-ATSK-004-L01	8392	435770	6230257	Bruce Glacier member	Felsic volcanoclastic rock	173.6 ± 1.7 Ma	ca. 183 Ma, ca. 189 Ma

influenced petrogenesis of Bruce Glacier member rhyolites. Data presented herein confirms Mesozoic inherited zircon in Bruce Glacier member felsic volcanic rocks (Table 2). Circa 200-183 Ma xenocrystic zircons were likely derived from the underlying Betty Creek Formation (Fig. 3) or related Texas Creek plutonic suite rocks (e.g., Logan et al. 2000 and references therein). Circa 218-213 Ma inheritance is consistent with derivation from the underlying Stuhini Group and related Stikine plutonic suite (ca. 225-210 Ma: Logan et al., 2000 and references therein).

U-Pb ages from the Bruce Glacier member agree with limits provided by the Aalenian radiolaria and Bajocian ammonites and brachiopods in overlying strata (Lewis et al., 2001). However, deposition of the Treaty Ridge member, which is characterized by non-volcanic strata, appears to partially overlap Bruce Glacier member volcanism. This suggests that either the Treaty Ridge Formation was deposited in a coeval basin that was somehow isolated from Betty Creek and Iskut River formations volcanic products, or that Treaty Ridge Formation needs to be re-examined in more detail (cf. Lewis et al., 2001).

5. Conclusion

Rhyolitic rocks from the Eskay member are discriminated from broadly coeval Bruce Glacier member volcanic rocks (Fig. 3) on the basis of Al-Ti-Zr ratios (Childe, 1996; Roth et al., 1999; Lewis, 2013). Previous studies in the Eskay anticline demonstrated that the Eskay member is only exposed on the western limb of the anticline, whereas the eastern limb comprises Bruce Glacier member, which displays Al/Ti ratios of <100. The samples that we dated have low Al/Ti ratios (Anderson, unpublished data), suggesting that the Bruce Glacier member is widespread in the MacTagg anticlinorium (Fig. 2). Although definitive Eskay member rocks have not been identified outside of the Eskay anticline, age-equivalent submarine felsic volcanic rocks are aurally extensive and locally voluminous in the MacTagg anticlinorium (Fig. 2; Lewis, 2013) and adjacent areas (Evenchick et al., 2004; Evenchick and McNicoll, 2002; Alldrick et al., 2005). Age-equivalent rocks also host volcanogenic massive sulphide deposits in the Anyox Pendant (Evenchick and McNicoll, 2002) and north of Eskay Creek mine (Alldrick et al., 2005). The presence of known VMS mineralization outside of the Eskay area indicates that much of the Upper Hazelton Group remains prospective for mineralization.

Acknowledgments

Sample collection and data acquisition were funded by the Geological Survey of Canada Targeted Geoscience Initiative Program (2004-2005). This is a contribution to the Geological Survey of Canada Geomapping for Energy and Minerals "Characterization of volcanic and intrusive rocks across the BC-Yukon border" activity. We thank JoAnne Nelson and Carol Evenchick for suggestions that improved this manuscript. This is ESS Contribution number 20140352.

References cited

- Alldrick, J.D., 1993. Geology and metallogeny of the Stewart mining camp, northwestern B.C. British Columbia Ministry of Energy, Mines and Petroleum Resources, British Columbia Geological Survey Bulletin 85, 105 p.
- Alldrick, D. J., Nelson, J. L., and Barresi, T., 2005, Tracking the Eskay Rift through northern British Columbia: geology and mineral occurrences of the upper Iskut River area. In: Geological Fieldwork 2004, British Columbia Ministry of Energy, Mines and Petroleum Resources, British Columbia Geological Survey Paper 2005-1, pp. 1-30.
- Anderson, R.G., 1993. A Mesozoic stratigraphic and plutonic framework for northwestern Stikinia (Iskut River area), northwestern British Columbia, Canada. In: Dunne, G.C., and McDougall, K.A. (Eds.), Mesozoic paleogeography of the western United States, II. Society of Economic Paleontologists and Mineralogists, Pacific Section, Los Angeles, CA. pp. 477-494.
- Anderson, R. G., and Thorkelson, D. J., 1990, Mesozoic stratigraphy and setting for some mineral deposits in Iskut River map area, northwestern British Columbia. Geological Survey of Canada Paper 90-1E, 131-139.
- Ash, C.H., MacDonald, R.J.W., and Friedman, R.M., 1997. Stratigraphy of the Tatogga Lake area, northwestern British Columbia (NTS 104H, 12, 13; 104G/9, 16). In: Geological Fieldwork 1996, British Columbia Ministry of Energy, Mines and Petroleum Resources, British Columbia Geological Survey Paper 1997-1, pp. 283-290.
- Brown, D.A., Gunning, M.H., and Greig, C.J., 1996. The Stikine project: geology of western Telegraph Creek map area, northwestern British Columbia (NTS104G/5, 6, 11W 12 and 13). British Columbia Ministry of Energy, Mines and Petroleum Resources, British Columbia Geological Survey Bulletin 95, pp. 183.
- Brown, D.A., Logan, J.M., Gunning, M.H., Orchard, M.J., and Bamber, W.E., 1991. Stratigraphic evolution of the Paleozoic Stikine Assemblage in the Stikine and Iskut rivers area, northwestern British Columbia. Canadian Journal of Earth Sciences 28, 958-972.
- Childe, F.C., 1994. Radiogenic isotopic investigations of the Eskay Creek volcanic hosted massive sulphide deposit, British Columbia, Canada. United States Geological Survey Circular 1107, 58p.
- Childe, F.C., 1996. U-Pb geochronology and Nd and Pb isotope characteristics of the Au-Ag-rich Eskay Creek volcanogenic massive sulfide deposit, British Columbia. Economic Geology, 91, 1209-1224.
- Cohen, K.M., Finney, S.C., Gibbard, P.L. & Fan, J.-X., 2013. The ICS International Chronostratigraphic Chart. Episodes 36, 199-204.
- Colpron, M. and Nelson, J.L., 2011. A Digital Atlas of Terranes for the Northern Cordillera. British Columbia Geological Survey GeoFile 2011-11.
- Evenchick, C. A., and McNicoll, V. J., 2002, Stratigraphy, structure, and geochronology of the Anyox Pendant, Northwest British Columbia, and implications for mineral exploration. Canadian Journal of Earth Sciences 39, 1313-1332
- Evenchick, C.A., McMechan, M.E., McNicoll, V.J. and Carr, S.D., 2007. A synthesis of the Jurassic-Cretaceous tectonic evolution of the central and southeastern Canadian Cordillera: exploring links across the orogeny. In: Sears, J.W., Harms, T.A., and Evenchick, C.A. (Eds.), Whence the mountains? Inquiries into the evolution of orogenic systems: a volume in honour of Ramond A. Price. Geological Society of America Special Paper 433, pp. 117-145.
- Evenchick, C.A., McNicoll, V.J., and Snyder, L.D., 2004. Stratigraphy, geochronology, and geochemistry of Georgie River area, northwest British Columbia, and implications for mineral exploration. Canadian Journal of Earth Sciences, 41, 199-216.
- Evenchick, C. A., Poulton, T. P., and McNicoll, V. J., 2010, Nature

- and significance of the diachronous contact between the Hazelton and Bowser Lake Groups (Jurassic), north-central British Columbia. *Bulletin of Canadian Petroleum Geology* 58, 235-267.
- Gagnon, J.F., Barresi, T., Waldron, J.W.F., Nelson, J.L., Poulton, T.P., and Cordey, F., 2012. Stratigraphy of the upper Hazelton Group and Jurassic evolution of the Stikine terrane, British Columbia. *Canadian Journal of Earth Sciences*, 49, 1027-1052.
- Hart, C. J. R., 1997. A transect across Northern Stikinia: Geology of the Northern Whitehorse map area, Southern Yukon Territory (105D/13-16. Exploration and Geological Services Division Bulletin, Yukon region, 8, 113p.
- Kyba, J. and Nelson, J.L., 2015. Stratigraphic and tectonic framework of the Khyber-Sericite-Pins mineralized trend, lower Iskut River, northwest British Columbia. In: *Geological Fieldwork 2014*, British Columbia Ministry of Energy and Mines, British Columbia Geological Survey Paper 2015-1, this volume.
- Lewis, P.D., Toma, A., and Tosdal, R.M., 2001. Metallogensis of the Iskut River Area, Northwestern British Columbia. Mineral Deposits Research Unit Special Publication Number 1, University of British Columbia, 337 p.
- Lewis, P.D., 2013. Iskut River area geology, northwest British Columbia (104B/08, 09, 10 & part of 104B/01,07,11). *Geoscience British Columbia report 2013-05*, 1:50,000-scale.
- Lewis, P.D., Mortensen, J.K., Childe, F., Friedman, R., Gabites, J., Ghosh, D., and Bevier, M.L., 2001. Chapter 9 - Geochronology Data Set. In: Lewis, P.D., Toma, A., and Tosdal, R.M., (Eds.), *Metallogensis of the Iskut River Area*, Northwestern British Columbia: Mineral Deposits Research Unit Special Publication Number 1, University of British Columbia, pp.89-96.
- Logan, J.M., Drobe, J.R., and McClelland, W.C., 2000. Geology of the Forrest Kerr-Mess Creek area, northwestern British Columbia (NTS 104B/10,15 & 104G/2 & 7W). British Columbia Ministry of Energy and Mines, Energy and Minerals Division, British Columbia Geological Survey Branch, Bulletin 104: 163p.
- Lowe, G.W., 2004. Preliminary lithostratigraphy of the Laberge Group (Jurassic), south-central Yukon: Implications concerning the petroleum potential of the Whitehorse trough. In: Esmond, D.S., and Lewis, L.L. (Eds.), *Yukon Exploration and Geology 2003*. Yukon Geological Survey, pp. 129-142.
- Ludwig, K.R., 2003. User's manual for Isoplot/Ex rev. 3.00: a Geochronological toolkit for Microsoft excel. Special Publication, 4, Berkeley Geochronology Centre, Berkeley, 70 p.
- Mihalynuk, M., Zagorevski, A., and Cordey, F., 2012. Geology of the Hoodoo Mountain area (NTS 104B/14). In: *Geological Fieldwork 2011*, British Columbia Ministry of Forests, Mines and Lands, British Columbia Geological Survey Paper 2012-1, pp.45-67.
- Monger, J.W.H., 1977. Upper Paleozoic rocks of the western Canadian Cordillera and their bearing on Cordilleran evolution. *Canadian Journal of Earth Sciences* 14, 1832-1859.
- Nelson, J. L., and Colpron, M., 2007. Tectonics and metallogeny of the British Columbia, Yukon and Alaskan Cordillera, 1.8 Ga to the present. In: Goodfellow, W. D. (Eds.), *A Synthesis of Major Deposit-Types, District Metallogeny, the Evolution of Geological Provinces, and Exploration Methods*. Geological Association of Canada, Mineral Deposits Division Special Publication, pp. 755-791.
- Nelson, J., and Kyba, J., 2014. Structural and stratigraphic control of porphyry and related mineralization in the Treaty Glacier – KSM – Brucejack – Stewart trend of western Stikinia. In: *Geological Fieldwork 2013*, British Columbia Ministry of Energy and Mines, British Columbia Geological Survey Paper 2014-1, pp. 111-140.
- Nelson, J., Colpron, M., and Israel, S., 2013. The Cordillera of British Columbia, Yukon and Alaska: tectonics and metallogeny. In: Colpron, M., Bissig, T., Rusk, B., and Thompson, J.F.H., (Eds.), *Tectonics, Metallogeny, and Discovery - the North American Cordillera and similar accretionary settings*. Society of Economic Geologists, Special Publication 17, pp. 53-109.
- Roth, T., Thompson, J. F. H., Barrett, T. J., 1999. The precious metal-rich Eskay Creek Deposit, northwestern British Columbia. *Reviews in Economic Geology*, 8, 357-373.
- Sircombe, K.N., 2004. AGEDISPLAY: an Excel workbook to evaluate and display univariate geochronological data using binned frequency histograms and probability density distributions. *Computers and Geosciences*, 30, 21-31.
- Stern, R.A., 1997. The GSC Sensitive High Resolution Ion Microprobe (SHRIMP): analytical techniques of zircon U-Th-Pb age determinations and performance evaluation: In *Radiogenic Age and Isotopic Studies*, Report 10, Geological Survey of Canada Current Research 1997F, pp.1-31.
- Stern, R.A., and Amelin, Y., 2003. Assessment of errors in SIMS zircon U-Pb geochronology using a natural zircon standard and NIST SRM 610 glass. *Chemical Geology*, 197, 111-146.
- Souther, J. G., 1972. Telegraph Creek map-area, British Columbia (104 G): Geological Survey of Canada Paper 71-44, 38 p.
- Thorkelson, D. J., Miller, D. M., Mortensen, J. K., Marsden, H., Taylor, R. P., and Busby, C., 1995. Age and tectonic setting of Early Jurassic episodic volcanism along the northeastern margin of the Hazelton Trough, northern British Columbia. *Geological Society of America Special Paper*, 299, 83-94.
- Tipper, H.W., and Richards, T.A., 1976. Jurassic stratigraphy and history of north-central British Columbia. *Geological Survey of Canada Bulletin* 270, 73 p.

Mapping hydrothermally altered rocks with Landsat 8 imagery: A case study in the KSM and Snowfield zones, northwestern British Columbia

Tian Han^{1, a} and JoAnne Nelson¹

¹ British Columbia Geological Survey, Ministry of Energy and Mines, Victoria, BC, V8W 9N3

^a corresponding author: Tian.Han@gov.bc.ca

Recommended citation: Han, T., and Nelson, J., 2015. Mapping hydrothermally altered rocks with Landsat 8 imagery: A case study in the KSM and Snowfield zones, northwestern British Columbia. In: Geological Fieldwork 2014, British Columbia Ministry of Energy and Mines, British Columbia Geological Survey Paper 2015-1, pp. 103-112.

Abstract

Mapping hydrothermally altered rocks, which are common indicators of mineralization, is integral to reconnaissance mineral exploration. Multi-spectral moderate-resolution satellite remote sensing has long-been applied to map altered rocks, offering wide spatial coverage, low cost, and simple image analysis. Most previous studies have been in un-vegetated arid or semi-arid areas. Use of this technique in much of the Canadian Cordillera faces the challenge of extensive cover by vegetation, ice, snow, and water along with high relief. We use Landsat 8 imagery, generated in August, 2013, of the Iskut region in northwestern British Columbia, a recently deglaciated area with abundant porphyry copper-related gossans, to develop a regional map depicting hydrothermal alteration. Integrated with ground observations of rock type, alteration, vegetation, and overburden at 100 field sites, traditional spectral unmixing image analysis was only partly successful in discriminating the spectral responses of altered and unaltered rocks. However, screening for the influence of topography (slope and aspect) was more successful. Our image-derived alteration map matched observations at 83% of the field sites. Altered rocks were unrecognized by spectral unmixing at 17% of the field sites, likely reflecting weak alteration or limited exposure of altered rocks. Based on these preliminary results, spectral unmixing of Landsat-8 images that account for high-relief topography is a potential tool to identify alteration haloes in less well known mineralized areas of British Columbia.

Keywords: Hydrothermal alteration mapping, remote sensing, Landsat 8, spectral unmixing, altered rock, image analysis, topography

1. Introduction

Given the common proximity of hydrothermally altered rocks to mineral deposits, regional mapping of exposed altered rocks by remote sensing has proven a useful complement to field exploration (Sabins, 1999). Multi-spectral moderate-resolution satellite remote sensing imagery, such as offered by NASA's Landsat satellites, has been used for regional mineral exploration since the early 1970s, which culminated in 1999 with the operation of ASTER (Advanced Space-borne Thermal Emission and Reflection Radiometer) onboard NASA's Terra satellite. A number of studies have demonstrated the utility of these data in geological mapping. Rowan et al. (1974) working in Goldfield, Nevada developed band-ratio and color-composite methods to enhance visibility of hydrothermally altered rocks, methods that have become the standard approach for geological applications. Loughlin (1991) analyzed Landsat Thematic Mapper (TM) images near the Gold Bar deposit in Nevada, generating a map highlighting hydrothermal alteration assemblages, including hydroxyl-bearing and iron-oxide minerals. Mars and Lawrence (2006) used ASTER images to map argillic- and phyllic-altered rocks near porphyry copper deposits in the Zagros magmatic arc of Iran. Gabr et al. (2010) used ASTER images from Abu-Marawat (Egypt) to separate mineralized and un-mineralized rocks based on abundance of secondary iron-oxide minerals.

Although extensively altered rocks can be identified visually using colour aerial photographs or high-resolution images, multi-spectral moderate-resolution satellite images: 1) provide

broad spatial coverage, yielding a synoptic view across entire hydrothermal systems; 2) capture both visible and shortwave infrared spectra (where many mineral-related absorption features reside; van der Meer, 2004); 3) can generally be obtained at no cost; and 4) can be quantitatively analyzed at a regional scale. In the summer of 2013, the United States Geological Survey (USGS) released images acquired by the Operational Land Imager (OLI) and Thermal Infrared Scanner (TIRS) onboard the Landsat 8 satellite, which was launched by NASA earlier in the year. The Landsat-8 images are enhanced relative to previous generations by the addition of aerosol and cirrus bands (Table 1), improved signal-to-noise ratios using a pushbroom imager, and high-radiometric resolution that uses 12-bit quantization. These enhancements hold promise for geological applications, including alteration mapping.

The present study is the first attempt to use Landsat 8 OLI and TIRS images to map hydrothermally altered rocks in the Cordillera of British Columbia. Hitherto, Landsat-based alteration mapping studies have mainly focused on arid or semi-arid areas with abundant un-vegetated bedrock exposures (e.g., Rowan et al., 1974; Loughlin, 1991; Mars and Lawrence, 2006; Gabr et al., 2010). Extensive cover by vegetation, snow, ice, and water bodies, along with high relief pose problems for alteration mapping based on analyzing multi-spectral moderate-resolution images across much of the Canadian Cordillera. Our study examines the area near the Kerr-Sulphurets-Mitchell (KSM) and Snowfield zones in northwestern British Columbia (Fig. 1), where recent deglaciation has created broad exposures

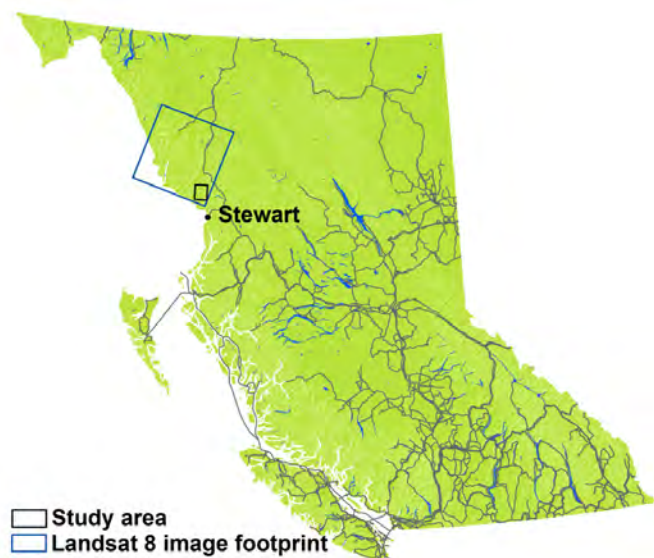


Fig. 1. Location of study areas and area covered by Landsat 8 image.

of bedrock, including alteration zones. Herein we describe steps to streamline image processing and analysis and to integrate ground observations with satellite imagery. We use spectral unmixing image analysis to distinguish altered rocks from unaltered rocks and other substances and to produce a map outlining the regional distribution of hydrothermal alteration.

2. Study area and ground observations

The Kerr-Sulphurets-Mitchell (KSM) and Snowfield zones are approximately 60 kilometres north of the town of Stewart, in northwestern British Columbia (Figs. 1, 2). In this region, porphyry-style systems are expressed as extensive gossans (Fig. 3). Recent deglaciation has resulted in widespread bedrock and colluvial exposures, creating a natural laboratory to compare outcrop geology and satellite imagery. Fieldwork was conducted in the summer of 2013 during regional bedrock

mapping (Nelson and Kyba, 2014). Detailed observations were made in four areas, near the Bruce and Treaty glaciers, and in the Iron Cap and Snowfield alteration zones (Fig. 2). Most outcrops near Bruce and Treaty glaciers are of unaltered rock, in many cases partly covered with lichen, moss, heather, and sedge grasses, and thin Quaternary gravels. These outcrops were used as standards to compare with the intensely altered rocks of the Iron Cap and Snowfield gossans. Iron Cap displays potassic, phyllic and silica-clay-sericite alteration, whereas Snowfield displays quartz-sericite-pyrite-clay and advanced argillic assemblages. Different alteration assemblages create outcrops of different morphology. For instance, silica-pyrite alteration produces resistant cliff outcrops, whereas clay-rich alteration assemblages result in extensive colluvium.

Ground observation sites (Fig. 2) were selected to represent the diversity of rock surfaces in terms of alteration, exposure, slope, and aspect, all of which influence spectral responses captured by satellite sensing instruments. Most of the sites have an area of 900 m² or more, large enough to be captured as a single pixel (30 m x 30 m) on the Landsat 8 OLI image. Site locations were established using hand-held GPS (with a ~3 m accuracy). After the fieldwork, we created a reference library that combines ground observations with spectra derived from the Landsat 8 image in a spatial database (Fig. 4) for current and future remote sensing mapping.

3. Landsat 8 image and preprocessing

Landsat 8 is equipped with the Operational Land Imager (OLI) and the Thermal Infrared Sensor (TIRS), which are able to collect up to 550 multispectral images daily (Irons et al., 2012; USGS, 2013a). Each image covers an area with dimensions of 170 km (north-south) by 183 km (east-west). Landsat 8 images, available to the public since July 2013, can be downloaded from several USGS websites, including the Earth Explorer (USGS, 2013b). The images are available at different processing levels (referred to as products). In the Level 1T product, used in the current study, raw images were

Table 1. Landsat 8 instrument bands.

Band #	Band name	Wavelength (µm)	Spatial resolution (m)
1	Coastal aerosol	0.43 - 0.45	30
2	Blue	0.45 - 0.51	30
3	Green	0.53 - 0.59	30
4	Red	0.64 - 0.67	30
5	Near Infrared (NIR)	0.85 - 0.88	30
6	Shortwave Infrared (SWIR) 1	1.57 - 1.65	30
7	Shortwave Infrared (SWIR) 2	2.11 - 2.29	30
8	Panchromatic	0.50 - 0.68	15
9	Cirrus	1.36 - 1.38	30
10	Thermal Infrared (TIRS) 1	10.60 - 11.19	100
11	Thermal Infrared (TIRS) 2	11.50 - 12.51	100

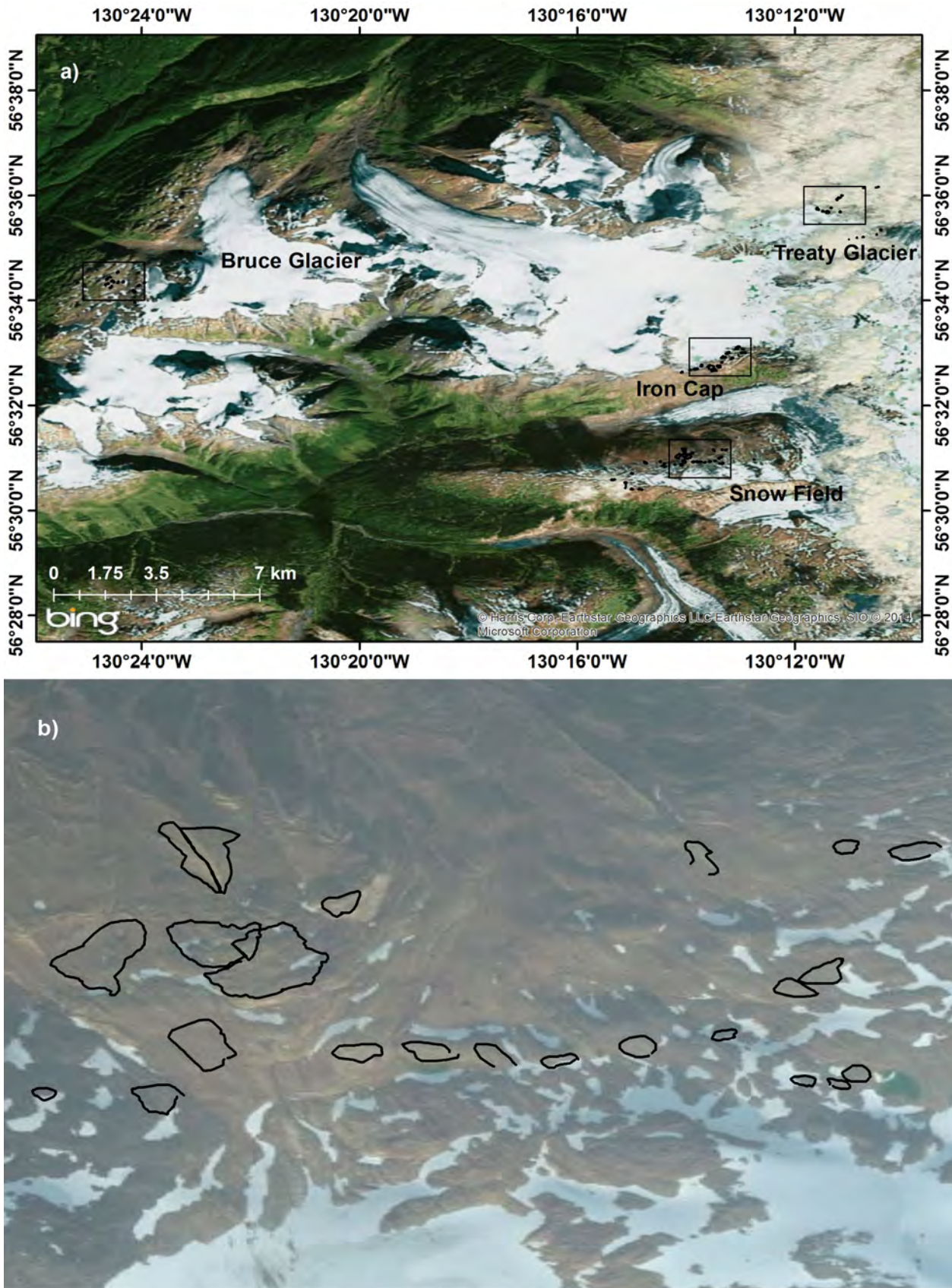


Fig. 2. a) Study areas near Bruce Glacier, Treaty Glacier, Iron Cap, and Snow Field (indicated by black rectangles). **b)** Enlarged image of field sites near the Snow Field camp (in black polylines). Zone 9N, NAD 83.



Fig. 3. Well-exposed altered rocks (silica-pyrite alteration) close to the Iron Cap camp (424998E, 626796N). Person (circled) for scale. Zone 9N, NAD 83.

processed for systematic radiometric and geometric correction using ground control points and the corresponding Digital Elevation Model (USGS, 2013c).

The Landsat 8 image used in this study (path 55 and row 20; Fig. 5) was captured on Aug. 3, 2013 under excellent

weather conditions (< 10% of cloud cover) while fieldwork was underway. The image was downloaded in a package containing 11 band images (in GeoTIFF), 1 quality assessment band image (in GeoTIFF), and 1 metadata file (in ASCII). Once the package was downloaded, the band images were processed as described below.

3.1. Spectral sub-setting

Because OLI band 8 (panchromatic) was designed for visualization and band 9 (cirrus) was for high-altitude cloud detection, they were excluded from further analysis. We created a nine-band image stack, including OLI bands 1 – 7 and TIRS bands 10 - 11 (Table 1).

3.2. Reflectance conversion

Level 1T images consist of Digital Numbers (DN) lacking physically meaningful units. They were converted to reflectance, representing the ratio of the radiation reflected off a surface to the radiation striking it. This conversion is commonly needed for quantitative remote sensing as it accounts for solar conditions (illumination, geometry, and intensity) when the images were acquired. The reflectance conversion was carried out using the method specified in USGS (2013e). Per pixel solar angles were used for more accurate reflectance

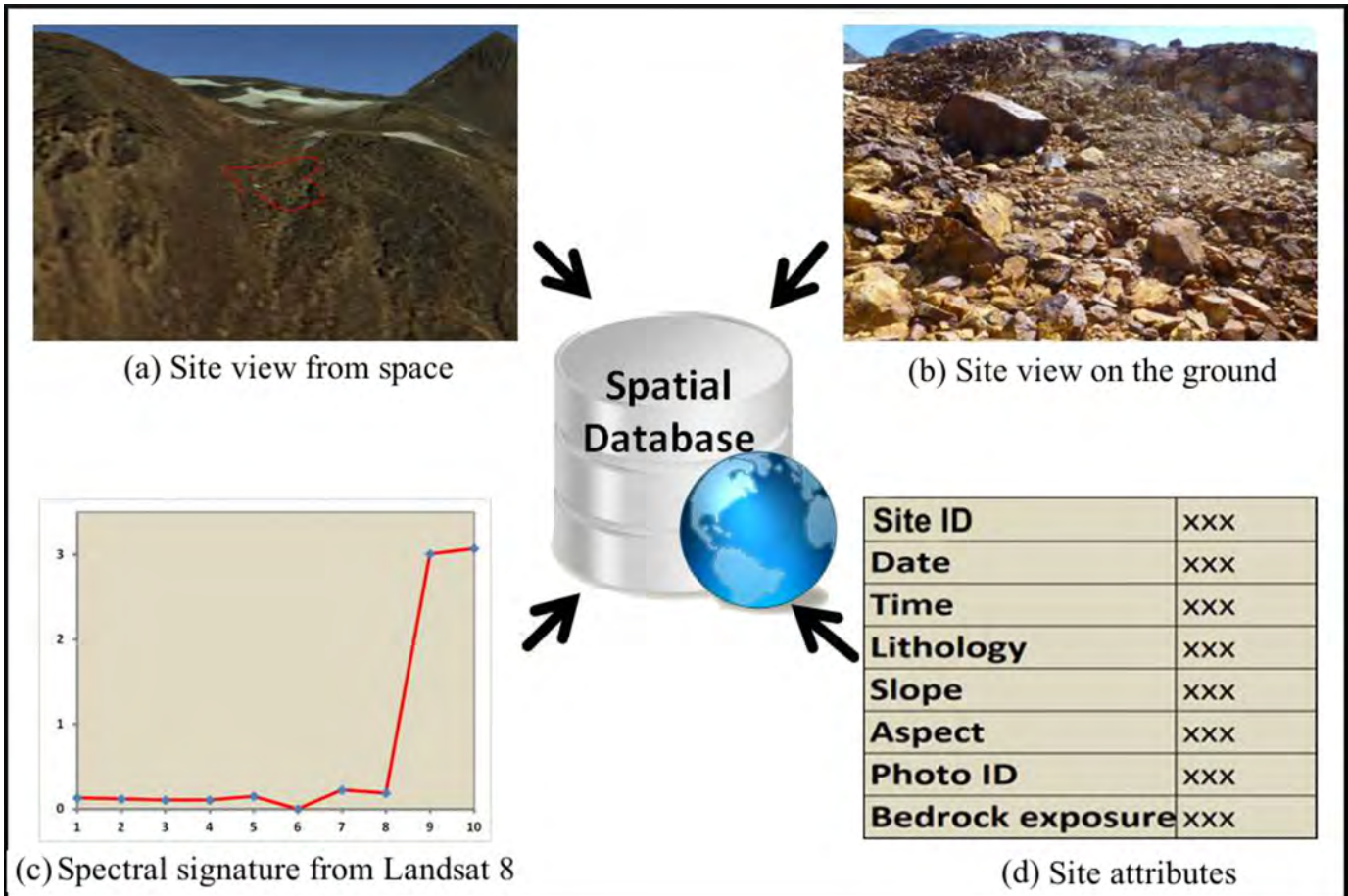


Fig. 4. Conceptual model to develop spectral library for alteration mapping.

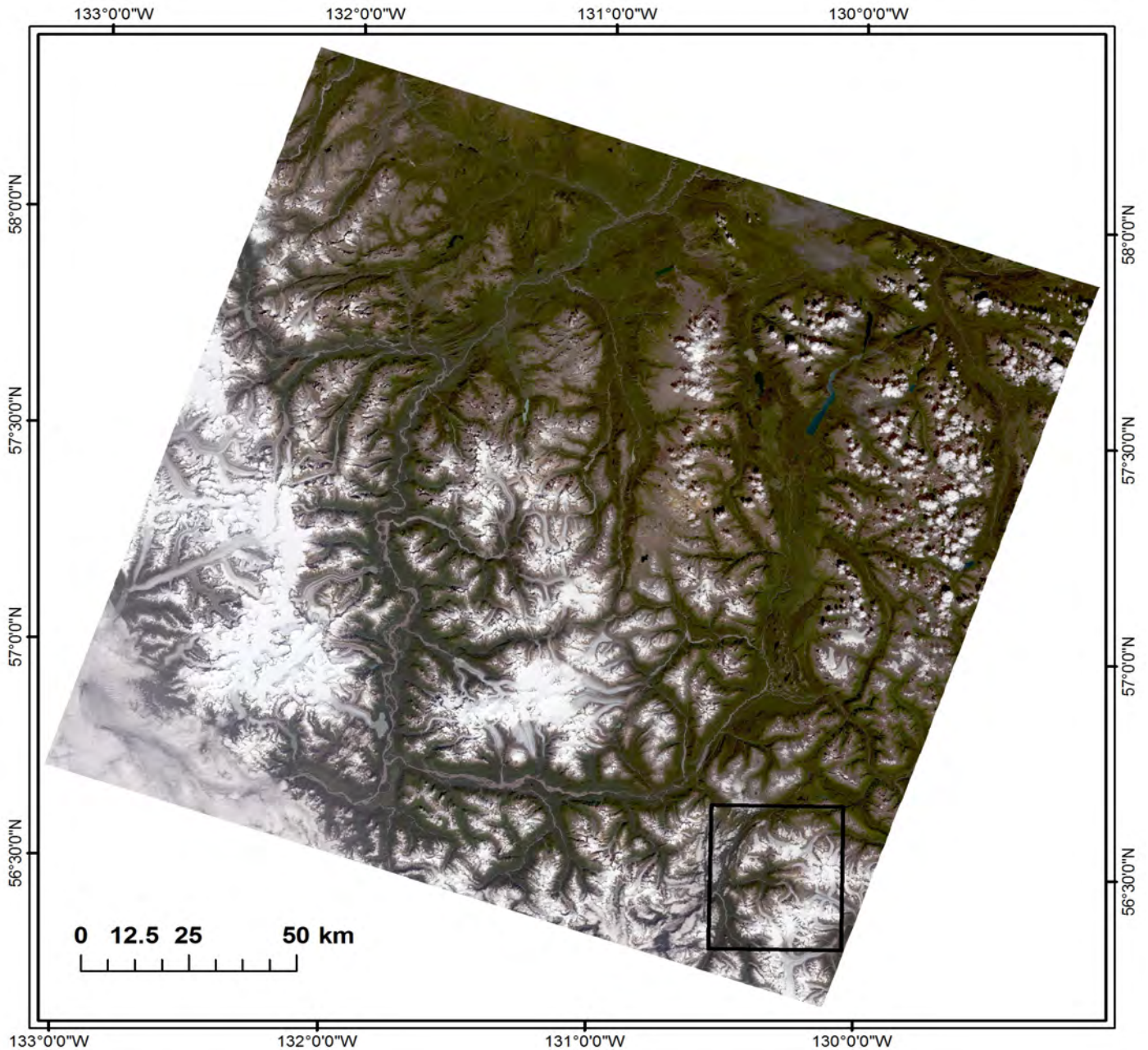


Fig. 5. Landsat 8 level 1T image; study area indicated by black rectangle.

calculation. Because the interaction between solar radiation and gases and aerosols in the atmosphere is still included after the conversion, this step is more accurately called top of atmosphere (TOA) reflectance conversion. This interaction happens more prominently in bands with wavelengths shorter than 1000 nm. Similarly, the 2 TIRS bands were converted to at-satellite brightness temperature using the parameters and formula in USGS (2013d).

3.3. Masking

Because the bare Earth surface was the only land cover of interest in this study, materials (water bodies, ice, snow, cloud and shadow, and vegetation) were masked out from further

image analysis. This masking was necessary to reduce image spectral variability arising from different land covers and to focus attention on the bare earth surface. The mask was created using information retrieved from the cirrus band, quality assessment band, and NDVI (Normalized Difference Vegetation Index) calculated using the TOA reflectance band images.

4. Image analysis

Incident solar radiation interacts with surface materials through electronic transitions, charge-transfers, and vibrational processes (Hunt, 1977). This interaction exhibits itself as absorption features (shown as dips in reflective spectral

profiles) that extend across spectral ranges including visible and near infrared (VNIR), shortwave infrared (SWIR), and thermal infrared (TIR). Captured as images by remote sensing instruments, the reflected and emitted energy spectra can be used to identify those substances with diagnostic absorption features.

Some minerals and mineral assemblages in hydrothermally altered rocks have distinctive absorption features. For example, alunite and clay minerals such as illite, kaolinite, and montmorillonite have distinctive absorption features at ~2100 nm and their spectral responses peak at ~1700 nm (Sabins, 1999). Iron oxide and sulphate minerals commonly show low reflectance close to ultraviolet or blue but strong reflectance near red (Rencz, 1999), which gives them a rusty colour in a natural colour image. This observation led to the development of band-ratioing technique for visualizing hydrothermal altered rocks. For example, the ratio image of Landsat TM band 5 (1550 – 1750 nm) over band 7 (2090 – 2350 nm) is able to distinguish areas with high concentrations of alunite and clay, where pixels in the image appear bright. The ratio image of band 3 (630 – 690 nm) over band 1 (450 – 515 nm) reveals areas where iron minerals are abundant (van der Meer, 2004).

Although the band-ratioing approach works reasonably well for visualization, it is inadequate for mapping, or other quantitative applications. The bandwidth assumed by optical multispectral remote sensing instruments is usually greater than 50 nm, which is too broad to unambiguously distinguish the individual spectral absorption features associated with specific alteration minerals. Also, many band-ratioing algorithms use only two or three bands even though multispectral images offer many more bands than that. Hence the image analysis approach we adopted in this study uses all nine bands together, taking advantage of the complete spectral information borne by the Landsat 8 image. As described below, feature extraction is the first step in this image analysis. This is followed by a spectral unmixing procedure to separate the spectra of altered rocks from other substances and derive a map for altered rock distribution.

4.1. Feature extraction

Between-band correlation is apparent among adjacent Landsat 8 band images, which degenerates the effectiveness of many image analysis methods, including the spectral unmixing employed in this study, which rely on image covariance matrix (Landgrebe, 2003). Feature extraction is a linear transformation that mitigates the correlation by projecting band images into a new space where the resultant images are orthogonal and arranged in terms of decreasing eigenvalues (representing information content) of the image covariance matrix. In this study, we used the Minimum Noise Fraction (MNF) for feature extraction.

4.2. Spectral unmixing

The Landsat 8 OLI band images have a spatial resolution

of 30 metres, and each pixel of an image covers an area of 900 m² (30 m x 30 m) on the ground. Generally, any given area of this size will be covered by different materials, referred to as endmembers, such as altered bedrock, unaltered bedrock, glacial till, gravel, and vegetation. Spectral unmixing is a method to determine the areal proportion occupied by such individual endmembers in each pixel. In this study, exposed altered rock is the endmember of interest. Altered rock spectra are extracted from the Landsat 8 image based on the GPS tracks collected during fieldwork. The endmember spectra of the exposed altered rocks are used as the ‘knowns’ in spectral unmixing, against which the Landsat 8 image pixel spectra, treated as the ‘unknowns’, are compared and unmixed.

4.3. Altered rock mapping

The result of the spectral unmixing is an image, called endmember abundance image, composed of pixels whose value represents the areal proportion (between 0 and 1) that a specific endmember occupies within that pixel. Brighter pixels in this image indicate areas where greater portions of the corresponding endmember occur. Using altered bedrock as the endmember, spectral unmixing generates an altered rock abundance image in which pixels with large proportions of altered rocks (> 0.6) are selected and labelled as the altered rock-dominated pixels. This image can then be used as a map to show the geographic distribution of the altered bedrocks across the entire Landsat 8 image.

4.4. Validation

Before accepting the generated altered rock abundance image, we validated the image using ground observations at altered rock sites. Because parts of these sites were used as the training data during the spectral unmixing process outlined above, we also checked the abundance image for altered rocks against the high-spatial resolution image offered through Microsoft Bing Web Map Service (WMS) where some highly altered rocks are visible.

5. Results and discussion

The effectiveness of the spectral unmixing described above depends on clearly distinguishing the spectra of altered bedrock from those of the other substances. Separating the altered rock spectra from those of water, snow, ice, and alpine vegetation is straightforward, because they have markedly different spectral shapes. Although separating altered and unaltered rocks is commonly more problematic, in some cases the distinction is clear. For example, outcrops of unaltered volcanic rock with local black lichen and patches of moss display spectra that differ from iron-stained, silica-clay-altered volcanic rock lacking vegetation (Fig. 6). Similarly, the spectra displayed by well-stratified, fine-grained siltstones and mudstones differ from clay-altered volcanic breccias (Fig. 7).

We further investigated spectral separation quantitatively using a spectral angle calculation (Clark et al., 1990). As there were 9 bands included in our image, each pixel spectrum

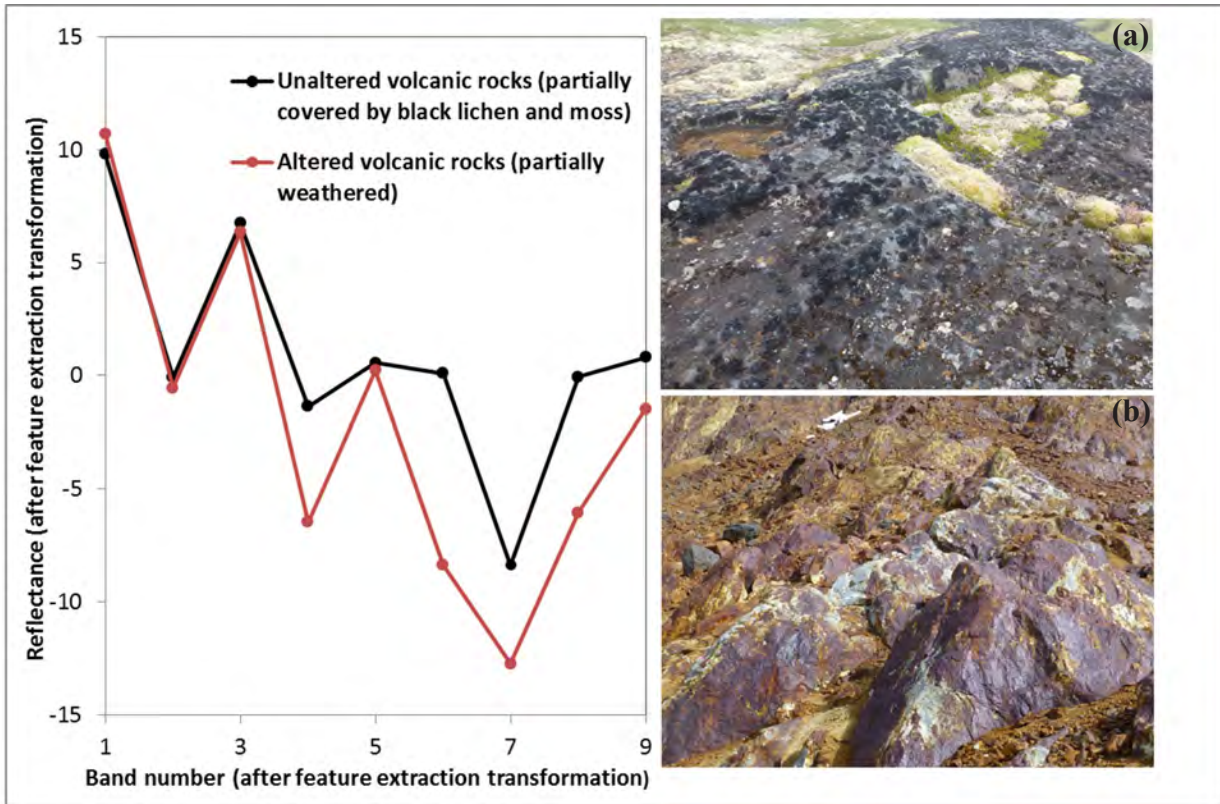


Fig. 6. Spectral comparison between a) unaltered volcanic rocks (width of photo is ca. 50 m; centred at 413364E, 6270411N) and b) altered volcanic rocks (width of photo is ca. 60m; centred at 424979E, 6266848N). Zone 9N, NAD 83.

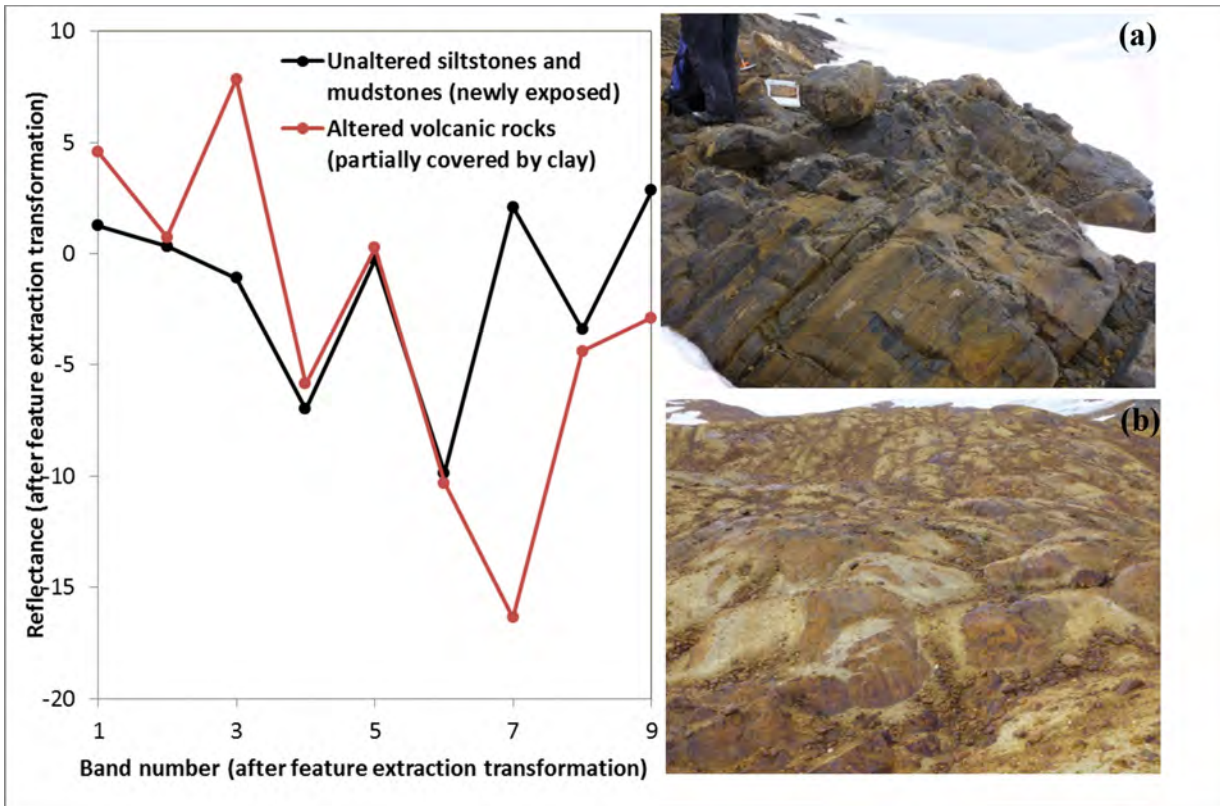


Fig. 7. Spectral comparison between a) unaltered fine-grained, well-stratified sedimentary rocks (width of photo is ca. 50 m; centred at 426939E, 6273494N) and b) altered volcanic rocks (width of photo is ca. 100m; centred at 424324E, 6264633N). Zone 9N, NAD 83.

(extracted from the image) was considered as a vector in a 9-dimensional space. The spectral separability between any two pixel spectra was evaluated by calculating the angle (θ) between the two vectors (representing the two pixel spectra). The formula for θ is:

$\theta = \cos^{-1} \left(\frac{a \cdot b}{|a||b|} \right)$ where a and b are the two spectrum-representing vectors. Two groups of pixel spectra were assembled; one included 25 field sites of unaltered rocks and the other 43 sites of altered rocks. The average spectrum was calculated for each group and used as the endmember.

Using spectral angle calculation, we found that the angle between the two average spectra representing the altered and unaltered rocks is 17° , showing that the altered and unaltered spectra are separable at the group level. However, between-member spectral angles within each group varied considerably around its group average. The angle between the average spectrum of the altered rock group and each member spectrum ranges between 4 and 26° . For the unaltered rock group, the angle ranges between 7 and 28° . An angle overlap exists between the altered and unaltered rock spectra. These spectra are therefore not completely separable using only the spectral information derived from the Landsat 8 image; some altered rocks would be mistakenly identified as unaltered rocks and vice versa.

Considering the high relief of the study area, topography could be a factor that contributes significantly to the spectral response and shape of the altered and unaltered rocks, and may worsen the spectral separability (Gitas and Riano et al., 2003; Devereux, 2006). For this reason, slope and aspect images derived from the TRIM DEM (GeoBC, 2014) were brought in as additional information to characterize the terrain and to assist the spectral unmixing operation. The 43 altered field sites were assigned to eight categories (Table 2) based on their slope and aspect. The average spectrum was calculated within each category and designated as the endmember spectrum with the specific slope and aspect values. The spectral angle between the average spectrum and each member spectrum within each category was then recalculated. The range of angles across all categories (between 4 and 19°), is significantly narrower than the range without topographic categorization (between 4 and 26°). Taking into account the topographic factors of slope and aspect helped to separate the altered and unaltered rock spectra.

Upon spectral unmixing, the slope and aspect of each pixel

Table 2. Field site categories by slope and aspect (the compass direction that a slope faces).

Category	Slope (degree)	Aspect (degree)
1	0 - 20	0 - 89
2	21 - 45	0 - 89
3	0 - 20	90 - 179
4	21 - 45	90 - 179
5	0 - 20	180 - 269
6	21 - 45	180 - 269
7	0 - 20	270 - 359
8	21 - 45	270 - 359

being unmixed were read out first, which was followed by selecting the endmember (altered rock) spectrum in the same slope and aspect category. Both the spectrum of the pixel being unmixed and the endmember spectrum were fed into the unmixing process. This gave rise to a topographic decision-assisted spectral unmixing method, where the decision was made based on pixel's slope and aspect. Following through the entire process of image processing and analysis, a map was generated outlining areas of significant alteration, which was rendered on top of a high-resolution Microsoft Bing WMS image (Fig. 8).

We verified our alteration map with ground observations from 100 field sites. Ground and remotely sensed observations agreed at 83 of the sites, but 17 sites where altered rocks are exposed were misidentified as containing unaltered rocks. The misidentified sites have either weak surficial expression of alteration or exposure that covered only a small part of an image pixel. As further verification, the alteration zones identified by the Landsat-8 data correspond well with colour anomalies recording red to orange gossans on the Microsoft Bing WMS image (Fig. 8b).

6. Conclusions and further work

This trial study demonstrates that analysis of a Landsat 8 image based on spectral unmixing can be effective for mapping hydrothermally altered rocks. This method was able to address the influence of topography on the surface spectral response, an important consideration in high-relief terrains such as the Cordillera. Including topographic factors in spectral unmixing helped distinguish altered and unaltered rock spectra, which helped produce a more accurate map.

Image processing and analysis for alteration mapping include several steps that can be streamlined by a semi-automated process (Fig. 9). Because a single Landsat 8 image covers an area with dimensions of $\sim 183 \times 170$ km, this method has the potential to quickly and inexpensively identify areas of altered rock and guide regional mineral exploration. The method may be of particular value in remote, recently deglaciated regions of northwestern British Columbia.

Future work might aim at collecting more detailed field data to enhance the spectral library, including rock spectra from the field, rock surface roughness, percentage of bedrock exposure, and topography. These data are vital to characterize the altered and unaltered rocks and to better separate their pixel spectra. Because the Landsat 8 image used in this study was only corrected to the top of atmospheric reflectance, atmospheric contaminations remain in the image, which may blur the spectral boundary between the altered and unaltered rocks. Pixel-based full atmospheric correction is preferred for further work.

Landsat 8 has a 30-metre spatial resolution and ~ 50 -nm spectral resolution for its OLI channels. These resolutions may be sufficient for regional work, but are inadequate for property-scale mapping. Using images with the higher spatial and spectral resolutions, such as those acquired by Worldview 3

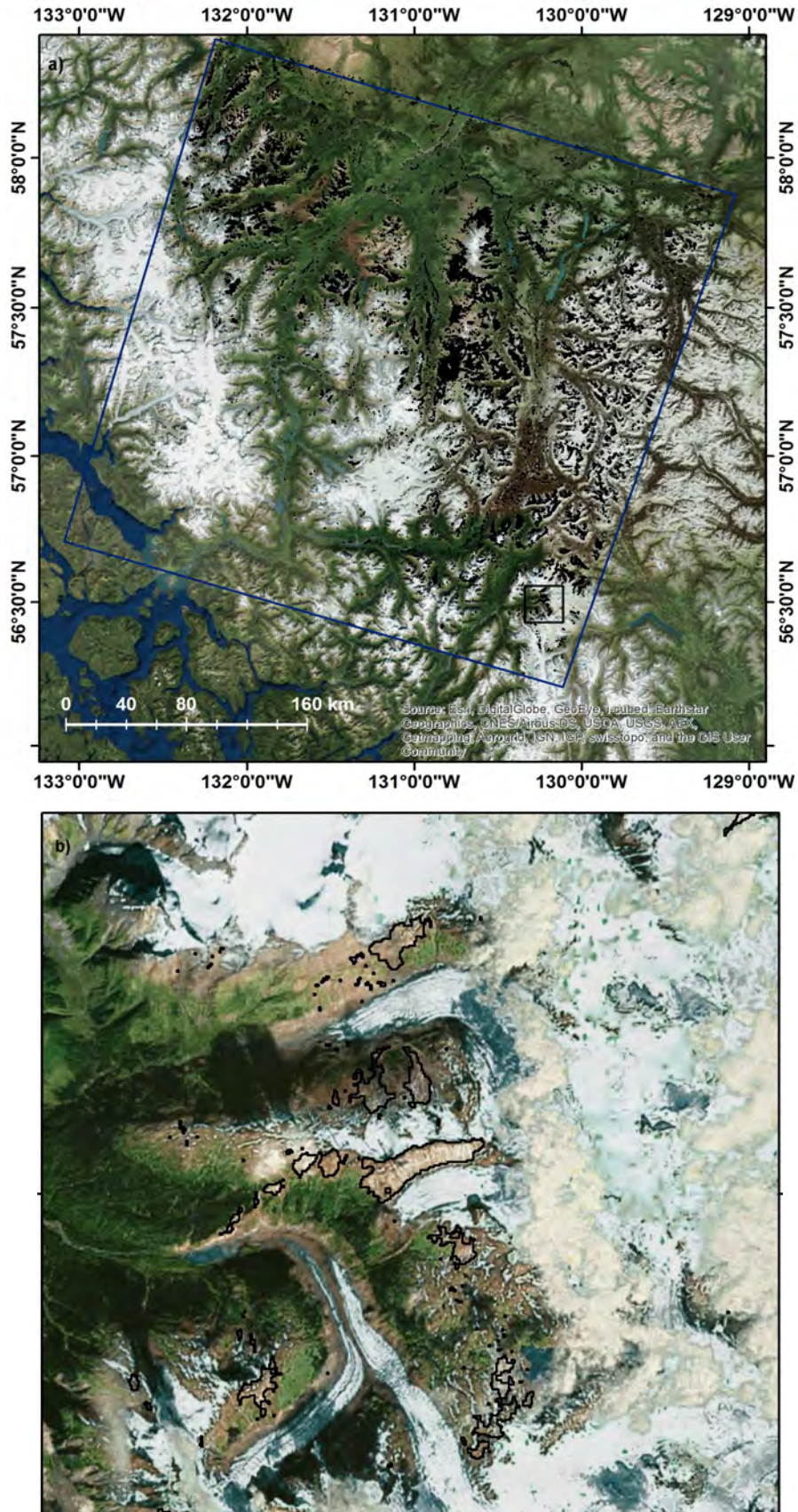


Fig. 8. a) Altered rock (in black) distribution plotted on Microsoft Bing WMS image. Blue rectangle marks the area of Landsat 8 image used in this study. **b)** Landsat 8 image mapped altered rocks (in black polylines) indicated by the black rectangle in a).

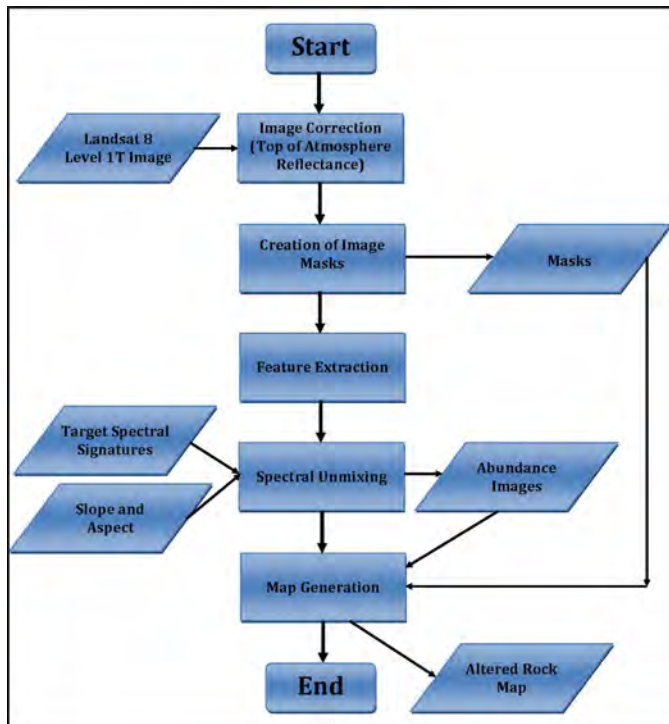


Fig. 9. Landsat 8 image processing and analysis for alteration mapping.

(Kruse and Perry, 2013) or airborne platforms, may be more appropriate for property-scale work, because they have the capacity to map not only altered rocks but hydrothermal mineral assemblages or even individual minerals. Potentially, property-scale image-based multispectral alteration maps could be used in conjunction with core spectrometer logs to create three-dimensional alteration mineral zoning models.

Acknowledgments

We thank L. Aspler (British Columbia Geological Survey) and O. Niemann (Department of Geography, University of Victoria) for reviews of an early draft.

References cited

- Clark, R.N., King, T.V.V., Kleijwa, M., Swayze, G.A. and Vergo, N., 1990. High spectral resolution reflectance spectroscopy of minerals. *Journal of Geophysical Research*, 95, 12653–12680.
- Gabr, S., Ghulam, A., and Kusky, T. 2010. Detecting areas of high-potential gold mineralization using ASTER data. *Ore Geology Reviews*, 38, 59–69.
- GeoBC, TRIM Program, <http://geobc.gov.bc.ca/base-mapping/atlas/trim/>. Accessed: July 14, 2014.
- Gitas, I.Z., and Devereux, B.J., 2006. The role of topographic correction in mapping recently burned Mediterranean forest areas from Landsat TM images. *International Journal of Remote Sensing*, 27, 41 – 54.
- Hunt, G.R. 1977. Spectral signatures of particulate minerals, in the visible and near-infrared. *Geophysics*, 42, 501–513.
- Irons, J. R., Dwyer, J. L., and Barsi, J. A., 2012. The next Landsat satellite: The Landsat data continuity mission. *Remote Sensing of Environment*, 122, 11–21.
- Kruse, F. A., and Perry, S. L., 2013. Mineral mapping using simulated Worldview-3 short-wave-infrared imagery. *Remote Sensing*, 5, 2688 – 2703.

- Landgrebe, D.A., 2003. *Signal theory methods in multispectral remote sensing*, John Wiley & Sons, Inc. New Jersey, 323p.
- Loughlin, W.P., 1991. Principal component analysis for alteration mapping. *Photogrammetric Engineering & Remote Sensing*, 57, 1161–1169.
- Mars, J.C., and Rowan, L.C., 2006. Regional mapping of phyllic- and argillic-altered rocks in the Zagros magmatic arc, Iran, using Advanced Spaceborne Thermal Emission and Reflection Radiometer (ASTER) data and logical operator algorithms. *Geosphere*, 2, 161–186.
- Nelson, J., and Kyba, J. 2014. Structural and stratigraphic control of porphyry and related mineralization in the Treaty Glacier – KSM – Brucejack – Steward trend of western Stikinia. In: *Geological Fieldwork 2014*, British Columbia Ministry of Energy and Mines, British Columbia Geological Survey Paper 2014-1, pp. 111–140.
- Rencz, A. N. 1999. *Manual of remote sensing: Remote sensing for the earth sciences*, John Wiley & Sons, 47p.
- Riano, D., E. Salas, C. J., and Aguado, I., 2003. Assessment of different topographic corrections in Landsat-TM data for mapping vegetation types, *IEEE Transactions on Geoscience and Remote Sensing*, 4, 1056–1061.
- Rowan, L.C., Wetlaufer, P.H., Goetz, A.F.H., Billingsley, F.C., and Stewart, J.H. 1974. Discrimination of rock types and detection of hydrothermally altered areas in south central Nevada by the use of computer-enhanced ERTS images. *USGS Professional Paper*, 883, 35p.
- Sabins, F. F., 1999. Remote sensing for mineral exploration. *Ore Geology Reviews*, 14, 157–183.
- USGS, 2013a. Frequently asked questions about Landsat missions: http://landsat.usgs.gov/band_designations_landsat_satellites.php Accessed Aug. 22, 2014.
- USGS, 2013b. Earth Explorer: <http://earthexplorer.usgs.gov/> Accessed Aug. 20, 2014.
- USGS, 2013c. Landsat 8 data products: <http://landsat.usgs.gov/landsat8.php>, last access: Aug. 20, 2014.
- USGS, 2013d. Using the USGS Landsat 8 Product: http://landsat.usgs.gov/Landsat8_Using_Product.php Accessed Aug. 20, 2014.
- van der Meer, D. F. 2004. Analysis of spectral absorption features in hyperspectral imagery. *International Journal of Applied Earth Observation and Geoinformation*, 5, 55 – 68.
- van der Meer, D. F., Harald, M. A., van der Werff, F. J. A., van Ruitenbeek, C. A., Hecker, W. H., Bakker, M. F., Noomen, M., van der Meijde, E., Carranza, J. M., Boudewijn de Smeth, J., and Woldai, T., 2012. Multi- and hyperspectral geologic remote sensing: A review. *International Journal of Applied Earth Observation and Geoinformation*, 14, 112 – 128.

Fieldwork in the Sylvester allochthon, Cassiar Mountains, British Columbia: Investigations of the Rapid River tectonite and the Slide Mountain terrane

James J. Ryan^{1, a}, JoAnne Nelson², and Cees van Staal¹

¹ Geological Survey of Canada, Vancouver, BC, V6B 5J3

² British Columbia Geological Survey, Ministry of Energy and Mines, Victoria, BC, V8W 9N3

^a corresponding author: jryan@nrcan.gc.ca

Recommended citation: Ryan, J.J., Nelson, J.L., and van Staal, C., 2015. Fieldwork in the Sylvester allochthon, Cassiar Mountains, British Columbia: Investigations of the Rapid River tectonite and the Slide Mountain terrane. In: Geological Fieldwork 2014, British Columbia Ministry of Energy and Mines, British Columbia Geological Survey Paper 2015-1, pp. 113-128.

Abstract

Back-arc extension during Devonian-Mississippian eastward subduction beneath the western flank of ancestral North America led to separation of Yukon-Tanana terrane from Laurentia, and opening of the Slide Mountain marginal ocean basin. Rocks exposed in imbricated thrust sheets of the Sylvester allochthon record the opening and closing of this marginal basin. At the highest structural level in the allochthon, the Rapid River tectonite is interpreted as a remnant of Yukon-Tanana basement. Pre-Late Devonian deformation in the Rapid River tectonite may represent collision of an exotic arc terrane with the outer peri-Laurentian margin that was the precursor to east-dipping subduction. Preliminary observations indicate that at least part of the Rapid River tectonite has a protolith of mafic mylonite and marble, possibly representing parts of a primitive arc. At two localities the tectonite is intruded by late synkinematic diorite/gabbro-tonalite-trondjemite plutons, one of which has been previously dated (ca. 362 Ma). Limited shear-sense indicators in the mylonite show top-to-the-northwest displacement. Thrust panels in the lower part of the Sylvester allochthon expose ultramafic-gabbro-supracrustal complexes that represent the youngest pre-accretionary phase in the YTT-Slide Mountain system. Near Zus Mountain northeast of the Cassiar townsite, and near Blue Dome 20 kilometres to the north, partly serpentized harzburgite tectonites form the lower parts of thrust panels within the Slide Mountain terrane. These tectonites are overlain by interlayered peridotite tectonite, lherzolite, dunite, and gabbro; all are cut by trondjemite dikes. The trondjemite dikes cut previously serpentized hosts, suggesting their emplacement during or after exhumation. At Zus Mountain, a large gabbro body overlies the ultramafites. At the Blue Dome section, seafloor deposits of locally pillowed basalt and radiolarian chert directly overlie the ultramafic rocks. This section also contains polymictic conglomerates with mainly 1 to 5 cm-sized angular clasts derived from subjacent units. Mafic clasts contain an internal ductile deformation fabric. The conglomerates indicate exhumation and erosional unroofing of previously deformed rocks, possibly along penecontemporaneous faults. Notably lacking are the sheeted dike complexes that intervene between ultramafic and supracrustal sections found in classical ophiolites. The Sylvester rocks may not have formed through 'normal' sea-floor spreading. Instead, they more closely resemble sections formed at slow-spreading ridges or hyperextending margins where the subcontinental mantle is exhumed by low-angle detachment faults. A previously dated (ca. 268 Ma) trondjemite dike from the Zus Mountain area is coeval with similar dikes in Slide Mountain ophiolites in the Yukon, but significantly younger than supracrustal successions elsewhere in the Slide Mountain terrane. The late ocean opening documented in the Sylvester allochthon and the Yukon was broadly coeval with ocean closing elsewhere, as ocean crust was consumed by westerly subduction beneath the Yukon-Tanana terrane.

Keywords: Sylvester allochthon, Slide Mountain terrane, Yukon-Tanana terrane, Rapid River tectonite, Devonian, Permian, ophiolites

1. Introduction

This report summarizes two weeks of fly camp-based fieldwork in the Cassiar Mountains of northern British Columbia (Fig. 1) aimed at assessing two elements of the Sylvester allochthon: 1) the timing, nature, and tectonic cause of deformation in the Rapid River tectonite and 2) the history of ophiolites in the Slide Mountain terrane as a constraint on timing and mechanisms of basin formation. Work from two camps in the Dalton Creek-Four Mile River and Cry Lake areas (Fig. 1) investigated the Rapid River tectonite, the highest structural slice in the Sylvester allochthon. It rests structurally on 'Division III', an imbricated sequence of Paleozoic arc-related rocks, which in turn structurally overlies the imbricated marginal basin assemblage of the Slide Mountain terrane

(Nelson, 1993). Nelson and Friedman (2004) correlated the Rapid River tectonite to mainly siliciclastic rocks of the Snowcap assemblage, which forms the basement of the Yukon-Tanana terrane (Colpron et al., 2006). Intruded by at least one Late Devonian (ca. 362 Ma) late synkinematic pluton (Gabrielse and Harms 1989; Gabrielse et al., 1993), the Rapid River tectonite offers a rare opportunity to study Devonian tectonic processes, which in most of the peri-Laurentian terranes have been obscured by Mississippian and younger deformation processes.

We also examined well-exposed ultramafic-mafic complexes of the Slide Mountain terrane in the Zus Mountain and Blue Dome areas (Fig. 1). The focus of this fieldwork was to evaluate if these complexes represent dismembered ophiolite

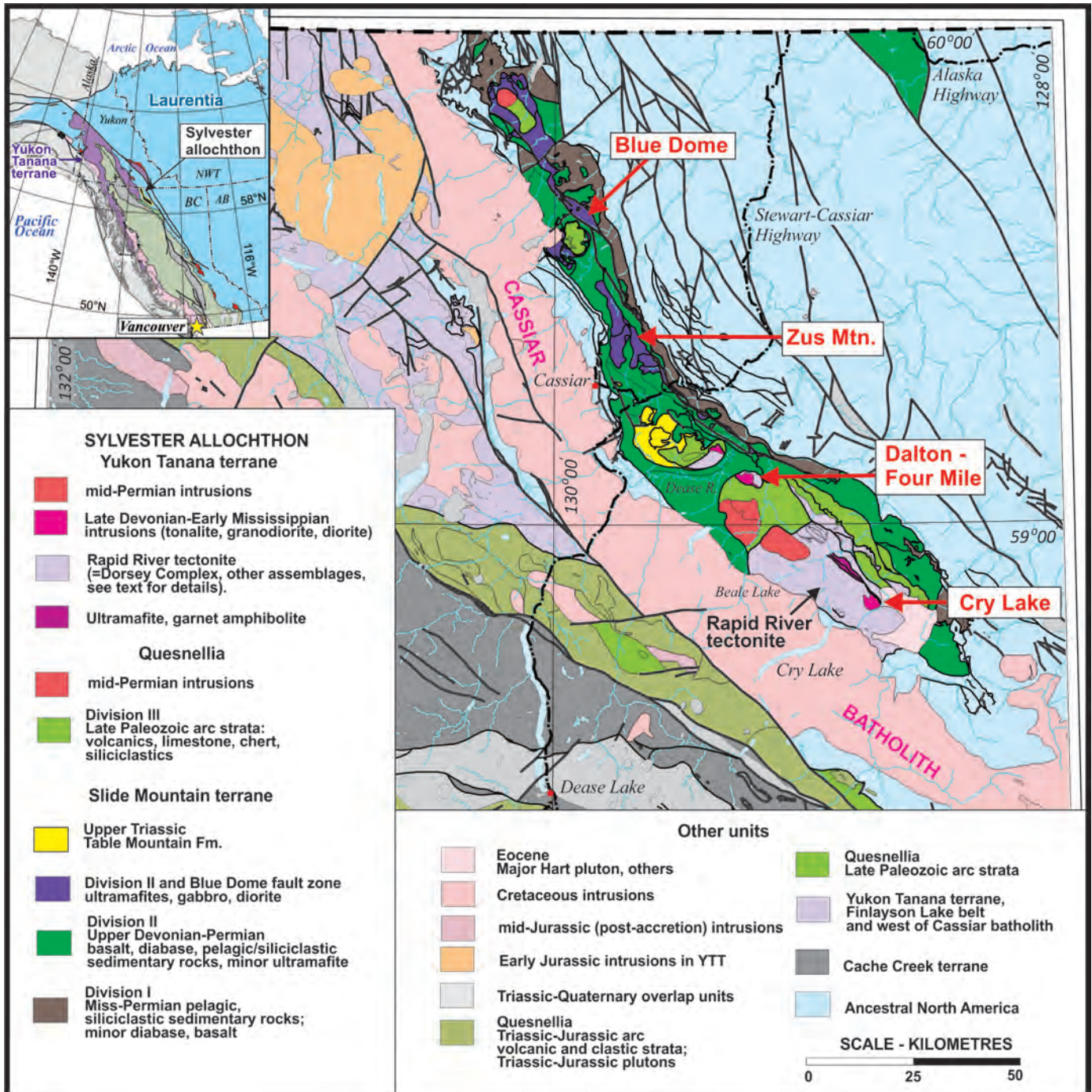


Fig. 1. Location of the Sylvester allochthon and 2014 study sites. General geology from Nelson and Friedman (2004).

massifs formed from ‘normal’ ocean-spreading or if they constitute Alpine-type peridotites formed during magma-poor hyperextension that exhumed mantle onto the seafloor (Manatschal et al., 2011).

2. The Rapid River tectonite and synkinematic intrusions

The Rapid River tectonite, first recognized in the Dalton-Four Mile area by Harms (1990), is an assemblage of mainly siliceous rocks that display ductile strain at a high structural level in the Sylvester allochthon. Gabrielse (1998) included

this assemblage in a unit of tectonized mafic metavolcanic rocks, chloritic phyllite, marble, siliceous cataclasite, and mylonitized intrusive rocks between Dease River and Cry Lake, which he tentatively correlated with the parautochthonous Kootenay terrane of southeastern British Columbia. However, the structural position of the unit above the Slide Mountain terrane indicates that it is allochthonous. It was assigned to the Yukon-Tanana terrane by Nelson and Friedman (2004), based on similarities between the amphibolite-facies, siliciclastic-metabasalt-ultramafic assemblage near Beale Lake in the

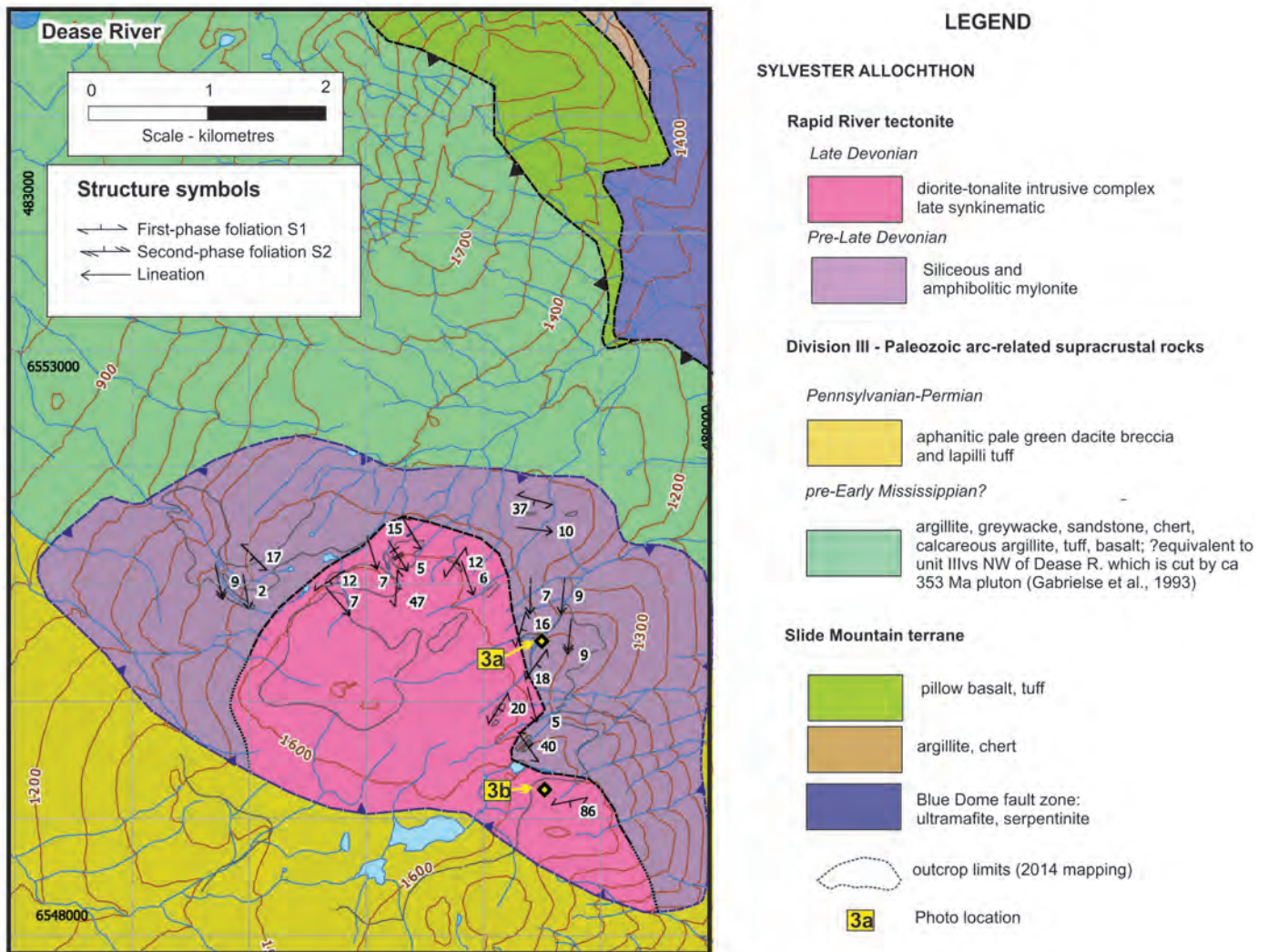


Fig. 2. Dalton Creek-Four Mile River area geology. Geology from Gabrielse and Harms (1989) updated with our 2014 mapping. UTM Zone 9, NAD 83.

Sylvester allochthon (Nelson and Lepage, 2002) and the Dorsey complex west of the Cassiar batholith (Fig. 1). It is likely however, given the variety of lithologies it includes, that the Rapid River tectonite comprises more than one assemblage. It is intruded by synkinematic plutons of known (Four Mile; Gabrielse et al., 1993) and suspected (Cry Lake, Gabrielse, 1998) Devonian age.

Our work focused on: 1) constraining the age of early deformation in the Rapid River tectonite; 2) evaluating if the tectonite is equivalent to the Dorsey complex (Snowcap assemblage) or if other assemblages are present; and 3) establishing the kinematic history and origin of the tectonite. We therefore focused on the two areas in which Devonian plutons are known or suspected to exist.

2.1. Dalton-Four Mile area

Tectonised rocks in the Dalton-Four Mile area include both siliceous and mafic mylonites (Fig. 2). Both are extremely fine grained, tectonically layered on mm to cm-scale, and display well-developed stretching lineations, indicating that they

accommodated high strain. Rare relict textures in the siliceous mylonite indicate a tonalitic protolith (Fig. 3a). The foliation is gently dipping except near the margins of the allochthon, and the stretching lineation plunges shallowly southward (160-180°, Fig. 2). Local shear bands and sigma porphyroclasts indicate a top-to-the north-northwest sense of shear. Lineation trends are considerably more northerly than the northwesterly folds and lineations that developed in the Sylvester allochthon and underlying Laurentian strata as it was assembled and emplaced on the continent margin. A sample of the mylonitized tonalite was collected for U-Pb geochronology to establish the early deformation history of the Rapid River tectonite.

The Dalton-Four Mile pluton (Figs. 2, 3b), mapped by Gabrielse and Harms (1989), yielded a ca. 362 Ma U-Pb zircon crystallization age, with significant ca. 2.23 Ga inheritance (Gabrielse et al., 1993). It occupies a higher structural position than the tectonite. The pluton grades downward from mainly hornblende diorite into tonalite and trondhjemite, and appears to form a sheeted sill complex. At its lower contact, plutonic rocks interfinger with the tectonite, clearly cutting the early foliation.

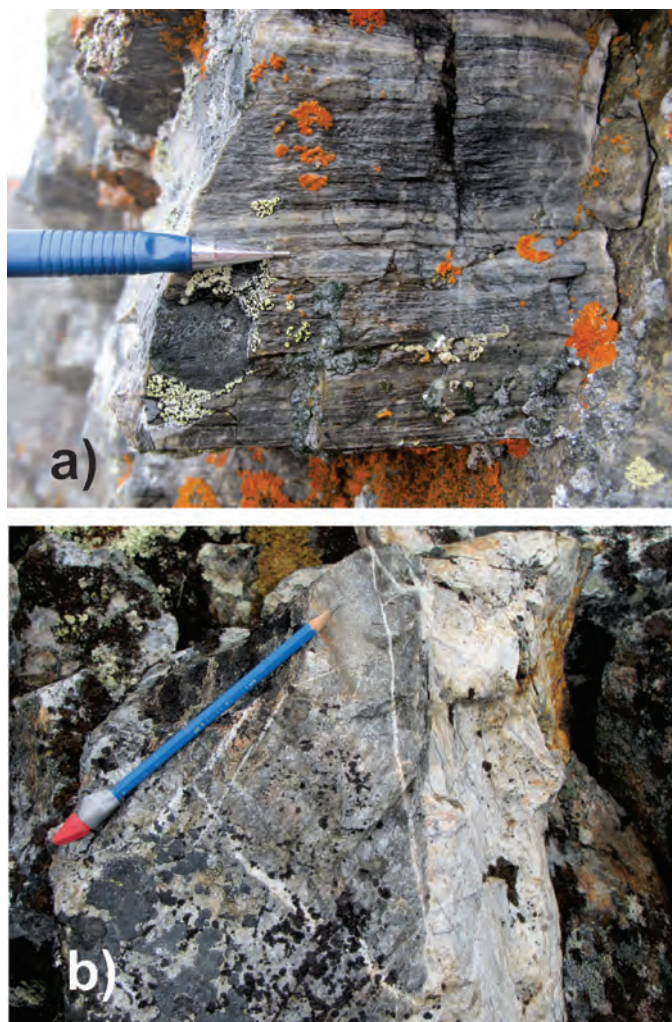


Fig. 3. Rapid River tectonite and Late Devonian intrusion in Dalton-Four Mile area. **a)** Mylonitized tonalite sill 'siliceous tectonite' (487498 E, 6550515 N). **b)** Late-stage post-kinematic aplite dike cutting foliated diorite of Late Devonian pluton, pencil aligned parallel to foliation (487522 E, 6549248 N). UTM Zone 9, NAD 83.

Some phases display well-developed stretching lineations and a weak to moderate foliation, whereas others are unfoliated and crosscut fabrics (Fig. 3b). We agree with Gabrielse and Harms (1989) that it was emplaced late in the kinematic history of the tectonite. We collected a sample from this body for U-Pb geochronology to better separate crystallization from inherited zircon fractions and obtain a more precise emplacement age.

2.2. Cry Lake area

In the Cry Lake area, the Rapid River tectonite consists mostly of heterogeneous, layered to laminated, fine-grained mylonitized amphibolite (Figs. 4, 5a), with scattered lenses of marble and calc-silicate (Fig. 6). The interpreted protolith is a mainly basaltic succession with small limestone lenses. Also present are layered siliceous mylonites and mylonitized tonalites similar to those in the Dalton-Four Mile area. Mylonitic fabrics are steeply dipping and northwesterly striking (Fig. 4). The stretching lineation, somewhat less well developed than

in the Dalton-Four Mile area, trends northwest, parallel to the hinge lines of major folds. Sinistral shear-sense indicators (shear bands; Fig. 5b) were observed at two locations. Map relationships (Fig. 4) suggest that an originally gently dipping tectonite fabric was steepened by later folding. Based on simple unfolding of the shallowly plunging folds in the Cry Lake area, the fabrics in the Rapid River tectonite would have had a top-to-the-northwest sense of shear, in common with the Dalton-Four Mile area.

The tectonite assemblage is intruded by an unnamed diorite-gabbro body. Within 50 metres of its margins, this body and the Rapid River tectonite are cut by abundant tonalitic to trondhjemitic dikes and sills. The main body consists mostly of hornblende-plagioclase-bearing diorite or gabbro (Fig. 5c). The hornblende crystals tend to be equant, possibly pseudomorphous after pyroxene. Patches of hornblendite may be replacements of clinopyroxenite; hornblendite also occurs as xenoliths in intrusive breccias. Hornblende increases in modal abundance near the xenoliths. The body is an intrusive complex that comprises multiple phases of varying composition and texture. Although generally undeformed, it is cut by discrete, narrow, high-strain zones. Although the diorite-gabbro lacks obvious free quartz, we collected a sample for U-Pb zircon geochronology to establish the upper limit to when the Rapid River tectonite was deformed.

Three phases of dikes can be recognized within 50 m of the upper contact between the main mafic pluton and the Rapid River tectonite. The earliest phase dikes are hornblende-phyric dacite, and are more deformed (e.g. boudinaged) than the later two sets (Fig. 5d). Bladed hornblende phenocrysts help define the foliation, and some are augen shaped. The second dike set is characterized by leucotonalite aplite, and lesser medium-grained tonalite (Fig. 5d). The first two dike phases were deformed at elevated temperature (Fig. 5e). Their emplacement may not have been greatly separated in time. A third set of crosscutting thin leucocratic aplite (trondhjemitic?) dikes are the least deformed, although they exhibit minor syn-magmatic shear offsets (Fig. 5d). The progressive nature of the deformation suggests that the dikes are late syn-kinematic. The first two phases of dikes and apophyses of the diorite are folded, and axial planes of the folds (Fig. 5f) are generally parallel to the steep overall fabric in the Rapid River tectonite at this locality. We collected a trondhjemitic sample from the late syn-tectonic, second-phase aplite for U-Pb geochronology.

3. Ophiolites in the Slide Mountain terrane

The Slide Mountain terrane represents the remnants of a mid- to late-Paleozoic back-arc ocean basin that opened between Laurentia and the arc-frontal Yukon-Tanana terrane (eg., Murphy et al., 2006; Piercey et al., 2006; Nelson et al., 2006). To further evaluate relationships between the Yukon-Tanana terrane and the ancient North American margin, and to consider the history of rifting and sea-floor spreading recorded by the Slide Mountain terrane, we examined extensive ultramafic-mafic complexes in the Zus Mountain and Blue Dome areas

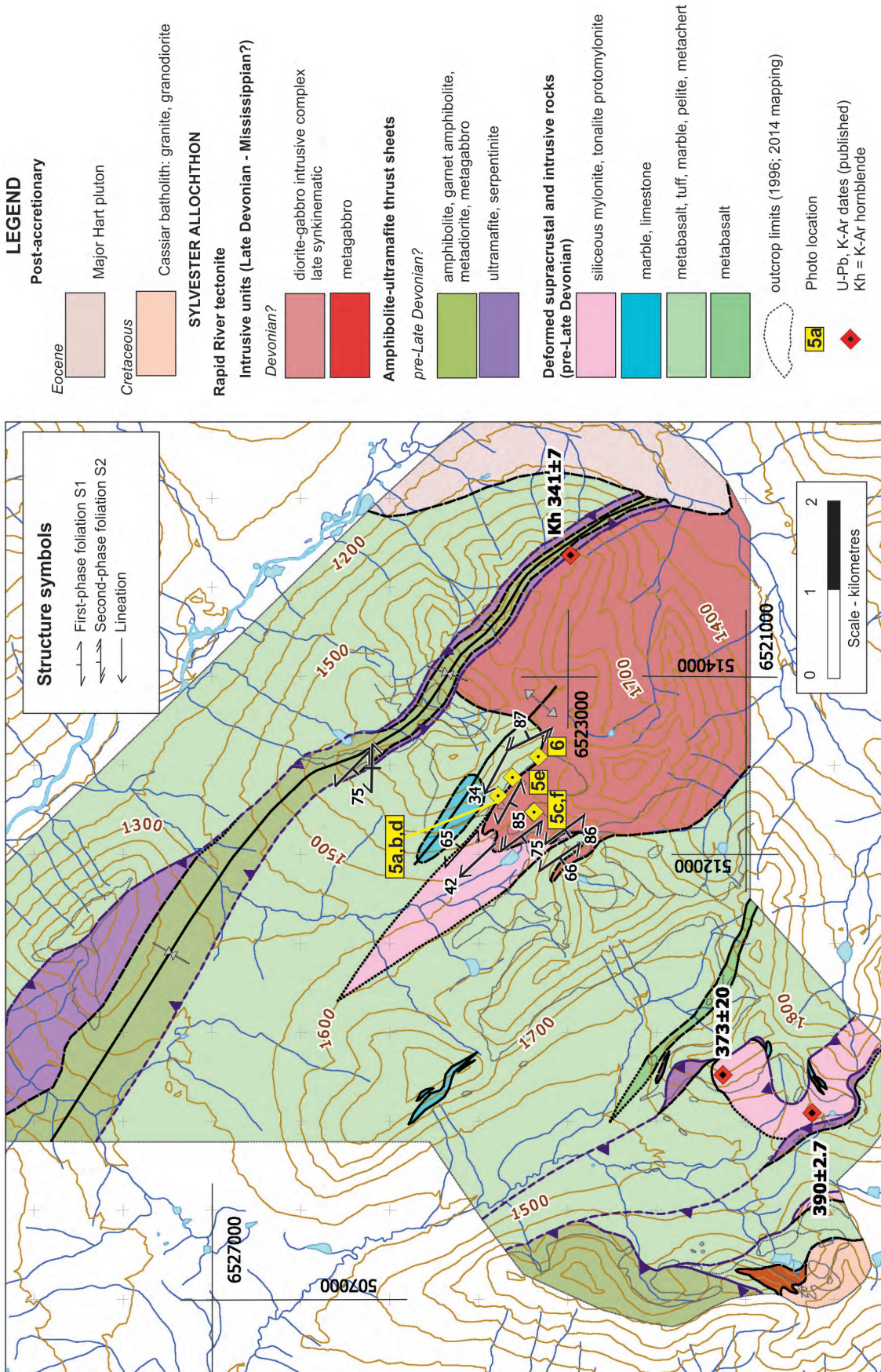


Fig. 4. Cry Lake area geology. Geology from Gabrielse (1994, 1998), J. Nelson, unpublished mapping, 1996, and our 2014 observations.

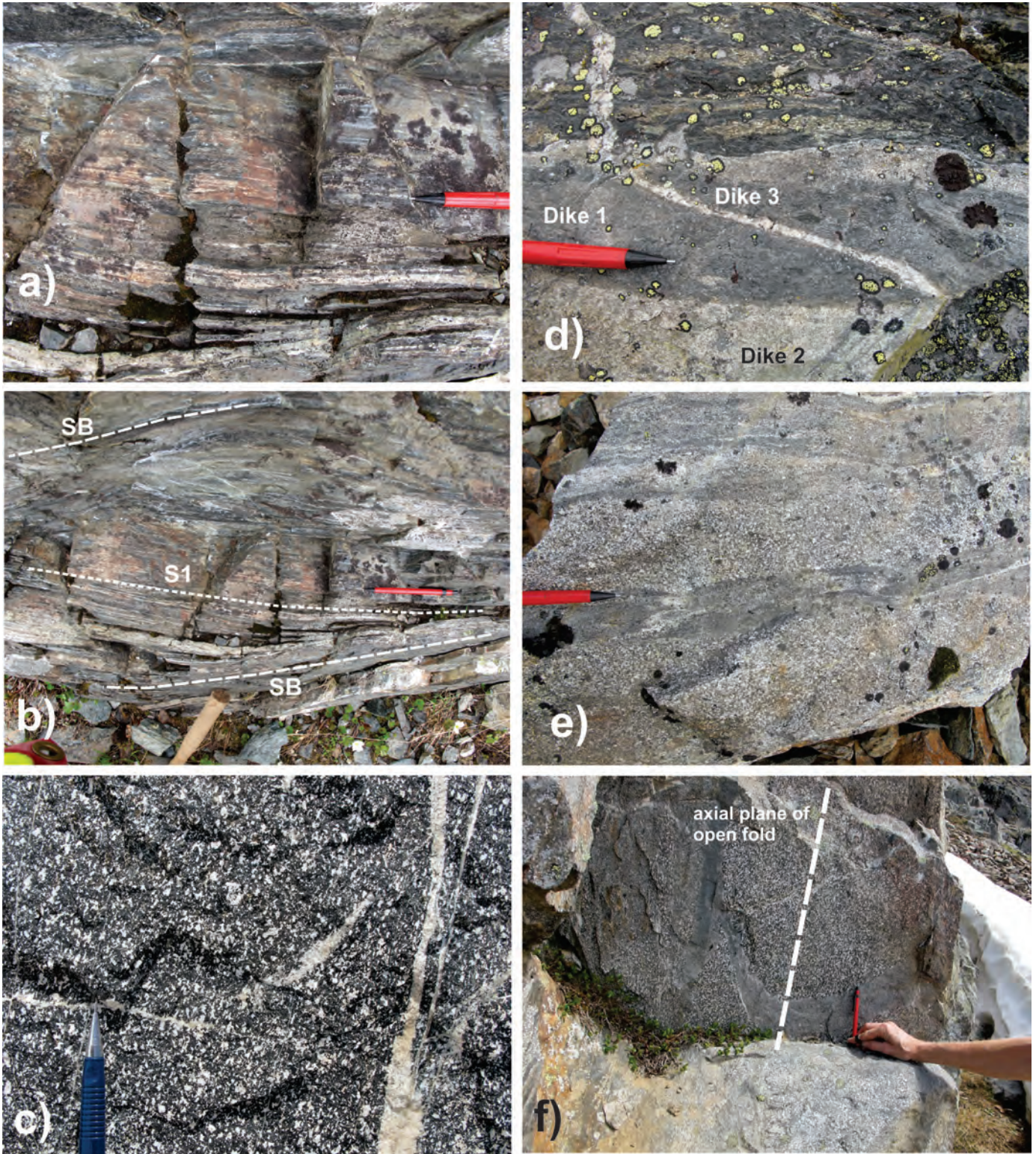


Fig. 5. Cry Lake tectonites and phases of late synkinematic pluton. **a)** Mylonitic amphibolite schist (512660 E, 6523782 N). **b)** Sinistral sense of shear recorded by large-scale shear bands in amphibolite of the Rapid River tectonite (512660 E, 6523782 N). **c)** Coarse-grained, diorite in main body of pluton; weak foliation defined by alignment of plagioclases from lower left to top right (512476 E, 6523377 N). **d)** Three generations of dikes cut the tectonite foliation. Dike 1 is folded and well foliated, and some hornblende crystals are augen-shaped, Dike 2 is moderately foliated tonalite, Dike 3 is very weakly foliated, cross-cutting leucotonalite aplite (512660 E, 6523782 N). **e)** Multi-phase dioritic intrusions at contact between diorite and tectonite; the dikes are synkinematic, with ductile sub-solidus fabrics (512865 E, 6523620 N). **f)** Coarse diorite phase of the pluton, with weak shape fabric parallel to axial plane of fold. Finer-grained dikes are also folded with the same axial plane. This phase of folding may have steepened the attitudes of the high strain fabric of the Rapid River tectonite (512479 E, 6523383 N).

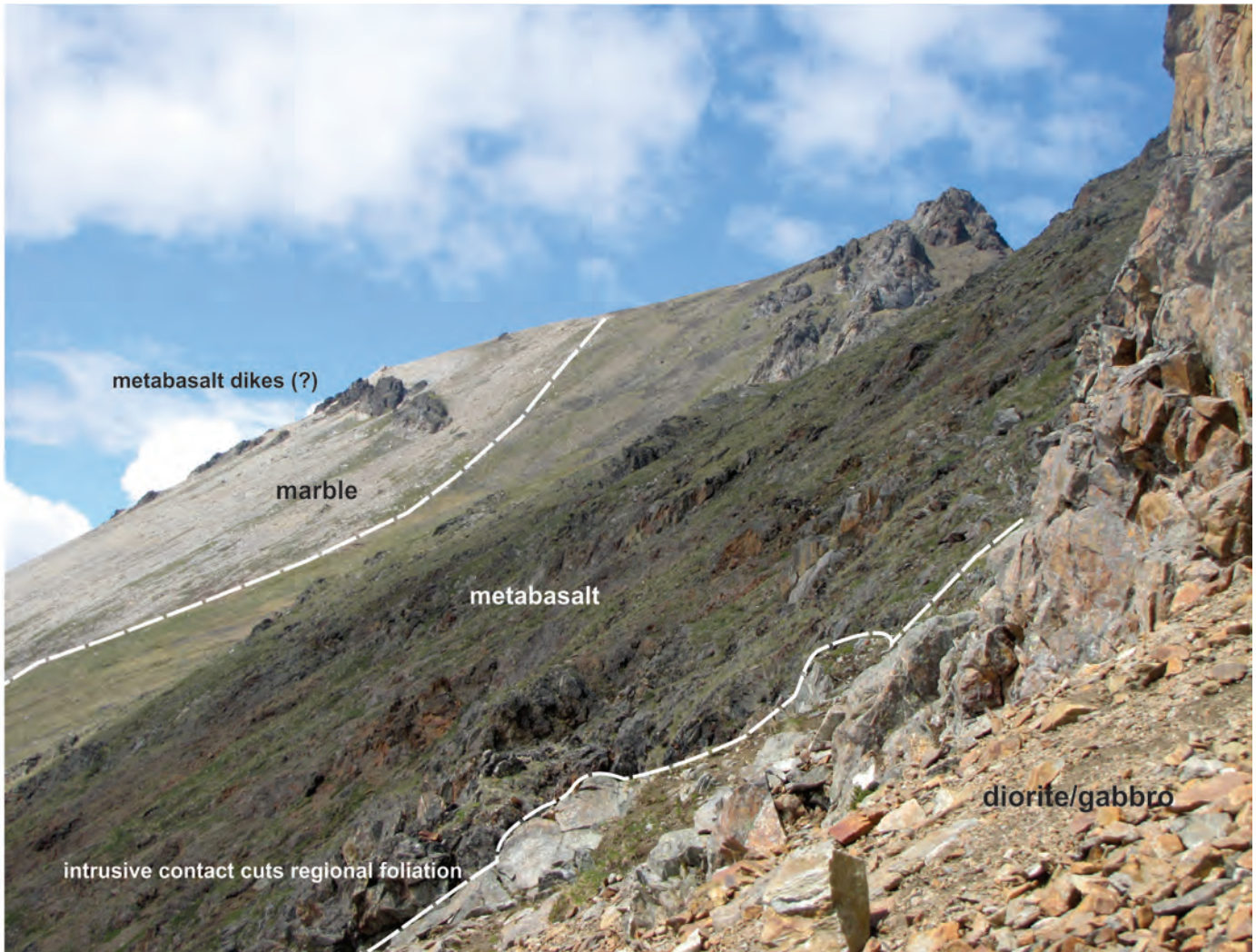


Fig. 6. Looking northwest from contact of synkinematic pluton into Rapid River tectonite (513100 N, 6523330 N). Dark, foliated rocks are mylonitized metabasalts. Marble body on ridge is cored by metabasalt. Axis of isoclinal antiform passes through it (Fig. 4). Pluton cuts across foliation, but is locally ductilely sheared and contact appears to be folded along with host rocks, with detail shown in Fig. 5f.

of the Sylvester allochthon (Fig. 1). We focus on establishing the tectonic setting and origin of these complexes, testing if they represent classical ophiolites formed by ‘normal’ sea-floor spreading; or rather at slow spreading ridges or hyperextending margins where subcontinental mantle is exhumed by low-angle detachment faults.

3.1. Zus Mountain area

The Sylvester allochthon east and north of the Cassiar townsite (Fig. 1) contains two imbricated ultramafite-gabbro complexes (Nelson and Bradford, 1993). The base of the lowest imbricate (Cassiar complex; age unknown) hosts the past-producing Cassiar asbestos mine. We interpret that this imbricate reappears in the valley of Quartzrock Creek (Fig. 7). West of Quartzrock Creek, this sheet is structurally overlain by a second imbricate containing the Zus Mountain ultramafite and gabbro (Fig. 7). The Zus Mountain ultramafite is a typical serpentinitized mantle tectonite composed of heavily serpentinitized harzburgite (Fig. 8a) to lherzolite. The ultramafic

rocks are characterized by well-stretched pyroxene crystals, and are Cr-spinel bearing. Dunite forms patchy bodies and dikes with diffuse margins (Fig. 8b). Common in the upper part of the ultramafite are dikes of leucogabbro and trondjemite. One of the trondjemite dikes has yielded a U-Pb age of ca. 268 Ma (Gabrielse et al., 1993; Figs. 4, 8c). Above the ultramafite, forming the upper ridges and peak of Zus Mountain, is a large body of gabbro (30% clinopyroxene-70% calcic plagioclase; Fig. 9). It displays distinct compositional layering parallel to its basal contact, particularly a prominent pale-coloured band (Fig. 9) that we interpret as a leucogabbro sill along a fault. The gabbro displays a foliation defined by a strong preferred dimensional orientation of apparently unbroken pyroxene and plagioclase that may be of high-temperature origin. Rocks in a gully immediately north of the gabbro (Fig. 7) appear to mark a northwest-dipping cataclastic fault zone that may signify late movement along the gabbro-ultramafite contact. This contact is also exposed along an old exploration road on the eastern side of the study area, where serpentinite near the contact displays

LEGEND

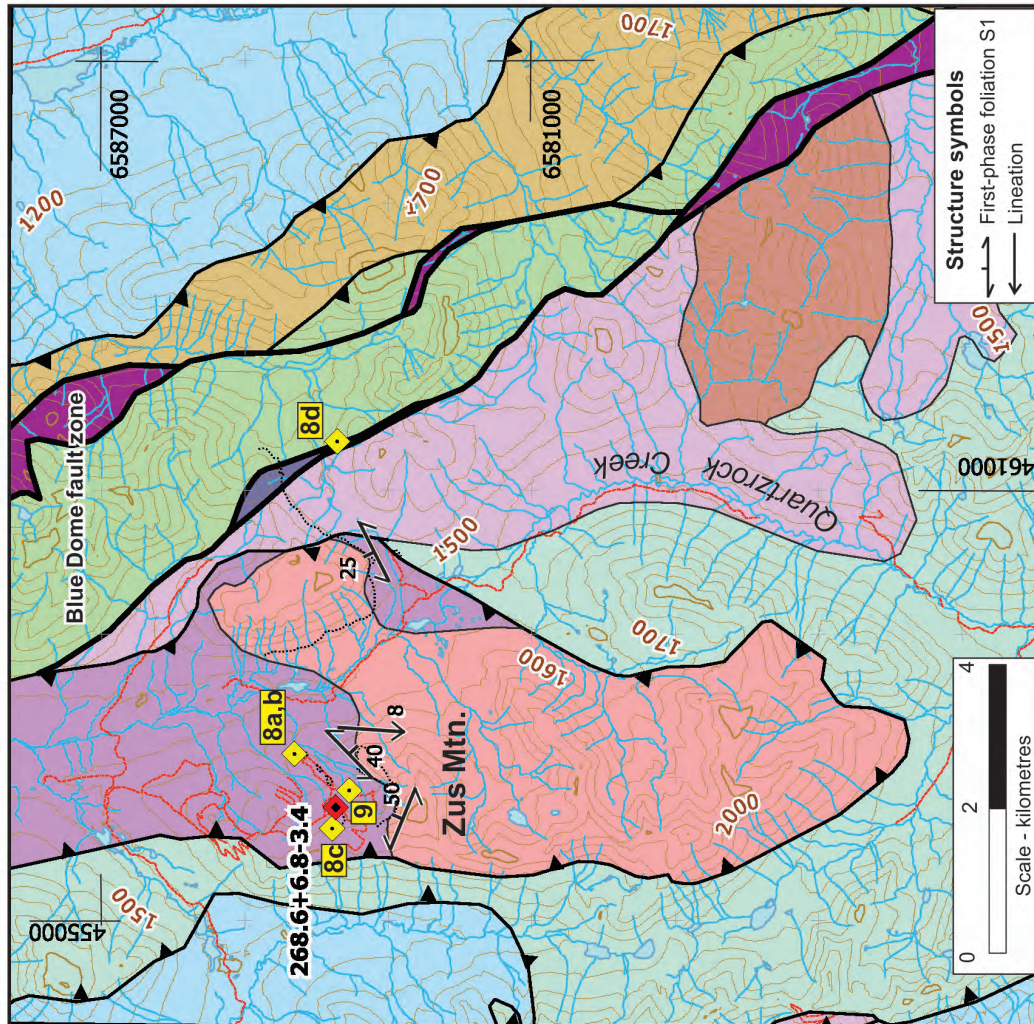
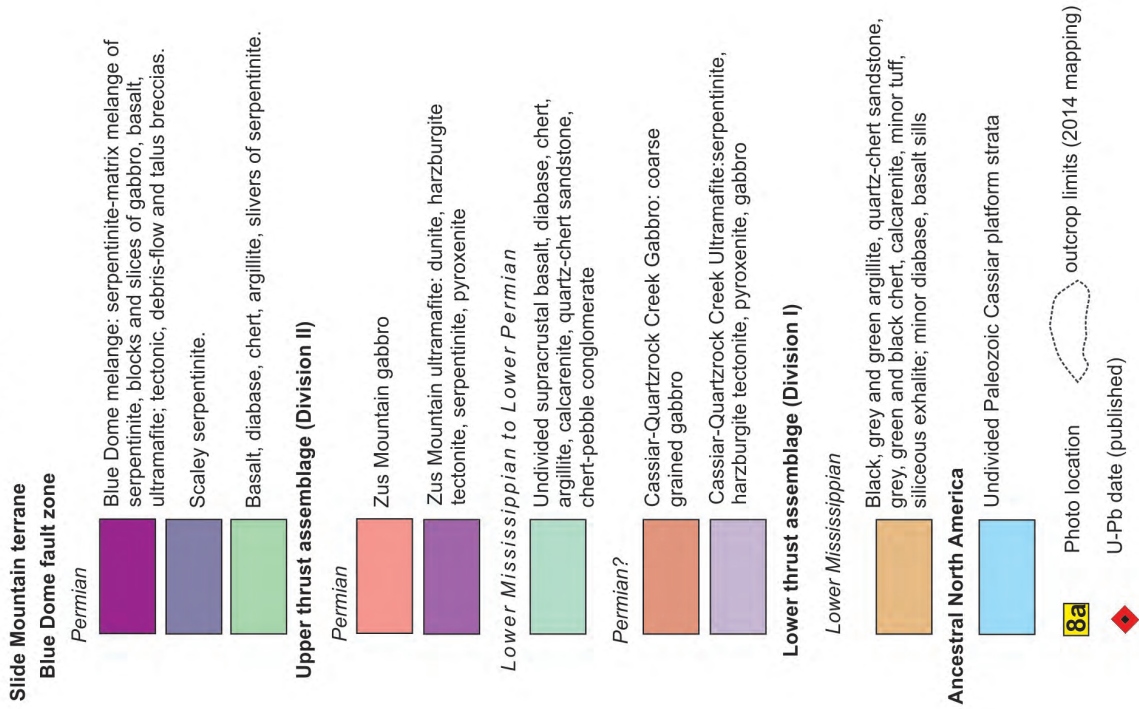


Fig. 7. Zus Mountain area geology. Note: cataclasite exposure in small gully is located between Fig. 9 photo site and S1 symbol with 40° dip. Geology from Nelson et al. (1989). UTM Zone 9, NAD 83.

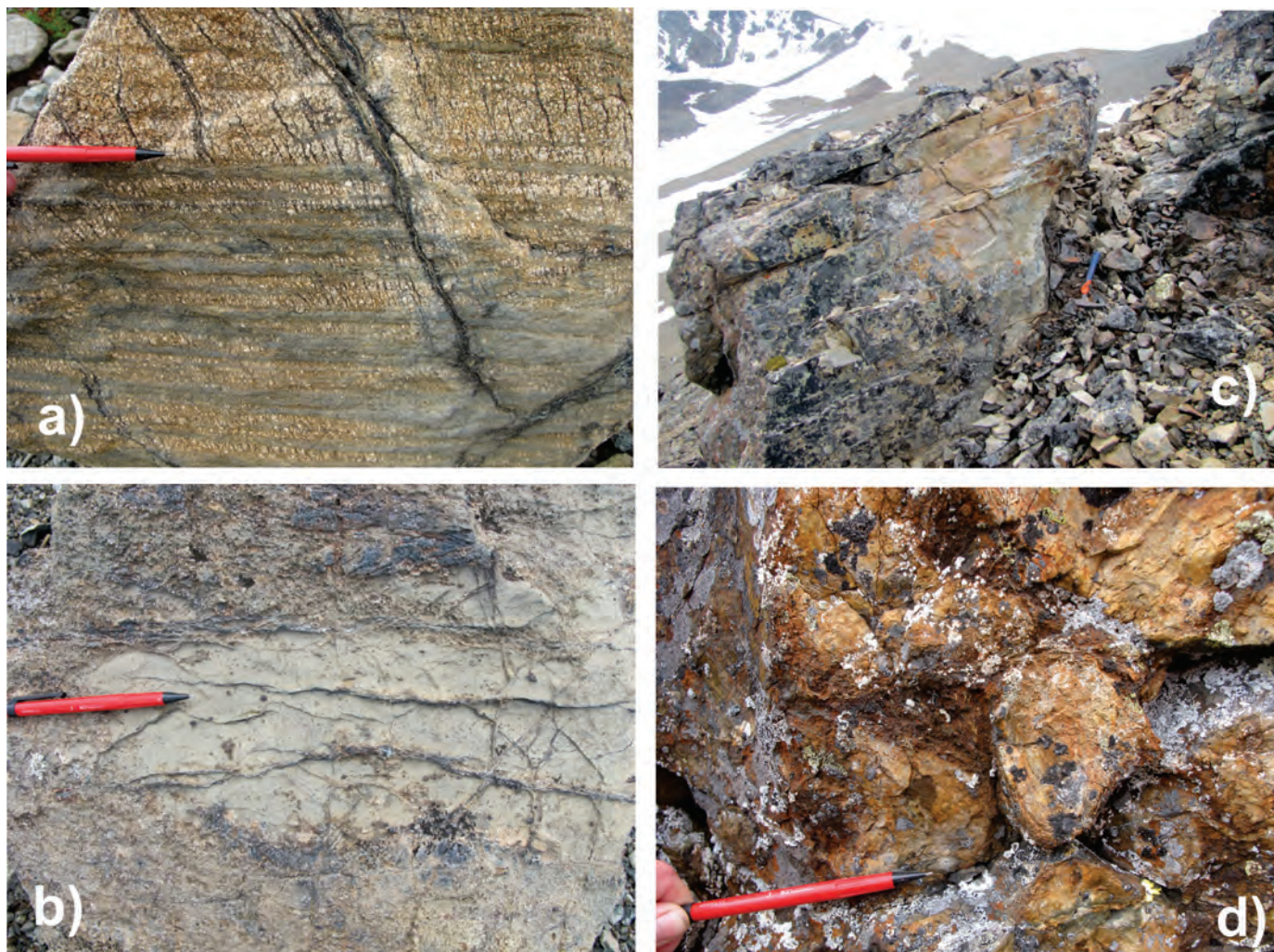


Fig. 8. Zus Mountain ultramafite, gabbro, and related phases. **a)** Well-banded serpentinitized harzburgite (mantle tectonite), with chrysotile veins; relict domains of stretched pyroxene (457326 E, 6584312 N). **b)** Chromite-bearing patchy dunite vein intruded into harzburgite (457326 E, 6584312 N). **c)** Middle Permian trondjemite dike (ca. 268 Ma) cuts serpentinitized ultramafite, chilled curvilinear margin above hammer (456581 E, 6583735 N). **d)** Concentric-zoned basalt pillows with thin selvages, hyaloclastite (brown patches) preserved in pillow interstices (461684 E, 6583714 N).

strong carbonate-quartz alteration (listwanitized).

Also on the eastern side of the study area, the structural contact between the Cassiar complex and Zus Mountain rocks in the overlying imbricate is marked by a thin chert unit (Fig. 7). In the Cassiar complex, below and to the east of the chert, is an extensive body of harzburgite with stretching lineations defined by bastite pseudomorphs after pyroxene. As at Zus Mountain, the harzburgite exhibits patches of Cr-spinel-bearing dunite intrusions. To the east, across the steeply dipping Blue Dome fault zone, are prehnite-pumpellyite facies basaltic flows with local well-preserved pillow structures (Fig. 8d). The marked contrast in strain between the little-deformed pillow basalts, and the more highly deformed chert-argillite horizons, suggests that the chert horizons may have been weak layers that accommodated shear displacement.

3.2. Blue Dome area

The objectives of our work in the Blue Dome area (Fig. 10) were to: 1) better characterize a well-exposed oceanic crustal section that lies between strands of the Blue Dome fault (Nelson et al., 1988); 2) better define the tectonic significance of the Blue Dome fault; and 3) determine the kinematics and nature of the fault movement(s) accommodated by the Blue Dome fault. As described below, a west to east transect along 'Liguria' ridge (Fig. 10) documents a mantle to sea floor transition.

The structurally lower, western end of the Liguria ridge is underlain by serpentinitized ultramafic rocks varying between lherzolite and harzburgite compositions, and generally preserving 1-2 cm partial or complete pseudomorphs after pyroxene (Fig. 11a). Interlayering of dunite and lherzolite was observed. Some peridotites are strongly deformed, with stretched and augen-shaped pyroxene crystals and bastite pseudomorphs (Fig. 11b), textures that are compatible with



Fig. 9. The Zus Mountain ultramafite-gabbro complex. Foreground ultramafite contains abundant pods and patches of dunitite. The rugged cliffs are in the overlying layered gabbro; leucogabbro sill indicated by arrow follows igneous layering and fabric. View to south from 456700 E, 6583600 N.

the high-temperature deformation regime in which mantle tectonites develop. These rocks have abundant serpentine veins throughout. Trondhjemite dikes cut the well-deformed peridotites, unfoliated lherzolite, and previously brecciated serpentinite. Some of the dikes define parallel arrays spaced at 50 to 100 m wide intervals (Fig. 11c). In contrast, other more shallowly dipping dikes in serpentinite exhibit highly irregular apophyses (Fig. 11d), possibly due to emplacement in a near-surface, thoroughly hydrated host. Although trondhjemite intrusion postdates at least some serpentinization, these apophyses suggest that intrusion was synchronous with motion on exhumation-related faults that brought rocks to higher levels in the crust where they were susceptible to serpentinization. Dating of the dikes would therefore be a proxy for the time of exhumation, and we collected several samples of trondhjemite for U-Pb dating. At one locality the trondhjemite is coarse grained and spatially associated with coarse-grained (pegmatitic) leucogabbro (Fig. 11e). Pegmatitic varieties of the trondhjemite have coarse (1 cm) quartz phenocrysts (Fig. 11f).

At structurally higher levels along the Liguria ridge transect, the abundance of diabase dikes and/or sills increases. Locally, the diabases appear brecciated. Upward, plagioclase-phyric basalts transition to basalt flows that are locally pillowed (Fig. 12a) and brecciated. Some of the basalt is variolitic. Local chert bodies (interlayers?) contain radiolaria. The volcanic flows and radiolarian-bearing chert signify that this part of the transect represents seafloor deposits stratigraphically overlying exhumed mantle.

At the eastern end of the transect is a strand of the Blue Dome fault. Near it, brecciated gabbro-diabase is cut by dense swarms of minor faults and zones of cataclasis (Fig. 12b), infilled by reticulated quartz-plagioclase veins that could be related to the trondhjemites seen immediately to the west. Some cataclasis zones appear to have significant offsets (e.g., 3 cm wide with at least 3 m of offset; Fig. 12c). These zones are intruded by basaltic dikes with chilled margins, that are also faulted, but with much less offset (Fig. 12d), suggesting that, although synkinematic, they postdate the main episode of cataclastic

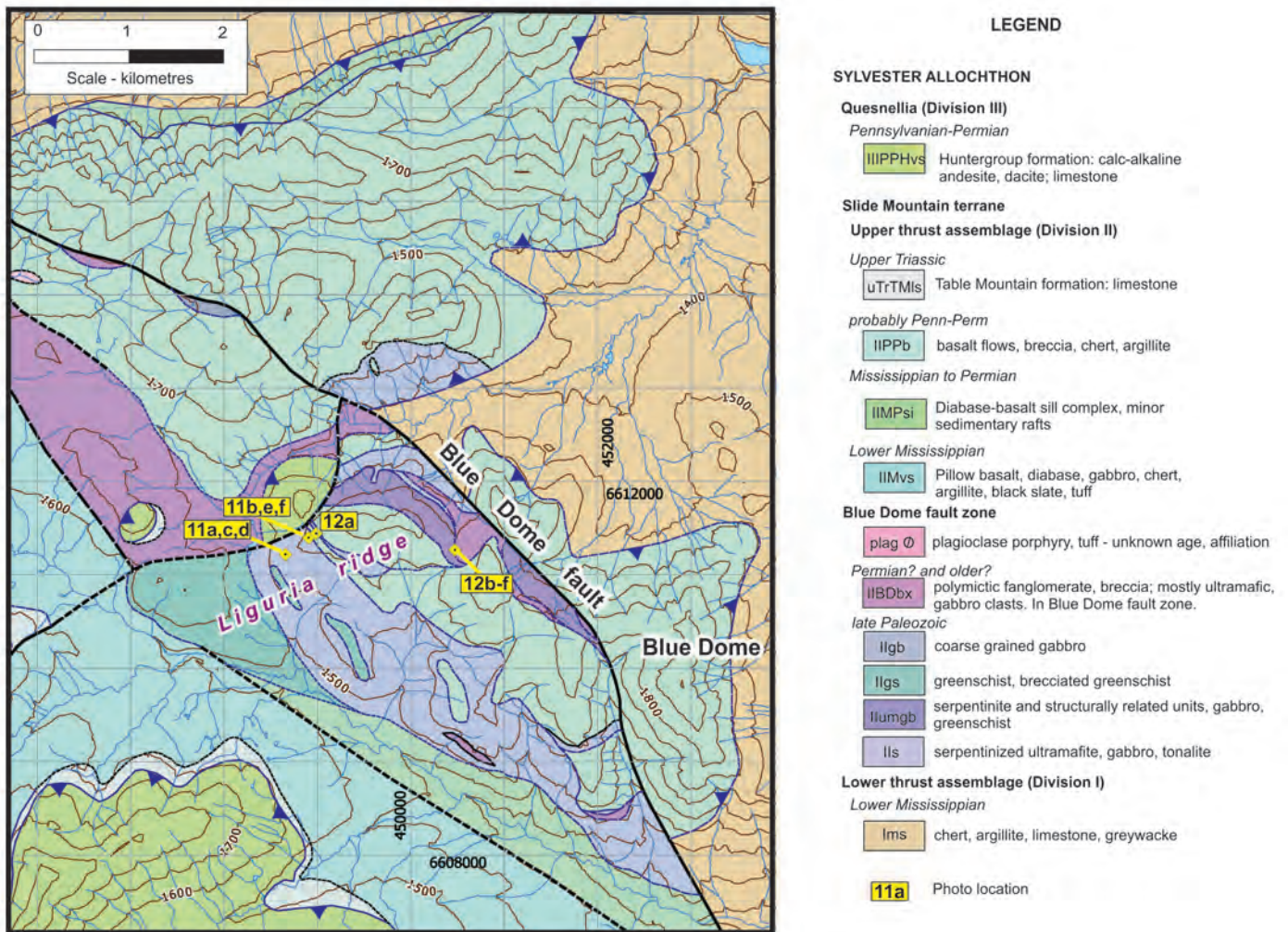


Fig. 10. Blue Dome area geology; from Nelson et al. (1988). UTM Zone 9, NAD 83.

faulting. It is possible that the basalt dikes are feeders to the pillow basalts observed at higher levels and, if so, indicate that basaltic effusion was broadly synchronous with movement on this fault strand.

Immediately east of the cataclastic zone in the gabbro-diabase unit is a lens of polymictic conglomerate up to 70 m thick (Fig. 10). The conglomerate contains angular (locally rounded), 1-5 cm clasts, supported by a sandstone matrix (Fig. 12e). Local sandstone layers separate conglomeratic beds (Fig. 12f). The clast suite consists of abundant intermediate plutonic rocks, basalt, gabbro, and very rare ultramafites. Significantly, the mafic clasts generally contain an internal foliation, pointing to unroofing of previously deformed rocks and penecontemporaneous faulting. Some gabbro-diabase clasts exhibit textures similar to the cataclasites exposed only 20 m to the west. We interpret that this unit represents sedimentation related to a fault scarp recorded by the cataclastic gabbro. Although ultramafic clasts are very rare at this locality, ultramafic rocks are exposed elsewhere along the Blue Dome fault and constitute the predominant clasts in breccias and ophicalcites (Nelson and Bradford, 1993), likely reflecting deeper levels of exhumation and erosion.

4. Discussion

4.1. Rapid River tectonite

The Rapid River tectonite in the Cry Lake and Dalton-Four Mile areas consists mainly of amphibolite-facies, mylonitized mafic volcanic rocks with sparse marble lenses. The highly siliceous felsic bands structurally intercalated with the supracrustal tectonites are mylonitized felsic intrusions and, to a lesser extent, metamorphic segregations and/or veins; evidence of a sedimentary origin is lacking. The mafic protolith of this assemblage is in marked contrast to the prominent siliciclastic rocks in Dorsey assemblage in the Beale Lake area between Cry Lake and the Four Mile River area (Fig. 1) west of the Cassiar batholith (Nelson and Friedman 2004). Hence we consider that the Rapid River tectonite is a distinct tectonostratigraphic assemblage (cf. Nelson and Friedman, 2004), perhaps recording relatively shallow-water, volcanic-rich deposition in a primitive, pre-Late Devonian arc. Possible analogues include the basaltic Knob Hill complex and metaigneous Trail gneiss, which are part of the Devonian and older Okanagan subterrane of southern Quesnellia in southeastern British Columbia (Simony et al., 2006; Massey, 2007).

The Rapid River tectonite is characterized by a high-



Fig. 11. Blue Dome area rocks and rock relationships. **a)** Pyroxene-phyric harzburgite; pyroxene partly altered to bastite (448657 E, 6611219 N). **b)** Peridotite tectonite with shaped pyroxene augen and chromite (448905 E, 6611399 N). **c)** Set of planar trondhjemite dikes (arrows) cutting lherzolite breccia (448657 E, 6611219 N). **d)** Apophyses of trondhjemite dike cutting serpentinitized lherzolite breccia (448657 E, 6611219 N). **e)** Coarse-grained, pegmatitic hornblende leucogabbro spatially associated with trondhjemite (448905 E, 6611399 N). **f)** Pegmatitic trondhjemite (with cm-scale quartz phenocrysts) from a 10 m-thick intrusive sheet. (448905 E, 6611399 N).

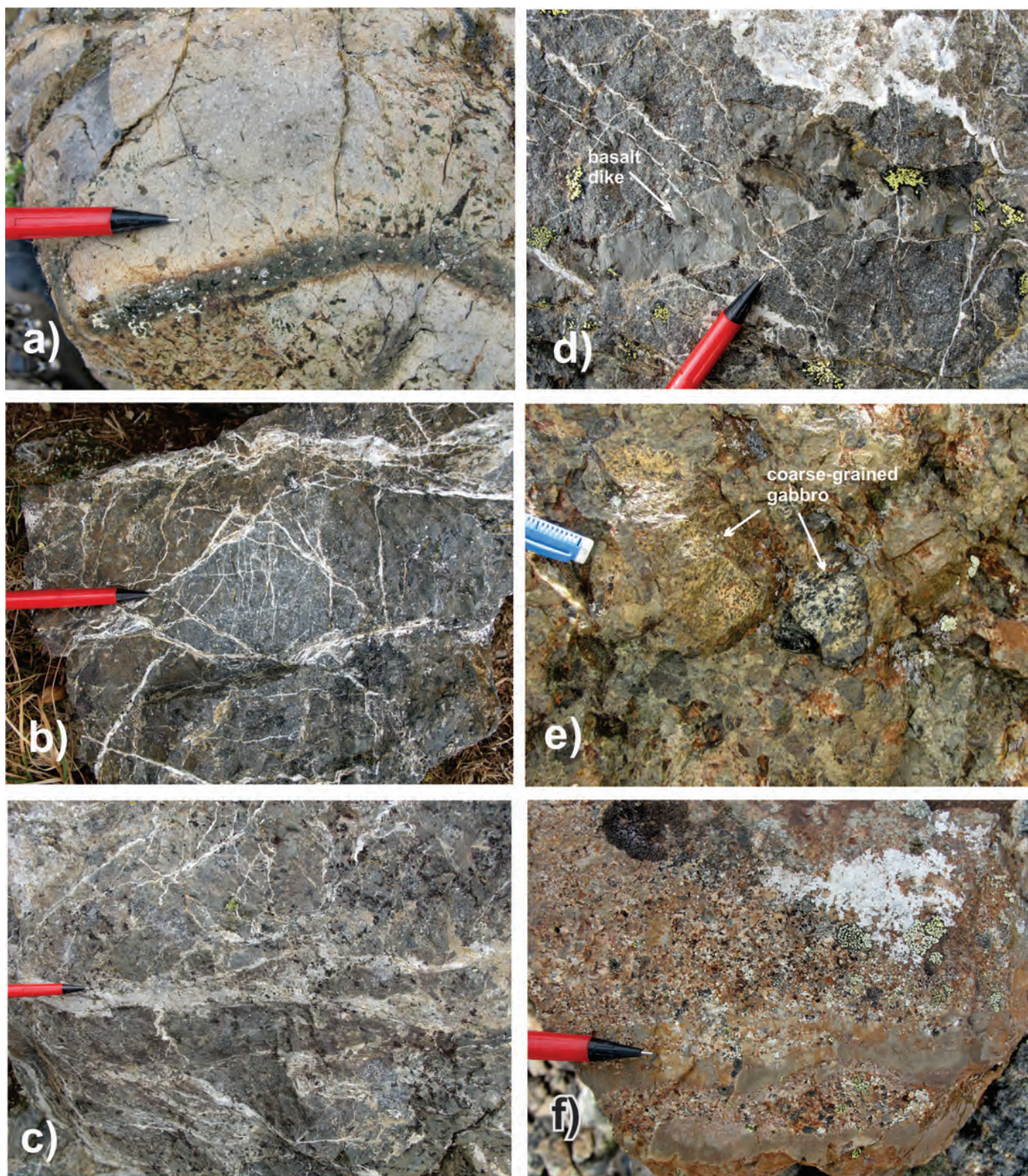


Fig. 12. Blue Dome area rocks and rock relationships, continued. **a)** Plagioclase-phyric basalt to andesite; dark-toned pillow selvage below pen. (448986 E, 6611444 N). **b)** Brecciated, cataclastically deformed gabbro-diabase; fractures and small shears healed with white plagioclase-quartz. **c)** Cataclastic breccia zone with significant offsets in gabbro-diabase. (450473 E, 6611266 N). **d)** Grey basalt dike cuts brecciated gabbro-diabase but shows minor brittle offsets on small shears filled with white quartz-feldspar (450473 E, 6611266 N). **e)** Moderately sorted, polymictic conglomerate with predominantly angular clasts in a sandstone matrix. Two coarse-grained gabbro clasts indicated (450473 E, 6611266 N). **f)** Interstratified polymictic granulestone and sandstone. (450473 E, 6611266 N).

strain, well-developed L-S fabric, indicating strong non-coaxial deformation, typical of a major ductile shear zone. What remains uncertain is if the shear zone accommodated contractional or extensional strain and which geological bodies were juxtaposed across it.

We note the following significant similarities between the Dalton-Four Mile and Cry Lake intrusive complexes: 1) both are mafic intrusions with more felsic marginal phases; 2) both are layer-parallel on a large and small scale; and 3) both are late syn-kinematic. Therefore our current interpretation is that both plutonic complexes are part of a single suite, which includes the 362 Ma granitoid dated by Gabrielse et al. (1993). This assertion will be tested by additional geochronological studies. The samples we collected for geochronology will also help to better constrain the duration of the non-coaxial deformation accommodated by this tectonite. Previous work in the area indicates that the protoliths of mylonitic intrusive rocks are as old as 390 Ma (Nelson and Friedman, 2004). It is possible that the high-strain deformation recorded by the Rapid River tectonite represents an early collision between an arc-related terrane of unknown provenance (represented by the mafic-marble tectonites and Early Devonian intrusions) and the leading edge of the Laurentian margin, the remnants of which may be represented by the Dorsey complex. This postulated collision would have been before the main onset of Late Devonian-Mississippian (363-345 Ma) arc activity built upon the substrate of the Yukon Tanana terrane (cf. Piercey et al., 2006), predating the generally accepted time of subduction initiation along the western margin of Laurentia.

4.2. Ophiolites in the Slide Mountain terrane

Ultramafic-mafic complexes in the Slide Mountain terrane contain heavily serpentinized harzburgite to lherzolite, locally preserving serpentine (after elongated olivine) and bastite (after pyroxene crystals or aggregates) pseudomorphs. Such rocks are typical of mantle tectonites (Mercier and Nicolas, 1975). The rocks are commonly Cr-spinel bearing and locally contain patches and dikes of dunite and pyroxenite. Small intrusive bodies of leucogabbro to trondhjemite are relatively abundant, but layered mafic-ultramafic cumulates and sheeted dikes typical of oceanic lower crust are notably absent. In general, the Zus Mountain, Cassiar and Blue Dome ultramafic bodies appear to be fragments of exhumed lithospheric mantle that became the substrate to the products of syn-rifting mafic magmatism, mainly represented by mafic plutonic rocks but also by basalts. Lithospheric extension is clearly expressed along the Blue Dome fault zone, which may be a zone of synvolcanic extensional faults, rather than simply a fossil transform fault as previously suggested (Nelson, 1993).

Sparse leucogabbro and trondhjemite intrusive samples from the Slide Mountain terrane in the Sylvester allochthon and southern Yukon have yielded mainly Permian ages between 274 and 265 Ma (Gabrielse et al., 1993; Murphy et al., 2006; van Staal et al., 2012 and unpublished results), which are a proxy for the time of mantle exhumation and related mafic magmatism

during early seafloor development. These ages are anomalously young relative to Late Devonian to Early Permian volcanic rocks of the Slide Mountain terrane that indicate that Slide Mountain ocean started to open in the Late Devonian-Mississippian and continued opening through the Pennsylvanian-Early Permian (Nelson, 1993). However, detailed examination of radiolaria and conodont data (Appendix 1 in Nelson and Bradford, 1993) suggests that ocean sedimentation and basalt volcanism were not continuous from early Mississippian to Permian. Rather, separate Mississippian and Late Pennsylvanian-Early Permian pulses appear to be separated by a notable gap during the Early to Middle Pennsylvanian, ending before the 274-265 Ma intrusive cluster. The evidence for Middle Permian hyperextension and the onset of proto-oceanic crust formation at that time suggest that the existing tectonic models are in need of modification. Possibly, distinct Mississippian and Permian basins, currently grouped together in the Slide Mountain terrane, record different episodes of subsidence separated by poorly defined episodes of basin inversion.

5. Conclusions

Field investigations in the Sylvester allochthon in 2014 provide new insights into the evolution of late Paleozoic arc-back-arc systems of western Laurentia. The Rapid River tectonite in the Dalton-Four Mile and Cry Lake areas has a protolith of mafic mylonite and marble. These rocks may signify part of a primitive arc that was mylonitized and then intruded by late synkinematic diorite/gabbro-tonalite-trondhjemite plutons. One of the plutons has previously been dated at ca. 362 Ma. This deformation was part of a tectonic event that set the stage for initiation of arc magmatism on the western Laurentian margin, followed by opening of the Slide Mountain back-arc ocean basin.

The ultramafic part of ophiolite complexes in the Slide Mountain terrane in the Zus Mountain and Blue Dome areas comprises a lower part of serpentinized harzburgite tectonite that is overlain by interlayered peridotite tectonite, lherzolite, dunite, and gabbro, all cut by trondhjemite dikes. Some trondhjemites cut previously-serpentinized hosts, and probably were emplaced during mantle exhumation. At Zus Mountain, a large gabbro body overlies the ultramafites. In the Blue Dome section, basalt, diabase, radiolarian chert and polymictic conglomerates overlie the ultramafites and were probably deposited shortly after their exhumation onto the seafloor. Lacking is an intervening unit of sheeted dikes, such as found in classical ophiolites, implying that the ophiolites did not form through 'normal' sea floor spreading. They more closely resemble slow-spreading ridges or hyperextending margins where the subcontinental mantle is exhumed by low-angle detachment faults. A ca. 268 Ma trondhjemite dike from the Zus Mountain area is coeval with similar dikes in Slide Mountain ophiolites of the Yukon, but significantly younger than the basaltic flow and sedimentary sequences elsewhere in the Slide Mountain terrane. The late (ca. 275-265 Ma) sea-floor spreading of the Slide Mountain ocean was broadly coeval

with sea-floor closing, as oceanic crust subducted beneath the eastern margin of YTT and generated ca. 273-239 Ma eclogites (Erdmer et al., 1998).

Continued petrological and geochronological investigation of samples from the mafic-ultramafic complexes of the Slide Mountain and Yukon-Tanana terranes in Yukon and northern British Columbia will better document the genesis and setting of these tectonically important rock packages which, in turn, will help establish the evolution of the peri-Laurentian margin through mid- to late Paleozoic time.

Acknowledgments

We thank Maurice Colpron of the Yukon Geological Survey for geological insights and productive collaboration during field activities. We thank Trans North Helicopters and pilot Nick Falloon for excellent flight services to the project. This work was carried out under the Crustal Blocks activity (Ancient faults and their controls on mineralization in northern BC and southern Yukon) of the Geomapping for Energy and Minerals program (GEM 2) Cordilleran Project, which was initiated in 2014 by the Geological Survey of Canada, in partnership with the British Columbia Geological Survey and Yukon Geological Survey. We thank Hu Gabrielse for his leadership and expertise over the years, in mapping the geology of the Cassiar Mountains and for setting the stage for this follow-up geological investigation. John Chapman is thanked for completing a critical review of the report. This is ESS Contribution number 2014035.

References

- Devine, F.D., 2005. Geology of the southern Campbell Range, southeastern Yukon: implications for the tectonic evolution of Yukon-Tanana terrane. M.Sc. thesis, Carleton University, Ottawa, Ontario, 136 p.
- Devine, F.D., Carr, S.D., Murphy, D.C., Davis, W.J., Smith, S. and Villeneuve, M., 2006. Geochronological and geochemical constraints on the origin of the Klatsa metamorphic complex: implications for Early Mississippian high-pressure metamorphism within Yukon-Tanana terrane. In: Colpron, M. and Nelson, J.L. (Eds.), *Paleozoic Evolution and Metallogeny of Pericratonic Terranes at the Ancient Pacific Margin of North America*, Canadian and Alaskan Cordillera. Geological Association of Canada, Special Paper 45, pp. 107-130.
- Erdmer, P., Ghent, E.D., Archibald, D.A. and Stout, M. Z. 1998. Paleozoic and Mesozoic high-pressure metamorphism at the margin of Ancestral North America in central Yukon. *Geological Society of America Bulletin*, 110, 615-629.
- Gabrielse, H., 1994. Geology of Cry Lake (104I) and Dease Lake (104J/E) map areas, north central British Columbia. Geological Survey of Canada, Open File Map 2779, scale 1:50 000.
- Gabrielse, H., 1998. Geology of Cry Lake and Dease Lake map areas, north-central British Columbia. Geological Survey of Canada, Bulletin 504, 147 p.
- Gabrielse, H. and Harms, T.A., 1989. Permian and Devonian plutonic rocks in the Sylvester allochthon, Cry Lake and McDame map areas, northern British Columbia. In: *Current Research Part E*, Geological Survey of Canada Paper 89-1E, pp. 1-4.
- Gabrielse, H., Mortensen, J.K., Parrish, R.R., Harms, T.A., Nelson, J.L., and van der Heyden, P., 1993. Late Paleozoic plutons in the Sylvester Allochthon, northern British Columbia; In: *Radiogenic Age and Isotopic Studies*, Report 7, Geological Survey of Canada, Paper 93-2, pp. 107-118.
- Harms, T.A. 1990. Complex tectonite suite in the Sylvester allochthon. Geological Association of Canada, Program and Abstracts. v. 15, p. A-54.
- Manatschal, G., Sauter, D., Karpoff, A.M., Masini, E., Mohn, G. and Lagabriele, Y. 2011. The Chenaillet Ophiolite in the French/Italian Alps: An ancient analogue for an oceanic core complex? *Lithos*, 124, 169-184.
- Massey, N.W.D. 2007. Boundary project: Rock Creek area (NTS 082/02W, 03E), southern British Columbia. In: *Geological Fieldwork 2006*. B.C. Ministry of Energy, Mines and Petroleum Resources, British Columbia Geological Survey Paper 2007-1, pp. 117-128.
- Mercier, J.-C. C. and Nicolas, A. 1975. Textures and fabrics of upper-mantle peridotites as illustrated by xenoliths from basalts. *Journal of Petrology*, 16, 454-487.
- Murphy, D.C., Mortensen, J.K., Piercey, S.J., Orchard, M.J., and Gehrels, G.E., 2006. Mid-Paleozoic to early Mesozoic tectonostratigraphic evolution of Yukon-Tanana and Slide Mountain terranes and affiliated overlap assemblages, Finlayson Lake massive sulphide district, southeastern Yukon. In: Colpron, M. and Nelson, J.L. (Eds.), *Paleozoic Evolution and Metallogeny of Pericratonic Terranes at the Ancient Pacific Margin of North America*, Canadian and Alaskan Cordillera. Geological Association of Canada, Special Paper 45, pp. 75-105.
- Nelson, J.L. 1993. The Sylvester allochthon: upper Paleozoic marginal basin and island arc terranes in northern British Columbia. *Canadian Journal of Earth Sciences*, 30, 631-643.
- Nelson, J.L., Harms, T., Bradford, J.A., Green, K.C. and Marsden, H. 1988. Geology and patterns of mineralization, Blue Dome map area, British Columbia (104P/12). British Columbia Ministry of Energy, Mines and Petroleum Resources, British Columbia Geological Survey Open File 1988-10, scale 1:25 000.
- Nelson, J.L., Bradford, J.A., MacLean, M. and Maddison, L. 1989. Geology and metallogeny of the Cassiar and McDame map areas, British Columbia (104P/3, 5). British Columbia Ministry of Energy, Mines and Petroleum Resources, British Columbia Geological Survey Open File 1989-9, 4 sheets, scale 1:25 000.
- Nelson, J.L. and Bradford, J.A., 1993. Geology of the Midway-Cassiar area, northern British Columbia (104O, 104P). British Columbia Ministry of Energy, Mines and Petroleum Resources, British Columbia Geological Survey Bulletin 83, 94 p., geologic map, scale 1:100 000.
- Nelson, J.L. and Friedman, R., 2004. Superimposed Quesnel (late Paleozoic-Jurassic) and Yukon-Tanana (Devonian-Mississippian) arc assemblages, Cassiar Mountains, northern British Columbia: Field, U-Pb and igneous petrochemical evidence. *Canadian Journal of Earth Sciences*, 41, 1201-1235.
- Nelson, J., and Lepage, L.D. 2002. Geology and mineral occurrences, Beale Lake map area (NTS 104I/14N). British Columbia Ministry of Energy and Mines, British Columbia Geological Survey Open File Map 2002-6, scale 1:50 000.
- Nelson, J., Harms, T., Bradford, J., Green, K., and Marsden, H., 1988. Blue Dome map area (104P/12); geology and metallogeny. British Columbia Ministry of Energy, Mines and Petroleum Resources, British Columbia Geological Survey Open File 1988-10, 6 sheets, scale 1:25 000.
- Piercey, S.J., Nelson, J.L., Colpron, M., Dusel-Bacon, C., Simard, R.-L., and Roots, C.F., 2006. Paleozoic magmatism and crustal recycling along the ancient Pacific margin of North America, northern Cordillera. In: Colpron, M. and Nelson, J.L. (Eds.), *Paleozoic Evolution and Metallogeny of Pericratonic Terranes at the Ancient Pacific Margin of North America*, Canadian and Alaskan Cordillera. Geological Association of Canada, Special Paper 45, pp. 281-322.
- Simony, P. S., Sevigny, J. H., Mortensen, J. K. & Roback, R. C.

2006. Age and origin of the Trail Gneiss Complex: Basement to Quesnel terrane near Trail, southeastern British Columbia. In: Colpron, M. & Nelson, J. L. (Eds.) Paleozoic evolution and metallogeny of pericratonic terranes at the ancient Pacific margin of North America, Canadian and Alaskan Cordillera. Geological Association of Canada, Special Paper 45, pp. 505-515.

van Staal, C., Escayola, M., McClelland, W., Petrie, M., Gilotti, J. and Ryan, J.J., 2012. Some comments on the Paleozoic tectonic history of the Yukon-Tanana terrane –Slide Mountain trane system. 2012 Cordilleran Tectonics Workshop Abstracts, February 24-26, 2012, Victoria, BC, p. 57.

Preliminary geology of the Shrimpton Creek area (NTS 092H/15E, 16W) Southern Nicola Arc Project

Mitchell G. Mihalynuk^{1, a}, Larry J. Diakow¹, James M. Logan², and Richard M. Friedman³

¹ British Columbia Geological Survey, Ministry of Energy and Mines, Victoria, BC, V8W 9N3

² JLoGeologic, Victoria, BC, V8L 5Z9

³ Pacific Centre for Geochemical and Isotopic Research, University of British Columbia, Vancouver, BC, V6T 1Z4

^a corresponding author: Mitch.Mihalynuk@gov.bc.ca

Recommended citation: Mihalynuk, M.G., Diakow, L.J., Logan, J.M., and Friedman, R.M., 2015. Preliminary geology of the Shrimpton Creek area (NTS 092H/15E, 16W) Southern Nicola Arc Project. In: Geological Fieldwork 2014, British Columbia Ministry of Energy and Mines, British Columbia Geological Survey Paper 2015-1, pp. 129-163.

Abstract

Geological maps and analytical results of the Southern Nicola Arc Project (SNAP) change the way that we view the evolution of southern Quesnel terrane. Nicola arc rocks host the Copper Mountain mine to the south and the Highland Valley and Afton mines to the north of the SNAP study area. Nicola Arc has been classically thought of as Late Triassic, felsic in the west, and relatively unaffected by contractional deformation. Our work indicates that magmatism is older (~238 Ma) than previously known and that the oldest dated Nicola Group rocks are felsic units in the central part of the arc. Felsic volcanism is not restricted to the classical 'Western belt' where it is now well dated at 224 to 225 Ma. Here we report on the Shrimpton area (NTS 092H/15E, 16W) where the oldest rocks are inferred to be turbiditic strata of the Eastern siliciclastic succession, which underlie the eastern map boundary. Near the western map boundary, the youngest dated Nicola Group rocks are volcanic sandstones. Zircons from the basal beds and a crosscutting dike limit deposition to between ~208 and ~201 Ma. These strata are capped by andesitic volcanic rocks of the 'Tillery unit'. Between the Eastern succession and the Tillery unit, we mapped volcanic and sedimentary units that can be traced for ten km or more. Many of these units have been assigned to one of three successions: 'Paradise', 'Shrimpton' and 'Harmon'. Thick volcanic conglomerates comprise the 'Paradise succession'. 'Shrimpton succession' includes finer clastic rocks, but also more arc-proximal, distinctive, apatite- biotite- and quartz-phyric tuffaceous rocks of the 'Zig unit'. These contain probable syngenetic Cu-Ag mineralization dated at ~210 Ma. Above the Shrimpton succession is the fossiliferous 'Hendriks limestone' of probable Norian age. It is incised by a regional unconformity upon which the Harmon succession was deposited, starting with the polymictic 'Shea conglomerate'. A return to arc construction is recorded by the Voght unit: coarse bladed feldspar porphyry flows that are intercalated with volcanic sandstone, mostly deposited above beds containing the >208 Ma detrital zircons. Overlying the Nicola Group is the 'Bates unit', an enigmatic chert pebble conglomerate with no known local source. Andesite to rhyolite of the Spences Bridge Group (~103-104 Ma) probably overly Bates conglomerate, loosely constraining its age to between 201 Ma and 104 Ma. Evidence for contractional deformation that regionally affects strata as young as Middle Jurassic (~170 Ma) is widespread. However, older deformation is also inferred from regional unconformities within the Nicola Group, and north-northeast synkinematic fabrics in the Late Triassic Allison pluton. Nicola arc rocks and their prolific porphyry deposits have been the primary target for mineral exploration in the area, but significant mineralization is also present in younger magmatic units, like the Osprey batholith (155-165 Ma) and the Otter intrusions (~53 Ma) that cut Nicola arc rocks. Examples are gold veins at the Siwash mine and, 8 km to the south, intense clay alteration around quartz stockworks containing pyrite-sphalerite-galena-chalcocopyrite at the Snowstorm prospect. Pyrite-sphalerite-galena-chalcocopyrite mineralization mapped 6 km east of the Snowstorm is not recorded in MINFILE. If related, it gives significant dimension to the magmato-hydrothermal system.

Keywords: porphyry copper gold, volcanogenic massive sulphide, gold vein, Miner Mountain, Siwash mine, Par prospect, Snowstorm prospect, Princeton, Merritt, Nicola Group, Spences Bridge Group, Princeton Group, Chilcotin Group, paleogeography

1. Introduction

Fieldwork in the prolifically mineralized southern Nicola belt (Figs. 1, 2) extended over about six months split between the summers of 2013 and 2014. New exposures and access arising from extensive clear-cut timber harvesting during salvage operations following the Mountain Pine Beetle infestation significantly benefit our geological mapping program. Such access was mostly lacking during creation of the benchmark geological work in the area at least three decades ago (Schau, 1968; Christopher, 1973; Lefebure, 1976; Preto, 1979; Monger, 1989). Herein we present new map, stratigraphic, geochronologic, structural, and mineral deposit data collected to better understand the evolution of the Nicola arc and the

major controls of mineralization. Our aim is to illuminate further exploration opportunities in a mining camp that, for 50 years, has contributed significantly to the wealth of British Columbians through copper and gold production.

2. Geography and Geological setting

On the dissected plateau between the Coast-Cascades ranges and orographic desert of the Interior Plateau, exposures of Nicola arc rocks are sparse. Only along steep valleys and glacially scoured ridges are continuous exposures found. However, extensive networks of logging roads and two highways provide excellent access to almost all parts of the map area. Away from roads, foot travel is easy through typically dry,

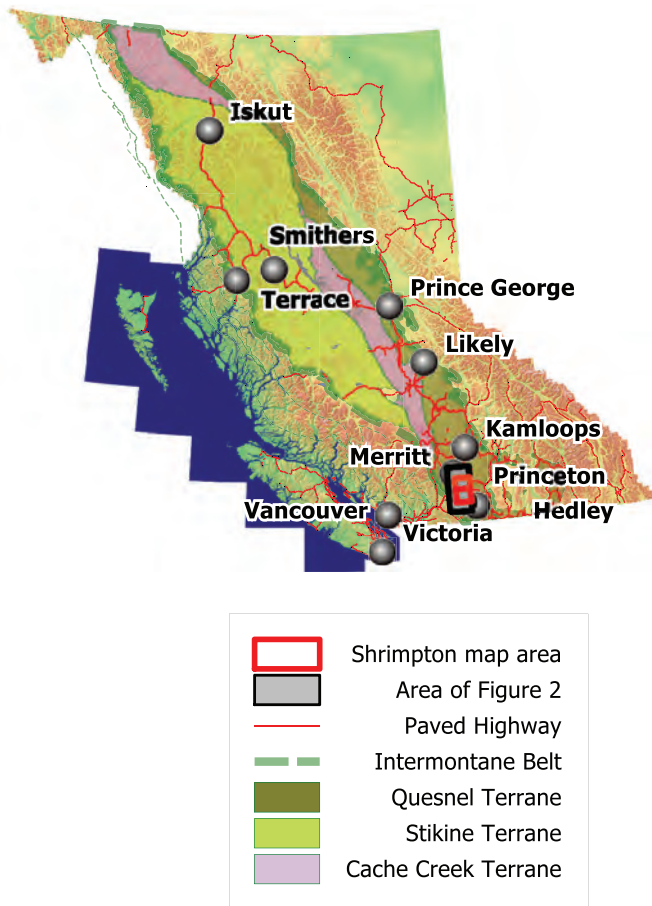


Fig. 1. Physiographic and tectonic setting of the Southern Nicola Arc Project (SNAP) study area between Princeton and Merritt.

open pine forests, and grassland.

Tributaries of three south-flowing creeks drain the southern map area. From west to east they are: Otter, Shrimpton (flows into Summers Creek via Missezula Lake), and Siwash (Fig. 3). Most of the northern map area is within the Quilchena Creek drainage, which eventually flows north into Nicola Lake. An exception is the northwest map area, which drains into Voght Creek, and eventually, the Coldwater River at Kingsvale (Fig. 2).

Nicola arc is constructed on basement rocks of a composite island arc belonging to the Quesnel terrane that contains fossils as old as Late Silurian (Read and Okulitch, 1977). The basement arc probably began life at the distal margin of western North America in the Devonian (Monger et al., 1972; Monger, 1977; Mihalynuk et al., 1994; Ferri, 1997). A back-arc basin apparently formed as this arc was rifted from its continental margin homeland (Harms, 1986; see discussions in Ferri, 1997; Mihalynuk et al., 1999; and citations therein). As the back-arc basin grew to oceanic proportions, the relicts of which are known by various names, most commonly 'Slide Mountain' in the south and 'Angayucham' in the north, Quesnellia became isolated from North America permitting colonization of endemic organisms, the remains of which are

not seen in adjacent parts of cratonic North America (Ross and Ross, 1983 and 1985; Belasky et al., 2002). The Slide Mountain basin began to close in the Permian (Struik and Orchard, 1985), probably initiated as a consequence of plate tectonic readjustments following the final closing of the Rheic Ocean (Nance et al., 2012) on the far side of North America. Quesnel and Stikine terranes started to be swept up against North America in the Late Triassic, which was accelerating westward with fragmentation of Pangea and growth of the new Atlantic Ocean. Both terranes were repatriated with the North American continental margin by the Early Jurassic (~185 Ma, Nixon et al., 1993); but final buckling and entrapment of exotic oceanic rocks of the Cache Creek between Quesnel and Stikine terranes was not completed until the Middle Jurassic (Ricketts et al., 1992; Monger and Ross, 1971; Mihalynuk et al., 1994; ~172 Ma, Mihalynuk et al., 2004). After the Middle Jurassic, rocks of the Quesnel arc were deformed during oblique collisions of the microcontinental Insular Superterrane (Monger et al., 1982) and then a massive oceanic plateau (Livaccari et al., 1981; Liu et al., 2010) that shuffled rocks along the ancestral continental margin, southward and then northward (Enkin, 2006; Sigloch and Mihalynuk, 2013). Quesnel, Stikine, and much of the Insular superterrane were finally pinned to North America by arc collisions in the Eocene (Bordet et al., 2013; Sigloch and Mihalynuk, 2013). Much of the southern Cordillera has since experienced extension (Brown and Journeay, 1987), giving rise to the landscape from which modern topography was inherited. Accurate reconstruction of the prolifically mineralized Late Triassic arc cannot be achieved without first restoring the effects of Jurassic to Eocene (and younger?) deformation.

Major volcanosedimentary successions of the Nicola arc (Fig. 4) were established through the pioneering works of Rice (1947), Schau (1968); Preto (1979) and Monger (1989), as compiled by Massey et al. (2005). They include the Nicola Group (Late Triassic), Spences Bridge Group (Early Cretaceous), Princeton Group (Eocene), and Chilcotin Group (Miocene-Pliocene). Most volcanic units have intrusive counterparts (Figs. 2, 3).

3. Nicola Group

Nicola Group strata in the Shrimpton Creek area belong mainly to the 'Central' and 'Eastern' belts of Preto (1979). Lithologies typical of the 'Western belt' have been mapped west of the Shrimpton area (Diakow and Barrios, 2008). Herein we focus on a transect across the northern part of the Shrimpton map area. From east to west, we recognize the Eastern belt (Preto, 1979) and subdivide much of the Nicola Group into the Eastern siliciclastic, Paradise, Shrimpton, and Harmon Lake successions, which define an overall trend from deep-water lithofacies to more arc-proximal lithofacies (Fig. 4). In the northwest part of the map area, the Harmon Lake succession includes the 'Shea polymictic conglomerate', the 'Voght unit' which consists of interbedded coarse bladed plagioclase porphyry flows and epiclastic redbeds, and is capped by 'Tillery' andesitic breccias (Fig. 4). Previous mappers assigned the

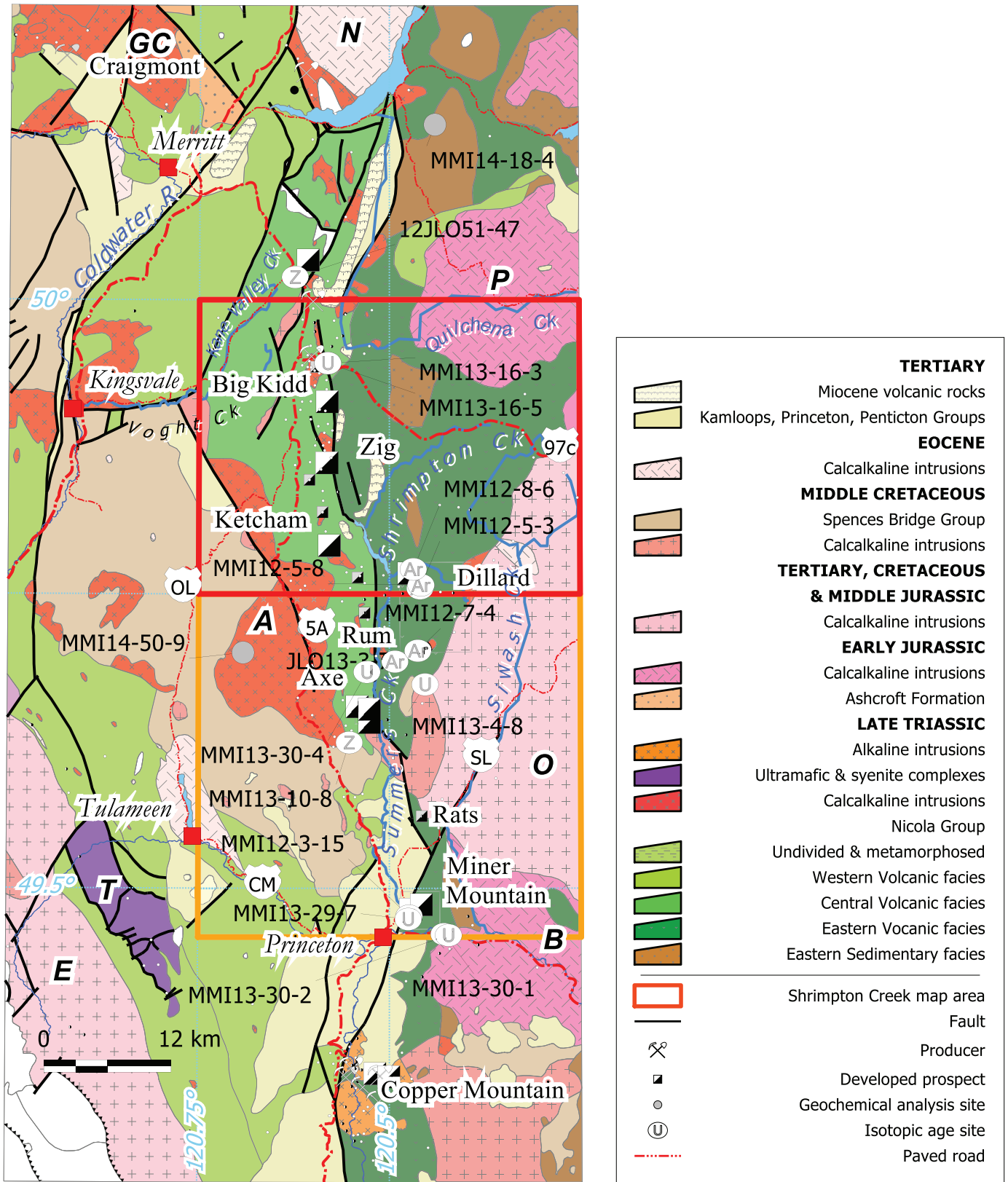
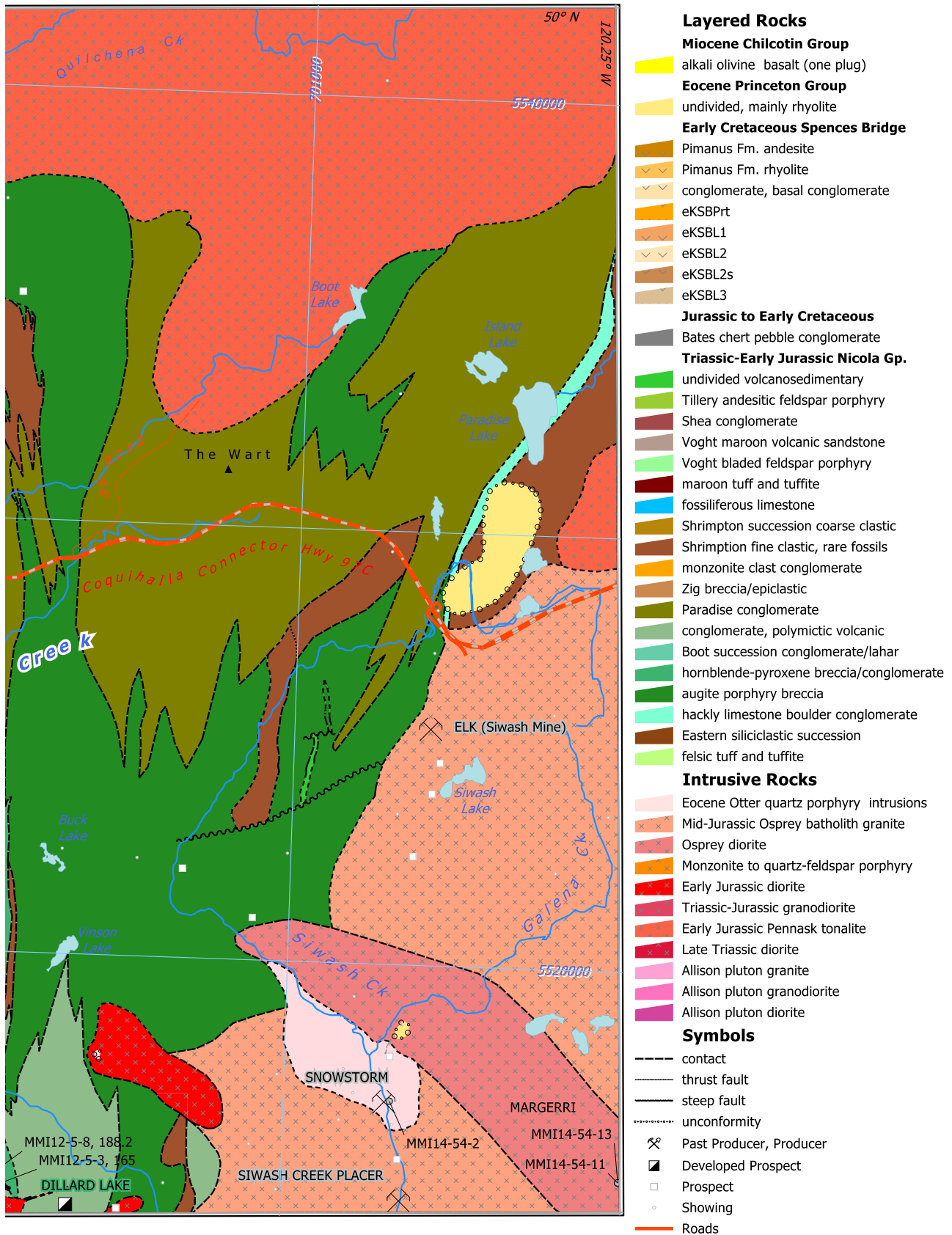


Fig. 2. Geological setting of field mapping, between Princeton and Merritt. Extents of Preto's (1979) Eastern belt (mafic submarine volcanic and sedimentary rocks), Central belt (arc axis, mafic volcanic and coeval intrusive rocks) and Western belt (intermediate to felsic volcanic and sedimentary rocks) are shown for reference, as adapted from Massey et al. (2005). Abbreviations denote major plutons: A = Allison Lake, B = Bromley, BI = Boulder intrusion, E = Eagle, GC = Guichon Creek, N = Nicola, O = Osprey Lake, P = Pennask, S = Summers Creek, T = Tulameen Complex. See Figure 1 for context. Orange box = 2013 mapping, red box = 2014 mapping.



Fig. 3. Simplified map of the Shrimpton Creek area. Compilation includes geological information from Monger (1989, regional framework), Preto (1979, mainly including areas between Shrimpton Creek and Highway 5A); Bergy (1999, PAR property); Gourlay (1991, ZIG property); and Nelson and Walker (1972, ZIG area).



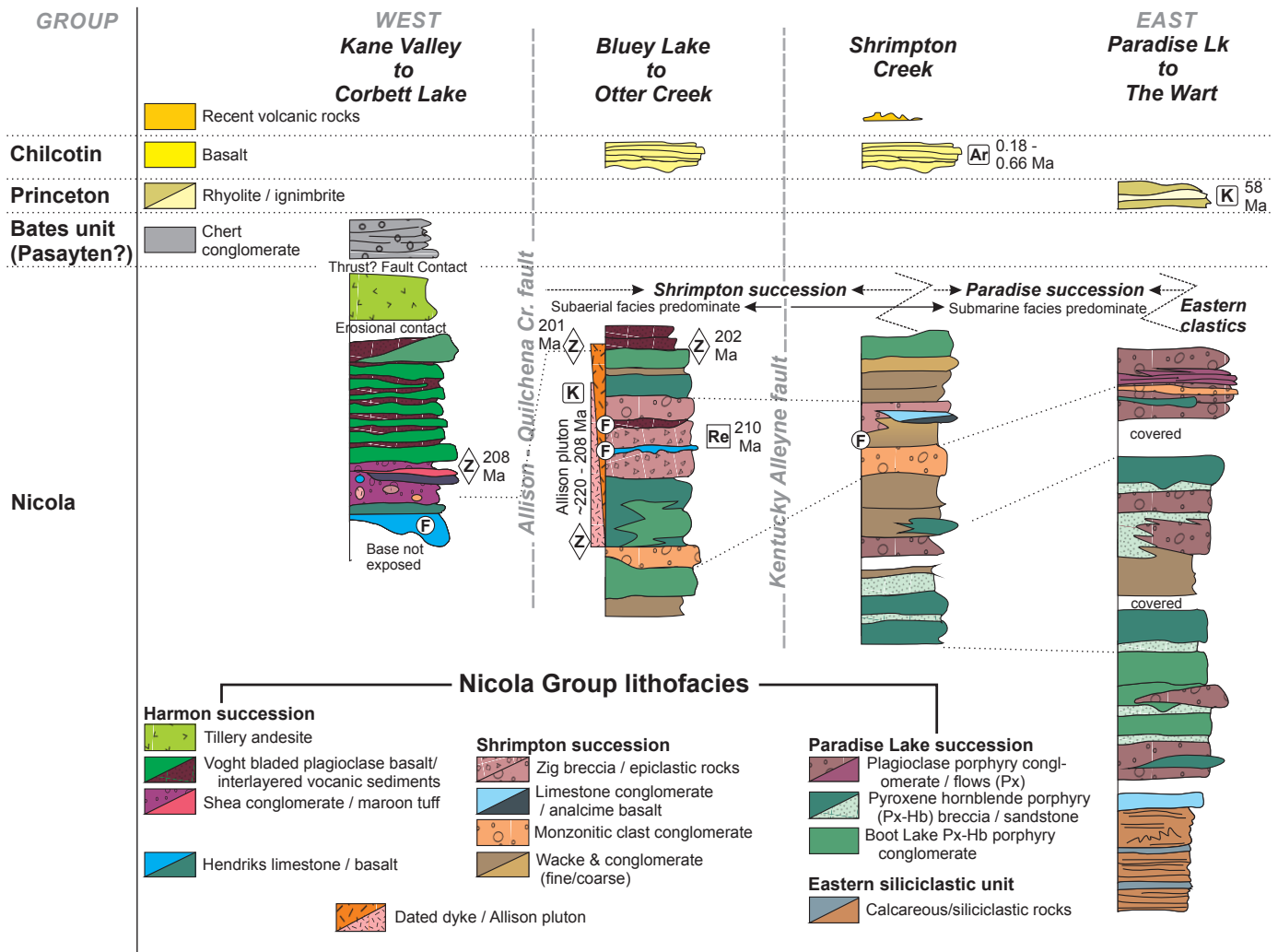


Fig. 4. Stratigraphic relations in the Shrimpton Creek area. Shapes overprinted with F, Ar, K, Re and Z indicate age control: macrofossils (F, age determinations pending), and isotopic ages: $^{40}\text{Ar}/^{39}\text{Ar}$ cooling age (Ar), K-Ar cooling age (K), Re-Os age (Re), and zircon detrital zircon ages (Z), or crystallization ages (Z on a black background). Older Allison Lake pluton ages are inferred from detrital zircons in overlying basal Early Cretaceous Spences Bridge conglomerate (cf. Mihalynuk et al., 2014).

Harmon succession to either the Upper Triassic (Monger, 1989) or Lower Cretaceous (Preto, 1979). New geochronology from the base of the succession (see below) establishes deposition in the Late Triassic to early Jurassic, at least 14 million years later than the youngest strata locally dated in the Nicola Group. The Harmon Lake succession lies unconformably above a carbonate unit of presumed Late Triassic age; herein named, the Hendriks limestone, and is faulted against younger, chert-rich conglomerate well exposed where incised by Bates Creek (unit 9 of Preto, 1979; unit Ks of Monger, 1989), and herein named the Bates conglomerate (Fig. 4).

In the eastern part of the map area, the Eastern fine siliciclastic succession is siltstone and sandstone that is capped by marble-clast-bearing conglomerate beds referred to herein as the ‘hackly carbonate unit’. This unit is stratigraphically overlain by the Paradise succession which, at its base, is a conglomerate and coarse sandstone unit derived from augite

and lesser hornblende-phyric mafic volcanic rocks. These strata pass upwards with gradual reduction in hornblende concentration into the main Paradise succession composed predominantly of medium-grained pyroxene-phyric mafic volcanic rocks interfingering with conglomerate derived from augite-feldspar-rich volcanic porphyries, and lesser monzonite-sourced conglomerate.

The Shrimpton succession gradationally overlies the Paradise succession, and is represented by predominantly immature volcanic-derived sandstone with locally intercalated monzonitic-clast conglomerate, and scant, thin flows of analcime-bearing basalt. A resistant subunit consisting mainly of monzonitic clasts can be mapped for kilometres. A unit similar in appearance, but containing distinctive grains of biotite, apatite and quartz, is well exposed around the Zig prospect (Fig. 3) and is herein called the ‘Zig unit’. Epiclastic strata containing clasts of Zig unit form mappable

layers in the Shrimpton succession which extends as far west as the Kentucky-Alleyne Fault (Fig. 3). West of this fault, in the Fairweather Hills (Fig. 3), basaltic flows, conglomerates and laharic breccias, interpreted as subaerial deposits, are the predominant Nicola Group lithologies (Lefebure, 1976). Although the current study conducted several traverses through the Fairweather Hills and found the conglomerates contained broadly similar lithologies as those in the Paradise succession, our work there is insufficient to reliably correlate with strata further east.

3.1. Eastern siliciclastic unit

Fine-grained siliciclastic strata were recognized east (Rice, 1947; Monger, 1989; Ray and Dawson, 1994) and south (Mihalynuk et al., 2014a) of the Shrimpton map area. We found that at least 410 m of these strata can be mapped on low ridges east of Paradise Lake, before they are lost eastward under cover or to intrusion of the Pennask batholith (Fig. 3). Batholith intrusion caused widespread thermal metamorphism, manifested mainly as bleaching of beds to shades of white and grey, increased induration and pyrrhotite disseminations.

Thin- to medium-bedded (0.5 to 30 cm thick) siltstone, sandstone, argillite and lesser granule to pebble conglomerate weather grey, white and rust. Medium-thick beds of sandstone with a calcareous matrix weather distinctively, but are a minor constituent. Shallow trough and ripple cross stratification are uncommon, although well-developed locally; most beds are parallel laminated and graded, commonly with scoured bases, typical of distal turbidites. Flame and ball and pillow structures are common and local zones of intense syndepositional disruption by gravity sliding and/or water escape are common (Fig. 5).

The hackly carbonate conglomerate unit forms the westernmost exposure of the Eastern unit. The conglomerate consists of spherical to tabular clasts up to boulder size. In some places, the clasts have weathered recessively leaving the hackly, sandy matrix behind (Fig. 6). Clasts are predominantly



Fig. 5. Irregular top of a ~0.4 m thick disrupted bed in the eastern sedimentary succession is the product of soft-sediment deformation.



Fig. 6. Carbonate clast-bearing conglomerate at the top of the eastern sedimentary succession. Carbonate clasts, up to boulder size, weather recessively relative to sandstone matrix, yielding a hackly appearance.

white, medium-crystalline marble; much less abundant are laminated, contorted siltstone and augite porphyry fragments, up to boulder size. Continuous outcrops expose a thickness of only ~8 m, but finer-grained conglomerates can be found across a covered interval that could overlie ~200 m of strata assuming persistent dips and no structural omission or duplication. Although the upper contact of conglomerate unit is not exposed, augite porphyry clasts and sandstone interbeds with pyroxene grains suggest a conformable transition to pyroxene and hornblende-bearing epiclastic rocks of the overlying Boot Lake unit of the Paradise succession.

The Eastern fine siliciclastic unit may be correlative with the Stemwinder Formation, which is relatively well constrained by microfossil ages as Late Carnian to Late Norian in age (Ray et al., 1993) and is interpreted to have been deposited in a back arc basin (Ray and Dawson, 1994).

3.2. Paradise Lake succession

Widespread in the northeastern quadrant of the study area, the Paradise succession crops out between younger batholiths, and it expands westward attaining a cross-strike breadth presumed to exceed 13 km. In northern and southeastern regions, the Pennask (Early Jurassic) and Osprey (Middle Jurassic) batholiths crosscut and locally metamorphose Paradise stratigraphy to pyroxene hornfels facies.

The lower part of the Paradise succession (referred to herein as the Boot Lake unit) consists mainly of hornblende-bearing conglomerate with fine clastic interbeds and sparse lava flows. The upper part of the Paradise succession underlies the region west and southwest of The Wart. Where coarse augite-phyric lava flows, a hallmark of the Nicola Group, predominate and are interleaved with lesser conglomerate and finer clastic rocks, they are included in the augite-phyric flow unit (see e.g., Mihalynuk et al., 2014),

The upper contact of the Paradise succession, observed locally

in the northwest, is gradational. Mafic flows are interlayered with sandstone that increases in proportion upsection into predominantly siliciclastic rocks of the Shrimpton succession. The age of the Paradise succession is uncertain. However, limestone clasts in conglomerate near the top of the unit might be derived, in part, from carbonate units in the Nicola Group west of Summers Creek Fault that contain conodonts of Late Carnian to Middle Norain age.

3.2.1. Boot Lake unit

The Boot lake unit comprises as much as one-third of the entire Paradise succession, and is exposed north of the Coquihalla Highway, between The Wart and the Eastern succession. Because of discontinuous outcrop, the thickness of the Boot Lake unit is uncertain. However, if the mainly west-dipping succession is not duplicated, it could be more than 4 km thick. The unit consists of conglomeratic and finer sedimentary strata composed predominantly of plagioclase and pyroxene with or without hornblende-phyric clasts (Fig. 7). In most places, the conglomerate forms massive layers composed of open framework cobbles and boulders, commonly with local bedded intervals of granule-size and finer clastic rocks. The clasts are mostly subangular to subrounded and are composed mainly of textural variants of fine- and medium-grained hornblende-augite plagioclase-phyric extrusive volcanic rock.

About 2 kilometres west of Paradise Lake, an interval more than 100 metres thick consists primarily of interbedded sandstone and siltstone with coarse augite and hornblende grains. A thin flow containing coarse hornblende prisms locally underlies a siltstone that contains a rare bivalve, which may indicate marine sedimentation. Higher in the section, conglomeratic beds reappear interlayered with sandstone; however, notably present are hornblende prisms, some up to 1 cm long, in the matrix and as clasts of hornblende-augite phyric mafic flows. Rare pebbles from a pyroxenite intrusion have also been observed. The clastic rocks are arranged in parallel



Fig. 7. Polymictic conglomerate of the Boot Lake unit containing only mafic, arc-derived clasts.

thin and thick beds with interlaminations and contain rip-up clasts at the base of some coarse sandstone beds. Channels in sandstone infilled with granule conglomerate grading to sandstone suggest stratigraphic younging toward the northwest.

3.2.2. Augite-phyric lava flows

Westward from The Wart for approximately 9 km to the inferred upper contact of the Paradise succession, the conglomerate generally lacks hornblende and comprises interbeds within more prominent lava flow sections. In this broad transect, the succession is particularly well exposed in newly harvested timber blocks along the west-facing slope of a prominent ridge trending north to its highest point at The Wart. Everywhere, the volcanic rocks consist of fine- and medium-grained porphyries containing plagioclase as the predominant phenocryst and ubiquitous augite, which is commonly altered to chlorite. The porphyritic texture and aphanitic groundmass of these volcanic rocks suggest a flow origin. Amygdaloidal flows occur at several isolated localities. At the northwestern extent of the Paradise succession, northwest of Pothole Creek, mafic flows occur exclusively; the conglomeratic beds pinch out farther southeast of this area.

Conglomerates west of The Wart differ from those between Paradise and Boot lakes only in the apparent greater clast diversity and significantly reduced or absent hornblende grains. Augite-plagioclase basalt porphyry flow remains the most abundant clast type, with the addition of pink fine-grained hornblende?-plagioclase phyric dacite and vesicular basalt clasts. Monzonitic clasts with fine-grained texture and brownish red color are abundant in exposures along Coquihalla Highway, from the point where the 88 Road passes under the highway, east towards The Wart summit (Fig. 3).

The southwestern extent of the Paradise succession in the Shrimpton Creek area is on a broad ridge between Buck and Missezula lakes. Here cobble-boulder conglomerate interlayered with coarse sandstone interbeds occupies a section inclined northwest that apparently overlies a thick sequence of augite-porphyry flows exposed to the southeast. Farther southwest towards Missezula Lake, a lateral lithologic change in the unit corresponds with the prevalence of hornblende-bearing clast conglomerate, locally associated with hornblende-augite-phyric lavas. Rare cobbles of grey limestone in conglomerate at three isolated localities between the Coquihalla highway and Missezula Lake may mark a stratigraphic level near the top of the Paradise succession.

We speculate the Paradise succession aggraded in a segment flanking the Nicola arc where relatively low relief prevailed. The clastic detritus, rich in mineral constituents and clasts resembling the flows were likely derived from immediately surrounding volcanic rocks and were presumably recycled and resedimented periodically (Fig. 8). The presence of more exotic clasts including porphyritic dacite, limestone and monzonite requires input from more distant sources that mixed with locally derived detritus.



Fig. 8. Orange-weathering augite-phyric autobreccia (under hammer) to conglomerate (left) transition demonstrates an immediately local source for some of the Paradise succession conglomerate facies.

3.3. Shrimpton succession

The Shrimpton succession is a predominantly siliciclastic unit consisting of: 1) feldspathic sandstone, granule- to cobble-conglomerate, siltstone, and siliceous argillite; 2) lenses of monzonite clast-bearing conglomerate; and 3) analcime-bearing lava flows (Figs. 9, 10). It is exposed mainly on ridges adjacent to Shrimpton Creek and extending north of the Coquihalla Highway to beyond Pothole Creek (Fig. 3). An easily accessed exposure showing the main lithologies of the succession is at the Loon Lake junction on the Coquihalla Highway. Here interlayered wacke, siltstone, argillite and impure limestone are folded and separated by high-angle faults from conglomerate with sparse monzonitic clasts.

The contact between the Shrimpton and Paradise successions is marked by a transition of interlayered mafic flows and sandstones; the base of the Shrimpton succession, exposed north of Pothole Creek is arbitrarily placed at the lowest sandstone interbed. The upper contact is also gradational and, east of Summers Creek, is presumed to be above a bed of monzonite clast-bearing conglomerate that is interleaved with clastic rocks containing mineral pyroclasts characteristic of the Zig unit.

3.3.1. Feldspathic wacke and conglomerate

Feldspathic wacke, and conglomerate (Fig. 9a) are the most widespread components of the succession. Bedded sandstones north of Pothole Creek form continuous sections up to 450m thick in which beds dip moderately west-southwest. Farther south, exposures at the Coquihalla highway, Loon Lake Junction display strongly folded strata and outcrop-scale thrust faults (see below), introducing the possibility of larger contractional structures that have not been recognized in forested outcrops. Typically, siltstone and siliceous argillite occupy relatively thin, well-bedded intervals in otherwise massive, thickly bedded sandstones. Dark grey and black limestone is scarce, typically

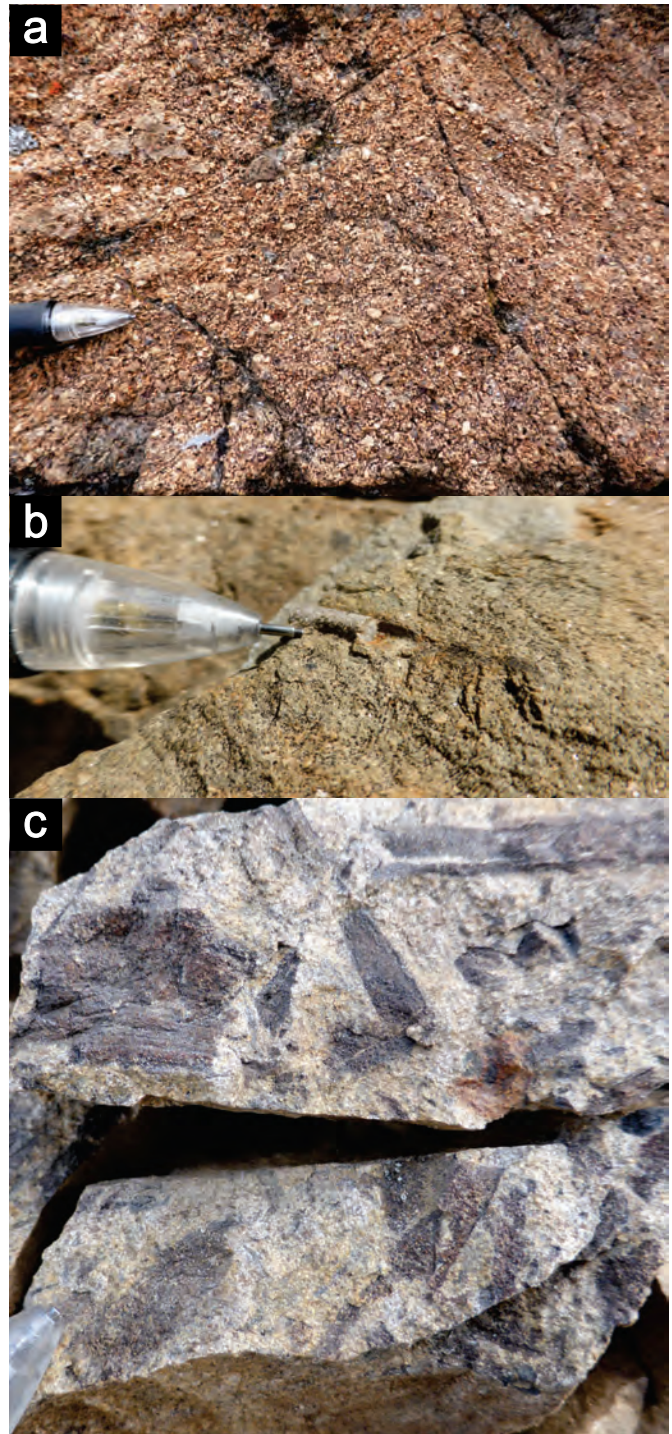


Fig. 9. Shrimpton succession. **a)** Pink-weathering, texturally and compositionally immature granule- conglomerate bed with mainly pink monzonitic debris. **b)** Crinoid stem in fine-grained calcareous sandstone. **c)** Medium-grained feldspathic wacke with carbonized plant debris.

in thin beds that locally contain fossils, including small bivalves, ammonoids, and crinoid stems that indicate marine sedimentation. Crinoids stems also occur in fine calcareous sandstone (Fig. 9b), in sections of coarser wacke containing

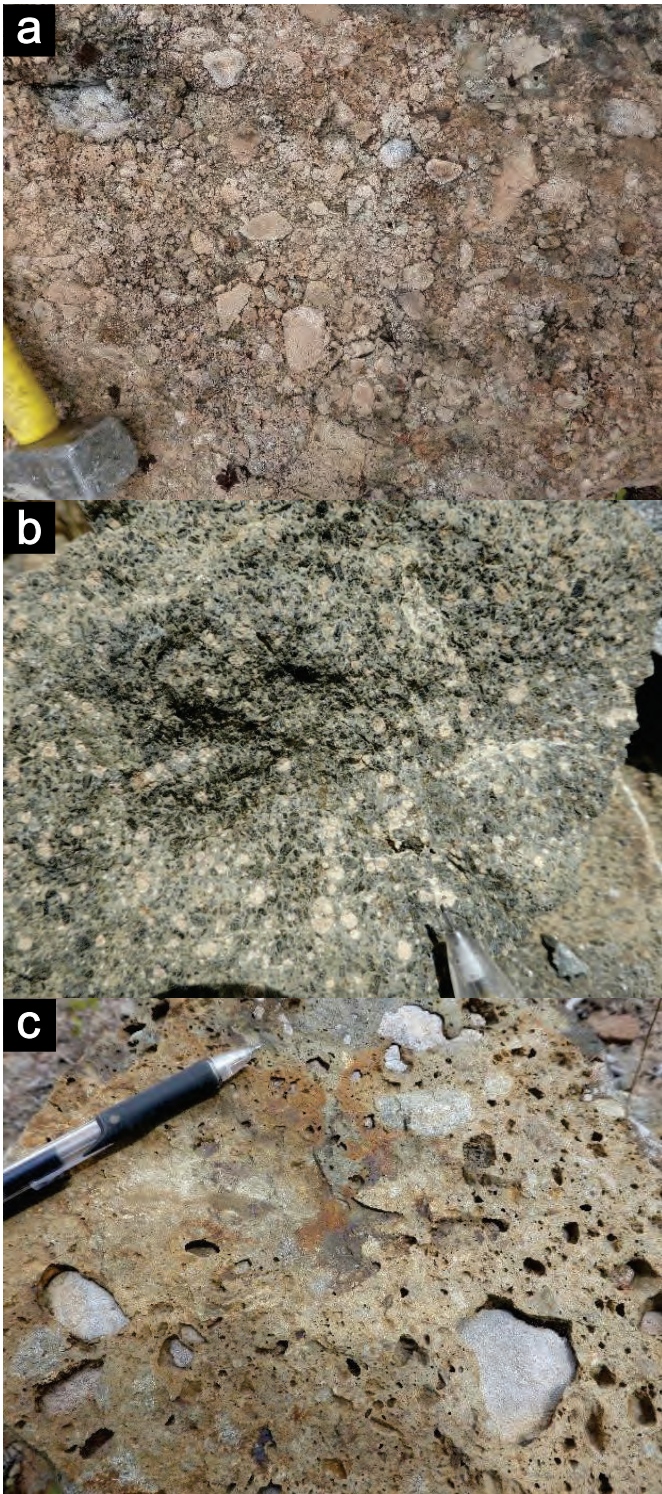


Fig. 10. a) Angular to rounded monzonitic clasts in Shrimpton succession conglomerate. b) Pyroxene (dark green to black) and analcime (rounded, light pink-tan) porphyry flow. c) Conglomerate interbed in Shrimpton sandstone, feldspar-rich sandstone matrix weathering in positive relief relative to limestone clasts.

locally abundant coaly layers with fossils of swamp grass (Fig. 9c), indicating transitional marine (brackish) deposition.

3.3.2. Monzonite clast conglomerate

East of Shrimpton Creek, local heights of land are underlain by resistant, massive conglomerate lenses conspicuously rich in pink to orange-weathering monzonitic clasts (Fig. 10a). One lens is up to 320 m thick and extends along strike for more than 10 km. Smaller lenses occur upsection, or as structural repeats. Upper and lower contacts of these conglomerate lenses grade into coarse sandstone. Rounded to angular monzonitic clasts are relatively uniform in composition and contain medium-grained, tabular feldspar that averages around 20%. The clasts are in a recessive ash-rich matrix that contains pyroxene, hornblende, biotite and rare quartz grains. Biotite occurs as medium-grained, golden, silver, or grey-green altered booklets, comprising as much as 4% of the rock, but typically less than 0.5%. Medium- to fine-grained quartz eyes are subhedral and smoky. They are irregularly distributed, typically sparse (<0.1%), but rarely can comprise as much as 2% of decimeter-thick layers. This unit appears to be the source of large glacial erratic boulder train 20 km to the south. A similar unit is distinguished by the presence of up to ~1%, fine- to medium-grained prismatic apatite. It is referred to as the 'Zig unit' (see below).

3.3.3. Analcime basalt flows

Analcime-pyroxene-phyric lava flows (Fig. 10b) just a few m thick are locally interleaved with sandstone and siltstone typical of the Shrimpton succession. Three isolated occurrences appear to occupy a specific interval west of the monzonitic clast conglomerate lenses. Locally adjacent to the flows are carbonate layers and conglomerates containing angular carbonate boulders (Fig. 10c). Intercalation of analcime pillow breccia and tuffaceous layers of estimated dacite to trachyte composition indicates synchronous sedimentation and at least some submarine arc volcanism, raising the possibility of volcanogenic massive sulphide accumulations. Sparse sulphide pebbles composed mainly of pyrrhotite and pyrite with traces of chalcopyrite are conspicuous constituents of resistant sedimentary units capping the ridge immediately east of the Kentucky-Alleyne Fault at Bluey Lake.

3.3.4. Zig unit

The Zig unit consists of variably reworked heterolithic breccia and lapilli tuff with continuously exposed thicknesses in excess of 150 m. The unit is the main host to mineralization at the Zig prospect immediately west of Bluey Lake. Diagnostic of Zig unit volcanic rocks are biotite, quartz, and red apatite prisms that combined usually comprise <2 % of rock matrix, with more abundant medium-grained tabular feldspar and fine-grained pyroxene. Volcanic clasts vary from red to dark green, very fine-grained or aphanitic. Possible hypabyssal accidental fragments are light pink holocrystalline monzonite, hornblende diorite and rare hornblende-biotite ?lamprophyre. Locally, the unit is strongly bleached and displays epidote alteration; pyroxene is typically replaced by chlorite, and fine-grained idiomorphic magnetite crystals are oxidized to hematite. Near the Nor 30 occurrence, the unit includes muddy maroon tuffite

that contains angular to well-rounded pebbles and cobbles of conspicuous diorite clasts representing up to 20% of the clast population, as well as sparse limestone clasts. Irregular beds of siltstone to arkosic sandstone and maroon mudstone are common. Sand grains are composed of plagioclase, lesser pyroxene and rare olivine(?). Fine-grained magnetite, replaced by hematite locally, comprises as much as 15% of the matrix. These magnetite-rich beds continue laterally for up to 400 m and may be more than 5 m thick. Poor sorting, weak clast alignment, and contorted bedding within this subunit are most consistent with deposition primarily as laharic flows.

3.3.5. Age of the Shrimpton succession

Tuffaceous sandstone layers interpreted to be near the top of the Shrimpton section contain biotite, apatite, and quartz and are interpreted as remnants of pyroclastic fallout associated with the Zig unit. If this correlation is correct, the age of the upper part of the Shrimpton succession may be ~210 Ma, the Re-Os age of mineralization associated with the Zig unit (unpub. data). Biochronology of the Shrimpton succession is pending identification of several ammonoid specimens and prospective conodont samples obtained from two limestone localities in the lower part of the succession.

3.4. Fairweather Hills laharic breccia and conglomerate

Ridges east of Highway 5a and west of Kentucky-Alleyne Fault, between Miner Lake in the south and Tule Lake in the north cover an area referred to as the Fairweather Hills. Here, Upper Triassic Nicola strata were mapped in detail at 1:6,000-scale as part of a M.Sc. thesis (Lefebure, 1976), following previous work by Christopher (1973) and Preto (1974). During this study we elected to not duplicate this earlier mapping, conducting traverses only to the edges of the Fairweather Hills, and isolated spot checks.

Lefebure (1976) shows Nicola stratigraphy broken by primary longitudinal block faults and smaller transverse faults. Across the longitudinal structures are significant changes in Nicola group facies and thickness. A medial fault block is underlain by mafic flows and lahars, interbedded in sub-equal amounts, with a cumulative thickness estimated at 1100 m. In flanking fault blocks, thicknesses decrease; to the east, lahars are predominant and to the west, lahars are interlayered with volcanic conglomerate, sandstone, and minor limestone. Mafic flows contain varying proportions of plagioclase and augite phenocrysts, as porphyries and amygdaloidal varieties, commonly accompanied by autoclastic breccia. Lahars in the medial block contain clasts mainly of augite-plagioclase basalt porphyry with abundant monzonitic and locally dioritic intrusive rocks. The lahars to the east contain mainly andesite and basalt porphyry, and lesser diorite clasts. To the west, basaltic rocks are predominant, with few sedimentary clasts. In general, these laharic deposits show poor sorting of mainly rounded to subrounded clasts.

3.5. Hendriks limestone

Typically massive white and light grey to tan-weathering, fossiliferous limestone attains thicknesses of at least 240 m along both sides of the Kane Valley. Bedding is locally distinct where intercalated with arc detritus, basalt flow or hyaloclastite debris, and dips away from the valley axis, which is slightly oblique to the broad, faulted, anticlinal hinge (Fig. 3). Upper parts of the unit, particularly south of the Tillery Road, contain bivalve-rich micritic limestones with exquisite fossil preservation, or reworked fossils in coquinas. Colonial coral heads more than a metre across can be discerned, especially where recrystallization is weakest, south of Tillery Road. Identification of fossils collected is pending.

The limestone is intercalated with volcanic rocks and conglomeratic lenses derived from volcanic terrain. One volcanic flow unit occupies a consistent position near the top of the limestone. It is a grass green aphanitic basalt flow and flow breccia with poorly developed pillows. Abundant fine chlorite amygdales are characteristic. Hyaloclastitic debris of the same composition form planar interbeds with the limestone.

Hendriks limestone has not been traced northeast or southwest beyond exposures in the Kane and Voght valleys. It appears that it was removed in both directions below a regional unconformity.

Siliciclastic rocks at the base of the overlying Harmon succession yield a detrital zircon maximum depositional age of about 208 Ma (see below). This age also establishes the Hendriks limestone as older, and presumably of Late Triassic age. The nearest Upper Triassic limestone outcrop to the Hendriks limestone is about 6.5 km to the north-northeast (Diakow and Barrios, 2008). It can be traced an additional several km farther north to near Sugarloaf Mountain where Preto (1979) mapped it as one of multiple limestone beds that locally contain early Norian fossils. This limestone section is succeeded above by a thin quartz-bearing dacite tuff from which a U-Pb zircon crystallization age of ~224 Ma was recently obtained (Diakow, unpub. data). If a provisional correlation is made between limestones near Sugarloaf Mountain and Kane Valley, they are somewhat older, and potentially bracket a hiatus in Nicola Group deposition, represented by the unconformable surface on the Hendriks limestone, between ~224 and ~208 Ma.

3.6. Harmon succession

The Harmon succession is a new stratigraphic division proposed for semi-continuous, sedimentary and volcanic strata. Where thickest northeast of Harmon Lake, it is conservatively estimated to be more than 2 km thick. Conglomeratic strata at the base of the succession comprise the lowest of four lithostratigraphic units. Here called the 'Shea conglomerate', it is thought to underlie a significant part of the valley bottom, apparently thickest at Shea Lake; however outcrops are few and widely spaced. Overlying units are: a lower undivided andesitic volcanic unit, 'Voght' bladed-plagioclase basalt porphyry flows and sandstone, and the 'Tillery' andesite unit.

The Harmon succession was included as part of Lower

Cretaceous stratigraphy (Preto, 1979), and as previously mapped, extends north of the Shrimpton Creek map area to Mount Nicola. Geological mapping by Monger (1989) assigned this succession to the Upper Triassic Nicola Group, including it within the Central belt. We interpret that the succession is confined between regional unconformities, the lower cuts into Hendriks limestone with a presumed Late Triassic age, and the upper is overlain by a chert conglomerate unit, herein named Bates conglomerate, possibly of Middle Jurassic to Early Cretaceous age.

3.6.1. Shea conglomerate

Oxidized, reddish maroon polymictic granule to boulder conglomerate is locally in direct contact with mafic flow rocks intercalated with the Hendriks limestone. Its thickness is highly variable, generally thicker and more widespread in Kane Valley and from Shea Lake area southward in Voght Valley, and very thin or absent in faulted blocks adjacent to Voght Creek and the Tillery Road.

Typically poorly sorted, the clasts are oxidized red and well rounded, varying from pebbles to boulders, and consisting of diverse lithologies that include: augite and hornblende-bearing volcanic porphyries; aphanitic and flow-laminated rhyolite and welded tuff; white and grey massive and sparsely fossiliferous limestone; monzonite, granodiorite, diorite and granite; and scarce chert and argillite. Except for chert, all of the clasts resemble lithologies found nearby in the Nicola Group or Late Triassic comagmatic plutonic phases. Undoubtedly, the conglomerate represents erosion of Nicola Group stratigraphy. In addition, boulders containing the distinctive mineral components characteristic of the Zig formation are recognized.

Sandstone and conglomeratic layers composed of granule and pebbles occur throughout massive, coarse conglomerate, generally as discontinuous spaced interbeds displaying parallel stratification and graded structure. Shea conglomerate is intercalated with maroon, mostly aphanitic to finely feldspar-phryic lapilli ash tuff.

Rare exposure of coarse-grained, pyroxene-plagioclase porphyry lava flow forms an interlayer locally or directly underlies Shea conglomerate. This flow, well exposed in a Coquihalla Highway cut across from Corbett Lake, consists of 40 m of coarse pyroxene-plagioclase-phryic and amygdaloidal basalt that is sharply overlain by Shea conglomerate with sandstone interbeds. It is distinguished by up to 30% plagioclase laths between 3-5 mm (locally >1 cm) long, and 2-5% pyroxene up to 3 mm diameter. Amygdaloidal texture, imparted by rounded and irregular white crystalline quartz amygdales, occurs only at the base and in a reddish oxidized zone at the top, which identifies the volatile-rich margins of a solitary flow. Lava displaying identical texture, observed at a locality in the Kane Valley, is considered to overlie Shea conglomerate which crops out about 5m lower, with the contact concealed in a grassy slope. Clasts of bladed-feldspar basalt porphyry observed in the Shea conglomerate might be derived from these lavas.

3.6.2. Lower, undivided andesitic volcanic rocks

This unit comprises andesitic lava flows, and minor sandstone and lesser conglomerate. Although the outcrops are small and isolated, they consistently occupy a general position topographically higher than Shea conglomerate and below overlying distinctive bladed plagioclase flows. Thickness of the unit varies along strike, suggested by apparent thinning towards the north, and absence of correlative strata in faulted stratigraphy near Tillery Road. The unit is at least 350 m thick, based on an approximate contact with underlying Shea conglomerate and overlying bladed-plagioclase basalt porphyry.

Mainly andesite flows with porphyritic and amygdaloidal textures, the unit contains 15-25% plagioclase between 1 and 3mm long, and 1-3% pyroxene phenocrysts up to 1.5mm that locally display red oxidation. The amygdaloidal rocks also contain similar phenocrysts, in addition to rounded and irregular quartz amygdales. Conglomeratic beds contain rounded cobbles and smaller clasts apparently derived from andesitic volcanic rocks.

3.6.3. Voght bladed plagioclase basalt porphyry flows and clastic rocks

Multiple, bladed-feldspar porphyry lava flows forming resistant ridges, locally separated by interflow sandstones, overlie the lower andesite unit. The unit is exposed on both sides of the Kane Valley. The best exposures are on the southeast valley side where recessive sandstone generally identified by red soil and angular chips marks the base of a lava succession containing at least 13 successive flows. The flows range in thickness from <5 to ~70 m and the unit might have a cumulative thickness of as much as 850 m.

The lowest flow member is the coarsest, with euhedral plagioclase laths up to 1.5 cm and larger glomerocrysts randomly dispersed in a dark green-black groundmass (Fig. 11 a). Passing up through this flow there is a gradual reduction in the length of plagioclase laths to between 4-7 mm and an overall increase in abundance to around 25-30%. Finer grained pyroxene phenocrysts typically account for less than 10%. Vesiculation is quite variable throughout; most are filled by laumontite and commonly rimmed by chlorite. The highest flow unit mapped contains relatively rare amygdales, composed either of white opalescent or crystalline quartz, that are up to 5 mm diameter, and sparse medium-grained plagioclase in a very finely felted to aphanitic blue-green groundmass. Upper parts of this highest unit show an oxidized, deep red colour (Fig. 11b). Rare exposures of maroon epiclastic beds immediately above some flow units include concentrations of scoraceous bladed-porphyry fragments.

Poorly exposed red-brown laminated and graded sandstone and siltstone occupy intervals up to 20 m thick between successive lavas. Interflow conglomerate with bladed-porphyry clasts is exposed at one locality in west Kane Valley (Fig. 11c). A sill origin for some of these flows was suspected by Preto (1979); however, there is no evidence of thermally

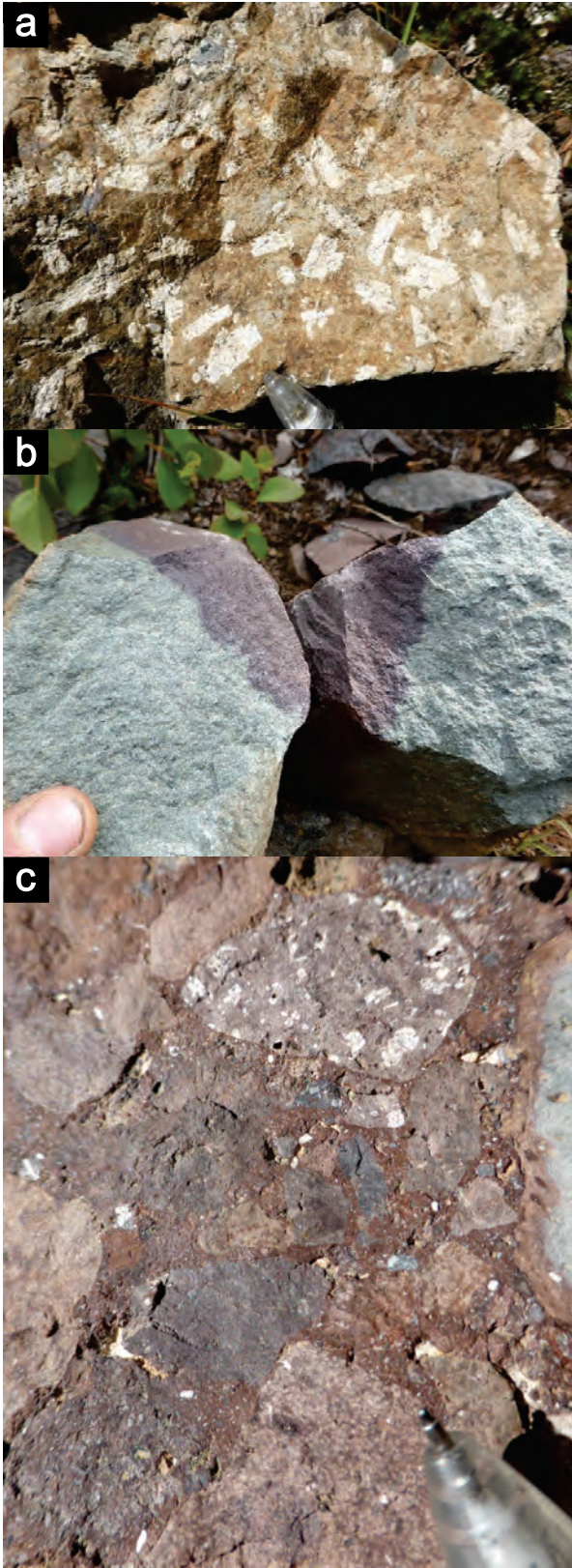


Fig. 11. Harmon succession, Voght unit bladed porphyry unit. **a)** Lowest flow, with very coarse bladed plagioclase. Plagioclase grain size decreases upsection. **b)** Highest flow with hematite staining. **c)** Intraformational conglomerate includes cobbles of coarse bladed feldspar porphyry.

altered interflow sediments, as might be expected by a massive injection of basalts.

The bladed-plagioclase basalt porphyry, although distinctive, is not restricted to the Harmon succession. Basalts with similar texture and overall appearance also have been observed at the base of the basal Shea conglomerate. In the Nicola Group, bladed-plagioclase basalt flows are not uncommon. For example, in the Paradise succession, they accompany highly vesiculated lavas in an area south of the Elkhart junction on the Coquihalla Highway (Fig. 3). Boulders also occur in conglomerate near the Axe deposit (Fig. 2).

3.6.4. Tillery andesites

The uppermost unit of the Harmon succession consists of fine- and medium-grained andesite porphyry and amygdaloidal lava flows, and relatively minor conglomerate and sandstone. Inclusion of this unit at the top of the Harmon succession is based on the relationship between a solitary exposure composed of underlying Voght strata that are abruptly replaced upsection by extensive andesite lava flows. The unit name originates from the general region of Voght Creek and the Tillery Road, where it is most extensive. North of the Tillery Road, the unit wedges out and has been removed by a combination of erosion and reverse faulting (Fig. 3), resulting in its absence in the homoclinal section east of Harmon Lake. Tillery andesites are unconformably overlain by Bates conglomerate, as exposed on an east-facing slope south of the Tillery Road.

Lava flows displaying fine and medium porphyritic and amygdaloidal textures comprise most of the unit. The porphyritic flows contain 20-30% plagioclase generally less than 3mm long, and rare pyroxene phenocrysts. Amygdaloidal flows generally form thin members in the more prevalent porphyritic flows, however, they predominate in eastern exposures of the unit, attaining an estimated thickness of more than 400 m near the contact with overlying Bates conglomerate, south of Tillery Road. Amygdaloids in the rock consist mainly of white quartz and an unidentified white zeolite with radiating habit. Uniform, fine- and medium-grained tabular feldspar porphyry breccia (Fig. 12) occurs locally as do conglomerate and sandstone layers. The conglomerate contains mainly cobbles of plagiophytic flows, like those that characterize the Tillery unit. Near the base of the unit, are dense vitreous, banded flows up to 4 m thick. Rare feeder dikes to these flows display highly irregular margins.

Data to directly constrain the minimum age of the Tillery andesite are lacking.

3.7. Nicola Group interpretation

Early workers recognized that Nicola volcanic arc rocks are flanked to the east and west by sedimentary strata (Campbell, 1966; Schau, 1968). The Shrimpton Creek area lacks evidence of an underlying basement like the Harper Ranch Group to the north, near Kamloops, which comprises mainly erosional relicts of a Late Devonian to Late Mississippian arc (Beatty et al., 2006). To the east, the Chaperon Group has been interpreted



Fig. 12. Harmon succession, Tillery unit feldspar porphyry breccia.

as a narrow Permian rift deposit formed on attenuated North American crust and correlative to the Harper Ranch Group (Thompson et al., 2006). To the south, the Anarchist Group (Middle Devonian to Early Permian) is interpreted as an 80 to 90 m.y. record of mid ocean ridge basalt to intra-oceanic tholeiitic arc formation (Massey and Dostal, 2013), strongly contrasting with the interpreted paleotectonic setting of the Chaperon Group.

Thus far, our detrital zircon analyses have failed to reveal a single Precambrian zircon, more consistent with an intraoceanic arc than with a continental arc origin. If an intra-oceanic arc setting is correct, distal background sedimentation was likely pelagic, overwhelmed by input from the emergent Nicola arc, and increasingly more volcanic and less sedimentary in character with proximity to the arc axis. Remarkably fresh tuffaceous sediment containing euhedral pyroxene, hornblende and olivine (see Boot Lake succession) indicate little residence time between original pyroclastic deposition, erosion and redeposition. Almost all primary volcanic units, such as coarse flow breccias or flows, are intercalated with sedimentary rocks, some of which contain marine fossils, unequivocal evidence of submarine deposition.

At least three erosional surfaces can be identified in the Nicola arc in the Shrimpton Creek area: above the Hendriks limestone, overlain by the Shea conglomerate of probable Late Norian age; above the Voght volcanic sandstone unit, approximately at the Triassic-Jurassic boundary; and above the Tillery andesite unit, probably sometime in the Early Jurassic. All may be correlative with similar erosional events observed along the length of the Quesnel and Stikine arcs (e.g. Logan and Mihalynuk, 2014).

4. Bates conglomerate

Massive tabular beds of distinctive, well-rounded black chert granule to boulder conglomerate comprise the Bates unit. Poorly developed beds are typically decimetres to a few metres thick with rubbly black surfaces that commonly display a weak, rusty red patina. The Bates unit is at least 420 m thick and extends from near Courtney Lake, ~17 km southwards to where it is beveled off by the modern erosional surface near the uplifted northern margin of the Late Triassic Allison Lake pluton. About 10 km farther south, the Spences Bridge Group

(Early Cretaceous) directly overlies the Allison Lake pluton without any intervening Bates unit rocks.

Only in some of the northern exposures, near Tinmilsh Lake, do cobbles and boulders of lithologies other than black chert comprise a significant proportion of the unit, including altered light grey granitoid and dark green volcanic rocks and black siltstone. Here the unit weathers orange, probably due to carbonate alteration, and is faulted and interleaved with well-cleaved argillite and siltstone. Except for these northern outcrops, which probably represent the lowest exposed parts of the unit, the predominance of chert clasts suggests a very restricted source region, with no contribution from currently local sources. A widespread source of chert is unknown in the Shrimpton Creek area. Cache Creek complex to the west and Slocan Group to the east are both sources of chert that may have been exposed during orogenesis in the Middle to Late Jurassic (see “Structure” below).

5. Spences Bridge Group (Early Cretaceous): Lodwick succession

The Spences Bridge Group is exposed over an area of 50 km² west of Highway 5A (Figs. 2, 3), where it is conterminous with a broader northwest-trending volcanic field at Shovelnose Mountain to the northwest (Diakow and Barrios, 2008), and southeast towards Princeton (Mihalynuk, et al. 2014a). Herein we mainly use stratigraphic nomenclature from Thorkelson and Rouse (1989) and Diakow and Barrios (2009).

We use the informal name ‘Lodwick succession’ for sections of the Pimainus Formation, (the basal unit of the Spences Bridge Group) best exhibited in the general vicinity of Lodwick Lake.

The Lodwick sequence is subdivided into three distinctive subaerially erupted rock units, which collectively conform to a regionally consistent eruptive pattern, albeit with local variability, that is observed throughout the Early Cretaceous volcanic tract between Princeton and Shovelnose Mountain. Initial volcanic deposits consist of an andesitic flow unit (Unit eKSBL1), succeeded sequentially by two felsic units (Units eKSBL2 and eKSBL3). The lower felsic unit consists of a solitary rhyodacitic pyroclastic flow and associated epiclastic deposits, conformably overlain by a dacitic flow unit. The Coalmont Road transects this sequence, and particularly good sections of the felsic components and related sedimentary rocks are adjacent to the road descending into, and forming the cliffs of Otter Creek valley.

Because of the scattered nature of small exposures comprising the andesite unit, its overall thickness is indeterminate; however, consistent spatial relationships confirm that it is stratigraphically lower than the felsic units. In general, the felsic units and associated epiclastic deposits thicken progressively to the northwest, attaining a maximum thickness at Otter Creek valley. Where the Coalmont Road crosses Otter Creek, dacite flows of the uppermost unit (Unit eKSBL3) form prominent columnar joints in cliffs more 75 m high. Nearby, these flows appear to abut the underlying rhyodacite ash-flow tuff and interfinger with epiclastic rocks, across a steep depositional contact.

Towards the northwest, beyond Otter valley, the felsic units either disappear or thin dramatically. This geometry suggests that the felsic units preserve a synvolcanic paleochannel. The dacite flow unit is restricted to several thin outliers outcropping nearby, and presumably resting conformably on the underlying andesite unit.

5.1. Andesites (Unit eKSBL1)

Andesitic lava flows and scant lapilli interbeds that comprise this unit typically weather to small, widely spaced, solitary outcrops. Distribution of these rocks extends from low-relief terrain along the western margin of the Allison pluton at Highway 5A westward to higher elevation near Lodwick Lake, where the upper contact with overlying rhyodacitic ashflow tuff is observed at one location. In the east, andesite exposures are scattered over 5 km close to granitic rocks of the Allison pluton, although contacts are not exposed. However, at nearby Gladstone Lake, andesite flows distributed over about 1 km² and surrounded by plutonic rocks presumably represent an outlier unconformable on the Allison pluton. In glacially sculpted terrain covered by thick till north of Otter Creek, midway between Highway 5A and the Coalmont Road, isolated andesite outcrops protrude through till close to topographically higher outcrops of chert-bearing conglomerate. Although the contact is concealed, it is interpreted as a steeply inclined sub-andesite unconformity that cuts into the Bates conglomerate unit (see above).

The flows are olive green, and typically display porphyritic textures imparted by 20–25% medium-grained plagioclase and up to several percent pyroxene (partly replaced by chlorite). Amygdaloidal varieties, locally with white opalescent silica amygdules, are rare. West of the Coalmont Road, andesites differ from those farther southeast near the Allison pluton in that flow breccia is more widespread and generally associated with oxidized maroon lavas containing an earthy green mineral, tentatively identified as celadonite, and chalcedonic silica infilling fractures and small cavities. These flows closely resemble those of unit PS1 comprising the basal flows of the Pimainus Formation in the adjoining Shovelnose Mountain area (Diakow and Barrios, 2008).

5.2. Rhyodacite lapilli tuff and derived epiclastic rocks (Units eKSBL2 and eKSBL2s)

Felsic volcanic fragmental and epiclastic rocks make up this unit. Widely distributed throughout the Johnny-Thalia-Lodwick lakes area, the relative volume of the epiclastic rocks apparently exceeds that of the tuffs. Here, the epiclastic rocks contain rock and crystal detritus that is similar to pyroclasts found in the tuffs. Although these tuffs continue northward to Otter Creek, the interlayered epiclastic rocks apparently terminate on the south side of the valley.

5.2.1. Rhyodacite tuff (Unit eKSBL2)

Unit eKSBL2 depositionally overlies andesitic rocks of unit eKSBL1 north of Lodwick Lake. The unit consists

predominantly of dacitic to rhyodacitic lapilli tuffs and rare rhyolitic ash tuff and laminated flows. These tuffs display a light green matrix that supports a variety of lithic fragment types. Most fragments are angular and subangular <3 cm to 10 cm in diameter, although block-size fragments occur (particularly in some eastern exposures). The clasts consist of varicolored, fine-grained volcanic porphyries and fewer, but diagnostic, flow-laminated and aphanitic dacite-rhyolite, collapsed pumiceous rhyolite, and pinkish fine- to medium-grained granitic rocks, some of which resemble phases of the Allison pluton. Also diagnostic are trace to 2% quartz and biotite. The tuff commonly contains m-scale interbeds of pebble conglomerate and sandstone with local parallel stratification.

The tuff unit is believed to have originated as a pyroclastic flow that has undergone minimal compaction. These rocks closely resemble unit PS4, a thick and widespread mainly pyroclastic unit at Shovelnose Mountain (Diakow and Barrios, 2008).

5.2.2. Conglomerate and sandstone (Unit eKSBL2s)

Conglomerate with sandstone interbeds underlie tuffs of unit eKSBL2 east of Lodwick Lake. This clastic unit thickens westward where conglomerate interfingers with tuff. Conglomerate forms thick, massive beds composed mainly of poorly sorted, polymictic and matrix-supported clasts. The clasts vary from subangular to well-rounded cobbles and sparse boulders that can reach 45 cm diameter (typically <20 cm). Planar bedded sandstone, locally with abundant carbonaceous plant debris, and granule-pebble layers form m-thick interbeds.

A conglomeratic and sandstone succession, lithologically distinct from that near Lodwick Lake, is faulted against andesite of unit eKSBL1 at its northern extent, adjacent to the Coalmont Road. Sandstone and siltstone from this unit underlie and, in part, interfinger with tuffs of unit eKSBL2 farther south in the Otter Creek valley. The conglomerate is a massive layer more than 30 m thick with self-supporting poorly sorted angular and subrounded boulders (up to 1.5 m in diameter). The clasts consist of andesite, porphyritic dacite and abundant flow-laminated rhyolites. Bedded sandstone and siltstone containing thin carbonaceous-rich layers occurs locally above the deposit.

This coarse clastic bed appears to locally overlie a comparatively finer siliciclastic sequence exposed in a series of cuts along the Coalmont Road. The sequence displays dark green, planar beds and characteristic weathering to rounded surfaces with conchoidal fracturing. It is composed of thickly bedded granule-pebble conglomerate alternating with medium and coarse sandstone and thinly bedded and interlaminated siltstones. The sandstones are composed mainly of plagioclase, some pyroxene and rare quartz. Structures in the rocks include graded bedding, small-scale channels, and ball and pillow structures. Plant debris is widespread in the finer grained layers, including rare tree stems up to 5 cm in diameter.

Based on the stratigraphic position relative to felsic tuffs and similar clast lithologies, the conglomerates in the vicinity of Lodwick Lake correlate with unit PS2 of the Pimainus

Formation at Shovelnose Mountain (Diakow and Barrios, 2008). A comparison of the siliciclastic units north of Otter Creek valley with those to the south near Lodwick Lake, indicates they occupy the same relative stratigraphic position, although significant lithologic differences exist, implying differing provenance. Conglomerates in the south contain clasts identical to lithic and crystal fragments found in tuffs of unit eKSBL2, implying periodic erosion and resedimentation of tuff deposits. In addition, the presence of ubiquitous granitic clasts in Unit eKSBL2 (see above) suggests a potential source for minor granitic detritus in conglomerates of unit eKSBL2s. North of Otter valley the finer clastic components contain sparse pyroxene, which may have been derived from andesites near the base of the Spences Bridge Group. The coarse boulder conglomerate contains abundant flow-laminated rhyolite, probably derived locally from voluminous flows in the Pimainus Formation at Shovelnose Mountain.

5.3. Dacite flow (Unit eKSBL3)

Dacite lava flows comprise the uppermost unit of the Spences Bridge Group in the Lodwick succession. The distribution and thickness of the unit is influenced by differential uplift in blocks separated by three steeply dipping north-south faults. Most widespread in the central block, the unit is continuous, forming cliffs north of Thalia Lake to Otter Creek valley. Conservatively estimated to be between 30 and 80 m thick in this segment, the flow unit dramatically thins north of the Otter Creek valley. The east-west extent of the unit is limited by a sub-horizontal outlier covering about 5 km² in the western block and it abruptly terminates at the fault marking the margin of the eastern block.

The lower contact of the unit is consistent throughout the region as a shallow, north-inclined plane, sharply separating the dacite from underlying unit eKSBL2 tuffs and eKSBL2s epiclastic rocks. On the northwest side of Thalia Lake, the contact is marked by a 2 m-thick hornblende-dacite porphyry flow not seen elsewhere in the unit. This distinctive flow directly overlies thinly bedded quartz and biotite-bearing unit eKSBL2s sandstone.

The dacite is remarkably uniform in appearance, typically forming cliffs exhibiting columnar joints. It weathers orange, and breaks into either blocky or slab-like pieces. The porphyritic texture is diagnostic, imparted by 15-20% subhedral feldspar up to 4 mm long and fewer feldspar glomerocrysts distributed evenly throughout the groundmass. Mafic minerals might be present as greenish anhedral grains in the rock; however, they are too small to identify macroscopically. Thin laminated flows were observed locally.

Although the dacite is generally unaltered, at a solitary location in a 50 m² area, fresh chalky clay minerals replace plagioclase phenocrysts and the groundmass. Where this alteration increases in intensity the porphyritic texture is obliterated, thereby yielding a dense off-white rock that is easily confused with an aphanitic rhyolite. White and translucent banded chalcedony, some with a central open cavity lined with

drusy quartz, comprise rare veinlets observed crosscutting the dacite flows.

Massive dacite has not been mapped elsewhere in the Spences Bridge Group. It may represent a solitary flow that exhibits pronounced thinning northwest over 7 km, suggesting that the vent might originally have been located farther south in an unmapped area. Based on the present distribution of the dacite, an inferred general flow path towards the northwest appears to coincide with a distinctive flow laminated rhyolite (unit PS6) which presently forms a broad lobe extending from higher elevation on Shovelnose Mountain, towards the southeast to its present terminus within 1 km of the closest dacite outlier. Because of their close proximity we speculate that these felsic flows once coalesced and are temporally equivalent.

6. Princeton Group (Eocene)

Only a few outliers of Princeton Group volcanic rocks are exposed in the Shrimpton Creek map area. The largest of these is between the western map boundary and McCullough Creek (west of Davis Lake, Fig. 3). These rocks apparently rest on an unconformity above the Spences Bridge Group to the west and in possible fault contact with the Allison pluton to the east. Smaller erosional remnants occur in the northeastern map area where they are mainly shallowly dipping, sparsely amygdaloidal rhyodacitic flows. Princeton Group volcanic strata are well dated near Princeton (Ickert et al., 2009) as between 53 and 47 Ma, (early part of Eocene, Cohen et al., 2013).

6.1. Rhyodacite flow outliers

Except where well-exposed in roadcuts, outcrops of rhyodacite flows form low-relief, tan to light grey and platy weathering, glacially sculpted mounds. Flows are very fine-grained to aphanitic with sparse, medium-grained feldspar phenocrysts and glomerocrysts. Vesicles are typically sparse and are locally filled with a soft, amber-coloured mineral along with chlorite and chalcedonic quartz. Some vesicles are not infilled by mineral matter.

6.2. Quartz-biotite rhyolite

Quartz-biotite-phyric ash flow crops out in two restricted areas in the eastern Shrimpton Creek area. South of Vinson Lake, a probable intrusive unit with a matrix lithologically similar to the ash flows is interpreted as a feeder.

White-weathering outcrops contain smoky quartz as fractured and rounded eyes (up to 20%); vitreous medium-grained plagioclase (up to 25%); orthoclase as altered, chalky white, medium-grained crystals (up to 15%) and sparse megacrysts to 1 cm diameter; and fine- to medium-grained golden to black biotite (3%). Beautiful flow banding of a white, ash-rich matrix locally contains ~3 % flattened and weakly welded grey pumice lapilli. Sparse accidental granodiorite fragments (Fig. 13) confirm that the tuff postdates crystallization of the adjacent batholith, from which the fragments were most likely derived.

Roadbed outcrops between Dillard and Vinson Lakes are



Fig. 13. Princeton Group. Quartz-eye, biotite-bearing rhyolite with accidental fragments of granodiorite.

lithologically similar to the ash flow, but lack flow banding and fragmented crystals, and are much coarser grained, with up to 15% coarse smoky quartz eyes and 5-20% euhedral anorthite crystals up to 3 cm by 10 cm. These textural differences are attributed to an intrusive origin, likely a feeder of the ash flows. As constrained by the distribution of rhyolite porphyry and surrounding granitic outcrops, the feeder is more than 65 m, but less than 1100 m in diameter.

7. Miocene to Recent basalt

Two ages of young basaltic flows occur in the Shrimpton Creek area: pre- and post- Quaternary.

Basalt flows infilling paleovalleys that have been inherited by the modern Shrimpton Creek-Missezula Lake and the Kentucky-Alleyne drainages, are capped by Quaternary deposits in which glaciated boulders derived from the flows can be a predominant component. Most extensive of these basalt units are horizontal, massive to columnar jointed flows, typically 2 to 5 m thick. They display scoraceous, brecciated bottoms with vesicle content decreasing toward the flow center. Vesicle pipes are common. Green to amber, medium to coarse olivine phenocrysts with irregular and commonly iridescent fractures comprise up to 1% of the rock. A very fine mat of plagioclase with interstices filled by black glass, or coated by glass that surrounds angular void spaces, are typical matrix types. Similar flows units occur as sporadic relicts in the Summers Creek area where they have been more fully described by Mihalynuk et al. (2014a), and are correlated with the Chilcotin Group of Miocene to Pliocene age (Mathews, 1989). They have been isotopically dated in the Coalmont area (Fig. 2) as 9 and 9.2 ± 1.8 Ma (Late Miocene; Mathews, 1989; recalculated by Breitsprecher and Mortensen, 2004), but those are apparently much older than rocks in the Shrimpton Creek area, which have $^{40}\text{Ar}/^{39}\text{Ar}$ step heating plateau ages of 0.2 ± 0.5 to 0.66 ± 0.03 Ma (Sluggett, 2008). Such young ages confirm the relative age assignments of the older “plateau” and “valley basalts” by Rice

(1947). Here we follow the usage of Rice (1947) and include all intra-glacial basalt flows as “valley basalt”. Recent basalts are treated separately.

Recent basalt occurs as highly scoraceous blocky tuff and spatter less than a m thick that are irregularly distributed atop about one hectare of Quaternary till and gravels east of Shrimpton Creek. Spatter cements the gravel that it came into direct contact with. Some granitic clasts entrained in the spatter fused to crystal mush with a quenched glass matrix. Droplets and mm veneers of spatter coat boulders; some granitoid boulders display spalled spatter rinds. Charcoal remains of trees are preserved where they were engulfed in scoraceous flow (Fig. 14), and imprints of other burnt organic matter, including growth rings, record where these organic materials have eroded away. No evidence of a vent was found; however, where the unit appears thickest it has been disturbed during construction of a logging landing, and any relict of a vent may have been infilled.

8. Intrusive units

Intrusive rocks in the study area include Late Triassic to Middle Jurassic plutons (Fig. 3) and dikes interpreted as coeval with Spences Bridge Group volcanic rocks (late Early Cretaceous). Late Triassic intrusions along the axis of the central Nicola belt, (as defined by Preto, 1979) include the polyphase Allison pluton (204 ± 10 to 207 ± 10 Ma, K-Ar hornblende and muscovite cooling ages in Preto, 1979; recalculated by Breitsprecher and Mortensen, 2004; and detrital zircons in Mihalynuk et al., 2014b) in the southwest part of the Shrimpton Creek map area, and numerous undated dioritic bodies such as at the Big Kid and Ketchan prospects, all interpreted as part of the ~205 Ma Copper Mountain suite (Logan and Mihalynuk, 2014). The northeastern and eastern parts of the study area are underlain by the Pennask batholith (Early Jurassic; 194 ± 1 Ma) and western parts of the Osprey Lake K-feldspar megacrystic granite batholith (166 ± 1 Ma;



Fig. 14. Highly scoraceous Recent basalt with charcoal wood fragments (pen tip).

U-Pb zircon ages from Parrish and Monger, 1992; and the ~160-164 Ma ages from zircons reported here). An extensive, north-trending dike swarm in the Summers Creek map area is correlated with the 104 Ma Spences Bridge Group to the west (Diakow and Barrios, 2009) and the 'Mine dikes' along strike to the south at Copper Mountain (103 ± 0.3 Ma, Mihalynuk et al., 2010; also known as 'Candy Stripe dikes'). This correlation is confirmed by geochronology (see below) but these dikes are largely unknown in the Shrimpton Creek area. One possible exception is east of Shrimpton Creek where a restricted, weak swarm of dikes with the same mineralogy, and up to ~10 m thick, are mapped north of Buck Lake (too small to show on Fig. 3). A series of quartz-feldspar porphyry dikes and stocks that cut the Osprey Lake batholith and are associated with gold mineralization at the Siwash mine, have returned K-Ar cooling ages that cluster around 53 Ma (Armstrong and Peto, 1981 and Hunt and Roddick, 1990; recalculated in Breitsprecher and Mortensen, 2005).

8.1. Allison pluton

The Allison pluton underlies the southwest corner of the Shrimpton sheet where it is nonconformably overlain by the Spences Bridge Group (Figs. 2, 3). It is a composite body consisting of northeast-trending zones in which diorite and granite predominate.

Felsic phases range from pink, coarse-grained granite with smoky quartz, to medium-grained, white-weathering tonalite. Mafic phases range from quartz diorite (Fig. 15a) to hornblende-plagioclase pegmatite (Fig. 15b), and tend to be varitextured. Younger phases tend to be more felsic, but irregular contacts between mafic and felsic phases, chilling of mafic against felsic phases (Fig. 15c), and zones with abundant mafic enclaves in granitic phases, suggest comingling of melts.

8.2. Pennask batholith

White-weathering, medium- to coarse-grained hornblende-biotite granodiorite to tonalite of the Pennask batholith (Fig. 16) crops out across the northeast corner of the map area (Figs. 2, 3). Wide spaced joints, up to 1 or 2 m in places, create blocky outcrops on scarps, or gently rounded outcrops on glaciated surfaces. Plagioclase (30-50%), orthoclase (<20%) and quartz (30-40%) can be subidiomorphic, relatively fresh biotite forms medium to coarse booklets and intergranular mats and is generally more abundant than hornblende (8-15% combined). Hornblende may appear dusty due to incipient chlorite alteration and is locally subtrachytic, outlining an igneous flow fabric. Fine-grained magnetite and fine to medium-grained titanite comprise 1-2% and 0.5% of the rock respectively.

8.3. Osprey Lake batholith

The Osprey Lake batholith covers more than 1100 km² between Peachland and the southwest corner of the Shrimpton map area (only ~95 km² are in the map area). Granite is the most common phase, forming white to pinkish-grey, rounded to blocky outcrops. K-feldspar megacrysts comprise 20 % of



Fig. 15. a) Pegmatitic hornblende diorite. One of a series of northeast-trending zones in the Allison pluton. b) Foliated dioritic border phase of the Allison pluton includes rafts of foliated diopside skarn, and is cut by synkinematic dikelets of quartz diorite. c) Cuspate-lobate contact between comagmatic diorite and granodiorite, Allison pluton.



Fig. 16. Typical salt and pepper Pennask tonalite, here with minor grey-green fault planes lined by chlorite.

the rock over broad areas. They are up to 5 cm long, and may display growth zones outlined by hornblende microlites; they tend to have light-coloured rims. Medium- to coarse-grained plagioclase, orthoclase, grey quartz, biotite and hornblende comprise the matrix. Plagioclase and pinkish matrix K-feldspar comprises ~60% of the rock volume. Biotite forms 3-5 mm euhedral to subhedral books comprising ~10% of the rock, and medium-grained hornblende is ~6%. Accessory minerals identifiable in hand sample include euhedral, honey brown titanite (0.5-1%) and magnetite. Enclaves of hornblende diorite are common. Magnetic susceptibilities range between 20 and 38 $\times 10^{-5}$ SI. A strong thermal-metamorphic halo 0.5 km or more wide is developed around this massive body.

8.4. Spences Bridge “Mine dikes”

An extensive set of dikes trends north, subparallel to the western contact of the Bromley pluton (Fig. 2). They are porphyritic, with phenocrysts of K-feldspar, plagioclase, quartz and chloritized hornblende in varying combinations. Some dikes are 10 m or more thick and have been interpreted as co-genetic with the Bromley pluton. On the basis of composition and a preliminary U-Pb isotopic age determination, Mihalynuk et al. (2014b) suggested a correlation between the ‘Mine dikes’ and Spences Bridge Group, a correlation confirmed by further U-Pb geochronology (see below).

8.5. Otter intrusions

A coarse orthoclase-quartz porphyritic intrusion extending northwest from the confluence of Galena and Siwash Creeks, underlies about 5 km². Most parts of the intrusion are pyritic, clay altered, and weather white, yellow and rust. In many localities hematite occurs as fine disseminations and pseudomorphically replaces octahedra of magnetite. The intrusion appears to be gradational with lithologically similar parts of the Osprey batholith, but is part of much younger east-trending belt of stocks that have yielded K-Ar ages of ~53 Ma

(Hunt and Roddick, 1990; Armstrong and Peto, 1981). Dikes included with the Otter intrusions cut the Osprey batholith at the Siwash mine and are interpreted as syn-mineralization.

9. Geochronology

Presented here are completed isotopic analyses on zircons extracted from samples collected during mapping: four analyzed by U-Pb isotopes by Chemical Abrasion-Thermal Ionization Mass Spectroscopy (CA-TIMS), and two analyzed by Laser Ablation (LA) ICP-MS. Geochronological results for 15 samples collected during fieldwork in 2014 are pending.

9.1. Methodology

Abridged methodologies are presented here. Complete procedures are reported in the references cited and in companion publications (Mihalynuk et al., 2014b; Mihalynuk et al., 2015).

9.2. Zircon CA-TIMS

CA-TIMS procedures described here are modified from Mundil et al., 2004, Mattinson, 2005 and Scoates and Friedman, 2008. Rock samples undergo standard mineral separation procedures; zircons separates are handpicked in alcohol. The clearest, crack- and inclusion-free grains are selected, photographed and then annealed at 900°C for 60 hours. Annealed grains are chemically abraded and then spiked with a ²³³⁻²³⁵U-²⁰⁵Pb tracer solution (EARTHTIME ET535), and then dissolved. Resulting solutions are dried and loaded onto Re filaments (Gerstenberger and Haase, 1997).

Isotopic ratios are measured by a modified single collector VG-54R or 354S thermal ionization mass spectrometer equipped with analogue Daly photomultipliers. Analytical blanks are 0.2 pg for U and 1.0 pg for Pb. U fractionation was determined directly on individual runs using the ET535 mixed ²³³⁻²³⁵U-²⁰⁵Pb isotopic tracer. Pb isotopic ratios are corrected for fractionation of 0.23%/amu, based on replicate analyses of NBS-982 reference material and the values recommended by Thirlwall (2000). Data reduction employed the Excel™-based program of Schmitz and Schoene (2007). Standard concordia diagrams are constructed and regression intercepts, weighted averages calculated with Isoplot (Ludwig, 2003). All errors are quoted at the 2 σ or 95% level of confidence, unless otherwise noted. Isotopic dates are calculated with the decay constants $\lambda^{238}=1.55125E^{-10}$ and $\lambda^{235}=9.8485E^{-10}$ (Jaffe et al, 1971). EARTHTIME U-Pb synthetic solutions are analysed on an on-going basis to monitor the accuracy of results.

9.3. Zircon LA-ICPMS

Zircons analyzed using laser ablation (LA) ICP-MS methods, employ techniques as described by Tafti et al. (2009). Instrumentation at the PCIGR comprises a New Wave UP-213 laser ablation system and a ThermoFinnigan Element2 single collector, double-focusing, magnetic sector ICP-MS. All zircons greater than about 50 microns in diameter are picked from the mineral separates and were mounted in an epoxy puck along with several grains of the Plešovice (337.13 \pm 0.13 Ma,

Sláma et al., 2007), and Temora2 (416.78 ±0.33 Ma) zircon standards and brought to a very high polish. Prior to analysis, the surface of the mount was washed for 10 minutes with dilute nitric acid and rinsed in ultraclean water. The highest quality portions of each grain selected for analysis are free of alteration, inclusions, or possible inherited cores. Line scans rather than spot analyses are employed in order to minimize elemental fractionation during the analyses. A laser power level of 40% and a 25 µm spot size are used. Backgrounds are measured with the laser shutter closed for ten seconds, followed by data collection with the laser firing for approximately 35 seconds. The time-integrated signals are analysed using Iolite software (Patton et al, 2011), which automatically subtracts background measurements, propagates all analytical errors, and calculates isotopic ratios and ages. Corrections for mass and elemental fractionation are made by bracketing analyses of unknown grains with replicate analyses of the Plešovice zircon standard. A typical analytical session at the PCIGR consists of four analyses of the Plešovice standard zircon, followed by two analyses of the Temora2 zircon standard five analyses of unknown zircons, two standard analyses, five unknown analyses, etc., and finally two Temora2 zircon standards and four Plešovice standard analyses. The Temora2 zircon standard was analysed as an unknown in order to monitor the reproducibility of the age determinations on a run-to-run basis. Final interpretation and plotting of the analytical results employed the ISOPLOT software of Ludwig (2003).

9.4. Geochronology results

Geochronology results for four CA-TIMS and two LA-ICPMS analyses are presented in Figures 17 to 21, and Tables 1 to 8. Complete raw data tables, cathode luminescence imagery of zircons, and ancillary plots such as those that show detrital zircon isochrons can be found in Mihalynuk et al., 2015. Most of the results are for samples collected in 2013 and only a cursory description of the units sampled is presented here. For more detailed descriptions see Mihalynuk et al. (2014a).

9.4.1. Missezula Mountain rhyolite: Sample MMI13-30-4

Sample MMI13-30-4 (Table 1; Fig. 17) was collected from pyritic felsic lapilli tuff on the east flank of Missezula Mountain. It was a second attempt to date the unit; only a few zircon fragments were obtained from a more massive ignimbritic section to the south (“rusty rhyolite lapilli tuff” in Mihalynuk et al., 2014a), and they provided inconclusive results.

An age of 238.1 ±0.3 Ma is calculated based upon two overlapping fractions on concordia. Slightly discordant older grains may include an inherited older zircon component. To our knowledge, this is the oldest isotopic age obtained from the Nicola Group volcanic rocks. Felsic strata in the western belt tend to cluster around 224 Ma (Diakow, unpub data).

9.4.2. Dike in Voght unit redbeds: Sample MMI13-16-5

Sample MMI13-16-5 (Table 2; Fig. 18a) was collected from a fine-grained dike that cuts red volcanic sandstone (Fig. 18b).

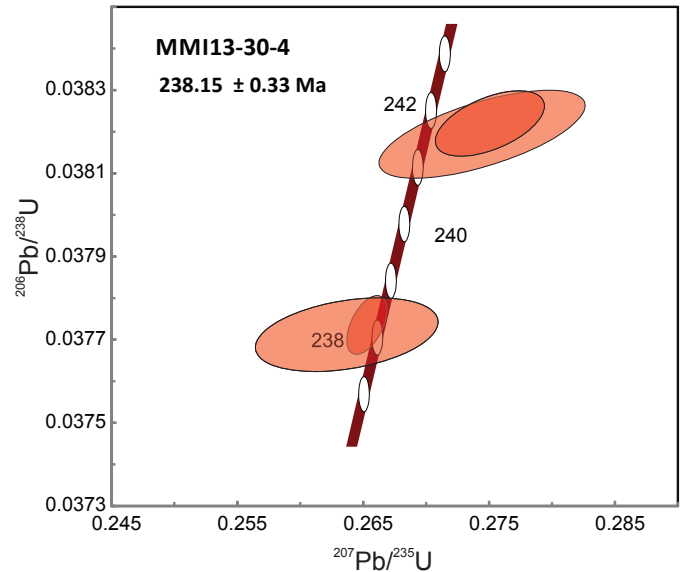


Fig. 17. Thermal Ionization Mass Spectrometric (TIMS) analysis of zircon U-Pb from sample MMI13-30-4 of felsic lapilli tuff on Missezula Mountain. An age of 238.1 ±0.3 Ma is based on two overlapping fractions on concordia. Slightly discordant older grains may include an inherited zircon component. Data point error ellipses are 2σ.

Four grains were run and these overlap concordia at 201 and 199 Ma. The more precise age is obtained from the older 2-grain cluster at 201 +0.3/-0.4 Ma; however, a circa 199 Ma age is also consistent with the age of the enclosing strata with a detrital zircon maximum depositional age (DZMD) of 202 ±4 Ma (see MMI13-16-3, below).

9.4.3. Bromley pegmatite: Sample MMI13-30-1

Sample MMI13-30-1 (Table 3; Fig. 19) Bromley pluton does not crop out in the Shrimpton Creek map area. However, we include new geochronological data from the southeast Summers Creek map area (Fig. 2) from pegmatitic dikes that are presumably related to the main medium-grained, hornblende-biotite granodiorite pluton. These dikes cut the biotite hornfels halo that extends ~500 metres away from the pluton (garnet occurs within a few tens of metres of the contact). Pegmatite dike intrusion appears to have been synchronous with extensional faulting within the thermometamorphic halo, and, on the basis of widespread Tertiary extension across the Summers Creek map area, the pegmatite was assumed by Mihalynuk et al. (2014a) to be Eocene. However four zircons extracted from the pegmatite, all clustering on concordia, yield an integrated age of 193.6 ±0.3 Ma. This is the same age (within error) as a previous U-Pb age determination of the Early Jurassic Bromley pluton (193 ±1 Ma, Parrish and Monger, 1992).

9.4.4. Mine dike swarm at Similkameen River: Sample MMI13-30-2

Sample MMI13-30-2 (Table 4; Fig. 20) is from a swarm of north-trending quartz-feldspar porphyry dikes (Fig. 20a). This

Table 1. U-Th-Pb isotopic data for sample MM113-30-4.

Sample	Compositional Parameters										Radiogenic Isotope Ratios						Isotopic Ages																		
	Wt.	U	Pb	Th	$^{206}\text{Pb}^*$	mol %	Pb*	Pb _c	^{206}Pb	^{204}Pb	^{208}Pb	^{207}Pb	^{206}Pb	^{235}U	% err	^{238}U	% err	^{207}Pb	^{206}Pb	corr.	^{207}Pb	^{235}U	% err	^{238}U	% err	^{207}Pb	^{206}Pb	corr.	^{207}Pb	^{235}U	% err	^{238}U	% err		
	(a)	(j)	(i)	(b)	(c)	(c)	(c)	(c)	(c)	(d)	(e)	(e)	(e)	(f)	(f)	(e)	(e)	(f)	(e)	(f)	(g)	(g)	(f)	(f)	(g)	(g)	(f)	(f)	(g)	(g)	(f)	(f)	(g)	(g)	(f)
MM113-30-4																																			
A	0.002	57	2.4	0.340	0.1985	97.07%	10	0.50	632	0.110	0.052008	2.681	0.273832	2.848	0.038187	0.268	0.651	285.77	61.30	245.75	6.22	241.58	0.63												
C	0.003	115	4.2	0.137	0.5757	99.28%	38	0.34	2572	0.043	0.050702	0.506	0.263172	0.574	0.037645	0.181	0.511	227.32	11.70	237.22	1.22	238.22	0.42												
D	0.001	91	3.4	0.017	0.1289	96.87%	9	0.30	591	0.005	0.050382	2.571	0.261314	2.640	0.037617	0.226	0.346	212.64	59.56	235.73	5.55	238.05	0.53												
E	0.001	121	4.9	0.299	0.1541	97.86%	13	0.28	862	0.097	0.052102	1.400	0.274545	1.496	0.038217	0.198	0.536	289.88	31.99	246.32	3.27	241.77	0.47												

(a) A, B etc. are labels for fractions composed of single zircon grains or fragments; all fractions annealed and chemically abraded after Mattinson (2005) and Scoates and Friedman (2008).
 (b) Model Th/U ratio calculated from radiogenic $^{208}\text{Pb}/^{206}\text{Pb}$ ratio and $^{207}\text{Pb}/^{235}\text{U}$ age.
 (c) Pb* and Pbc represent radiogenic and common Pb, respectively; mol % $^{206}\text{Pb}^*$ with respect to radiogenic, blank and initial common Pb.
 (d) Measured ratio corrected for spike and fractionation only. Mass discrimination of 0.25%/amu based on analysis of NBS-982; all Daily analyses.
 (e) Corrected for fractionation, spike, and common Pb; up to 0.5 pg of common Pb was all assumed to be procedural blank: $^{206}\text{Pb}/^{204}\text{Pb} = 18.50 \pm 1.0\%$; $^{207}\text{Pb}/^{204}\text{Pb} = 15.50 \pm 1.0\%$; $^{208}\text{Pb}/^{204}\text{Pb} = 38.40 \pm 1.0\%$ (all uncertainties 1-sigma).
 (f) Errors are 2-sigma, propagated using the algorithms of Schmitz and Schoene (2007) and Crowley et al. (2007).
 (g) Calculations are based on the decay constants of Jaffey et al. (1971). $^{206}\text{Pb}/^{238}\text{U}$ and $^{207}\text{Pb}/^{206}\text{Pb}$ ages corrected for initial disequilibrium in $^{230}\text{Th}/^{238}\text{U}$ using Th/U [magma] = 3.
 (h) Corrected for fractionation, spike, and blank Pb only.
 (i) Nominal fraction weights estimated from photomicrographic grain dimensions, adjusted for partial dissolution during chemical abrasion.
 (j) Nominal U and total Pb concentrations subject to uncertainty in photomicrographic estimation of weight and partial dissolution during chemical abrasion.

Table 2. U-Th-Pb isotopic data for sample MM113-16-5.

Sample	Compositional Parameters										Radiogenic Isotope Ratios						Isotopic Ages																		
	Wt.	U	Pb	Th	$^{206}\text{Pb}^*$	mol %	Pb*	Pb _c	^{206}Pb	^{204}Pb	^{206}Pb	^{207}Pb	^{206}Pb	^{235}U	% err	^{238}U	% err	^{207}Pb	^{206}Pb	corr.	^{207}Pb	^{235}U	% err	^{238}U	% err	^{207}Pb	^{206}Pb	corr.	^{207}Pb	^{235}U	% err	^{238}U	% err		
	(a)	(i)	(j)	(b)	(c)	(c)	(c)	(c)	(c)	(d)	(e)	(e)	(e)	(f)	(f)	(e)	(e)	(f)	(e)	(f)	(g)	(g)	(f)	(f)	(g)	(g)	(f)	(f)	(g)	(g)	(f)	(f)	(g)	(g)	(f)
MM113-16-5																																			
A	0.0041	122	4.0	0.307	0.6558	98.55%	20	0.79	1273	0.098	0.050503	0.520	0.219094	0.578	0.031464	0.172	0.473	218.23	12.03	201.16	1.06	199.70	0.34												
B	0.0034	108	3.5	0.268	0.4838	98.14%	15	0.76	990	0.084	0.049671	0.971	0.216801	1.044	0.031656	0.162	0.515	179.61	22.62	199.24	1.89	200.91	0.32												
C	0.0052	50	1.7	0.273	0.3420	97.36%	10	0.76	699	0.086	0.049634	3.048	0.214731	3.240	0.031377	0.313	0.640	177.90	71.06	197.51	5.81	199.16	0.61												
D	0.0035	109	3.6	0.247	0.5026	97.91%	13	0.88	882	0.079	0.050469	1.664	0.220507	1.771	0.031688	0.196	0.580	216.64	38.53	202.33	3.25	201.11	0.39												

(a) A, B etc. are labels for fractions composed of single zircon grains or fragments; all fractions annealed and chemically abraded after Mattinson (2005) and Scoates and Friedman (2008).
 (b) Model Th/U ratio calculated from radiogenic $^{208}\text{Pb}/^{206}\text{Pb}$ ratio and $^{207}\text{Pb}/^{235}\text{U}$ age.
 (c) Pb* and Pbc represent radiogenic and common Pb, respectively; mol % $^{206}\text{Pb}^*$ with respect to radiogenic, blank and initial common Pb.
 (d) Measured ratio corrected for spike and fractionation only. Mass discrimination of 0.25%/amu based on analysis of NBS-982; all Daily analyses.
 (e) Corrected for fractionation, spike, and common Pb; up to 0.5 pg of common Pb was assumed to be procedural blank: $^{206}\text{Pb}/^{204}\text{Pb} = 18.50 \pm 1.0\%$; $^{207}\text{Pb}/^{204}\text{Pb} = 15.50 \pm 1.0\%$; $^{208}\text{Pb}/^{204}\text{Pb} = 38.40 \pm 1.0\%$ (all uncertainties 1-sigma). Excess over blank was assigned to initial common Pb, using the Stacey and Kramers (1975) two-stage Pb isotope evolution model at 200 Ma.
 (f) Errors are 2-sigma, propagated using the algorithms of Schmitz and Schoene (2007) and Crowley et al. (2007).
 (g) Calculations are based on the decay constants of Jaffey et al. (1971). $^{206}\text{Pb}/^{238}\text{U}$ and $^{207}\text{Pb}/^{206}\text{Pb}$ ages corrected for initial disequilibrium in $^{230}\text{Th}/^{238}\text{U}$ using Th/U [magma] = 3.
 (h) Corrected for fractionation, spike, and blank Pb only.
 (i) Nominal fraction weights estimated from photomicrographic grain dimensions, adjusted for partial dissolution during chemical abrasion.
 (j) Nominal U and total Pb concentrations subject to uncertainty in photomicrographic estimation of weight and partial dissolution during chemical abrasion.

Table 3. U-Th-Pb isotopic data for sample 30-1.

Sample	Compositional Parameters										Radiogenic Isotope Ratios						Isotopic Ages						
	Wt.	U	Pb	Th	$^{206}\text{Pb}^*$	mol %	Pb*	Pb _c	^{206}Pb	^{208}Pb	^{207}Pb	^{206}Pb	^{207}Pb	^{206}Pb	^{207}Pb	^{206}Pb	^{207}Pb	^{206}Pb	^{207}Pb	^{206}Pb			
	mg	ppm	ppm	ppm	U x 10 ⁻¹³ mol	$^{206}\text{Pb}^*$	Pb _c	(pg)	^{204}Pb	^{206}Pb	^{206}Pb	% err	^{235}U	% err	^{238}U	% err	corr.	corr.	±	±	±	±	
(a)	(i)	(j)	(b)	(c)	(c)	(c)	(c)	(d)	(c)	(e)	(f)	(e)	(f)	(e)	(f)	(e)	(f)	(g)	(f)	(g)	(f)	(g)	(f)
MM113-30-1																							
C	0.0009	931	26.2	0.031	1.0678	99.68%	82	0.29	5868	0.010	0.050512	1.672	0.212824	1.656	0.030558	0.384	0.076	218.61	38.68	195.92	2.95	194.04	0.73
D	0.0008	459	13.1	0.030	0.4670	99.28%	36	0.28	2585	0.010	0.050257	1.527	0.211531	1.550	0.030527	0.271	0.174	206.90	35.40	194.84	2.75	193.84	0.52
E	0.0002	3198	93.5	0.042	0.8124	98.69%	20	0.90	1410	0.013	0.050089	0.873	0.210430	0.911	0.030469	0.131	0.354	199.13	20.27	193.91	1.61	193.49	0.25
F	0.0002	955	28.5	0.015	0.2427	97.92%	12	0.42	889	0.005	0.049899	1.547	0.209706	1.609	0.030480	0.261	0.313	190.29	35.99	193.31	2.83	193.55	0.50

(a) A, B etc. are labels for fractions composed of single zircon grains or fragments; all fractions annealed and chemically abraded after Mattinson (2005) and Scoates and Friedman (2008).
 (b) Model Th/U ratio calculated from radiogenic $^{208}\text{Pb}/^{206}\text{Pb}$ ratio and $^{207}\text{Pb}/^{235}\text{U}$ age.
 (c) Pb* and Pb_c represent radiogenic and common Pb, respectively; mol % $^{206}\text{Pb}^*$ with respect to radiogenic, blank and initial common Pb.
 (d) Measured ratio corrected for spike and fractionation only. Mass discrimination of 0.25%/amu based on analysis of NBS-982; all Daly analyses.
 (e) Corrected for fractionation, spike, and common Pb; up to 0.9 pg of common Pb was all assumed to be procedural blank: $^{206}\text{Pb}/^{204}\text{Pb} = 18.50 \pm 1.0\%$; $^{207}\text{Pb}/^{204}\text{Pb} = 15.50 \pm 1.0\%$; $^{208}\text{Pb}/^{204}\text{Pb} = 38.40 \pm 1.0\%$ (all uncertainties 1-sigma).
 (f) Errors are 2-sigma, propagated using the algorithms of Schmitz and Schoene (2007) and Crowley et al. (2007).
 (g) Calculations are based on the decay constants of Jaffey et al. (1971). $^{206}\text{Pb}/^{238}\text{U}$ and $^{207}\text{Pb}/^{206}\text{Pb}$ ages corrected for initial disequilibrium in $^{230}\text{Th}/^{238}\text{U}$ using Th/U [magma] = 3.
 (h) Corrected for fractionation, spike, and blank Pb only.
 (i) Nominal fraction weights estimated from photomicrographic grain dimensions, adjusted for partial dissolution during chemical abrasion.
 (j) Nominal U and total Pb concentrations subject to uncertainty in photomicrographic estimation of weight and partial dissolution during chemical abrasion.

Table 4. U-Th-Pb isotopic data for sample MM113-30-2.

Sample	Compositional Parameters										Radiogenic Isotope Ratios						Isotopic Ages								
	Wt.	U	Pb	Th	$^{206}\text{Pb}^*$	mol %	Pb*	Pb _c	^{206}Pb	^{208}Pb	^{207}Pb	^{206}Pb	^{207}Pb	^{206}Pb	^{235}U	% err	^{238}U	% err	corr.	corr.	±	±	±	±	
	mg	ppm	ppm	ppm	U x 10 ⁻¹³ mol	$^{206}\text{Pb}^*$	Pb _c	(pg)	^{204}Pb	^{206}Pb	^{206}Pb	% err	^{235}U	% err	(f)	(e)	(f)	(e)	(f)	(g)	(f)	(g)	(f)	(g)	(f)
(a)	(i)	(j)	(b)	(c)	(c)	(c)	(c)	(d)	(e)	(e)	(f)	(e)	(f)	(e)	(f)	(e)	(f)	(e)	(f)	(g)	(f)	(g)	(f)	(g)	(f)
MM113-30-2																									
A	0.0069	95	1.7	0.325	0.4440	97.34%	11	1.00	694	0.105	0.048478	1.740	0.108545	1.859	0.016239	0.169	0.728	122.65	40.97	104.63	1.85	103.84	0.17		
B	0.0054	174	3.1	0.402	0.6355	97.90%	14	1.12	880	0.130	0.048627	0.960	0.109044	1.027	0.016264	0.144	0.522	129.90	22.57	105.09	1.03	104.00	0.15		
C	0.0061	104	1.8	0.384	0.4307	97.61%	12	0.87	775	0.123	0.048001	1.206	0.107446	1.289	0.016235	0.141	0.620	99.30	28.53	103.63	1.27	103.81	0.15		
D	0.0053	145	2.6	0.357	0.5206	96.92%	9	1.36	600	0.116	0.048814	1.501	0.109463	1.587	0.016264	0.203	0.480	138.92	35.23	105.47	1.59	104.00	0.21		
E	0.0041	213	3.9	0.453	0.5928	97.48%	12	1.26	734	0.146	0.048578	2.021	0.109048	2.122	0.016281	0.268	0.431	127.53	47.54	105.09	2.12	104.11	0.28		

(a) A, B etc. are labels for fractions composed of single zircon grains or fragments; all fractions annealed and chemically abraded after Mattinson (2005) and Scoates and Friedman (2008).
 (b) Model Th/U ratio calculated from radiogenic $^{208}\text{Pb}/^{206}\text{Pb}$ ratio and $^{207}\text{Pb}/^{235}\text{U}$ age.
 (c) Pb* and Pb_c represent radiogenic and common Pb, respectively; mol % $^{206}\text{Pb}^*$ with respect to radiogenic, blank and initial common Pb.
 (d) Measured ratio corrected for spike and fractionation only. Mass discrimination of 0.25%/amu based on analysis of NBS-982; all Daly analyses.
 (e) Corrected for fractionation, spike, and common Pb; up to 1.0 pg of common Pb was assumed to be procedural blank: $^{206}\text{Pb}/^{204}\text{Pb} = 18.50 \pm 1.0\%$; $^{207}\text{Pb}/^{204}\text{Pb} = 15.50 \pm 1.0\%$; $^{208}\text{Pb}/^{204}\text{Pb} = 38.40 \pm 1.0\%$ (all uncertainties 1-sigma). Excess over blank was assigned to initial common Pb, using the Stacey and Kramers (1975) two-stage Pb isotope evolution model at 104 Ma.
 (f) Errors are 2-sigma, propagated using the algorithms of Schmitz and Schoene (2007) and Crowley et al. (2007).
 (g) Calculations are based on the decay constants of Jaffey et al. (1971). $^{206}\text{Pb}/^{238}\text{U}$ and $^{207}\text{Pb}/^{206}\text{Pb}$ ages corrected for initial disequilibrium in $^{230}\text{Th}/^{238}\text{U}$ using Th/U [magma] = 3.
 (h) Corrected for fractionation, spike, and blank Pb only.
 (i) Nominal fraction weights estimated from photomicrographic grain dimensions, adjusted for partial dissolution during chemical abrasion.
 (j) Nominal U and total Pb concentrations subject to uncertainty in photomicrographic estimation of weight and partial dissolution during chemical abrasion.

Table 5. U-Th-Pb isotopic data for sample MMI13-29-7.

Compositional Parameters										Radiogenic Isotope Ratios						Isotopic Ages							
Wt.	U	Pb	Th	$^{206}\text{Pb}^*$	mol %	Pb*	Pb _c	^{206}Pb	^{207}Pb	$^{206}\text{Pb}/^{207}\text{Pb}$	^{206}Pb	^{235}U	% err	^{238}U	% err	corr.	^{207}Pb	^{206}Pb	^{206}Pb				
mg	ppm	ppm	ppm	$\times 10^{-13}$	mol	Pb _c	(pg)	^{204}Pb	^{206}Pb	^{206}Pb	^{206}Pb	^{235}U	% err	^{238}U	% err	coef.	^{235}U	^{238}U	^{238}U				
(a)	(j)	(j)	(b)	(c)	(c)	(c)	(c)	(d)	(e)	(e)	(e)	(e)	(f)	(e)	(f)	(f)	(g)	(f)	(g)	(f)			
MMI13-29-7																							
A	0.001	1291	47.9	0.814	1.3746	98.93%	31	1.20	1733	0.258	0.050017	0.910	0.220188	0.956	0.031928	0.141	0.396	195.77	21.14	202.07	1.75	202.61	0.28
B	0.001	252	9.2	0.743	0.4670	98.69%	24	0.51	1408	0.235	0.049784	1.545	0.218264	1.651	0.031797	0.159	0.691	184.93	35.97	200.46	3.00	201.79	0.32
C	0.001	741	12.3	0.415	0.3304	97.88%	14	0.59	873	0.133	0.048040	1.627	0.101294	1.736	0.015292	0.168	0.672	101.24	38.47	97.97	1.62	97.84	0.16
D	0.000	657	12.6	0.444	0.1326	95.25%	6	0.54	390	0.140	0.047577	6.321	0.105971	6.706	0.016154	0.447	0.871	78.31	150.07	102.27	6.52	103.30	0.46
E	0.000	1175	45.0	0.833	0.3102	97.79%	15	0.58	839	0.266	0.050372	0.889	0.219953	0.970	0.031669	0.190	0.506	212.21	20.61	201.87	1.78	200.99	0.37

(a) A, B etc. are labels for fractions composed of single zircon grains or fragments; all fractions annealed and chemically abraded after Mattinson (2005) and Scoates and Friedman (2008).

(b) Model Th/U ratio calculated from radiogenic $^{208}\text{Pb}/^{206}\text{Pb}$ ratio and $^{207}\text{Pb}/^{235}\text{U}$ age.

(c) Pb* and Pb_c represent radiogenic and common Pb, respectively; mol % $^{206}\text{Pb}^*$ with respect to radiogenic, blank and initial common Pb.

(d) Measured ratio corrected for spike and fractionation only. Mass discrimination of 0.25‰/amu based on analysis of NBS-982; all Daly analyses.

(e) Corrected for fractionation, spike, and common Pb; up to 1.2 pg of common Pb was all assumed to be procedural blank: $^{206}\text{Pb}/^{204}\text{Pb} = 18.50 \pm 1.0\%$; $^{207}\text{Pb}/^{204}\text{Pb} = 15.50 \pm 1.0\%$;

$^{208}\text{Pb}/^{204}\text{Pb} = 38.40 \pm 1.0\%$ (all uncertainties 1-sigma).

(f) Errors are 2-sigma, propagated using the algorithms of Schmitz and Schoene (2007) and Crowley et al. (2007).

(g) Calculations are based on the decay constants of Jaffey et al. (1971). $^{206}\text{Pb}/^{238}\text{U}$ and $^{207}\text{Pb}/^{206}\text{Pb}$ ages corrected for initial disequilibrium in $^{230}\text{Th}/^{238}\text{U}$ using Th/U [magma] = 3.

(h) Corrected for fractionation, spike, and blank Pb only.

(i) Nominal fraction weights estimated from photomicrographic grain dimensions, adjusted for partial dissolution during chemical abrasion.

(j) Nominal U and total Pb concentrations subject to uncertainty in photomicrographic estimation of weight and partial dissolution during chemical abrasion.

Table 6. U-Th-Pb isotopic data for sample MMI13-4-8.

Compositional Parameters										Radiogenic Isotope Ratios						Isotopic Ages							
Wt.	U	Pb	Th	$^{206}\text{Pb}^*$	mol %	Pb*	Pb _c	^{206}Pb	^{207}Pb	$^{206}\text{Pb}/^{207}\text{Pb}$	^{206}Pb	^{235}U	% err	^{238}U	% err	corr.	^{207}Pb	^{206}Pb	^{206}Pb				
mg	ppm	ppm	ppm	$\times 10^{-13}$	mol	Pb _c	(pg)	^{204}Pb	^{206}Pb	^{206}Pb	^{206}Pb	^{235}U	% err	^{238}U	% err	coef.	^{235}U	^{238}U	^{238}U				
(a)	(j)	(j)	(b)	(c)	(c)	(c)	(c)	(d)	(e)	(e)	(e)	(e)	(f)	(e)	(f)	(f)	(g)	(f)	(g)	(f)			
MMI13-4-8																							
A	0.0190	48	1.3	0.566	0.9530	99.68%	96	0.25	5801	0.180	0.049214	0.163	0.171247	0.234	0.025237	0.130	0.738	158.05	3.82	160.50	0.35	160.67	0.21
B	0.0052	224	6.1	0.458	1.2500	99.15%	36	0.86	2181	0.145	0.049192	0.413	0.174538	0.473	0.025733	0.157	0.524	157.00	9.67	163.35	0.71	163.79	0.25
C	0.0032	338	9.1	0.424	1.1561	99.20%	37	0.76	2322	0.135	0.049234	0.395	0.174107	0.456	0.025648	0.154	0.540	159.01	9.25	162.98	0.69	163.25	0.25
D	0.0045	313	8.4	0.456	1.5045	99.36%	47	0.79	2886	0.145	0.049269	0.299	0.174317	0.360	0.025660	0.144	0.588	160.66	6.99	163.16	0.54	163.33	0.23
E	0.0032	165	4.5	0.509	0.5628	98.91%	28	0.49	1701	0.161	0.048968	1.321	0.172604	1.407	0.025565	0.144	0.636	146.30	30.96	161.68	2.10	162.73	0.23

(a) A, B etc. are labels for fractions composed of single zircon grains or fragments; all fractions annealed and chemically abraded after Mattinson (2005) and Scoates and Friedman (2008).

(b) Model Th/U ratio calculated from radiogenic $^{208}\text{Pb}/^{206}\text{Pb}$ ratio and $^{207}\text{Pb}/^{235}\text{U}$ age.

(c) Pb* and Pb_c represent radiogenic and common Pb, respectively; mol % $^{206}\text{Pb}^*$ with respect to radiogenic, blank and initial common Pb.

(d) Measured ratio corrected for spike and fractionation only. Mass discrimination of 0.25‰/amu based on analysis of NBS-982; all Daly analyses.

(e) Corrected for fractionation, spike, and common Pb; up to 0.9 pg of common Pb was all assumed to be procedural blank: $^{206}\text{Pb}/^{204}\text{Pb} = 18.50 \pm 1.0\%$;

$^{208}\text{Pb}/^{204}\text{Pb} = 38.40 \pm 1.0\%$ (all uncertainties 1-sigma).

(f) Errors are 2-sigma, propagated using the algorithms of Schmitz and Schoene (2007) and Crowley et al. (2007).

(g) Calculations are based on the decay constants of Jaffey et al. (1971). $^{206}\text{Pb}/^{238}\text{U}$ and $^{207}\text{Pb}/^{206}\text{Pb}$ ages corrected for initial disequilibrium in $^{230}\text{Th}/^{238}\text{U}$ using Th/U [magma] = 3.

(h) Corrected for fractionation, spike, and blank Pb only.

(i) Nominal fraction weights estimated from photomicrographic grain dimensions, adjusted for partial dissolution during chemical abrasion.

(j) Nominal U and total Pb concentrations subject to uncertainty in photomicrographic estimation of weight and partial dissolution during chemical abrasion.

Table 7. Laser ablation analysis results for sample 12JLO51-4.

Age estimates with 1 sigma uncertainty (Ma)							
Analysis No.	$^{207}\text{Pb}/^{235}\text{U}$		$^{206}\text{Pb}/^{238}\text{U}$		$^{207}\text{Pb}/^{206}\text{Pb}$		
	Ma	$\pm 1\sigma$ Error	Ma	$\pm 1\sigma$ Error	Ma	$\pm 1\sigma$ Error	
PL1	338.7	5.49	337.4	2.62	334.3	40.78	
12JLO51-4	2	223.3	5.48	221.5	2.19	284	59.18
	3	220.3	15	220.2	4.95	232.8	155.74
	4	219.3	22.42	222.2	6.18	203.2	233.62
	5	223	6.6	224.1	2.54	251.3	70.16
	6	215.8	12.54	212.4	4.09	374.3	132.62
	7	221.7	8.65	218.6	2.9	228.2	92.3
	8	219.3	13.9	218.7	4.72	152.7	145.64
	9	229.2	9.7	222.3	3.21	298.3	98.9
	10	217.2	13.73	217.2	4.55	243.7	145.69
	11	226.7	12.22	216.8	3.8	272	124.97
	12	208.1	11.23	208	3.78	301.5	124.39
	13	229.7	6.48	228.9	2.58	228.3	66.6
	14	227.3	13.32	224	4.78	388	128.95
	15	225.8	20.58	221.5	6.96	291.7	199.81
	16	231.2	11.49	230.6	4.2	225.2	112.9
	17	241.9	14.58	233.6	5.26	473	131.21
	18	229.6	11.65	226.8	4.13	217	115.93
	19	225.3	11.39	222	4.02	243.7	115.46
	20	225.4	13.82	224	4.59	259.3	139.47
	21	225.8	15.62	226.9	5.56	147.4	156.54
	22	231.7	14.89	227.4	5.26	420.7	141.07
	23	215	11.68	215.9	4.04	300.8	123.41
	24	208.6	9.08	210.6	3.47	192.2	99.75

Table 8. U-Th-Pb isotopic data by laser ablation for sample MMI13-16-3.

Grain Number	$^{207}\text{Pb}/^{235}\text{U}$		$^{206}\text{Pb}/^{238}\text{U}$		CE *vs**	$^{206}\text{Pb}/^{238}\text{U}$		$^{207}\text{Pb}/^{206}\text{Pb}$		$^{207}\text{Pb}/^{235}\text{U}$	
	$\pm 2\sigma^*$	$\pm 2\sigma^{**}$	$\pm 2\sigma$	$\pm 2\sigma$		$\pm 2\sigma$	$\pm 2\sigma$	$\pm 2\sigma$	$\pm 2\sigma$	$\pm 2\sigma$	$\pm 2\sigma$
MMI13_16_3_1	0.212	0.020	0.03297	0.0016	0.079557	208.9	9.8	0.0491	0.004	197	16.0
MMI13_16_3_2	0.239	0.020	0.03313	0.0015	0.17834	209.9	9.3	0.0529	0.004	214.8	16.0
MMI13_16_3_3	0.225	0.019	0.0328	0.0015	0.28517	207.9	9.4	0.0495	0.004	202.9	16.0
MMI13_16_3_4	0.2276	0.017	0.03268	0.0014	0.21927	207.5	8.7	0.0507	0.003	208	14.0
MMI13_16_3_5	0.233	0.017	0.03324	0.0014	0.56452	210.7	8.8	0.0512	0.003	212.5	14.0
MMI13_16_3_6	0.2182	0.018	0.03195	0.0014	0.30674	202.6	8.9	0.0501	0.003	199.2	15.0
MMI13_16_3_7	0.2383	0.017	0.03421	0.0015	0.65598	216.7	9.3	0.05133	0.003	217.8	14.0
MMI13_16_3_8	0.2277	0.017	0.03361	0.0015	0.39965	213	9.3	0.0495	0.003	208.5	14.0
MMI13_16_3_9	0.2389	0.017	0.03429	0.0014	0.37134	217.5	9.0	0.0507	0.003	216.9	14.0
MMI13_16_3_10	0.2284	0.018	0.03286	0.0015	0.18967	208.3	9.5	0.0504	0.003	209.4	15.0
MMI13_16_3_11	0.2138	0.016	0.03191	0.0014	0.36845	202.4	8.7	0.0489	0.003	196.6	13.0
MMI13_16_3_12	0.2359	0.018	0.03477	0.0018	0.72474	220.2	11.0	0.0484	0.003	215	14.0
MMI13_16_3_13	0.224	0.017	0.0331	0.0015	0.66294	209.8	9.6	0.0489	0.003	205.6	14.0
MMI13_16_3_14	0.224	0.018	0.03358	0.0016	0.33965	212.8	9.7	0.0486	0.003	205.9	15.0
MMI13_16_3_15	0.2199	0.017	0.03286	0.0014	0.34091	208.3	8.9	0.0478	0.003	202.2	14.0
MMI13_16_3_16	0.25	0.025	0.034	0.0017	0.30709	215.3	11.0	0.0531	0.005	224	20.0
MMI13_16_3_17	0.2336	0.018	0.03401	0.0017	0.6308	215.5	11.0	0.0494	0.003	213.1	14.0
MMI13_16_3_18	0.225	0.019	0.03308	0.0015	0.35251	209.7	9.4	0.0486	0.003	205.6	15.0
MMI13_16_3_19	0.239	0.030	0.0359	0.0022	0.096084	227	13.0	0.0522	0.007	214	24.0
MMI13_16_3_20	0.232	0.019	0.03292	0.0015	0.12325	208.7	9.5	0.0516	0.003	211.9	15.0

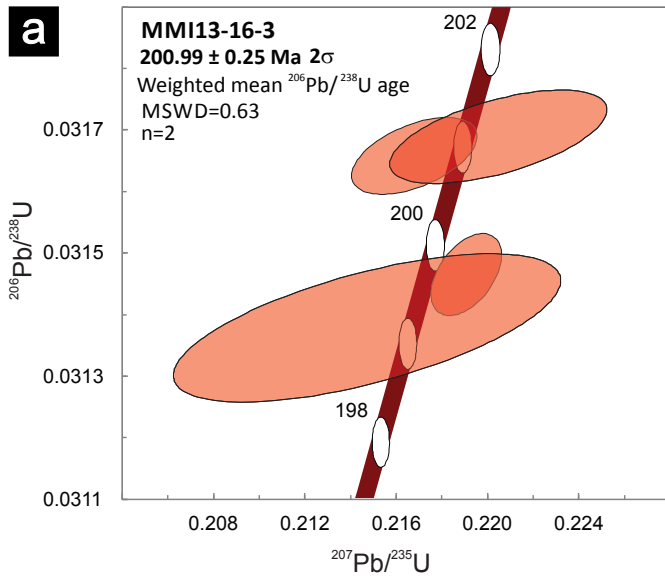


Fig. 18. a) Thermal Ionization Mass Spectrometric (TIMS) analysis of zircon U-Pb from sample MMI13-16-3 of dike in b) yields an age of 202 ± 4 Ma based on two overlapping fractions on concordia. Slightly younger grains are discordant. Data point error ellipses are 2σ . **b)** Near-vertical, fine-grained dike cuts maroon and green volcanic sandstone and granule conglomerate (black arrow marks southeast contact).

swarm was previously mapped as part of the Bromley pluton, but the lithologic character and dike orientation more closely resemble those of the ‘Mine dikes’, well exposed to the south, and dated at 102.9 ± 0.3 Ma at the Copper Mountain mine (Mihalynuk et al., 2010). To confirm this reassignment, we collected a sample for age determination. Analysis of 5 grains extracted show that they mutually overlap concordia at 103.9 ± 0.2 Ma with no hints of inheritance (Fig. 20b), and are most likely genetically related to the Mine dike swarm.

9.4.5. Southwest Zone, Miner Mountain: Sample MMI13-29-7

Following previous unsuccessful attempts at U-Pb dating of

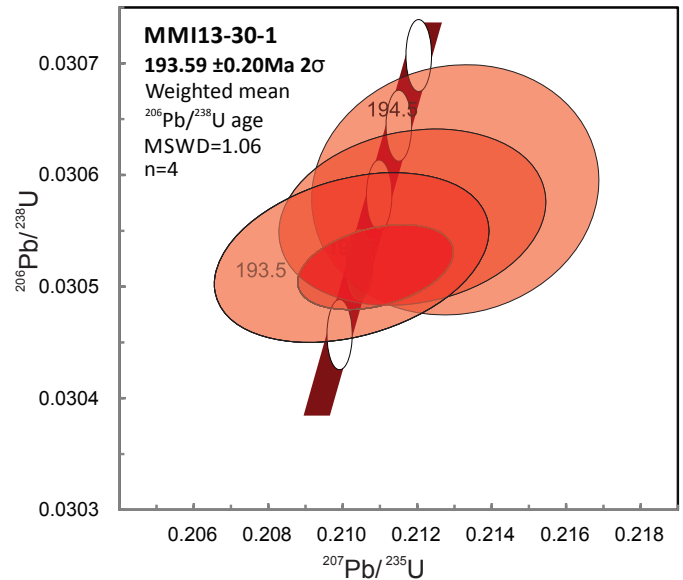


Fig. 19. Thermal Ionization Mass Spectrometric (TIMS) analysis of zircon U-Pb from sample MMI13-30-1 of pegmatitic dikes west of the Bromley pluton. An age of 193.6 ± 0.3 Ma is based on four overlapping fractions on concordia.

intrusions at Miner Mountain due to zircon poor-lithologies, we processed two boxes of core from the Southwest Zone that had been sawn in half (drillhole DDH13, 3.45 m to 11.11 m). Only 7 zircon grains were recovered (five were faceted and 2 subrounded, Fig. 21a), five of these survived chemical abrasion pre-treatment and were analysed (Fig. 21b; Table 5). They yielded a broadly bimodal spread of results: three overlap concordia at ca. 200-203 Ma ($\text{Th}/\text{U} = 0.74\text{-}0.83$), and two at ca. 98-103 Ma ($\text{Th}/\text{U} = 0.42\text{-}0.44$). The older population is interpreted as having inherited xenocrystic material and the younger as largely primary magmatic zircon that records the crystallization of this intrusion. The more subtle spread of ages within each of the two groupings may be due to minor Pb loss not mitigated through chemical abrasion pre-treatment, a physical mixture of populations (minor older cores in younger grains or younger rims on older grains), or a combination of the two. It is not possible with the current data to confidently choose between these possibilities, so we conservatively assign a crystallization age of $\sim 100 \pm 3$ Ma for this rock, with ~ 200 Ma inheritance.

9.4.6. Osprey Lake batholith: Sample MMI13-4-8

Sample MMI13-4-8 (Table 6; Fig. 22) is from grey-weathering, porphyritic granodiorite that cuts and thermally metamorphosed flow-banded rhyolite and andesite breccia in the headwaters of Swanson Creek. Mihalynuk and Logan (2014a) mapped the volcanic package as Early Cretaceous because of strong similarity and continuity with the suite of rocks farther west (e.g. Monger, 1989) and interpreted the porphyritic intrusion as belonging to the younger Summers Creek suite of intrusions, which has returned K-Ar cooling ages of ~ 98 Ma (Preto, 1979; recalculated in Breitsprecher

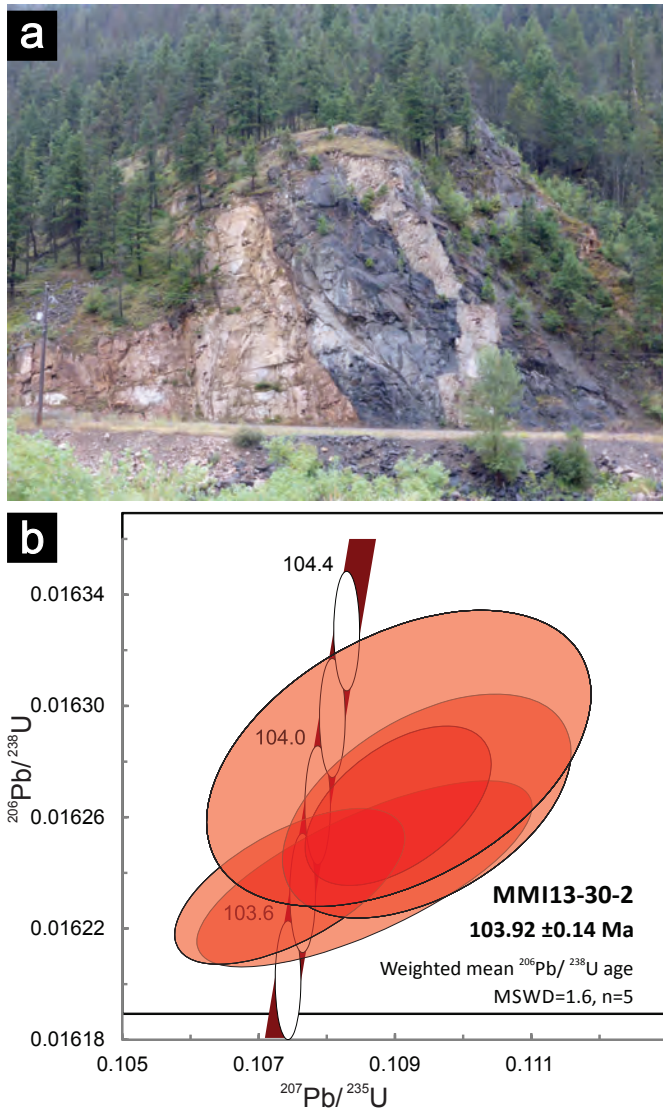


Fig. 20. a) View to south, across the Similkameen River; north-trending 'Mine dikes' (pink) cut dark green volcanosedimentary Nicola Group country rocks. **b)** Concordia plot shows cluster of 5 grains analyzed from 'Mine dike' sample MMI13 30-2 at 103.9 ± 0.2 Ma.

and Mortensen, 2005). However, zircons extracted from the intrusion overlap concordia between 160 Ma and 164 Ma (Fig. 22a) requiring the volcanic package to be Late Jurassic or older. To ensure that the TIMS ages were not erroneously old as a consequence of older xenocrystic cores, 11 grains were examined by cathodoluminescence (Fig. 22b) and the rims and cores of 10 grains were analyzed by laser ablation (LA-ICPMS). Neither cathodoluminescence, nor laser dating revealed any evidence of cores or strong overgrowths. Rather, these analyses confirm the TIMS ages with a weighted age for 9 of the 10 zircons at 162 ± 2 Ma (range from 156–167 Ma ± 5 Ma for individual analyses; see Mihalynuk et al., 2015 for the complete dataset). One grain yielded a slightly younger age ($\sim 145 \pm 5$ Ma); however there is no evidence of younger, ~ 100 Ma rims on any of the zircons.

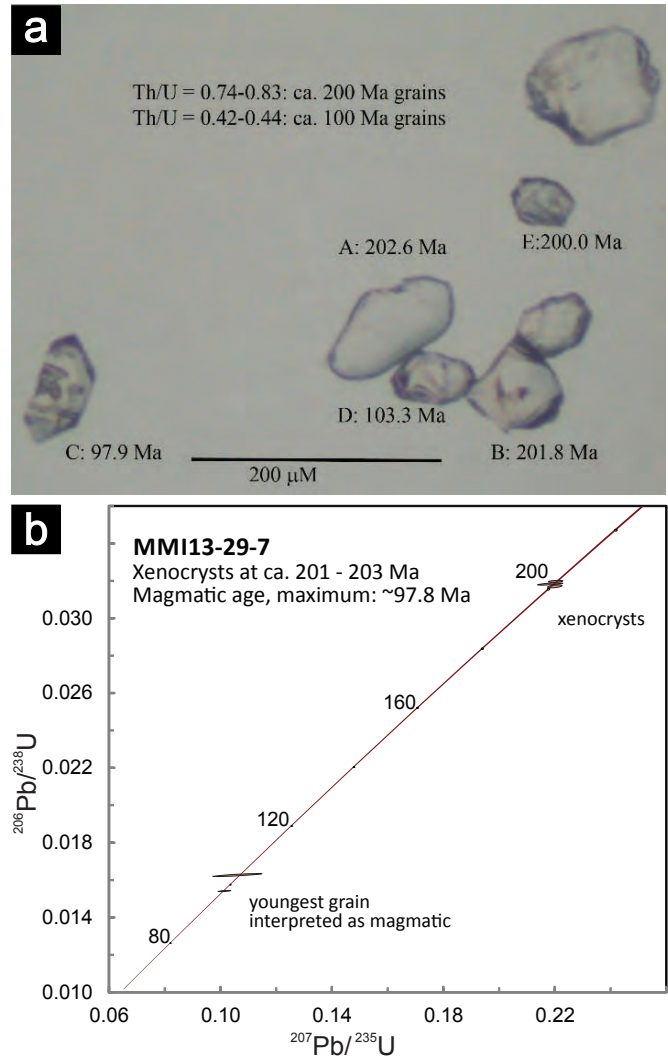


Fig. 21. a) Photomicrograph of zircons from sample MMI13-29-7 of drill core intersected by drilling at Miner Mountain, southwest zone prior to chemical abrasion. **b)** Thermal Ionization Mass Spectrometric (TIMS) analysis of zircon U-Pb. Multiple fractions lie on concordia. The age of this intrusion is most likely ~ 98 Ma; it contains ~ 200 Ma xenocrystic zircons.

We have collected the rhyolite with the aim of confirming a previously unrecognized older felsic volcanic package in the Swanson Creek area as required by the age data. A corollary is that the porphyritic intrusion is part of the huge Osprey Lake batholith with a U-Pb crystallization age of 166 ± 1 Ma (Parrish and Monger, 1992). Analyses are pending.

9.4.7. Detrital zircon analysis of Voght unit sandstone: Samples JLO12-51-4 and MMI13-16-5

Two samples of maroon sandstone (Tables 7 and 8; Fig. 23) interpreted to bracket deposition of the Voght unit, were collected from sites along the Coquihalla Highway that are separated by ~ 9 km. The samples were submitted for detrital zircon analysis by LA-ICPMS to determine maximum depositional ages as given by the youngest zircon. In active

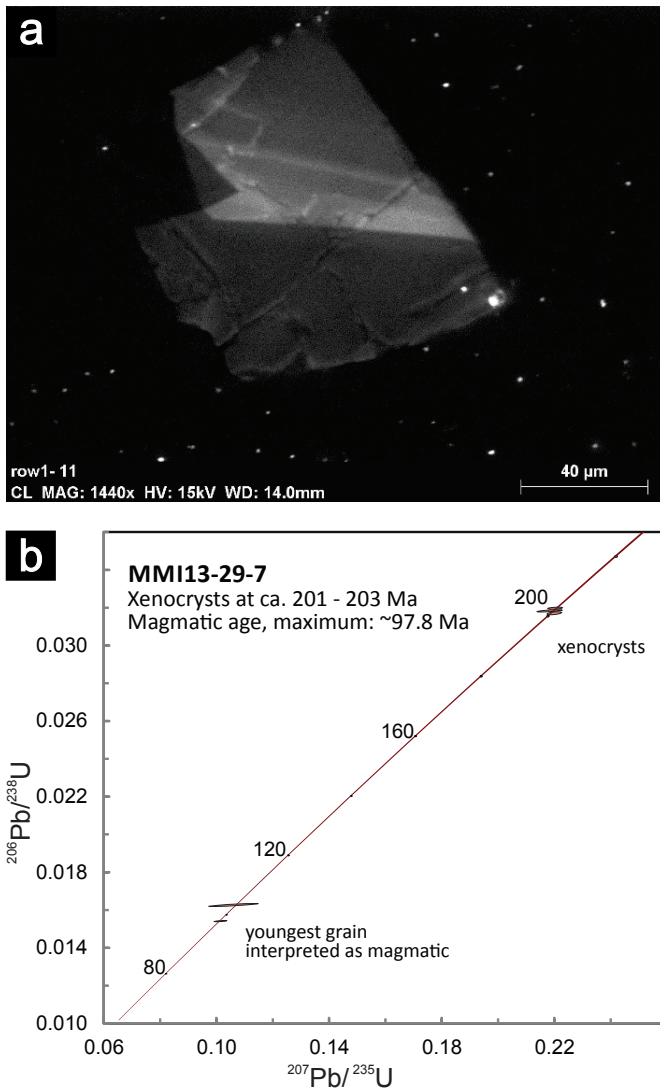


Fig. 22. **a)** Concordia plot for sample MMI13-4-8 of porphyritic granodiorite. **b)** Cathodoluminescent image of a zircon extracted for follow-up LA-ICPMS dating. Growth bands are visible, but evidence of overgrowths or a xenocrystic core are lacking.

volcanic terranes, the age of the youngest detrital zircons commonly closely corresponds to the actual depositional age, given the error of the analytical technique and time scale uncertainties (e.g. Evenchick et al., 2010).

Twenty zircons were analyzed from each sample and the age of youngest zircons date the Voght unit between 208 ± 4 Ma (Fig. 23a) and 202 ± 4 Ma (Fig. 23b). Including 1σ errors, this age spans most of the late Norian (Late Triassic) through to the Hettangian (earliest Jurassic, IUGS timescale, Cohen et al., 2013). However, the younger age is further constrained as being older than $201 +0.3/-0.4$ Ma, based on the TIMS age determination of the cross-cutting dike (sample MMI13-16-5; Fig. 18a, see above), making the entire Voght section Late Triassic. Pillow breccia intercalated with the inferred older part of the succession, is probably of Middle Norian age (~208 Ma).

10. Structure

Evidence for contractional deformation can be found at all scales in layered rocks of the Shrimpton map area. However, the lack of continuous exposures means that large-scale structures must be inferred from regional strike and dip information combined with outcrop distribution patterns. For example, a faulted, open, north-northeast-trending, mountain-scale anticlinal hinge that occupies the Kane Valley has been defined by tracing out a previously unmapped carbonate unit. This anticline parallels the general structural grain in the region (Fig. 3).

Observations of outcrop-scale folds are mostly limited to new exposures, mainly roadcuts. Massive bedrock incisions along the Coquihalla Connector (Highway 97C) are especially instructive because the highway cuts across strike. For example, west of the Loon Lake turnoff are excellent new exposures of folded strata and near-bedding parallel fault zones interpreted as thrust faults (Fig. 24a). Most thrusts appear to cut up section to the east. An exception to east-directed thrust faults are those interpreted to carry Triassic strata westward over the Bates unit. Because most thrust faults cannot be traced along strike, amounts of shortening across them are unconstrained.

Ductile fabrics are developed in the thermal metamorphic halo around the Early Jurassic Pennask batholith, but are lacking, except within tens of m of the contact around the even more extensive Osprey batholith. For example, within about 1km of the Pennask contact, incipient chlorite-actinolite schistosity is developed in the Boot Lake unit of the Paradise succession, along with discrete dextral and sinistral shear zones (Fig. 24b).

Most ocean lithosphere subduction beneath volcanic arcs today is non-orthogonal. Such oblique subduction results in strain partitioning: the normal component causes shortening concentrated in the accretionary complex and forearc, and the arc-parallel component causes transverse faulting concentrated along the hot, weak, arc axis (McCaffrey et al., 2000). Shortening in the Nicola arc accretionary complex is recorded by Cache Creek Group rocks exposed well to the west of the map area (Savona to Cache Creek; Monger and McMillan, 1989). Transverse faulting expected along the arc axis is probably recorded by the Summers and Allison creeks faults; possibly long-lived, steep fault systems that have long been recognized (Preto, 1979, Monger, 1989, and others). This >160km-long fault system is suspected to have focused emplacement of mineralized Late Triassic plutons (Preto, 1979). However, the question of the amount of offset has not been addressed.

Distinctive biotite-quartz-apatite-phyrlic volcanic units of the Zig unit, and clastic rocks derived from it, have not been recognized south of the Shrimpton area (e.g. Preto, 1979; Mihalynuk et al., 2014), nor are we aware of the unit having been mapped to the north (e.g. Preto, 1967, 1979; Kwong, 1987; Logan and Mihalynuk, 2005a, b). Assuming that these workers have not overlooked the distinctive rock units, it would appear that the units do not extend tens to hundreds

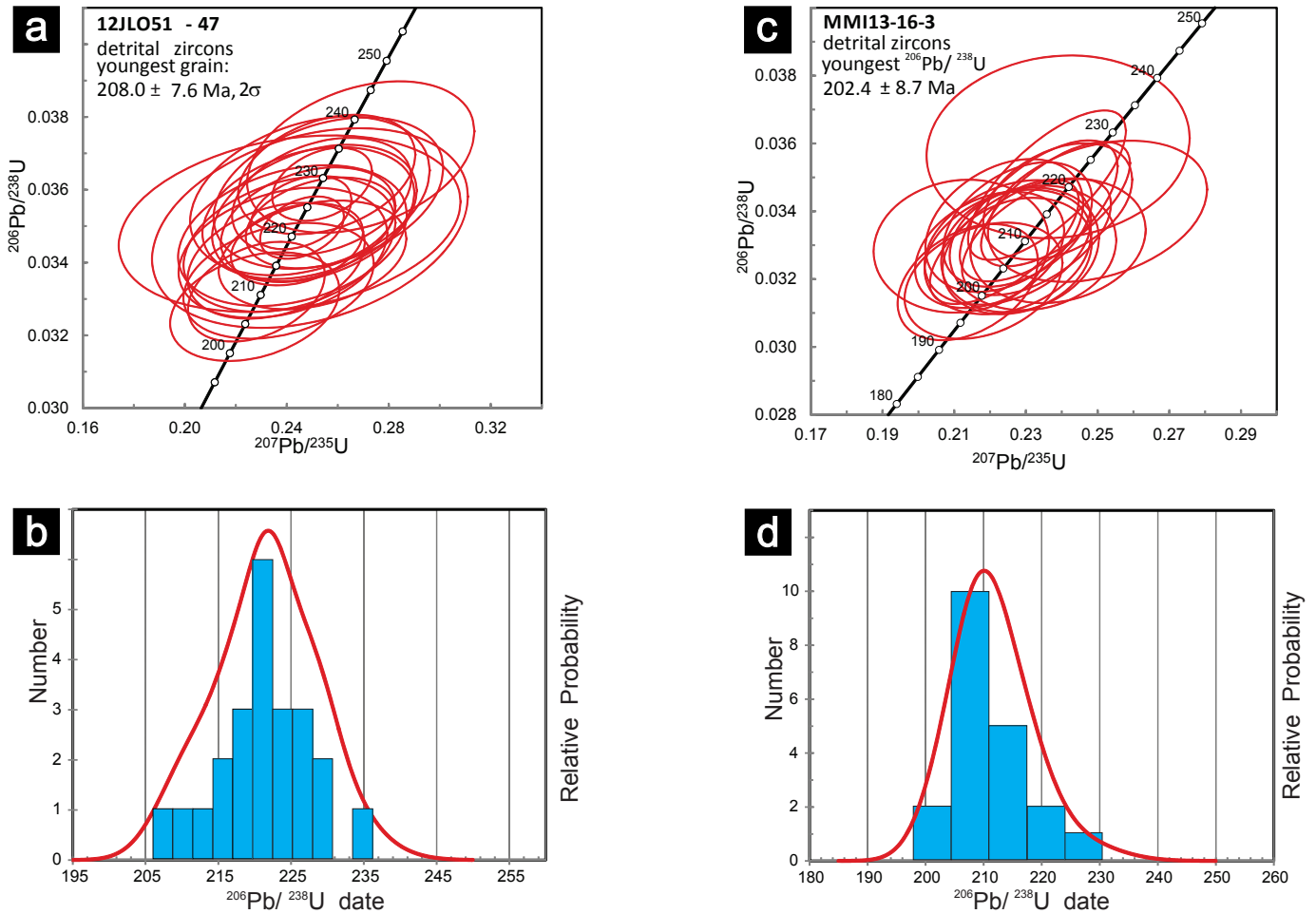


Fig. 23. a) Concordia plot and b) histogram of detrital zircon ages from the approximate base of the Voght unit maroon volcanic sandstone. c) Concordia plot and d) histogram of detrital zircon ages from the upper Voght unit. Both samples are Late Triassic (229-201 Ma; Cohen et al., 2013).

of kilometres along the arc. Rather, the Zig unit and derived clastic rocks may be restricted to the Shrimpton area on both sides of northern strands of the Summers Creek Fault, known as the Kentucky-Alleyne Fault through much of the Shrimpton Creek map area. This is an important observation, because if accurate, it severely limits offset on the fault. Although offset on Summers Creek Fault was apparently insufficient to displace the Zig unit and derived clastic units, offset prior to Zig unit deposition is unconstrained. Kentucky-Alleyne Fault strands must swing west of the Pennask batholith, as is shown by Preto (1979), because the trace of the batholith's southern contact can now be extended almost as far west as Pothole Lake (Fig. 3).

At the southern border of the Shrimpton map area, the Allison Creek Fault cuts the Allison pluton, appears to juxtapose Spences Bridge Group with the intrusion, and may have been active during deposition of the Cretaceous volcanic succession, as discussed by Mihalynuk et al. (2014a). Amounts of Late Triassic and younger offset on the Allison Creek fault are limited by the amount of apparent offset of the Allison pluton. Because the pluton is elongated subparallel to the fault (Fig. 3) and intrusive contacts with country rocks are largely obscured

by cover, the amount of apparent lateral offset along the Allison Creek fault cannot be estimated with certainty. However, it is probably less than 10 km.

11. Mineralization

More than 100 years of active exploration in the Shrimpton area has resulted in discovery of more than 130 MINFILE occurrences. One of the first showings to be explored in the Aspen Grove Copper Camp was the Big Sioux. It was staked in 1899, developed by underground workings and produced hand-sorted ore containing copper minerals that included chalcopyrite, bornite, malachite, chalcocite and cuprite. Historical mineral production since those early days reportedly came from three mineral deposit types; placer gold (Shrimpton Creek, MINFILE 092HNE180 and Siwash Creek, MINFILE 092HNE290), Au-quartz veins (Elk, (Siwash Mine) MINFILE 092HNE096) and alkalic porphyry Cu-Au-Ag (Big Sioux, MINFILE 092HNE073 and Copper Star, 092HNE036).

Major exploration and development programs were completed by three mining companies in the Shrimpton area in 2014. Bulk sample mining, begun in 2013 by Gold Mountain



Fig. 24. **a)** Folding and thrust faulting of Shrimpton succession wacke unit west of the Loon Lake turnoff, Coquihalla Highway. Thrust fault (red dotted line) juxtaposes near-vertical beds in footwall against subhorizontal beds in hanging wall. **b)** Incipient foliation in hornblende-pyroxene conglomerate of the Boot Lake unit.

Mining Corp. at their Elk Project (Siwash Mine), was completed this fall with shipment of 6668 tonnes of mineralized material expected to yield an average grade of 17.3 g/t Au (Gold

Mountain Mining Corporation, 2014). The Au-Ag mineralized pyritic quartz veins are thought to be Tertiary and related to Otter intrusions (Pooley et al., 2011). Fjordland Exploration Inc. completed a preliminary soil sampling and 2070 m surface trenching program (East Dillard) followed by a 14-hole, 5,574 m diamond drill program on both Dillard East and Dillard West porphyry copper-gold targets, approximately 15 km southwest of the Elk Project. Kaizen Discovery Inc. carried out a diamond drilling program at their Par prospect (described below), following-up on the results of a 2013 geological mapping and sampling program completed by West Cirque Resources Ltd. (Kaizen Discovery Inc., 2014).

We limit our discussion below primarily to undocumented, possibly new, occurrences and to existing MINFILE occurrences with new observations or geochemical analyses (Table 9) to report.

11.1. Par prospect (MINFILE 092HNE169)

Kaizen Discovery Inc. completed 2,012 metres of diamond drilling in four holes that tested 880 metres of potential VMS mineralized strike length on their Par prospect, in

Table 9. ICP-MS analytical results for select samples and elements.

StatNum	Type	UTM E	UTM N	Ag	As	Au	Ba	Bi	Co	Cs	Cu	Fe	Hg	In	Mn	Mo	Ni	Pb	Re	S	Sb	Se	Te	Zn
				ppb	ppm	ppb	ppm	ppm	ppm	ppm	ppm	%	ppb	ppm	ppm	ppm	ppm	ppm	ppb	%	ppm	ppm	ppm	ppm
GMc14-05-13	1.3m chip	687575	5513992	387	5.9	54.8	33	0.23	13.8	2.76	287.33	4.95	51	<0.02	116	2.09	23	2.52	8	2.7	0.39	1.8	1.05	18.1
GMc14-05-13b	20cm chip	687575	5513992	450	44.7	23.6	93.6	0.16	10.3	8.01	136.75	3.81	120	0.05	938	1.27	21	3.39	7	1.25	3.37	0.7	0.51	29.2
GMc14-61-3	Assay grab	670558	5502382	303	4.8	73.8	26.6	1.57	20.9	0.19	178.14	3.71	<5	0.04	216	0.27	36	1.88	1	2.65	0.14	0.4	0.94	26.3
MM14-02-6	3m chip	672712	5532632	3767	37.7	3.6	46.1	0.37	23.8	0.3	>10000.00	3.12	121	<0.02	756	0.95	12	1.11	2	0.07	0.65	0.9	0.29	55.2
MM14-09-7	Assay grab	681991	5524340	269	2.1	1.3	153.5	0.16	17.7	2.48	153.91	3.26	<5	0.03	978	1.15	26	2.82	2	0.24	0.39	1.6	0.03	50.2
MM14-18-4	chip	682905	5558331	68084	27.3	322.8	17.8	0.48	10.8	0.18	>10000.00	6.53	73	0.11	684	117.1	11	35.29	<1	0.27	1.11	8.8	7.12	106.9
MM14-19-6	Assay grab	685541	5517303	282	0.8	122.2	37.6	0.04	12.8	1.63	466.75	3.09	16	<0.02	446	0.11	5.6	0.59	<1	<0.02	<0.02	<0.1	0.08	40
MM14-24-12	Assay grab	676868	5516880	1209	21.6	170.1	547.4	0.05	24.6	0.18	4765.58	5.67	15	<0.02	1476	0.84	5.3	15.91	<1	0.03	0.1	1.8	<0.02	161.2
MM14-39-1	Assay grab	678706	5521179	53	3.5	1.8	14.9	<0.02	8	0.41	252.91	2.13	34	<0.02	659	0.21	3.4	1.93	<1	0.06	0.24	<0.1	0.05	34.2
MM14-41-07	Assay grab	676505	5525203	250	19.9	3.3	84.9	0.14	17.1	1.48	3294.72	4.19	8	0.03	1106	0.47	8.9	2.7	<1	<0.02	0.21	<0.1	<0.02	88.5
MM14-41-10	Assay grab	675935	5525883	112	7.8	4.5	23.5	0.03	7.5	0.07	12.69	2.87	107	<0.02	469	3.12	2.3	6.92	5	1.38	0.3	0.4	0.04	22
MM14-50-09b	Assay grab	666460	5507872	86078	15.5	5	4134.1	0.96	16.4	4.22	1758.81	2.61	628	<0.02	416	0.27	55	996.8	2	0.1	135.9	0.2	0.37	482.7
MM14-50-09c	Assay grab	666460	5507872	28464	2.3	4.4	5399.3	0.26	10	3.89	541.77	1.99	151	<0.02	229	0.46	28	194	<1	0.09	19.65	<0.1	0.14	256.4
MM14-50-10	Assay grab	666492	5507891	255	4.9	2.8	60	0.04	80.4	18.11	51.27	6.36	<5	0.02	734	0.7	334	18.55	<1	<0.02	1.67	<0.1	0.03	301.9
MM14-50-11	Assay grab	666450	5507870	>100000	21.5	2	>10000.0	0.55	5	1.07	1900.27	1.01	430	0.02	223	0.82	20	4714	<1	0.06	217.9	0.2	0.61	194.6
MM14-52-07	Assay grab	666944	5505292	243	<0.1	0.5	313.1	0.05	1.4	0.06	17.05	1.52	<5	<0.02	68	10.02	1.1	10.02	22	0.22	0.59	0.4	0.06	8.8
MM14-54-02	Assay grab	692527	5516847	21564	16.6	75.2	15.8	4.58	10.3	0.58	1425.57	5.52	425	22.69	814	2.91	1.4	874	2	7.33	3.81	2.7	0.22	>10000.0
MM14-54-11	Assay grab	698019	5515139	2422	2.1	<0.2	30.5	0.18	11.7	0.4	62.47	3.6	14	0.03	8382	0.26	41	3257	<1	1.28	0.61	<0.1	0.1	3242.4
MM14-54-13a	Assay grab	698021	5515146	388	0.5	1.1	9.4	0.12	4	0.11	3.92	1.63	<5	<0.02	>10000	2.95	12	544.7	<1	0.93	0.17	<0.1	0.03	543.8
MM14-54-13b	Assay grab	698021	5515146	295	0.8	1.1	58.5	0.04	6.8	0.39	15.9	2.17	<5	<0.02	5530	19.2	7.6	130.5	2	0.76	0.31	<0.1	0.02	411.7
MM14-50-10	grab dup	666492	5507891	273	4.6	1.4	64.6	0.03	68.8	19.24	49.85	6.74	<5	<0.02	729	0.56	351	19.28	<1	<0.02	1.68	<0.1	<0.02	302.1
MM14-50-10	grab dup	666492	5507891	285	5.1	1.1	66.2	<0.02	74.1	19.09	48.67	7.13	<5	<0.02	782	0.63	376	19.17	<1	<0.02	1.64	<0.1	<0.02	312.1
Detection Limit				2	0.1	0.2	0.5	0.02	0.1	0.02	0.01	0.01	5	0.02	1	0.01	0.1	0.01	1	0.02	0.02	0.1	0.02	0.1

southeast Shrimpton Creek map area. The mineralization and alteration observed in core indicates at least two styles of mineralization; a hybrid high-level porphyry-high sulfidation epithermal system; and volcanogenic massive sulfides (Kaizen Discovery Inc., 2014). The alkalic porphyry/breccia type Cu-Au-Mo mineralization appears to be superimposed on the early synvolcanic mineralization. Mineralization includes massive to semi-massive intervals of copper, zinc, silver, gold and molybdenum-bearing sulphides. It is contained in broad intervals of intense silicification, and phyllic and advanced argillic alteration zones in high-level quartz-feldspar porphyry intrusions and related felsic volcanic and volcanoclastic rocks (Kaizen Discovery Inc., 2014).

11.2. Ketchan Lake North prospect (MINFILE 092HNE115)

The Ketchan Lake North porphyry Cu-Au-Ag-Pd±Pt prospect is in the southeast part of the Shrimpton Creek map area, where maroon pyroxene-olivine-analcite phytic volcanic rocks are intruded by a high-level, northwest-trending alkaline monzodiorite intrusion, (Ketchan Lake stock; Fig. 25). Pyroxene-biotite diorite and hornblende±pyroxene monzodiorite to monzonite are the main intrusive phases; mineralization is focused in the monzonite. Sub-circular breccia pipes with magnetite-healed breccias and elevated Cu and Au values intrude the intrusive complex. Analyses of two samples of Ketchan Lake mineralization were reported in Mihalynuk et al. (2014a). Sample JLO13-23-8 (Zone 10, NAD83; 676833 E, 5516535 N) is a brecciated hornblende monzonite healed by anastomosing K-spar and magnetite and overprinted by shallow, east-trending epidote fracture fillings and replacement zones. Sample JLO13-23-9 (Zone 10, NAD83; 676763 E, 5516564 N) is a pervasive K-spar and albite altered monzonite cut by mm to cm steep, north-trending veinlets of chalcopyrite±pyrite with pink K-spar vein selvages. Higher gold and silver values have a direct relationship to higher copper values. Analyses of Ketchan Lake mineralization also reveals some of the highest Pt (35 ppb) and Pd (323 ppb) values in the study area (Mihalynuk et al. 2014a, Table 1).

The Ketchan Lake stock is one of several alkalic intrusive centers in the Shrimpton map area, including Big Kidd (Fig. 2; MINFILE 092HNE074). All are undated but are presumed correlative with the alkalic Copper Mountain Intrusive Suite (<205 Ma) that hosts the Copper Mountain, New Afton and Mount Polley mines in southern British Columbia.

11.3. Snowstorm prospect (MINFILE 092HNE032)

The Snowstorm prospect, also known as the Siwash Creek property, is classified in MINFILE as a shear-related vein. However, little evidence of a major shear zone is present: mineralization occupies dilatant quartz-calcite-sphalerite-galena±chalcopyrite vein stockworks and is broadly related to strongly clay altered porphyritic ‘Otter intrusion’. The base metal veins at the Snowstorm may have formed distal to a buried porphyry system, a model that has been partly tested by Cu and Mo geochemical surveys (Banks, 1980) and a regional

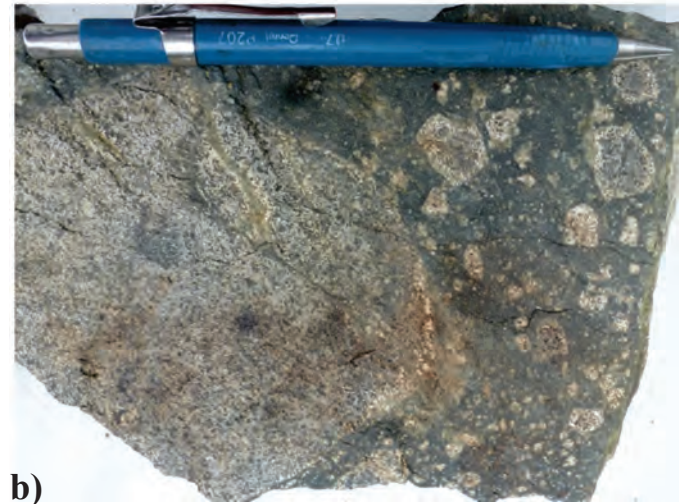
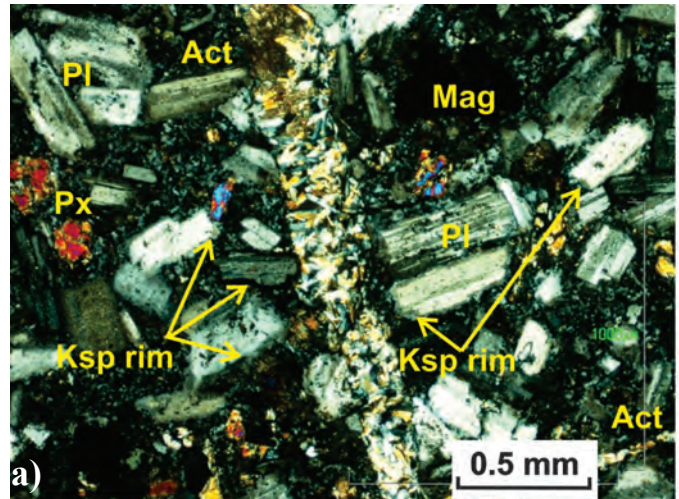


Fig. 25. a) Photomicrograph of Ketchan Lake stock. Pyroxene-hornblende and stubby plagioclase porphyritic monzodiorite flooded by secondary K-spar and cross-cut by actinolite and calcite (violets), cross polarized light. **b)** Chlorite+magnetite matrix supported monzodiorite intrusive breccia.

drilling campaign by Brenda Mines (Groves, 1989).

Old dumps, tracks and collapsed adits are relicts of underground mining dating to 1917, when most work entailed drifting along the veins. According to Groves (1989), 27 tons of ore shipped to Trail in 1927 yielded 3 oz. gold, 3,379 oz. silver, and 1,578 lbs of lead. We sampled well-mineralized vein material on surface from above the collapsed main adit (Fig. 3; sample MMI14-54-02). It contained element values consistent with the observed sulphide mineralogy: i.e. >10,000 ppm Zn, 874 ppm Pb, 21.6 ppm Ag, and significantly, 22.7 ppm In (Table 9). Indium does not form primary mineral deposits but elevated values commonly accompany sphalerite mineralization (Briskey, 2005).

11.4. Margerri

Chocolate-coloured carbonate-cemented breccia of fine feldspar porphyry dikes and clay-altered, pyritic quartz-feldspar porphyry locally contains mm-thick veinlets of galena, sphalerite, and chalcopryite at the Margerri showing (Fig. 26a). Analysis of three mineralized samples range up to 0.32% Zn, 0.32% Pb and 2.4 ppm Ag. Alteration mineralogy and intrusive texture of the porphyry are similar to the host porphyry at the Snowstorm (Fig. 26b). Analysis of predominantly matrix material (Table 9, MMI14-54-13a) returned >1% Mn, 1.6% Fe and 2.83% Ca, suggesting that the matrix material comprises a brown weathering Mn-Fe oxide intergrown with calcite. Margerri is not catalogued in MINFILE, and there is no indication that it has been sampled previously; although any sample collection markings may have been removed because the breccia is in a small borrow pit, actively being used as road ballast. Approximately 100 m to the north, similar mineralization is exposed at a logging landing (Fig. 26c).

11.5. DaBren

In the northwestern part of the Summers Creek map area, broken outcrops along the Pike Mountain logging road (Fig. 2; Mihalynuk et al., 2014a) include blocks of quartz \pm carbonate-barite veins up to 35 cm thick. Quartz contains outlines of bladed, 1 to 2 cm-long crystals interpreted to be silicified carbonate. Mineralization occurs as blebs and discontinuous veinlets of sphalerite and chalcopryite and dark grey, vein-parallel banding. Analysis of mineralized samples returned Pb and high Ag values, perhaps indicative of argentiferous galena (Table 9, MMI12-50-09b, c: up to 0.5% Ba, 0.17% Cu, 0.1% Pb, 0.04% Zn and 86 ppm Ag). Our samples returned only low Au contents (up to 5 ppb). This epithermal precious metal vein occurrence is not catalogued in MINFILE.

11.6. Leeman

Rubbly, rust and copper-stained quartz vein scree occurs near the crest of a low glacial ridge in the grassland between Quilchena and the northeast corner of the Shrimpton map area (Fig. 2). Excavation of the vein revealed that it is up to 35 cm thick and has chalcopryite along banded margins and a cockscomb interior. Host rocks are tan, well-bedded cherty argillite and siltstone. A composite chip sample was taken across the vein from two sites separated by ~3 m. ICP-MS analysis (MMI14-18-4; Table 9) shows that the vein contains elevated Au (0.3 ppm), Ag (68 ppm), Cu (>1%) and Zn (0.01%). This precious and base metal-rich vein is not catalogued in MINFILE.

12. Conclusions

Geological fieldwork between Princeton and Merritt in 2014 extended 2013 mapping in the Summers Creek area northward to the Shrimpton Creek area, covering NTS sheets 092H/15E and 16W. Field and laboratory results arising from this work have changed the way we perceive the Late Triassic arc and its overlying strata.

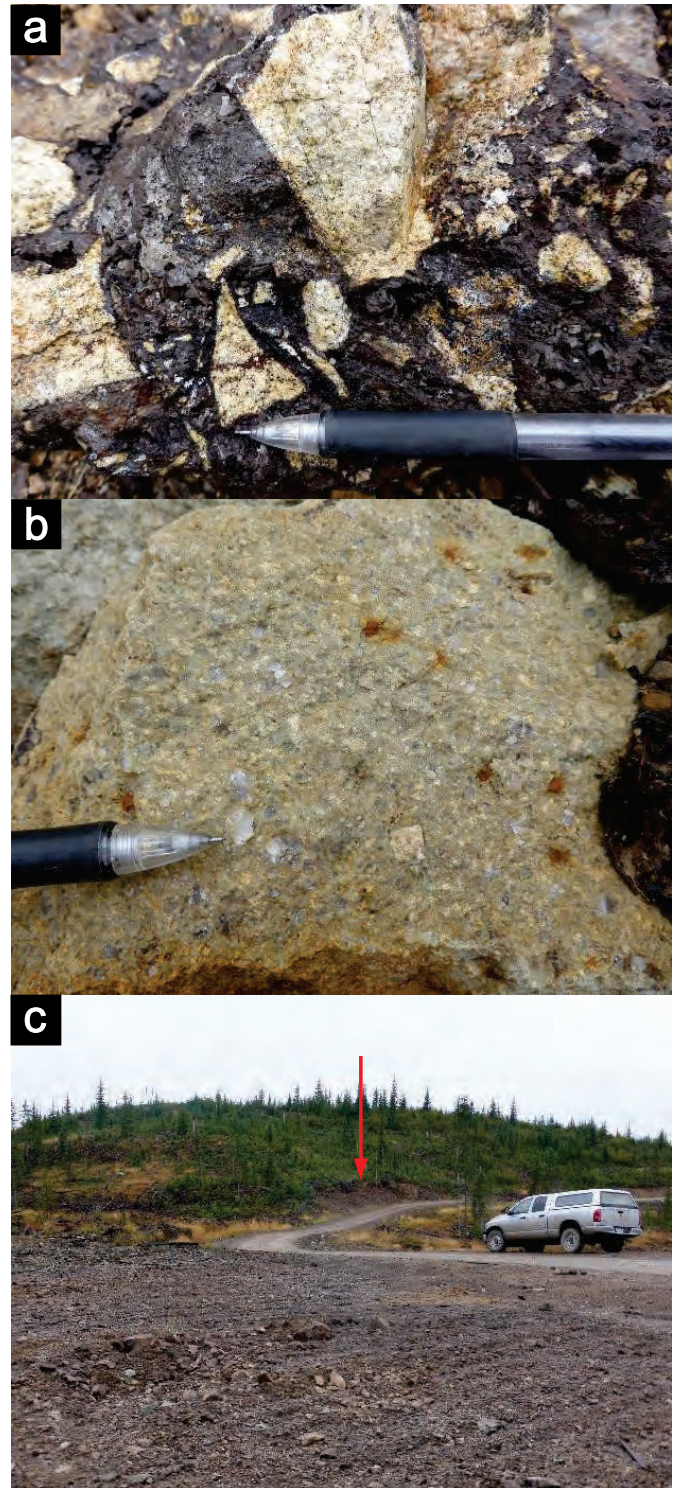


Fig. 26. a) Chocolate-coloured Mn-Fe oxide and carbonate interstitial to angular fragments of altered quartz-feldspar porphyry. b) Clay-altered quartz-feldspar porphyry is similar to host rocks at the Snowstorm prospect. c) Main mineralized breccia in borrow pit at Margerri is beyond the corner in the road (arrow) and similar mineralization is found as disturbed subcrop at the logging landing in the foreground.

Nicola arc strata are both older and younger than previously recognized. A new U-Pb crystallization age of ~238 Ma from a rhyolite tuff in the Central belt (Preto, 1979) is the oldest dated unit in the Nicola Group.

Felsic volcanism, previously thought to be characteristic of Preto's (1979) Western belt extends into the Central belt.

The 'Zig unit', a newly recognized distinctive biotite-quartz-apatite porphyry, and clastic rocks derived from it, span the Summers Creek fault, limiting significant motion on the fault to before ~210 Ma.

A marker succession recognized in the Kane Valley permits definition of a regional anticline.

Mainly eastward-vergent contractional deformation is recorded by thrust faults and folds that are well displayed in sedimentary successions.

Three base and precious metal vein occurrences not catalogued in MINFILE were encountered during 2014 mapping. The extent and importance of these occurrences has yet to be determined, but they are indicative of the mineral potential still to be uncovered in the southern Nicola arc.

Acknowledgments

We are indebted to past workers in the southern Nicola arc, especially J.W.H. Monger and V.A. Preto, both of whom have generously shared their time and knowledge with us in the field. Discussions and property and drill core visits with Siwash geologists, Brad Benoit and Oliver Saunders, and Tyler Ruks of Kaizen Discovery Inc. greatly aided our understanding of the Siwash gold deposit and the Par prospect.

References cited

- Armstrong, R. L., and Peto, P., 1981. Eocene quartz-feldspar porphyry intrusions west of Okanagan Lake, southern B.C.: K-Ar dates and Sr isotopic composition. *Northwest Geology*, 10, 13-19.
- Banks, P.C., 1980. Geological and geochemical surveys on the Siwash Creek copper property. In: British Columbia Ministry of Energy, Mines, and Petroleum Resources, Assessment Report 7,987.
- Beatty, T.W., Orchard, M.J., Mustard, P.S., 2006. Geology and tectonic history of the Quesnel Terrane in the area of Kamloops, British Columbia. In: Colpron, M. and Nelson, J.L., (Eds.), *Paleozoic Evolution and Metallogeny of Pericratonic Terranes at the Ancient Pacific Margin of North America*, Canadian and Alaskan Cordillera: Geological Association of Canada, Special Paper 45, pp. 483-504.
- Belasky, P., Stevens, C.H., and Hanger, R.A., 2002. Early Permian location of western North American terranes based on brachiopod, fusulinid, and coral biogeography. *Palaeogeography, Palaeoclimatology and Palaeoecology*, 179, 245-266.
- Bergey, W.R., 1999. Report on geological survey, PAR claims. In: BC Ministry of Energy, Mines, and Petroleum Resources, Assessment Report #25,965.
- Bordet, E., Mihalynuk, M.G., Hart, C.J.R., Mortensen, J.K., Friedman, R.M., and Gabites, J., 2013. Chronostratigraphy of Eocene volcanism, central British Columbia. *Canadian Journal of Earth Sciences*, 51, 56-103. doi:10.1139/cjes-2013-0073
- Breitsprecher, K., Mortensen, J.K., 2004. BCAGE 2004A-1: A database of isotopic age determinations for rock units from British Columbia. British Columbia Ministry of Energy and Mines, British Columbia Geological Survey Open, Open File 2004-3.
- Briskely, J.A., 2005. Indium in zinc-lead and other mineral deposits: a reconnaissance survey of 1118 Indium analyses published before 1985. United States Geological Survey, Open-File Report 2005-1209, 8p.
- Brown, R., and Journeay, J., 1987. Tectonic denudation of the Shuswap metamorphic terrane of southeastern British Columbia. *Geology*, 15, 142-146. doi:10.1130/0091-7613(1987)15<142:TDO TSM>2.0.CO;2
- Campbell, R.B., 1966. Tectonics of the south central cordillera of British Columbia. In: *Tectonic History and Mineral Deposits of the Western Cordillera*. Canadian Institute of Mining, Special Volume, 8, pp. 61-72.
- Christopher, P.A., 1973. Preliminary geological map of the Aspen Grove area, British Columbia, BC Ministry of Energy Mines and Petroleum Resources, British Columbia Geological Survey Preliminary Map No. 10.
- Cohen, K.M., Finney, S.C., Gibbard, P.L., and Fan, J.X., 2013. The ICS international chronostratigraphic chart. *Episodes*, 36, 199-204.
- Crowley, J.L., Schoene, B. and Bowering, S.A., 2007. U-Pb dating of zircon in the Bishop Tuff at the millennial scale. *Geology*, 35,, 1123-1126.
- Diakow, L.J. and Barrios, A., 2008. Geology, Spences Bridge Group southwest of Merritt, British Columbia (parts of NTS 092H/14, 15 and 092I/2,3); BC Ministry of Energy Mines and Petroleum Resources, British Columbia Geological Survey Open File 2008-8, 1:50 000 scale.
- Diakow, L.J. and Barrios, A., 2009. Geology and mineral occurrences of the mid-Cretaceous Spences Bridge Group near Merritt, southern British Columbia (parts of NTS 092H/14, 15; 092I/2, 3). In: *Geological Fieldwork 2008*, British Columbia Ministry of Energy Mines and Petroleum Resources, British Columbia Geological Survey Paper 2009-1, pp. 63-79.
- Enkin, R.J., 2006. Paleomagnetism and the case for Baja British Columbia. In: Haggart, J.W., Enkin, R.J., and Monger, J.W.H. (Eds.), *Paleogeography of the North American Cordillera: Evidence For and Against Large-Scale Displacements*. Geological Association of Canada, Special Paper 46, 233-253.
- Evenchick, C.A., Poulton, T.P. and McNicoll, V.J., 2010. Nature and significance of the diachronous contact between the Hazelton and Bowser Lake groups (Jurassic), north-central British Columbia. *Bulletin of Canadian Petroleum Geology*, 58, 235-267.
- Ferri, F., 1997. Nina Creek Group and Lay Range Assemblage, north-central British Columbia: remnants of late Paleozoic oceanic and arc terranes. *Canadian Journal of Earth Sciences*, 34, 854-874. doi:10.1139/e17-070
- Fjordland Exploration Inc., 2014. Fjordland and Sumac Drill 153 Metres Grading 0.20% Copper and 0.09 g/t Gold on Dillard Property, Southern British Columbia, press release, November, 18, 2014, <http://www.fjordlandex.com/news/nr14-13.pdf>.
- Gerstenberger, H., and Haase, G., 1997. A highly effective emitter substance for mass spectrometric Pb isotopic ratio determinations. *Chemical Geology*, 136, 309-312.
- Gold Mountain Mining Corporation, 2014. Gold Mountain bulk sample lot 2 gold grade at 22.8 gpt: Gold Mountain Mining Corporation, press release, November 17, 2014, http://www.aumtn.com/cms/wpcontent/uploads/2014/11/2014_11_17_Gold_Mountain_Press_Release_Bulk_Sample_Lot_2_Gold_Grade_22_gpt.pdf.
- Gourlay, A.W. 1991. Zig property reverse circulation percussion drilling. In: BC Ministry of Energy, Mines, and Petroleum Resources, Assessment Report #21,406.
- Grove, E.W., 1989. Geological report & work proposal on the Siwash creek property. In: British Columbia Ministry of Energy, Mines, and Petroleum Resources, Assessment Report, 19.
- Harms, T.A., 1986. Structural and tectonic analysis of the Sylvester allochthon, northern British Columbia; implications for paleogeography and accretion. Ph.D. Thesis, University of

- Arizona.
- Henderson, M.A., Mihalynuk, M.G., Creaser, R.A., and Logan, J.M., 2015. Microthermometry and Re-Os age of Cu-Ag mineralization at the Zig prospect, southern Quesnel Terrane. In: Geological Fieldwork 2014, British Columbia Ministry of Energy, Mines and Natural Gas, British Columbia Geological Survey Paper 2015-1, (this volume).
- Hunt, P.A., and Roddick, J.C., 1990. A compilation of K–Ar ages: report 19. In: Radiogenic Age and Isotopic Studies, Report 3. Geological Survey of Canada, Paper 89-02, 153-190.
- Ickert, R.B., Thorkelson, D.J., Marshall, D.D., and Ullrich, T.D., 2009. Eocene adakitic volcanism in southern British Columbia: remelting of arc basalt above a slab window. *Tectonophysics*, 464, 164-185.
- Jaffey, A.H., Flynn, K.F., Glendenin, L.E., Bentley, W.C., and Essling, A.M., 1971. Precision measurement of half-lives and specific activities of ²³⁵U and ²³⁸U. *Physics Review*, C4, 1889-1906.
- Kaizen Discovery Inc., 2014. Kaizen Discovery announces positive results of phase-one drilling at Aspen Grove Copper Project in British Columbia, Canada: multiple potential targets established for 2015 phase-two drilling. Kaizen Discovery Inc. press release, December, 10, 2014. http://www.kaizendiscovery.com/s/news_releases.asp?ReportID=687190&_Type=News-Releases&Title=Kaizen-Discovery-announces-positive-results-of-phase-one-drillingbrat-Aspen
- Kwong, Y.T.J., 1987. Evolution of the Iron Mask batholith and its associated copper mineralization: British Columbia Ministry of Energy, Mines and Petroleum Resources, British Columbia Geological Survey, Bulletin 77, 55p.
- Lefebvre, D.V., 1976. Geology of the Nicola Group in the Fairweather Hills, B.C., M.Sc. Thesis, Queen's University, 179p.
- Liu, L., Gurnis, M., Seton, M., Saleeby, J., Müller, R.D., and Jackson, J.M., 2010. The role of oceanic plateau subduction in the Laramide orogeny. *Nature Geoscience*, 3, 353-357.
- Livaccari, R.F., Burke, K., and Sengor, A.M.C., 1981. Was the Laramide orogeny related to subduction of an oceanic plateau? *Nature*, 289, 276-278.
- Logan, J.M. and Mihalynuk, M.G., 2005a. Regional geology and setting of the Cariboo, Bell, Springer and Northeast porphyry Cu-Au zones at Mount Polley, south-central British Columbia. In: Geological Fieldwork 2004, British Columbia Ministry of Energy and Mines, British Columbia Geological Survey Paper 2005-1, 249-270.
- Logan, J.M., and Mihalynuk, M.G., 2005b. Porphyry Cu-Au deposits of the Iron Mask batholith, southeastern BC. In: Geological Fieldwork 2004, British Columbia Ministry of Energy and Mines, British Columbia Geological Survey Paper 2005-1, 271-290.
- Logan, J.M., and Mihalynuk, M.G., 2014. Tectonic controls on early Mesozoic paired alkaline porphyry deposit belts (Cu-Au-Ag-Pt-Pd-Mo) within the Canadian Cordillera. *Economic Geology*, 109, 827-858.
- Ludwig, K.R., 2003. Isoplot 3.09: a geochronological toolkit for Microsoft Excel. Berkeley Geochronology Center, Special Publication 4, Berkeley.
- Massey, N.W.D., MacIntyre, D.G., Desjardins, P.J., and Cooney, R.T., 2005. Digital Geology Map of British Columbia: Whole Province. British Columbia Ministry of Energy, Mines, and Natural Gas, British Columbia Geological Survey, GeoFile 2005-1.
- Massey, N.W.D., and Dostal, J., 2013. Geochemistry of metabasalts from the Knob Hill complex and Anarchist Group in the Paleozoic basement to southern Quesnellia. British Columbia Ministry of Energy, Mines, and Natural Gas, British Columbia Geological Survey, GeoFile 2013-1.
- Mathews, W.H., 1989. Neogene Chilcotin basalts in south-central British Columbia: geology, ages, and geomorphic history. *Canadian Journal of Earth Sciences*, 26, 969-982. doi:10.1139/e89-078
- Mattinson, J.M., 2005. Zircon U-Pb chemical abrasion (CA-TIMS) method: combined annealing and multi-step partial dissolution analysis for improved precision and accuracy of zircon ages. *Chemical Geology*, 220, 47-66.
- McCaffrey, R., Zwick, P.C., Bock, Y., Prawirodirdjo, L., Genrich, J.F., Stevens, C.W., Puntodewo, S.S.O. and Subarya, C., 2000. Strain partitioning during oblique plate convergence in northern Sumatra: geodetic and seismologic constraints and numerical modeling. *Journal of Geophysical Research*, 105, 28,363-28,376.
- Mihalynuk, M.G., Nelson, J. and Diakow, L., 1994. Cache Creek terrane entrapment: oroclinal paradox within the Canadian Cordillera. *Tectonics*, 13, 575-595.
- Mihalynuk, M.G., Erdmer, P., Ghent, E.D., Archibald, D.A., Friedman, R.M., Cordey, F., Johannson, G.G., and Beanish, J., 1999. Age constraints for emplacement of the northern Cache Creek terrane and implications of blueschist metamorphism. In: Geological Fieldwork 1998, British Columbia Ministry of Energy, Mines and Petroleum Resources, British Columbia Geological Survey Paper 1999-1, 127-141.
- Mihalynuk, M., Erdmer, P., Ghent, E.D., Cordey, F., Archibald, D.A., Friedman, R.M., and Johannson, G.G., 2004. Coherent French Range blueschist: subduction to exhumation in <2.5 m.y.? *Geological Society of America Bulletin*, 116, 910-922.
- Mihalynuk, M.G., Logan, J., Friedman, R.M., and Preto, V.A., 2010. Age of mineralization and 'mine dykes' at Copper Mountain alkaline copper-gold-silver porphyry deposit (NTS 092H/07), south-central British Columbia. In: Geological Fieldwork 2009, British Columbia Ministry of Energy, Mines and Petroleum Resources, British Columbia Geological Survey Paper 2010-1, 163-172.
- Mihalynuk, M.G., Logan, J.M., 2013a. Geological setting of Late Triassic Cu-Au porphyry mineralization at Miner Mountain, Princeton. In: Geological Fieldwork 2012, British Columbia Ministry of Energy, Mines and Natural Gas, British Columbia Geological Survey Paper 2013-1, 81-96.
- Mihalynuk, M.G., Logan, J.M., 2013b. Geological setting of Late Triassic Cu-Au porphyry mineralization at the Dillard-Primer prospects near Merritt. In: Geological Fieldwork 2012, British Columbia Ministry of Energy, Mines and Natural Gas, British Columbia Geological Survey Paper 2013-1, 97-114.
- Mihalynuk, M.G., Logan, J.M., Diakow, L.J., Friedman, R.M., and Gabites, J., 2014a. Southern Nicola Arc Project (SNAP): preliminary results. In: Geological Fieldwork 2013, British Columbia Ministry of Energy and Mines, British Columbia Geological Survey, Paper 2014-1, 29-57.
- Mihalynuk, M.G., Friedman, R.M., Gabites, J.E., Logan, J.M., 2014b. Southern Nicola Arc Project 2013: Geochronological data. British Columbia Ministry of Energy and Mines, British Columbia Geological Survey, GeoFile 2014-3.
- Mihalynuk, M.G., Friedman, R.M. and Logan, J.M., 2015. Southern Nicola Arc Project 2014: geochronological data. British Columbia Ministry of Energy and Mines, British Columbia Geological Survey, GeoFile 2015-2.
- Monger, J.W.H., 1989. Geology, Hope, British Columbia. Geological Survey of Canada, Map 41-1989, sheet 1, scale 1:250 000.
- Monger, J.W.H. and McMillan, W.J., 1989. Geology, Ashcroft, British Columbia (92I). Geological Survey of Canada, Map 42-1989, sheet 1, scale 1:250 000.
- Monger, J.W.H., and Ross, C.A., 1971. Distribution of fusulinaceans in western Canadian Cordillera. *Canadian Journal of Earth Sciences*, 8, 259-278.
- Monger, J.W.H., Price, R.A., and Tempelman-Kluit, D.J., 1982. Tectonic accretion and the origin of the two major metamorphic and plutonic belts in the Canadian Cordillera. *Geology*, 10, 70–75.
- Mundil, R., Ludwig, K.R., Metcalfe, I., and Renne, P.R., 2004. Age and timing of the Permian mass extinctions: U/Pb dating of closed-

- system zircons. *Science*, 305, 1760-1763.
- Nance, R.D., Gutiérrez-Alonso, G., Keppie, J.D., Linnemann, U., Murphy, J.B., Quesada, C., Strachan, R.A., and Woodcock, N.H., 2012. A brief history of the Rheic ocean. *Geoscience Frontiers*, 3, 125–135.
- Nelson, W. and Walker, J.T., 1972. Combined Geological and Geophysical Report on the Adonis Property. In: BC Ministry of Energy, Mines, and Petroleum Resources, Assessment Report #04495.
- Nixon, G.T., Archibald, D.A., Heaman, L.M., 1993. ^{40}Ar - ^{39}Ar and U-Pb geochronometry of the Polar is Alaskan-type complex, British Columbia: precise timing of Quesnellia-North America interaction. In: Geological Association of Canada, Mineralogical Association of Canada, Annual Meeting, Program with Abstracts, Waterloo, ON, Canada, pp. A76.
- Parrish, R.R., Monger, J.W.H., 1992. New U-Pb dates from southwestern British Columbia. Geological Survey of Canada, Paper 91-2, Radiogenic Age Isotopic Studies Report, 5, 87-108.
- Patton, C., Hellstrom, J., Paul, B., Woodhead, J., and Hergt, J., 2011. Iolite: freeware for the visualization and processing of mass spectrometry data. *Journal of Analytical Atomic Spectroscopy*, 26, 2508-2518.
- Pooley, R., Lomas, S., Hawthorn, G., and Alexander, R.B., 2011. NI 43-101 technical report for a preliminary economic assessment on the Elk Gold Project, Merritt, British Columbia, Canada: prepared for Almaden Minerals and Beanstalk Capital Inc., 141p.
- Preto, V.A., 1979. Geology of the Nicola Group between Merritt and Princeton: British Columbia Ministry of Energy, Mines and Petroleum Resources, British Columbia Geological Survey, Bulletin 69, 90p.
- Ray, G.E., and Dawson, G.L., 1994. The geology and mineral deposits of the Hedley gold skarn district, southern British Columbia. British Columbia Ministry of Energy, Mines and Petroleum Resources, Bulletin 87, 156p.
- Ray, G.E., Webster, I.C.L., Dawson, G.L., and Ettliger, A.D., 1993. A geological overview of the Hedley gold skarn district, southern British Columbia (92H). In: Geological Fieldwork 1992, British Columbia Ministry of Energy, Mines and Petroleum Resources, British Columbia Geological Survey Paper 1994-1, 269-279.
- Read, P.B., and Okulitch, A.V., 1977. The Triassic unconformity of south-central British Columbia. *Canadian Journal of Earth Sciences*, 14, 606-638.
- Rice, H.M.A., 1947. Geology and mineral deposits of the Princeton map area, British Columbia. Geological Survey of Canada, Memoir 243, 136p.
- Ricketts, B.D., Evenchick, C.A., Anderson, R.G., and Murphy, D.C., 1992. Bowser Basin, northern British Columbia: constraints on the timing of initial subsidence and Stikinia-North America terrane interactions. *Geology*, 20, 1119-1122.
- Ross, C.A., and Ross, J.R.P., 1983. Late Paleozoic accreted terranes of western North America. In: Stevens, C.H. (Ed.), *Pre-Jurassic Rocks in Western North American Suspect Terranes*. Society of Economic Paleontologists and Mineralogists, 7-22.
- Ross, C.A., and J.R.P. Ross., 1985. Carboniferous and Early Permian biogeography. *Geology*, 13, 27-30.
- Schau, M.P., 1968. Geology of the Upper Triassic Nicola Group in south central British Columbia. Ph.D. Thesis, The University of British Columbia, Vancouver, Canada, 211 p.
- Schmitz, M.D., and Schoene, B., 2007. Derivation of isotope ratios, errors, and error correlations for U-Pb geochronology using ^{205}Pb - ^{235}U -(^{233}U)-spiked isotope dilution thermal ionization mass spectrometric data. *Geochemistry, Geophysics, Geosystems*, 8, Q08006. doi:10.1029/2006GC001492
- Scoates, J.S. and Friedman, R.M., 2008. Precise age of the platiniferous Merensky Reef, Bushveld Complex, South Africa, by the U-Pb ID-TIMS chemical abrasion ID-TIMS technique, *Economic Geology*, 103, 465-471.
- Sigloch, K., Mihalynuk, M.G., 2013. Intra-oceanic subduction shaped the assembly of Cordilleran North America. *Nature*, 496, 50-56.
- Sláma, J., Košler, J., Condon, D.J., Crowley, J.L., Gerdes, A., Hanchar, J.M., Horstwood, M.S.A., Morris, G.A., Nasdala, L., Norberg, N., Schaltegger, U., Xchoene, B., Tubrett, M.N., and Whitehouse, M.J., 2007. Plešovice zircon - A new natural reference material for U-Pb and Hf isotopic microanalysis. *Chemical Geology*, 249, 1-35.
- Sluggett, C.L., 2008. Quaternary alkaline and calc-alkaline basalts in southern British Columbia: mixed signals from mantle sources above the southern edge of the Juan de Fuca-Pacific slab window. M.Sc. thesis, Simon Fraser University, Vancouver, Canada, 153p.
- Struik, L.C., Orchard, M.J., 1985. Late Paleozoic conodonts from ribbon chert delineate imbricate thrusts within the Antler Formation of the Slide Mountain terrane, central British Columbia. *Geology*, 13, 794-798.
- Tafti, R., Mortensen, J.K., Lang, J.R., Rebagliati, M., and Oliver, J.L., 2009. Jurassic U-Pb and Re-Os ages for newly discovered Xietongmen Cu-Au porphyry district, Tibet: implications for metallogenic epochs in the southern Gangdese Belt. *Economic Geology*, 104, 127–136.
- Thirlwall, M.F., 2000. Inter-laboratory and other errors in Pb isotope analyses investigated using a ^{207}Pb - ^{204}Pb double spike, *Chemical Geology*, 163, 299-322.
- Thompson, R.I., Glombick, P., Erdmer, P., Heaman, L.M., Lemieux, Y., and Daughtry, K.L., 2006. Evolution of the ancestral Pacific margin, southern Canadian Cordillera: insights from new geologic maps. In: Colpron, M., and Nelson, J.L. (Eds.), *Paleozoic Evolution and Metallogeny of Pericratonic Terranes at the Ancient Pacific Margin of North America*, Canadian and Alaskan Cordillera. Geological Association of Canada, Special Paper 45, 433-482.
- Thorkelson, D.J., and Rouse, G.E., 1989. Revised stratigraphic nomenclature and age determinations for mid-Cretaceous volcanic rocks in southwestern British Columbia. *Canadian Journal of Earth Sciences*, 26, 2016-2031.

Carlin-type geochemical signal in lake and stream sediments from the Kechika trough, north-central British Columbia

Alexei S. Rukhlov^{1,a}, Tian Han¹, JoAnne Nelson¹, Adrian S. Hickin¹, and Filippo Ferri²

¹British Columbia Geological Survey, Ministry of Energy and Mines, Victoria, BC, V8W 9N3

²Ministry of Natural Gas Development, 1810 Blanshard Street, Victoria, BC, V8W 9N3

^acorresponding author: Alexei.Rukhlov@gov.bc.ca

Recommended citation: Rukhlov, A.S., Han, T., Nelson, J., Hickin, A.S., and Ferri, F., 2015. Carlin-type geochemical signal in lake and stream sediments from the Kechika trough, north-central British Columbia. In: Geological Fieldwork 2014, British Columbia Ministry of Energy and Mines, British Columbia Geological Survey Paper 2015-1, pp. 165-188.

Abstract

Statistically robust treatment of multi-element geochemical data using simultaneous regression analysis, principal components analysis, and weighted sum indices can reveal economically significant anomalies that might otherwise be masked. Robust analysis of data from the National Geochemical Reconnaissance and the Regional Geochemical Survey programs document Au±As±Hg±Tl±Sb enrichment in stream and lake sediments from the Kechika trough, a long-lived (Neoproterozoic to Paleozoic) deep-water basin in north-central British Columbia. A similar enrichment is found in stream sediments sourced from recently discovered Carlin-type gold and realgar occurrences in Selwyn basin, the northward continuation of Kechika trough in the Rackla belt of east-central Yukon. In both areas, anomalous values are spatially related to platform to deep-water basin transitions and to extensional structures that originated during basin subsidence and then reactivated as thrusts during regional shortening. These anomalies and geologic setting are comparable to those of Carlin-type gold deposits of the Great Basin in Nevada. The Kechika trough may hold potential for Carlin-type deposits.

Keywords: Kechika trough, Selwyn basin, Carlin-type, Regional Geochemical Survey, stream- and lake-sediment geochemistry

1. Introduction

Eocene Carlin-type gold deposits (CTGD's) of the Great Basin in Nevada are some of the most prolific in the world (Muntean et al., 2011). In these deposits, gold occurs primarily in fine-grained (1-5 µm) arsenian pyrite and as µm-sized particles disseminated in quartz that are hosted by Paleozoic silty carbonate and siliceous sedimentary rocks altered by decarbonatization, silicification (jasperoid) and argillization processes. Enrichment in As-Hg-Tl-Sb±Te reflects realgar, orpiment, and stibnite in late-stage calcite veins that locally contain barite. Controlled both by stratigraphy and structure, the Carlin deposits have notably low Ag and base metal contents relative to spatially associated Paleozoic sedimentary exhalite (SEDEX) and Mesozoic to Cenozoic intrusion-related deposits. A widely accepted genetic model for CTGDs is lacking; both magmas and crust have been proposed as sources for auriferous fluids. Nonetheless, the Carlin deposits appear to mark intense hydrothermal activity from renewed magmatism in Great Basin between 42 and 34 Ma, during a change from regional shortening to extension (Arehart, 1996; Muntean et al., 2011).

Gold and realgar showings with similar stratigraphic and structural controls have recently been discovered in Proterozoic to Paleozoic strata of Selwyn basin in the Rackla belt, east-central Yukon (Fig. 1; ATAC Resources Ltd., 2010; Arehart et al., 2013; Tucker et al., 2013). These discoveries raise the possibility of similar occurrences in the Kechika trough, the southward continuation of Selwyn basin in north-central British

Columbia (Fig. 1; Poulsen, 1996). This study evaluates multi-element stream- and lake-sediment geochemical data to test the Carlin-type potential of the Kechika trough. These data were generated by the National Geochemical Reconnaissance (NGR; Friske et al., 1991a, b; Héon, 2003; Day et al., 2009; Jackaman, 2011b) and Regional Geochemical Survey (RGS; Jackaman et al., 1996; Lett et al., 1996; Cook et al., 1997, 1999; Jackaman, 2011a) programs. Our robust statistical treatment, which is validated by identifying geochemical signatures at known Carlin-type showings in the Rackla belt, highlights similar geochemical anomalies in the Kechika trough, suggesting that it holds potential for similar deposits.

2. Regional setting

2.1. Kechika trough

The Kechika trough, in the Foreland Fold and Thrust belt of the northern Canadian Cordillera, is a long-lived, deep-water basin that formed between the MacDonald platform to the east and the Cassiar platform to the west (Fig. 1; Gabrielse, 1962; 1963a, b; 1998; Ferri et al., 1999). Northward it connects to, and shares stratigraphic and structural elements with, the Selwyn basin in Yukon Territory (Fig. 1). The Kechika trough was filled with fine-grained, deep-water deposits that are equivalent to platform strata to the east. The oldest rocks in the basin include Neoproterozoic rift-related siliciclastic rocks (Hyland Group and Gataga volcanic rocks). The youngest strata consist of Cenozoic conglomerates, sandstones, and mafic volcanic rocks. Most of the study area is underlain by Cambrian to early

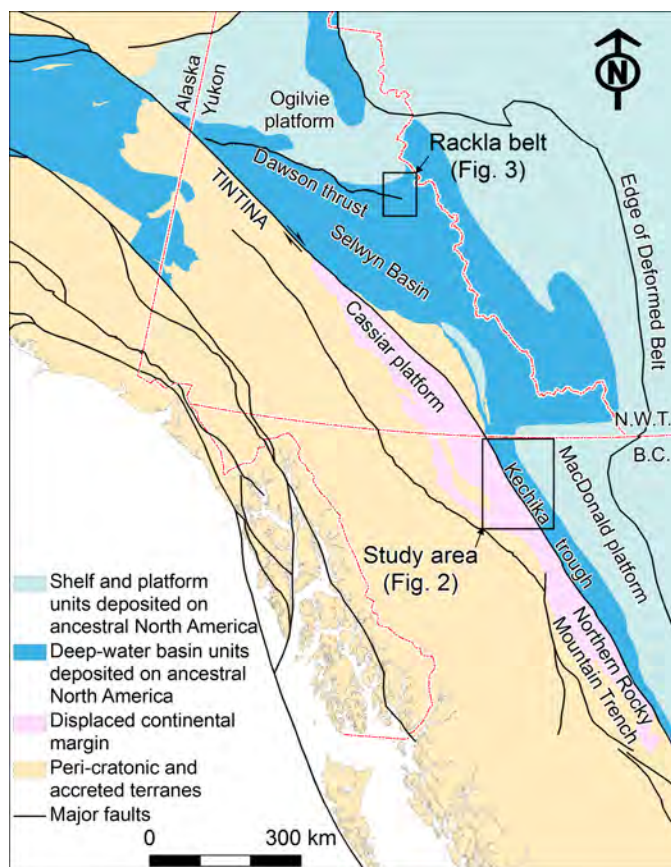


Fig. 1. Simplified geology and locations of Kechika trough study area in north-central British Columbia and the Rackla belt of Carlin-type Au mineralization in east-central Yukon.

Mississippian fine-grained siliciclastic and carbonate rocks (Gog, Kechika, Road River and Earn groups). Minor intrusive rocks include Early Paleozoic mafic sills and dikes and small Early Cretaceous to Eocene (?) granitic feldspar porphyry stocks, dikes and sills (Fig. 2).

Transitions from platform to deep-water sedimentation were probably controlled by syndepositional growth faults. Episodes of extension during the Paleozoic terminated at the end of the early Jurassic with the onset of compressional tectonics, which generated the predominantly easterly vergent thrusts and folds that characterize the northern Rocky Mountains. Some thrusts appear to be reactivated growth faults. For example, eruption of the Gataga volcanic rocks (ca. 690 Ma) was localized along a syndepositional fault; reactivated slip with a reverse sense during Jura-Cretaceous thrusting juxtaposed these rocks against strata as young as Devonian (Ferri et al., 1999).

SEDEX barite±sulphide mineralization is the most important mineral deposit type in the Kechika trough. These stratiform Zn-Pb-Ag-Ba deposits are in Cambrian, Middle Ordovician, Lower Silurian, and Upper Devonian strata (Fig. 2). The most significant are hosted by Upper Devonian shales, cherts, and slates in the lower part of the Earn Group. These include the Cirque (Stronsay), Driftpile Creek, Akie, Bear and Mount Alcock deposits. The trough also contains porphyry and skarn W-Mo±Cu mineralization related to early Cretaceous

intrusions (e.g., Boya showings) and sulphide vein Ag-Pb-Zn-Cu mineralization (Ferri et al., 1999).

2.2. Rackla belt

The Rackla belt is on the northern edge of Selwyn basin (Fig. 1). Most of the area is underlain by deep-water basin to shelf and slope strata. They consist of fine-grained siliciclastic and carbonate rocks, ranging from Neoproterozoic (Yusezyu, Algae, and Narchilla formations of the Hyland Group) to Devonian-Mississippian (Earn Group) and locally Carboniferous to Triassic strata (Fig. 3). Cambrian to Devonian platformal carbonate rocks overlie the Neoproterozoic strata north of the long-lived Dawson thrust zone and the Kathleen Lakes fault (Chakungal and Bennett, 2011; Colpron et al., 2013). Late Cretaceous and Paleocene felsic intrusions occur throughout Selwyn basin to the west and south of the area (Hart et al., 2004; Thiessen et al., 2012).

Similar to the Kechika trough, platform to deep-water basin transitions in the Rackla belt were controlled by syndepositional structures, as indicated by significant changes in thickness of Neoproterozoic strata across north-trending faults. Changes in Neoproterozoic to Paleozoic stratigraphy across the Dawson and Kathleen Lakes faults suggest fault reactivation in the Paleozoic, and during Mesozoic folding and thrusting (Colpron et al., 2013).

Long-lived faults, combined with favourable carbonate host strata at the shelf-slope transition, localized mineralization. Neoproterozoic fine-grained siliciclastic and carbonate rocks host most of the Carlin-type gold and realgar mineralization discovered to date (Osiris, Isis, Conrad and Pharaoh zones; ATAC Resources Ltd., 2010; Arehart et al., 2013). The Carlin-type mineralization is spatially associated with Mississippi Valley-type Ag-Pb-Zn occurrences hosted by both Proterozoic and Paleozoic carbonate rocks (Chakungal and Bennett, 2011). The Earn Group (Devonian-Mississippian) controls SEDEX and volcanogenic massive sulphide (VMS) barite and Pb-Zn-Ag±Cu occurrences (e.g., Marg deposit). Nearby Cretaceous intrusions of the Tombstone suite are associated with intrusion-hosted and skarn W±Cu mineralization (Chakungal and Bennett, 2011). The Tiger Au deposit, in Silurian to Devonian carbonate rocks with basalt intercalations, lies west of the Nadaleen trend of Carlin-type occurrences and is probably related to the Paleocene Rackla granitic pluton (Thiessen et al., 2012).

3. Data sources and methods

3.1. Regional geochemical survey database

Since 1976, the joint federal National Geochemical Reconnaissance (NGR) and provincial Regional Geochemical Survey (RGS) programs have been carried out in British Columbia and Yukon to aid exploration and development of mineral resources. Sample collection, preparation, and analytical protocols are strictly specified and carefully monitored to ensure consistent data regardless of the area, year of survey, or analytical laboratory (Friske and Hornbrook,

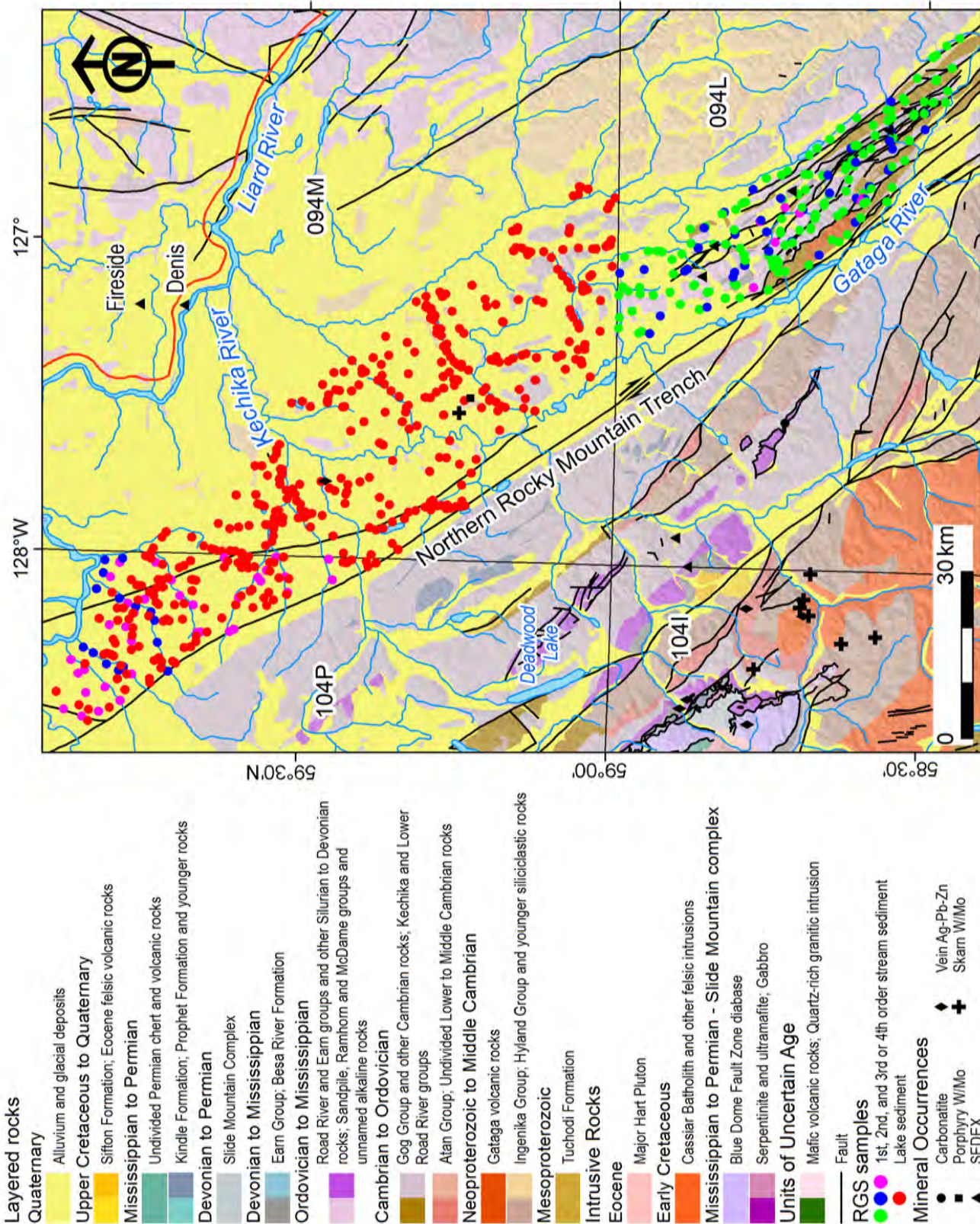


Fig. 2. Geology, selected Regional Geochemical Survey lake- and stream-sediment sample locations, and mineral occurrences, Kechika trough study area, north-central British Columbia. Geology after Gabrielse (1962; 1963a, b; 1998), and Ferri et al., (1999).

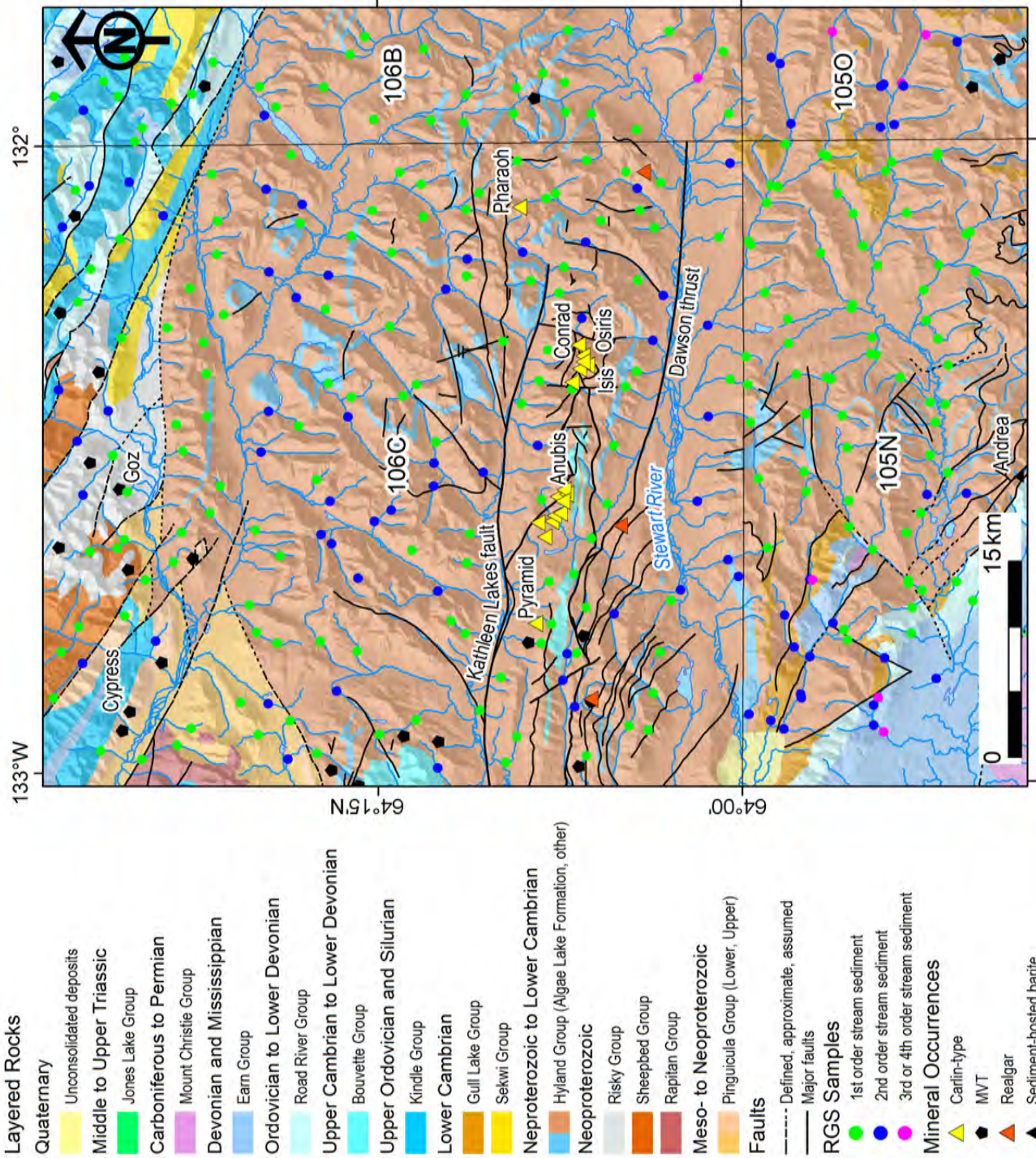


Fig. 3. Geology, selected National Geochemical Reconnaissance stream-sediment sample locations, and mineral occurrences, Rackla belt, east-central Yukon. Geology after Blusson (1974), Gordy and Makepeace, (1999), Chakungal and Bennett (2011), Colpron (2012), and Colpron et al. (2013).

1991).

The data for this study are derived from NGR and RGS stream- and lake-sediment geochemical surveys covering the Kechika trough of north-central British Columbia (total 644 samples) and the Rackla belt of Carlin-type occurrences in east-central Yukon (total 304 samples). To provide representative geochemical data for the catchment basin upstream, samples of fine-grained (<0.18 mm) sediment were collected from lakes at an average density of about 1 site per 11.2 km² and from streams at an average density of about 1 site per 7–13 km². These data include determinations for up to 63 analytes, field observations, and sample locations.

3.2. Raw data

We used multi-element determinations by aqua-regia extraction with inductively coupled plasma mass/emission spectrometry (ICP-MS/ES) finish, and instrumental neutron activation analysis (INAA). Analytical results below lower detection limits (DL) were set to half the minimum lower DL value and those above the upper DL were set to that DL value. The number of censored values less than the lower DL is generally <15% of the total number of determinations for most analytes, with the exception of Au by INAA, Co, Cs, Eu, Hf, Lu, Rb, Ta, Tb, Te, Ti and W for which 18–98% of the total number of values are ≤DL (Table 1).

Elsewhere (Rukhlov et al., 2014) we provide full appendices summarizing statistics for samples from the Kechika trough and the Rackla belt, grouped by sample medium, stream order, and bedrock geology. Univariate histograms, Tukey box plots and probability plots show typical positively skewed distributions of raw data for most analytes (Rukhlov et al., 2014). We used stream order as a rough approximation of catchment basin size to evaluate downstream dilution effects (Hawkes, 1976). The RGS sediments from third- and fourth-order streams have much lower concentrations of Al, Mg, P and most trace metals, and much higher Cr, Na, Ti and Ta concentrations than those from first-order streams due to the dilution by increased input of total sediment in the larger catchment basins (Rukhlov et al., 2014). Stream sediments derived primarily from thick, relatively far-travelled glacial and alluvial sediments in large catchment basins may miss the geochemical signal from material eroded from more immediate catchment basin slopes due to the decoupling effect (Fletcher, 1997; Heberlein, 2013).

Variable sample media and catchment basin geology may also influence sediment composition and cause background variations that can mask signals of mineralization (e.g., Bonham-Carter and Goodfellow, 1986). The RGS sediments show significant variations of Al, Bi, Ca, Ce, Hf, Pb, Rb, S, Sr and Th concentrations related to underlying geology. These elements, along with Br, Cr, Cs, rare-earth elements (REE) and Se, also have different concentrations in lake and stream sediments (Rukhlov et al., 2014).

3.3. Data standardization

To correct for the above effects, the raw analytical data were

Table 1. Summary of analytical detection levels (DL) for selected RGS data.

Analyte	Minimum DL	Values ≤DL (%) ¹
Ag	2 ppb	0.3
Al	0.01 wt %	0.9
As	0.1 ppm	5.6
Au	0.2 ppb	13.6
Au INAA	2 ppb	60.1
Ba INAA	50 ppm	0.5
Bi	0.02 ppm	11.1
Br INAA	0.5 ppm	3.5
Ca	0.01 wt %	0.3
Cd	0.01 ppm	0.3
Ce INAA	3/5 ppm	8.6
Co INAA	1/5 ppm	30.4
Cr INAA	5/20 ppm	7.1
Cs INAA	0.5/1 ppm	32.3
Cu	0.01 ppm	0.3
Eu INAA	0.2/1/2 ppm	46.6
Fe INAA	0.01 wt %	0
Ga	0.1 ppm	3.8
Hf INAA	1 ppm	22.9
Hg	5 ppb	2.1
K	0.01 wt %	8.3
La INAA	0.5/2 ppm	0.3
Lu INAA	0.05/0.2 ppm	19.6
Mg	0.01 wt %	0.3
Mn	1 ppm	0.3
Mo	0.01 ppm	0.3
Na INAA	0.01 wt %	0.2
Ni	0.1 ppm	0.5
P	0.001 wt %	0.3
Pb	0.01 ppm	0.3
Rb INAA	5/15 ppm	21.6
S	0.01/0.02 wt %	8.1
Sb	0.02 ppm	0.4
Sc INAA	0.1/0.2 ppm	0.7
Se	0.1 ppm	6.1
Sm INAA	0.1 ppm	4.8
Sr	0.5 ppm	0.3
Ta INAA	0.5 ppm	50.7
Tb INAA	0.5 ppm	50.9
Te	0.02 ppm	35.0
Th INAA	0.2 ppm	2.3
Ti	0.001 wt %	17.7
Tl	0.02 ppm	9.8
U INAA	0.5 ppm	0.4
V	2 ppm	6.3
W	0.1/0.2 ppm	98.1
Zn	0.1 ppm	0.3

Notes:

Determinations are by aqua regia extraction with inductively coupled plasma mass spectrometry or emission spectrometry finish and by instrumental neutron activation analysis (INAA) where indicated. ¹Per cent of total 948 values except for Au by inductively coupled plasma mass spectrometry (total 655 values).

log₁₀-transformed to a more normally distributed form, and levelled using the Z-score method, first by sample medium and stream order and then by underlying bedrock in iGAS® software. Z-scores convert data to units of standard deviation using the median as a robust estimate of the mean and the interquartile range (IQR) multiplied by 0.7413 as a robust

estimate of standard deviation (SD). IQR is the difference between the 75th and 25th percentiles and covers approximately 50% of the data distribution (Garrett and Grunsky, 2001). After the transformation all levelled groups have a mean of zero and a SD of 1. The robust Z-score levelling preserves true outliers and is defined as follows:

$$Z = (\text{Input Value} - \text{Median of group}) / [\text{Interquartile Range of group}] * 0.7413$$

Comparison of univariate raw and standardized data shows that the logarithmic transformation coupled with the robust Z-score levelling results in a de-skewed and statistically equivalent dataset (Rukhlov et al., 2014). All interpretations of the RGS data presented below are based on the standardized values.

4. Multi-element interpretation of Carlin-type signal

The standardized data were evaluated for Carlin-type geochemical signals using coincident As±Hg±Tl±Sb±Au anomalies, regression analysis, principal components analysis (PCA), and weighted sum (WS) index to test for geochemical patterns found in the Nevada type area (Patterson and Muntean, 2011). The model Carlin-type geochemical signatures in stream and lake sediments were validated by predicting the known Carlin-type occurrences of the Rackla belt.

4.1. Coincident pathfinder anomalies

Elevated concentrations of As±Hg±Tl±Sb±Au in regional stream and lake sediments that are underlain by favourable geology could signal Carlin-type mineralization (Tucker et al., 2013). In Figures 4 to 7, we illustrate sediment samples having As-Hg-Sb and As-Hg-Tl values greater than the 95 percentile and Au percentile ranks for the Kechika trough and the Rackla belt. Coincident As±Hg±Tl±Sb±Au anomalies highlight the main clusters of Carlin-type showings of the Rackla belt. Notably, Sb is less significant in samples nearest to the Carlin-type occurrences, similar to the geochemical signature of many Carlin deposits in Nevada (Patterson and Muntean, 2011).

Many stream and lake sediment samples in the Kechika trough also have As±Hg±Tl±Sb±Au concentrations greater than the 95 percentile. In the southeast part of the study area (NTS 094L) is a cluster of stream-sediment samples with elevated As±Au, Hg±Au, As-Hg, Hg-Tl, Sb-Tl, As-Tl-Sb, and As-Hg-Tl-Sb concentrations (Figs. 4 and 6). The only sample that shows coincident As-Hg-Tl-Sb anomalies is from a first-order catchment that is underlain by variably graphitic, calcareous, and pyritic, fine-grained siliciclastic and carbonate rocks, containing siliceous and baritic exhalites of the Earn Group. However, interpretation of these pathfinder signals may be obscured by nearby MVT, VMS, and SEDEX mineralization (Ferri et al., 1999; Chakungal and Bennett, 2011) at shelf-slope transitions.

4.2. Regression analysis

Late-stage realgar and orpiment are important spatial

indicators of Carlin deposits in Nevada (Arehart, 1996) and the Rackla belt (Arehart et al., 2013; Tucker et al., 2013). As vs. S regression analysis on the RGS data provides an effective way to test for these indicators in the stream and lake sediments. Compared to a regular least-squares regression, a robust regression using the least median of squares (LMS) method of Rousseeuw and Leroy (1987) better models most of the data and enhances the identification of anomalies by down-weighting outlying data points. The method uses the following algorithm.

1. Randomly select many sub-groups, with the minimum size of each sub-group being equal to the number of response variables plus 1.
2. Calculate squared residuals (r^2) for all data using regression equations determined for each sub-group.
3. Calculate the residual (r_i) for each sample using the regression equation that gives the minimum median squared residual.
4. Estimate a preliminary standard deviation (s^0) of the minimum median squared residuals.
5. Assign a weight of 1 to samples having standardized residual, $r_i/s^0 < 3.0$, and a weight of 0 to the rest of samples.
6. Repeat a robust estimate of the standard deviation (s^*) of the minimum median squared residuals on just the samples that had been assigned a weight of 1 in the previous step.
7. Assign a weight of 1 to samples having standardized residual, now calculated as $r_i/s^* < 3.0$, and a weight of 0 to the rest of samples.
8. Perform the least-squares regression on the samples having a weight of 1.
9. Calculate the final standardized residuals for all the data based on the regression solution in step 8.

Figure 8a shows the results of As vs. S regression analysis using the LMS method on the standardized RGS data. All but one of the stream and lake sediment samples with the standardized residuals of >3.0 fall along the realgar/orpiment control line on the As vs. S plot in terms of the raw concentrations (Fig. 8b). The only outlier is a lake sediment sample (Anomaly number 11; Rukhlov et al., 2014) containing 8.0 wt % S and 295 ppm As. These ‘indicator mineral’ standardized residuals mark two lake sediment and one stream sediment samples in the Kechika trough (Fig. 9), and highlight the main clusters of the Carlin-type occurrences and a number of new targets in the Rackla belt (Fig. 10).

4.3. Principal components analysis (PCA)

Robust PCA describes the variation within a multivariate dataset using a few derived functions, termed “principal components” (PC1, PC2, etc.), which are not biased by outliers (Campbell, 1980). The principal components are linear transformations of input variables representing perpendicular best-fit lines through the variation for all variables. The first few principal components account for most of the variance

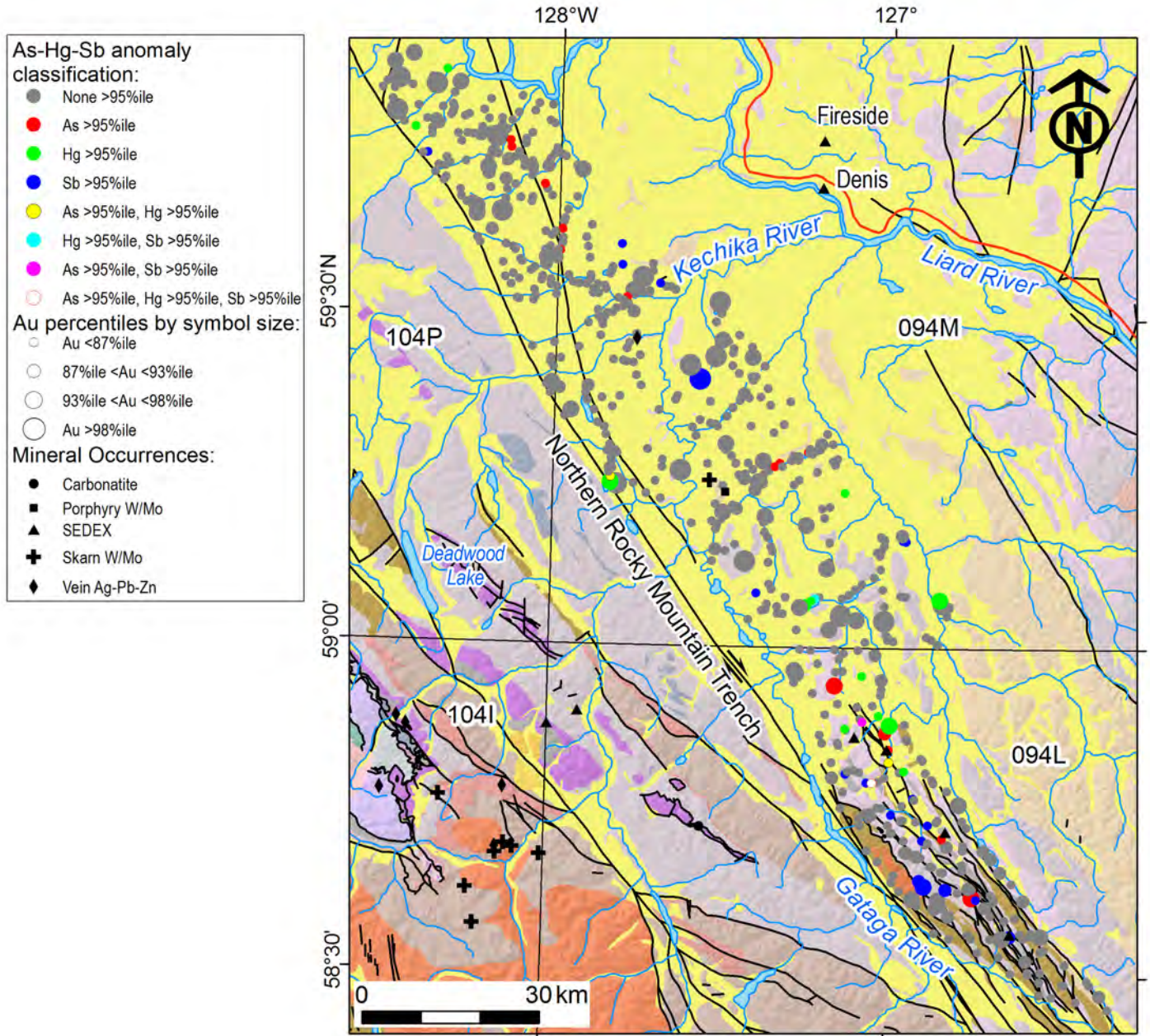


Fig. 4. As-Hg-Sb >95 percentiles, and Au anomalies (percentiles by symbol diameter) from RGS lake- and stream-sediment samples, Kechika trough. Rock legend as in Figure 2.

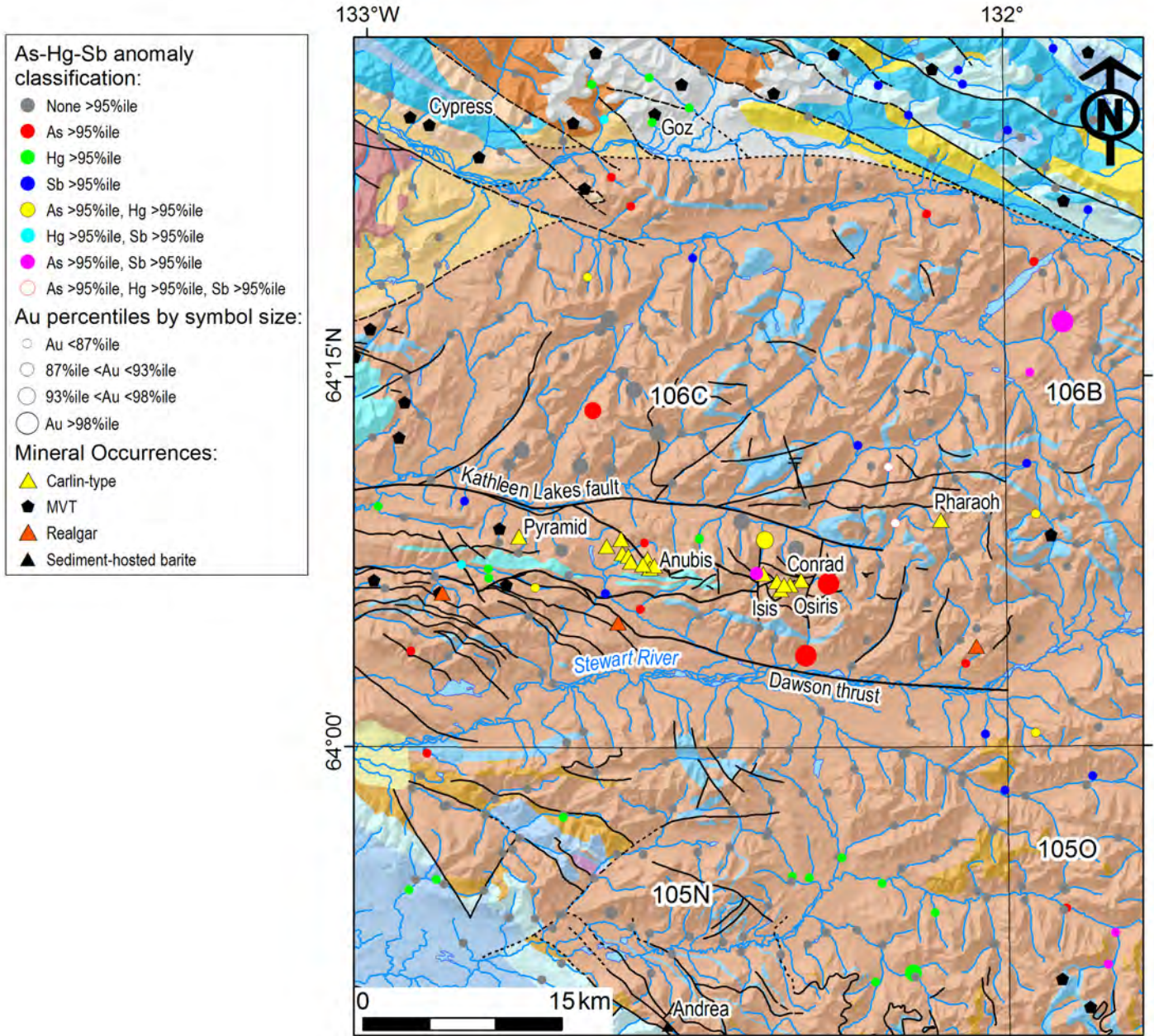


Fig. 5. As-Hg-Sb >95 percentiles, and Au anomalies (percentiles by symbol diameter) from NGR stream-sediment samples, Rackla belt. Rock legend as in Figure 3.

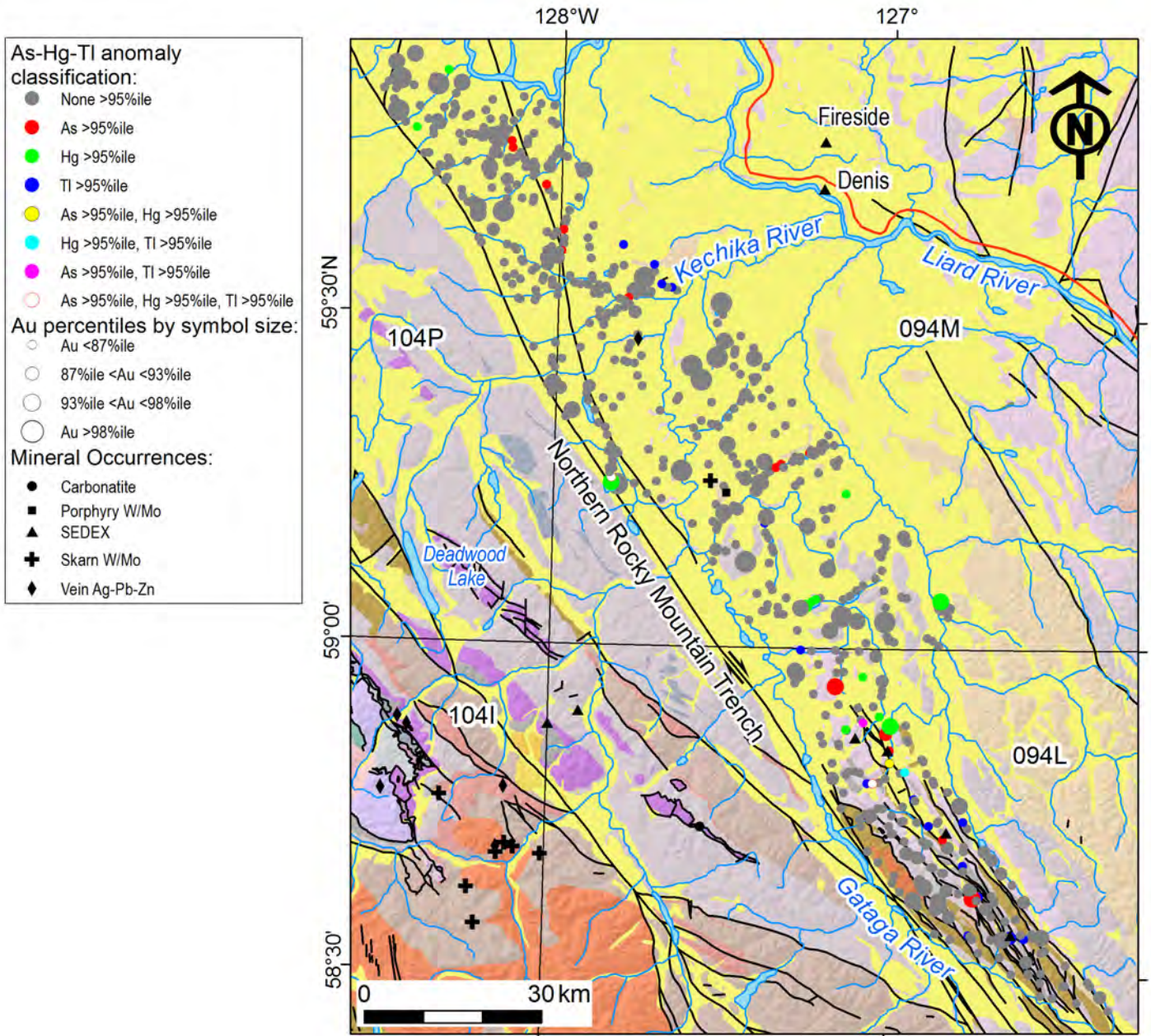


Fig. 6. As-Hg-Tl>95 percentiles, and Au anomalies (percentiles by symbol diameter) from RGS lake- and stream-sediment samples, Kechika trough. Rock legend as in Figure 2.

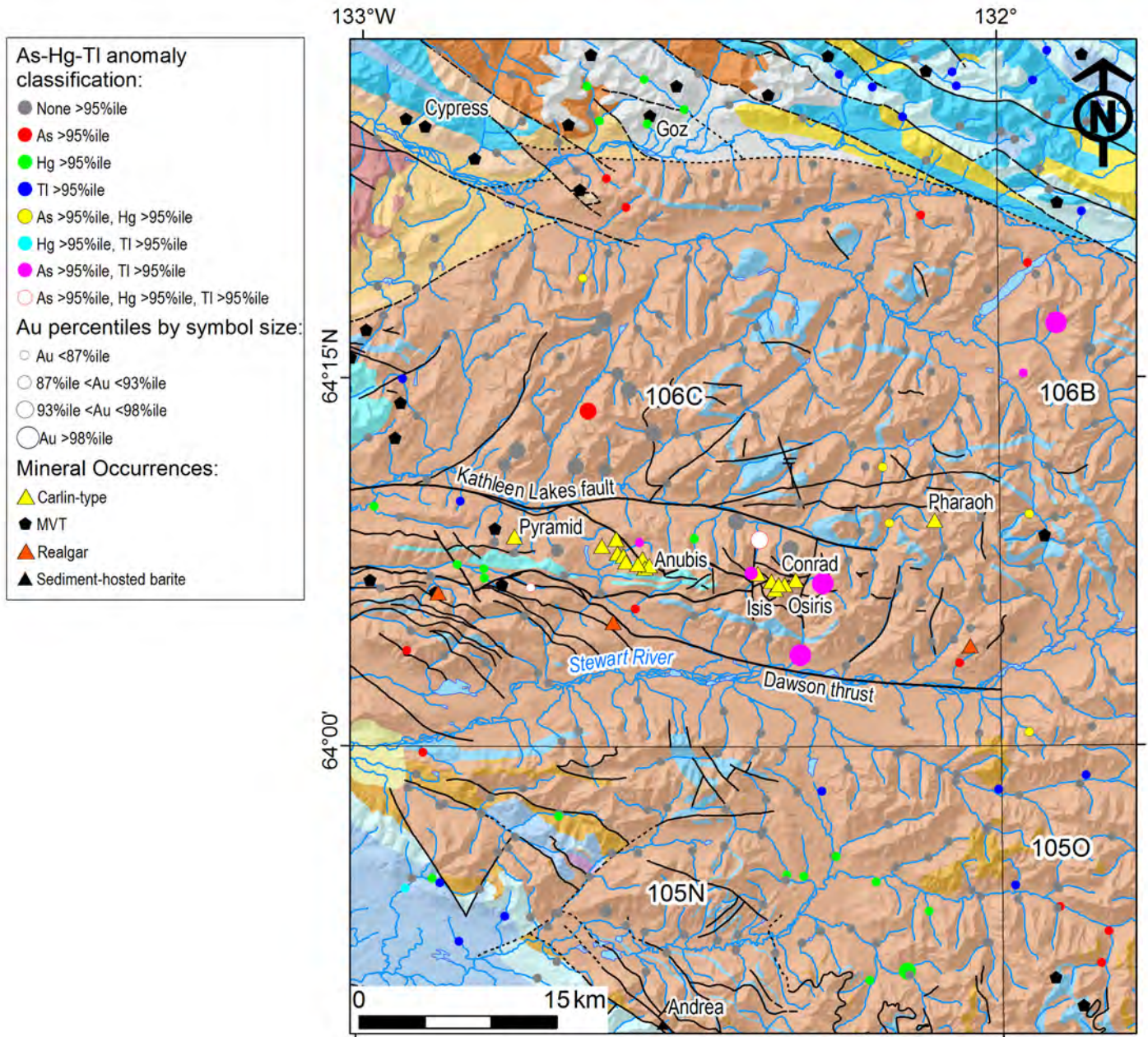


Fig. 7. As-Hg-Tl>95 percentiles, and Au anomalies (percentiles by symbol diameter) from NGR stream-sediment samples, Rackla belt. Rock legend as in Figure 3.

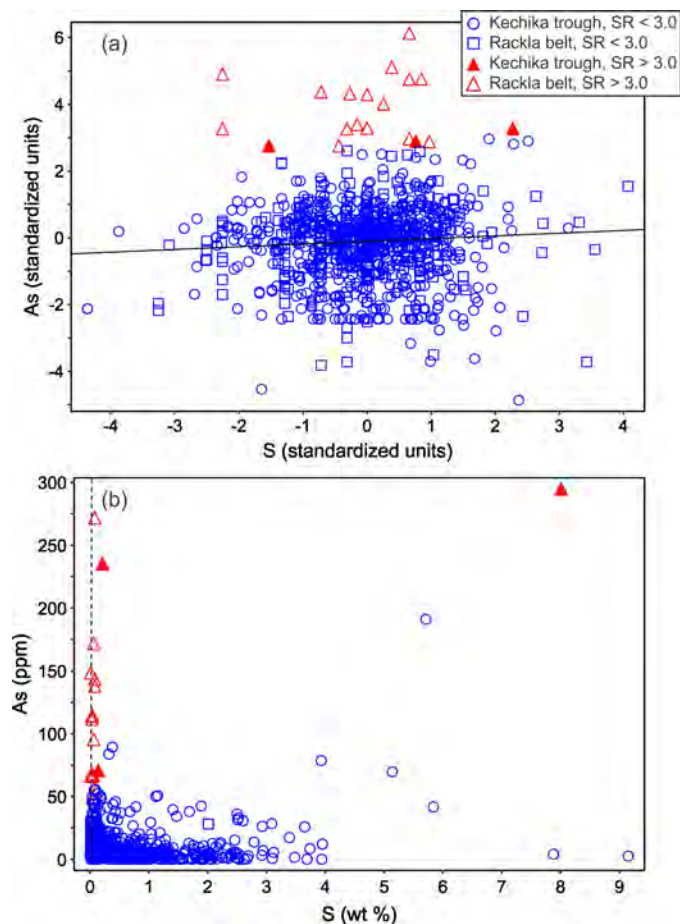


Fig. 8. As vs. S scatter plot for lake- and stream-sediment samples from the Kechika trough, and the Rackla belt. **a)** Standardized values showing the results of robust regression analysis. **b)** Raw concentrations indicating possible realgar control in the samples having standardized residuals (SR) > 3.0.

and, therefore, capture the essential information in the original multi-dimensional dataset of the input variables (Rock, 1988).

We performed PCA on the standardized RGS data in iOGAS® software using a 46-element correlation matrix (Table 2). To minimize the impact of outliers on the principal components, the correlation matrix was calculated by weighting each of the samples by their robustly estimated Mahalanobis distance using a low outlier rejection algorithm. This method assigns low weights to outlying samples to minimize their influence on the correlation calculation, but then projects the outliers onto the robustly determined principal components (Campbell, 1980).

The robust PCA best discriminates the stream-sediment samples derived from Carlin-type showings of the Rackla belt in terms of the second (PC2) and the fourth (PC4) principal components, which total to ~16.6% of the variation in the original dataset (Table 3). On the PC4 vs. PC2 diagram (Fig. 11), data points that fall in the narrow field defined by this group of stream sediments have a similar multi-element, Carlin-type signature. They include one lake sediment sample,

underlain by Cambrian–Ordovician carbonate and fine-grained siliciclastic strata of the Kechika Group in Kechika trough (Fig. 12), and a number of stream-sediment samples in the Rackla belt (Fig. 13).

A circle plot of scaled loadings of each variable to PC2 and PC4 shows a loose cluster of As, Hg, Tl, Te, Ba and Ag (Fig. 14). Sb plots away from this Carlin-type cluster. Similar geochemical signatures characterize many Carlin deposits in Nevada (e.g., Patterson and Muntean, 2011).

4.4. Weighted sum index (WS)

WS index uses a priori knowledge of mineralization to model its multi-element signature by a single linear function. The index is similar to the first principal component in PCA, but the relative weights for each element are assigned by the user, rather than being determined from the covariance or correlation matrix (Garrett and Grunsky, 2001).

Table 4 lists the model parameters for WS index of a Carlin-type signature in the RGS stream- and lake-sediment samples. Elements chosen for the WS index show the largest absolute loadings to a Carlin-type factor derived from the factor analysis on >6,400 drill-core samples from the Jerritt Canyon district in Nevada (Patterson and Muntean, 2011). Relative importance is assigned for each element based on their Carlin-type factor loadings. For instance, As, Hg, and Tl, which show the maximum loadings to the Carlin-type factor, are given 5 times more weight than Ag, Fe, and W, which are more characteristic of background (Table 4). Positive importance signifies elevated concentrations of pathfinder elements associated with the Carlin-type model and negative importance indicates diagnostic depletions. The relative importance values are converted into weights by dividing each importance by the square root of the sum of the squares of all of the importance values, so that the sums of the squares of the weights equal unity. The WS index score for each sample is then calculated as a sum of these weights multiplied by the normal scores for each corresponding element included in the index. The normal score for each element is obtained using robust estimates of the mean (median) and the SD (IQR*0.7413) and the Z-score levelling equation given above (Garrett and Grunsky, 2001).

In the Kechika trough study area, five stream-sediment and three lake-sediment samples show the Carlin-type WS index scores >98 percentile (Fig. 15). These samples are underlain by Paleozoic and older fine-grained siliciclastic and carbonate rocks of the Earn, Road River, Kechika, and Hyland groups. The stream sediments with the WS scores >98% percentile also predict the main clusters of the Carlin-type showings and highlight a few additional targets in the Rackla belt (Fig. 16).

4.5. Summary of multi-element modelling of Carlin-type signal in stream and lake sediments

The coincident elevated concentrations of pathfinder elements, standardized residuals >3.0 from robust As vs. S regression analysis, and principal components analysis and weighted sum index scores highlight a Carlin-type signal in 11

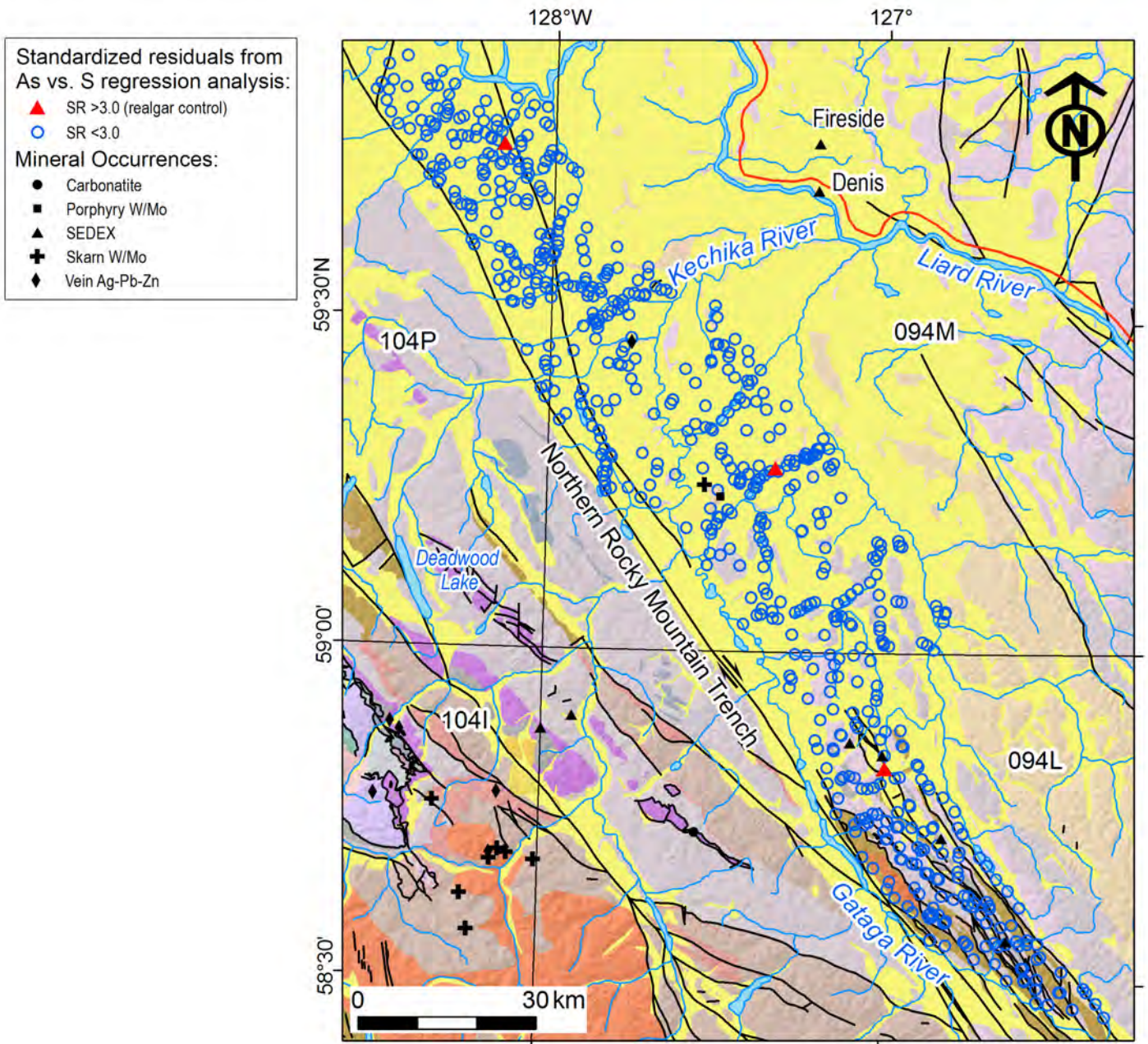


Fig. 9. As vs. S robust regression analysis on the RGS data, Kechika trough, highlighting standardized residuals (SR) >3.0, which may indicate realgar. Rock legend as in Figure 2.

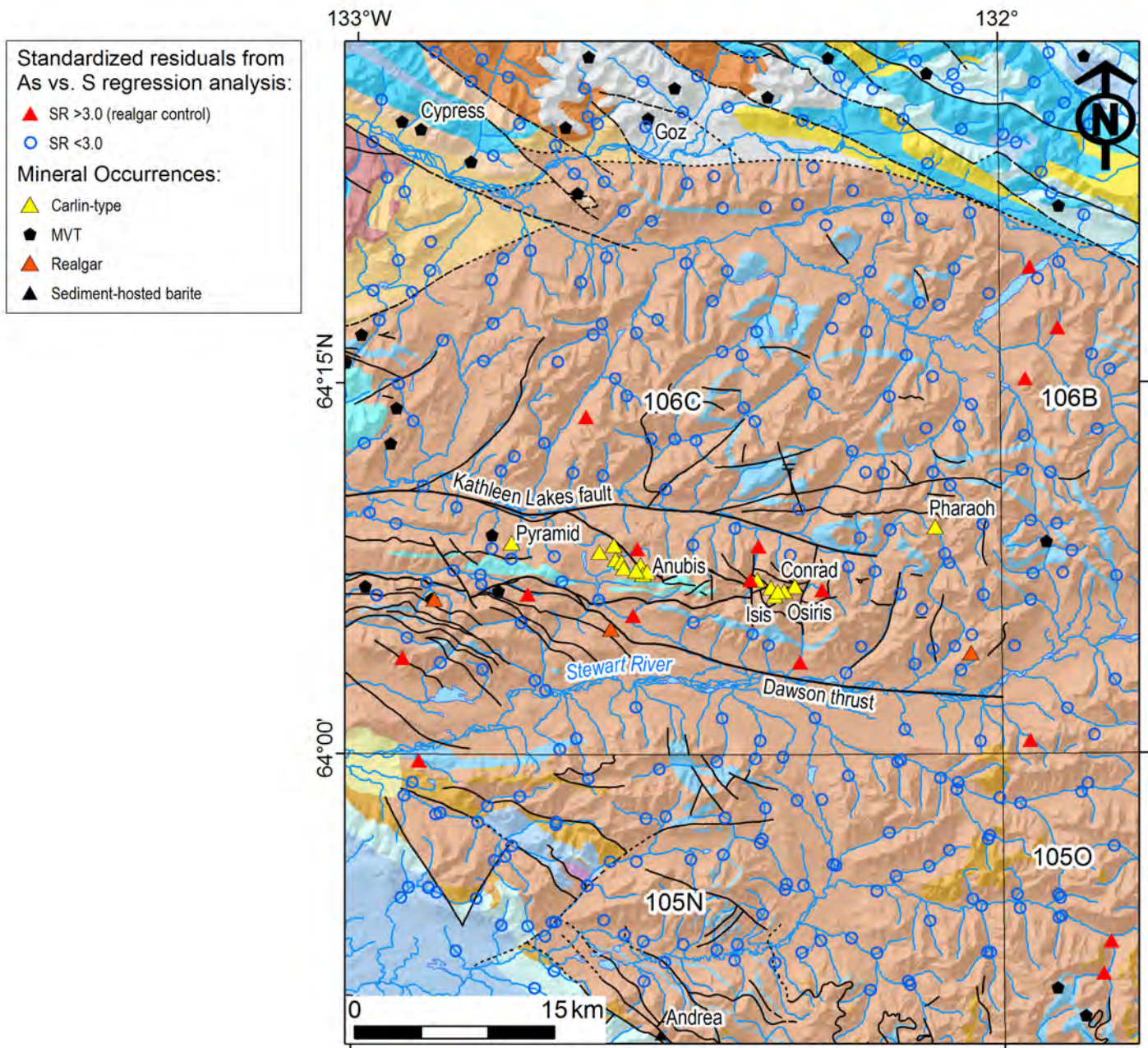


Fig. 10. As vs. S robust regression analysis on the NGR data, Rackla belt, highlighting standardized residuals (SR) >3.0, which may indicate realgar. Rock legend as in Figure 3.

Table 3. Results of robust PCA for the second and fourth principal components that best discriminate stream sediments associated with Carlin-type occurrences of the Rackla belt, east-central Yukon.

Principal Component	PC2		PC4	
	Eigenvectors ¹	Scaled coordinates ⁴	Eigenvectors ¹	Scaled coordinates ⁴
Au	0.11	0.27	-0.01	-0.01
Ag	0.19	0.46	0.12	0.18
Al	-0.09	-0.21	-0.20	-0.28
As	0.07	0.16	0.31	0.43
Bi	-0.12	-0.28	-0.02	-0.03
Br INAA	0.15	0.36	-0.19	-0.27
Ca	0.09	0.22	-0.03	-0.05
Cd	0.28	0.67	0.04	0.06
Ce INAA	-0.12	-0.28	-0.04	-0.05
Co INAA	-0.07	-0.16	-0.03	-0.05
Cr INAA	0.00	0.01	0.01	0.02
Ba INAA	0.09	0.22	0.13	0.19
Cs INAA	-0.04	-0.10	0.05	0.07
Cu	0.14	0.32	0.05	0.07
Eu INAA	-0.12	-0.29	0.26	0.36
Fe INAA	0.02	0.04	0.03	0.04
Ga	-0.09	-0.21	-0.25	-0.35
Hf INAA	-0.12	-0.29	-0.01	-0.01
Hg	0.21	0.51	0.22	0.31
K	0.05	0.11	-0.09	-0.12
La INAA	-0.10	-0.25	-0.05	-0.08
Lu INAA	-0.06	-0.15	-0.02	-0.02
Mg	0.02	0.04	-0.16	-0.23
Mn	0.05	0.12	0.04	0.06
Mo	0.32	0.76	-0.03	-0.05
Na INAA	-0.13	-0.31	-0.35	-0.50
Ni	0.16	0.39	0.05	0.06
P	0.15	0.34	0.00	0.00
Pb	-0.07	-0.16	-0.02	-0.03
Rb INAA	-0.08	-0.20	-0.02	-0.03
S	0.23	0.54	-0.24	-0.34
Sb	0.31	0.74	0.01	0.01
Sc INAA	-0.07	-0.16	-0.06	-0.09
Se	0.29	0.68	-0.15	-0.21
Sm INAA	-0.11	-0.27	-0.05	-0.07
Sr	0.10	0.24	-0.07	-0.10
Ta INAA	-0.04	-0.10	0.08	0.11
Tb INAA	-0.04	-0.10	0.23	0.33
Te	0.13	0.30	0.12	0.17
Th INAA	-0.13	-0.31	-0.01	-0.02
Ti	0.12	0.29	-0.31	-0.44
Tl	0.20	0.47	0.09	0.13
U INAA	0.19	0.45	-0.21	-0.30
V	0.17	0.40	-0.06	-0.08
W	0.04	0.10	-0.34	-0.48
Zn	0.25	0.60	0.07	0.11
Eigenvalues ²		5.6		2.0
Variation Score (%) ³		12.3		4.3

Notes:¹Contributions of input variables to the best-fit line or principal component.²Variance of contributions within the principal component.³Proportion of variance captured by the principal component.⁴Loadings or lengths of the contributions from original variables scaled to the variance (eigenvalue) so that each principal component has a length of 1 (Fig. 14).

The input variables are log10-transformed and levelled values of original analytical determinations by inductively coupled plasma mass spectrometry or emission spectrometry and instrumental neutron activation analysis (INAA). The second and fourth principal components scores in the sediment samples are calculated as follows:

$$\text{PC2} = -0.12*\text{Eu} - 0.031*\text{Tb} + 0.046*\text{W} + 0.11*\text{Au} + 0.29*\text{Ag} - 0.15*\text{Al} + 0.084*\text{As} - 0.22*\text{Bi} + 0.14*\text{Br} + 0.099*\text{Ca} + 0.38*\text{Cd} - 0.22*\text{Ce} - 0.041*\text{Co} + 0.0086*\text{Cr} + 0.14*\text{Ba} - 0.016*\text{Cs} + 0.27*\text{Cu} + 0.031*\text{Fe} - 0.14*\text{Ga} - 0.24*\text{Hf} + 0.27*\text{Hg} + 0.058*\text{K} - 0.19*\text{La} - 0.12*\text{Lu} + 0.017*\text{Mg} + 0.063*\text{Mn} + 0.40*\text{Mo} - 0.26*\text{Na} + 0.27*\text{Ni} + 0.23*\text{P} - 0.12*\text{Pb} - 0.097*\text{Rb} + 0.22*\text{S} + 0.44*\text{Sb} - 0.12*\text{Sc} + 0.34*\text{Se} - 0.22*\text{Sm} + 0.11*\text{Sr} - 0.018*\text{Ta} + 0.19*\text{Te} - 0.26*\text{Th} + 0.098*\text{Ti} + 0.25*\text{Tl} + 0.24*\text{U} + 0.277*\text{V} + 0.40*\text{Zn} + 1.1484.$$

$$\text{PC4} = 0.26*\text{Eu} + 0.17*\text{Tb} - 0.36*\text{W} - 0.0068*\text{Au} + 0.19*\text{Ag} - 0.34*\text{Al} + 0.39*\text{As} - 0.042*\text{Bi} - 0.18*\text{Br} - 0.036*\text{Ca} + 0.060*\text{Cd} - 0.070*\text{Ce} - 0.020*\text{Co} + 0.025*\text{Cr} + 0.20*\text{Ba} + 0.020*\text{Cs} + 0.092*\text{Cu} + 0.061*\text{Fe} - 0.39*\text{Ga} - 0.014*\text{Hf} + 0.28*\text{Hg} - 0.11*\text{K} - 0.096*\text{La} - 0.030*\text{Lu} - 0.17*\text{Mg} + 0.050*\text{Mn} - 0.041*\text{Mo} - 0.71*\text{Na} + 0.077*\text{Ni} + 0.0034*\text{P} - 0.039*\text{Pb} - 0.021*\text{Rb} - 0.24*\text{S} + 0.013*\text{Sb} - 0.10*\text{Sc} - 0.18*\text{Se} - 0.10*\text{Sm} - 0.075*\text{Sr} + 0.034*\text{Ta} + 0.18*\text{Te} - 0.022*\text{Th} - 0.26*\text{Ti} + 0.12*\text{Tl} - 0.27*\text{U} - 0.087*\text{V} + 0.12*\text{Zn} + 0.6941.$$

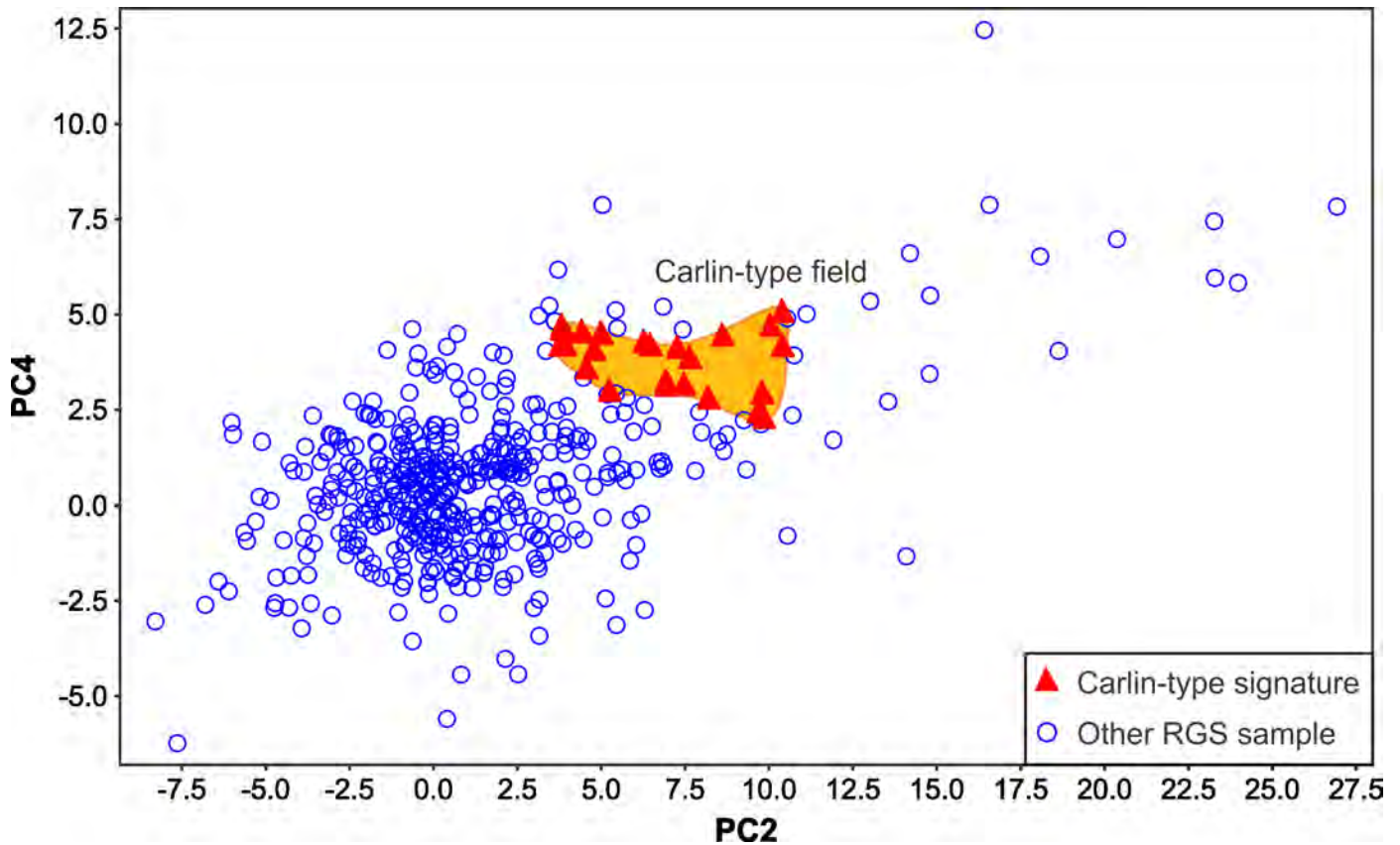


Fig. 11. Discrimination diagram showing Carlin-type field in terms of the second vs fourth principal components derived from the log-transformed and levelled NGR and RGS data for lake and stream sediments from the Kechika trough and the Rackla belt using robustly estimated multi-element correlation matrix (Table 2). The PC2 and PC4 total to 16.6% of variation score in the original dataset (Table 3).

Table 4. Model parameters for weighted sum index of Carlin-type signal in the RGS/NGR lake- and stream-sediment samples from the Kechika trough, and the Rackla belt.

Element	W	Ag	As	Au	Ca	Fe	Hg	La	Sb	Sr	Te	Tl
Method ¹	ICPMS	ICPMS	ICPMS	ICPMS	ICPMS	INAA	ICPMS	INAA	ICPMS	ICPMS	ICPMS	ICPMS
Loading ²	0.37	0.35	0.77	0.79	-0.14	0.31	0.85	-0.15	0.42	-0.18	0.58	0.83
Importance ³	1	1	5	5	-1	1	5	-1	2	-1	3	5
Weight ³	0.092	0.092	0.46	0.46	-0.092	0.092	0.46	-0.092	0.18	-0.092	0.27	0.46

Notes:

¹ICPMS, aqua-regia extraction with inductively coupled plasma mass spectrometry finish; INAA, instrumental neutron activation analysis.

²Carlin-type Factor loadings derived from the factor analysis on >6,400 multi-element analyses of drill-core samples from the Jerritt Canyon district of CTGDs in Nevada (Patterson and Muntean, 2011).

³Assigned relative importance values and their weights are based on the Carlin-type factor loadings. See text for details.

The Carlin-type WS index score for each sample is calculated using the standardized analytical data on the stream and lake sediments as follows:

$$WS = 0.258*W + 0.0929*Ag + 0.469*As + 0.541*Au - 0.0972*Ca + 0.0948*Fe + 0.468*Hg - 0.0943*La + 0.187*Sb - 0.0937*Sr + 0.336*Te + 0.436*Tl + 0.0730.$$

stream- and lake-sediment samples from the Kechika trough (Fig. 17). Applied to stream sediments of the Rackla belt, these geochemical models consistently confirm the known Carlin-type occurrences in the area (Fig. 18), thus validating their effectiveness for evaluating Carlin-type potential. The stream and lake sediments with a Carlin-type signal contain up to 272 ppm As, 31 ppm Sb, 13.9 ppm Hg, 1.3 ppm Tl, 0.22 ppm Te,

and 46 ppb Au (Rukhlov et al., 2014). The geochemical patterns and concentrations of pathfinder elements in these sediments are comparable to those of mineralized halos near the Carlin deposits in Nevada (Patterson and Muntean, 2011).

5. Kechika trough: highlights and conclusions

Regional stream- and lake-sediment geochemical surveys

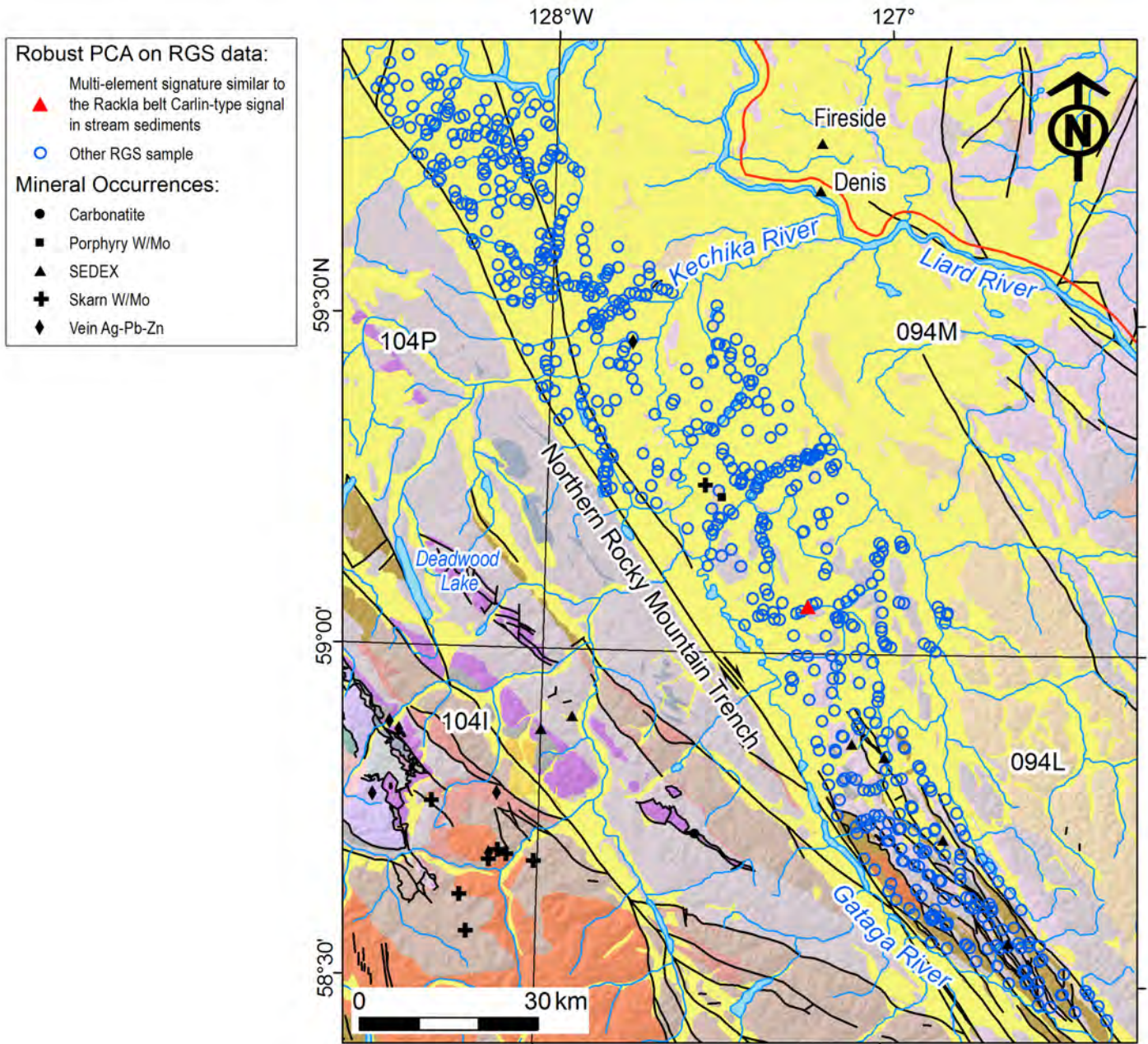


Fig. 12. Robust PCA on the RGS data, Kechika trough, highlighting multi-element Carlin-type signatures in samples with second and fourth principal component scores similar to those from the Rackla belt. Other symbols as in Figure 2.

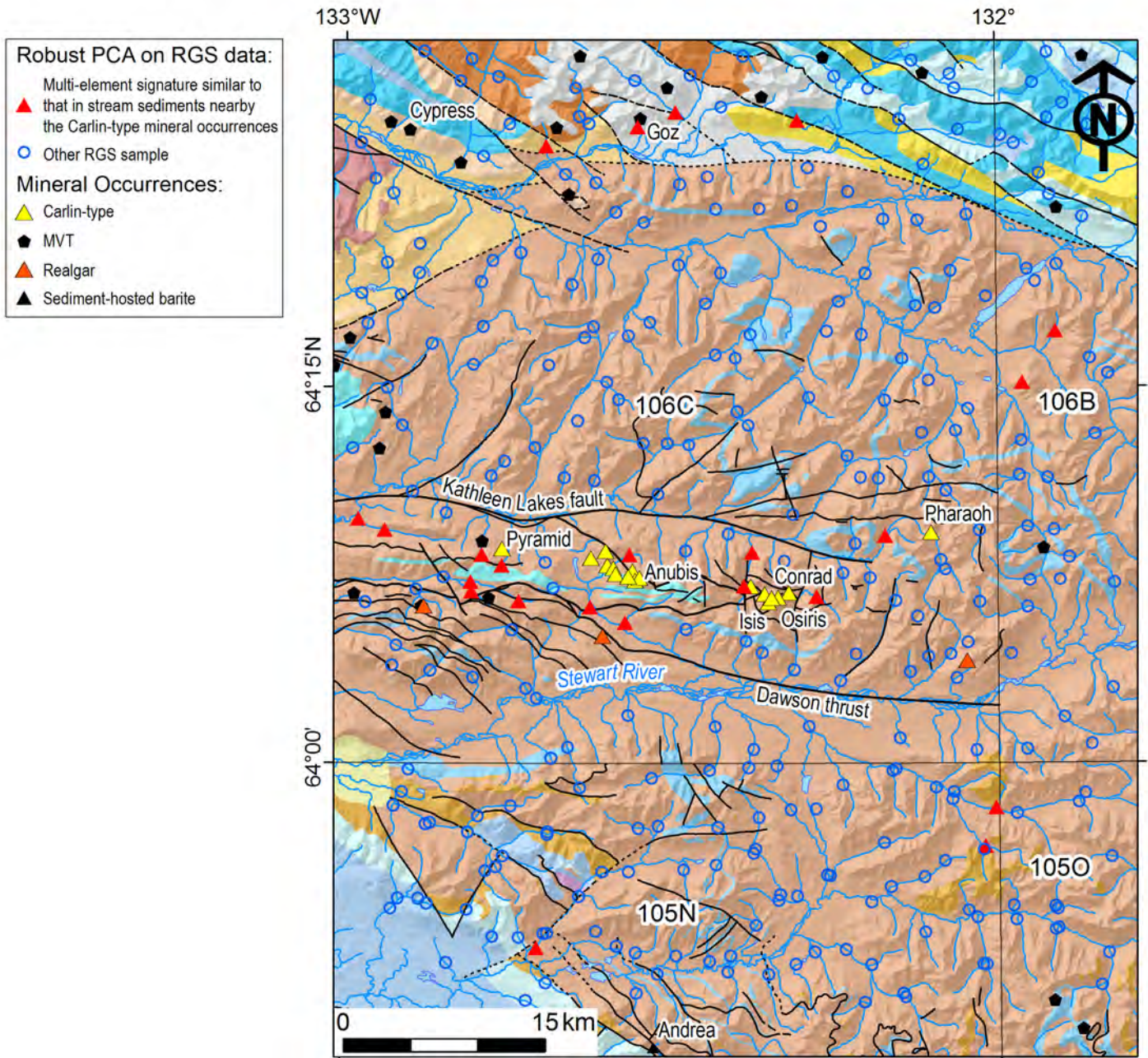


Fig. 13. Robust PCA on the NGR data, Rackla belt, highlighting multi-element Carlin-type signatures in samples with second and fourth principal component scores similar to those in samples nearby the Carlin-type mineral occurrences in the area. Rock legend as in Figure 3.

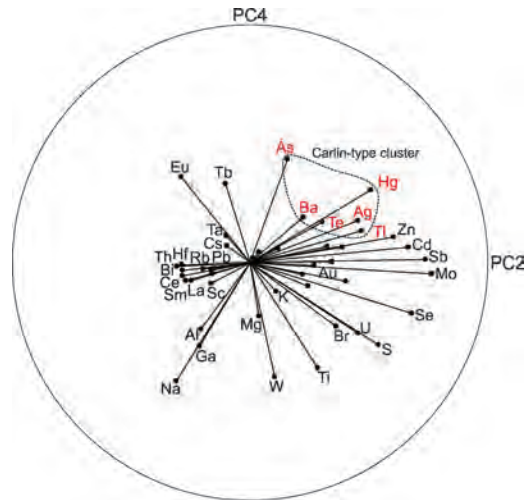


Fig. 14. Circle plot of scaled contributions (loadings) of each variable to PC2 and PC4 derived from robust PCA on the log10-transformed and levelled RGS and NGR data for lake- and stream- sediments from the Kechika trough and the Rackla belt (Table 3). As, Hg, Tl, Te, Ba and Ag form a Carlin-type cluster (outlined). Analytes plotting closer to the unit circle (e.g., As, Hg and Tl) have higher loadings and are better represented by these components. Ca, Co, Cr, Cu, Fe, Lu, Mn, Ni, P, Sr, and V have relatively low loadings and are not labelled for clarity.

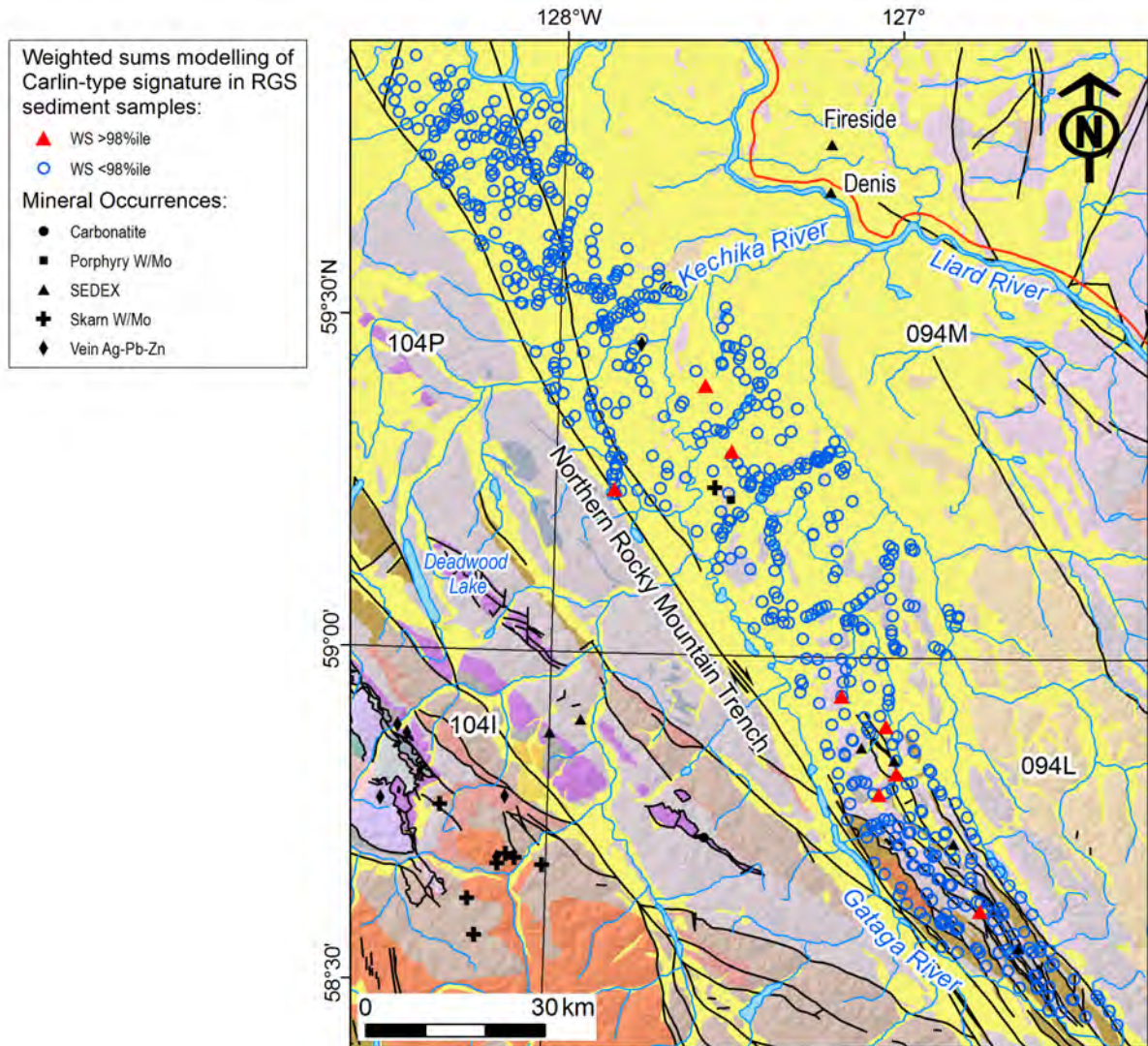


Fig. 15. Weighted sum index (WS) modelling of Carlin-type signature in the RGS sediments, Kechika trough (Table 4). Samples having the WS scores >98 percentile are highlighted. Rock legend as in Figure 2.

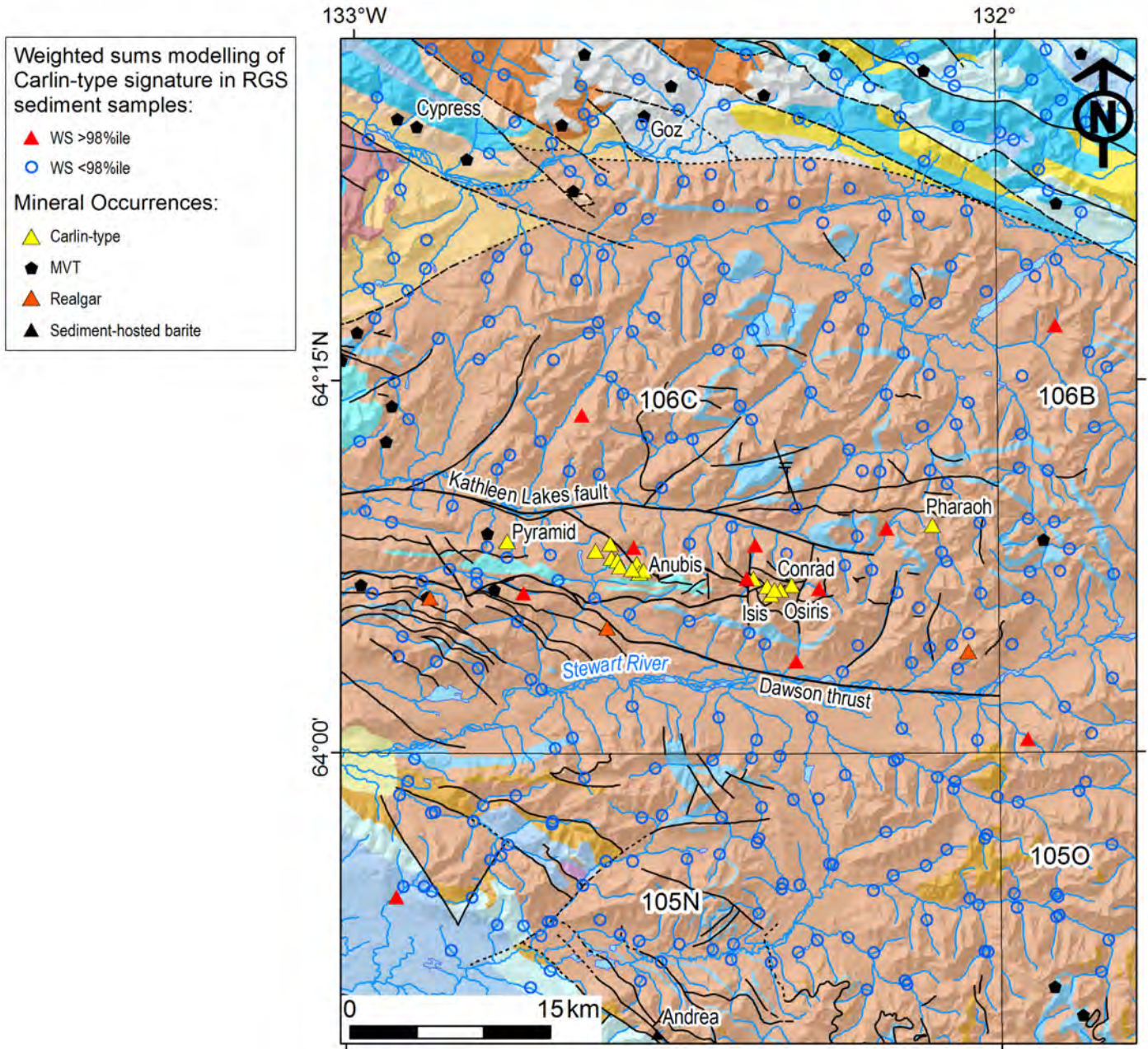


Fig. 16. Weighted sum index (WS) modelling of Carlin-type signature in the NGR stream sediments, Rackla belt. Samples having the WS scores >98 percentile (highlighted) predict the Carlin-type occurrences in the area. Rock legend as in Figure 3.

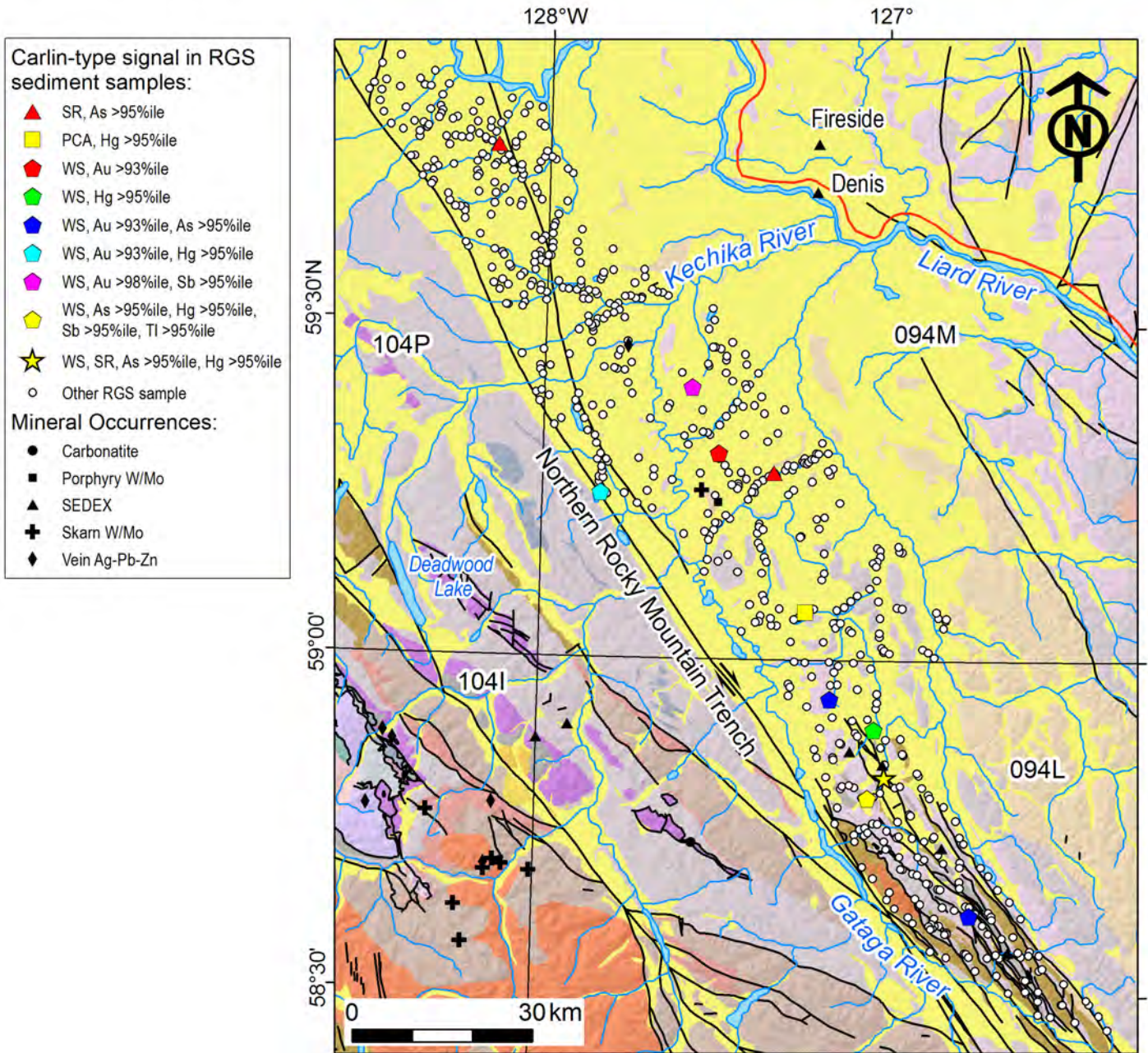


Fig. 17. RGS samples with interpreted Carlin-type signatures, Kechika trough (Appendix 4). Catchment basins for the anomalous stream-sediment samples are smaller than their map symbols. Rock legend as in Figure 2.

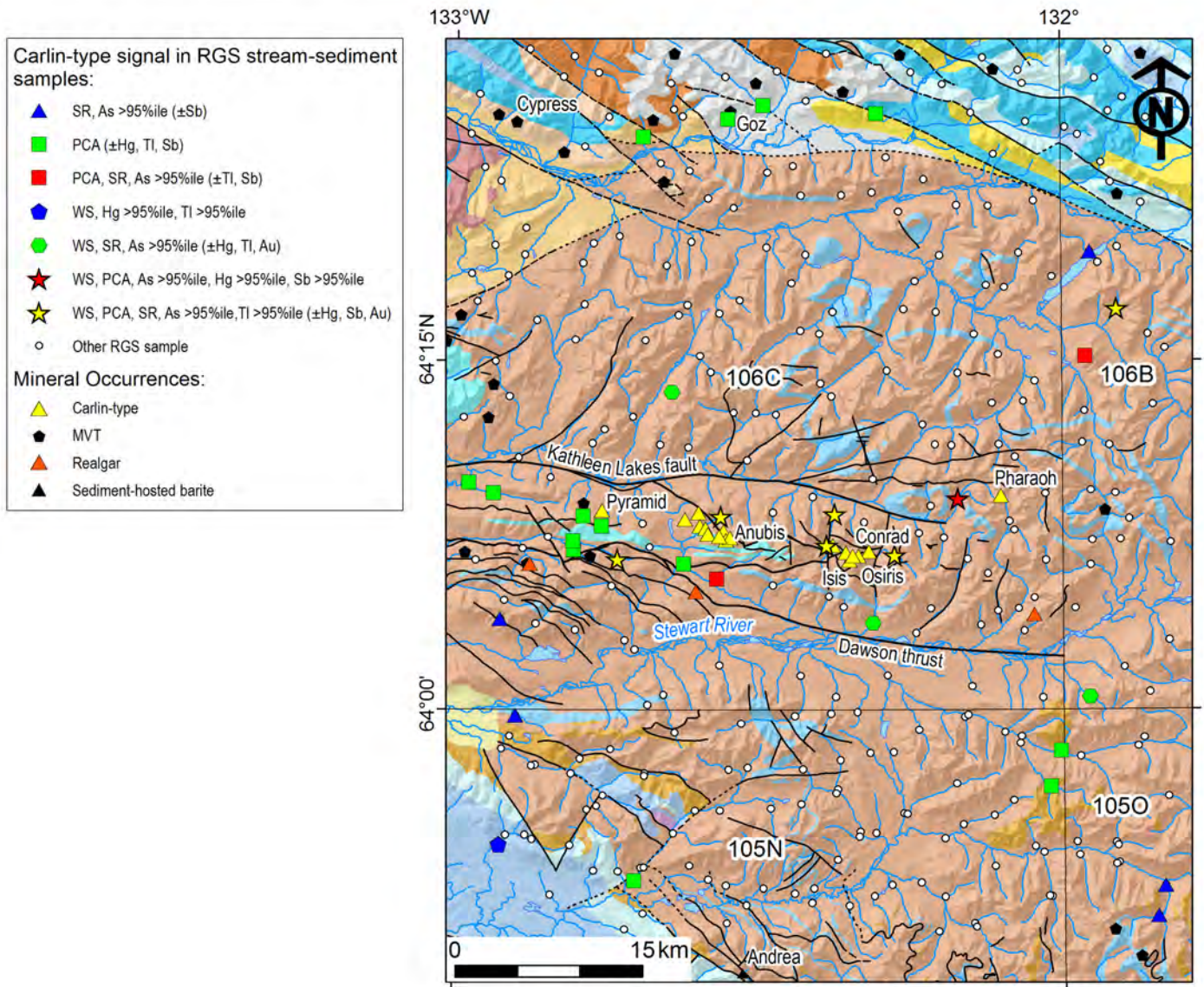


Fig. 18. NGR samples with interpreted Carlin-type signatures, Rackla belt (Appendix 4). Rock legend as in Figure 3.

can be used to identify areas that have potential for Carlin-type deposits (Tucker et al., 2013). Interpretation of raw analytical data is enhanced by standardization methods that normalize analyses, and by levelling procedures to account for sample medium, catchment basin size, and bedrock geology.

Coincident elevated concentrations of As±Hg±Tl±Sb±Au in sediments may be related to Carlin-style mineralization. However, because of nearby MVT, VMS-SEDEX, intrusion-related, and other types of base- and precious metal mineralization in the Kechika trough (Ferri et al., 1999) and the Rackla belt (Chakungal and Bennett, 2011) this interpretation is unclear.

Multi-element modelling of standardized RGS data using robust PCA and WS index scores and 'indicator mineral' regression analysis enhance the Carlin-type geochemical signal in sediments and independently confirm known Carlin-type deposits in the Rackla belt. Applied to the western flank of Kechika trough, these models highlight 11 lake and stream sediment samples that show the Carlin-type signatures (Fig. 17). These samples are underlain by fine-grained siliciclastic and carbonate rocks in the footwall of a thrust. South of the study area, Lett (2001) reported up to 147 ppb Au, 20 ppm As, 975 ppb Ag and 59 ppm Sb in black siliciclastic rocks of the Gunsteel Formation, north of the Bear mineral occurrence (NTS 094F 024). The elevated gold- and pathfinder-element bedrock anomalies, coupled with stratigraphic and structural similarities with the Rackla belt, suggest that Kechika trough holds potential for kindred Carlin-type deposits. The eastern margin of the Kechika trough has yet to be evaluated.

6. Exploration applications and future work

Carlin-type signals in low sample density stream and lake sediments mark new exploration targets in the Kechika trough. The Paleozoic and older fine-grained siliciclastic and carbonate rocks in this area also host numerous SEDEX Pb-Zn-Ba deposits and at least one known intrusion-related W-Mo stockwork-skarn deposit (e.g., Ferri et al., 1999). Exploration work might focus on bedrock and surficial geology mapping of the target catchment basins, complemented by geochemical surveys to locate favourable replacement and breccia zones near long-lived faults. Realgar, orpiment, and stibnite overprinting auriferous As-rich pyrite are the best indicators of Carlin-type mineralization (Tucker et al., 2013). However, exploration in the northern part of Kechika trough (parts of NTS 94M and 104P) has previously been limited by extensive drift cover and poor exposure. Drift prospecting and till geochemistry coupled with indicator mineralogy could aid interpretation of the geochemical anomalies.

Acknowledgments

We thank Yao Cui (British Columbia Geological Survey), Dani Alldrick (former British Columbia Geological Survey), and Maurice Colpron (Yukon Geological Survey) for useful comments. Thorough review by Larry Aspler (British Columbia Geological Survey) and Ray Lett (British Columbia Geological

Survey) significantly improved this paper.

References

- Arehart, G.B., 1996. Characteristics and origin of sediment-hosted disseminated gold deposits: a review. *Ore Geology Reviews* 11, 383-403.
- Arehart, G.B., Ressel, M., Carne, R., Muntean, J., 2013. A comparison of Carlin-type deposits in Nevada and Yukon. In: *Tectonics, Metallogeny, and Discovery: The North American Cordillera and Similar Accretionary Settings*, M. Colpron, T. Bissig, B.G. Rusk, and J.F.H. Thompson (eds.), Society of Economic Geologists, Inc., Special Publication 17, pp. 389-401.
- ATAC Resources Ltd., 2010. ATAC Resources Makes a New Gold Discovery On its Rau Gold Project - Yukon. July 29, 2010. Accessed online from ATAC Resources Ltd. (<http://www.atacresources.com/s/NewsReleases.asp?>), October 07, 2014.
- Blusson, S.L., 1974. Five geological maps of northern Selwyn Basin (Operation Stewart), Yukon Territory and District of Mackenzie, N.W.T. Geological Survey of Canada, Open File 205.
- Bonham-Carter, G.F., Goodfellow, W.D., 1986. Background corrections to stream geochemical data using digitized drainage and geological maps: Application to Selwyn Basin, Yukon and Northwest Territories. In: *Exploration for ore deposits of the North American Cordillera*, C.E. Nichols (ed.), *Journal of Geochemical Exploration* 25 (1-2), p. 139-155.
- Campbell, N.A., 1980. Robust procedures in multivariate analysis. I: Robust covariance estimation. *Applied Statistics* 29, 231-237.
- Chakungal, J., Bennett, V., 2011. New bedrock geology of Mount Mervyn map sheet (106C/04) and mineral potential for the South Wernecke mapping project. In: *Yukon Exploration and Geology 2010*, K.E. MacFarlane, L.H. Weston and C. Relf (eds.), Yukon Geological Survey, p. 55-87.
- Colpron, M., 2012. Preliminary geological map of the Mount Ferrell area (106C/3), central Yukon. Yukon Geological Survey, Open File 2012-11, 1:50 000 scale.
- Colpron, M., Moynihan, D., Israel, S., Abbott, G., 2013. Geological map of the Rackla belt, east-central Yukon (NTS 106C/1-4, 106D/1). Yukon Geological Survey, Open File 2013-13, 1:50 000 scale.
- Cook, S.J., Jackaman, W., Friske, P.W., Day, S.J., Coneys, A.M., Ferri, F., 1997. Regional lake sediment and water geochemistry of the northern Kechika Trough, British Columbia (NTS 94M/2, 3, 4, 5, 6, 12; 104P/8, 9, 10, 15, 16). British Columbia Ministry of Employment and Investment, British Columbia Geological Survey Open File 1997-15, Geological Survey of Canada Open File 3499, 31 p.
- Cook, J., Jackaman, W., Friske, P.W., Day, S.J., Hall, G.E.M., Coneys, A.M., 1999. Geochemistry of Alkaline Lake Waters of the Northern Kechika Trough, British Columbia (NTS 94M/2, 3, 4, 5, 6, 12; 104P/8, 9, 10, 15, 16). British Columbia Ministry of Energy and Mines, British Columbia Geological Survey Open File 1999-6, Geological Survey of Canada Open File 3704, 47 p.
- Cui, Y., Katay, F., Nelson, J.L., Han, T., Desjardins, P.J., Sinclair, L., compilers, 2013. British Columbia Digital Geology. British Columbia Ministry of Energy and Mines, British Columbia Geological Survey, Open File 2013-4.
- Day, S.J.A., McCurdy, M.W., Friske, P.W.B., McNeil, R.J., Hornbrook, E.H.W., Lynch, J.J., Durham, C.C., Gross, H., Galletta, A.C., 2009. Regional stream sediment and water geochemical data, Lansing Range area, east central Yukon (NTS 105N). Geological Survey of Canada, Open File 6272, Yukon Geological Survey, Open File 2009-27, 11 p.
- Ferri, F., Rees, C., Nelson, J., Legun, A., 1999. Geology and mineral deposits of the northern Kechika trough between Gataga River and the 60th parallel. British Columbia Ministry of Energy and Mines, British Columbia Geological Survey Bulletin 107, 122 p.

- Fletcher, W.K., 1997. Stream sediment geochemistry in today's exploration world. In: *Geophysics and Geochemistry at the Millennium. Proceedings of Exploration 97: Fourth Decennial International Conference on Mineral Exploration*, A.G. Gubbins (ed.), Prospectors and Developers Association of Canada, p. 249-260.
- Friske, P.W.B., Hornbrook, E.H.W., 1991. Canada's National Geochemical Reconnaissance programme. *Transactions of the Institution of Mining and Metallurgy*, London, Section B 100, 47-56.
- Friske, P.W.B., Hornbrook, E.H.W., Lynch, J.J., McCurdy, M.W., Gross, H., Galletta, A.C., Durham, C.C., 1991a. National Geochemical Reconnaissance stream sediment and water data, east central Yukon (NTS 105N). Geological Survey of Canada, Open File 2363, 140 p.
- Friske, P.W.B., Hornbrook, E.H.W., Lynch, J.J., McCurdy, M.W., Gross, H., Galletta, A.C., Durham, C.C., 1991b. National Geochemical Reconnaissance stream sediment and water data, east central Yukon (NTS 105O; parts of 105P). Geological Survey of Canada, Open File 2364, 140 p.
- Gabrielse, H., 1962. Kechika map area. Geological Survey of Canada, Preliminary Map 42-1962, 1:253,440 scale.
- Gabrielse, H., 1963a. Rabbit River map area. Geological Survey of Canada, Preliminary Map 46-1962, 1:253,440 scale.
- Gabrielse, H., 1963b. McDame map area, Cassiar District, British Columbia. Geological Survey of Canada, Memoir 319, 138 p.
- Gabrielse, H., 1998. Geology of Cry Lake and Dease Lake map areas, north-central British Columbia. Geological Survey of Canada, Bulletin 504, 147 p.
- Garrett, R.G., Grunsky, E.C., 2001. Weighted sums - knowledge based empirical indices for use in exploration geochemistry. *Geochemistry: Exploration, Environment, Analysis* 1, 135-141.
- Gordey, S.P., Makepeace, A.J., compilers, 1999. Yukon bedrock geology in Yukon digital geology. Geological Survey of Canada, Open File D3826/ Indian and Northern Affairs Canada, Exploration and Geological Services Division, Yukon, Open File 1999-1(D).
- Grunsky, E.C. 2007. The interpretation of regional geochemical survey data. In: *Advances in Regional-Scale Geochemical Methods, Proceedings of Exploration 07: Fifth Decennial International Conference on Mineral Exploration*, B. Milkereit (ed.), Geological Survey of Canada, Paper 8, p. 139-182.
- Hart, J.R., Mair, J.L., Goldfarb, J.R., Groves, I.G., 2004. Source and redox controls on metallogenic variations in intrusion-related ore systems, Tombstone-Tungsten Belt, Yukon Territory, Canada. *Transactions of the Royal Society of Edinburgh. Earth Sciences* 95, 339-356.
- Heberlein, D.R., 2013. Catchment basin analysis and weighted sums modelling: enhanced interpretation of RGS data using examples from map sheets NTS 105M, 105O and part of 105P. Yukon Geological Survey, Open File 2013-16, 18 p.
- Héon, D., compiler, 2003. Yukon Regional Geochemical Database 2003 - Stream sediment analyses. Exploration and Geological Services Division, Yukon Region, Indian and Northern Affairs Canada.
- Hawkes, H.E., 1976. The downstream dilution of stream sediment anomalies. *Journal of Geochemical Exploration* 6, p. 345-358.
- Jackaman, W., Lett, R., Sibbick, S., 1996. Geochemistry of the Gataga Mountain area. British Columbia Ministry of Employment and Investment, British Columbia Geological Survey Open File 1996-18, 194 p.
- Jackaman, W., 2011a. Northern BC Sample Reanalysis Project. *Geoscience BC, Report 2011-2*, 11 p.
- Jackaman, W., 2011b. Regional stream sediment geochemical data Nidderly Lake, Yukon (105O & P). Yukon Geological Survey, Open File 2011-30, 116 p.
- Lett, R., 2001. Geochemical exploration models Vol 2: Shale hosted Pb-Zn-Ag deposits in NE BC (94F/13, 94K/4 and 94L/1). British Columbia Ministry of Energy, Mines and Petroleum Resources, British Columbia Geological Survey Open File 2001-07, 74 p.
- Lett, R., Jackaman, W., Sibbick, S., 1996. Spring water and spring sediment geochemistry of the Gataga Mountain area (parts of 94L/7, 8, 9, 10, 11, 14, 15). British Columbia Ministry of Employment and Investment, British Columbia Geological Survey Open File 1996-30, 27 p.
- Muntean, J. L., Cline, J. S., Simon, A. C., Anthony, A. L., 2011. Magmatic-hydrothermal origin of Nevada's Carlin-type gold deposits. *Nature Geoscience* 4, 122-127.
- Patterson, L.M., Muntean, J.L., 2011. Multi-element geochemistry across a Carlin-type gold district: Jerritt Canyon, Nevada. In: *Great Basin Evolution and Metallogeny*, R. Steininger and B. Pennell (eds.), Geological Society of Nevada 2010 Symposium, Reno, NV, United States, DEStech Publications, Lancaster, PA, United States, p.1119-1151.
- Poulsen, K. H., 1996. Carlin-type gold deposits and their potential occurrence in the Canadian Cordillera. In: *Geological Survey of Canada, Current Research 1996-A*, p.1-9.
- Rock, N.M.S., 1988. *Numerical Geology: A Source Guide, Glossary and Selective Bibliography to Geological Uses of Computers and Statistics*. Lecture Notes in Earth Sciences 18, Springer-Verlag, Berlin, 427 p.
- Rousseeuw, P.J., Leroy, A.M., 1987. *Robust Regression and Outlier Detection*. Series in Applied Probability and Statistics, Wiley-Interscience, New York, 329 p.
- Rukhlov, A.S., Han, T., Nelson, J., Hickin, A., Ferri, F., 2014. Supplementary data for Carlin-type geochemical signal in lake and stream sediments from Kechika trough, north-central British Columbia. British Columbia Ministry of Energy and Mines, British Columbia Geological Survey GeoFile 2014-10.
- Thiessen, E.J., Gleeson, S.A., Dufrane, S.A., Carne, R.C., Dumala, M., 2012. Upper age constraint and paragenesis of the Tiger zone, Rau property, central Yukon. In: *Yukon Exploration and Geology 2011*, K.E. MacFarlane and P.J. Sack (eds.), Yukon Geological Survey, p. 151-164.
- Tucker, M.J., Hart, C.J.R., Carne, R.C., 2013. Geology, alteration, and mineralization of the Carlin-type Conrad zone, Yukon. In: *Yukon Exploration and Geology 2012*, K.E. MacFarlane, M.G. Nordling, and P.J. Sack (eds.), Yukon Geological Survey, p.163-178.

Concentration of carbonatite indicator minerals using a Wilfley gravity shaking table: A case history from the Aley carbonatite, British Columbia, Canada

D.A.R. Mackay¹, G.J. Simandl^{1,2,a}, P. Luck², B. Grcic³, C. Li³, M. Redfearn³, and J. Gravel⁴

¹ School of Earth and Ocean Sciences, University of Victoria, Victoria, BC, V8P 5C2

² British Columbia Geological Survey, Ministry of Energy and Mines, Victoria, BC, V8W 9N3

³ Bureau Veritas Commodities Canada Ltd., Inspectorate Metallurgical Division, 11620 Horseshoe Way, Richmond, BC, V7A 4V5

⁴ ACME Analytical Laboratories, 9050 Shaughnessy St., Vancouver, BC, V6P 6E5

^a corresponding author: George.Simandl@gov.bc.ca

Recommended citation: Mackay, D.A.R., Simandl, G.J., Luck, P., Grcic, B., Li, C., Redfearn, M., and Gravel, J., 2015. Concentration of carbonatite indicator minerals using a Wilfley gravity shaking table: A case history from the Aley carbonatite, British Columbia, Canada. In: Geological Fieldwork 2014, British Columbia Ministry of Energy and Mines, British Columbia Geological Survey Paper 2015-1, pp. 189-195.

Abstract

A Wilfley shaking table was used to concentrate specialty metal indicator minerals, with an emphasis on Nb- and REE-bearing minerals. This paper presents an assessment of the Wilfley shaking table using a synthetic sample and natural samples from the Aley carbonatite drainage area. The Wilfley shaking table successfully concentrated key indicator minerals from stream-sediment samples from the Aley carbonatite drainage area. The key carbonatite indicator minerals (in order of importance) are: pyrochlore, columbite-(Fe); fersmite, REE-fluorocarbonates; monazite; apatite; and possibly magnetite, Na- and K-amphibole, and Na pyroxene. The concentrations of these minerals correlate with the concentrations of pathfinder elements (Nb, Ta, LREE [La, Ce, Pr, and Nd], Ba, Sr, P, U, and Th) in the Aley stream sediments. Relative to unprocessed sediments, the Wilfley table concentrated Nb by 4.8 times, Ta by 3.6 times, and LREE by 3.9 times. This indicates that heavy minerals previously identified as potential indicators were successfully concentrated by the Wilfley shaking table. High coefficients of determination ($R^2 > 0.85$) between the raw stream sediment and Wilfley concentrates for Nb, Ta, LREE, Y, Th, U, and Fe content indicate the targeted heavy minerals were consistently concentrated and Wilfley table treatment preserves the carbonatite geochemical signature.

Keywords: indicator minerals, heavy mineral separation, carbonatite, niobium, tantalum, rare-earth elements, specialty metals

1. Introduction

Indicator minerals are effective tools to explore for covered or poorly exposed ore deposits, and methods for their use in regional studies are well established (McCurdy et al., 2006, 2009; McClenaghan, 2011). The 250 μm –2.0 mm size fraction is commonly examined, and Wilfley-type tables are used to pre-concentrate minerals before heavy liquid separation, isodynamic magnetic separation, and hand picking (McClenaghan, 2011).

Indicator minerals for carbonatite-related specialty metal deposits are: Nb-bearing minerals (pyrochlore, columbite-[Fe], and fersmite), monazite, zircon, REE-fluorocarbonates (bastnaesite and synchysite), apatite, sulphates (barite-celestine) and potentially, magnetite, Na-K amphiboles, Na-pyroxenes, and allanite (Table 1). Herein we use sediment samples from streams draining the Aley carbonatite (Fig. 1) to determine if Wilfley tables can effectively concentrate carbonatite indicator minerals to a degree that additional processing is unnecessary before using Quantitative Evaluation of Minerals by SCANning electron microscopy (QEMSCAN) to establish quantitative mineralogy.

2. Aley carbonatite

The Aley carbonatite is 290 km north of Prince George, British Columbia (Fig. 1), and outcrops over a 3 x 3.5 km



Fig. 1. Location of the Aley carbonatite (yellow star) in British Columbia, Canada.

area (Mäder, 1986; McLeish, 2013). The Aley carbonatite is the most important Nb-deposit in the Canadian Cordillera with

Table 1. Potential carbonatite indicator minerals. Expected ranges in pathfinder element content (oxide Wt.%) are for minerals from carbonatites. From Bühn et al. (2001), Belousova et al. (2002a, b), Atencio et al. (2010), Anthony et al. (2014), and Mackay and Simandl (2014c).

Mineral Name	Chemical Formula	Density (g/cm ³)	Nb ₂ O ₅	Ta ₂ O ₅	TREO	Y ₂ O ₃	P ₂ O ₅	ThO ₂	SrO	BaO	U ₃ O ₈	ThO ₂
Pyrochlore	(Ca,Na) ₂ (Nb,Ti,Ta) ₂ O ₆ (O,OH,F)	4.2-6.4	34.2-86.8	tr-4.3	2.6-6.0	n.a.	n.a.	n.a.	n.a.	n.a.	n.a.	n.a.
Columbite-(Fe)	(Fe ²⁺ ,Mn)(Ta,Nb) ₂ O ₆	5.3-7.3	46.8-81.2	tr-31.2	n.a.	n.a.	n.a.	n.a.	n.a.	n.a.	n.a.	n.a.
Fersmite	(Ca,Ce,Na)(Nb,Ta,Ti) ₂ (O,OH,F) ₆	4.69-4.79	66.0-70.1	tr-16.9	4.8	2.9	n.a.	n.a.	n.a.	n.a.	n.a.	n.a.
Monazite	(Ce,La,Nd,Th)PO ₄	4.8-5.5	n.a.	n.a.	59.2	n.a.	27.4	11.6	n.a.	n.a.	0.4	11.6
Zircon	ZrSiO ₄	4.6-4.7	n.a.	n.a.	0.1-4.4	n.a.	n.a.	n.a.	n.a.	n.a.	tr	n.a.
Bastnaesite	Ce(CO ₃)F	4.95-5.00	n.a.	n.a.	73.6-78.1	n.a.	n.a.	n.a.	n.a.	n.a.	n.a.	n.a.
Synchysite	Ca(Ce,La)(CO ₃) ₂ F	3.90-4.15	n.a.	n.a.	47.8	0.5	n.a.	n.a.	n.a.	n.a.	n.a.	n.a.
Apatite	Ca ₅ (PO ₄) ₃ (OH,F,Cl)	3.16-3.22	n.a.	n.a.	0.5-5.5	n.a.	35.7-40.4	tr-0.1	0.4-4.5	tr-1.0	n.a.	tr-0.1
Barite	BaSO ₄	4.48	n.a.	n.a.	n.a.	n.a.	n.a.	n.a.	n.a.	65.4-65.7	n.a.	n.a.
Celestine	SrSO ₄	3.9-4.0	n.a.	n.a.	n.a.	n.a.	n.a.	n.a.	56.2-56.4	n.a.	n.a.	n.a.
Magnetite	Fe ²⁺ Fe ³⁺ ₂ O ₄	5.1-5.2	n.a.	n.a.	n.a.	n.a.	n.a.	n.a.	n.a.	n.a.	n.a.	n.a.
Arfvedsonite	Na ₃ [(Fe ²⁺ ,Mg) ₄ Fe ³⁺]Si ₈ O ₂₂ (OH) ₂	3.44-3.45	n.a.	n.a.	n.a.	n.a.	n.a.	n.a.	n.a.	n.a.	n.a.	n.a.
Richterite	Na(Ca,Na)(Mg,Fe ²⁺) ₅ Si ₈ O ₂₂ (OH) ₂	3.09	n.a.	n.a.	n.a.	n.a.	n.a.	n.a.	n.a.	n.a.	n.a.	n.a.
Aegirine	NaFe ³⁺ Si ₂ O ₆	5.50-5.54	n.a.	n.a.	n.a.	n.a.	n.a.	n.a.	n.a.	n.a.	n.a.	n.a.
Allanite	(Ce,Ca,Y) ₂ (Al,Fe ²⁺ ,Fe ³⁺) ₃ (SiO ₄) ₃ (OH)	3.3-4.2	n.a.	n.a.	32.0	5.5	n.a.	n.a.	n.a.	n.a.	n.a.	n.a.

n.a. = not applicable; tr = trace; TREO = total rare earth oxides

a measured plus indicated resource of 286 million tonnes at 0.37% Nb₂O₅, with a cut-off grade of 0.20% Nb₂O₅ (Simpson, 2012). It is hosted by greenschist-facies metasedimentary rocks. The main body of the Aley carbonatite is dolomitic and is surrounded by a volumetrically minor calcite-carbonatite rim (Mäder, 1986; McLeish, 2013). Minerals of economic interest include fersmite, columbite-(Fe), and pyrochlore; common accessories include apatite, pyrite, magnetite, biotite/phlogopite, and calcite (Mäder, 1986; Kressell et al., 2010; McLeish, 2013; Mackay and Simandl, 2014a). The carbonatite is surrounded by a zone of fenitized (Na and K hydrothermally altered) country rock containing richterite, arfvedsonite, aegirine, and albite.

3. Summary of previous work

Twelve stream sediment samples were collected from the stream draining the Aley carbonatite area (Mackay

and Simandl, 2014a). Samples were dry sieved into eight size fractions (>4 mm, 2–4 mm, 1–2 mm, 500 µm–1 mm, 250–500 µm, 125–250 µm, 63–125 µm and <63 µm). The dry sieved 125–250 µm size fraction (herein referred to as ‘raw sample’) was determined to be ideal for carbonatite exploration in British Columbia, based on high concentrations of carbonatite pathfinder elements relative to the other size fractions (Luck and Simandl, 2014; Mackay and Simandl, 2014a, b). An approximately 10 g split of each raw sample was milled, prepared in standard X-ray diffraction sample cups, and analyzed using a Thermo Scientific Niton® FXL-950 as described by Luck and Simandl (2014). Samples with large amounts of material (>300 g) in the 125–250 µm fraction were split for processing on the Wilfley table.

4. Wilfley mineral separator

Wilfley shaking tables separate silt and sand sized material

based on mineral density (e.g., Sivamohan and Forssberg, 1985; Stewart, 1986; McClenaghan, 2011). Testing and optimization of operating conditions for the Mine & Smelter Supply Co. Wilfley shaking table (#13 table, 457 x 1016 mm) was performed using a synthetic standard, which contained 500 g of material made up of magnetite (40 g), garnet (30 g), fluorite (60 g), and quartz (370 g). Magnetite was selected as a proxy for heavy minerals targeted as carbonatite indicators. Synthetic standard components were milled to the same grain size range (125–250 μ m) as identified previously for testing (Luck and Simandl, 2014; Mackay and Simandl, 2014a, b). Several runs with synthetic standards were performed, and operating parameters were optimized based on magnetite concentrations (a magnet was used to recover magnetite from concentrate). The main operating parameters for a Wilfley shaking table are: table inclination and slope, wash-water flow rate, material feed rate, table speed, and stroke amplitude (Razali and Veasey, 1990; Manser et al., 1991). Separation of material is also affected by feed grade and feed density. The table was set with an 8° incline, 3° slope, 10 mm stroke, and

table speed of 250 rpm for all samples. Water flow was kept constant for all samples at 18 L/min based on optimization using synthetic standards. Optimized parameters increased the magnetite yield by 3.7 times.

4.1. Processing procedure

Dry sieved (125–250 μ m size fraction) stream-sediment samples varying from 380.4–938.4 g (Table 2) were mixed into a slurry with water and gradually washed from a container into the sample feeder (Fig. 2) using a water hose. Material moves in the direction of shaking across the table surface and diagonally down the table slope. Denser material (concentrate) is carried farthest left along the table ridges, while the least dense material is washed off the bottom of the table (Fig. 3). Launder trays were positioned to collect the concentrate, middlings, and tailings. Suspended particles were allowed to settle and excess water was decanted from concentrates, middlings, and tailings. Samples were dried overnight at 90°C then weighed for quality control, allowing samples to be reconstituted and reprocessed if needed. After processing, concentrate, middlings, and tailings

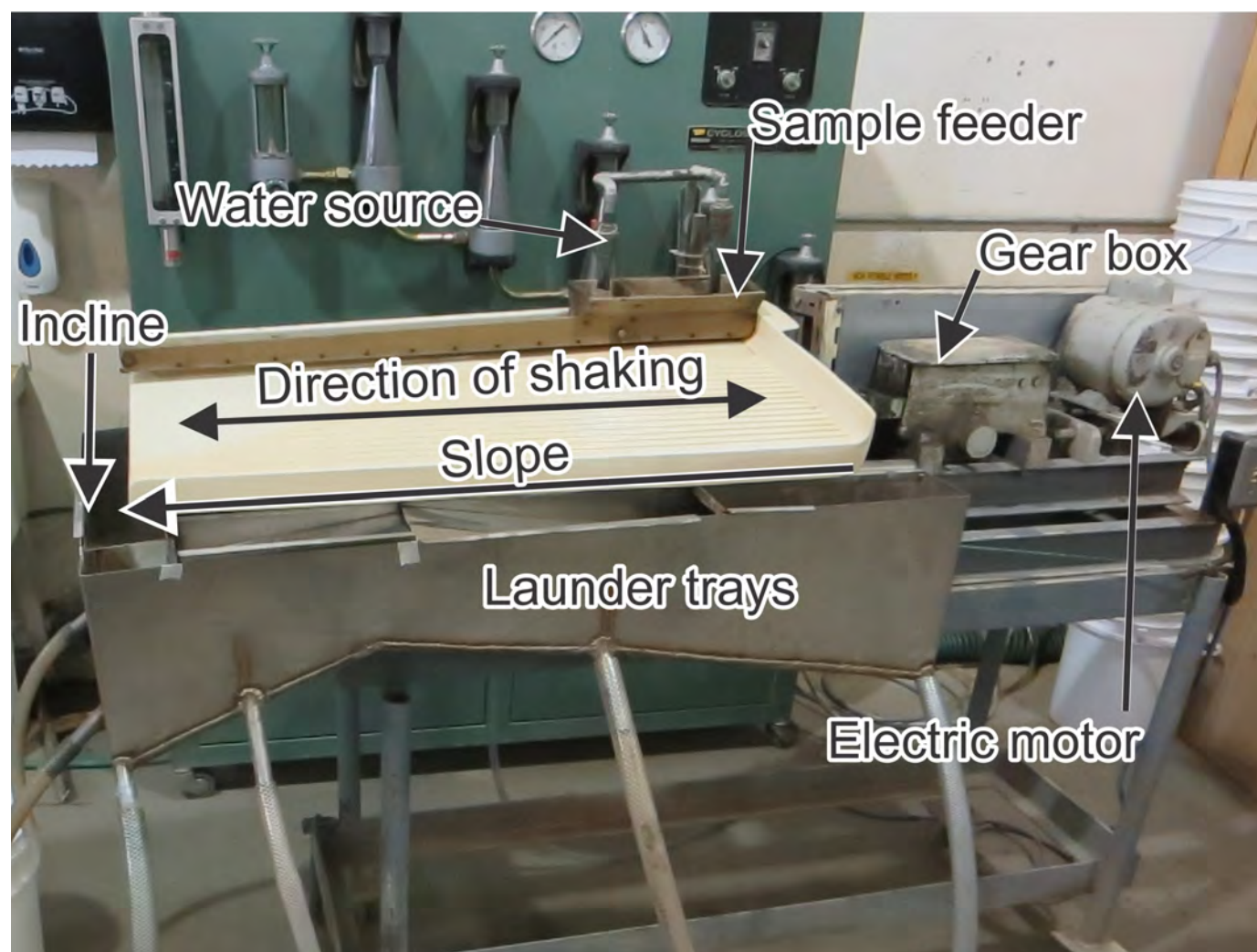


Fig. 2. Wilfley shaking table with adjustable launder trays. Slope and incline axes (angle from horizontal) are shown.

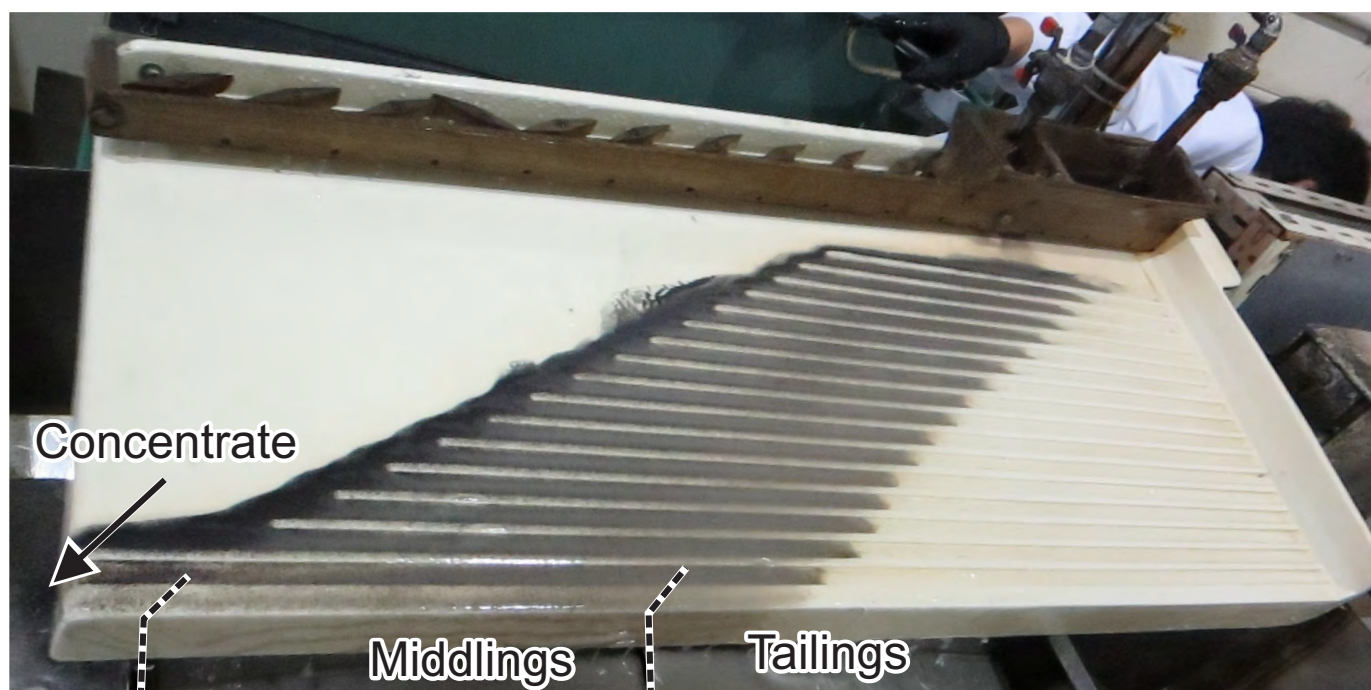


Fig. 3. Close-up of the Wilfley table. Heavy minerals (black) are separated from middlings and tailings as material moves from the top-right to bottom-left.

Table 2. Selected major and minor elemental composition (ppm) of the 125–250 μm size fraction of stream sediments from the Aley area, analysed by portable XRF. Phosphorous content was determined by lab analysis using fused bead, acid digestion, and ICP-AES analysis. Modified from Mackay and Simandl (2014a).

Sample no.	Split Size (g)	Nb	Ta	LREE	La	Ce	Pr	Nd	Y	Ba	Sr	P*	U	Th	Fe	Ca
AL-13-01	380.4	3495	79	2602	596	936	346	724	72	670	711	10822	26	266	40852	78201
AL-13-07	383.1	615	23	1690	316	505	289	580	34	244	688	6327	6	68	22375	160338
AL-13-10	510.1	5543	110	4879	1280	1918	520	1161	104	505	944	14619	40	376	65852	154081
AL-13-16	938.4	5246	101	4229	1083	1648	470	1028	93	910	745	12000	36	355	59782	156997
AL-13-18	503.7	3311	78	2763	662	1025	355	721	71	688	747	10997	26	255	42845	166097

*Lab analysis by fused bead, acid digestion, and ICP-AES analysis

were analysed by portable X-ray fluorescence (XRF) using the method described by Luck and Simandl (2014) and Mackay and Simandl (2014a).

5. Results of Wilfley table separation and geochemical analysis

Wilfley table separation of the 125-250 μm size fraction of stream-sediment samples from the Aley carbonatite drainage produced a range in proportions of concentrates (10.0-18.3 wt.%), middlings (48.8-68.8 wt.%), and tailings (11.0-38.2 wt.%; Fig. 4). Due to minor loss of material during processing, the proportion of concentrate, middlings, and tailings do not total 100%. Relative to raw samples (Table 2), the Nb content of Wilfley concentrates (Table 3) increased by 3.9-5.6 times (average of 4.8; Fig. 5a). Similarly, Ta increased by 2.3-4.9

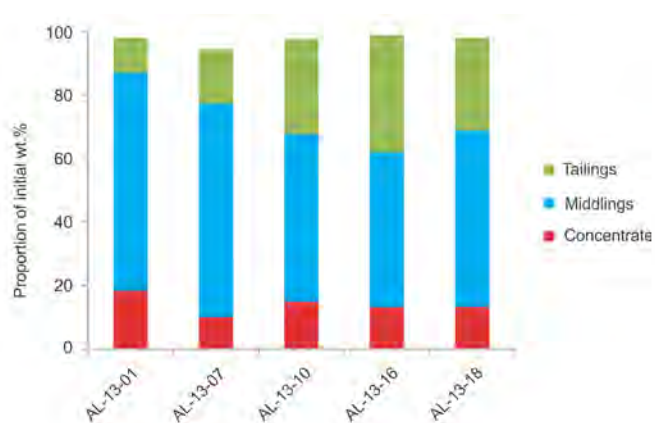


Fig. 4. Proportion of original wt.% in Wilfley table concentrates, middlings, and tailings for Aley carbonatite area stream sediments.

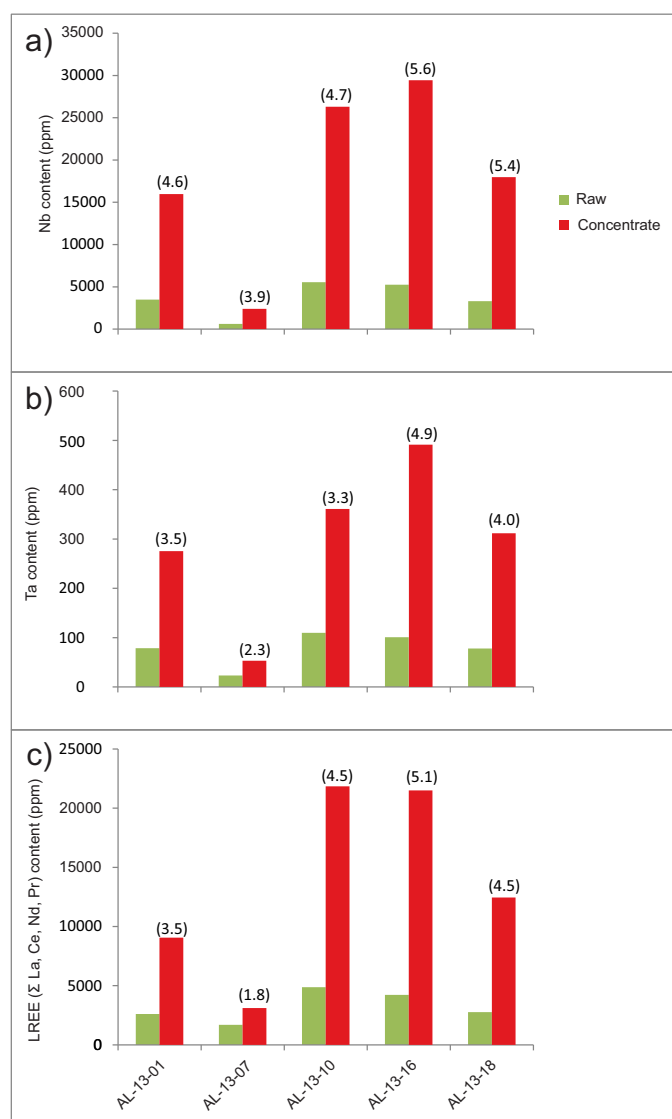


Fig. 5. Comparison of **a)** Nb, **b)** Ta, and **c)** LREE (Σ La, Ce, Nd, Pr) concentrations in Wilfley table concentrates relative to corresponding raw samples from Aley. Concentration factors for each element or group of elements for individual samples are shown in parentheses.

times (average of 3.6; Fig. 5b) and LREE content increased by 1.8-5.1 times (average of 3.9; Fig. 5c). The portable XRF used in this study reports phosphorous values above 10000 ppm as below detection limit, hence P was determined by fused bead, acid digestion and inductively coupled plasma atomic emission spectroscopy (ICP-AES; Tables 2 and 3). Phosphorous content of Wilfley concentrations increased by 1.8-2.4 times (average of 2.2) relative to raw samples.

6. Discussion of Wilfley table heavy mineral separation

Relatively high coefficients of determination in raw samples versus Wilfley table concentrates for Nb ($R^2=0.96$; Fig. 6a) and Ta ($R^2=0.85$; Fig. 6b) suggest consistent concentration of Nb- (\pm Ta) bearing minerals (pyrochlore, columbite-(Fe), and fersmite). Similarly, high coefficients of determination for LREE ($R^2=0.96$; Fig. 6c) and Y ($R^2=0.94$; Fig. 6d) suggest that REE-fluorocarbonates, monazite, and other REE-bearing minerals were successfully concentrated by the Wilfley table treatment. High coefficient of determination ($R^2=0.98$) between Zr and LREE content of Wilfley table concentrates indicates zircon is a possible LREE-bearing indicator mineral for carbonatite exploration. Iron also shows a high coefficient of determination ($R^2=0.97$) suggesting the effective concentration of magnetite, hematite, and columbite-(Fe). The low coefficient of determination ($R^2=0.01$; Fig. 6e) for Sr content in concentrates and raw samples and a low concentration factor (average of 1.2) from Wilfley table processing indicate that Sr in stream sediments was not concentrated in a predictable way. Coefficients for Ba ($R^2=0.93$; Fig. 6f), Th ($R^2=0.95$), and U ($R^2=0.95$) in raw samples and Wilfley table concentrates indicate that the carbonatite signature in stream sediments is preserved following Wilfley table concentration.

7. Conclusions

The Wilfley shaking table successfully concentrated carbonatite pathfinder elements in the 125–250 μ m size fraction of stream-sediment samples from the Aley carbonatite drainage. Niobium content of Wilfley table concentrates increased relative to raw samples by a factor of 4.8 (in the

Table 3. Selected major and trace element composition (ppm) of Wilfley table concentrates from the Aley area, analysed by portable XRF. Phosphorous was determined by fused bead, acid digestion, and ICP-AES analysis.

Sample no.	Nb	Ta	LREE	La	Ce	Pr	Nd	Y	Ba	Sr	P*	U	Th	Fe	Ca
AL-13-01	15977	275	9058	2528	3885	769	1876	238	1473	988	25964	112	926	128372	164276
AL-13-07	2387	53	3107	754	1156	374	823	71	251	888	14837	14	184	37174	206324
AL-13-10	26293	361	21845	6692	10006	1367	3779	368	1055	943	26052	147	1209	265897	126498
AL-13-16	29441	491	21493	6516	9902	1370	3706	396	3327	861	24743	162	1371	273248	118279
AL-13-18	17983	312	12451	3621	5534	904	2392	274	1912	1006	26663	109	993	167279	155281

*Lab analysis by fused bead, acid digestion, and ICP-AES

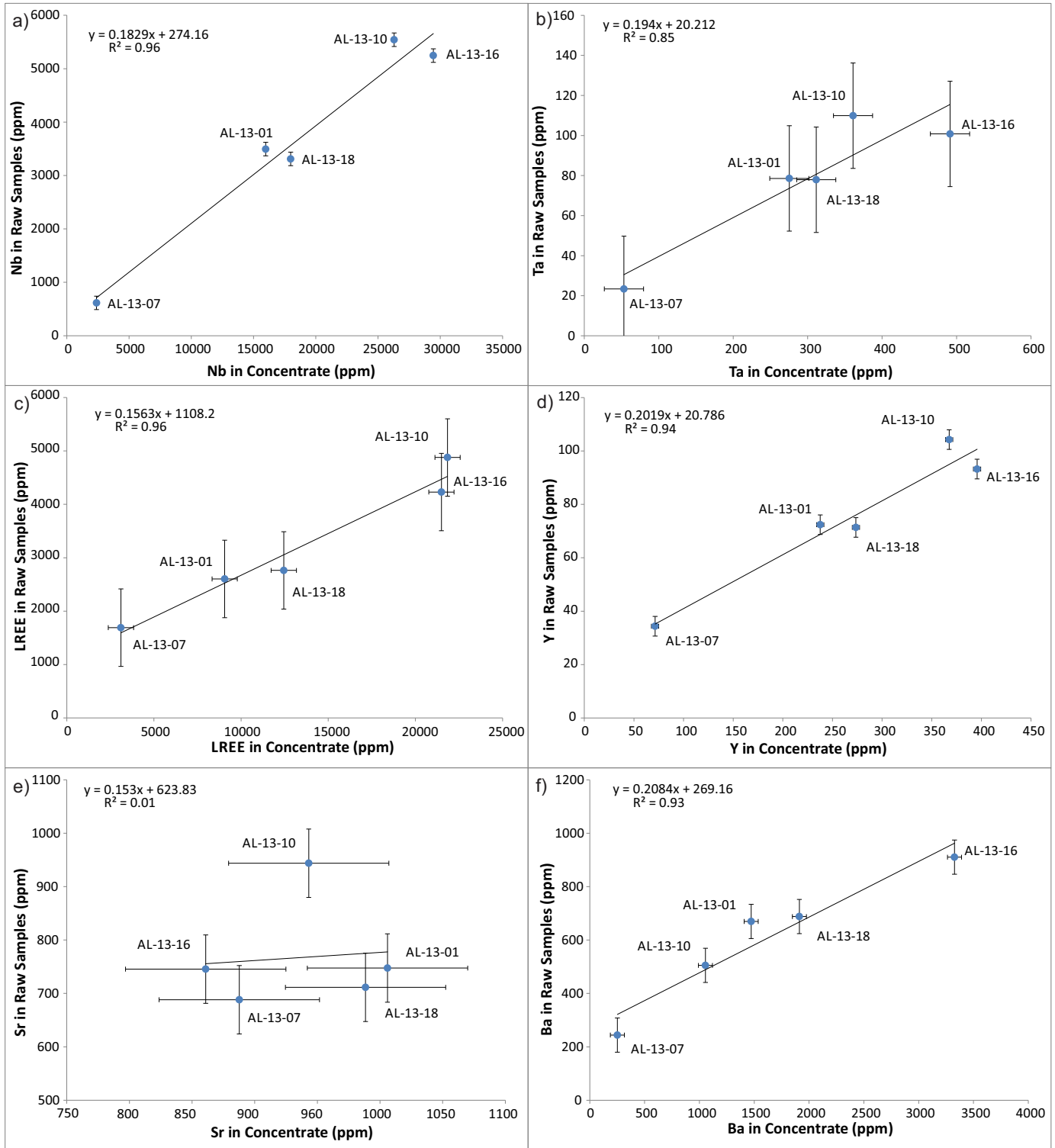


Fig. 6. Comparison of Wilfley table concentrates relative to raw samples from the Aley carbonatite. **a)** Nb. **b)** Ta; for raw samples Ta is near the lower detection limit, resulting in large errors relative to the concentrates. **c)** LREE; error propagation for \sum LREE results in larger margins relative to La, Ce, Pr, and Nd individually. **d)** Y. **e)** Sr. **f)** Ba. Error bars (2σ) are based on repeated analyses of standards as described in Luck and Simandl (2014).

range of 600–30000 ppm). Similarly, Ta increased by 3.6 times (in the range of 20–500 ppm), and LREE by 3.9 times (in the range of 1700–22000 ppm). This indicates that the

Wilfley table effectively concentrates the Nb-, Ta-, and LREE-bearing heavy minerals targeted by this study (e.g. pyrochlore, columbite-[Fe], fersmite, REE-fluorocarbonates, monazite,

zircon, apatite, and allanite). High coefficients of determination between pathfinder element concentrations in raw samples and Wilfley table concentrates suggests predictable relationships between indicator mineral counts in raw sediments and Wilfley table concentrates. A QEMSCAN study is in progress to test this.

Acknowledgments

This project was funded by the Targeted Geoscience Initiative 4 (2010–2015), a Natural Resources Canada program. The Specialty Metal component of this program was carried out collaboratively the Geological Survey of Canada and the British Columbia Geological Survey. Dr. Maria Holuszko (University of British Columbia, Norman B. Keevil Institute of Mining Engineering) provided many helpful and constructive comments and suggestions that improved the manuscript. Bureau Veritas Commodities Canada Ltd., Inspectorate Metallurgical Division and Acme Analytical Laboratories are thanked for access to laboratory equipment and the expert advice of their staff. Helicopter and logistical support during sampling from Taseko Mines Limited and a scholarship from Geoscience BC to the first author are also greatly appreciated.

References

- Anthony, J.W., Biduaex, R.A., Bladh, K.W., and Nichols, M.C., 2014. Handbook of mineralogy. Mineralogical Society of America, Chantilly, U.S.A., <<http://www.handbookofmineralogy.org/>> Accessed December 29, 2014.
- Atencio, D., Andrade, M.B., Christy, A.G., Gieré, R., and Kartashov, P.M., 2010. The pyrochlore supergroup of minerals: nomenclature. *The Canadian Mineralogist*, 48, 673-698.
- Belousova, E.A., Griffin, W.L., O'Reilly, S.Y., and Fisher, N.I., 2002a. Apatite as an indicator mineral for mineral exploration: trace-element compositions and their relationship to host rock type. *Journal of Geochemical Exploration*, 76, 45-69.
- Belousova, E.A., Griffin, W.L., O'Reilly, S.Y., and Fisher, N.I., 2002b. Igneous zircon: trace element composition as an indicator of source rock type. *Contributions to Mineralogy and Petrology*, 143, 602-622.
- Bühn, B., Wall, F., and Le Bas, M.J., 2001. Rare-earth element systematics of carbonatitic fluorapatites, and their significance for carbonatite magma evolution. *Contributions to Mineralogy and Petrology*, 141, 572-591.
- Kressall, R., McLeish, D.F. and Crozier, J., 2010. The Aley carbonatite complex – Part II petrogenesis of a Cordilleran niobium deposit. In: Simandl, G.J., and Lefebure, D.V. (Eds.), *International workshop on the geology of rare metals*, November 9-10, 2010, Victoria, Canada. *Extended Abstracts Volume*. British Columbia Ministry of Energy and Mines, British Columbia Geological Survey, Open File 2010-10, pp. 25-26.
- Luck, P. and Simandl, G.J., 2014. Portable X-ray fluorescence in stream sediment chemistry and indicator mineral surveys, Lonnie Carbonatite Complex, British Columbia. In: *Geological Fieldwork 2013*, British Columbia Ministry of Energy and Mines, British Columbia Geological Survey, Paper 2014-1, pp. 169-182.
- Mackay, D.A.R., and Simandl, G.J., 2014a. Portable X-ray fluorescence to optimize stream sediment chemistry and indicator mineral surveys, case 1: Carbonatite-hosted Nb deposits, Aley carbonatite, British Columbia, Canada. In: *Geological Fieldwork 2013*, British Columbia Ministry of Energy and Mines, British Columbia Geological Survey, Paper 2014-1, pp. 183-194.
- Mackay, D.A.R. and Simandl, G.J., 2014b. Portable X-ray fluorescence to optimize stream sediment chemistry and indicator mineral surveys, case 2: Carbonatite-hosted REE deposits, Wicheeda Lake, British Columbia, Canada. In: *Geological Fieldwork 2013*, British Columbia Ministry of Energy and Mines, British Columbia Geological Survey, Paper 2014-1, p. 195-206.
- Mackay, D.A.R. and Simandl, G.J., 2014c. Geology, market and supply chain of niobium and tantalum—a review. *Mineralium Deposita*, 49, 1025-1047.
- Mäder, U.K., 1986. The Aley carbonatite complex. Unpublished Master of Science thesis, University of British Columbia, 176 p.
- Manser, R.J., Barley, R.W., and Wills, B.A., 1991. The shaking table concentrator – the influence of operating conditions and table parameters on mineral separation – the development of a mathematical model for normal operating conditions. *Minerals Engineering*, 4, 369-381.
- McClenaghan, M.B., 2011. Overview of common processing methods for recovery of indicator minerals from sediments and bedrock in mineral exploration. *Geochemistry: Exploration, Environment, Analysis*, 11, 265-278.
- McCurdy, M.W., Kjarsgaard, I.M., Day, S.J.A., McNeil, R.J., Friske, P.W.B. and Plouffe, A., 2009. Indicator mineral content and geochemistry of stream sediments and waters from northeast British Columbia (NTS 94A, 94B, 94G, 94H, 94I, 94K, 94N, 94O, 94P). British Columbia Ministry of Energy and Mines, Geological Survey of British Columbia, Report 2009-2 and Geological Survey of Canada, Open File 6311, 19 p.
- McCurdy, M.W., Prior, G.J., Friske, P.W.B., McNeil, R.J., Day, S.J.A. and Nicholl, T.J., 2006. Geochemical, mineralogical and kimberlites indicator mineral electron microprobe data from silts, heavy mineral concentrates and water from a national geochemical reconnaissance stream sediment and water survey in northern and southwestern Buffalo Head Hills, northern Alberta (parts of 84B, 84C, 84F, and 84G): Alberta Energy and Utilities Board, Alberta Geological Survey, Special Report 76 and Geological Survey of Canada Open File 5057, 11 p.
- McLeish, D.F., 2013. Structure, stratigraphy, and U-Pb zircon-titanite geochronology of the Aley carbonatite complex, northeast British Columbia: Evidence for Antler-aged orogenesis in the foreland belt of the Canadian Cordillera. Unpublished Master of Science thesis, University of Victoria, 131 p.
- Razali, R. and Veasey, T.J., 1990. Statistical modelling of a shaking table separator – part one. *Minerals Engineering*, 3, 287-294.
- Simpson, R.G., 2012. Technical report - Aley carbonatite niobium project. Taseko Mines Limited, 66 p. <<http://www.sedar.com>> Accessed December 29, 2014.
- Sivamohan, R. and Forssberg, E. 1985. Principles of tabling. *International Journal of Mineral Processing*, 15, 281-295.
- Stewart, R., 1986. Routine heavy mineral analysis using a concentrating table. *Journal of Sedimentary Research*, 56, 555-556.

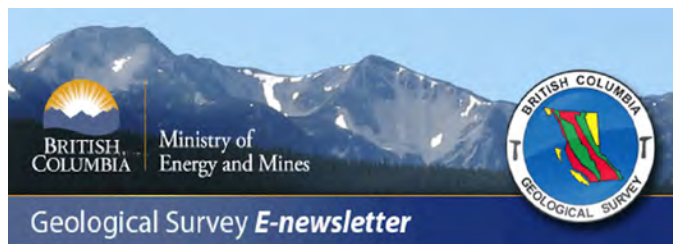
Appendix: British Columbia Geological Survey publications, 2014

All BCGS publications are available for download, free of charge, from:

www.empr.gov.bc.ca/Mining/Geoscience/PublicationsCatalogue/Pages/default.aspx

To receive notification of our latest releases email:

Geological.Survey@gov.bc.ca



Geoscience Maps

GM 2014-1

Ferby, T., 2014. Surficial geology of the Nadina River area (NTS 093E/15), 1:50,000 scale.

GM 2014-2

Ferby, T., 2014. Surficial geology of the Colleymount area (NTS 093L/01), 1:50,000 scale.

GM 2014-3

Nelson, J., Diakow, L.J., Mahoney, J.B., Gehrels, G.E., van Staal, C.R., Karl, S., Pecha, M., and Angen, J.J., 2014. Geology of the north and mid-coast regions, British Columbia (Parts of NTS 103-A, -G, -H, -I and -J), (also Geological Survey of Canada Open File 7604), 1:150,000 scale.

Open Files

OF 2014-1

Britton, J., Jago, P., Katay, F., Kyba, J., Li, G., Madu, B., and Northcote, B., 2014. Operating Mines and Selected Major Exploration Projects in British Columbia, 2013.

OF 2014-2

Ferby, T., 2014. Basal till potential of the Nadina River area (NTS 093E/15). (also Geoscience BC Map 2014-09-01), 1:50,000 scale.

OF 2014-3

Manor, M.J., Wall, C.J., Nixon, G.T., Scoates, J.S., Pinsent, R.H., and Ames, D.E., 2014. Preliminary Geology and Geochemistry of the Giant Mascot Ultramafic-Mafic Intrusion, Hope, Southwestern British Columbia (also Geological Survey of Canada Open File 7570), 1:10,000 scale.

OF 2014-4

Ferby, T., 2014. Basal till potential of the Colleymount area (NTS 093L/01), British Columbia (also Geoscience BC Map 2014-09-02), 1:50,000 scale.

OF 2014-5

Mihalynuk, M.G., Logan, J.M., Diakow, L.J., Martha A. Henderson, M.A., Jacob, J., and Watson, A.K.G., 2014. Allison Creek area preliminary geology NTS 92H/9W & 10E (and parts of adjacent sheets north and south).

OF 2014-6

Sacco, D., Ferby, T., and Jackaman, W., 2014. Basal till potential of the Clusko River map area (NTS 093C/09), British Columbia (also Geoscience BC Map 2014-06-01), 1:50,000 scale.

OF 2014-7

Sacco, D., Ferbey, T., and Jackaman, W., 2014. Basal till potential of the Clisbako River map area (NTS 093B/12), British Columbia (also Geoscience BC Map 2014-06-02), 1:50,000 scale.

OF 2014-8

Sacco, D., Ferbey, T., and Jackaman, W., 2014. Basal till potential of the Marmot Lake map area (NTS 093B/13), British Columbia. (also Geoscience BC Map 2014-06-03), 1:50,000 scale.

OF 2014-9

Sacco, D., Ferbey, T., and Jackaman, W., 2014. Basal till potential of the Toil Mountain map area (NTS 093C/16), British Columbia. British Columbia (also Geoscience BC Map 2014-06-04), 1:50,000 scale.

OF 2014-10

Sacco, D., Ferbey, T., and Jackaman, W., 2014. Basal till potential of the Suscha Creek map area (NTS 093F/01), British Columbia (also Geoscience BC Map 2014-06-05) 1:50,000 scale.

OF 2014-11

Sacco, D., Ferbey, T., and Jackaman, W., 2014. Basal till potential of the Coglistiko River map area (NTS 093G/04), British Columbia (also Geoscience BC Map 2014-06-06), 1:50,000 scale.

OF 2014-12

Sacco, D., Ferbey, T., and Jackaman, W., 2014. Basal till potential of the Pelican Lake map area (NTS 093G/05), British Columbia, (also Geoscience BC Map 2014-06-07), 1:50,000 scale.

OF 2014-13

Sacco, D., Ferbey, T., and Jackaman, W., 2014. Basal till potential of the Euchiniko River map area (NTS 093F/08), British Columbia, (also Geoscience BC Map 2014-06-08), 1:50,000 scale.

OF 2014-14

Sacco, D., Ferbey, T., and Jackaman, W., 2014. Basal till potential of the Chilako River map area (NTS 093G/12), British Columbia, (also Geoscience BC Map 2014-06-09), 1:50,000 scale.

OF 2014-15

Sacco, D., Ferbey, T., and Jackaman, W., 2014. Basal till potential of the Hulatt map area (NTS 093G/13), British Columbia, (also Geoscience BC Map 2014-06-10), 1:50,000 scale.

GeoFiles

GF 2014-1

Logan, J.M., and Schiarizza, P., 2014. Rayfield River major oxide, trace and rare earth element geochemical data.

GF 2014-2

Mihalynuk, M.G., Logan, J.M., and Diakow, L.D., 2014. Southern Nicola Arc Project 2013: Geochemical data.

GF 2014-3

Mihalynuk, M.G., Friedman, R.M., Gabites, J.E., and Logan, J.M., 2014. Southern Nicola Arc Project 2013: Geochronological data.

GF 2014-4

Luck, P., and Simandl, G.J., 2014. Stream sediment geochemical/indicator mineral orientation survey, Lonnie Nb Prospect, British Columbia, Canada (poster).

GF 2014-5

Mackay, D.A.R. and Simandl, G.J., 2014. Stream sediment orientation survey, Aley carbonatite niobium deposit, British Columbia, Canada, (poster).

GF 2014-6

Mackay, D.A.R. and Simandl, G.J., 2014. Fine-tuning stream sediment chemistry and indicator mineral methodology in exploration for carbonatite-related REE targets, Wicheeda Lake, BC, Canada. British Columbia Geological Survey, (poster).

GF 2014-7

Mackay, D.A.R. and Simandl, G.J., 2014. Columbite-tantalite and pyrochlore as indicator minerals for specialty metal deposits, (poster).

GF 2014-8

Rukhlov, A., Han, T., Hickin, A., and Ferri, F., 2014. Carlin-type gold in British Columbia? (poster).

GF 2014-9

Cui, Y., 2014. Integration and delivery of British Columbia digital geology.

GF 2014-10

Rukhlov, A.S., Han, T., Nelson, J., Hickin, A., Ferri, F., 2014. Supplementary data for Carlin-type geochemical signal in lake and stream sediments from Kechika trough, north-central British Columbia.

GF 2014-11

Henderson, M.A., Mihalynuk, M.G., Sigloch, K., Johnston, S.T., and Shephard, G.A., Jurassic to Recent tectonic evolution of North America: A preliminary model using GPlates software.

Information Circulars

IC 2014-1

Britton, J., Katay, F., Jago, P., Kyba, J., Li, G., Madu, B., and Northcote, B., 2014. Provincial summary exploration and mining in British Columbia in 2013.

IC 2014-2

Dominion Coal Block Infographic.

IC 2014-3

Opportunities to Explore Infographic.

IC 2014-4

Northcote, B. Madu, B., Schroeter, T., and Li, G., 2014. Gold production and resources in British Columbia, 1890-2013.

IC 2014-5

British Columbia coal industry overview 2013.

IC 2014-6

Simandl, G., Paradis, S., and Luck, P., 2014. Refractory minerals in British Columbia, Canada, 2014.

IC 2014-7

British Columbia Geological Survey.

IC 2014-8

Opportunities to explore.

IC 2014-9

Online databases at the British Columbia Geological Survey.

Peer-reviewed journal publications

Angen, J.J., van Staal, C.R., Lin, S., Nelson, J.L., Mahoney, B., Davis, D.W. and McClelland, W.C., 2014. Timing and kinematics of shear zone deformation in the western Coast belt: Evidence for mid-Cretaceous orogen-parallel extension. *Journal of Structural Geology*, 68, 273-299.

Bell, K., Zaitsev, A.N., Spratt, J., Fröjdö, S., Rukhlov, A.S. in press. Elemental, lead and sulphur isotopic compositions of galena from Kola carbonatites, Russia - implications for melt and mantle evolution. *Mineralogical Magazine*.

Bordet, E., Mihalynuk, M.G., Hart, C.J.R., Mortensen, J.K., Friedman, R.M., and Gabites, J., 2014. Chronostratigraphy of Eocene volcanism, central British Columbia. *Canadian Journal of Earth Sciences*, 51, 56-103.

Colpron, M. and Nelson, J., 2014. Terrane (definition). *Encyclopedia of Marine Geosciences*, Springer-Verlag, DOI 10.1007/978-94-007-6644-0_214-1.

Logan, J., and Mihalynuk, M.G., 2014. Tectonic controls on paired alkaline porphyry deposit belts (Cu-Au ±Ag-Pt-Pd-Mo) within the Canadian Cordillera. *Economic Geology*, 109, 827-858.

Mackay, D.A.R., and Simandl, G.J., 2014. Geology, market and supply chain of niobium and tantalum-a review. *Mineralium Deposita*, 49, 1025-1047.

Mackay, D.A.R., and Simandl, G.J., in press. Pyrochlore and columbite-tantalite as indicator minerals for specialty metal deposits.

Geochemistry: Exploration, Environment, Analysis.

- Paradis, S., Keevil, H., Simandl, G.J., and Raudsepp, E. in press. Carbonate-hosted nonsulphide Zn-Pb mineralization of southern British Columbia, Canada. *Mineralium Deposita*.
- Simandl, G.J., 2014. Geology and market-dependent significance of rare earth element resources. *Mineralium Deposita*, 49, 889-904.
- Simandl, G.J., Fajber, R., Paradis, S., 2014. Portable X-ray fluorescence in the assessment of rare earth element-enriched sedimentary phosphate deposits. *Geochemistry: Exploration, Environment, Analysis*, 14, 161-169.
- Simandl, G. J., Stone, R. S., Paradis, S., Fajber, R., Reid, H. M., Grattan, K., 2014. An assessment of a handheld X-ray fluorescence instrument for use in exploration and development with an emphasis on REEs and related specialty metals. *Mineralium Deposita*, 49, 999-1012.
- Simandl, G. J., Paradis, S., Stone, R. S., Fajber, R., Kressall, R., Grattan, K., Crozier, J., and Simandl, L.J., 2014. Applicability of handheld X-ray fluorescence spectrometry in the exploration and development of carbonatite-related niobium deposits: a case study of the Aley carbonatite, British Columbia, Canada. *Geochemistry: Exploration, Environment, Analysis*, 14, 211-221.
- Stoppa, F., Rukhlov, A.S., Bell, K., Schiazza, M., and Vichi, G., 2014. Lamprophyres of Italy: early Cretaceous alkaline lamprophyres of Southern Tuscany, Italy. *Lithos* 188, 97-112.
- Tochilin, C.J., Gehrels, G.E., Nelson, J., and Mahoney, J.B., 2014. U-Pb and Hf isotope analysis of detrital zircons from the Banks Island assemblage (coastal British Columbia) and southern Alexander terrane (southeast Alaska). *Lithosphere*, 6, 200-215.

Contributions to partner publications

- Celis, M.A., Bouzari, F., Bissig, T., Hart, C.J.R., and Ferbey, T., 2014. Petrographic characteristics of porphyry indicator minerals from alkali porphyry copper-gold deposits in south-central British Columbia (NTS 092, 093). In: *Geoscience BC Summary of Activities 2013*, Geoscience BC Report 2014-1, pp. 53-62.
- Ferbey, T., Plouffe, A., and Anderson, R.G., 2014. An integrated approach to search for buried porphyry-style mineralization in central British Columbia using geochemistry and mineralogy: a TGI-4 project. *Geological Survey of Canada Current Research 2014-2*, 12 p. doi:10.4095/293130
- Hashmi, S., Ward, B.C., Plouffe, A., Ferbey, T., and Leybourne, M., 2014. Geochemical and mineralogical dispersal in till from the Mount Polley Cu-Au porphyry deposit, central British Columbia, Canada. *Geological Survey of Canada Open File 7589* (poster). doi:10.4095/293682
- Plouffe, A., Ferbey, T., and Anderson, R.G., 2014. Till composition and ice-flow history in the region of the Gibraltar Mine: developing indicators for the search of buried porphyry mineralization. *Geological Survey of Canada Open File 7592*, (poster). doi:10.4095/293839
- Ryan, J.J., van Staal, C.R., Haggart, J.W., and Nelson, J.L., 2014. Report of activities for ancient faults and their controls on mineralization in northern British Columbia and southern Yukon: GEM2 Cordillera Project. *Geological Survey of Canada Open File 7700*, 18 p., doi:10.4095/295503
- Sacco, D.A., Jackaman, W., and Ferbey, T., 2014. Targeted geochemical and mineralogical surveys in the TREK Project area, central British Columbia (parts of NTS 093B, D, F, G). In *Geoscience BC Summary of Activities 2013*. *Geoscience BC Report 2014-1*, pp. 19-34.
- Zagorevski, A., Mihalynuk, M.G., Joyce, N., and Martin, K., 2014. Characterization of volcanic and intrusive rocks across the British Columbia-Yukon border, GEM 2 Cordillera. *Geological Survey of Canada Open File 7697*, 10 p., doi:10.4095/295465